Fawu Wang · Tonglu Li (Eds)

Landslide Disaster Mitigation in Three Gorges Reservoir, China

Springer

Environmental Science and Engineering
Subseries: Environmental Science

Series Editors: R. Allan • U. Förstner • W. Salomons

Fawu Wang · Tonglu Li (Eds.)

Landslide Disaster Mitigation in Three Gorges Reservoir, China

Springer

Editors
Dr. Fawu Wang
Kyoto University
Disaster Prevention Research Inst.
Research Centre on Landslides
Gokasho, Uji, Kyoto 611-0011
Japan
wangfw@landslide.dpri.kyoto-u.ac.jp

Prof. Tonglu Li
Chang'an University
School of Geological
   Engineering and Geomatics
No.126 Yanta Road
Xi'an 710054
People's Republic of China
dcdgx08@chd.edu.cn

Cover design: Integra Software Services Pvt. Ltd.

Printed on acid-free paper

Foreword

The purpose of the Three Gorges project is to construct a large dam, forming a large-scale water reservoir in the valley. When the final design reservoir water level is reached, the length of the reservoir will be longer than 660 km, which extends from the dam site at Sandouping town to Maoer-Xia Gorge in Chongqing City. The reservoir crosses the low–medium mountainous area consisting of the fold zone from Sinian system to Mesozoic Erathem, which is distributed in Hubei Province, Hunan Province, Yunnan Province and Chongqing City, to the low mountainous area formed by the fold zone ranging from the Triassic to the Jurassic Periods, which is distributed in the eastern part of Chongqing City. Generally, the reservoir area can be divided into two parts. The eastern part is from Sandouping town to Baidicheng in Fengjie County, with a length of 160 km. In this part, three portions consisting of limestone formed the narrow Three Gorges. Between the Three Gorges are two portions consisting of clastic rocks forming wide valleys. At the dam site are the Pre-Sinian System crystal rocks. In the Three Gorges parts, thick bulk limestone and dolomite are mainly distributed, sandwiching thin layers of sandstone and shale. The mountain height at the gorge areas is about 600–1,200 m, and the width at those areas is only 200–300 m. The geomorphology characterized by high mountains and deep valleys formed the famous three gorges, namely, Qutang Gorge in the west, Wu Gorge in the middle, and Xiling Gorge in the east. The Xiling Gorge is divided into eastern part and western part. The dam site is located between the eastern part and western part of Xiling Gorge. The upstream valley of the dam site consists of gneiss and mixture rock of the Pre-Sinian system, with 16-km long, wide valley. One of the two wide valley areas sandwiched by the three gorges is the Zigui basin valley formed in the Jurassic Period; the other was formed by shale during the Silurian Period. The width of the river in both areas is about 300–400 m, with a mountain height of 500–800 m. The slopes in these areas are relatively gentle. The western part extends from Baidicheng to Maoer-Xia Gorge, with a length of 490 km. It crosses the eastern part of the Sichuan–Chongqing basin, which features low mountains formed by fold zones during the Triassic to Jurassic Periods. The height of the mountain ridges is about 300–600 m, and the valley width is about 500–1,000 m. The bank slope height is about 100–300 m, with a gentle slope of 15–30°. In the part from Baidicheng to Fengdu County town, the length of which is 270 km, the Yangtze River flows along the axis of the Yunyang Syncline and the

Fengdu Anticline which consists of thick red sandstone and shale of the Jurassic Period. The bank slopes in this part are almost dip-structured slopes. In the part from Fengdu to the end of the reservoir, Maoer-Xia Gorge, the Yangtze River mainly crosses the northeast ward comb-style fold. When the river crosses the core part of the anticline which features limestone of the Triassic Period, small and short gorges were formed. These gorges distributed among the relatively wide valley. The main tributaries, such as the Daning-he River, Xiangxi-he River and Meixi-he River, are also in high mountains and steep gorges landscapes.

Meteorologically, the reservoir is located in the Western Hubei Province, and the Chongqing heavy rainfall area. The average annual precipitation is 1,100 mm. The rainfall generally concentrates in summer, and the maximum daily precipitation is between 150 and 240 mm. Also in summer, the rain likely continues for several days.

Summarizing the above features, the Three Gorges area has conducive environments of topography, geomorphology, rock mass structure, valley structure, and climate conditions for the formation of landslides. As a result, landslides have occurred in this area extensively. The major work to study the stability of bank slopes of the Three Gorges Reservoir is to investigate the landslide distribution in this area, and assess the stability of the bank slopes. In the regions with dense population such as towns and villages, and those parts with main traffic lines, it is especially important to investigate and study the large-scale landslides.

The investigation and research on large-scale landslides was emphasized from the first period when the pre-investigation of geology in the Three Gorges area for dam construction began in the 1950s. 1956–1967 was the first working period. Under the leadership of the Three Gorges Geological Team of the former Geology and Mineral Resource Ministry, and General Survey Team of Yangtze River Watershed Managing Office of Hydro-power Ministry (later the name was changed to Yangtze River Water Power Committee), members from Beijing College of Geology, Changchun College of Geology and Chengdu College of Geology participated in a 1:100,000-scale engineering geology survey in the reservoir area, and pointed out nine large-scale landslides such as the Xintan landslide, and five potential risky rock mass such as the Lianziya cliff. It is concluded that the part including the Xintan landslide and Lianziya cliff is a dangerous part with a low level of stability for bank slopes. The second time period dates from 1968 to 1983. The main work in this period was to conduct a detailed investigation in the above-mentioned dangerous part. The topographic survey and exploration was conducted by the General Survey Team of the Yangtze River Water Power Committee and the Hydrogeology and Engineering Geology Team of Hubei Province. The deformation monitoring was conducted by the Landslide and Rockfall Investigation Office of Xiling Gorge (established by Scientific and Technological Committee of Hubei Province). Thereafter, a deformation monitoring system was also established at the Huanglashi landslide, while other large-scale landslides with obvious deformation were undergoing monitoring for early warning. In 1985, the reactivation of the Xintan landslide was predicted successfully, and the loss caused by the landslide was mitigated to a very low level of occurrence. There was nobody killed by the landslide.

In 1982, the western part of the Baota landslide reactivated and formed the Jipazi landslide. In addition, Xintan landslide reactivated in 1985. Both of them formed major geo-hazards, and counter-measures to prevent further disaster should be implemented. There is especially the need for further discussion on the Three Gorges project itself. From 1983 to 1988, a period just before the dam construction, a new period started for the investigation of bank slope stability and landslides in the reservoir area. Counter measure works were conducted on the Jipazi landslide, the Xintan landslide, and the Lianziya risky cliff. From 1989 when the dam construction started, the exploration, monitoring, and counter measure works were continued. At the same time, landslide investigation works were also applied to a wider area including tributaries that have valleys characterized by relatively lower stability.

From 1983, the research on geology and earthquakes in the Three Gorges area, including bank slope stability assessment and landslide investigation, was reinforced by the Department of Environmental Geology, Ministry of Geology and Mineral Resource. The Hydrogeology and Engineering Geology Team of Hubei Province, Nanjiang Hydrogeology and Engineering Geology Team in Sichuan Province, Chengdu Center of Hydrogeology and Engineering Geology, General Survey Team of Yangtze River Water Power Committee, Landslide and Rockfall Investigation Office of Xiling Gorge of Hubei Province conducted excellent work. China University of Earth Science (Wuhan), Changchun College of Geology and Chengdu College of Geology actively participated in the landslide research in the area. From Changchun College of Geology, Guangjie Li, Mancao He, Jianping Chen, Lei Nie, Jingshan Bo, Chuanzheng Liu, Xinsheng Li, Huiming Bao, Dianqiang Chen, Fawu Wang, Tonglu Li, Yonggang Jia, Bingjian Ling, Minghui Liu, Hongjun Liu, Yan Liang, Tingkai Nian participated the field investigation and data analyses and obtained significant results. Notably, Mancao He completed the stability assessment of the Jipazi landslide, and his work was included in the final report. For the prediction of the Xintan landslide, Chuanzheng Liu estimated the sliding area and sliding mass volume, pointed out the sliding route and direction, and predicted the dangerous area correctly. His analysis was used for the final prediction, and an appreciation letter was sent to Changchun College of Geology from the Scientific and Technological Committee of Hubei Province.

Through nearly 40 years of investigation in the Three Gorges area, a general knowledge was established for the landslide distribution, and mechanism and the stability of the major landslides in this region. In the whole area, there are 392 landslides with a volume larger than 10,000 m^3. Among them, 57% (222 landslides) have high stability, 22% (88 landslides) have medium stability, and 21% (82 landslides) have low stability. Along the main stream of the Yangtze River in the reservoir area, there are 170 landslides and 86 rockfalls. Among the 170 landslides, there are 3 super large-scale landslides with volumes larger than 1×10^8 m^3, 29 large-scale landslides with volumes between 1×10^7 and 1×10^8 m^3, 42 medium-large landslides with volumes between 1×10^6 m^3 and 1×10^7 m^3, 62 medium landslide with volumes between 1×10^5 and 1×10^6 m^3, and 34 small-scale landslides with volumes smaller than 1×10^5 m^3.

The three super large-scale landslides are the Fanjiaping landslide, the Gaojiazui landslide, and the Taibaiyan landslide. The Fanjiaping landslide is located 8 km

east of Badong County town, and has a volume of 1.1×10^8 m^3. The Gaojiazui landslide is located on the south bank near the Yunyang County town, and has a volume of 1.3×10^8 m^3. The Taibaiyan landslide is located near Wanzhou City, and has a volume of 1×10^8 m^3. All of the three super large-scale landslides were stable before water impoundment, and now they are also remaining stable after the current impoundment. Among the 29 large-scale landslides, there are 8 landslides with low stability. They are the Xintan landslide, Jipazi landslide, Huanglashi landslide, Daping landslide, the Zuojituo landslide, the Cicaotuo landslide, Sandengzi landslide, and Yunyang Chengxi landslide. The first three landslides, the Xintan landslide, Jipazi landslide, and Huanglashi landslide especially, also have high risk. Due to the counter measure works from the 1980s, their stabilities were improved greatly. For all of the eight large-scale landslides with low stability (due to their volumes) are between 1×10^7 and 1×10^8 m^3, the workloads were quite heavy. Besides, the other 21 large-scale landslides along the main stream of the Yangtze River have relatively higher stability. They are remaining stable even after the current water impoundment. Among the medium large-scale landslides, medium-scale landslides and small-scale landslides, about 80% have higher stability. Only 20% of them have low stability. However, it is very important to pay attention to the dip-structure red-layer slopes distributed from Yunyang to Wanzhou, where large-scale landslides occurred frequently.

Among the 86 rockfalls along the main stream of the Yangtze River, there are 4 sites with large volumes. Three of them are located on the south bank of Wushan County town, and one is located near Wanzhou City town. The three large-scale rockfalls in Wushan are (1) the Baiheping rockfall with a volume of 4.6×10^7 m^3, which is the largest rockfall in the Three Gorges area, but was stable before the impoundment. It is also remaining stable after the current impoundment, (2) the Yaqianwan rockfall with a relatively smaller volume of 1.4×10^7 m^3. However, its stability is low, and rockfalls occasionally have occurred in this site. Close attention should be paid to this site; (3) the Dawan rockfall with a volume of 1,200 m^3. It is stable even after the current water impoundment. The rockfall located in Wanzhou City town is the Diaoyaping rockfall with a volume of 1.7×10^7 m^3. It is stable now and has low risk.

The most dangerous potential rockfall is the above-mentioned Lianziya rockfall, which is located on the south bank of the main stream of the Yangtze River. This cliff consists of limestone of the Carboniferous and Permian Periods. At the bottom of the limestone is a coal seam. The cliff facing the river is 700 m long and 200–250 m high. The limestone was cut by fissures and joints into many blocks. Among the risky rock blocks, South-1 block and South-2 block have a volume of 9×10^5 and 2×10^4 m^3, respectively. The possible fall locations are the valleys in the east side. Because they cannot fall directly into the river, the risk is relatively low. However, their fall will have negative influence on the North-3 block, which has a volume of 2.5×10^6 m^3. If South-1 and South-2 blocks fall down, the North-3 block will face the Yangtze River directly. The risk will be increased greatly, because the mountain structure here is a dip structure with a low angle of the coal seam, which is the potential sliding plane. Fortunately, the fissures in the rear part did not reach the

coal seam, and the North-3 block is also connected to the main mountain body. The possibility for the whole block sliding is relatively low. The most dangerous part of the cliff is the block cut by Fissure T9. This block has a volume of 1.2×10^6 m^3. It will slide into the main stream along a weak layer of carbonated shale. According to the deformation monitoring data, the monitoring point at the top of the Lianziya cliff moved north to the Yangtze River at an annual rate of 1.6 mm. The counter measure works on this potential rockfall were conducted before the water impoundment.

Now, the Three Gorges dam has been completed for 2 years, and the water level will reach the design water level, 175 m in 2009. The investigations of the landslide and risky rockmasses, and the monitoring and counter measure works are also ongoing. After the impoundment of the reservoir, some landslides were reactivated, and some slopes began to deform. It is also very important to conduct research and monitoring on the landsliding phenomenon for the purpose of disaster mitigation, and pay attention to the tsunami caused by the landslides.

My students, Fawu Wang and Tonglu Li, are trying to compile the research on landslides in this area in a book, written in English. It is a very significant work. This book reminded me of the active investigation life when I was young, and the time when I worked as a member of the National Expert Team on Geology and Earthquake for the project. I hope what we have done and what the young generation will do can contribute to the disaster mitigation in this important project.

I hope people have interest in the Three Gorges project could benefit from information found in this book. Also I would like to express appreciation for the kind support of the authors in this book and for their great contributions. For those who want to know more about the landslides in this region, I will like to recommend the Final Report on Geology and Earthquake submitted by National Expert Team for the Three Gorges project published in June 1988, the Comprehensive Report on Types of Bank Slope and their Stability in the Three Gorges dam reservoir finished by Chengdu Center on Hydrogeology and Engineering Geology, Nanjiang Hydrogeology and Engineering Geology Team of Sichuan Province, and Hubei Province Hydrogeology and Engineering Geology Team under the technical advice of the National Expert Team on Geology and Earthquake published in 1995.

Zhoudi Tan

Former Professor of Changchun College of Geology
October 2008, Changchun, China

Preface

The Yangtze River is the largest river in China, and the Three Gorges section is one of the most beautiful parts of the river. In order to harness the hydropower of the Yangtze River, a dream was envisioned by Mr. Sun Yat-Sen, the first president of China. In 1918, Sun Yat-Sen suggested in his book, Strategy for State, "a dam should be set here to let ships go downstream and use the water resource as power". Through the efforts of the Chinese people the dream came true after 100 years. Begun in 2004, the Three Gorges dam construction was completed in 2006, and the dam operation will become fully functional in 2009, when the reservoir water level will reach the maximum height of 175 m. Before the dam construction, the water level at the Three Gorges dam site was 90 m. An increase of 85 m of slowly rising water in a reservoir with a length of about 660 km from the dam to its terminus at Chongqing City has greatly impacted the environment. The impact on the geo-environment, especially the instability phenomenon and landslides, was given great attention, because landslides not only affect the people living on the bank slopes but also affect navigation and shipping on the river. In addition, the sliding masses moving into the reservoir will have negative effects on the lifetime of the reservoir itself. Because of the importance of this consideration, bank slope stability and landslide problems have been, and will continue to be studied systematically. The studies can be divided into two periods seperating in June 2003, when the first reservoir impoundment was conducted for partial operation. To summarize, the studies before the impoundment were concentrated on landslide site identification, and instability evaluation of existing landslides; while in the period after the impoundment, the studies shifted to landslide monitoring and prediction of landslides caused by water-level changes during the reservoir operation. The purposes of the studies for the two periods are the same, which is to acquire sufficient data and information for landslide disaster mitigation.

The idea to edit this book was initiated by the interest of non-Chinese colleagues. Whenever we presented our research in the Three Gorges area, others always wanted to know more. The Three Gorges area is a mysterious and challenging area for them. As a result, this book aims to present the landslide studies in the Three Gorges dam reservoir area for the two periods before and after the impoundment. Chinese experts on landslides learned much about landslides in this area as a result of the great project. It is very important to document these important experiences. A comparison

between the works before the impoundment and after the impoundment is also very interesting because the great change of the water level in the reservoir provides a dynamic challenge for the landslide disaster mitigation. This book will document the dynamics of slope failures and subsequent mitigation, providing a beginning for innovative ways to cope with the complexity of the problems.

In order for this book to present the real level of Chinese experts on landslides in this area, authors from different organizations were invited to contribute chapters. They are from Yangtze River Management Committee, Land and Resource Ministry, Chinese Academy of Sciences, and some major universities. All of these organizations are involved in the landslide studies in the Three Gorges area and have contributed to this book. We hope this book can represent the magnitude of the national-level research on landslides that is occurring in this important area.

In reference to the content, some chapters address regional characters of landslides, and some chapters present case studies. Some methodological studies with application to this area were also included. We believe that the scientific progress obtained from both the geologic and engineering practices are fully presented in this book.

Editing the book in English is a great adventure for our two Chinese editors, as we do not have lengthy experience in English-speaking countries. At this point, we would like to give our sincere appreciation to Ms. Lynn Highland of The United States Geological Survey. She made a trip to the Three Gorges area in 2007, and investigated some typical landslides. She checked all of the chapters, correcting for English usage and grammar. For some chapters, she made suggestions to authors to revise the chapter in order to make them more understandable. It is she who makes the book possible. Without her kind help, we would not be confident of whether our target readers, the people in western countries would fully understand it or not.

Finally, we would like to convey our appreciation for the financial support from MEXT, Japan, and NSFC, China, through the scientific research grants (No. JSPS-18403003, Project leader: Fawu Wang, and No. NSFC-40772181, project leader: Ping Li) and the technical support from Birke Dalia from Springer-Verlag.

Fawu Wang   Kyoto, Japan
Tonglu Li   Xi'an, China, October 2008

Contents

Part I   Regional Properties of Landslides

Part II Case Studies for Typical Landslides

Part III   New Methodologies Applied in this Area

Contributors

Jianguang Bai State Key Laboratory of Geo-hazard Prevention and Geo-environment Protection, Chengdu University of Technology, Chengdu 610059, China

Huiming Bao Department of Civil Engineering, Guilin University of Technology, Guilin 541004, Guangxi, China, bhm@glite.edu.cn

Jianjun Chen State Key Laboratory of Geo-hazard Prevention and Geo-environment Protection, Chengdu University of Technology, Chengdu 610059, China

Lide Chen Yichang Center of the China Geological Survey, Yichang 443003, China, brianchenlide@yahoo.con.cn

Zhoufeng Chen Yichang Center of China Geological Survey, Yichang, 443003, China

Qinglu Deng Faculty of Engineering Geology, China University of Geosciences, Wuhan 430074, China, dengqinglu@263.net

Simeng Dong State Key Laboratory of Geo-hazard Prevention and Geo-environment Protection, Chengdu University of Technology, Chengdu 610059, China

Xiating Feng State Key Laboratory of Geomechanics and Geotechnical Engineering, Institute of Rock and Soil Mechanics, the Chinese Academy of Sciences, Wuhan 430071, China

Youlong Gao China University of Geosciences, Wuhan 430074; Center for Hydrogeology and Environmental Geology, CGS, Baoding, Hebei 071051, gemcgao@163.com; gemcgaoyl@263.net

Jinliang Han Geomechanics Institute of China Academy of Geological Sciences, Beijing 100081, P.R. China

Xinli Hu China University of Geosciences (Wuhan), Lumo Road, Wuhan 430074, China

Bolin Huang Yichang Geology and Mineral Research Institute, Ministry of Land and Resources, P.R.C., Yichang 443003, China

Runqiu Huang State Key Laboratory of Geo-hazard Prevention and Geo-environment Protection (Chengdu University of Technology), Chengdu 610059, China

Zhitao Huo Yichang Center of the China Geological Survey, Yichang 443003, China

Wenxing Jian Faulty of Engineering, China University of Geosciences, Wuhan 430074, China, wxjian@cug.edu.cn; wxjian0506@yahoo.com

Xiaohui Kang Department of Civil Engineering, Guilin University of Technology, Guilin 541004, Guangxi, China

Gang Li China University of Geosciences, Wuhan 430074; Center for Hydrogeology and Environmental Geology, CGS, Baoding, Hebei 071051

Ping Li School of Geological Engineering and Geomatics, Chang'an University, Xi'an, Shaanxi Province, China 710054

Shaojun Li State Key Laboratory of Geomechanics and Geotechnical Engineering, Institute of Rock and Soil Mechanics, The Chinese Academy of Sciences, Wuhan 430071, China, sjli@whrsm.ac.cn

Tiefeng Li China Institute for Geo-Environmental Monitoring, Beijing 100081, China

Tonglu Li School of Geological Engineering and Geomatics, Chang'an University, Xi'an, Shaanxi Province, China 710054, dcdgx08@chd.edu.cn

Jianfa Lian China Institute for Geo-Environmental Monitoring, Beijing 100081, China

Xiao Lin Institute of Tibetan Plateau Research, Chinese Academy of Sciences, Beijing, 100085, China

Chuanzheng Liu China Institute for Geo-Environmental Monitoring, Beijing 100081, China, liucz88@sohu.com

Yanhui Liu China Institute for Geo-Environmental Monitoring, Beijing 100081, China

Xianqi Luo Key Laboratory of Geological Hazards on Three Gorges Reservoir Area, Ministry of Education, China Three Gorges University, Yichang 443002, China

Heping Ma Guanghan Institute of Geological Engineering Exploration, Guanghan, Sichuan, China

Xuan Mo Department of Civil Engineering, Guilin University of Technology, Guilin 541004, Guangxi, China

Xuanming Peng Yichang Geology and Mineral Research Institute, Ministry of Land and Resources, P.R.C., Yichang 443003, China

Jianping Qiao Key Laboratory of Geo-surface Process and Mountain Hazards, Institute of Mountain Hazards and Environment, Chinese Academy of Science, Chengdu 610041, China, jpqiao@imde.ac.cn

Shengwu Qin College of Construction Engineering, Jilin University, Changchun 130026, China

Jian Shen China University of Geosciences (Beijing), Beijing, 100083, China

Jusong Shi Geomechanics Institute of China Academy of Geological Sciences, Beijing 100081, P.R. China

Lin Shi Geomechanics Institute of China Academy of Geological Sciences, Beijing 100081, P.R. China

Jianmin Tan Yichang Institute of Geology and Mineral Resources, China Geological Survey, Yichang, Hubei, 443003

Huiming Tang China University of Geosciences (Wuhan), Lumo Road, Wuhan 430074, China, tanghm@cug.edu.cn

Minggao Tang State Key Laboratory of Geo-hazard Prevention and Geo-environment Protection (Chengdu University of Technology), Chengdu 610059, China

Fawu Wang Research Centre on Landslides, Disaster Prevention Research Institute, Kyoto University, Gokasho, Uji, Kyoto 611-0011, Japan, wangfw@landslide.dpri.kyoto-u.ac.jp

Hongde Wang China University of Geosciences, Wuhan 430074; Center for Hydrogeology and Environmental Geology, CGS, Baoding, Hebei 071051

Huabin Wang School of Civil Engineering and Mechanics, Huazhong University of Science & Technology, Wuhan 430074, P.R. China; Hubei Key Laboratory of Control Structure, Huazhong University of Science & Technology, Wuhan 430074, P.R. China

Meng Wang Key Laboratory of Geo-surface Process and Mountain Hazards, Institute of Mountain Hazards and Environment, Chinese Academy of Science, Chengdu 610041; Graduate University of Chinese Academy of Sciences, Beijing100049

Shangqing Wang China Three Gorges University, Key Laboratory of Geological Hazards on Three Gorges Reservoir Area, Ministry of Education, Yichang, China, 443002

Shimei Wang Key Laboratory of Geological Hazards on Three Gorges Reservoir Area of Education Ministry, China Three Gorges University, Yichang 443002, China, wwsm3044@yahoo.com.cn

Xueping Wang Faculty of Resources, China University of Geosciences, Wuhan 430074, China

Yang Wang China University of Geosciences, Wuhan, Hubei, 430074, China, wangyangcug@126.com

Zhijian Wang Key Laboratory of Geological Hazards on Three Gorges Reservoir Area, China Three Gorges University, Yichang 443002, China

Baoping Wen China University of Geosciences (Beijing), Beijing, 100083, China

Mingsheng Wen China Institute for Geo-Environmental Monitoring, Beijing 100081, China

Jian Wu Key Laboratory of Geological Hazards on Three Gorges Reservoir Area, Ministry of Education, China Three Gorges University, Yichang 443002, China

Shuren Wu Geomechanics Institute of China Academy of Geological Sciences, Beijing 100081, P.R. China, shrwu@sohu.com

Yuhua Wu Three Gorges Exploration and Research Institute, Yangtze River Hydraulic Management Committee, China

Chengren Xiong China University of Geosciences (Wuhan), Lumo Road, Wuhan 430074, China

Fuxing Xu Three Gorges Exploration and Research Institute, Yangtze River Hydraulic Management Committee, China

Guoqing Xu Qingdao Geotechnical Investigation and Research Institute, Qingdao, Shandong, 266033, China

Ping Xu Department of Geological Engineering, Chang'an University, Xi'an, Shaanxi Province, China 710054

Qiang Xu State Key Laboratory of Geo-hazard Prevention and Geo-environment Protection (Chengdu University of Technology), Chengdu 610059, China, xuqiang_68@126.com

Guofu Xue Three Gorges Exploration and Research Institute, Yangtze River Hydraulic Management Committee, China, shingtonxue@126.com

Xiuyuan Yang Center for Hydrogeology and Environmental Geology, CGS, Baoding, Hebei 071051

Zongji Yang Institute of Mountain and Environment, Chinese Academy of Science, Chengdu, Sichuan, 610041, China

Kunlong Yin Faulty of Engineering, China University of Geosciences, Wuhan 430074, China

Qingjie Yin Key Laboratory of Geological Hazards on Three Gorges Reservoir Area of Education Ministry, China Three Gorges University, Yichang 443002, China

Shunde Yin State Key Laboratory of Geomechanics and Geotechnical Engineering, Institute of Rock and Soil Mechanics, the Chinese Academy of Sciences, Wuhan 430071, China

Wei You Department of Civil Engineering, Guilin University of Technology, Guilin 541004, Guangxi, China

Wencheng Yu Department of Civil Engineering, Guilin University of Technology, Guilin 541004, Guangxi, China

Yongzhi Yu Three Gorges Exploration and Research Institute, Yangtze River Hydraulic Management Committee, China

Zhongping Zeng College of Public Administration, Huazhong University of Science and Technology, Wuhan 430074, P. R. China, z.p.zeng@tom.com

Changliang Zhang Department of Geological Engineering, Chang'an University, Xi'an, Shaanxi Province, China 710054

Junyi Zhang China University of Geosciences, Wuhan 430074; Center for Hydrogeology and Environmental Geology, CGS, Baoding, Hebei 071051

Yeming Zhang Yichang Center of the China Geological Survey, Yichang 443003, China

Yongshuang Zhang Geomechanics Institute of China Academy of Geological Sciences, Beijing 100081, P.R. China

Youliang Zhang State Key Laboratory of Geomechanics and Geotechnical Engineering, Institute of Rock and Soil Mechanics, the Chinese Academy of Sciences, Wuhan 430071, China

Zhenhua Zhang Key Laboratory of Geological Hazards on Three Gorges Reservoir Area, Ministry of Education, China Three Gorges University, Yichang 443002, China, zenithzhang@sina.com

Pinggen Zhou China Institute of Hydrogeology and Engineering Geology Exploration, Beijing100081, China, zhoupg@mail.cigem.gov.cn

Top-Author Biographies

Fawu Wang is assistant professor of landslides at Disaster Prevention Research Institute, Kyoto University. He obtained a doctorate degree in science from Kyoto University in 1999. Prior to joining Kyoto University in 2004, he worked as a lecturer and associate professor at Kanazawa University, Japan, and as a lecturer at Changchun College of Geology, China. He has been working on challenging problems in landslides, such as the mechanism of rapid and long runout landslides, the transference mechanism from landsliding to flow-sliding, motion prediction of landslides, marine landslides, and landslides triggered by earthquakes, heavy rainfall, and water impoundment. His primary research interests are to clarify the common mechanisms of landslides initiated by different triggers, and to find a way to predict the occurrence and motion of landslides, for the purpose of landslide disaster mitigation.

Tonglu Li is professor at Chang'an University, China. He completed his PhD in 1992 at Xi'an College of Geology (now united to Chang'an University). Since then, he has worked in the university up until now. He has been a visiting academic at the University of Adelaide, Australia, during the period of January to June 1996. His research work involves several fields. He has completed the active faults investigation and the assessments of the earth crust stability for the area around the Three Gorges dam, the Offshore Area of Qinghuangdao City, China, and compiled the Map of the Regional Engineering Stability of China. Currently, his work is focused on landslides and the engineering of slopes. His research interests are the three-dimensional equilibrium method for slope stability assessment, and the interaction between the stabilizing structure and the rock and soil. He has completed many of the investigations and control designs of the landslides for the hydro-electric power projects including the Three Gorges Reservoir, highway projects and lifeline projects, and the high cut slopes at some nuclear power plants.

Chuanzheng Liu is a senior engineer at the professor level at China Institute for Geo-Environment Monitoring (CIGEM). He received his bachelor's and master's degree in engineering geology in 1983 and 1986 at Changchun College of Geology, followed by a PhD in 1992. Since 1992, he has been working on CIGEM. He served as vice director of department on environmental geology and director of department on geo-hazard monitoring at one time or another. At present, he serves as deputy

engineer in chief at CIGEM. He has been involved in a great deal of projects in China over 20 years, such as reservoir-induced earthquakes, regional earth crust stability, landslide control engineering, early warning of geo-hazards, and management countermeasures of geo-hazard mitigation. His research interests include prevention for geo-hazards and assessment of geo-environments.

Guofu Xue is the chief geologist of Three Gorges project (TGP) and Wudongde Hydropower Station (WHS) in China. He is also the director of geological supervision for four of the largest hydropower stations in China; two of them are under construction. He graduated from The Changjiang University of Engineering in 1965. As a visiting scholar, he studied at McMaster University in Canada and took some short courses at Western Kentucky University, Waterloo University, and University of Missouri – Rolla from 1981 to 1983. He has taken charge of more than 30 national key scientific and technological sub-projects on the stability of high slopes, dam foundations, reservoir banks, and regional geotectonic stability and has lead the geological investigation and study for nine large-scale bridges crossing the main stream of the Yangtze River and more than 1,000 km major levees of the Yangtze River from 1991 to 2002. Since 1991, he has been involved in consultation, and evaluation or inspection of about 30 engineering projects or research programs. He is the author or co-author of 6 academic books on regulations issued by ministry, 20 papers, and about 100 technical reports. He was the winner of the State Golden and Silver Prize of Engineering Design and Investigation, First Class of State Award of Science and Technology Progress, First Class Provincial or Ministerial Awards of Engineering Design and Investigation from 1996 to 2004.

Huiming Tang is now a professor and vice president of China University of Geosciences (Wuhan) and chairman of academic committee of the university. Also, he serves as a vice president of the engineering geology committee, China. He received his PhD in engineering geology from China University of Geosciences in 1992, and had successfully conducted cooperative research as a research fellow and visiting scholar at Imperial College of Sciences & Technology, UK. His primary research interests include controlling of geological disasters, and engineering geological simulation. He has successfully accomplished more than 40 research programs, including NSF Projects for China, UK-China International Co-operative Projects, National key research Projects for geological disasters in the reservoir area of the Three Gorges, for example. He has won five national-level and five ministry-level awards of China.

Xuanming Peng is director of Qingdao Institute of Marine Geology, China Geological Survey (CGS). Before he moved to his current position in December 2008, he worked as a deputy director of Yichang Institute of Geology and Mineral Resource, CGS. He received his bachelor's degree in engineering geology in 1986 at Changchun College of Geology, and PhD from China University of Geosciences (Beijing) in 2005. He has finished many research projects on geo-hazard evaluations in western China and the Three Gorges dam reservoir area, land use policy in landslide-prone areas, and protection of geo-environment, establishing a geo-park, and city relocation.

Qiang Xu is a professor at Chengdu University of Technology, Sichuan, China. He completed his PhD in 1997 at Chengdu University of Technology and was a lecturer after he finished his degree. Currently, he is in charge of the College of Environmental and Civil Engineering as dean and as deputy director of the State Key Laboratory of Geo-hazards Prediction and Environment Protection. His research interests include evaluation and forecasting of geo-hazards caused by slope collapses and landslides and the remediation work, for which he has a great deal of experience in Sichuan Province. He is involved in several large projects in Sichuan Province including the large landslides that occurred in Danba town, several other landslides and sub-hazards evaluation projects. He participated in more than 10 national-level research projects and was awarded the first prize for one of those projects as well as awarded the excellence in geological engineering in Sichuan Province. After the May 12, 2008 Wenchuan Earthquakes, Sichuan Province, he participated in the remediation works in Beichuan, Qingchuan, Yingxiu areas as a member of a group of experts. He also edited the Plan for Geo-hazards Prevention after the Wenchuan Earthquakes, as a chief editor.

Jianping Qiao is researcher at Institute of Mountain Hazards and Environment (IMHE), CAS, China, and the chief of the landslide research division. He received his BSc degree in geophysics in 1980 at Chinese Scientific and Technical University. He has been studying landslide for 28 years and his major research fields are focused on landslide formation mechanism, landslide distribution regularity, landslide hazard assessment, and earthquake-induced landslides. He has been awarded a national special government allowance. At the same time, he is visiting professor at Southwest Jiaotong University of China, academic and technological leader of Sichuan Province, landslide professional committee leader of China disaster prevention association, vice chairman of Sichuan geography association, deputy director of debris flow and landslide professional committee of China Soil and Water Conservation Society, Sichuan Seismological Society executive director and member of a group of experts for the project, "Prevention and Treatment Engineering to Landslide and High Cutting Slope in Second and Third Phases in Three Gorges Region" established by National Development and Reform Commission and State Council Three Gorges Project Construction Committee Executive Office.

Baoping Wen is professor at China University of Geosciences (Beijing). She obtained her first degree in Engineering Geology at Chengdu University of Technology, China in 1984, followed by her MS degree at Chang'an University in 1989. She completed her PhD at the University of Hong Kong in 2002. From 1984 to 1986, she worked at Northwest Institute of Investigation and Design for Hydropower Project as a site engineer in engineering geology. From 1989 to 1998, she worked in China Institute of Geo-Environment Monitoring and was involved in several research projects related to geological hazards, particularly landslides. She also worked at Tsinghua University for 2 years as a postdoctoral fellow. She has wide research interests in many aspects associated with landslide mechanism and hazard mitigation, including slope stability analysis, landslide monitoring, and evolution of landslide slip zone in terms of microstructure and shear strength variations,

landslide mapping, and landslide risk assessment. Currently she is involved in several projects about mechanisms of large-scale landslides in the Three Gorges area and loess plateau region, China.

Shimei Wang is a professor at Institute of Geological Disaster Prevention of China Three Gorges University. She obtained her bachelor's (1988) and master's (1991) degree in engineering geology from Changchun College of Geology and PhD (2007) in hydraulic structure from Wuhan University. As a visited scholar supported by China Scholarship Council, she visited Moscow State University of Civil Engineering for 1 year in 2004. Her major research domains include rock and soil mechanics, mechanism of geological disasters, and forecasting. She has been involved in a lot of scientific researches projects, such as National Science & Technology Pillar Program, and National Natural Science Foundation projects. She took the responsibility to establish the unsaturated soil and soil rheology laboratories in her institute.

Wenxing Jian is a professor at China University of Geosciences (Wuhan). He got his BS in geology and exploration of coal mines in 1989, MS in structural geology in 1992, and PhD in Geotechnical Engineering in 1998 in China University of Geosciences. In 1992, he joined the China University of Geosciences. He had conducted some research in the Disaster Prevention Research Institute, Kyoto University, Japan, as a postdoctoral research fellow from 1999 to 2001, and visited the Department of Civil and Environmental Engineering, Virginia Tech, USA as a visiting research scholar from 2006 to 2007. His research interests include slope stability, soil mechanics, laboratory and in situ testing, geological engineering, and numerical modeling. He has done much research on the mechanism, prevention methods, and monitoring technique of landslides in the Three Gorges Reservoir, China.

Lide Chen is senior researcher at the Yichang Institute of Geology and Mineral Resources, China Geological Survey. He completed his studies in geology in 1991 at the Peking University. For a long time, he worked on regional geology survey and geo-hazard survey. In recent years, his projects are related to the regional geology and geo-hazard in Daning-he River water-compensation engineering area in middle route of south-to-north water transfer project.

Qinglu Deng is professor at the China University of Geosciences (Wuhan). He received his BSc and MSc degrees in geology in 1984 and 1987, and obtained his PhD in engineering geology in 1998 from the China University of Geosciences. He participated in slope geo-hazard survey and research of some new relocation sites for relocated towns in the Three Gorges Reservoir area early in the middle 90s in the 20th century. His research interest is especially on the deformation process of large landslide before landsliding, and he has found several large landslides which are characterized by pre-sliding deformation system in the Three Gorges Reservoir area. He also carried out much work on geo-hazard risk evaluation and protection for Zhongxian-Wuhan gas pipe lines in recent years.

Zhenhua Zhang is a lecturer in China Three Gorges University. He received his bachelor's degree in hydraulic and hydro-power engineering in 2001 at Wuhan University of Hydraulic and Electric Engineering, followed by his master's degree in disaster mitigation and protection engineering in 2004 at China Three Gorges University. He completed his PhD in 2008 at Institute of Rock and Soil Mechanics, the Chinese Academy of Sciences. He visited Kaiserslautern Applied Technology University in Germany for cooperative research in 2006. Now he is working in the Institute of Geological Hazards Mitigation and Control, China Three Gorges University. He has been involved in several large projects on slope stabilization, construction on underground power stations, and prediction and forecasting of landslides in the Three Gorges Reservoir area. His research interests include slope stability, and prediction and forecasting of landslides in reservoirs.

Shangqing Wang is a professor at China Three Gorges University. He received his bachelor's degree in Geodetic Engineering in 1977 at Wuhan University. Now he is working at Institute of Geological Hazards Mitigation and Control, China Three Gorges University, China. He has been involved in several large projects on monitoring and forecasting of rockfalls and landslides in the Three Gorges Reservoir area. His research interests include slope stability, and prediction and forecasting of rockfall and landslides in reservoirs.

Yang Wang is associate professor at the China University of Geosciences (Wuhan). He received his bachelor's degree in geotechnical engineering in 2000, followed by a PhD in geological engineering at the China University of Geosciences in 2005. His doctoral theses dealt with the research on speed of the landslide and water wave hazard in reservoir, and some key problems such as initial water wave characteristics generated by landslides, and the propagation and runup of the water wave. He has been involved in several large projects on water waves generated by landslides, landslide stabilization, and prediction and evaluation for landslide hazard. His research interests include water waves generated by the landslides, landslide stability, landslide probability analysis, prediction method for landslides and numerical simulation.

Shaojun Li is associate professor at the Institute of Rock and Soil Mechanics, the Chinese Academy of Sciences. He got his bachelor's and master's degree of geological engineering at China University of Sciences in 1997 and 2000, respectively, followed by a PhD in Geotechnical Engineering in 2005. From 2000 to 2007, he has worked at the Institute of Rock and Soil Mechanics, the Chinese Academy of Sciences. In 2007 and 2008, he received funding from the Chinese Academy of Sciences and conducted collaborations as a visiting researcher at the University of Dundee, UK. He has been involved in nearly 10 high-level national research projects relevant to slope safety evaluation and prediction such as dam site slopes at Longtan Hydropower station in Guangxi, Bazimen landslide in Fujian, and some reservoir slopes in Three Gorges. His research interests include in situ monitoring and testing, slope reinforcement, pile–slope interaction, centrifuge modelling and computing learning methods in geotechnical engineering.

Huiming Bao is a professor at Guilin University of Technology, China. He worked at Louisiana State University as a visiting scholar from 2006 to 2007, received a PhD in transportation engineering from Chang'an University in 2003, and received the ME and BE in engineering geology from Changchun Collage of Geology in 1988 and 1985, respectively. Aiming at increasing safety and reducing cost and based on the experience and theory of many years, he led and completed the project of landslide prevention design for the relocated city in Shuanglong Town, Wushan County in Three Gorges region of the Yangtze River. In addition, he is paying attention to the development of civil engineering, and studied the application of fuzzy mathematics, fractal theory, neural networks, and rough set in civil engineering. Now, he is working on the project of Road Performance of Sisal Fiber Concrete, and studying the application of rough set theory in road and slope engineering.

Zhongping Zeng is a post-doctoral research fellow at Huazhong University of Science and Technology, China. He received his first degree in geology in 1993, followed by a master's degree in remote sensing geology in 1996. From 1996 to 2003, he worked at Computer Center of Fujian Province (FJCC) and Remote Sensing Center of Fujian Province (FJRSC) at Fuzhou City, China. At FJRSC, as Head of Image Processing Division, he was responsible for remote sensing image applications. He visited TELESPAZIO LTD, Italy, for a flood hazard risk assessment project in 1997. He has been involved in several large projects, involving remote sensing interpretation of land use, government database design and software development, and an E-government project. In 2006, he completed his PhD in Cartography and Geographic Information Engineering at China University of Geosciences (Wuhan). He carried out some landslide hazard risk evaluation projects for the Three Gorges areas using remote sensing technology. His research interests include public security, disaster safety monitoring, and disaster prediction.

Youlong Gao is a senior engineer and is assistant to the Director of Geological Hazard Researching Department of Hydrogeology Environmental Geology Center, China Geological Survey. He received his first degree in Eastern China College of Geology, and became a candidate for PhD in China University Geosciences in 2005. He has concentrated on prevention and countermeasure techniques in geologic hazards, such as investigating and estimating geologic hazards, evaluating and management of geo-hazard risk, and optimizing and integrating solutions for geo-hazard monitoring instruments and techniques. He has been involved in several large projects in China, such as Lianziya potential dangerous rock mass control, geo-hazard research in counties located in mountain areas.

Zongji Yang received his BSc degree in geography at Sichuan Normal University in 2004. Now he is a PhD candidate at the Institute of Mountain Hazards and Environments of Chinese Academy of Sciences. His research interest focuses on both risk assessment of landslides and early warning methods rainfall-induced landslides. He applied information the entropy method to find objective weight of factor index model for landslide hazard assessment and zonation. He has studied the relationship between landslide occurrence and precipitation. In recent years, he devotes him-

self to work on landslide hazard assessment and geological mechanism research in Three Gorges. This work involves studies of the mechanism and regulation of landslide distribution in the Three Gorges area and the site-specific research of typical landslides.

Pinggen Zhou is a senior engineer and professor at China Institute for Geo-Environment Monitoring (CIGEM). He received his bachelor's degree in hydrogeology and engineering geology in 1985 at Changchun College of Geology, followed by his MS degree of engineering geology at Chinese Academy of Geology in 1988. He completed his PhD in engineering geology at the Institute of Geology of Chinese Academy of Sciences in 1997. Since 1988, he has been working on CIGEM. He served as vice director of Department on Geo-hazard Monitoring. At present, he serves as director of Department on Geo-hazard Survey and Monitoring at CIGEM. He participated in slope geo-hazard survey and research for some new relocation sites for relocated towns in the Three Gorges Reservoir area, early in the mid-1990s. His research interest is especially on the deformation process and countermeasures for large landslides induced by rainfall and reservoir impounding. Currently, he is in charge of the project concerning the study of early warning for rainfall-induced landslides at Ya'an City of Sichuan Province, which serves as a pilot study in China.

Introduction: The Scenary of Three Gorges, from Downstream to Upstream

Fawu Wang

At the end of June 2008, the author took a tourist ship through the Three Gorges dam and Reservior, from the downstream area to the upstream area. The voyage began at the end of the Three Gorges (the eastern part of the Xiling Gorge), passed the dam, and the western part of the Xiling Gorge, through Wu Gorge, and ending finally, at the Qutang Gorge (the first gorge of the Three Gorges).

The dam reservoir is named the Three Gorges because the dam is located in the famous Three Gorges area, although the reservoir extends further westward to Chongqing City for a total length of 660 km (Fig. 1).
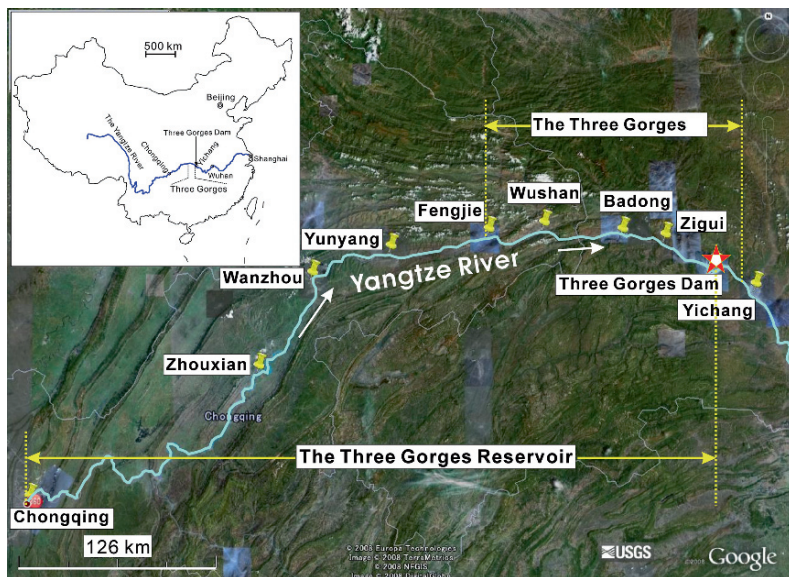
Fig. 1 Site map of the Three Gorges Reservoir

F. Wang (✉)
Research Centre on Landslides, Disaster Prevention Research Institute, Kyoto University, Gokasho, Uji, Kyoto 611-0011, Japan
e-mail: wangfw@landslide.dpri.kyoto-u.ac.jp

The following shows a sampling of the scenary, encompassing the topography, landslide and potential dangerous rock cliffs, and the dam itself, as an introduction to the research section of this book.

Photo 1 (Xiling Gorge eastern part) The end of the eastern part of Xiling Gorge. The cliff is formed by limestone. The measurement shows the water level of the downstream area of the Three Gorges at 65 m a.s.l

Photo 2 (Xiling Gorge eastern part) White houses were built near the water level and in front of the steep limestone cliffs

Photo 3 (Xiling Gorge eastern part) Tourist ship anchored at the exit of a tributary of the Yangtze River

Photo 4 (Xiling Gorge eastern part) Traditional houses are located at the exit of the Yangtze River's tributary

Photo 5 (Xiling Gorge eastern part) Steep limestone cliffs in the Xiling Gorge. Near the river is a ship manufacturing facility

Photo 6 (Xiling Gorge eastern part) The Xiling Bridge crossing the Yangtze River. It is the first bridge located downstream of the Three Gorges dam

Photo 7 (Three Gorges dam) The Three Gorges dam

Photo 8 (Three Gorges dam) "The Three Gorges dam," in Chinese

Photo 9 (Three Gorges dam) This wedge, now located at the dam visitor's center, was used to stop the river flow at the initial stage of the dam construction

Photo 10 (Three Gorges dam) A chunk of bedrock taken from the river bed at the dam site of the Three Gorges dam is displayed at the visitor's center

Photo 11 (Xiling Gorge western part) A wide-angle view in front of the Three Gorges dam

Photo 12 (Xiling Gorge western part) The limestone cliff in the western part of the Xiling Gorge

Photo 13 (Xiling Gorge western part) The site of the Xintan landslide that occurred in 1985. Because of the successful failure prediction based on monitoring, no one was killed by the large-scale landslide. It has been preserved as a visitor's site for geo-hazard education, after the gradation was performed

Photo 14 (Xiling Gorge western part) The Lianziya potential dangerous limestone cliff. It is located on the opposite bank of the Xintan landslide. Countermeasure works such as anchors were applied to reinforce the part near the river. This area is the narrowest part of the Three Gorges

Photo 15 Wu Gorge is famous for the high and steep mountain cliff. The *arrow* points to the Goddess peak

Photo 16 The pervasive limestone cliffs in the Wu Gorge
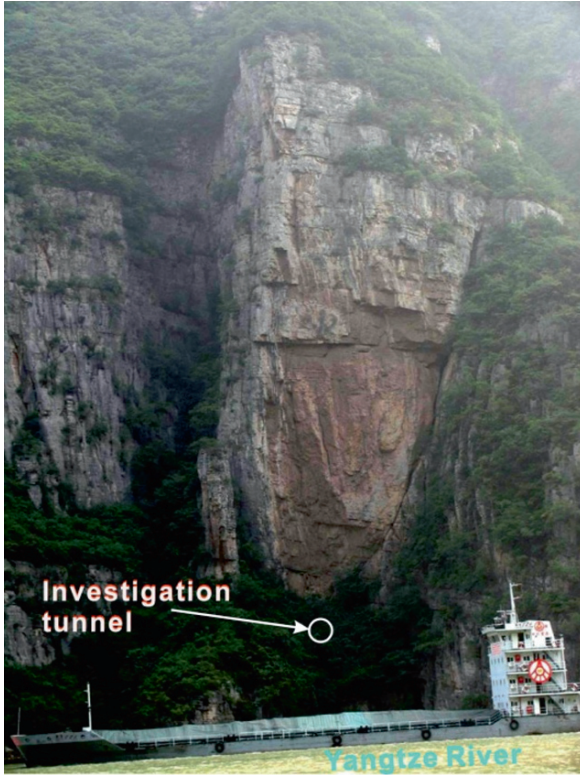
Photo 17 The Jianchuandong potential dangerous rockmass located in the Wu Gorge. A cargo ship was passing by the cliff

Photo 18 Landslide formed by colluvium from the limestone cliff, located in the far mountain, between Wu Gorge and Qutang Gorge

Photo 19 The gently sloping bank between Wu Gorge and Qutang Gorge. There are many landslides located in this area

Photo 20 Countermeasure works applied to the landslide between Wu Gorge and Qutang Gorge

Photo 21 This landslide surface is densely populated by villagers (between Wu Gorge and Qutang Gorge)

Photo 22 The Entrance of the Qutang Gorge. Here is the starting point of the Three Gorges. It is famous for the gorgeous massive cliff. The scenery is used for illustrations on Chinese currency

Photo 23 The green water in Shenlongxi stream, a tributary of the Yangtze. The exposed zone without green was formed by washing of the previously increased water level of the reservoir

Part I
Regional Properties of Landslides

Chapter 1
Geo-hazard Initiation and Assessment in the Three Gorges Reservoir

Chuanzheng Liu, Yanhui Liu, Mingsheng Wen, Tiefeng Li, Jianfa Lian, and Shengwu Qin

Abstract   Geo-hazard study results for the Three Gorges reservoir of Yangtze River are presented at three geographical scales: first, at the largest scale, is the geo-hazard investigation and evaluation of the whole reservoir area, which involves 19 counties (54462 km^2); secondly, at a mid-level scale, is the initiation mechanism of complex slopes (landslides) in the Three Gorges section of the Yangtze River (about 4000 km^2); lastly, at the small scale, research on the fan-shaped slope of Badong county new town was studied to ascertain its geologic characteristics, landslide initiation factors, and geo-environmental quality.

Keywords   The Three Gorges reservoir of the Yangtze River · China · Geo-hazards · Landslides · Badong slope system · Gravity initiation · Geo-environmental quality

Introduction

Since the 1990s,we have been studying the geo-hazards of the Three Gorges reservoir on the Yangtze River and obtained scientific data for three geographic levels of scale, the largest of which consists of the whole Three Gorges reservoir encompassing 19 counties. At the mid-level scale, the Three Gorges segment of the reservoir was studied, and at a smaller scale, the slope stability evaluation for the New town of Badong County is presented.

Regional Assessments of Geo-hazards

Based on the compiled analyses of the existing papers and literature about mitigation of geological hazards (Aleotti & Chowdhury 1999, Carrara 1983, Haruyama & Kitamura 1984, Yin & Yan 1987, Baeza & Corominas 1996, Carrara et al. 1992,

C. Liu (✉)
China Institute for Geo-Environmental Monitoring, Beijing 100081, China
e-mail: liucz@mail.cigem.gov.cn

Aleotti et al. 2000, Michael-Leiba 2000, Ragozin 2000, Elliott & Gori 2000), the authors have set up a new assessment system for regional geological hazards.

Problems and Concepts

Basic Problems

The assessment for regional geological hazards addresses four basic problems as follows:

(1) The status of geological hazards at present, which reflects types, quantity, distributive area, and space volume;
(2) A correct description of geological environments as they relate to geological hazards which consists of landforms, morphological features, vegetation forms and degree of coverage, elements and structure of geologic bodies, groundwater distribution, and the dynamic background in relation to the earth's regional crust;
(3) Evaluation of the potential geological hazards induced by various kinds of triggering factors, such as rainfall, earthquake, and all forms of human activity;
(4) How to mitigate geological disasters which include impacts on human, property, infrastructure projects, and the living environment.

Basic Concepts

Four basic concepts are put forth, which include "distribution degree," "potentiality degree," "dangerous degree," and "harmful degree" of regional geo-hazards as they relate to the above four problems (Liu & Yang 2001, Liu et al. 2004a).

Concept 1 "distribution degree" of geological hazards is a reflection of the development of geological disasters in the region which involves the numerical distribution, the area distribution, and the size distribution of geological hazards.

Concept 2 "potentiality degree" of geological hazards is an evaluative parameter that describes conditions using a combination of geo-environmental aspects.

Concept 3 "dangerous degree" for geological hazards expresses a quantitative possibility that occurs in a certain period of time due to some kind of triggering factors (natural or human made). In certain situations, "dangerous degree" can be used as an early warning index for levels of geological hazards.

Concept 4 "harmful degree" of geological hazards reflects a result that results in casualties, economic loss, and environmental destruction. It can be used as a basis to set up a disaster prevention and mitigation plan for a region.

Evaluation Method for Geological Hazards Regional Analysis

A regional geological hazards evaluation framework can be established by applying the analyses of "distribution degree," "potentiality degree," "dangerous degree," and "harmful degree" (Liu et al. 2004a).

"Distribution Degree" of Geological Hazards

"Distribution degree" of geological hazards is the function of regional disaster frequency (f), area (s), and volume (v):

$$F = f(f, s, v) \tag{1.1}$$

In order to reflect the actual situation of the establishment of geological hazard "distribution degree" computational model, the first aspect of nondimensional treatment or normalization for the above-mentioned three indicators is applied.

1. *Disaster frequency ratio*: To set up unit i for the regional disaster frequency f_i, cell area of S_i, the frequency of disaster unit density ρ_{fi}; the entire study area with an area of S, the total number of disasters for the f, the frequency of the total density of ρ_f, then

The i unit disaster frequency ratio

$$R_{fi} = \rho_{fi}/\rho_f$$
$$\rho_{fi} = f_i/S_i; \quad \rho_f = f/S$$

2. *Geological hazard area modulus ratio*: To set up unit i with an area of the distribution of disaster—si, unit area of S_i, within unit i the disaster area modulus ρ_{si}; the entire study area for the S, at a total area of disaster s, with a total area of module for ρ_s, then

Unit i area modulus ratio

$$R_{si} = \rho_{si}/\rho_s$$
$$\rho_{si} = s_i/S_i; \quad \rho_s = s/S$$

3. *Geological hazard volume modulus ratio*: To set up unit i of the total volume for the disaster point vi, unit area of S_i, i unit the size of the disaster modulus ρ_{vi}; the entire study area has a total area of S, the total volume for the disaster point v, the total volume modulus ρ_v, then

Unit i volume modulus ratio R_{vi}

$$R_{vi} = \rho_{vi}/\rho_v$$
$$\rho_{vi} = v_i/S_i; \quad \rho_v = v/S$$

So, (1.1) changes to

$$F_i = f(R_{fi}, R_{si}, R_{vi}) \tag{1.2}$$

R_{fi}, R_{si}, and R_{vi} are "distribution factors."

A general equation (1.3) can be established by the practice of combining a large number of geological disasters in the Three Gorges reservoir area and comprehensive studies.

$$F_i = R_{fi} + R_{si}^{\frac{1}{2}} + R_{vi}^{\frac{1}{3}} + r \tag{1.3}$$

F_i – "distribution degree" of unit i;
R_{fi} – Disaster frequency ratio of unit i;

R_{si} – Geological hazard area modulus ratio of unit i;
R_{vi} – Geological hazard volume modulus ratio of unit i;
r – Amended index, generally 1.5–2.0.

Because of the omission or too much emphasis on "people-oriented" aspects, the regional investigations of geological hazards could lead to many parts of the disaster that were not investigated, which are the "blind spots" or the "out area." The Eq. (1.3) was amended in order to make up for the "blind spot" defects. Taking into account regional disaster points higher than the harm caused by the size and volume, consideration was given to the role of the three amendments to increase the amended index of r.

"Potentiality Degree" of Geological Hazards

"Potentiality degree" is the basis of various geological disaster trends such as early warning, and it can provide the basic indicators to a single or a combination early warning. Specific value calculation is based on the development factor and basic factor.

Equation can be written as:

$$Q = (q_1, q_2, q_3, \ldots \ldots, q_n) \tag{1.4}$$

$q_1, q_2, q_3, \ldots \ldots, q_n$ are the values of reflection of potential geological hazards.

For composite index model, (1.4) can be written in style:

$$Q_i = \sum_{j=1}^{n} a_i b_j \tag{1.5}$$

$i = 1, 2, \ldots, m$; $j = 1, 2, \ldots, n$;
Q_i – "potentiality degree" of unit i;
j – evaluation factor;
a_i – assignment of j factor in unit i;
b_j – weight of evaluation factor j;
m – number of evaluation units;
n – number of evaluation factors.

The portfolio of geo-environmental elements is basic factors, including the frequency ratio, area modulus ratio, and volume modulus ratio and are integral parts of the basic factors as a response of the potential. Because it is a response of the potential and also can reflect the fragility of the geological environment, the "development factor" is also known as the "response factor."

"Dangerous Degree" of Geological Hazards

"Dangerous degree" is calculated based on analysis of "potentiality degree," then the trigger factors are considered, and the mathematical model becomes consistent with the "potentiality degree" computing model.

Using the composite index model,

$$W_i = \sum_{j=1}^{p} a_i b_j \qquad (1.6)$$

$i = 1, 2, \ldots, m; \; j = 1, 2, \ldots, p;$
W_i – "dangerous degree" of unit i;
j – evaluation factor;
a_i – assignment of j factor in unit i;
b_j – weight of evaluation factor j;
m – number of evaluation units;
p – number of evaluation factors.

According to actual data of the regional geological hazards investigation and experience, discriminate factors of "dangerous degree" calculation are divided into three categories: basic factor, response factor, and trigger factor. The assignment of trigger factor is based on the geological hazard history of the study area, especially the statistical analysis of the different factors that lead to different sections of the failure threshold range. Calculated "dangerous degree" can be used as an early warning indicator when a numerical trigger factor is known.

"Harmful Degree" of Geological Hazards

"Harmful degree" of geological hazards is the social attributes expressions of geological hazards. Focus on the "harmful degree" and the vulnerability of human life and property in disaster-stricken areas, and quantitative indicators, shows the expression as follows:

$$R = R(r_1, r_2, r_3, \ldots\ldots, r_n) \qquad (1.7)$$

$r_1, r_2, r_3, \ldots\ldots$, where r_n is the value of the reflection of geological hazards.
    In general, the damage from geological hazards is expressed as the casualties, the loss of the value, and environmental damage effects that cannot be measured by currency. "Harmful degree" is written in the general model of evaluation unit:

$$R_i = W_i \times V_i \qquad (1.8)$$

R_i – Unit harmful degree;
W_i – Unit dangerous degree;
V_i – Unit disaster–vulnerability index.

$$V_i = \omega_1 V_{1I} + \omega_2 V_{2I} + \omega_3 V_{3I} + \cdots\cdots + \omega_n V_{nI}$$

$V_{1I}, V_{2I}, V_{3I}, \cdots\cdots, V_{nI}$ are the indicators of vulnerability of all types of body; $\omega_1, \omega_2, \omega_3, \cdots\cdots, \omega_n$ are the respective weights.

The Division Methods of Geological Hazard Evaluation

The results of regional geological hazard evaluation are classified from low to high. First, we chose a number of selected units (box, natural search or district) based on a general scale evaluation, calculation of the unit with a set of quantitative factors (quantitative), combining the unit which results in a number close to the value of its kind, that is, the map Merger spot – the traditional clustering method, based on the space adjacent to the clustering coefficient and so on.

This method is repeated until the objective of the work is reached. The idea is that the different levels of units are compared to a different factor in the working process and it uses quantitative expression if possible.

This study uses the combined method of spot map, according to the calculations of "distribution degree," "potentiality degree," "dangerous degree," and the "harmful degree", and it combines the units which are adjacent or close to the same level, forming the corresponding zoning map.

Evaluation of Geological Disasters in the Three Gorges Reservoir Area

The survey of geological disasters in the Three Gorges reservoir comprises an area encompassing longitude 106°–111°, latitude 29°–31°21′. The administrative divisions are those that occur across the 19 counties (districts) of Chongqing Municipality and Hubei Province, including the Yichang, Xingshan, Zigui and Badong counties in Hubei Province, Wushan, Wuxi, Fengjie, Yunyang, Wanzhou, Kaixian, Zhongxian, Shizhu, Yubei, Banan, Chongqing city urban area, Changshou, Fengdu, Fuling, and Wulong counties or districts in Chongqing Municipality, and the total area of the comprehensive investigation assessment is about 54462 km^2 (Fig. 1.1).
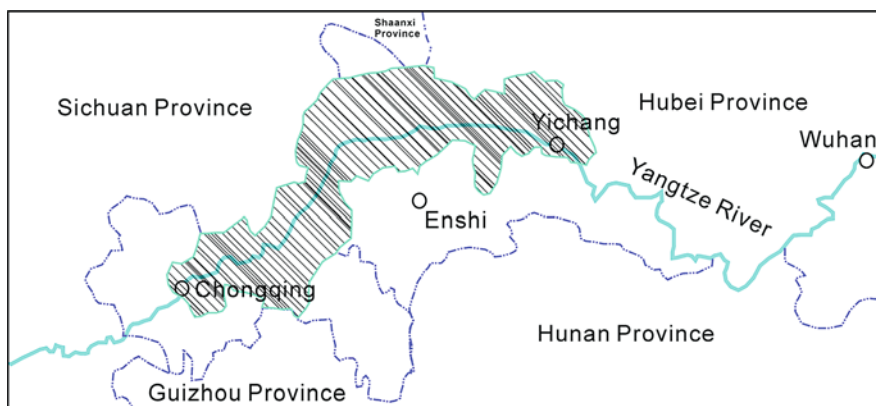
Fig. 1.1 Geo-hazard survey location of the Three Gorges reservoir region on the Yangtze River

Overall Features of Geological Disasters

The main targets of assessing geological disasters in the Three Gorges reservoir area survey are landslide and collapse, the perilous rock masses (unstable slope or deformed slope), debris flows, ground collapse, and cracking and collapse of reservoir banks. The scale of the investigation is 1:100,000 and a map in scale of 1:50,000 was used.

There are 7,068 points in the actual survey of geological disasters in the Three Gorges reservoir area; 5,706 points were found and registered, including 3,830 landslides, accounting for 67% of the total; landslides numbering 549, accounting for 9.6% of the total; 90 mudslides, accounting for 1.6% of the total; 85 incidences of ground collapse, accounting for 1.5%, 45 areas showing cracks, accounting for 1%; and 1107 unstable slopes, accounting for 19.3% of the total. The largest number of existing geological disasters is minimal , composed of 5,706 points, 3,658 were registered, accounting for 64.11%; and 93 points are giant geological disasters, which are 1.6% of the total number (Fig. 1.2).
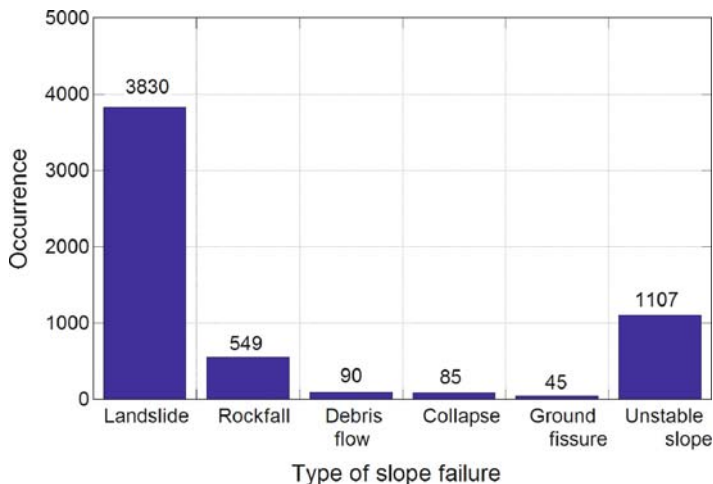
Fig. 1.2 Number distribution of geo-hazard types in the Three Gorges reservoir region

Calculation and Analysis of Assessment

The spatial database and layered graphics database using digital terrain is a 1:250,000 Base Map in MapGIS of Three Gorges reservoir area that is based on the data from 19 counties (districts) survey. Through statistics obtained by research of geological disasters and terrain (elevation, slope), water system, vegetation, rock groups of geologic engineering, active geological structures, slope type, rainfall distribution, seismic activity, evaluation of the regional development factor, basic factor, trigger factor, and vulnerability factor system of geological disasters in the Three

Gorges reservoir area were identified. A 2.5 km × 2.5 km (figure – 1 cm × 1 cm) grid throughout the region (a total of 9,309 grids), the numerical distribution of "distribution degree," "potentiality degree," "dangerous degree," and "harmful degree" were calculated, and entered onto the corresponding zoning map using interpolation methods (Liu et al. 2004b).

1. *Distribution degree calculation*: According to the results of regional geological disasters "distribution degree," and considering various hazard factors and the actual situation in the Three Gorges reservoir area, the development degree of geological disasters in the Three Gorges reservoir area is divided into four categories: the development of geological disasters indicating none (0–3), low growth (3–6), normal area (6–9), and high growth (≥ 9).

By viewing all levels of district size disaster distribution and percentage of geological disasters in the Three Gorges reservoir area, "distribution degree," it can be ascertained that the development zones have their own different characteristics (Table 1.1).

2. *Potentiality degree calculation*: According to survey data and the actual results of geological disasters in the Three Gorges reservoir area, the basis factor and response factor of geological disasters are the discriminate factors of the "potentiality degree" calculation (Table 1.2).

Calculated by the composite index model, the "potentiality degree" curve jumps to 1.6, 2, 2.4, and 2.8, using the four points to divide the Three Gorges reservoir area into five geological disaster potential (degrees) districts: great (>2.6), rather high (2.3–2.6), high (2–2.3), low (1.6–2), and rather low (0–1.6) (Table 1.3).

"Potentiality degree" division results are inosculated with geological background, terrain, and other factors, and the division results can be considered as the disaster forecast foundation for the geological danger forecast for the Three Gorges reservoir area and additionally, geological disaster early warning.

3. *Dangerous degree calculation*: "Dangerous degree" must be calculated using composite index model, and in addition, using the basic factor and response factor, we also need to establish a trigger factor system (Table 1.4). "Dangerous degree" exponential curve calculated by the composite index model corresponds to the interval changes 2.2 and –2.4, 2.5–2.6, 2.8–3, and 3.4–3.5. The whole region will be divided into five risk areas indicated by the results of the analysis and the study of "potential degree" distribution: great (>3.5), rather high (3.2–3.5), high (2.8–3.2), low (2.4–2.8), and rather low (1.5–2.4) (Table 1.5).

Table 1.1 Geo-hazard "distribution degree" division

Distribution degree	None	Low	Normal	High
Hazard points	7	1599	1641	2459
Area(km^2)*	39425	9318.75	5456.25	3981.25
Points/km^2	0.00019	0.17160	0.30064	0.61769

*Grid unit includes the reservoir area outside the boundary of the grid area.

Table 1.2 Weighted basic and response factors of geo-hazard in the Three Gorges reservoir area

Discrimination factor			Unit	Discriminate parameter value*					Weight
Basic level	High level								
Basic factor	Terrain	Altitude	M / Assign	<250 / 5	250–400 / 4	400–600 / 3	600–1000 / 2	>1000 / 1	0.06
		Slope gradient	Assign / °	<10 / 4	10–25 / 5	25–40 / 3	40–60 / 2	>60 / 1	0.1
		Slope type	Code / Assign	I / 2	II / 3	III / 4	IV / 5	V / 1	0.07
		Gulch density	km / Assign	0–2 / 1	2–3.5 / 2	3.5–5 / 3	5–6.5 / 4	>6.5 / 5	0.07
	Vegetation	Cover degree	% / Assign	<10 / 2		10–50 / 3		>50 / 1	0.04
	Rock group	Type	Code / Assign	HM / 2	HC / 3	HD / 4	SD / 5	SQ / 1	0.15
		Geologic structure	Developed degree / Assign	Intensity / 5	Rather intensity / 4	Normal / 3	Rather feebleness / 2	Feebleness / 1	0.06
Response factor		Disaster frequency ratio	Assign	0–1 / 1	1–2 / 2	2–4.5 / 3	4.5–8 / 4	>8 / 5	0.07
		Disaster area modulus ratio	Assign	0–1 / 1	1–2 / 2	2–3 / 3	3–4 / 4	>4 / 5	0.04
		Disaster area capacity modulus ratio	Assign	0–1 / 1	1–2 / 2	2–3 / 3	3–4 / 4	>4 / 5	0.04

*Discriminate parameter value is valid in the 2.5 km ×2.5 km calculating range.

Table 1.3 "Potentiality degree" division characteristics

Code	Name	PP	Area percentage(%)	Annotation
1	Level 1	0–1.6	9.56	Rather low
2	Level 2	1.6–2	29.71	Low
3	Level 3	2–2.3	29.70	Rather high
4	Level 4	2.3–2.6	24.41	High
5	Level 5	>2.6	6.62	Great

Table 1.4 Weighted induced factors of geo-hazard in the Three Gorges reservoir area

Trigger factor									
Rain capacity	1 day max	mm	<150	150–200	200–250	250–300	>300		
		Assign	1	2	3	4	5		0.05
	3days max	mm	<200	200–400	400–600	600–800	>800		
		Assign	1	2	3	4	5		0.08
	On average a year	mm	<1000	1000–1200	1200–1400	1400–1600	>1600		
		Assign	4	5	3	2	1		0.06
Earthquake intensity	Intensity		IV	V	VI	VII			
	Assign		2	3	4	5			0.03
Human activity			Great	High	Normal	Rather low	Low		
	Assign		5	4	3	2	1		0.08

Table 1.5 "Dangerous degree" division characteristics

Code	Name	DP	Area percentage(%)	Annotation
5	Level 5	>3.5	5	Great
4	Level 4	3.2–3.5	17	Rather high
3	Level 3	2.8–3.2	35	High
2	Level 2	2.4–2.8	28	Low
1	Level 1	1.5–2.4	15	Rather low

Table 1.6 Weighted vulnerability factors of geo-hazard in the Three Gorges reservoir area

	Distinguishing factor								
	Basic level	High level	Unit/km²	Discriminate parameter value					Weight
Vulnerability factor	Population density			<100	100–200	200–400	400–650	>650	
			Assign	1	2	3	4	5	0.4
	Property			–	–	–	–	–	
			Assign						0.3
	Engineering facility			–	–	–	–	–	
			Assign						0.3

Table 1.7   Geo-hazard "harmful degree" division

Harmful degree	HP	Area percentage(%)	Annotation
Level 1	0–0.5	15.94	Low
Level 2	0.5–0.8	34.01	Rather low
Level 3	0.8–1.2	33.62	High
Level 4	1.2–1.4	11.37	Rather high
Level 5	>1.4	5.06	Great

4. *Harmful degree calculation*: According to the actual situation in the study area, the selected vulnerability factors are population density, property value, and engineering facilities (Table 1.6). The deficiency of the information on property and engineering facilities resulted in only the evaluation of population density to be selected as the vulnerability factor. According to the changes in population density and disaster point distribution, the population density is divided into five sectors, and was assigned as, the population density of up to 5, and a minimum of 1. The actual calculations only took into consideration, population density multiplied by the 1/10 of the assignment from small to big according to discriminate population density and no weighted calculation, as shown in Table 1.7.

The study divided five "harmful degree" levels to consider the actual situation in the Three Gorges reservoir area. The calculation was evaluated as great (>1.4), rather high (1.2–1.4), high (0.8–1.2), low (0.5–0.8), and rather low (0–0.5).

Disaster Prevention Measures

According to the calculation and division of "distribution degree," "potentiality degree," "dangerous degree," and "harmful degree" results, economic and social development planning, immigration relocation planning, and other factors affecting the Three Gorges reservoir area, different levels or different types of zones would be delineated. Level 3 "dangerous degree" and "harmful degree" in the area are for general prevention. Level 4 and level 5 "dangerous degree" in the area is focused on early warning, respectively, for 2708 km^2 and 9209 km^2. Level 4 and level 5 "harmful degree" areas have a major distribution, of 2741 km^2 and 6159 km^2.

Initiation Mechanism of Complex Slope in the Three Gorges

The initiation mechanism of complex slopes in the Three Gorges of the Yangtze River is not only a simple academic problem but also an emergency requirement for resettlement projects and reservoir banks protection, involving the basic problems such as the geological environmental quality and engineering construction capacity. It would be much more useful to expand our hazard assessments to be more inclusive of these factors, and not to simply continue to study landslide processes, only.

Facts and Viewpoints

Basic Facts

The attitude of the stratum in the Wanzhou area is gentle, but there are a large number of landslides. Resettlement and reconstruction are impacted by several landslides, such as the Taibaiyan landslide, Diaoyanping landslide, Pipaping landslide, Anlesi landslide, Caojiezi landslide, and Yuhuanguan landslide.

Landslide disasters are serious along the Yangtze River in Yunyang county, and there are many large bedrock landslides. The Baotaping landslide is one of the four landslides with volumes that are more than 1×10^9 m^3 in the reservoir area, and the stability of its middle and back part is worth researching. The new location of Yunyang is away from the landslides group in the old city, but there are still landslides in Saiba, where the attitude of the stratum is gentle.

City construction of Fengjie county shows that the slope stability gradually decreases from west to east, and the landform is cut acutely. In the process of the new county city construction, large-area accumulation bodies with complex structures whose initiation is undefined are found. Because of the scarcity of geological evaluations addressing reasonable development, the new county city is 13 km long, and it has eight pieces of construction. There is no unambiguous geological assessment verdict in Baotaping and the old city extending to Sanmashan, road along the river, and junction road area, so as a result, new county locations have been changed several times.

Slope structure in Wushan is that of uncompaction. In the construction process of the new city resettlement, it was found that the geological foundation and the characteristics of roads, bridges, and building grounds are complex. The component, structure, initiation, and stability of slope rock mass and soil are key problems. Wushan is considered to be a typical spot of "down-slope overlapping." Unusual clay with carbon is found, indicated by drilling, but there is rubble above and clay underneath. This phenomenon occurs in Fengjie, which shows that there was an absonant component during normal evolution.

The new location of Badong County town has been selected three different times and moved twice. The new location of Badong county city was first determined in Huangtupo in 1982, but it was found that there was a huge ancient landslide (Huangtupo landslide), during the investigation process in 1988, so the location had to be re-selected. Badong county city center was planned to be located in Yuntuo in 1992, but the location had to be moved once again because of the abnormal geological body. The government agency center of Badong county city was planned for Xirangpo, in the third location selection in 1996.

Scientific Knowledge

The resettlement locations of cities in Three Gorges reservoir area have been changed many times because the geological composition of the environment and the structure and failure initiation of geological bodies assessed by engineering

excavation are unclear. In addressing this problem, some scholars propose different conceptions, such as characterizing the geology as for instance, "compound accumulation body," "down-slope overlapping," "landslide," "loose deposits," "cataclastic rock mass," "ancient collapse of underground river," or "corrosion settlement body." Due to the lack of systemic analysis and the limitations of individual viewpoints, these conceptions are unlikely to be unified descriptions, anytime soon.

For these viewpoints, down-slope overlapping, proposed by Cui Zhengquan, an engineer, has involved decades of observation. But there is a lack of evidence for ascribing this activity to global earthquakes, landslides, and floods of 200,000 years ago.

Liu CZ proposed the conception of "compound accumulation body" based on decades of site investigation and research in Three Gorges. It is the general name of a slope composed of bedrock, ancient collapse deposits, ancient collapse and landslides, and quaternary deposition. He ascribes the initiation to the abnormal reservoir bank rebuilding that occurred when the ancient Chuanjiang River was connected with the Xiajiang River at Qutang Gorge in Fengjie county, forming a unified Yangtze River (Liu 2000, 2005).

Regional Geological Evidence

Regional Geological Structure

There is geological evidence that the ancient Chuanjiang River was connected with the Xiajiang River at Qutang Gorge in Fengjie county to form a unified Yangtze River (Fig. 1.3). Three Gorges is mostly in the junction of the Chuandong fold belt, the Dabashan arc, and the west part of the Huaiyang Mountain shape reflex arc. Fengjie is the dividing point of regional sedimentary facies, in the west, which is mostly Jurassic red beds, and in the east, mostly Triassic carbonate rock (Chen 1993). In geomorphology evolution history, it is a karst collapse region in Fengjie, where a world-famous spectacle occurred, Tiankeng and Difeng. Before connection, the Caotang River which belongs to the Chuanjiang river system flowed west, while the Daxi River which belongs to the Xiajiang river system flowed east. These two rivers cut through the Qiyue Mountain anticline and the Qutang Gorge formed, and thus, the unified Yangtze River came into being (Fig. 1.3) (Tian 1996).

Neo-tectonic Stress Field in the Three Gorges Region Inversed Analysized by River System

Formation and development of modern topography and geomorphology are controlled and affected directly by neo-tectonic movement. River systems are very sensitive to neo-tectonic movement, and its morphology has important significance in determining the neo-tectonic stress field. The method that calculates neo-tectonic stress fields, utilizing regional river system statistics, is more and more important (Koleback & Scheidegger 1977, Liu 1993a, Qin et al. 2006).
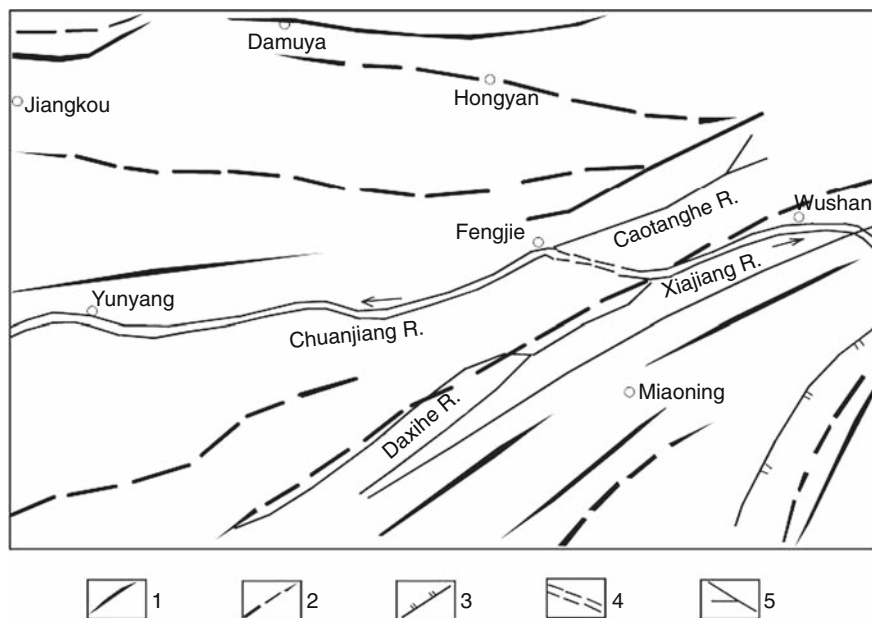
Fig. 1.3 Structural outline map in the connected area between Chuan and Xiajiang rivers. 1 – Anticline; 2 – sysncline; 3 – faults; 4 – Qutang Gorge at present; 5 – water system (simplified from Tian 1996)

After arranging the river system data, the node coordinate of every river broken line can be obtained through the second development of MAPGIS software utilizing visual basics. Then a line is fit, the slope and arctangent of which is obtained through linear fitting using the least square method. River system-dominant trends can be calculated utilizing the azimuth of the fitting line and river length, obtained from the river file. It is then that the principal compressive stress can be obtained.

The dominant direction of the neo-tectonic stress field in the Three Gorges is the NE direction, and it is in a NW direction in A2 and B5. Stress field distribution shows the inherent neo-tectonic movement, which is the inherent activity of an old fault. The NE direction is dominant showing that NE is the direction of principal compressive stress. The neo-tectonic stress field in the Three Gorges appears to be in a NE direction, about 42°.

River System Fractal Character

According to fractal theory, based on GIS technology, utilizing the box-counting method with the digital topographic map, the fractal dimension of Three Gorges can be calculated (Mandelbrot 1982, Liu 1993b). Side length (km) ε=165.40, 82.70, 41.35, 20.675, 10.34, 5.17, 2.58, and 1.29. Box counts are 2, 8, 28, 94, 336, 1133, 3276, and 7846 respectively. The fractal dimension of the river system in Three Gorges is 1.7239, and the correlation coefficient is 0.9985063.

Generally, the fractal dimension of a river system reflects the development degree of the river system, and the difference of fractal dimension reflects the developmental difference in degree of watershed topography. According to the fractal dimension calculation applied to river systems of China, the critical fractal dimension of watershed topography development stage is $D = 1.6$, when $D < 1.6$ is reached, watershed topography is in a young stage. When $1.6 < D \leq 1.89$ is reached, watershed topography is in a mature stage. When $1.89 < D \leq 2.0$, watershed topography is in a mature stage (He & Zhao 1996).

The fractal dimension of the river system in the Three Gorges is $D=1.7239$, so watershed topography is in a mature stage and the river system development has been basically completed. With the Three Gorges Project finished, river system erosion will slow down, and it will be in a weak erosion stage.

Supergene Dynamic Phenomenon

A series of supergene dynamic phenomenon show that the Fengjie–Wushan area has been an abnormal region of crustal movement since the middle Pleistocene.

1. *Terrace characteristics*: The longitudinal profile of terraces shows that terraces in the Fengjie–Wushan area are abnormal. From Jiangjin to Fengjie–Wushan, all terraces are mostly parallel to a kraurotic water line and change gently. But the inclination of a downstream terrace in the east of Fengjie–Wushan increases suddenly. Terraces intersect the kraurotic water line with a sharp angle, forming a turning point in the Fengjie–Wushan area (Fig. 1.4) (Shen 1965).
2. *Riverbed characteristics*: The water level gradient is 0.16–0.17 from Jiangjin to Fengjie. It is even higher, as much as 0.4, from Fengjie to Wushan, which is the
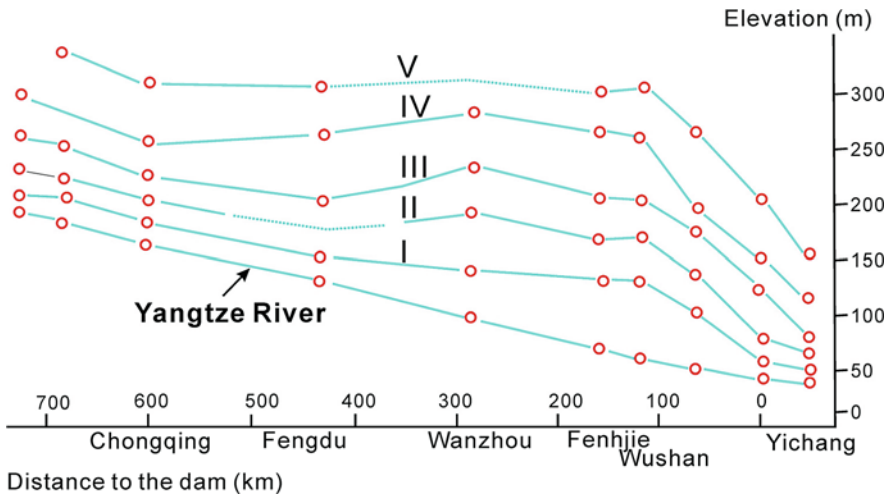

Fig. 1.4 River terrace altitude in the Three Gorges of Yangtze River

highest of the whole river. Tributaries of the Yangtze River also have greater riverbed gradient.

According to 1:12000 scale statistics in the Yangtze River channel, there are 141 shallow troughs, troughs, and deep troughs, 31 of which are lower than sea level and 30 are in Three Gorges. The lengths of shallow troughs, troughs, and deep troughs in Three Gorges account for 53.2% of the total length from Chongqing to Yichang, but the river length of the Three Gorges area is less than one third of the whole river (Table 1.8) (Yang 2006).

3. *Landslide activity*: Regarding elevation distribution, toe elevations of landslide are mainly between 60 and 200 m, and the back edge elevations are mainly between 60 and 200 m. The difference is generally 250–350 m, and the maximum is 730 m (Deng 2000). Dip angle of slip surface is generally 20°–40°. Ancient landslide dating in the junction region shows that nearly all the landslides happened in Q_2 or Q_3, coinciding with the warm and wet climate period (Zhang 1993). According to statistics, from Wanxian to Badong, landslides happened during 4 periods: $(35-45) \times 10^4$ a; $(25-30) \times 10^4$ a; $(8-15) \times 10^4$ a; and $(2-5) \times 10^4$ a (Fig. 1.5).

According to slip soil dating, the climax number of landslides happened in two periods: 40×10^4 YBP (years before the present) and $7-15 \times 10^4$ YBP. Landslides in Fengjie–Wushan took place mostly since the late Pleistocene, which shows that it was not a large-scale formation period before 15×10^4 YBP in Fengjie–Wushan. Both sides of Fengjie–Wushan are in a violent formation period that is a landslide period. After 15×10^4 YBP, Fengjie–Wushan entered a collapse and landslide period.

4. *Relationship between ancient collapse and landslides and the ancient Yangtze River*: Through geological investigation, deep erosion troughs were found on the toe of Baiyi'an ancient landslide and bedrock was not found at 18 m of elevation, which shows that the mainstream of the Yangtze River was closed to the Baiyi'an ancient landslide after a long period of landsliding (Liu et al. 2003). The stratum structure of the Baiyi'an ancient landslide also proves that the toe has always been

Table 1.8 Deep trough distribution in a section of Chongqing–Yichang section (Simplified from Yang 2006)

River section	Shallow trough*	Trough**	Deep trough***
Chongqing–Dahongjiang	1	5	0
Dahongjiang–Qingyanzi	5	0	0
Qingyanzi–Liushapo	0	14	0
Liushapo–Xinglongtan	9	0	0
Xionglongtan–Fengjie	3	13	1
Fengjie–Yichang	35	25	30
Total	53	57	31

*Shallow trough is 20 m lower than the river bed;
**Trough is 30 m lower than the river bed;
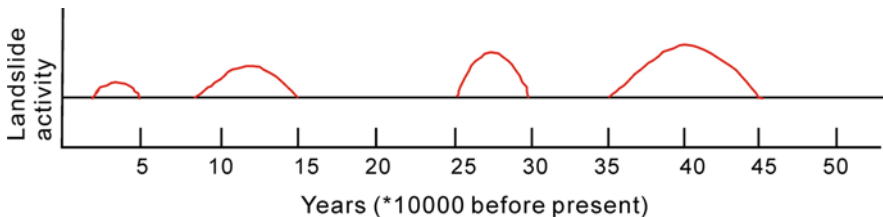***Deep trough is lower than sea level.

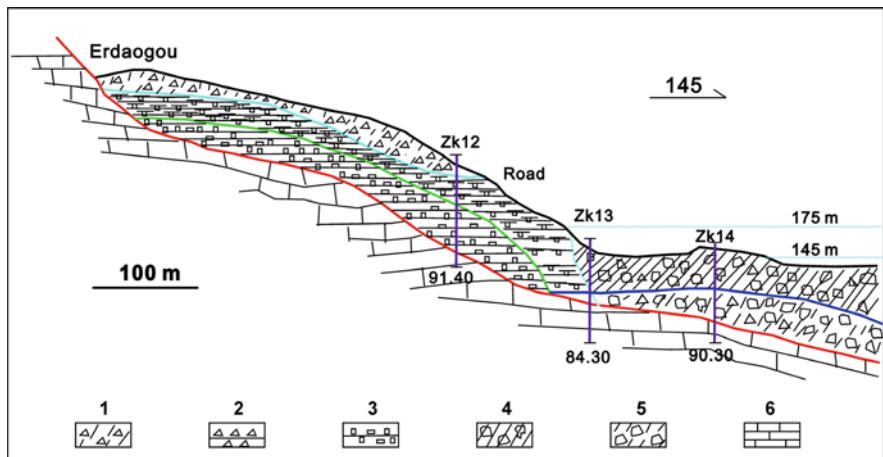**Fig. 1.5** Division of distribution periods for landslide activity

Fig. 1.6 Geological section of the Baiyi'an ancient landslide at the northern bank of the Yangtze River. 1 – soilaggregate; 2 – fractured rock mass; 3 – fractured rock mass in block; 4 – silty clay with fractured rock piece; 5 – cobble soil with sand; 6 – Triassic marlite

the bank of the ancient Yangtze River. Subsequently, a cut slope formed and was covered by diluvium at a later time (Fig. 1.6).

5. *Collapse relic-Yanyudui*: "Yanyudui" was always a huge stone in the Qutangxia Gorge of the Yangtze River, which was 30 m long, 20 m wide, and 40 m high. It was blown up by 20 tons of dynamite to remove the barrier in the winter of 1958. "Yanyudui" was a typical collapse relic, which showed that huge landslides and collapses had always taken place in Qutangxia (Fig. 1.7).

Ancient Chuanjiang River Connected with Ancient Xiajiang River Forming a Unified Yangtze River and Slope Evolution

In this chapter, for the sake of convenience, the section of the Yangtze River from Yibin to Fengjie is called the Chuanjiang River and the section of the Yangtze River from Fengjie to Yichang is called the Xiajiang River. These two rivers belonged to a different river system in history, so the linking up and the evolution of these

Fig. 1.7 Rock fall trace in Qutangxia Gorge – "Yanyudui," a huge stone (from Zhangzudao, photographed in 1956)

two rivers have important significance in engineering geology and environmental geology, which affect the quality of the geological environment, engineering construction capacity, and the ecological environment bearing capacity.

The Ancient Chuanjiang River and the Xiajiang River Linking up Was a Great Natural Event

Before linking up, the Chuanjiang River flowed west, while the Xiajiang River flowed east. These two rivers eroded headward in the direction of the Wushan–Qiyueshan area. After linking up, three dynamic water forces acted in a short time. These were, the "water saw" undercutting of Chuanjiang river on the top of the watershed, the headward erosion of the Xiajiang River, and an earthquake induced by underwater river collapse or karst collapse (Fig. 1.8).

These three processes caused a drastic reconstruction period and evolution process on the bank slopes of the river junction area. Under the action of "water saw," slopes in the junction area changed, as a result of physio-chemical action. Structure fracture is the basis of bank slope shaping. The unloaded, loose, and cracked geological body with the space created by "water saw" turned muddy and collapsed, and eventually the final version of the collapse body come into being. Erosion of limestone and gypsum rocks caused the karst collapse or overhead collapse to occur on the top of the riverbed. Thus, the underground river turned into a surface-flowing
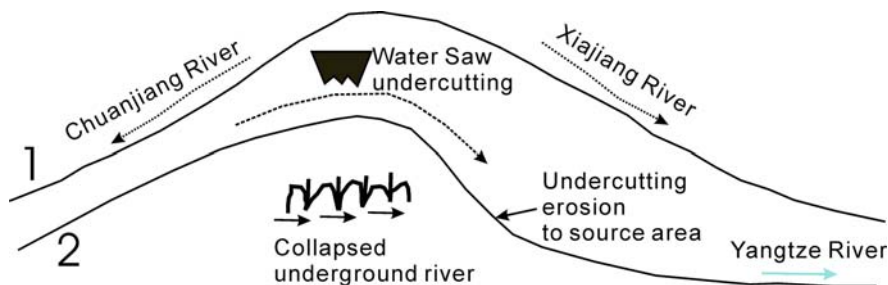
Fig. 1.8 The diagram of hydrodynamic action before and after the Chuanjiang River connected with the Xiajiang River in the Qutang Gorge segment of the Three Gorges at the Yangtze River. 1 – Geological processes before the Chuanjiang River connected with the Xiajiang River; 2 – geo-actions after the Chuanjiang River connected with the Xiajiang River, forming the Yangtze River

river. Surface collapse and landsliding contributed to the reformed process and over-lapped with the alluvial–diluvial actions. The process of bank slope formation can be described as mountain unloading, characterized by loose, cracked, tumultuous mud-collapse and landslide-terrace formation overlapping with an accumulation of compound formations. The process is repetitive.

Basically, erosional action is obviously more pronounced in the junction area of the two rivers rather than in the adjacent area. The main area is the Yunyang–Fengjie–Wushan–Badong area. Fengjie–Wushan is the most intensive area and Wanzhou, Yunyang, Badong are the affected zones. The chronological progression of these processes is 60×10^4 YBP–10×10^4 YBP, and they have evolved naturally since 10×10^4 YBP.

Geological Dynamic Background

In regard to regional geodynamics, China is located at the junction of the circum-Pacific tectonic region and Himalayan tectonic region. Subduction of the Pacific plate and extrusion activity of the Indian Oceanic plate in relation to the Pacific plate are the main geodynamic sources for mainland China. The Himalayan Mountains which are the highest mountains in the world, formed at the edge of the Indian Oceanic plate and Asian plate. A large ridge formation occurred, which is the Qinghai–Tibet Plateau. Convergence of these two active tectonic regions creates the tectonic framework and basic topographical configuration of China, which determines the diversity of geological environments and the frequency of geological disasters.

Research has proven that the Qinghai–Tibet Plateau has risen up quite a bit since the recent tectonic period and the west part of Sichuan became the second-level terrain step of China, which is the background for the Chuanjiang River connecting with the Xiajiang River. At the border of Sichuan province, Yunnan province and Tibet, the Nujiang River, the Lancangjiang River, and the Jinshajiang River flow parallel to one another. The Jinshajiang River changes a lot in Shigu town, and
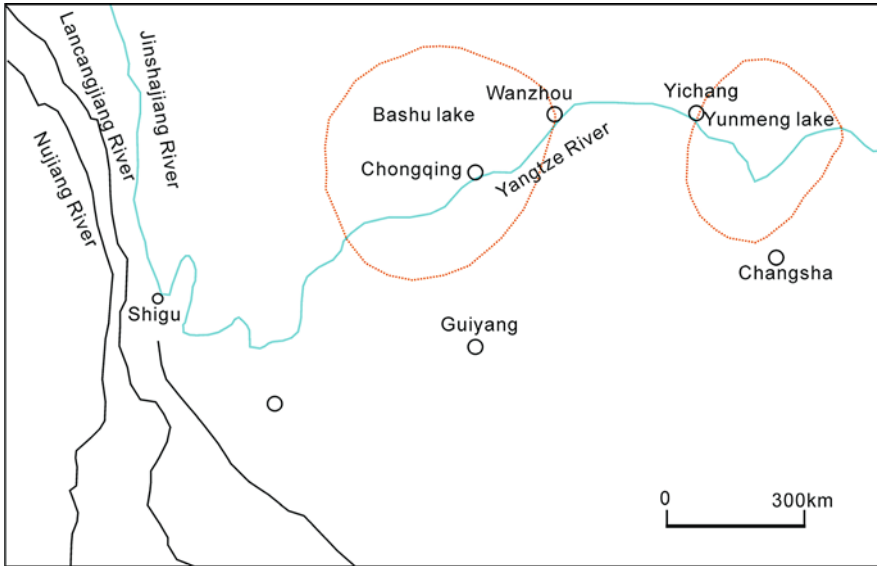
Fig. 1.9 Three rivers (Jinshajiang, Lanchangjiang, and Nujiang) flow in the same direction and converge to form the Yangtze River

Honghe River in the south of Shigu along the Ailao Mountains and is perhaps the relic of the Jinshajiang River flowing south. At the border of Sichuan province and Hubei province, the Xiajiang River belongs to a different river system; the west part belongs to Bashu ancient lake, while the eastern part belongs to Yunmeng ancient lake. Three Gorges allows the Xiajiang River to connect with Chuanjiang River (Fig. 1.9) (Liu 2000, 2005, Tian 1996, Shen 1965, Yang 2006, Lee 1924, Yang 1988).

The Complex Slope Failure Initiation and Assessment in Badong County

Statement of Problem

The initiation process of large complex slopes in the Three Gorges reservoir still does not have an acceptable evaluation, and the academic community also has not integrated knowledge of the characteristics of the fan-shaped slope at Badong new town in the Three Gorges reservoir, even if a few have researched micro-phenomenon survey to compare it with the "big question" from macroscopic-type research. This kind of "question" is the main reason for the new site selection and the numerous changes in location of Badong new town, and it is a typical instance

of new town planning that lacks the necessary research on regional engineering geology (Cui 1998, Liu et al. 2006a).

Throughout the course of about 20 years' planning and changes, Badong new town site has become five subzones, those of Huangtupo, Daping, Baitupo, Yuntuo, and Xiranpo, extending from the east to the west. Within the narrow, long area that is about 8 km in length and 1 km wide along the Yangtze River, the Badong big slope is divided into five slope units, delineated by four gullies (Aleotti & Chowdhury 1999, Haruyama & Kitamura 1984).

Reviewing history, the geological work during the course of planning and construction of Badong new town generally was dealt with passively, and the geological work was the guiding and leading evaluation approach for hazard studies and had not completely accounted for a through scientific investigation.

This one-sided approach did not adequately explain the complexities involved in assessing the hazard from landslides. The question about deep layers in the entire slide area of Badong big slope was put forward in 2002, and even then there were worries about whether there would be a calamitous hidden danger such as that which occurred at Vajont reservoir in Italy.

This research tries to address the mistaken aspects of the overall conclusion that is drawn from local phenomenon. Based on the analysis of morphological features and geological structures, the complex slope system of Badong was found to be the example for failure initiation and for the assessment of geologic environmental quality and dynamics.

Geological Characteristic of Badong Big Slope

Morphologic Features

(1) The morphologic features of the Badong big slope belong to the characteristic middle-low gorge area with areas of structural erosion. The mountain top elevation is 700–1230 m, and the elevation of the river before impoundment of the Three Gorges reservoir is 67.1 m. The Yangtze River flows across the edge of the Badong big slope becoming a northward arc, and the width of the river surface is 300–600 m, which is the relatively widest reach of the Three Gorges.

(2) The Badong big slope is a fan-shaped slope where the strike is nearly east–west and the incline is north. There are a series of deep and big gullies in the slope area, and the gullies pass through the slope from south to north and enter into the Yangtze River. The whole area was cut into five slope units, forming widths of from 1.3 to 1.7 km, the distribution being nearly south–north (Fig. 1.10).

(3) The gullies in the slope area are short and deep cut, merging into a single gulley, and many gullies have the same source. They reflect the numerous occurrences of landslide development under the control of the geological structure.

(4) The cross section of gully generally is a "V" type, the depth cut is 50–200 m, and the greatest depth is 350 m (Baiyangou). The cut depths of Tongpenxi and Huangjiagou are 20–150 m, they have many falls, and the catchment areas are both greater than 2 km^2. The lengths are both greater than 2 km.

Fig. 1.10 Aerial map of the Badong large slope (from China Aero Geophysical Survey & Remote Sensing Center for Land and Resources (AGRS), 2003.4)

(5) Terraces on the Yangtze River have rarely been found, indicating that the continuous downward erosion and the side directional hillside soil losses are large, occurring since the more recent period, and the phenomena of erosion gyration or landform erosion gyration are not found.

(6) There are many remnants of riverbed at Badong on the Yangtze River and they are lower than sea level – some places are even up to 11.8 m lower. They are lower than the erosion base-level generally, and this indicates that there are deep pools which resulted from vortex erosion.

(7) The trailing edge border of the big slope is an arc gulley which resulted from the differential erosion of the contact zone of soft rock and hard rock. It became the back border of the whole slope and the source of all gullies, and it controls the gulley situation within the slope.

(8) There are five water systems within the slope, from the west to the east known as, Huangjiadagou, Tongpenxi, Baiyangou, Sidaogou, and Toudaogou, and their fractal values are 1.051, 1.111, 1.124, 1.012, and 1.114. The water system fractal value of the whole fan-shaped area of Badong is 1.267. All the fractal values are less than 1.6, and it indicates that the river basin belongs to the young period of erosional development; the water systems do not develop sufficiently (He & Zhao 1996, Lian et al. 2006).

Stratum Combination

The Badong big slope is made up of four lithologies of the Badong group (T_2b) of the Triassic Period middle system; it is an interlayered combination of clastic rock and carbonate rock. The fourth section (T_2b^4) is red sand-mudstone, and it is mainly distributed in Hongshibao and at the exit of Huangjiagou, and is the remnant of

karyomere of the Guangdukou syncline. The third section (T_2b^3) is carbonate rock and is the main body of Badong big slope. It is generally a rock mass with moderate weathering, some parts are intensely weathered, and they present a fractured rock mass with fissure development. The second section (T_2b^2) is fuchsia mudstone and silt-mudstone, they are mainly distributed at an elevation of 430–460 m, the rock is easily weathered, and subject to softening and argillization, and it is one of the most slide-prone strata in the Three Gorges. The first section (T_2b^1) is gray matter mudstone interlayer with micrite and dolostone, with banding distributed on the trailing edge of the Badong big slope, and they have become the sources of gullies in the upper reaches or the border valleys of the whole slope. The third section Jialingjiang group (T_1j^3) of Triassic Period lower system is medium thickness seam dolomite–limestone and limestone, interlayered with angular gravel limestone. It makes up the base of the Badong big slope, exposed behind the mountain, becoming the first watershed.

The Quaternary-age material is made up of residual slope deposits – demise diluvial (Q^{el+dl}) and demise deposits ($Q^{col+del}$), and some parts develop alluvium–proluvium, manual deposits (Q^{ml}), and debris flow deposits (Q^{sef}).

The Vestige of Geological Structure

The regional geological structure of the Badong big slope is generally simple, in that it is the south wing of the Guangdukou syncline made up of a monoclinal mountain, and some small-scale relaxed folds or fold distortion with strong extrusion formed by the geological reconstruction in some parts of slope. The loosening relief fracture, kinky deformation of soft rock, and collapsed landslides are very developed. The syncline is broad and relaxed, and the axial plane is slightly inclined to the south. The dip angle of the north wing is 10°–25°, and the dip angle of the south wing is 20°–48°. The structural axis of the Guangdukou–Dongrangkou syncline occurs near the river at new town, at the river entrance of Baiyangou and Tongpenxi. The geological structure of the fan-shaped big slope of Badong new town is a monoclinal slope which is made up of the south wing of the syncline (Fig. 1.11) (Geological Bureau of Hubei Province 1997, Yangtze River Conservancy of Water Resource Committee 1997).

The Question About the "Badong Fracture"

1. *The geological facts*: The trailing edge of the Badong big slope is nearly developed along the strata division of the Jialingjiang group (T_1j^3) and the Badong group (T_2b^1). It trends as an arc negative in relief, the middle area of the Zhongyuan village as watershed, and the east and west side develop along the upper reaches of Huangjiadagou, Tongpenxi, Sidaogou, and Toudaogou, and it is also the source of the branch gully of Baiyangou. Along the trailing edge valley, there are some typical sites with extrusion vestiges.
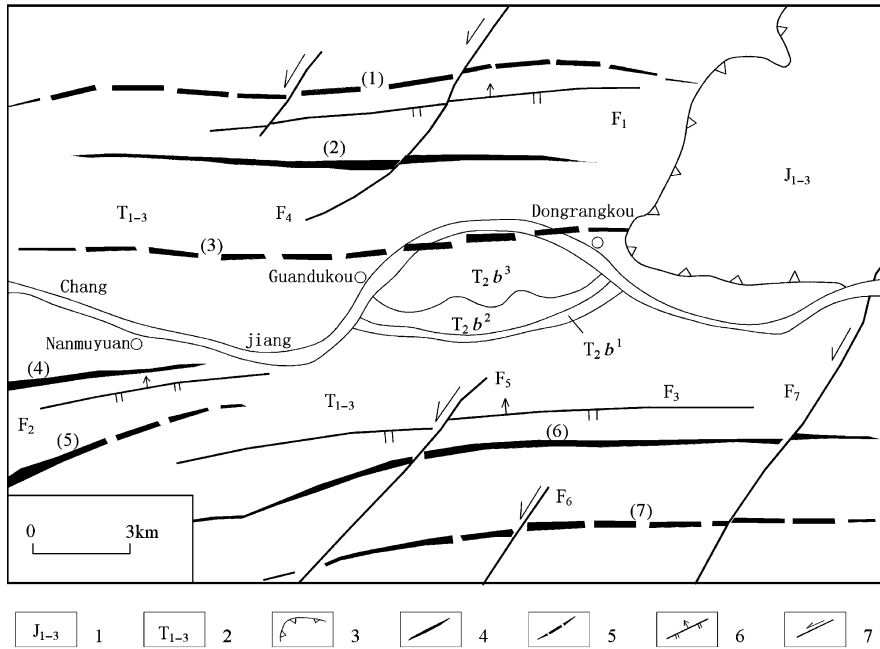
Fig. 1.11 Areal structure sketch of Badong slope in the Three Gorges of the Yangtze River. 1 – Jurassic System; 2 – Triassic System; 3 – continental deposit (Zigui) basin; 4 – anticline structure axis; 5 – syncline structure axis; 6 – reversed fault; 7 – shift fault. (1) – Huofeng syncline; (2) – Xiaogaoshan anticline; (3) – Guangdukou syncline; (4) – Nanmuyuan anticline; (5) – Duping syncline; (6) – Baifuping anticline; (7) – Fengcuiya syncline; F_1 – Guangyintang fault; F_2 – Bingshuijing fault; F_3 – Maluchi fault; F_4 – : Gongqiao fault; F_5 – Yeluchi fault; F_6 – Meiziya fault; F_7 – Niukou fault

a. The extrusion breccias were developed at the corner of Mutianwan at the 209 national road, the color is lark, the shale content is high, and the angular gravel sizes are different. The small size is 3–5 cm, and the big size is 10–15 cm, the edge angle of angular gravel is not clear, the angular gravel is round, and slickensides can be seen. The weathering relief of the surface layer is pronounced and was shown as argillization. The strike of the extrusion is $105°$, the incline is north, and the dip angle is $61°$. The hanging wall is argillaceous limestone of T_2b^1, and the footwall is interlayered and is composed of thick and thin limestone of T_1j^3.

   The highway slope to the north about 100 m on 209 national road is made up of a fuchsia mudstone sliver of T_2b^2, Kelly gray matter mudstone sliver and deep gray limestone block, without bedding and separation. The geological composition is collapse deposits.

b. The original breccia was found at the Jigongling (elevation 450 m) along the eastward end of the trailing edge border of Badong slope, and the breccia is crushed, loose, and unsupported. Its matrix is made from gray sand-

mudstone, argillaceous limestone, and limestone with non-rounded gravel. It is in the contact zone of the T_1j^3 and T_2b^1 stratum.

c. Toward the east, at the place where the Toudaogou passes through the trailing edge border of Badong slope (elevation 290 m), the limestone angular gravel and the tan marl are intermixed, and the angular gravel has some rounding. The diameter of the gravel is 5–10 cm, and it has been cemented into rock, but the soft rock gravel has been corroded into the porous areas

2. *Basic acquaintance*

a. The plane of the trailing edge border of Badong big slope is the result of tensile stress, and the trailing edge is expressed as transpression at the cross section. The Mutianwan extrusion is the local phenomena of transpression first and tension later. It is the result of a static landslide under gravity.

b. The breccia is corrosion-collapse breccia, and it was cemented into rock by the deposits resulting from collapse and landsliding. It is not the structure breccia, and the fracture phenomenon does not exist.

c. The width of the fractured zone of Mutianwan is 130–140 m, and it is composed of the deposits of collapse and landsides, as a fractured zone.

d. According to the ESR, the value is 30×10^4 a; it is consistent with the valley evolution of the Yangtze River and corresponds to the middle and late period of the middle Pleistocene (Liu et al 2006a).

e. There is creep indicated along the strata border of T_1j^3 and T_2b^1 of the whole slope.

f. "Badong fracture" does not pass through the river at both sides of the east and west, and it is only shown as a fold phenomenon.

Therefore, it is mistaken to take the local extrusion, corrosion-collapse breccias, and deposits of collapse and landsliding of the trailing edge border of Badong slope as facture structures.

Joint and "Fracture" of Slope Area

According to the data, the whole Badong slope has 62 data points referring to fractured zone width (Yangtze River Conservancy of Water Resource Committee 1997, Hubei Hydrogeology and Engineering Geology Team 2001). It is interesting to note that the site, structure, property, and width of the fractured zone were recorded in detail by predecessors, but the length was rarely mentioned. We can find that the width is less than 1 m accounting for 41.9% of the 62 data points, 1–5 m account for 32.3%, 5–10 m account for 11.3%, and greater than 10 m account for 14.5%.

Generally speaking, the width of the fault corresponds to its length, and it cannot be just the local geological behavior that the fractured zone reaches a certain width. It is through the local gravity function that the fractured zone width can be seen at cross section, as it rarely can be seen at the ground. Many "faults" of the Badong slope area described by predecessors were the vestiges of relief, extrusion

deformation, and collapse landslide; they are not the inner-dynamic structural cause of failure.

Geomechanics Model of Superficial Deformation and Damage

The superficial geological vestige of Badong slope can be summed up by six geo-mechanics damage models, reflecting the mountains with dip slope geological structure, quickly becoming a free face and thus, gravity lateral relief and collapse-landslide processes came into being under the action of quick corrosion and cutting by the flow of the Yangtze River.

1. *Lateral drawing crack model*: The main initiation of slope failure is human activity, such as excavation of building foundations or highway cut-slopes, and these may result in failure scarps occurring in a short time. This may result in mountain relief along the lateral direction. The rock mass may fall away along the fracture, and the block may slip or even form into a landslide (Fig. 1.12).
2. *"Avalanche type" collapse model*: The deformation type at the leading edge of the Badong slope can be found at every strata layer, but the contact zones of T_1j^3 and T_2b^1 and the rock mass distribution of T_2b^3 are typical, and they are generally shown as corrosion-collapse breccia deposits (Fig. 1.13).
3. *Surface layer weathering model*: Distributing near the river at the trailing edge of the Badong big slope, they are shown as an imbricate type at the geological cross section, and then developed into a small-scale rock fall phenomenon (Fig. 1.14).
4. *Lateral slip translation rupture model*: Mainly appears in the brittle rock mass distribution of T_2b^2 and T_2b^3. The translation fissures are dense in rows, and shown as a certain equidistance, and formed into fractured zone at the macrocosm (Fig. 1.15). This slope model is transformed, once sudden collapse occurs, and the avalanche-type destruction form will occur and become what is called a "fall and cover mass" (Cui 1998).
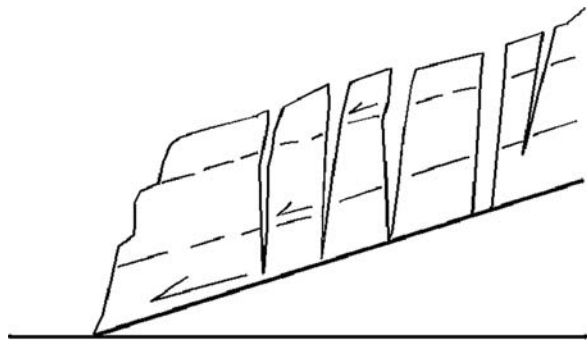

Fig. 1.12 Lateral drawing back failure

Fig. 1.13 "Avalanche type" collapse model
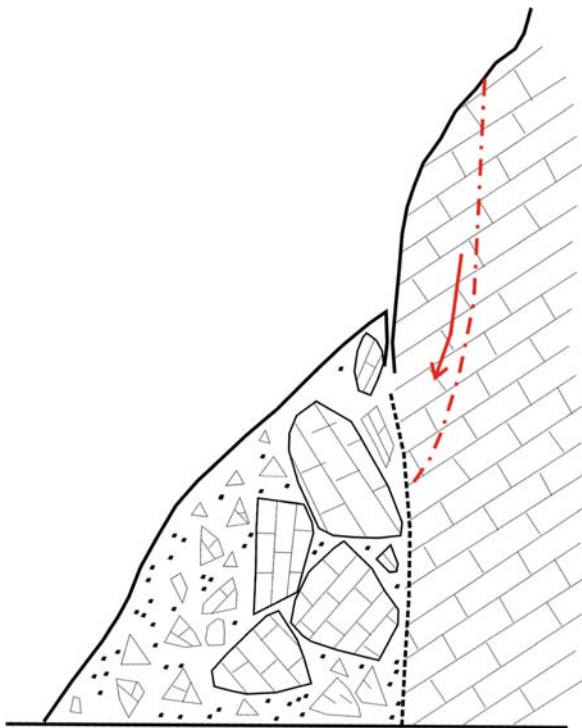
Fig. 1.14 Surface layer weathering model
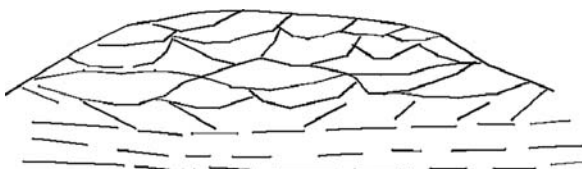
Fig. 1.15 Lateral slip translation rupture model
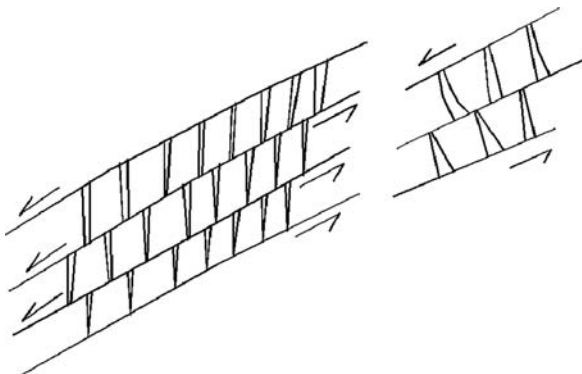
Fig. 1.16 Rock stratum breaking and shift model
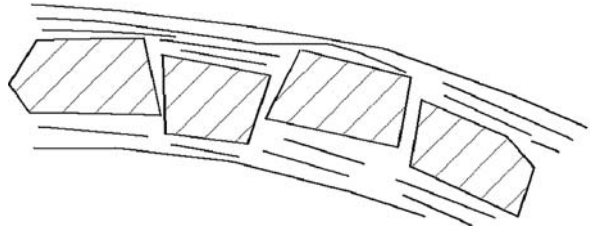
Fig. 1.17 Soft rock kink shear rupture model
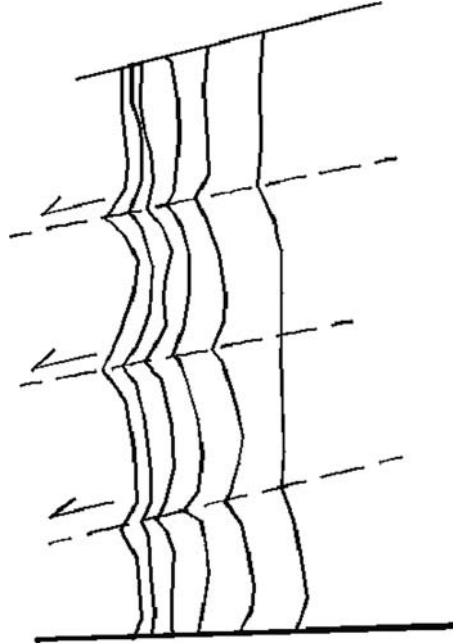
5. *Rock stratum breaking and shift model*: Mainly appears in the T_2b^3 marl interlayer occurring as a soft rock sandwich, interlaid with hard rock. This process also appears in the T_2b^2 marl interlayer distribution (Fig. 1.16).

6. *Soft rock kink-like shear rupture model*: Mainly appears in the T_2b^3 marl with thin-bed distribution. The interlayer slip cuts off the dense tension joint and appears as a kink effect (Fig. 1.17).

Badong Complex Slope System and Its Failure Initiation

Badong Complex Slope System

Based on the monoclinal mountain at the south wing of the Guandukou syncline, and given the strongly cutting erosion of the great geological incident of the Yangtze River run-through as the dynamic force, the complex slope system of Badong was

gradually formed by the process of local folding, layering slip, breaks with layers, many gullies with the same source, and a collapse-landslide formation, formed in stages and zones. Geological structure, initiation type, and space distribution in the Badong slope system can be divided into three layers, namely the deposit layer of surface layer collapse landslide, the middle bedrock layer with gullies and superficial geological vestige development, and a deep partial bedrock layer of a continuous and straightforward incline.

The surface layer is made up of the deposits of the landslide that happened in different areas and time, or human activity. Its Quaternary period deposits are relatively isolated and are easily subject to geological hazards. The middle bedrocks are made up of the T_2b^2, T_2b^3, and T_2b^4 bedrock mass that was cut by the Yangtze River and gullies, the layers are relatively integrated, but show a discontinuous characteristic due to the cutting by gullies. The layers generally are straightforward in inclination, and the geological vestige of local fold, layering slip, and fractures within layers are developed; it is the key layer for maintaining the superficial geological vestige. The deep part bedrocks under the middle bedrocks and above the T_1j^3 generally are a straightforward incline, and they mainly consist of T_2b^1, T_2b^2, and T_2b^3 that are not cut by gullies – the whole structures are continuous and integrated, and do not have the failure condition.

Taking the Tianxiangling–Zhaoshuling slope unit as an example, the western part of this slope unit is Huangjiawuchang, the landform where the elevation is between 200 and 275 m and is integrated and gentle, the slope angle is 5°–15°, and above 275 m, the slope angle is 15°–25°. The eastern part of the slope system is the famous Zhaoshuling ancient landslide. The landslide surface has three platforms, and their elevations are 150–200 m, 350–425 m, and 450–525 m. The top of the slope is Tianxiangling, and the elevation is 700–800 m, and the visible strata are T_2b^3 and T_2b^2 of the Badong group. The trailing edge of the slope passes through the Badong arc gully of which the lithology is T_2b^1 of the first section of Badong group. It is the highest mountain in the area with an elevation exceeding 800 m, and the lithology is T_1j^3 of the Jialingjiang group.

The material of the Zhaoshuling landslide mainly comes from T_2b^3, and some come from T_2b^2. There are mainly three kinds of landslide materials, namely, sliding rock mass, stone fragments with soil, and soil aggregate. The sliding rock mass mainly distributes at the elevation of 100–400 m. The rock mass shows bedded structure and keeps to a certain sequence. The thickness of the sliding mass is 34.6 m (Yun-13 hole) – 99.09 m (Yun-11 hole); the anterior part of the sliding mass overlaps the normal bedrock and appears at the boundary of T_2b^{3-1} and T_2b^2 repeatedly, in the vertical direction. Between the Yun-5 hole and Yun-21 hole, the sliding rock mass shows an anticlinal shape, and the geological characteristics around the edge of the sliding mass indicates that this original anticline is part of a large, dissolved cavern anticline, and the mass then slid to its current location. It can be inferred that the horizontal sliding distance is about 500 m. The sliding masses at the south of Yun-14 hole are mostly fragmented stone with soil (Fig. 1.18).
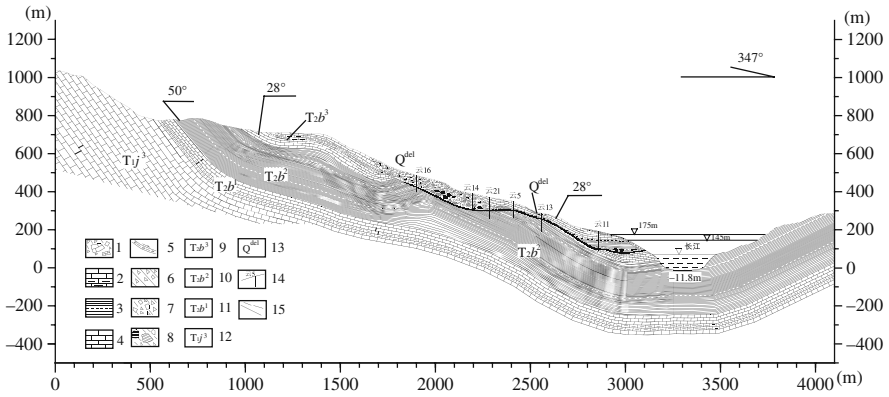
Fig. 1.18 Geological profile of Tianxiangling–Zhaoshuling. 1 – Gray limestone, fragmented stone with soil; 2 – limestone, marl; 3 – mudstone, siltstone, mud–siltstone; 4 – limestone; 5 – slip band; 6 – fragmeted stone; 7 – fragmented stone with soil; 8 – red mudstone, fragmentedstone with soil; 9 – the third section of Badong group; 10 – the second section of Badong group; 11 – the first section of Badong group; 12 – the third section of Jialingjiang group; 13 – landslide deposit; 14 – borehole; 15 – the boundary of strata and lithology

The strong corrosion and cutting actions resulted in the bed elevation of the trailing edge of the Zhaoshuling landslide to be –11.8 m, but the elevations of the shearing outlet of the landslide leading edge are all above 65 m. The elevation of the landslide trailing edge is below 600 m, and these correspond with the elevations of the leading edge and the trailing edge of the whole Three Gorges. The profile structures reflect that the main shear strata of the landslide are layered slip, and that the tangent sheaf is minor.

Initiation Theory of Gravity

(1) Basic condition

  a. A wing of the Guandukou syncline formed the monocline mountain, and it has the structure of an inclining slide.
  b. The engineering petro-fabric which makes up the monocline mountain is clastic rock of continental deposit alternating as soft and hard, having the biological clastic rock of shallow marine facies. They easily facilitate bedding slip and even a bend failure at the terrain condition with free space. Not sure what "free space" means.

(2) The geological structure of the slope

  a. The arc boundary of the Badong slope trailing edge shows differential weathering, or a valley (deep gulley) formed by wash, cementation of

   corrosion-collapse breccia, deposits of loosening collapse landslide, and
   pressure-twisting slip of interlayered gravity relief.

   b. There are small-scale folds, ruptures, and joints inside the Badong slope, and
      their extensive development caused the geo-mechanics failure phenomenon
      of superficial gravity relief, such as mountain loosening deformation.

   c. Collapse-landslide incidence of different periods is generally developed
      at the elevation between 65 and 600 m, and they correspond with bank
      slope landside distribution of the Three Gorges mainstream of the Yangtze
      River.

(3) Regional outside dynamic force

   The ancient Chuanjiang River and ancient Xiajiang River linking up into Yangtze
River caused the water to flow to the east. The flow increased severely and resulted
in a special period of supernormal wash, erosion, and cutting. This outside dynamic
force shaped the bank slope quickly, a steep free space formed and collapsed,
landslide or underground water collapse happened severely, and it resulted in a
local, unusual geological incident against the background of regional intermittent
ascension.
   The basic condition, inherent reason, and outside unusual dynamic force action
described above form the collection of evidence for the gravity failure initiation
theory of the Badong complex slope.
   The three levels of division actually provide a regulation of the slope develop-
ment in sequence with the Yangtze River's deep cutting and river valley widening.
The deep level can be developed into the middle level, and the middle level can
be developed into the superficial level. This is a geological course mainly based
on gravitational action that happened with many instances of loosening, relief, and
movement initiated with each other, due to the wash action by supernormal hydro-
dynamic forces and the formation of a steep, free-space slope.
   The Badong complex slope system is made up of three levels comprising the
geological body. Each slope unit and even each landslide area can be divided into
lower sliding sequences. The Zhaoshuling landslide and the Huangtupo landslide
can be divided into sliding blocks and slides of different scales and different period
(Shen 1965).

Numerical Simulation Analysis with FLAC^{3D}

According to the numerical simulation analysis with FLAC^{3D}, we found the follow-
ing results (Liu et al. 2007).

(1) With the special stratum lithology and geo-structure of Badong slope, gravity
     action could make the slope slide along the interface between T_2b^1 and T_1j^3
     (Fig. 1.19).
(2) There was no mechanical condition in the trailing edge of the Badong slope, so
     it could creep minimally and no deep sliding of the whole occurred.
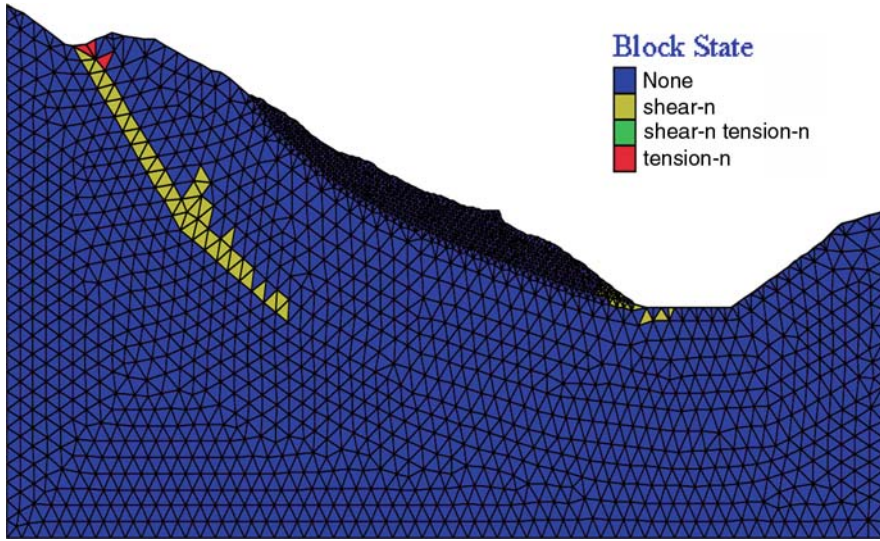
Fig. 1.19 Plastic zone distribution of the slope trailing edge

Regional Geo-environment Quality Assessment of the Badong Slope

Basic Idea

According to the application of geo-environmental sustainably and achievement of geo-hazard risk management, we should not limit our ideas to stability studies but should also research geo-environmental assessments to meet the requirements for an engineering construction program scale (1:10,000–1:50,000). To provide direction for carrying out the different types of regional geo-environmental assessment and to answer geological safety problems at the macrocosm scale, we gave the basic frame of regional geo-environmental assessment (Liu et al. 2006b).

Regional geo-environmental quality assessment, which is the acceptable degree of geo-environment in relation to people's activities, is the mutual goal. It is the primary objective of geo-environment for engineering.

Regional geo-environmental function division, which needs regional socioe-conomic development status and trend, is a functional division for the base components of geo-environmental quality assessments. With it, relevant engineering function division ideas and implementation can be obtained, for example, such activities as town building, basic infrastructure building and maintenance, rural community preservation, traffic control, and agricultural concerns such as woods, fruit trees, and vegetables. Regional geo-environmental capacity evaluation, which is based on relevant engineering types, scale, construction process, and operating characteristic, integrates the relationship between geo-environmental

and engineering construction. In different function zones, engineering construction capacity can be evaluated and its engineering bearing ability can be brought out.

Geo-hazard prevention risk management studies can evaluate geo-hazard risk probability and acceptability in the different function zones. Then, suggestions for alleviating geo-hazards can be formed. The theory base of risk management study is that geo-hazards such as landslide, debris flow, etc. behave as uncertainties but its uncertainty can be measured.

In practice, according to special engineering types in geo-environment function zone, engineering capacity evaluation and geo-hazard risk division should be carried out. Then, geo-hazard risk management suggestions can be given, which will be helpful to engineering safety.

Geo-environment Evaluation of Badong Slope

Twelve factors, such as altitude, gradient, gully density, slope type, engineering geological stratum sets, bedrock depth, etc., and their weight were used to evaluate the geo-environmental quality index of Badong slope. The method is an aggregate index model, shown in Table 1.9.

To find the threshold value of the geo-environmental quality index for its grades, typical zones were selected to check, and the following results were obtained: there were more landslides in two units, which had quality indexes that ranged from 2.4 to 3.0 and greater than 3.0. So, using this quality index, geo-environmental quality evaluation and division could be achieved (Liu et al. 2006).

The whole Badong slope area is 17.8832 km^2. In view of research and application, the Badong slope was divided into five grade quality zones. According to quality index distribution, quality index units could be merged and smoothed with MapGIS, then Badong slope quality evaluations were calculated (Table 1.10).

Geo-environmental function division, which was a new project, is the primary method advanced in the chapter. According to the geo-environmental quality division, the Badong slope was divided into, primarily, three grades of geo-environment function zones (Fig. 1.20).

Zone A, about 6.3728 km^2, 35.64% of the whole zone, includes grade-1 and grade-2 quality zones. Its geo-environmental capacity was the largest. The rock mass in zone A was stable, with bedrock exposed or buried in a shallow manner. Zone A could be extrapolated to include the town, where higher or multistory buildings could be constructed.

Zone B, about 6.0560 km^2, 33.86% of the whole zone, was a grade-3 quality zone. Its geo-environment capacity was in the middle, or medium. The rock mass in zone B was relatively stable, distributed in the slope's trailing edge, inconvenient for traffic but in a better natural condition, where forests or rural communities could be constructed. This zone could also be used for a wharf or port on the river bank.

Zone C, about 5.4544 km^2, 30.50% of the whole zone, included grade-4 and grade-5 quality zones. Zone C incorporated the main distribution of landslides,

Table 1.9 Value and weight of engineering geo-environmental quality evaluation factors

No.	Factor	Unit	Class and value					Weight
1	Altitude	m	<200	200–350	350–500	500–700	>700	0.06
		Value	5	1	2	3	4	
2	Gradient	°	<10	10–15	15–25	25–35	>35	0.14
		Value	1	2	3	4	5	
3	Gully density	mm/cm^2	<1.6	1.6–3.2	3.2–4.8	4.8–6.4	>6.4	0.06
		Value	1	2	3	4	5	
4	Slope type	Type	Reverse	Toeing	Exceed incline	Shorter incline	Equal incline	0.12
		Value	3	1	5	2	4	
5	Engineering stratum sets	Class	T_2b^3	T_2b^2	T_2b^4	T_2b^1	Q	0.16
		Value	1	2	3	4	5	
6	Bedrock depth	m	0–3	3–5	5–15	15–30	>30	0.10
		Value	1	2	3	4	5	
7	Immersed depth in 175 m water level	m	0–10	10–30	30–50	50–80	>80	0.05
		Value	5	4	3	2	1	
8	Rockmass property of 175 m–145 m water level zone	Class	Higher	High	Middle	Low	Lower	0.06
		Value	5	4	3	2	1	
9	Runoff and flood zone	Class	Higher	High	Middle	Low		0.08
		Value	4	3	2	1		
10	Deformation/stress concentration depth	m	0–10	10–30	30–50	50–80	>80	0.05
		Value	5	4	3	2	1	
11	People activity	Class	Forest	Brush/grass	Cultivated land	Building/road		0.08
		Value	1	2	3	4		
12	Seismic dynamic parameter	cm/s^2	90–95	95–100	100–110	110–120	>120	0.04
		Value	1	2	3	4	5	

Value 1 is the best quality, and 5 indicates the least quality.

Table 1.10 Index grades of the engineering geo-environment of Badong slope

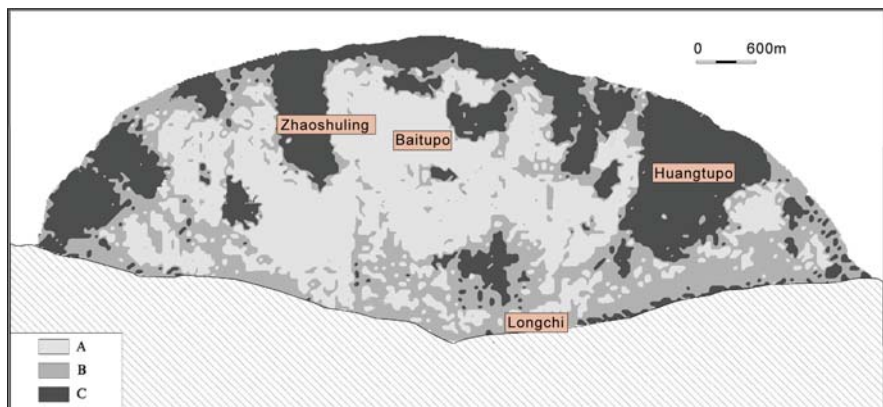| Quality grade	Index value (Q)	Unit number	Area (km^2)	Percent (%)
Grade-1	0.0–1.5	1204	1.9264	10.77
Grade-2	1.5–1.8	2779	4.4464	24.86
Grade-3	1.8–2.4	3785	6.0560	33.86
Grade-4	2.4–3.0	2298	3.6768	20.56
Grade-5	>3.0	1111	1.7776	9.94

Fig. 1.20 Geological environmental function division. A – large or larger capacity; B – middle capacity; C – low or lower capacity

where the geo-environmental capacity was lower. Rock mass in zone C was unstable; there is relaxed rock mass but good quality soil, in which gardens or vegetable planting could be laid out.

Conclusions

(1) It was feasible to advance and use the "Four degrees analysis" method for geo-hazard assessment by "distribution degree," "potentiality degree," "dangerous degree," and "harmful degree" in the Three Gorges.

(2) The ancient Chuanjiang River and the Xiajiang River linking up into Yangtze River was a great natural event, which was the principle factor forming the complex slopes. With the linking, complex bank slopes in the Three Gorges became "compound accumulation bodies," which resulted from three strong geological actions, i.e., undercutting of headwaters erosion, "water saw" undercutting, and underwater river collapses.

(3) The fan-shaped slope for Badong new town is a complex system. Badong complex slope system experienced sustaining gravity action, the so-called review

of gravity initiation. The action resulted from the River bank slope break-down which produced unloading and sliding with erosion, such as sustainable hypabyssal and hypergene rebuilding, in which occurred gradual undercutting by the Yangtze River, which formed into a monoclinal slope in the southern limb of the Guandukou–Dongrangkou syncline.

(4) Geo-environmental quality evaluation and function division, at the middle or larger scale of 1:10,000–1:50,000, were helpful for town planning. The research on the Badong complex slope gave typical examples.

References

Aleotti P, Baldelli P, Polloni G (2000) Hydrogeological risk assessment of the Po river basin (Italy). Landslides in Research, Theory and Practice, Thomas Telford, London, pp. 13–18

Aleotti P, Chowdhury R (1999) Landslide hazard assessment: summary review and new perspectives, Bulletin of Engineering Geology and the Environment, 58(1): 21–44

Baeza C, Corominas J (1996) Assessment of shallow landslide susceptibility by means of statistical techniques. In: Proceedings of 7th International Symposium Landslides, Trondheim, Vol. 1, pp. 147–152

Carrara A (1983) Multivariate models for landslide hazard evaluation. Mathematical Geology, 15(3): 403–426

Carrara A, Cardinali M, Guzzetti F (1992) Uncertainty in assessing landslide hazard and risk. ITC Journal, 2: 172–183

Chen XC (1993) Slope type and stability in the Three Gorges Reservoir. Sichuan Science and Technology Press (in Chinese)

Cui ZQ (1998) Main problems of environmental engineering geology in the Three Gorge hydraulic project the Yangtze River. Study to Natural Hazards Mitigation in China, Science and Technology Press (in Chinese)

Deng Qinglu (2000) Slope deformational structure: Badong County slope analysis. China University of Geosciences Press, Wuhan (in Chinese)

Elliott C, Gori P (2000) National landslide hazards mitigation strategy—A framework for loss reduction. Open-file report 00-450, U.S. Geological Survey

Geological Bureau of Hubei Province (1997) Regional hydro-geological investigation report, China (Badong Section) (in Chinese)

Haruyama M, Kitamura R (1984) An evaluation method by the quantification theory for the risk degree of landslides caused by rainfall. In: Proceedings of 4th International Landslides, Toronto, Vol. 2, pp. 435–440

He LH, Zhao H (1996) The fractal dimension of river networks and its interpretation. Scientia Geographica Sinica, 16(2): 124–128 (in Chinese)

Hubei Hydrogeology and Engineering Geology Team (2001) Engineering Geologic Investigation Report of Badong Huangtupo Landslide in Three Gorges Reservoir (in Chinese)

Koleback F, Scheidegger AE (1977) On the theory of evaluation of joint orientation measurement. Rock Mechanics, 9(4): 781–795

Lee JS (1924) Geology of the gorge district of the Yangtze River (from Yichang to Tzekuei) with special reference to the development of the gorges. Bulletin of the Geological Society of China, 3(3–4): 351–391

Lian JF, Liu CZ, Gao SR (2006) Research of fractal geometry characteristic on water system in gullies and valleys of Badong slope area in Three Gorges Reservoir Area. Site Investigation Science and Technology, 24(1): 25–28 (in Chinese)

Liu CZ (1993a) A discussion on the engineering geology environment evolution of surface crust of the Three Gorges Project area of Yangtze River. Journal of Hebei College of Geology, 16(1): 56–69 (in Chinese)

Liu CZ (1993b) The segregative characteristics of active fault system and its fractal geometry. Hydrogeology and Engineering Geology, 20(6): 16–19 (in Chinese)

Liu CZ (2000) The study on development process of slope in the connected part between Chuan and Xiajiang rivers in Yangtze River. The Chinese Journal of Geological Hazard and Control, 11(1): 50–54 (in Chinese)

Liu CZ, Yang B (2001) A new thought of surveying, evaluating, monitoring and forecasting for the geologic hazards in the Three Gorges on Yangtze River. Journal of Engineering Geology, 9(2): 121–126 (in Chinese)

Liu CZ, Li TF, Zou ZS (2003) Geological study on the Baiyi'an landslides in the three-gorges reservoir area. Journal of Engineering Geology, 11(1): 3–9 (in Chinese)

Liu CZ, Li TF, Cheng LP (2004a) A method to analyze four parameters (degree) for assessment and early warning on the regional geo-hazards. Hydrogeology and Engineering Geology, 31(4): 1–9 (in Chinese)

Liu CZ, Li TF, Wen MS (2004b) Assessment and early warning for geo-hazards in the three gorges reservoir region of Yangtze River. Hydrogeology and Engineering Geology, 31(4): 9–20 (in Chinese)

Liu CZ (2005) On the evolution of complex slopes in the Three Gorges of Yangtze River. Hydrogeology and Engineering Geology, 32(1): 1–6 (in Chinese)

Liu CZ, Liu YH, Lian JF (2006) Initiation mechanism study on Badong slope system in the Three Gorges of the Yangtze River. Geological Review, 52(4): 510–521 (in Chinese)

Liu CZ, Zhang MX, Liu YH (2006a) A System of geo-environment evaluation based on the sustainable land-use. Geosciences Frontier, 13(1): 242–245 (in Chinese)

Liu CZ, Liu YH, Lian JF (2006b) Evaluation of engineering geo-environment quality of Badong large slope area in Three Gorges Reservoir region of Yangtze River. Hydrogeology and Engineering Geology, 33(5): 1–8 (in Chinese)

Liu YH, Liu CZ, Li TF (2007) Numerical simulation for deformation mechanism and stability study of Badong large slope system in the Three Gorges Reservoir. Hydrogeology and Engineering Geology, 34(1): 47–52 (in Chinese)

Mandelbrot BB (1982) The Fractal Geometry of Nature. Freeman, San Francisco

Michael-Leiba M (2000) Quantitative landslides risk assessment of Cairns, Australia. Landslides in Research, Theory and Practice, Thomas Telford, London, pp. 1059–1064

Qin Shengwu, Liu CZ, Li GJ (2006) Neotectonic stress field in Three Gorges region inversed against river system by utilizing the improved GIS method. Global Geology, 25(2): 160–163 (in Chinese)

Ragozin AL (2000) Landslide hazard, vulnerability and risk assessment. Landslides in Research, Theory and Practice, Thomas Telford, London, pp. 1257–1262

Shen YC (1965) Valley Landform in the Upstream of Yangtze River. Science Press, Beijing (in Chinese)

Tian LJ (1996) Development history of valley in the Three Gorges. Southwest Jiaotong University Press (in Chinese)

Yang DY (1988) The origin and evolution of the three gorges of the Yangtze River. Journal of Nanjing University, 24(3): 466–474 (in Chinese)

Yang DY (2006) Landform process in Yangtze River. Geological Press, Beijing (in Chinese).

Yangtze River Conservancy of Water Resources Committee (1997) Badong new county address in Three Gorges Reservoir geological verification report (Detailed investigation stage) (in Chinese)

Yin KL, Yan TZ (1987) Regional landslides distribution and slope instability prediction. Earth Science: Journal of Wuhan University of Geosciences, 12(6): 631–638 (in Chinese)

Zhang NX (1993) Consequent rock slope analysis in the Three Gorges Reservoir. Earthquake Press, Beijing (in Chinese)

Chapter 2
Bank Slope Stability Evaluation for the Purpose of Three Gorges Reservoir Dam Construction*

Guofu Xue, Fuxing Xu, Yuhua Wu, and Yongzhi Yu

Abstract Through working on the classification of the reservoir bank slopes and their deformation mechanism, failure conditions, countermeasure on various types of slope failures, stability analysis and assessment of the bank slopes and large landslides, and monitoring and forecasting, this chapter summarizes the bank slope stability evaluation for the purpose of Three Gorges reservoir dam construction. The exploration and research methods for the evaluation of bank slope stability before the dam construction can be found in this chapter.

Along the two sides of the Three Gorges reservoir on the Yangtze River, there are more than 150 counties and towns. The reservoir is part of the Golden Waterway for outgoing transport from the southwest region of China. Bank slope stability of the reservoir is one of the major geological engineering and environmental geological problems which directly affect the dam construction, the navigation, and the safety of peoples' life and property in the area. The research on bank slope stability in this area has been conducted for more than 30 years since the 1960s. After collaborative research by many departments, many disciplines, with the application of multiple skills, and multiple orders, the problems of the bank slope stability under natural conditions and water storage conditions have been basically clarified and a set of theories and methods for investigation, research, analysis and assessment, monitoring and forecasting have been established.

The research on the bank slope stability of the Three Gorges reservoir includes classification of the reservoir bank slopes and their deformation mechanism, failure conditions, control factors of various types of bank slopes, stability analysis and assessment of the bank slopes and large landslides, risk assessment of the bank slope

G. Xue (✉)
Three Gorges Exploration and Research Institute, Yangtze River Hydraulic Management Committee, China

Investigation and research on stability of reservoir bank slopes	Study on geographical and geological environment of the reservoir bank slopes	Regional geologic features	Geomorphologic type unit
			Strata and distribution
			Geological structure
			Seismic activity
			Climate
			Hydrology
		Geological environment characteristics of the reservoir bank slopes	Basic characteristics of the rock and soil
			Characteristics of geological structure
			Geomorphologic features of river valley
			Characteristics of groundwater
			Dynamic environmental features
	Investigation and research on stability of the reservoir bank slopes	Type of the reservoir bank slopes	Level 1 division–Based on lithology in the reservoir bank slopes
			Level 2 division–Based on the relationship between river valley direction and attitude of strata.
		Research on evolution mechanism of the reservoir bank slopes	The main types and evolution mechanism of the reservoir bank slopes
			Analysis on evolution mechanical process of the reservoir bank slopes
			Present stability of the reservoir bank slopes
		Assessment of stability of the reservoir bank slopes	Stability determination of the different type of reservoir bank slopes
			Probability statistic (quantitative)analysis of the reservoir bank slopes
			Stability quantitative prediction and assessment of stability of the reservoir bank slopes
	Investigation and research on stability of the rock falls, landslides on the reservoir bank slopes	Type and distribution of the bank slope deformation	Landslide features
			Characteristics of rock falls and dangerous rocks
			Size of rock fall and landslide
			Characteristics of geography
			Relations with lithology
			Relationship with geological structure
		Structural Characteristics of rock fall and landslide	Type of rock mass
			Structural characteristics of rock mass
			Hydrogeological characteristics
			Physical and mechanical characteristics of the soil in sliding zone
		Analysis on evolution process of rock fall, landslide	Analysis on forming mechanism
			Special research on typical landslide
			Analysis on active age of landslide
		Analysis on reactivation mechanism of rock fall and landslide	Heavy storm-induced agencies
			River erosion
			Water level fluctuation
			Loading on the back top
			Human engineering activities
		Deformation monitoring of rock fall and landslide	Ground monitoring
			Underground monitoring
		Analysis on stability of rock fall and landslide	General geological analysis
			Stability Calculation and numerical analysis
		Prediction analysis on the risk by the reservoir bank slope failure	Impact on the reservoir storage capacity and lifetime
			Impact on construction and running of the hub buildings
			Impact on navigation
			Impact on resettlement of the towns and immigrants in the reservoir area

Fig. 2.1 Investigation and research approaches for the Three Gorges reservoir bank slope stability analysis

failure, and monitoring technique and forecasting models of bank slope deformation as shown in Fig. 2.1.

Types of Reservoir Bank Slopes and Assessment of the Stability Conditions

Types and Characteristics of the Reservoir Bank Slopes

Up to 5,000 km of bank slope length, including mainstream and tributaries of the Three Gorges reservoir, crossed different geomorphologies and tectonic units. The crystalline rocks, carbonate rocks, scattered rocks, and loose deposits compose the various geological types of the reservoir bank slopes. Deformation and damage to the bank slope are mainly controlled by the rock and soil types and their complexities, the slope form, structural planes and their relationship to the slope surface.

The Three Gorges reservoir bank slopes can be classified into four major types: soil slope, clastic rock slope, carbonate slope, and crystalline rock slope.

Based on the structure of rock and soil and the attitude of the rock and soil beds on the slopes, slopes can be further subdivided into sub-types:

I. Soil slope
    I_1 Alluvial and pluvial sand and gravel bank slope
    I_2 Slide and fall accumulations or breccias and fragments bank slope
    I_3 Thick residual and talus breccia and fragment bank slopes
II. Detritus rock slope and III carbonate slope
    II_1, III_1 Gentle bed slope (dip angle less than 10°)
    II_2, III_2 Transverse slope (the angle between rock dip and slope dip greater or equal to 60°)
    II_3, III_3 Consequent slope (the angle between rock dip and slope dip less or equal to 30°)
    II_4, III_4 Reverse slope (the angle between rock dip and slope dip greater or equal to 150°)
    II_5, III_5 Diagonal slope (the angle between rock dip and slope dip between 30° and 60° or between 120° and 150°)
    II_6, III_6 The rock slope of special structure (referring to the slope with broken rock or the slope with soft base)
IV. Crystalline rock slope
    IV_1 Magmatic rock slope with massive structure
    IV_2 Metamorphic rock slope with massive structure.

Among the reservoir bank slopes of the mainstream and major tributaries, the soil slope is 140.5 km long, accounting for 4.69% of the total length; bedded rock slope is 2,368.6 km long, which is 79.06% of the total length; layered carbonate slope is 454.5 km long, which is 15.18% of the total length; crystalline rock slope is 32 km

long, which is 1.07% of the total length. It should be noted that the width and the thickness of loose deposits of the soil slope composition are limited; the lower and the upper on the soil slope are still bedrock.

Assessment on Stable Conditions of the Reservoir Bank Slopes

The main types of deformation and damage along the reservoir bank slopes are bank slope rock falls and landslides. Bank slope rock falls mainly occur in the zone of river alluvial deposits, which distributes in small areas of small thicknesses and as long and narrow strips along the Yangtze River. After the reservoir storage, and exposure to long periods of saturation in water and effects of the fluctuation of the water level, the bank slope would experience small-size rock falls. In the trunk stream of the reservoir, there are only 13 sections of possible collapsed bank slopes for the total 12 km long area. The width of the predicted collapse zone is 20–86 m and the total volume of collapse is about 6 million m^3. The erosion of the bank slope surface is manifested as slow and long-term evolutionary processes. The most intuitive signs of the bank slope stable conditions (good or bad) are the developmental characteristics of landslides. When zoning by bank slope stable conditions, some of the main consideration factors are lithology and complex geological structure, types of rock structure, relation between attitude of rock bed and valley direction, deformation and damage degree, number and stability of the existing landslides, and possible changes under the effect of water level fluctuation. Based mainly on geological recognition combined with numerical analysis (mainly for stability of landslides), the stable conditions of the reservoir bank slopes can be divided into four types: good (A), general (B), poor (C), and bad (D) (Table 2.1).

Bank slope in a condition of good stability (A): Lithology and complex slope structure and slope shape are all of benefit to slope stability. Minor in deformation and damage degree, rare in the landslides with a size of more than 1 million m^3; good in the overall stability of existing landslides as well as few in number and small in size of possible newly created landslides during construction and operation of the reservoir. This type of bank slope is 4,271.4 km long, accounting for 85.8% of the total length.

Bank slope in general condition of stability (B): Lithology and complex slope structure and slope shape are all of benefit to slope stability. Medium in deformation and damage degree, rare in the landslides with size of more than 1 million m^3, these mostly belong to stable or generally stable ones. This type of reservoir bank slope is stable, on the whole. During the construction and operation of the reservoir, only a small number of medium- to small-sized landslides would be of poor stability and may fail. There are 76 sections of this type of reservoir bank slopes with the length of 354.5 km, accounting for 7.0% of the total length. These are 89 km long on the mainstream and 265.5 km on the tributaries.

Bank slope of poor stability (C): With soft rock or complex hard and soft rock, slope structure and slope shape have a greater effect on slope stability. This is mostly the case in the number of old landslides, but most of them are no longer active. Poor

Table 2.1 Types of slope stability conditions of the Three Gorges reservoir

Item	Stable condition of the bank slope		Number of sections	Total length	Percentage in the mainstream or the total tributaries in length	Development degree of landslides with a size of more than 1 billion m³			
	Code	Type				Count	Size	Average line density	Average line Module
Mainstream	D	Bad	6	16.1	1.2	16	24,934.0	0.99	1,548.7
	C	Poor	9	116.0	8.9	52	110,478.9	0.45	952.4
	B	General	5	89.0	6.9	22	131,56.5	0.25	147.8
	A	Good		1,078.9	83.0	46	21,659.6	0.04	20.1
Tributary	D	Bad	31	56.3	1.5	31	34,738.7	0.55	617.0
	C	Poor	93	165.2	4.5	95	57,519.4	0.58	348.2
	B	General	71	265.5	7.2	34	17,044.8	0.13	64.2
	A	Good		3,192.5	86.8	24	11,745.0	0.008	3.7

stability is in a small number of the landslides among the ones with volume of more than 1 million m³, they may be partially damaged during construction and operation of the reservoir. The bedrock bank slopes may partially collapse. There are 102 sections of this type of reservoir bank slopes with the length of 281.2 km, accounting for 5.6% of the total length. They are 116 km in length on the mainstream and 165.2 km long on the tributaries.

Bank slope in bad condition of stability (D): With soft rock or complex hard above and soft below rocks developing cracks. Slope structure and slope shape are primary conditions for deformation and damage. There is presently a higher degree of deformation and damage or large-size landslides that have reactivated recently (such as Jipazi landslide, Xintan landslide) or deformation is developing (such as Huanglashi landslide, Lanziya dangerous rock mass). In natural circumstances or construction and operation of the reservoir, serious falls and slides or local rock falls and slides may occur. There are 37 sections of this type of reservoir bank slopes with the length of 72.4 km, only accounting for 1.5% of the total length. These are 16.1 km long on the mainstream, accounting for 1.2% of the total mainstream bank slope length.

In addition, during the scientific and technological research on "the 5th Five-Year Plan," the "information quantities method," "logic information method," "fuzzy math method," "risk probability analysis," "numerical analysis," "multi-factor comprehensive evaluation," and other methods are applied for assessment and analysis of stability of partial reservoir bank slopes; the results are generally closed to the geological macro-reorganization, as shown in Table 2.2.

Table 2.2 Evaluation results of the bank slope stability on the Three Gorges reservoir

		Evaluation result	
No.	Evaluation method	Percentage of the bank slope of poor or bad stability	Percentage of the bank slope of general or good stability
1	The "information quantities method"	7.43	92.57
2	Logic information method	8.69	91.31
3	Fuzzy math method (Zhongxian to Jiangjin tributary)	0	100
4	Multi-factor comprehensive evaluation (reservoir until Fengjie)	12.7	87.3
5	Quantitative assessment for the important sections — Comprehensive assessment System Predicted diagnostic system	Mostly belong to stable type or generally stable type	

Rock Falls, Landslides, and Dangerous Rocks

The bank slope is composed of Quaternary loose accumulation and structural broken rocks and is a minor presence in the Three Gorges reservoir. The flow-related

damages such as mud–rock flow and debris flow are not widespread, and it may be of small size or sporadic occurrences. Therefore, the main deformation and damage to the Three Gorges reservoir bank slopes are rock falls, landslides, and a few of dangerous rocks in deformation condition, which are the main subjects that have been researched for stability.

Rock falls can be divided into two forms, rock falls and falls, based on their initiation. Landslides can be divided into two forms, rock landslides and loose deposit landslides, based on their lithology, of which the rock landslides can be further divided into two forms, those of bedding landslide and bed-cutting landslides, based on the relation between sliding surface and bedrock attitudes.

In total, there are 684 rock falls, landslides, and dangerous rocks with a size larger than 100,000 m^3 that are distributed on the 1,300 km long mainstream and the 3,679.5 km long tributary bank slopes of the Three Gorges reservoir. The total volume is 3.04 billion m^3, the average line density 0.14 km^{-1}, and the line module 61×10^7 m^3 km^{-1}. There are 215 landslides with the total size of 1.73 billion m^3, the average line density of 0.17 km^{-1}, and the line module of 133×10^7 m^3 km^{-1} on the mainstream, while there are 469 landslides with the total size of 1.31 billion m^3, the average line density of 0.13 km^{-1}, and the line module of 35.5×10^7 m^3 km^{-1} on the tributaries (Table 2.3).

Individual size of the landslides can be divided into four degrees according to the practices in the Three Gorges reservoir: huge size – size larger than 0.1 billion m^3, large size – size between 10 and 100 million m^3, medium size – size between 1 and 10 million m^3, and small size – size between 0.1 and 1 million m^3.

There are 4 huge landslides with a total size of 0.63 billion m^3 on the mainstream and tributary bank slopes, 53 large ones with a total size of 1.4 billion m^3, 263 medium ones with a total size of 0.88 billion m^3, and 364 small ones with a total size of 0.12 billion m^3. The small landslides take up 54% of the total in number, but only 4% for volume, which indicates that those sizes of more than 1 billion m^3 play a key role in the reservoir bank slope stability.

Counting by types, there are 552 landslides with a total size of 2.78 billion m^3, 126 rock falls with a total size of 0.25 billion m^3, 6 dangerous rocks with a total size of 7.86 million m^3, accounting for 80.7%, 18.4%, 0.9% in total number and 91.6%, 8.2%, 0.2% in total size respectively. Thus, the landslides, mostly bedrock bedding ones, are the main deformation and damage type affecting the reservoir bank slopes which have a total size of 1.89 billion m^3, accounting for 62% of the total size of landslides (Table 2.4).

The distribution of 57 huge and large landslides on the mainstream and tributaries of the Three Gorges reservoir is shown in Fig. 2.2, the size of them in Table 2.5.

Distribution Features of the Landslides

Geographical Distribution

Intensity of the landslides on the reservoir bank slopes is controlled by the conditions of lithology, geological structure stratigraphy, and so on. This is indi-

Table 2.3 Number and size of rock falls, landslides, and dangerous rocks on the bank slope of the Three Gorges reservoir

Ordering in size	Number/size (m^3)				Line density No. km^{-1}	Line module 10^{4}m^{3}km^{-1}
	<100 (small)	100–1,000 (medium)	1,000–10,000 (large)	>10,000 (huge)	Total	
Mainstream	79/2,644.1	105/38,425.9	28/87,449.6	3/44,333.0	215/172,852.6	0.17	133.0
Tributaries	285/9,619.0	158/49,269.7	25/52,758.3	1/19,020	469/13,066.9	0.13	35.5
Total	364/12,263.1	363/87,659.6	53/140,207.9	4/63,353	684/303,519.5	0.14 (average)	61.0 (average)

Table 2.4 Statistic of the rock falls, landslides, and dangerous rocks on the bank slopes of the Three Gorges reservoir

| Type		Landslide			Rock fall	Dangerous rock	Total
		Loose deposit landslide	Bedrock landslide				
			Bedding	Bed-cutting			
Mainstream	No.	22	101	40	48	4	215
	Size	11,488.5	133,563.4	14,224.5	13,029.2	547.0	172852.6
Tributaries	No.	203	92	94	78	2	469
	Size	31,494.6	55,512.0	31,626.5	11,792.5	239.3	130,666.9
The whole total	No.	225	193	134	126	6	684
	%	32.9	28.2	19.6	18.4	0.9	100%
	Size	42,983.1	189,075.3	45,851.0	24,821.6	786.5	303,519.5
	%	14.2	62.3	15.1	8.2	0.2	100%
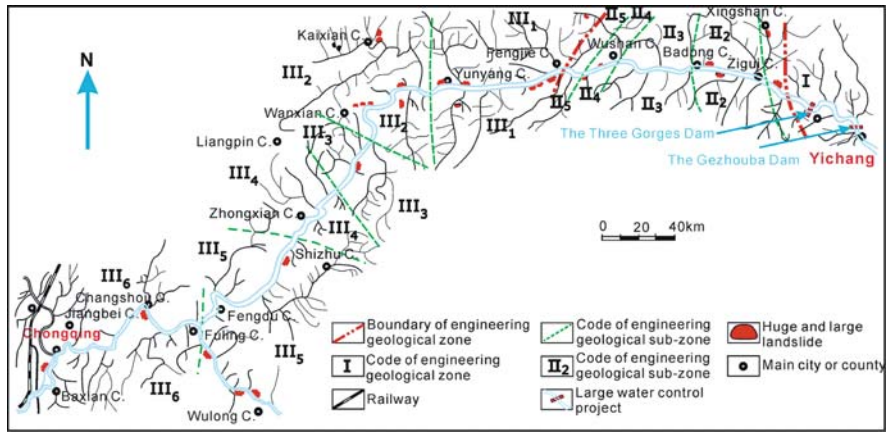
Fig. 2.2 Distribution of huge and large landslides on the Three Gorges reservoir bank slopes

cated by an evident regional deference that the large and medium landslides are concentrated in some areas while rare in other areas. For example, there is only one small rock fall on the approximately 50 km long bank slope from Sandouping to Xintan, a few landslides on the north bank slope from Yaowanxi to Shazhenxi, the Wuxia Gorge and Qutangxia Gorge, the valley from Taoyuan, Fengdu city to Chaotianmen Chongqing city, and no landslides on the 48 km long north bank slope from Sandengzi to Dahegou. The eight portions of the river bank slopes which are Shuping, Zigui county to Huanglashi, Badong county; Laoshucuo to Dawan, Huangguashu to Liujiawuchang, Wushan county; Baiyi'an, Fengjie county to Maohelin, Yunyang county; Baota to Xinlongtan, Yunyang county; Wanxian urban area; Daxikou to Shierchong, Wanxian city; Miaoshang, Zhongxian county to Chengjiadiaoya, Fengdu county, having total length of 151.6 km, make up 11.7%

Table 2.5 Huge and large landslides on the Three Gorges reservoir

| | The reservoir bank slopes on the mainstream | | |
	Landslide No.	Landslide name	Size ($10^4\,m^3$)
The mainstream of Yangtze River	2	Xintan	3,000
	8	Shuping	2,360
	14	Fanjiaping	12,500
	16	Huanglashi	1,800
		Huangtupo	4,080
	22	Zuojituo Rock fall	1,353
	27	Xiangjiawan	2,000
	31	Caojiawan rock fall	2,300
	43	Shuizhuyuan	1,700
	49	Liujiawuchang	1,791
	52	Baiyi'an	4,434
	53	Qiancaotuo	3,360
	57	Baihuanping	12,933
	59	Xinpu	6,000
	60	Outang	2,000
	66	Gulingzhen	18,900
	68	Baota	8,500
	69	Jipazi	1,500
	72	Yunyangxicheng	2,500
	76	Jiuxianping	5,220
	87	Yuhuangguan	4,887
	89	Caojiezi	2,283
	90	Anlesi	6,426
	91	Taibaiya	6,220
	92	Diaoyanping Rock fall	1,747
	99	Houcao	3,516
	119	Maoxuzi	3,368
	122	Longwangmiao	1,173
	126	Chengjia Diaoya	1,231
	135	Caofang	1,000
	139	Zhonggangjiaolu	1,420
Tributaries			
Xiangxi R.	16–32	Shifuosi	1,030
Guizhou R.	19–1	Kaziwan	3,360
	19–3	Wujiadaling	1,432
	19–7	Hujiawuchangwu	4,308
Daning R.	48–6	Zaibaozi	1,015.5
	48–18	Lianyuchi	1,020
Cuokaixia R.	69–3	Dawuchang	1,204
Daxi R.	75–4	Hualianshu	2,604
	75–10	Xiangshuitan	2,394
	75–11	Yinwozi	1,164
	75–14	Shijiawan	1,292
Meixi R.	78–15	Baiwafang	2,880
	78–16	Zhichangwan	1,612
	78–17	Longpo	19,020
Modao R.	105–3	Dashiban	1,075

Table 2.5 (continued)

	The reservoir bank slopes on the mainstream		
	Landslide No.	Landslide name	Size (10^4 m^3)
Xiaojiang R.	120–11	Wangjiayuanzi*	2,036
	120–12	Duoxiaoping	4,944
	120–14	Zhoujiayuanzi*	1,492
	120–15	Panjiayuanzi*	2,730
Xongjiagou R.	124–1	Wutongping	1,869.6
Bayangxi R.	125–2	Oujiaping	1,612.5
Huilongxi R.	132–1	Pijiayuanzihuapo	1,795
Wujiang R.	164–9	Wanbeituo	2,863.2
	164–21	Yangjiaotan	1,006
	164–23	Yangjiaozhen Rock fall	4,071
	164–28	Tukan Rock fall	2,128.2

*The reservoir will not affect.

of the whole mainstream, but the landslides on these bank slopes take up 48% in number and 84.4% in size of those on the whole mainstream.

Landslides on the tributary bank slopes mainly occur in the Xiangxi River, Guizhou River, Qingganhe River, Caotang River, Meixi River, and Wujiang River, which take up 44.3% in number and 63.4% in size, of those on the total number of tributaries.

Elevation of the Landslides Distribution

Most landslides occur close to the base of the Yangtze River. For over 97% medium or larger ones on the mainstream, their toes are near the dry water level of the Yangtze River; meanwhile for the 85% of those on the tributaries, their toes are near the river bed. The sliding surface of the Wanxian landslide group occurring in nearly horizontal rock beds has three elevation levels, 190–200 m, 214–224 m, and 240–250 m, corresponding to II – III terraces (Fig. 2.3).

Relationship with the Lithology and Stratigraphy

Rock masses are the material basis of rock falls and landslide formation. Different rock types differ in the intensity of rock fall and landslides. There are no large landslides in magmatic and metamorphic rock bank slopes. Deformation and damage on carbonate bank slopes are relatively weak, and the main damage form is rock falls. In the over 600 km long carbonate bank slope, the landslides account for only 8.2% in number and 5.6% in size of the total. In the 422 km long bank slopes with soft and hard inter-bedded clastic rocks and part carbonate rock having a weak base, the landslides are relatively extensive; their failure form is mainly large and medium,
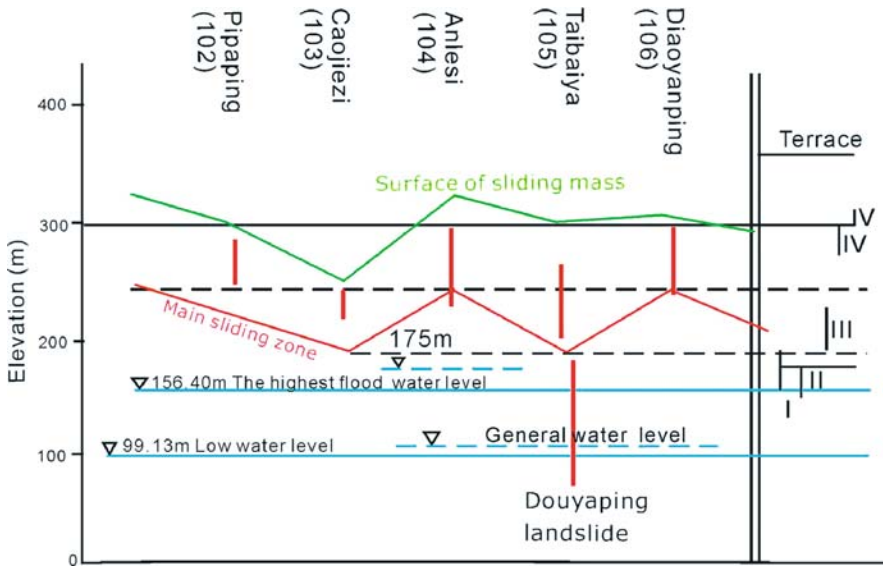
Fig. 2.3 Profile of sliding surface elevation of the old landslides in Wanxian city

which accounts for 87.3% in number and 91.1% in size of those on the total area of the bank slopes. Therefore, as to the distribution area, development extent, and possible damage of the landslides, the bank slopes with bedded clastic rocks rank a main status, and it is the most important area to study for reservoir bank slope stability.

Relationship with Geological Structure

The effect of deformation and damage of the reservoir bank slopes based on geological structure depends mainly on the relative relation between the direction of river flow and the attitude of geological structures. As river flow is consistent with a fold axis, it can form along a strike valley and continue mainly along bedding landslides which concentrate on the bedding dip slope of a syncline wing or a tilted end, such as Fengjie-Guling town and Baota-Xinglongtan bank slopes within the Guling syncline (Fig. 2.4). Meixihe bank slope within the Qumahe syncline and Jinzhuyuan-Tangjiawan within the Fengdu-Zhongxian syncline are all parts of synclines that converge to tilt up toward the east and close increasingly, where they form an "arm-chair" slope structure generally causing large-scale bedding landslides. Daxihe within the Wushan syncline, Taping-Liujiawuchang on the mainstream, Xiangxihe on the margin of the Zigui syncline, Shuping-Fanjiapingduan on the mainstream, and Qingganhe in the Caidianzi syncline are also the regions where landslides are concentrated.

In the river valleys which are cut along the vicinity of an anticline axis, not only landslides and rock falls have developed in the dip sides but a relatively large size
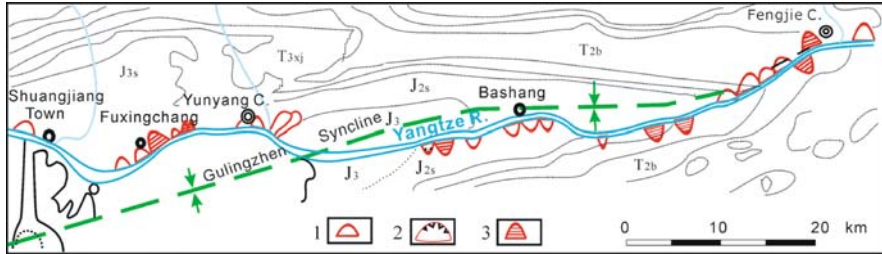
Fig. 2.4 Cases along bedding slope – those landslides developing in the wing or tilted end of syncline. 1 – The landslide with a size of less than 1 million m^3; 2 – the rock fall with a size of less than 10 million m^3; 3 – the landslide with a size of more than 10 million m^3

of landslide could occur in the other reverse dip sides as the cracks paralleling the river bank slope occur and converge with the cracks in other directions as well, based on certain lithologic conditions (e.g., Badong formation). Examples include the Shuping landslide in Zigui county, the Huanglashi landslide in Badong county, etc.

Another important reason for large landslides easily occurring in the core of the anticline in the Three Gorges area is that the anticlines often outcrop with weak shale and coal formation (Silurian, Ma'an Group in Permian) which forms a geological structure of a hard bed lying on a soft base which causes large dangerous rock masses (such as Lianziya dangerous rock mass) and cumulative blocks of rock falls as well as the triggering of large landslides, such as the Xintan landslide and the Xiangjiawan landslide.

In the canyons cutting across anticlines, as the attitude of rock beds drastically changed and small faults densely developed, the area is prone to rock falls and sliding deformation of the rock fall deposits, such as the landslides occurring at Zuojituo, Xiangjiawan, Baiheping, Yaqianwan, which are located in the axis of the Nanmuyuan and the Hengshixi anticlines (Fig. 2.5).

Relationship with the Structure of the River Bank Slope

The structure of the bank slope is a synthetic performance of stratigraphic lithology, geological structure, and valley geomorphology, which directly controls the distribution and development of landslides. The order of the landslide intensity ranging from strong to weak is as follows: dip-slope bedded bank slope, gentle dip and soft base bedded bank slope, reverse slope dip bedded bank slope, and other types. The damage is dominated by landslides that occur on slope dip bedded bank slope and by relative equivalent landslides, for other types of bank slopes. It can be concluded that landslides are evidently defined by the structure of the clastic bank slope, especially the slope dip bedded bank slope is a primary slope type for large landslides; the bank slope containing a soft base in a carbonate area is the zone with densest development of landslides and rock falls.
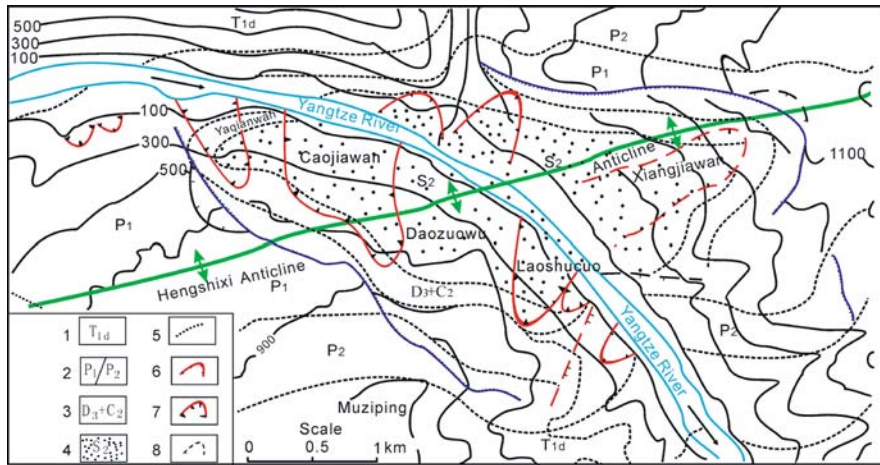
Fig. 2.5 Cases of rock falls concentrated in the anticline cores in the Gorges areas. 1 – Daye limestone in lower Triassic; 2 – limestone in Permian; 3 – sandstone in Devonian and limestone in Carboniferous; 4 – shale in Silurian; 5 – stratigraphic division line; 6 – landslide; 7 – rock fall; 8 – dangerous rock

Structural Characteristics of the Landslides

The greatest number of landslides occurred in loosely structured rock blocks with soil fill. The rock blocks vary in sizes mostly of 0.1–1.0 m in diameter, and larger than 10 m for the large ones. Because of ground water and surface water leaching, the clay content in the lower portion is increasing. As gravity grading and post-filling in the long-term accumulation of the rock falls, the majority may appear faintly discernible beddings.

The soil components of the landslide are controlled by the factors of stratigraphy, lithology, activation times, sliding velocity and run-out distance, variability in material composition, and braking intensity and can generally be divided into six types according to landslide structures (Table 2.6). Broadly speaking, from type 1 to type 5, it generally shows increase in activation times, sliding velocity and run-out distance and decrease in the entirety. For a single case, generally the extent of disintegration in the front and in the surface of the sliding mass is more serious than in the deep position.

Physical and Mechanical Properties of the Sliding Zone

Reactivation of landslides mostly occurs along the original sliding surface (zone), so it is of great significance to research the sliding zone.

Material Composition of the Sliding Zone

**Table 2.6** Structural types and characters of the sliding mass

No.	Structural types	Structural characters	Landslide types	Cases
1.	Massive structure	Sliding mass has a good entity of mainly the rock with massive structure, only the depression zone or the front has the rocks with scattered-broken structure.	Rock has beddings of near horizontal or gentle dip, along with bedding landslide.	Landslide of Jiuxianping and landslide group of Wanxian.
2.	Cataclastic-massive structure	There is 70% of sliding mass composition with massive cracked rock, only local part in the front is cataclastic-scattered structure. Colluvium and deluvium can be seen mainly in the rear.	Rock has beddings dipping to slope, with bedding sliding landslide.	Landslides of Baihuanping, Guling, Outang Houcao, etc.
3.	Scattered-cataclastic-massive structure	Rocks with massive-cracked structure are not up to 40%; scattered structure can be seen mainly on surface, in the front and rear or depression zone, with massive-cracked structure mostly located at the base.	With dip structure landslide and cut bedding rock landslide	Landslides of Fanjiaping, Liujiawuchang, Baota, and Cicaotuo.
4.	Cataclastic-scattered structure	Rocks with cataclastic structure and those with scattered structure contaminate each other, in proportion of 2:3, but scattered rocks are located mainly on the surface and in the front and rear.	Rock landslide or its reactivation part.	Landslides of Liulaiguan, Dawan, Jipazi, Xichen, and Taoyuan.
5.	Scattered with cataclastic structure	Rocks with scattered structure have more than 70% occurrence. Scattered rocks distribute mainly in the base or the rear of the sliding mass.	The old landslide reactivating for times. The sliding mass is composed of colluvium, deluvium, and underlying bedrock together reactivating times.	Landslides of Sandengzi, Huangshi, Daping, Anlesi, and Zhonggang.
6.	Scattered structure	Sliding mass is composed of the rock with scattered structure, basically.	The old landslide reacting for times or the deposits of landslides transformed to slides.	Landslides of Xintan, Liyutuo, Diaoya Ping

Mineral Composition

Mineral composition of sliding zones depends on the mother rocks, whose clay minerals and contents are the same as those in the mother rocks. By polarizing identification and differential thermal analysis, the soil in the sliding zone is mainly composed of clay minerals of an average content of 65% and the average content of detrital minerals is 35%. Clay minerals are mainly illite which occurs in an average of 45%, then crypto crystal clay, an average of 20% (Fig. 2.6). Micro-calcite, kaolinite, montmorillonite, and organic matter occur in small amounts. Detrital minerals are mainly quartz, mudstone, siltstone, and sandstone debris and are the second ones.

In addition, the clay mineral in the soil of the sliding zone depends upon the weathering intensity. In weathering crust, the shallower the buried depth, the longer is its history; the looser its structure, the higher is its clay content. Furthermore, the clay mineral content of the sliding zone is also related to the geomorphology and to the buried depth from where the sliding zone occurs.

Fig. 2.6 Mineral content in the sliding zones of the landslides on the mainstream of the Three Gorges reservoir
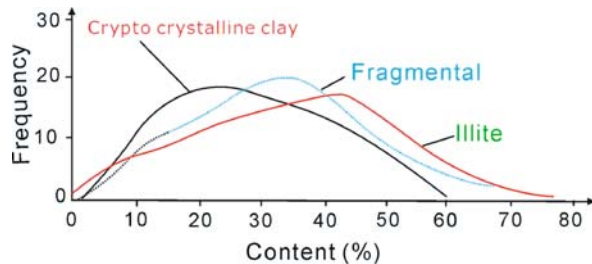
Grain Composition

Engineering geological properties of the sliding zone vary with its grain composition. The granular metric analysis for more than 100 specimens from the sliding zones of the landslides in the Three Gorges reservoir (Fig. 2.7) suggests that gravels and sand content show lognormal distribution with a relative concentrated distribution and little divergence, with the average content of 20%; silts and clays show normal distribution, but the former is high in divergence with the average content of only 25% and the latter is low with the average content of 35%. On the whole, fine grains in the sliding zone of the large landslides in the Three Gorges reservoir are rich; the main grain compositions are clays, and the soil is typically clayey.

Physical and Mechanical Properties

Physical Properties

The soil in the sliding zone is clay whose consistency can change into solid, plastic, and liquid states depending on its moisture content variation.

According to the statistical analysis of the test results for the soil in the sliding zone (Fig. 2.8), both plastic limit and liquid limit show lognormal distribution, with

Fig. 2.7 Content of various particles in the sliding zone of the landslides in the mainstream of the Three Gorges reservoir
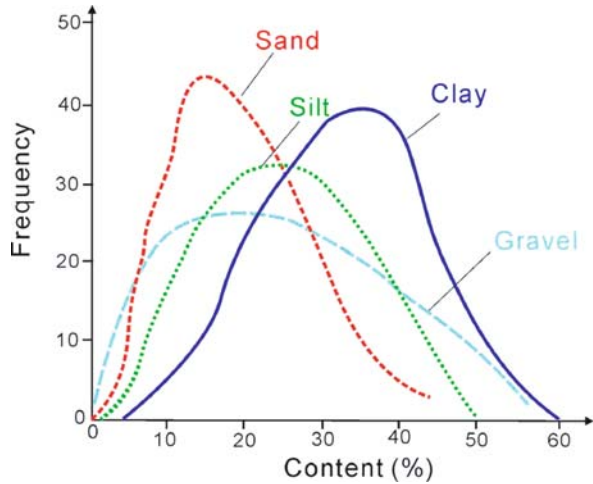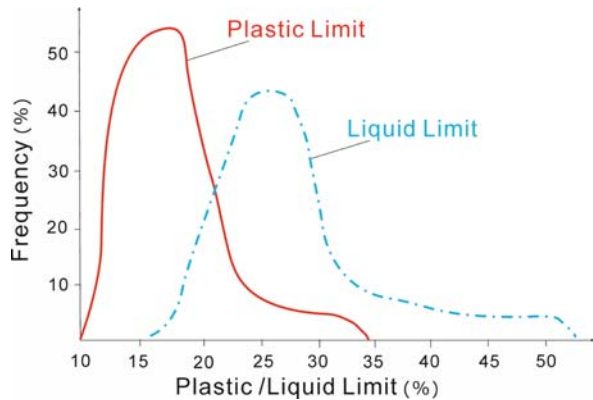

**Fig. 2.8** Distribution of plastic limit and liquid limit of the soil in the sliding zone

low divergence and the average value of 27.5% and 17.5%, respectively, the corresponding average plasticity index of 10%, the soil belongs to the clayey category.

Mechanical Properties

Mechanical properties of sliding soil include strength indexes and deformation indexes; the former are the essential parameters for calculating the landslide stability.

The statistical results of the shear strength are presented in Fig. 2.9; it indicates that peak strength shows normal distribution while residual strength shows lognormal distribution with low divergence for both. The average peak value of cohesion (c) is 12.22 kPa and that of friction angle (φ) is 16.78°, while the average residual value of cohesion (c) is 7.96 kPa and that of friction angle (φ) is 13.84°. The general regularity is that the shearing strength of the sliding zone decreases in the order of the sliding zones of the landslides and rock falls with hard rock

Fig. 2.9 Distribution of c and φ of the soil in the sliding zone
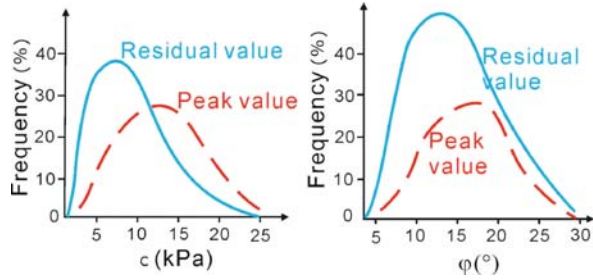
sliding bed (such as landslides of Zuojituo, Yaqianwan), those of the cut beddings landslides (such as landslides of Huanglashi, Shuping), those of rock falls with a shale rock base (such as rock falls of Baiheping, Xiangjiawan), those along bedding, and landslides controlled by coal seams (such as landslide of Fanjiaping), those of accumulative deposit landslides with shale base (such as landslide of Xintan), and along bedding landslide controlled by mudstone bed (such as landslides of Jipazi, Taibaiya, and Zhonggangjiaolu).

The main factors that affect the strength of sliding zones are granular composition, mineral composition, and water content. The effect on the friction angle is shown in Table 2.7 and Fig. 2.10.

To consider the comprehensive effect of various factors on residual strength, a couple model and a regression analysis are also carried out. The results present that

Table 2.7 Factors affecting the shearing strength of sliding zone

| Affecting factors		Affecting results
Clay content		The residual friction angle of sliding zones shows prominent negative correlation with clay content; it indicates that the higher the clay content, the stronger the water colloid cohesion, and lower the residual strength.
Mineral composition	Illite	Its content has nonlinear negative correlation with residual friction angle. Content of illite with 38% is the sensitive point (curve inflection point). As less than the point, the residual friction angle is sensitive to illite, while greater than the point, the sensitivity deceases.
	Cryptocrystalline soil	As the context is more than 40%, the effect to residual friction angle is apparent.
	Detrital minerals	Its content has linear negative correlation with residual friction angle.
Water content		Water content has clear nonlinear negative correlation with residual friction angle. There is a sensitive point near liquid limit (24%). Structure of the soil in the sliding occurs mutation when higher than this point.
Structure of the soil and roughness of the particle surface		The soil in the sliding zone with scales texture has low residual friction angle.
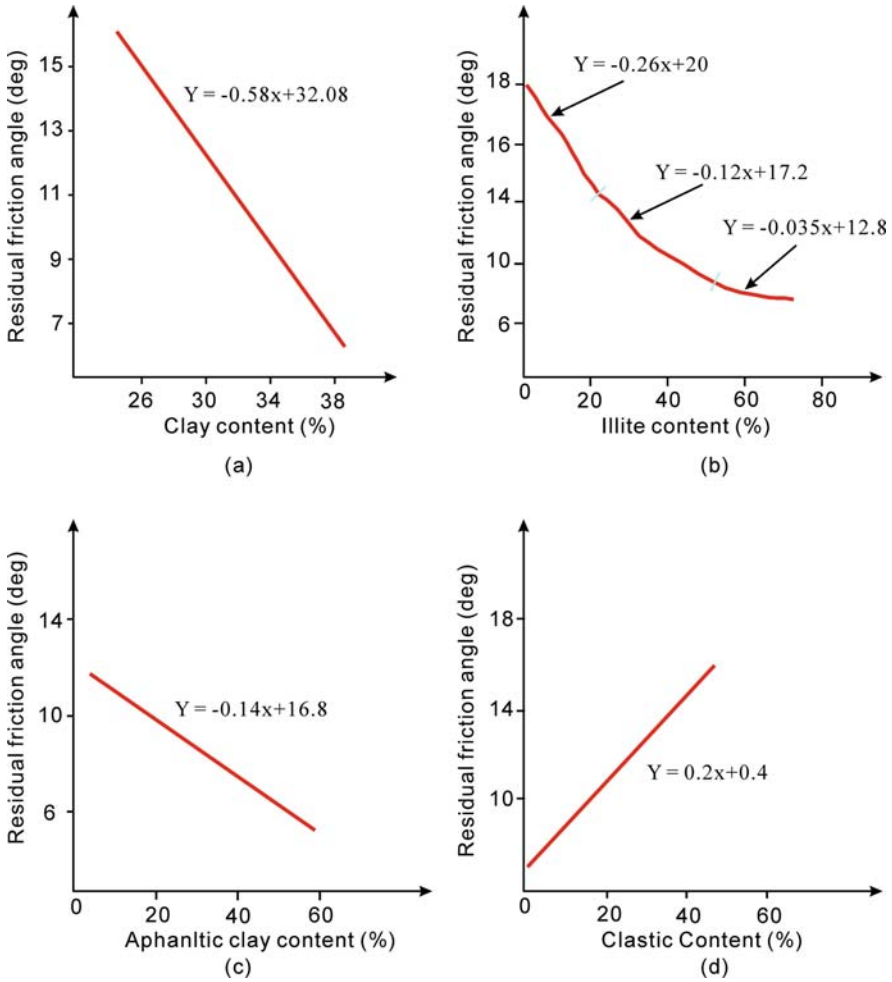
Fig. 2.10 Relations between residual friction angle and the content of clay, cryptocrystalline clay, and detrital mineral

as natural water content of the soil in sliding zone in couple model is near liquid limit, the estimated residual internal friction angle is similar to the one obtained by the consolidation undrained shearing test. The results of the couple model are satisfactory. By the regression model, we can see that the residual strength has linear negative correlation with the logarithm of clay content and of water content respectively, has linear positive correlation with plastic limit. Water content is the most sensitive factor affecting the residual strength of the soil in the sliding zone.

Microstructure Feathers of the Sliding Zone

According to the identification results by polarizing microscopy, microstructure characteristics of the soil in the sliding zone of the landslides in the region can be summarized as the structures of microscopic scale-like, crypto-crystal and microcrystal. Microscopic scale-like structure is the main type of soil in the sliding zone, in which the clay minerals are mostly scale-like illite, with a directional array, and the array direction has a small angle of intersection with the sliding surface. Contact among the soil particles is mainly face to face, and the attractiveness of the contact is weak and not firm. However, its water tight characteristic can result in water saturation of the sliding zone to cause the advantageous distribution of the weak microstructure planes. For crypto-crystal and microcrystal structures, the former is mainly dispersed crypto-crystal clays, with a few scale-like illites, and a trace of kaolinites, while the latter is mainly microcrystalline calcite, mostly in aggregates or dispersed, secondly it is crypto-clays and micro-scale-like illites.

Hydro-geological Characteristics of the Landslides

Landslides in the Three Gorges reservoir often contain ground water, where water-bearing capability, permeability, recharge and discharge conditions, and water level variation are the important factors affecting the present deformation and stability.

Landslides are mainly loose deposits, in which the ground water occurs mainly as pore water with the buried condition of phreatic aquifer. Also, there is fissure water in the rock with a massive structure. The conditions of the ground water movement and discharge are not only controlled by rock properties and structures but also affected by terrain, river water level, and hydrogeological characteristics of the underlying bedrocks.

Water-Bearing Capacity and Permeability of the Landslides

Water bearing capacity and permeability of the landslides are confined by material composition and structure type of the sliding mass and have a relatively high anisotropy.

Rock Fall Deposits

Rock fall deposits mainly distributed on the sides of deep and steep Gorges are generally composed of stiff and thick rock blocks, contain relatively less fill mud, mostly without water, and are of high permeability. According to borehole results, the rock fall deposits such as Qianya, Xiangjiawan, and Baiheping, contain water locally or in the front, with small water storage capacity and seasonal variation.

Landslide Deposits

Landslide deposits are an open hydrogeological structure on a slope, in which the ground water condition occurs as the relation between the slope runoff surface and

the slope sliding surface, that is, while the slope sliding surface is less than the slope runoff surface, the sliding mass contains water; on the contrary, it contains no water or partially contains water. According to exploration data, ground water gradients in typical and large landslides are generally 0.15–0.27.

Statistical results suggest that the aquifer in the landslide generally has four types:

(1) Ground water bearing. The landslide deposits are saturated annually, but the ground water depth varies in a large range with the type and the size of the sliding mass, the shape of the sliding bed, and the geomorphic position of the landslide. The dips of land surface and the sliding surface for this type of landslide are mostly less than 15°.

(2) Ground water bearing basically. Most of the landslide deposits are saturated annually, but a small part is saturated seasonally. The dips of land surface and sliding surface for this type of landslide are mostly less than 15°.

(3) Partially bearing ground water. A part of the landslide deposit is saturated annually; the other part is saturated seasonally. The land surface for this type of landslide is steep generally, with average dip angle more than 15° in most cases. Sliding surface is greater than 15° overall, mostly more than 20°.

(4) No ground water basically or ground water bearing in the front, seasonally. Most of the sliding mass has no water annually, and is only temporarily saturated during the rainy season. Both land surface and sliding surface for this type of landslide are steep, with dip angles larger than 20°. Most of the sliding mass locates above the flood level of the Yangtze River; in addition, the underlying bedrock has high permeability.

Permeability of landslide deposit obviously differs because of their structural variation. The stiff rocks with cataclastic structure (limestone, sandstone) present serious leakage in the drilling process and show relatively high permeability. The rock with scattered and cataclastic structure in general has low permeability, and the coefficient of permeability obtained by pumping test is 0.01–0.05 m/d.

Recharge and Discharge Conditions of Ground Water in the Landslides

Water sources of ground water recharge in rock fall and landslide deposits include rainfall, surface water (rivers, barrier lakes, paddy fields, etc.) and ground water from the vicinity, of which rainfalls and rivers are the main sources. As permeability of the landslide surface is low, water penetration is relatively homogenous and stable. As it is high and ground fissures exist, the conditions for ground water supply are preferable, and concentrated water supply in space and time may occur, which makes the ground water level rise suddenly, seriously affecting the stability of the landslide, often leading to landslide failure (such as Jipazi landslide).

Discharge conditions of ground water in rock fall and landslide deposits are related to their water convergent conditions, length, thickness, slope angle, cut

of gullies, permeability, and spatial attitude. There are about three cases of water drainage:

(1) *Poor drainage condition*: It is large in water convergent basins, not developed in gullies, or developed in gullies, and more in paddy fields and barrier lakes. Permeability of the rock fall and landslide deposits is low.
(2) *General drainage condition*: It is medium in water convergent basin, but developed in gullies; or small in water convergent basins, not developed in gullies. Permeability of the rock fall and landslide deposits is medium.
(3) *Good drainage condition*: It is small in water convergent basin, developed in gullies, or not developed in gullies but there are water-tight covers. Permeability of the rock fall and landslide deposits is good.

Ground Water Fluctuation and Its Affecting Factors

Ground water level in the rock fall and landslide deposits has seasonal fluctuations which are affected by the rainfall, and by both the rainfall and the river, in the front. Ground water fluctuations can be divided into sensitive and non-sensitive types.

(1) *Sensitive type*: It can be further divided into rainfall sensitive type and river sensitive type by the affected agent. For example, the Dabashi slide block of the Huanglashi landslide has the perched water table with a buried depth of 3–17 m and a water saturated thickness of 3.3–20 m. The range of ground water level change is 3–16.4 m, and the peak of spring water runoff has a 2-day delay of the peak of rainfall. The ground water level change in the front of Jipazi landslide is closely related to changes of the river water level, and its range is 20–44 m. See Figs. 2.11 and 2.12.
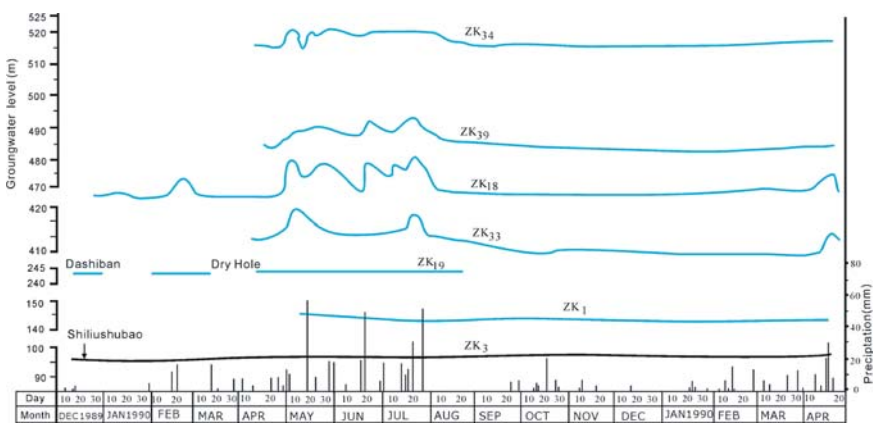

Fig. 2.11 Relationship between ground water level changes in the Huanglashi landslide and the precipitation
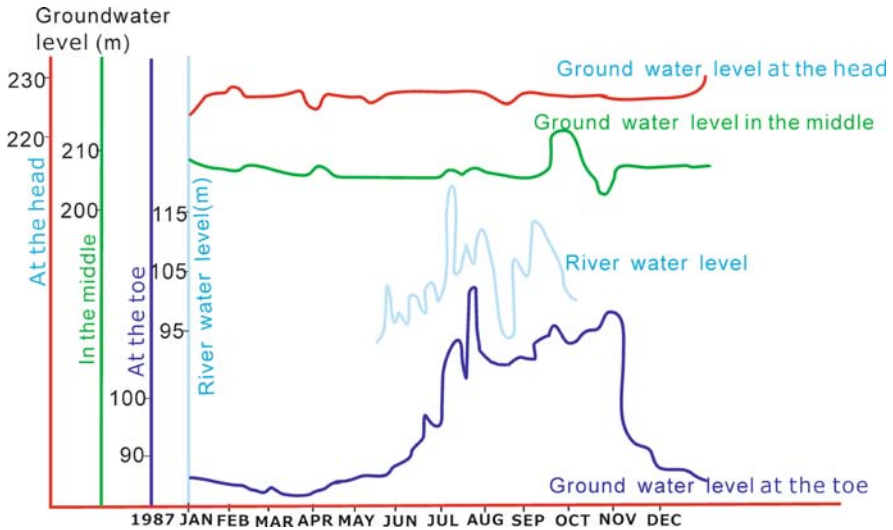
Fig. 2.12 Relationship between ground water level changes in the Jipazi landslide and the river level in 1987

(2) *Non-sensitive type*: Such as the landslides of Chengjiadiaoya and Maoxuzi, the range of ground water level change is 0.4–4.4 m. In addition, some landslides being good in water convergent condition, but poor in land surface permeability, belong to the non-sensitive type.

Looking at the long-term monitoring data, ground water level fluctuation in the typical and large landslide deposits has the following regularities:

(1) The landslide deposits with scattered and cataclastic structures are smaller in annual fluctuation of ground water level while those with massive structures are large.
(2) Those without the river affecting them are smaller in annual fluctuation of ground water level, on the contrary, are larger. According to monitoring information, annual water level fluctuation in boreholes is 1–3 m for the landslide deposits with scattered and cataclastic structures – up to 7–20 m for those affected by river water. It is 4–10 m for those with massive structures, up to 40 m for those affected by river water.

Formation Age of the Landslides

Besides exploring and researching the basic characteristics of the large landslides in the reservoirs, meanwhile, their formation time was also researched. The applied methods are as follows.

Determination of the Absolute Age for the Soil in the Sliding Zone

The age determination results of the soil formed in the sliding zone and the ruptures for the 10 landslides including Huanglashi are shown in Table 2.8. From the results, it can be seen that the ages for different landslides are quite different, but the following preliminary situations can be concluded:

(1) All that have their age determined are older than 8,000 years. Most of the sliding masses in the Three Gorges area are located along both sides of the mainstream and tributaries. Almost no large landslide occurring recently is noted, as the recently failed Jibazi and Xintan landslides are both reactivation of old ones. It seems that deformation and failure on the bank slopes of the Three Gorges reservoir have come to a quite period, after the end of activation.
(2) The absolute age of the soil in the sliding zones is determined mainly by ranges between 27 and 120 thousand years, and it is in accordance with the geological history of the Late Pleistocene (Q_3), the time when the landslides formed.
(3) Comparing the dated ages with the paleoclimate periods, most correspond to warm-humid periods, which show that the landslide formation has a close relationship to the warm-humid time of the paleoclimate.

Table 2.8 The age determination results of some landslides

Geological times	Age ($\times 10^4$a)	The sites for sampling specimens ($\times 10^4$a)
Holocene (Q_4)	Present–1.1	Zhaojiatuo (0.95), Huanglashi (0.8–1.2), Zhongang (1.2)
Late Pleistocene (Q_3)	1.1–13.0	The west of Yunyang county (2.7), Qingyanzi (1.4), Xintan, Jiuxianping, Huanglashi (3.7–6.4), Guling and Quchipan (7.5–13.0), Huanglashi (8.70 rupture)
Middle Pleistocene (Q_2)	13.0–73.0	Qiancaotuo, Daping (19.0), Baihuanping (29.0±), Wanxian landslide group (15.0–30.0)

Referring to the Terraces of Yangtze River Valley

From statistical analysis, the front of the sliding masses in the Three Gorges reservoir rests mostly between the first terrace and the low water level of the Yangtze River. The first terrace sediments and the erosion platform are commonly seen in the front of the sliding mass. Elevations of the main sliding zones and their fronts, for seven old landslides in Wanxian city, correspond to that of the first terrace, and those of land surfaces to the fourth to fifth terraces. From the facts, we may conclude that the sliding mass along the Yangtze River bank slopes was mainly formed in the middle or late Pleistocene, which basically coincides with the determined absolute age above.

Stability Assessment of the Sliding Masses

The main methods to evaluate the sliding mass stability include macro-geologic judgment, stability calculation, failure probability analysis, sensitivity analysis,

and fuzzy synthetic evaluation. Whether the results achieved from those methods are correct or not depends on the objectivity and reality for recognizing the factors affecting the stability of the sliding masses, especially in stability calculation, whether the boundary conditions of the slide masses are clear or the selected parameters for computing correctly, directly affects correction of the results. As it is difficult to ascertain landslide boundaries thoroughly and to obtain accurate parameters in practical work, multi-methods are applied for comprehensive assessment to obtain a relatively practical result.

Micro-geologic Judgment

By comparing many cases of landslide failure, it is realized that micro-geologic judgment of sliding mass stability should emphatically take into consideration the following main factors:

(1) With or without apparent deformation and reactivation symptom at present;
(2) Intensity of recent activation and status of post activation;
(3) Shape of the run-out surface and structures of the slope;
(4) Structure of the sliding mass and shape of the sliding surface;
(5) Material sources and the sizes contributing to the landslide material, from the head;
(6) Surface water infiltration and drainage conditions;
(7) Seismic effect and human activity intensity.

Of the factors mentioned above, traces of deformation are the primary mark for stability judgment. The geomorphic characteristics of the sliding mass, such as on-surface inclination, front-surface freedom, gully cuttings, and closed depressions, provide external marks for stability judgment. Dip direction, dip angle and shape of the sliding surface, and ratio of the resistant segment to the total length of the sliding surface are significant indicators for the sliding mass stability judgment, which needs in-site exploration to determine. The investigation of case histories suggested that the landslides with steep plane sliding surface have low stability; those with circular arcs are wave-like; broken line sliding surfaces have medium stability; and those with gentle, long horizontal segment sliding surfaces or with a reverse slope in the front thrust portion usually have good stability. Storm intensity, stream action, human activity, earthquake, and other dynamic environmental processes are the important triggering agents affecting the sliding mass stability.

Calculation by Limit Equilibrium Methods

In the limit equilibrium method calculating landslide stability, the method of inter-force transfer is the principle method used in China. The method considers not only the gravity of the sliding mass but also the hydrodynamic pressure and buoyant force or uplift force of the ground water. The five important landslides including Xintan are also checked with consideration of the potential seismic intensity as seven degrees.

The effects of rainfall and the river water level fluctuation on calculations are considered as following schemes:

(1) In dry seasons, there is no or less rainfall in the area, and the calculation is carried out in natural state;
(2) In rainy seasons, there is continuous rainfall or rainstorm in the area, and the calculation is carried out using a saturated state;
(3) The water level of the reservoir is considered according to the dry water level, 1% frequency of flood level before storage, limit level for flood control and the normal water level after storage, and other kinds of conditions, in the calculation. Also, there is the special circumstance where the water level drawdown from the normal water level decreases the level for purposes of flood control is also considered.

The parameters for calculating generally are determined by in situ test results, taking the mean values or weighted mean values. The shear strength of the sliding zone is the utmost factor for the calculation; therefore, the three methods of test, back analysis, and experienced analogy are applied to comprehensively determine them.

For the soil of the sliding zone below ground water level, the strength of the sliding zone is adopted to be the residual values of the consolidated-quick shearing tests where the water content is near the liquid limit. For that above of ground water level, the residual values of quick shearing test in natural water content are adopted.

For the recent reactivated landslides, such as the Xintan landslide and the Jibazi landslide, back analysis is adopted to presume the shearing strength. For the sliding mass without any specimens, parameters are chosen by comparing them with similar landslides.

Failure Probability Analysis

Failure probability analysis of the rock fall and landslide stability is characterized by Monte Carlo simulation analysis. The present study shows that c and φ values of the sliding zone are random variables obeying normal distributions, the factor of safety (K) being a certain function of c and φ is also a random variable. Using Monte Carlo analysis, a series of c and φ values are produced by simulation, and then the values are applied to the limit equilibrium method to obtain the factor of safety (K). Taking the probability of $K<1$ (the failure probability) and P as the index of the stability judgment, the criteria is suggested as $P<30\%$, stable; $P=30–60\%$, basic stable; $P=60–80\%$, poor stable; $P>80\%$, non-stable.

Sensitivity Analysis

Sensitivity analysis is the study of the sensitivity of a given parameter to the factor of safety by changing the one and keeping the others invariant in the stability

calculation. This analysis not only can ascertain the controlling factors of the stability but also be a supplement to the limit equilibrium and failure probability analysis.

There are two methods for sensitivity analysis:

(1) *Sensitivity analysis for the singles*: The method was carried out for 33 large and medium landslides on the mainstream and 26 large ones on the tributaries. The approach is to select the representative sliding section for a landslide, using the Sarma method to calculate the relation between the factor of safety with the different water level of reservoir, ground water level, seismic intensity (6 or 7 degree) and sudden drawing down of the reservoir water level to flood control limitation level, and so on. Then considering the factors based on the mother rock properties, the granular composition and the water content variation of the sliding zone or potential sliding zone or through engineering geologic analogy zone, to evaluate the variation range of the shearing strength parameters (c, φ), finally judging the stability of the landslides under various constitution of conditions (Fig. 2.13).

(2) *Sensitivity analysis of the main area affecting factors for the large ones*: Analysis and assessment of the sensitivity of landslide stability to friction angle of the soil in the sliding zone, dip angle of sliding surface, slope of the landslide surface, sliding resistant ratio (ratio of the resistant length to the total length of the sliding surface), saturated thickness ratio (ratio of the mean thickness of saturated portion to that of total sliding mass), submerged ratio (ratio of the length of the sliding surface submerged underwater to that of the total sliding surface), and daily maximum rainfall suggest that sliding-resistant ratio, slope of the landslide surface, dip angle
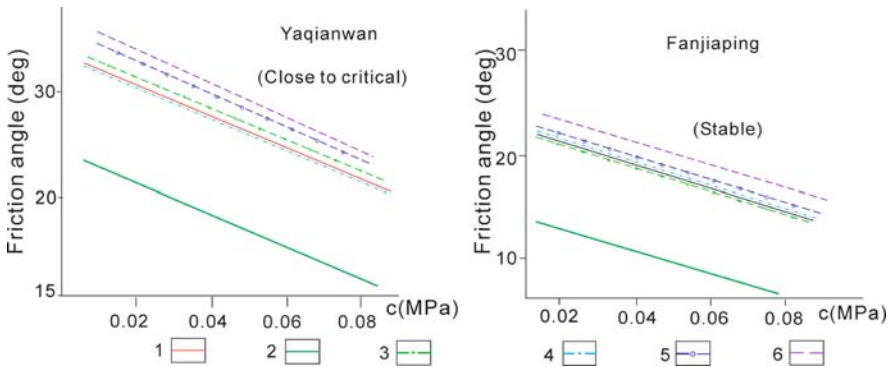

Fig. 2.13 Sensitivity analysis results of the landslide stability for two cases on the mainstream. 1 – Natural river water level, lower half portion of the slope saturated, 6 degree of seismic intensity; 2 – Natural river water level, no water in the slope, 6 degree of seismic intensity; 3 – Lower half portion of the slope saturated, 145 m reservoir water level, 6 degree of seismic intensity; 4 – Lower half portion of the slope saturated, 175 m reservoir water level, 6 degree of seismic intensity; 5 – Lower half portion of the slope saturated, 6 degree of seismic intensity, water level suddenly drawing down from 175 m to 145 m; 6 – Natural river water level, lower half portion of the slope saturated, 7 degree of seismic intensity

of sliding surface, submerged ratio, and friction angle are the most sensitive factors to landslide stability; daily maximum rainfall and saturated thickness ratio are the medium ones, and cohesion is the lowest one.

Fuzzy Comprehensive Evaluation

The 10 factors friction angle, impedance ratio, submerged ratio, saturated thickness ratio, dip angle of sliding surface, slope of landslide surface, active state, daily maximum rainfall, earthquake, and human activity were selected for fuzzy comprehensive evaluation. Consideration is given to not only the action of the internal and external dynamic agents but also the effect of the inner structures and outer morphology of the sliding mass.

For stability assessment of the landslides in the Three Gorges reservoir, the main approach is to use micro-geologic judgment. For the large and huge ones, various calculations and analysis methods were carried out. For a few potential unstable deforming rock masses which have been studied in detail (such as Lianziya dangerous rock mass, Huanglashi landslide), finite element simulation, discrete element simulation, and centrifugal model tests were applied. For the work mentioned above, stability of the landslides in the Three Gorges reservoir are divided into four degrees (a) stable, (b) fairly stable, (c) poor stability, and (d) unstable; the indicators for determining these categories are shown in Table 2.9.

After the comprehensive assessment of the 684 landslides with the size more than 100 thousand m^3 each in the mainstream and tributaries, in the natural state, it was found that there are 569 stable (a) or fairly stable (b) landslides with a total size of 262 million m^3, which accounts for 83.2% and 86.2% in number and in size of the total, respectively; 115 poor stability (c) and unstable (d) ones with a total size of 420 million m^3, accounted for 16.8% and 13.8% in number and size of the total, respectively. Of the landslides with size more than 1 million m^3; there were 64 of poor stability and unstable ones with the total size of 340 million m^3, accounted for 20% and 11.8% in number and in size of the total, respectively. All the huge ones and more than 85% large ones belong to the stable and fairly stable types in the reservoir area (Table 2.10). Therefore, stability of most landslides on the reservoir bank slopes is good or comparatively good.

Effect on the Rock Falls and Landslide by the Reservoir Impounding

After the Three Gorges reservoir begins impounding water, except for few landslides being either submerged totally or above the reservoir water level without the influence of the water fluctuation, most will be affected by variation of the water level. Effect on stability of the landslides by the water fluctuation depends on geographical position and the stability of the sliding mass, shape and elevation of the sliding surface, structure and material composition of the sliding mass, drainage condition of the slope, and the flood process of the reservoir. According to the three methods

Table 2.9 Criteria for stability classification of the landslides

Stability / Methods		Stable (a)	Fair stable (b)	Poor stable (c)	Non-stable (d)
Deformation and revival symptoms		No	No	No	Yes
Extensive activation recently		No	No	May be	May be
Geography	Height difference between the front and the back	Little	Fairly little	Fairly large	Large
	Slope of landslide surface	Gentle	Fairly gentle	Fairly steep	Fairly steep
Macro-geologic judgment	Slope structure — Firm or cemented extent	Well	Better	Fairly poor	Fairly poor–poor
	Attitude and character of sliding surface	Gentle, high strength	Fairly gentle, reverse segment is short, high strength	Fairly steep or gentle, fairly low strength	Fairly steep or gentle, low strength
	Characters of the rear portion — Material distribution	Little	Fairly little	More	More
	Back cliff	Stable, no significant erosion	Basically stable	Possible collapse	Possible collapse or forming
	Collapse activity	No	No	May be	Has

Table 2.9 (continued)

Stability Methods		Stable (a)	Fair stable (b)	Poor stable (c)	Non-stable (d)
Hydrogeology condition	Water convergent area	Small	Fairly small	Fairly large	Fairly large
	Infiltration condition	poor	Fairly poor	Fairly well	Well
	Drainage condition	Gullies developed and deep cut, good drainage conditions	Gullies developed, good drainage conditions	Not smooth in local drainage system	Not smooth in total or local drainage
Calculated factor of stability (K)		High	Not high	Little higher than 1	$K \leq 1$
Sensitivity analysis		The landslides keep stable state when the affecting factors change to worse tendency.	The landslides close to critical state when the affecting factors change to worse tendency.	The landslide is in critical state when the affecting factors change to worse tendency.	The landslide is worse than critical state when the affecting factors change to worse tendency.
Failure probability (P)		$\leq 30\%$	30–60%	60–80%	$\geq 80\%$
Fuzzy evaluation		Stable	Basically stable tends to be stable	Basically stable, tends to be unstable potentially	Unstable or unstable potentially

Table 2.10 Stability classification of the landslides with the size more than 1 million m³ in the Three Gorges reservoir (before storage)

River	Stability	1–10 million m³ (medium)		10–100 million m³ (large)		>100 million m³ (huge)		Landslides
		No./size	Proportion to the total (%)	No./size	Proportion to the total (%)	No./size	Proportion to the total (%)	>1 million m³
Mainstream	Poor stable (d)	6/2,172	5.7/5.7	1/1,800	3.6/3.6			Huanglashi, Lianziya, Yaqianwan, Yutang, Qianxigou, Dongzi, Wangyemiao –. totally 7.
	Fairly poor stable (c)	6/2,129	5.7/5.5	4/9,213	14.3/10.5			Zuojituo, Xiangjiawan, Ciancaotuo, Yunyangxicheng, Taping, Huangguashu, Sandengzi, Mmiaoping, Lishupin, Biaoganshang – totally 10.
	Basically stable (b)			5/19,380	17.9/22.2	1/12,933	33.2/29.2	Xintan, Huangtupo, Baiheping, Baihuanping, Baota, Jibazi, Shuping, Fanjiaping, Shuizhuyuan, Liujiawuchang, Baiyi'an, Xinwu, Outang, Guling, Jiuxianping, Yuhuangguan, Caojiezi, Anlesi, Taibaiya, Diaoyaping, Houzao, Maoxuzi, Longwangmiao, Chenjiadiaoyan, Caofang, Zhongangjiaolu, etc. – totally 119.
	Stable (a)	93/34,125	88.6/88.8	18/50,056	64.3/65.2	2/31,400	16.7/70.8	

Table 2.10 (continued)

River	Stability	1–10 million m³ (medium)		10–100 million m³ (large)		>100 million m³ (huge)		Landslides
Tributaries	Poor stability (d)	7/1,796	4.4/3.6	1/2,394	4.0/4.5			Xiangshuitan, Hujiacitang, Tianmachi, Paotongwan, Nianziping, Mahuanggou, Huangnibaping, Dalinba – totally 8.
	Fairly poor stable (c)	37/11,961	23.4/24.3	2/2,959	8.0/5.6			Yinwozi, Pijiayuanzi, Xiangxi town, Bazimen, Baofutai, Xiangxihe Mineral Bureau, Zhnegjiahe Coal Mine, Zigui Cement Plant, Sangshuping, Dengjiawan, Xindatian, etc. – totally 39.
	Basically stable (b)	50/17,436	31.6/35.4	11/21,386	44/40.5	1/19,020	100/100	Shifosi, Wujiadaling, Hujiawuchangwu, Zhaizibao, Lianyuchi, Shijiawan, Longpo, Wangjiayuanzi, Zhoujiayuanzi, Wanbeituo, Yangjiaotan, Yanjiao town, etc. – totally 62.
	Stable (a)	64/18,076	40.5/36.7	11/26,019	44/49.3			Kaziwan, Dawuchang, Hualianshu, Baiwafang, Zhichang, Dashiban, Duoxiaoping, Panjiayuanzi, Wutongping, Oujiaping, Tukan, etc. – totally 75.

of the reservoir operation, effects of the reservoir on the landslides have the two aspects as below.

Effect of the Normal Water Level

After water storage, the hydrogeological condition of the submerged part of the landslide will be changed; especially, change of the physical and mechanical properties of the sliding zone directly influences the landslide stability. However, change of the sliding zone strength is related to the material composition, permeability, natural underground water level, and other factors.

Study on the typical and huge landslides shows that, except for a few strong permeability landslides, in natural states, the sliding zones or potential sliding zones of most landslides are totally or partially below ground water level annually, and apparently the rising of the reservoir water level has no essential effect on the strength. But strength of the portions above ground water level for the sliding zones and the sliding masses composed of soil with breccias will be decreased after saturation. This negative condition should be considered in sensitivity analysis of the landslide stability.

By analysis, comparing the factor of safety before to after storage for the 37 typical and large landslides as the reservoir water level reaches the 175 m level and whether the strength change of the sliding zone and sliding mass is ignored, it is equivalent or there is a little increase for 44% after storage, a little decrease for 24% (3–10% decrease in the factor of safety), and a large decrease for 32% (11–30% decrease in the factor of safety). But of the ones experiencing decrease, only two have the factor of safety near to 1.0, and the others are all above 1.08. As indicated, the normal reservoir water level has influence on the landslide stability.

Effect of the Reservoir Water Level Fluctuation

There are two periods of prominent fluctuation as the Three Gorges reservoir routinely operates:

(1) Slow falling of water level before the flood season. In the 5 months from November to March, the water level in front of the dam falls from a normal level 175 m to the flood control limit level 145 m, with a 30 m reduction in velocity of about 0.2 m/d. Comparing the bank slopes of the reservoir to bank slopes in other parts of the world, there is no apparent effect on the entire stability of the reservoir bank slopes under such decreasing velocity, but it may induce sliding failure of some deformable masses with poor stability.

(2) Rapid falling in a small range. This is sudden drawdown of reservoir water level after a peak flood in flood season. Magnitude of the drawdown range depends on the flood amount and flood type. Take the 1954 flood for instance, the maximum drawdown of the water level in front of the dam was 17 m with the velocity of 1.2 m/d. This kind of large range and rapid falling of water level resulted from

simultaneously appearing torrential rain, and flood will be the important factor for the failure of the poorly stable and unstable landslides.

After reservoir storage, the effect of water level fluctuation on stability of the landslide can be basically recognized by sensitivity analysis, stability calculation for typical landslides, and drawing and analogy to the Gezhouba reservoir. Sensitivity analysis was carried out for the 28 large landslides on the mainstream in the case of extreme drawdown of the water level, only 7 of them decreased in stability compared to their natural state. For the 31 large and huge landslides on the mainstream, by the methods of macro-geologic judgment, stability calculation, failure probability analysis, and fuzzy comprehensive evaluation, it is shown that only one (Longwangmiao landslide) degraded from class b to class c, and degraded another one (Anlesi landslide) from class a to class b. While for the others, it was the same as in their natural state.

Hazard Assessment for Failure of the Reservoir Bank Slopes

Analysis of the Main Factors Inducing Hazards

The damage intensity by the river bank slope failure depends on the size of the sliding mass sliding into the river and the surge it would be inducing. If the mass sliding into the river was larger, it could destroy houses, farmland, public transportation, and communication facility; and obstruct or even disrupt the navigation of Yangtze River. A high surge would cause different degrees of dangers to various buildings, public accommodations, and farmland.

Estimation of the Size Sliding into River

Exploration and research on stability of the bank slopes and landslides of the Three Gorges reservoir suggest that water storage basically will not change the present condition of the rocky bank slopes. Most of the landslides with relatively good stability would keep entirely stable except some small-scale collapses in the water level variation zone. Some poor or fairly poor stable ones may destabilize locally, and a few in the process of deforming may failure entirely. Scattered alluvial and deluvial bank slopes may collapse to reach a new equilibrium state under water immersion and scouring, but the size of the collapse may be small. Therefore estimation of the volume of the sliding mass into river was mainly carried out for the single unstable ones.

The eight poor and fairly poor stable landslides, including Lianziya and Huanglashi, were studies to estimate the size of the slide into river, using formula calculation and case analogy.

The size of lip mass sliding into river can be estimated by the following equation:

$$V_{max} = \frac{S_{max}}{L_{max}} V$$

where

V_{max} – The maximum size of the sliding mass sliding into river (m³);
S_{max} – The maximum average sliding distance of the landslide (m);
L_{max} – The maximum length of the landslide (m);
V – Total size of the sliding mass (m³).

The Jibazi landslide in 1982 and the Xintan landslide in 1985 can be used as an analogy; as they slid into river, their size accounted for 1/8 and 1/11 of the total, respectively. The volumes of the material which slid into the river for the eight landslides are shown in Table 2.11.

Table 2.11 Estimation of the size of material sliding into the river for poor and fairly poor stable landslides on the mainstream of the Three Gorges reservoir

| Landslide name | The size sliding into river (×10⁴ m³) | | | Note |
| | Calculated value | Empirical value | | |
		1/8 of the total size	1/11 of the total size	
Lianziya dangerous rock mass	216	216	216	Assume the segment facing to the river slides into river
Huanglashi landslide	427	225	163.60	The volume of the sliding mass in the west part is considered as 1,800×10⁴ m³
Xiangjiawan landslide	127.49	250	181.82	
Yaqianwan rock fall	41.97	81.25	59	
Qiancaotuo landslide	271	420	305.45	
Sandengzi landslide	94.61	86.38	62.82	
Yuanyangxichen landslide	100.06	312.50	227.27	
Longwangmiao landslide	269.13	126.88	92.27	

Estimation of the Surge

Here, some methods for estimation of the height of the surge by landslides are applied for the Three Gorge Project.

Table 2.12 The results of the surge test for the Xintan landslide

| Times | Test conditions | | | | |
	Reservoir water level	The sliding size into water	Sliding velocity (m/s)	Flood discharge ($\times 10^4 \mathrm{m}^3/\mathrm{s}$)	Surge height in front of the dam
1	150	1,600	41.4	3	0.63
2	150	500	64.5	3	0.50
		1,600			1.00
3	130	500	67.5	3	0.75
		1,600			1.50
4	95	500	72.4	1.6	0.75
		1,600			1.38

(1) *By surge test*: Yangtze Scientific Research Institute used the hydraulic model for the head segment of the reservoir and selected a huge landslide (the Xintan landslide) and a dangerous rock mass (Lianziya) which are close to the dam and have poor stability at the time of the surge tests under different failure conditions, sliding sizes, and water levels. The results for the Xintan landslide are shown in Table 2.12.

It was found that the surge attenuation is influenced by the river, prominently. If the river has more meanders, tributaries, and brooks, it is favorable to the surge attenuation. It is especially evident in the upstream passing mender V-shape gorge, as the height of the surge attenuated rapidly. The surge height of the Xintan landslide was only 1.5 m up to the dam site when using the extreme conditions of the maximum sliding size and the highest sliding velocity for testing.

(2) *By surge calculation*: Calculated results using various formulas were compared to the real measured value of the 1985 Xintan landslide, and it is concluded that the method of the U.S. Corps of Civil Engineers is suitable to the characteristics of the Three Gorges reservoir. This method assumes that the sliding mass is emerged in a semi-infinite water body and the vertical falling distance is bigger than the water depth. Using a theory of gravity in a linear relation to the surface area, a calculation formula for surge height induced by landslide is derived. Supposing the eight poor and fairly poor stable landslides along the reservoir bank slopes had failed, the surge heights induced by them at the entry point (the opposite bank slope) Sandouping dam site and town nearby were calculated.

(3) *By case analogy*: The Xintan landslide, in June 1985, had 3.4 million m^3 of material sliding into the Yangtze River instantaneously. The surge reached 49 m in height at the entry point of the opposite bank slope, but it attenuated up and down the river rapidly. At 1 km downstream in the river, the surge height was 7 m, at 7.5 km was 2 m, at 11 km was 0.5 km, and no effect at the dam site. In the up-river, the surge height was 5 m at 4 km (Xiangxi town), and only 10 cm at 13 km (Zigui county) (Fig. 2.14).Other cases of landslides with surge-height measuring data also can be referred to.
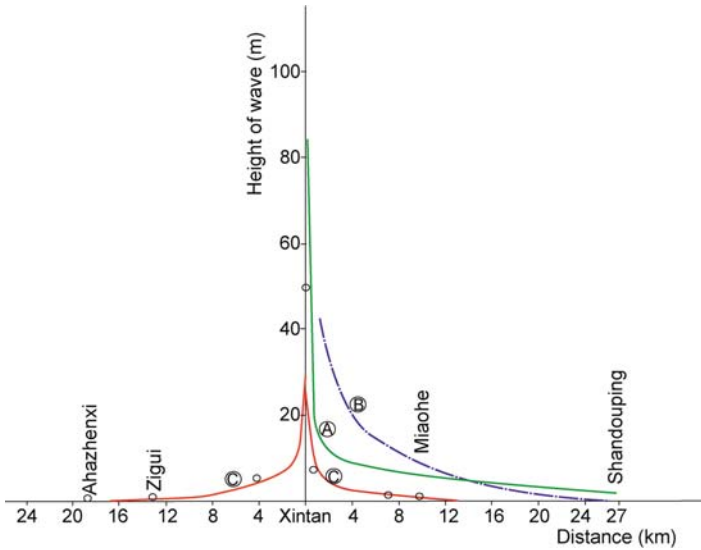
Fig. 2.14 The attenuation curve of surge height for the Xintan landslide. A – Calculated attenuation curve, size into river 16 million m³, velocity into water 100 m/s, water level 150 m; B – tested size into river 16 million m³, velocity into water 67 m/s, water level 130 m; C – measured attenuation curve on June 12, 1985 sliding

Analysis and Assessment for Potential Harm

Influence on Storage Capacity and Lifespan of the Reservoir

Comparing the size of rock and soil possibly sliding into the reservoir during bank slope failure with the total storage size, the intensity that the landslide deformation and failure have on the reservoir storage capacity can be evaluated.

The total size of the 684 landslides with each size larger than 100 thousand m³ distributing along the three gorges reservoir is 3.04 billion m³, even if they all failed and 1/8 of the total size slipped into river, the size into the water only accounted for 1% of the total water storage, and 2% of the dead water storage. Therefore, the landslides have no substantive influence to the storage capacity and lifetime of the reservoir if failure were to occur.

Influence on Construction and Operation of the Key Structures

The influence of reservoir bank slope failure on construction and operation of the key structures includes two aspects of direct and indirect influences.

(1) *Direct influence*: After years of detailed investigation, it is suggested that the front area of the dam is low hills and gentle slopes composed of crystalline rocks, neither large landslides nor the terrains, and geological conditions preferring large

landslides. There are no unstable bank slopes or landslides in the head segment of the reservoir directly threatening the stability of the key structures.

(2) *Indirect influence*: Neither poor nor fairly poor stable large and huge landslides exists; also, the geological conditions characterizing the landslides within 26 km long up river from the dam do not exist. Therefore, only the influence of the surge produced by unstable landslides 26 km away from the dam should be considered.

Poorly stable and deforming Lianziya dangerous rock mass and Xintan landslide, which are possible local failures, are 26–27 km away from the dam. Xintan landslide failed in 1985; the surge it produced attenuated rapidly downstream and basically vanished up to the dam site. In the future operational period, the possibility of the landslide reactivating as in 1985 is minor. But in the surge study, several conditions worse than those in 1985 sliding are assumed to be possible according to surge test and calculation, but the result represented that the highest surge up to the dam is only 2.7 m.

For Lianziya dangerous rock mass, supposing 2.16 million m^3 rock mass adjacent the river fell into the river at once, calculating the various schemes and with different methods, the surge heights up to the dam are all less than 2.0 m. Other landslides which may fail are all 65 km away from the dam site. Once they would fail and slip into the reservoir, the surge height up to the dam would be lower than above-documented ones. Thus surge caused by reservoir bank slope failure will not affect the construction and safety of the key structures.

Influence on Navigation

Influence on Navigation Before the Dam Was Built

In history, there were about 140 rapids in the Three Gorges reservoir segment, and investigation suggests that many of them were formed by landslides occurring in past history. After the Gezhouba reservoir storage, all the rapids down from Fengjie county were merged, in addition to many years of regulation; the shipping conditions of the channel had apparently been improved. But the conditions of the river bank slopes were not changed basically, the capability of controlling the failure of landslide to obstruct the navigation is still weak, and once a large landslide broken, it may result in serious navigation obstruction. Take 1982 Jipazi landslide for instance, where 2.3 million m^3 soil and rock masses slipped into the river, making the river bed experience uplift 30–40 m high. Most river section for navigation was occupied and the navigation was once obstructed. It has recovered after a large amount of regulation work. As to the Xintan landslide in 1985, 2.6 million m^3 soil and rock masses accumulated under water, extending forward into the river, 90 m wide and which occupied one third of the water area of the river section below the water level of 65 m (Gezhouba reservoir normal water level). Accounting for the river dry water level, it occupied about two thirds of the river section below water (Fig. 2.15). If Gezhouba reservoir had not raised the water level 20 m above the dry level, it might have lead to serious navigation obstruction.
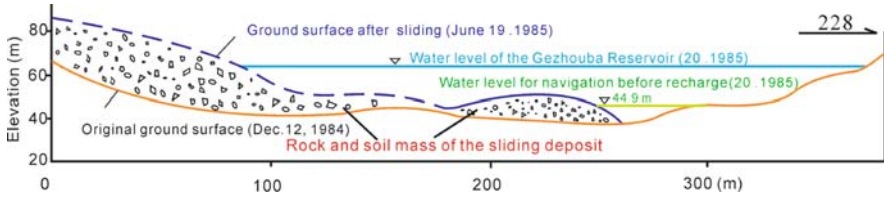
Fig. 2.15 Contrast of the channel sections before and after the Xintan landslide occurred

Referring to the above cases, without the Three Gorges reservoir, if the large or huge landslide with poor or fairly poor stability was a failure and only 1/8 and 1/11 of the total sliding mass slipped into the river, the soil and rock masses would occupy 50% of the river section under dry water level (Table 2.13), which would result in a serious navigation obstruction.

Effects by the Reservoir, to Navigation

As the reservoir formed, it will deepen the water depth 10 to 100 m, widen the water surface 200 to 800 m, increase the water area of the cross section 3–5 times. The possible size of the sliding masses sliding into the reservoir by failure of the poor and fairly poor landslides is generally thought to be 400–750 thousand m^3, at the most, about 4 million m^3. Considering the lowest reservoir water level, that is flood control limitation level, 135 m (earlier) and 145 m (latter), the area that the sliding masses occupied in serious segment takes up just 30% of the total water area of the cross section under water (Table 2.13). The rest of the area is far more than the area of the river section before the reservoir was built, so it basically does not affect the safety of the shipping channel. Therefore, the reservoir itself essentially mitigates the harmful effects of large and huge landslides to navigation.

Effects to Towns and Immigrant Settlement in the Reservoir Area

Most landslides along the reservoir bank slopes often are the main places for people to labor and live. In a natural state, because of natural agents and human activities, some deformation and unstable landslides have caused hazards to cities and public centers to some extent, and the old Xintan town was destroyed at a glance. Yunyang, Wanxian, Changshou, Xiangxi, etc. towns and cities have buildings damaged in different degree by landsliding and deformation after the Three Gorges reservoir was constructed, and the present deforming landslides may tend to aggravate the situation and would seriously destroy the buildings that are located.

Table 2.13 The volumes of the sliding mass accumulating under the water as the several large landslides in the Three Gorges reservoir were supposed failure entirely

| Landslide name | Percentage of the area soil and rock masses occupied under water to the original area under water in the river cross-section | | | | | | | |
| | 1/11 of the total in size into the water | | | | 1/8 of the total in size into the water | | | |
	Natural dry water level	135 m level	145 m level	175 m level	Natural dry water level	135 m level	145 m level	175 m level
Lianziya	88.1	31.5	28.5	20.0	65.5	15.4	13.5	8.8
Huanglashi	48.3	11.3	9.9	6.5	113.0	12.4	10.0	6.6
Yaqianwan	82.6	9.1	7.4	4.7	163.3	7.8	7.0	5.0
Xintan	88.1	5.6	5.0	3.6	46.0	20.3	17.4	10.6
Zuojituo	34.0	15.0	12.9	7.8	200.0	24.7	20.7	12.6
Xiangjiawan	144.0	17.8	14.9	9.1	212.0	21.6	18.1	11.5
Qiancaotuo	155.0	15.8	132	8.4	58.3	12.6	10.3	6.4
Sandengzi	43.3	9.4	7.7	4.8	139.0	32.9	27.6	17.8
Baota	103.0	24.3	20.4	13.1	48.1	10.2	8.3	5.0
Yunyangxicheng	35.2	7.4	6.0	3.6				

Note: Lianziya accounted for the 216 thousand m^3 adjacent to the river.

Table 2.14 Calculation result for the surge height caused by the landslides on the mainstream of the Three Gorges reservoir

Landslide name and location	Affected place	Distance (km)	Surge height (the highest surge on the opposite bank slope (m)/surge height in the affected place (m)					
			1/8 sliding into the reservoir			1/11 sliding into the reservoir		
			Previous river water level	135 m level	175 m level	Previous river water level	135 m level	175 m level
Xintan, Zigui	Sandouping dam site	27	>40/0.9–1.8	>40/0.89–1.6	>40/<1.5	40–59.5	40–45.9/	40.2/<1.2
Lianziya, Zigui	Sandouping dam site	27	>40/0.6–2	31–81.3/<0.7	23–70/0.6–2			
Daping, Badong	Badong county	5	45–63.1/2.3–4	25–42.3/1.5	13–32/0.9–3	39/1.9	22/1.3	11/1.0
Huanglashi, Badong	Badong county	1.5	50–71/7.5–11.8	20–44.8/0.7	33–65/4–9.5	50/10	38–50/8.7	33–50/8.1
Zuojituo, Badong	Badong county	17	35–>58/1–1.5	49–61/1.4	9.8–38/0.4–1	30.5/0.9	17/0.6	8.4/0.4
Caojiawan, Wushan	Wushan county	9	>50/1.5–1.8	49–61/1.4	35–50/1–1.1	>50/1–1.5	41/1.2	30/<1.0
Yaqianwan, Wushan	Wushan country	10	48–57.1	40–50/1.1	34–41/0.9–1	42–1.1	34/0.9	29/0.8
Yaqianwan, Wushan	Wushan county	9	41–54.7/1.1–2	20–42.8/0.6	9.7–37/0.4–1.5	33–0.9	16/0.5	8/0.3
Qiancaotuo, Fengjie	Fengjie county	5	48–57/1.4–3	25–44/1.2	8.4–38/0.6–2	41/1.2	21.6/1.0	7.1/0.5
Qiancaotuo, Fengjie	Fengjie county	12	42–50/1–1.5	31–60.4/0.9	22–53/0.7–1.2	34/0.9	26/0.7	19/0.4
Sandengzi, Fengjie	Yunyang county	>20	2.8/<0.2	1.9/<0.1	0.7/<0.1	2.4/<0.1	1.6/<0.1	0.6/<0.1
Lieloushan, Fengjie	Yunyang county	>20	17.5/0.7	14/0.6	10/0.5	15/0.6	12/0.5	8/0.4
Dongzi, Wanxian	Wanxian city	10	8.8/0.3	8.2/0.3	4/<0.2	7.5/<0.3	6.9/0.2	3.4/0.1
Wangyemiao, Fuling	Changshou county	10	8/0.3	7.4/0.2	3.6/<0.2	0.8/0.2	6.3/0.2	3/0.1

In addition, analysis and calculation (Table 2.14) suggested that the surge produced by the poorly stable landslide sliding into the reservoir is also an indirect threat to the towns and cities nearby, especially the surge produced by extensive sliding of the Huanglashi landslide close to Badong county. It can reach to 8–10 m high, and this factor should be considered in planning the new buildings in a new town.

Monitoring, Prediction, and Mitigation for the Main Landslides

Deformation Monitoring and Prediction for the Main Landslides

Monitoring of poor stable and deforming landslides is an available measure to forecast the failure exactly. For example, Xintan landslide failed in 1985 and the failure was successfully forecasted, which averted huge loss of lives and properties. The success is attributed to the 7 years of ground deformation monitoring. Systematic monitoring for the poor and fairly poorly stable landslides in the Three Gorges reservoir can provide an important base for failure prediction and control measures. At present, a deformation-monitoring network has been set up for the Xintan, Huanglashi, Jibazi, and Douyapeng landslides and the Lianziya dangerous rock mass. In cooperation with the new immigrants of the urban relocation of the reservoir area, an automatic monitoring system is going to be constructed all over the reservoir area.

There is a quite long process before a landslide failure, including appearance and extension of the surface fissures, formation and transfixion of the sliding surface, cracking and falling of the dangerous rock masses, etc. Therefore, the deformation monitoring commonly includes two aspects of ground monitoring and underground monitoring.

Ground Deformation Monitoring

The general methods for ground deformation monitoring are high precise triangulation network and collimation line method. Xintan, Huanglashi landslides, Lianziya dangerous rock mass, and Douyapeng deformed body were adapted to these methods of monitoring the ground deformation.

On the Xintan landslide before 1977, five collimation lines termed A, B, C, D, E parallel to the Yangtze River were set up on the sliding mass in the area between the attitude of 600 m and the riverside, of which, each line was composed of five points, and the endpoints were put on firm bedrock, and others were set in a line on the sliding mass. With deformation, part collimations became invalid, so another eight intersection monitoring points were added on the attitude of 600–900 m, a coffin corner monitoring network composed of seven stationary points on the outer margin of the landslide bedrock was constructed. Systematic and reliable data were collected for many years by monitoring, which provided the evidence for exact fore-

casting. This method is high in precision, simple in operation, and convenient for determining the displacement quickly. Monitoring of the vertical displacement was adapted to second-class level to make the measuring accuracy.

Comprehensive Survey Bureau, Yangtze River Committee used GPS to monitor the ground deformation of Baota (Jibazi) landslide in Yunyang county and Xiakouzhen landslide in Xingshan county, etc.

Besides monitoring for the deformation of the entire sliding mass, the relative displacement among the blocks on and below the surface of the sliding mass also should be monitored. As the case with Lianziya dangerous rock mass, 21 observational standard piers were set up at different blocks divided by cracks, and high-precision triangle measuring and second-class angle precision anterior intersection method were allied to record the displacement of each rock block. More than 30 relative displacement observation points were set up on the ground and in the cracks of the dangerous rock mass, and a crack meter extension rod, dial indicator, Spiral micrometer, precise level bubble, etc. were applied to measure the relative opening, closure, and vertical movement between blocks.

Deep Deformation Monitoring

Deep deformation monitoring is mainly used to determine the position and deformation characteristics of the sliding surface. At present, the most useful and comparatively economical apparatus is a borehole inclinometer. It is used for monitoring in Huanglashi landslide, and valuable data like the depth and displacement of the sliding surface, the correlation between displacement and rainfall, river water level, etc. were obtained (Fig. 2.16). Many borehole inclinometers were set up on Taibaiya, Anlesi, and Douyapeng landslides and on a deforming rock mass in Wanxian city to obtain fairly good observation data.

In addition, if conditions permitted, a tunnel could be excavated up to the sliding surface and high precise short-survey crosses could be set on the sliding surface to measure the relative displacement. The method was used on the Huanglashi landslide and it achieved a good effect. For deep monitoring in the Xintan landside, an F-12 style dislocation meter was used to monitor the relative displacement in the creep stage; a WL-30 pressure gauge was used to monitor the stress variation in the deep position; multi-points plumb, dislocation meter, adhesive wall-adhesive displacement meter, and crack needle installed on the shaft wall were used to measure the displacements of the sliding zone and sliding mass at different locations and depths.

Coordinating the monitoring of the landslide deformation, other items such as hydrology, meteorology, earthquake, and hydrogeology should also be observed simultaneously, as these data are significant in forecasting the deformation and development of landslides.
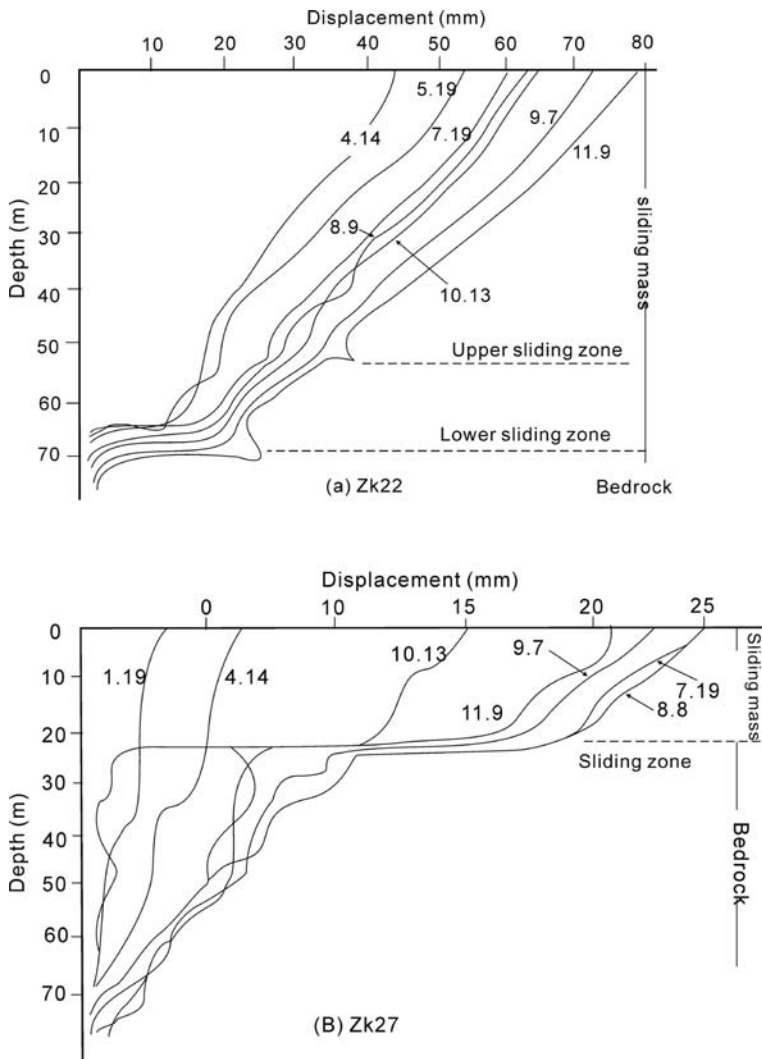
Fig. 2.16 The curves of displacement verses depth measured by borehole inclinometers in the Huanglashi landslide

Prediction

The aim of monitoring a landslide is to forecast its deformation and failure correctly and to make a decision for mitigation. The deformation process of a typical landslide can be divided into four stages. The initial stage is slow deformation, the following stage is apparent deformation, in this period, deformation trace can be seen on the ground, such as ground fissures, building cracks and incline, and these two stages last for a long time. The third stage is accelerating deformation, not only the
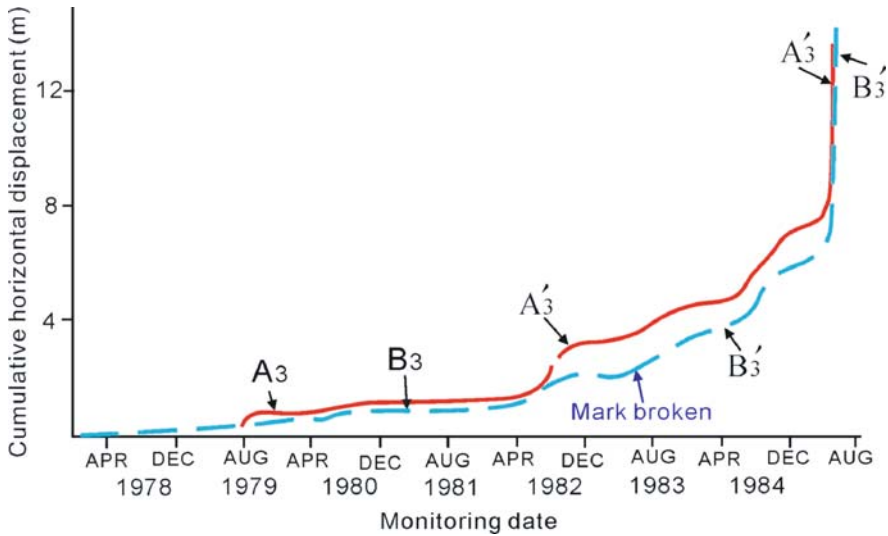
Fig. 2.17 Cumulative horizontal displacement curves on the observation lines A3-A3′ and B3-B3′ for the Xintan landslide

amount but also the velocity of the deformation increases with time. The last stage is failure of the landslide. Corresponding to deformation stages above, prediction of landslide failure can be divided into early prediction, medium-term prediction, short-term prediction, and critical sliding prediction. For example, the forecast for the Xintan landslide, before 1979 belongs to the category of early prediction, from 1979 to 1981 is medium-term prediction, from 1981 to 1984 is short-term prediction, and the critical sliding prediction started from March, 1985 (Fig. 2.17).

Treatment of the Landslides

The deforming hazardous landslides and dangerous rock masses should have measures taken to stabilize them. The design for stabilizing works should be based on the detailed investigation to pinpoint the main factors affecting the landslide stability and to avoid blindness. The main engineering mitigation measures include the following.

Water Drainage

The surface and the underground water usually are important factors affecting landslide stability, as most landslides happen in the rainfall period. Deformation monitoring shows that the majority of landslide deformation increases in the rainy season. Therefore, fixing the surface and underground drainage system is an important measure for enhancing landslide stability. For the Huanglashi landslide (Dashiban), for

example, the factor of safety decreases by 0.005–0.07 when underground water level rises every 0.1H (H is the water thickness within the sliding mass). Both the Huanglashi and the Jibazi landslides utilized valid drainage systems and the results are fairly good.

Unloading

For the landslide having much source material from the back and with down thrusting failure type, unloading on the top area is advisable to reduce the down sliding force and to enhance the stability.

Anchoring and Retaining

Generally, anchoring is applied to the reinforcement of dangerous rock masses and the stabilizing of small landslides. Reinforced structures are usually retaining walls and stabilizing piles to enhance landslide stability. In addition, under certain conditions (such as when the rock mass up and under the slip is fairly intact), resistant bolts crossing the sliding surface or other measures can be applied.

Multiple treatment measures were adopted for the reinforcement of Lianziya dangerous rock mass, which included surface water drainage ditches, local unloading, reinforcing by stabilizing piles for local shallow sliding, and pre-stressed anchor cables for the dangerous rock mass facing the river. Especially effective is a series of concrete bolts on the bottom of the dangerous rock mass to keep the mass from entirely settling and sliding.

Chapter 3
Research on the Characteristics and Slope Deformation Regularity of the Badong Formation in the Three Gorges Reservoir Area

Huiming Tang, Xinli Hu, Qinglu Deng, and Chengren Xiong

Abstract The Three Gorges reservoir area is characterized by widely distributed strata of the Badong formation, in which large-size landslides and deep-reaching loosely consolidated formations are likely to occur. Therefore, it is significant to reveal the mechanism and patterns of the large-size landslides that occur in the Badong formation for a better understanding of the development of the nature of deformation and process of formation of the deep-trending loose-slope stratum in the Wushan, Fengjie, and Badong renewal city zones. In this chapter, the geological characteristics of the rock mass of the Badong formation are analyzed on the basis of a systematic explanation of the rock mass strata, space variation of the lithological combinations as well as the space variation of stratum thickness, and structural deformation of the Badong formation. To demonstrate the basic law of long-term deformation of the Badong formation slopes and the patterns of later stage reformation and landslide evolution, the authors use the Huangtupo landslide as an example, as it is a typical failure in the Badong formation.

Introduction

The Three Gorges reservoir area is characterized by widely distributed strata of the Badong formation, in which large-size landslides and deep-reaching loosely consolidated formations are likely to occur. Therefore, it is significant to analyze the mechanism and patterns of the large-size landslides in the Badong formation for a better understanding of the development of the nature of deformation and process of formation of the deep, loosely consolidated stratum in the slopes in the Wushan, Fengjie, and Badong renewal city zones. Still, profound research on the character of

H. Tang (✉)
China University of Geosciences (Wuhan), Lumo Road, Wuhan 430074, China
e-mail: tanghm@cug.edu.cn

strata construction of the Badong formation is recognized as reliable and essential geological background information in terms of reservoir bank slope protection and other types of landslide mitigation for relevant areas of the Badong formation in the Three Gorges reservoir area (Wu 1996; Zong et al. 1996).

The research on the engineering characteristics of the Badong formation in the Three Gorges reservoir area covers the following aspects: the substantial composition and engineering properties, the physical–mechanical property of the rock and soil, the hydrogeological and geological structure of the slopes, and the dynamic characteristics of ground water in the rock mass. The relation between interaction of ground water–rock mass and slope deformation and destruction, the evidence of deformation of rock masses, the configuration of loosely consolidated formations, the features of the slope deformation, and the landslide evolution patterns are also included.

In this chapter, the geological engineering characteristics of the rock mass structure of the Badong formation are based on the systematic introduction of the rock mass of strata, space variation of the lithology combinations, space variation of stratum thickness, and structural deformation of the Badong formation. To demonstrate the basic law of long-term deformation and failure of the Badong formation slopes as well as the modes of later stage deformation and landslide evolution, the authors present the example of the Huangtupo landslide, a landslide that is typical of those occurring in the Badong formation.

Development Characteristics and Space Variation of the Strata of the Badong Formation in the Three Gorge Reservoir Area

The strata of the Badong formation fall into the categories of middle Triassic System (T_2b), with the overlying strata of upper Triassic System of Xujiahe formation (T_3xj, in Wushan and Fengjie) or Shazhenxi formation (T_3s in Zigui Basin) and the underlying strata of the lower Triassic System of Jialingjiang formation (T_1j).

The Lithology and Space Variation of Lithology Combinations of the Strata of the Badong Formation

The lithology and lithological combinations of the Badong formation are subject to space variation in terms of some differences.

The 1st section of the Badong formation (T_2b^1): Wholly of grey and dark grey, the lithological combinations consist of calcareous shale, dolostone, and pelmicrite containing marlite of medium to slight lamella, all of which are brecciated to various degrees. The rock mass in this area is subject to weathering and is of low strength for soft and sub-soft lithology, with no remarkable variation in different sections.

The 2nd section of the Badong formation (T_2b^2): Wholly of fuchsia and composed of combinations of mudstone and politic siltstone, with slight variation in

various sections; in Daxi of Wushan Mountain and Fanjiaping of Badong, the crimson clastic rock mass accounts for the absolute majority except for rare grey carbonate terrain; in Guojiaba and Shazhenxi of Zigui, the crimson clastic rock mass accounts for majority except for a few grey carbonate terrain on the top of the stratum; in the Changdang of the Fengjie, the crimson clastic rock mass accounts for the majority except for a certain amount of grey carbonate terrain.

The 3rd section of the Badong formation (T_2b^3): Unchanging color of terrain in various stratum sections in terms of light grey to dark grey, the majority of rock mass is shale containing muddy carbonate rock. The content of the muddy interlayer of the terrain is characterized by an unremarkable increase from the east to the west, and the majority of the stratum falls into hard rock.

The 4th section of the Badong formation (T_2b^4): Spatially, the section of the most prominent variation of lithology in the Badong and Zigui districts in the east, where the terrain of crimson clastic rock mass accounts for the majority and is subject to a sharp decrease to the west up to the Wushan Mountain area; by contrast, the muddy carbonate terrain increases remarkably, and the grey muddy carbonate terrain increases to an equivalence of clastic terrain to Fengjie district. The majority of strata fall into soft and sub-hard rock mass.

The 5th section of the Badong formation (T_2b^5): Wholly of light grey to celandine green from the east to the west, and the lithology is subject to slight variation in terms of dolomite in the lower stratum and pelmicrite in the upper stratum in Zigui, clay rock in the lower stratum and pelmicrite in the upper stratum in Badong, as well as muddy pelmicrite in the lower stratum and clay rock in the upper stratum in Wushan Mountain and Fengjie districts.

Space Variation of Stratum Thickness of Badong Formation

Figure 3.1 is the histogram of strata measured, generally, and it is characterized by thick stratum in the east and thin stratum in the west; for instance, the total thickness of stratum in Zigui is some 830 m and that in the Changdang village of Fengjie county is about 1420 m. The 4th section has the most remarkable variation of stratum thickness in terms of 274 m in Zigui to 590 m in Fengjie.

One common outcome as shown by the predecessors' information and measurements is that the horizontal stratum thickness of the Badong formation is unstable and subject to great variation. The spatial differences of stratum thickness of the Badong formation are attributed to three factors: different thickness of deposition, uneven denudation, and impact of subsequent structural deformation.

The Badong formation represents the deposition characteristics during the transition from typical neritic mesa strata (T_1j) to continental strata (T_3xj), with general deposition in the context of shore land–tidal flat and shore land–lagoon, including inter-tide and shore land mesa strata in local sections (mainly of T_2b^3). The deposition condition is characterized by longitudinal upward shake and transverse undulating fluctuation; the former results in featured alternating occurrence of stratum of muddy carbonate rock mass and muddy stone stratum, and the latter leads to variation of deposition facies and deposition thickness.
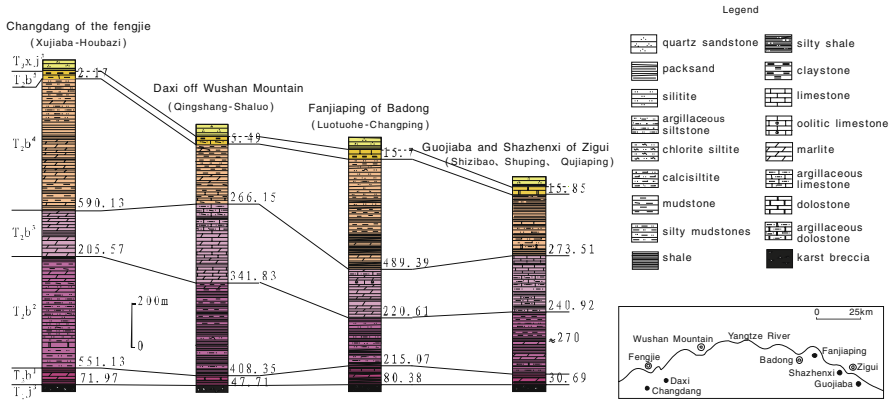
Fig. 3.1 Histogram for comparison of the strata measured in Fengjie–Wushan Mountain–Badong–Zigui of the Badong formation

The shake of longitudinal upward strata is incident to shake of raising and dropping of the crust, and local section is bare on the ground during the crust rise and subject to weathering denudation; due to the transverse undulating fluctuation of the earth surface, the ground is subject to denudation of various degrees, causing different thicknesses of residual strata.

Characteristics of Structural Deformation of Badong Formation

Cleavage

The cleavage structure of the Badong formation in the Three Gorges reservoir area is distinctive in terms of dense development and a constantly occurring strata layer, which, being weak and soft in structure, is all important in the course of the evolution of deformation and loss of stability of large-size slopes. In this section, emphasis shall be given to introducing the property of cleavage structure in the new city zone of Badong.

(1) *Attitude characteristics*: In the slope area of the Badong county, the cleavage runs in a steady manner from the old Xinling town to the new county of Xirang. Figure 3.2 is a rose diagram of the strikes drawn as per growth of 50 cleavages, and as illustrated, the predominant direction of cleavage running is evident (within the range of 80–100°), with a mean strike of 90.4° that is consistent to the extension direction of the fold axis in this area. The dip angle of the cleavage is closely related to strata lithology. The growth and the attitude of cleavage are variable corresponding to different positions of the fold and various lithology sections. The cleavage is nearly vertical at the fold core, which is generally in the opposite direction to the layers in the wing sides. Same-direction cleavage is only found in the 2nd section of the Badong formation, and the cleavage is featured by steep dip angle. In general,

Fig. 3.2 Rose diagram of cleavage strike in Badong county
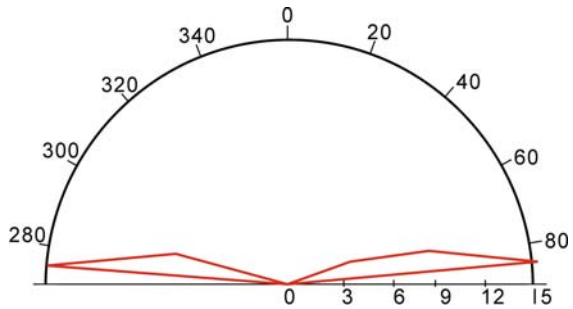
the angle between cleavage and stratum is great (72–90°) in the 3rd section of the Badong formation; that is less (36–60°) in the 2nd section of the Badong formation, an outcome of mud content of the rock mass in terms of higher content of mud and less angle.

(2) *Extent and pattern of cleavage development and relations between cleavage and stratum lithology*: The different stratum lithology has a remarkably diversified extent of cleavage development. For example, cleavage is hard to find in the Jialingjiang formation, but by contrast, the cleavages develop well in the 2nd and the 4th sections of the Badong formation in terms of the cleavage spacing generally of millimeter to centimeter levels; the cleavage is dense in the 3rd section in terms of cleavage spacing of centimeter to tens of centimeter levels as well as thinner stratum develops better than that of thicker one and stratum of higher content of mud develops better than that of lower content of mud; as for the 3rd section, the upper stratum develops better than the lower stratum. In addition, different position of one stratum has different type of cleavage. The cleavage of the 3rd section is typically noncontinuous in terms of separate interface between the cleavage composed of muddy (or sericite) membrane and muddy pelmicrite split rock; and the 2nd and the 4th sections are characterized by continuous cleavages, where the cleavage domain and split rock are hard to differentiate in the open except for visible flake-shape exfoliation along the length of cleavage which extends in the mantle rock.

(3) *Cleavage structure*: Emphasis is given to outdoor and indoor observations and research of the 3rd section, and the result shows gradual and fluctuating development of cleavage instead of a straight and flat face (Fig. 3.3), and the cleavage domain looks like a narrow and long lens. The thickness of the cleavage domain of a dark celadon muddy stratum ranges from nearly 1 to 5 mm; for more careful observation, this stratum is differentiable to several strata (muddy) of less thickness, sandwiched by thin layer of white and fine crystal calcite in the form of a multilayer pie. To observe this stratum under a microscope, the multilayer structure is clear, among which the muddy pelmicrite observed in the open is fine sericite flakes arrayed in a given direction, and the fine crystal calcite stratum develops vertical to the rock wall, with joints vaguely visible at the center (Fig. 3.4).

Fig. 3.3 Cleavage of muddy pelmicrite of the 3rd section of Badong formation

Fig. 3.4 Sketch of microscopic cleavage structure

Calcite veins

Argillaceous film   Marl
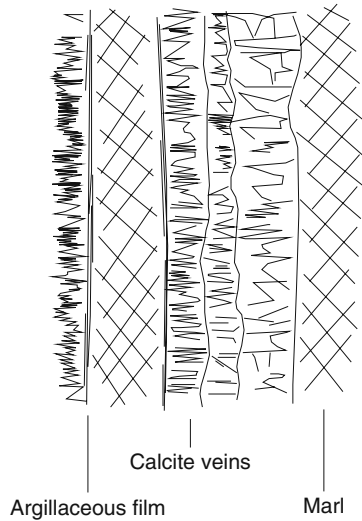
Joint

The joint develops well in the Badong county area, where the pattern of the valley is subject to impact by the joint. The joints in this area can be divided into four groups according to directions, namely, EW, SN, NNE, and NNW.

(1) *EW joint*: It belongs to a longitudinal joint, mainly found in the broad and smooth section from the Guandukou in the riverfront to the core of the syncline, where the joint is flat and straight and unfilled in most of the area as well as of moderate to smooth obliquity. This is a conjugate joint of *s* parallel intersecting line (east–west)

that is probably formed as a result of pressing stress field in adjacent to south–north direction.

(2) *SN joint*: It belongs to transverse joint and falls into shear joints and tension joints as per mechanical quality. The shear joint is steep, level, regular and extends afar (generally of tens to hundreds of meters), and the joint is isometric in transverse direction (normally with spacing of 500–600 m), and this joint group has impact on the valley of Badong county area. The tension joint develops mainly in hard rock mass with a steep joint face, and the face is irregular, nonlinear and generally extends to within tens of meters; most of the tension joints are of the branch end, with the gap filled by calcite range. According to statistics of more than 40 tension joints in the Sidaogou Valley, the mean strike of the joint is 5°, and the predominant direction is concentrated and nearly vertical to the cleavage side. In comparison to the shear joint of the same direction, it extends in shorter distance and is denser in terms of varied spacing within the range of 0.2–7 m.

(3) *NNE and NNW joints*: Both of them are generally in the pattern of conjugate joints and can be found in different lithological sections. Generally, the joints are dense and extend a short distance within the range of several centimeters to less than 20 m. Thus, the direction of main pressure stress in conjugate joints is northeast.

The conjugate joints, SN tension joint and EW joint reflect the stress field of the same structure, i.e., are the main stress adjacent to south–north direction. The SN shear joint probably falls into the group of conjugate joints in terms of direction, but both are hard to match in modeling.

Geological and Construction Property of the Rock Mass Structure in the Badong Formation

Property of Rock Mass Structure

Research on properties of the rock mass structure is accomplished mainly by means of statistics about structural planes and Monte Carlo simulation. Due to many stages of crust movement and impact of the Yangtze River cutting and eroding, the structure joint and unloading fissures of the rock mass of the Badong formation are well developed. The structure of the rock mass is composed only of these structural planes and rock blocks. Therefore, the dimension of structure mass and geometric property of the structure can be determined by means of an analog of combination characteristics, distribution and extension patterns, and the development condition of the structure planes, which is an effective method for studying the structural property of a rock mass.

The bedrock of an example outcrop in Badong county is selected as the section for surveying and statistics, and each of the geometric pattern parameters of each structural plane is measured using the linear statistical method, with nine measuring lines arranged in succession.

The principles of a Monte Carlo network analog are employed to draw the network diagram and networking diagram of bedrock structure planes within the area so as to determine the distribution chart of line density and RQD value of various directions of the section.

The following conclusions can be made through applying statistics of structure planes and network analogs of structure planes of rock mass:

(1) The research shows general development of 3–4 joint groups in the rock mass in this area, and the joints are characterized by steep slope angle (generally of 45–80°) in the directions of adjoining east, NNE, and near west.
(2) The variation of the attitude of the strata is remarkable and uneven, and the interlayer cleavage and secondary fold are well developed due to impact of the structure movement.
(3) Most of the joints are through structure planes, and the trace length measured is tens of meters and intersects with many groups of structural planes. By comparison, the trace length of other structure planes is less, with half the trace length of 1.0–5.0 m and a few of more than 5.0 m; according to the information collected by surveying and statistics, the width of most fissures between structure planes is less than 5 mm and within the range of 1–3 mm, and the fissures are rarely filled and are open. The joints in the muddy rock mass are short and small.
(4) The structural planes have large mean spacing, and remarkable differences exist between different groups of structure plane, generally of 30–300 cm, a minimum of 3 cm and a maximum of 650 cm. In general, the linear density of structure plane is 1.5–4.0 lines/m, some 0.24 lines/m in the least dense area and some 8.34 lines/m in the densest area, with directions of the most concentrated in 5–25°, 55–70°, 130–165° as well as directions of the most densest lines in 15–40°, 85–100°, and 115–170°.
(5) In this area, the RQD value is tremendous at the block diameter of 0.1 m, with mean RQD at various surveying points of more than 90%; and the RQD is less at the block diameter of 0.5–0.7 m, with remarkable differences between various surveying points; most of the values are more than 60%, showing that the rock mass is large in this area. The structure of the rock mass is featured by layered pattern or layered fracture patterns.

Physical–Mechanical Property of the Soft Layer

The physical–mechanical property of the soft layer is very much dependent upon the slope stability. As shown in Table 3.1, the landslide soil, muddy sandwich, and fault mud in the terrain weak zone are of fine granularity and fall into silty clay and have low values of shear strength (slow shear stress) C and ϕ.

Table 3.1 Analysis of physical–mechanical properties of the terrain weak zone and landslide zone of the Badong formation

Sample No.	Moisture content W %	Unit weight r g/cm³	Granule composition 0.25–0.1 %	0.1–0.05 %	0.05–0.01 %	0.01–0.005 %	0.005–0.002 %	Cohesion C kPa	Internal friction angle φ °	Classification according to composition
1#	18.4	1.95	4.7	2.0	15.0	32.4	45.9	20/10	11.3/14	Light silty clay
2#	30.4	1.74	4.6	7.0	23.7	23.8	40.9	88/72	32/31	Light silty clay
3#	11.1	1.95	5.1	3.4	47.3	22.0	22.2	70/60	32/33.7	Light silty clay
4#	37.2	1.45	4.3	3.1	14.8	30.4	47.4	5.0/5.0	12.5/10.3	Light silty clay
5#	16.6	1.69	0.5	4.3	30.8	18.0	46.4	10.0/5.0	19.2/18.4	Light silty clay
6#	11.4	1.89	23.6	8.6	22.6	12.3	32.9	5.0/5.0	19.9/19.7	Light silty clay

Engineering Properties of the Rock Mass

Physical–Mechanical Property of the Rock Mass

The basic physical–mechanical property of the rock of the Badong formation includes: (1) T_2b^2 and T_2b^4 muddy siltstone, the muddy rock is generally of soft rock and sub-soft rock, and most of T_2b^3 are of high strength, with saturated tension strength of more than 30 MPa, fall into sub-hard or extremely hard rock, and physical–mechanical property of T_2b^1 is between the two types of rock as mentioned above; (2) The mechanical strength is subject to impact of structure planes and density, for instance, the mechanical strength and density (minimum of ρ_d=2.3 g/cm^3) of thin marlite and calcareous muddy siltstone are the least, and their spacing rate is the highest (n is up to 1.93–4.72%); (3) The muddy rock varieties are subject to high intenerating, and the softening coefficient of most of the muddy rocks is less than 0.6; by contrast, the pelmicrite varieties are subject to weak intenerating and have softening coefficient of more than 0.75, showing greater impact of muddy rocks (e.g., silty rock, calcareous muddy siltstone, and muddy pelmicrite) to mechanical property; (4) According to the point load test, various types of rock have strong anisotropy, and the rock strength is estimated by the point load strength and the uniaxial strength of rock mass.

Mechanical Properties of the Structural Plane

(1) *Indoor shear test*: The test of the structural plane shows that the shearing strength of the terrain and that of the cleavage is approximately equivalent with identical lithology, and the shearing strength is slightly different with strata of various lithology; for instance, the T_2b^1 is thin marlite and subject to severe weathering, covered with muddy membrane on the surface, and its strength is comparatively lower than that of other groups of rock; C is generally of 5–15 kPa, ϕ is 20–30°, as to T_2b^3pelmicrite, C is 50–100 kPa and ϕ is 30–38°.

(2) *Inverse calculation of cuneiform body and statistics of the bedrock landslide*: According to research and statistics for the landslide of cuneiform body and bedrock of various types of rocks, the shearing strengths C and ϕ of various structure planes are calculated. A total occurrence of five cuneiform bodies are found mainly in the case of T_2b^2 fuchsia, a calcareous muddy siltstone; the sliding plane is composed of a layer and nearly vertical intersecting cleavage plane in all cases. The dimension of the cuneiform body is measured on the spot, and the stability coefficient formula of cuneiform body is applied. The shear strength of the landslide planes (layer and cleavage plane) can be worked out through a random choice of 4 of 5 landslides. Also, the calculated coefficient of shear strength of layers and that of cleavage plane of T_2b^2fuchsia calcareous muddy siltstone is approximately equivalent of $C_{layer}=C_{cleavage}$=6.8–12.8 kPa, $\overline{C}$=8.6 kPa; $\phi_{layer}=\phi_{cleavage}$=26–39.5°, $\overline{\phi}$=35°. The result is slightly less than the value (T_2b^2 layer C=110 kPa, ϕ=38°) of indoor shear test of the structure plane. According to research, the occurrences of landslide of cuneiform body in this area occur in the rainstorm season, when the strength of the

sliding plane is lowered due to rainwater saturation and lubrication, etc.; indoor tests are completed in dry conditions, hence the outcome of inverse algorithm is less than the test data.

Bedrock landslides occur mainly in strata of T_2b^3 and T_1j; in some sections and due to artificial excavation of the slope, the bedrock is bare, and the rock mass loses support, causing a bedrock landslide. This occurrence is similar to a single plane landslide of slope failure, when the slope angle of the sliding plane is approximately equivalent to its friction angle in the condition of limit balance. The approximate friction angle can be calculated through surveying a great amount of slope angles of various sliding planes. The mean friction angle of T_2b^3 pelmicrite $\bar{\phi} = 38°$, basically equivalent to that obtained in indoor shearing tests of the structure plane.

Estimation of Mechanical Parameters of Rock Masses

(1) *Evaluation of rock mass quality*: According to the engineering and geological property of rock masses, the rock mass is divided into four groups, and then evaluations of qualities of various rock groups are applied by means of classification of RMR and Q value (Table 3.2). The results of classification demonstrate that the rock mass qualities estimated with both methods of classification are basically equivalent.

(2) *Calculation of mechanical parameters of rock masses*: The deformation modulus E_m (Gpa) of various types of rock mass can be calculated by means of the RMR and Q values, as shown in Table 3.3. According to the RMR value of various types of rock mass, corresponding C_m and ϕ_m values can be looked up (Table 3.4). The mechanical parameters of various types of rock mass can be worked out by the Hock–Brown estimation method (Table 3.5).

Table 3.2 Classification of rock masses

Item	I	II	III	IV
Stratum lithology	T_2b^2, T_2b^4 siltstone and muddy siltstone	T_2b^3 pelmicrite	T_2b^3 marlite	T_2b^3, T_2b^1 pelmicrite and shale
Q classification	3.29	11.5	3.83	1.01
RMR classification	52	66	54	32
Rock type	Common quality	Good quality	Common quality	Poor quality

Table 3.3 Estimation of deformation modulus of rock masses

	I	II	III	IV
RMR value	52	66	54	32
E_m (GPa)	11.2	32	12.5	3.5
Q value	3.29	11.5	3.83	1.01
E_m (GPa)	12.9	26.5	14.5	0.11

Table 3.4 Strength parameters of rock masses calculated by the RMR classification method

		I	II	III	IV
	RMR value	52	66	54	32
Shear	C_m(kPa)	260	325	270	150
strength	ϕ_m (°)	31	38.0	32	22

Table 3.5 Estimation of mechanical parameters of rock masses by the Hock–Brown method

Rock group	Uniaxial stress strength σ_c (MPa)	Uniaxial stress strength σ_{mc} (MPa)	Uniaxial tension strength of rock mass σ_{mt} (MPa)	Parameters of shear strength of rock masses in different positive stresses	
				Cohesion (Mpa)	Friction angle (°)
				0 2 4 6 15	0 2 4 6 15
I	30	1.12	0.05	0.12 0.47 0.76 0.95 1.86	57 26 21 19 14
II	75	3.18	0.16	0.37 0.81 1.15 1.47 2.64	58 34 29 26 20
III	100	6.32	0.6	1.20 1.59 2.00 2.38 3.65	53 39 34 31 25
IV	20	0.2	0.01	0.03 0.34 0.51 0.69 1.21	61 18 15 13 10

Recommended Parametric Values for Mechanical Calculation of Rock Mass

In integrating various existing data as well as data concerning mechanical property and experience of identical rock mass in relevant adjoining areas and in consideration of factors such as geological and structural properties, etc., of various rock masses in the areas, we recommend the following parametric values for calculation of various rock masses and structure planes, as shown in Tables 3.6 and 3.7

Table 3.6 Recommended parametric values for mechanical calculation of rock masses

	T_2b^4	T_2b^3	T_2b^2	T_2b^1	T_1j^3	T_1j^2	T_1j^1
Density ρ(g/cm^3)	2.55	2.63	2.55	2.35	2.68	2.68	2.66
Deformation modulus E_m(GPa)	2.0	4.0	3.0	1.5	10.0	9.0	7.0
Poisson's ratio μ	0.3	0.25	0.3	0.35	0.2	0.2	0.25
Uniaxial stress strength σ_{mc} (MPa)	0.8	2.5	1.0	0.15	5.0	4.5	4.0
Uniaxial tension strength σ_{mt} (MPa)	0.03	0.50	0.05	0.01	0.5	0.45	0.4
Shear　　　C_m (kPa)	240	400	260	165	1100	1100	1000
strength　ϕ_m (°)	28	38	30	22	41	41	39

Table 3.7 Recommended parametric values for calculation of structure planes

Type of structure plane	Shear strength	
	C_j(kPa)	ϕ(°)
T_2b^3 mudstone layer	60	31
T_2b^3 mudstone cleavage plane	40	30
T_2b^2 calcareous muddy siltstone plane	20	31
T_2b^2 calcareous muddy siltstone plane cleavage plane	8	30
T_2b^1 marlite plane	8	25
T_1j pelmicrite plane	30	32

Typical Landslide of the Badong Formation – Deformation Mode of the Huangtupo Landslide

The Huangtupo landslide is located about 1 km upstream of the old Badong county of Hubei province, on the south bank of the Yangtze River, to the west of Erdaogou, and to the east of Sidaogou. In comparison to the adjoining areas, the Huangtupo is generally smooth in landform with two broad platforms. On one platform is the 1st Senior High School of Badong county and that of Badong Farm Machine factory; quaternary deposition almost accounts for the whole Huangtupo landslide, and beyond it, the bedrock predominates and the quaternary rock mass is sparsely distributed.

Geological Background

The main outcrop of the Huangtupo landslide and adjoining areas is muddy pelmicrite of the 3rd section of the Badong formation, and the outcrop behind the slope belongs to fuchsia marlite and muddy siltstone of the 2nd section of the Badong formation.

The Guandukou syncline is a main structure of this area (Fig. 3.5); the axial trace is adjacent to the east–west direction, a broad fold zone gradually widens, with an SN width of up to 6 km. The slope angles of both flanks are generally of 20–45° (Fig. 3.6). The Huangtupo landslide is in the south wing of the syncline of the dip slope.

The bedrock landslide muddy zone of the Badong formation in the new city zone is well developed. The area accelerating the initiation of the bedrock landslide
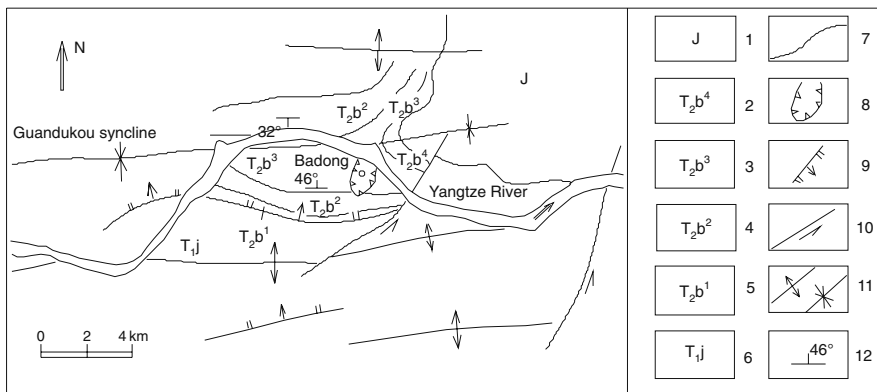
Fig. 3.5 Outline of the structure of Badong new city zone and adjoining areas. 1 – Jurassic System; 2 – the 4th section of the Badong formation; 3 – the 3rd section of the Badong formation; 4 – the 2nd section of the Badong formation; 5 – the 1st section of the Badong formation; 6 – Jialing River formation; 7 – sideline of lithology sections; 8 – landslide; 9 – normal fault; 10 – strike slip fault; 11 – fold (the left is anticline, and the right is syncline); 12 – terrain attitude
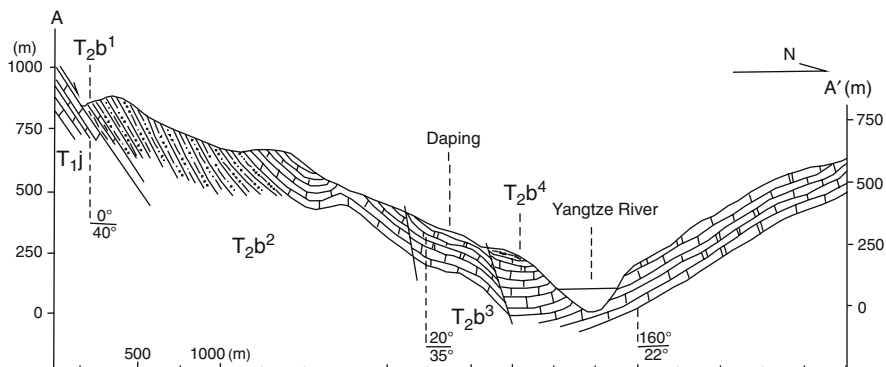
Fig. 3.6 Profile of Guandukou syncline

is where the interface of strong and weak terrains as well as a weak sandwich of the internal terrain locates, among which the former includes the interface between Jialing River stratum and the Badong formation as well as that between the 2nd and the 3rd sections of the Badong formation. The development of a fault of the Badong formation may be attributed to this bedrock landslide; and the latter develops mainly in the 3rd section of the Badong formation.

Figure 3.7 is a section of the Xirangpo Water Diversion Tunnel, where the terrain is formed by the 3rd section of the Badong formation, with length of the section plane of 210 m, wherein 14 bedding faults of various sizes are formed, and an average of one fault every 15 m develops, which is evidently, a dense development of faults; the landslide zones are of different thickness, with majority of the centimeter level and minority of more than 1 m.

The bedrock landslide zone is characterized by a muddy area, breccias muddy areas or breccias areas of low mechanical strength. Four sliding muddy areas in the tunnel are sampled for stress strength test, and the mean shearing strength obtained is $C=13.3$ kPa, $\phi=4°$.

The dip slope, bedrock landslide area, and cleavage contribute substantially to structural deformation during generation and development of the Huangtupo landslide.

Long-Term Deformation of the Slope

According to investigations of the deformation zones on both sides of Huangtupo landslide and the front edge of the riverfront, long-term slope deformation is found in terms of coincidence of toppling deformation and deep creep deformation (Fu & Cai 1996; Carey 1953; Savage & Varnes 1987; Zischinsky 1966).

(1) *Toppling deformation*: The loosely consolidated body of the Huangtupo landslide slopes eastward, and there is a wide area of rock mass of strong deformation,
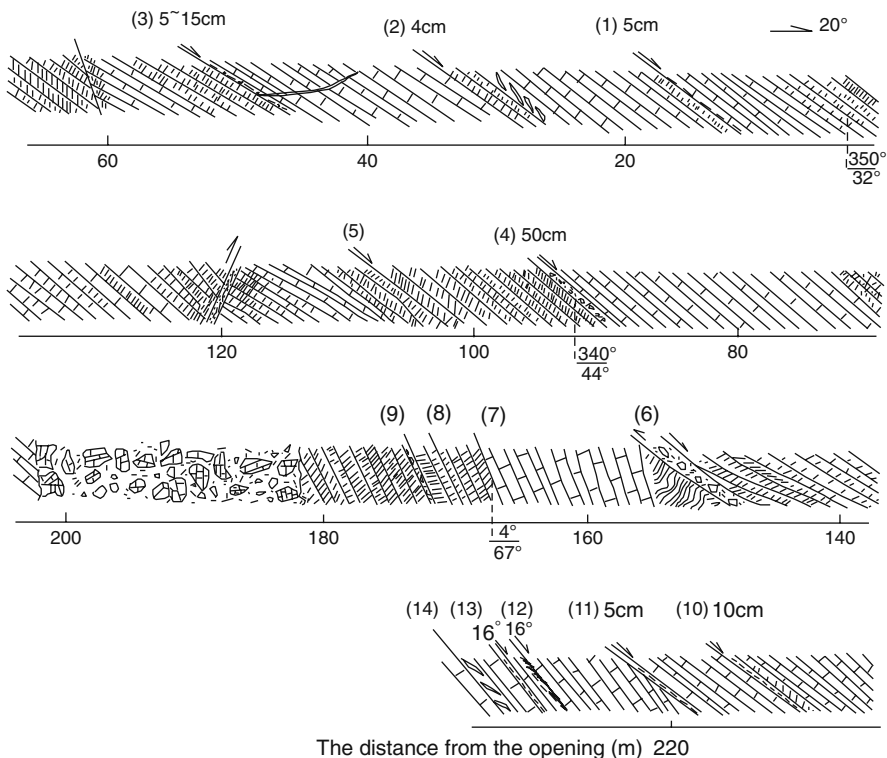
Fig. 3.7 Measured section of the water diversion tunnel on Xirang slope

characterized by toppling of rapidly developing axial cleavage (Fig. 3.8). The toppling deformation causes joint rock blocks to form in a staggered, rotating, and consequently toppling downgrade.

Although the terrain experiences strong toppling deformation, the terrain plane remains intact, and the toppled rock mass and the underlying non-toppled rock mass
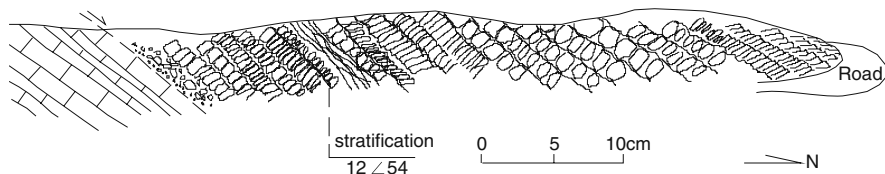
Fig. 3.8 Toppling deformation of cleavage in the east side of Huangtupo landslide
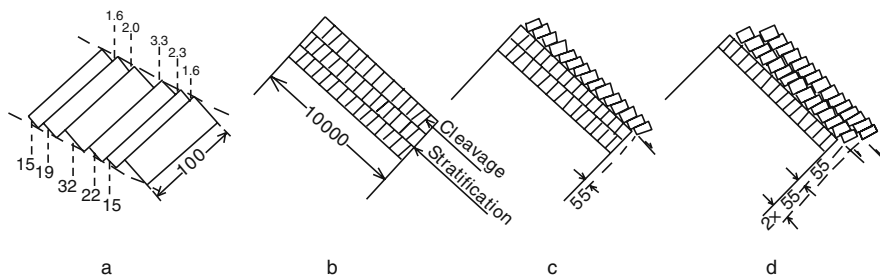
Fig. 3.9 Measurement and modeling of toppling and displacement of cleavage rock of the Emigration Bureau highway slope. a – Measurement of toppling of cleavage rock; the upper figure stands for staggering distance between cleavage rocks, and the lower figure stands for thickness of cleavage rock, in centimeter; b – cleaved single rock mass; c – toppling of cleavage of single rock mass; d – general effect of toppling of cleavage of multilayer rock mass

are separated by the sandwiched bedrock landsliding plane, and it is obvious that slippage of any long distance does not occur.

According to the rotation and staggering (Fig. 3.9a) of cleavage rock of the single terrain observed in this section, the sliding displacement of 0.55 m of the single terrain (assumed of 1.0 m of terrain thickness) of 100 m long in the front end caused by rock toppling can be estimated. Assuming that a terrain section with a thickness of 100 m (assumed of 1.0 m of terrain thickness, see Fig. 3.9b), the top terrain topples first and leads to displacement of 0.55 m in the front of the terrain (Fig. 3.9c); and then another terrain topples (Fig. 3.9d), also with displacement of 0.55 m in the front, when the front end of the upper terrain has a relative displacement of $2 \times 0.55 = 1.1$ m as per its original position $2 \times 0.55 = 1.1$ m; likewise, in the case of toppling of the 100 underlying terrains, the upper terrain has a relative displacement of $100 \times 0.55 = 55$ m.

In the case where the toppled rock masses fail to open along the joint, it causes longitudinal extension of the terrain, which is the cause of bedrock deformation before toppled and deformed terrains; longitudinal sliding is necessary for toppling in terms of space adjustment, and this is why there is often occurrences of displacement of development of toppled rock mass to the dip slope.

The toppled and reconstructed terrain at this observation point remains completely intact stratum; nevertheless, the toppled rock mass observed from the west side of the Huangtupo landslide is a transition of continual and intact stratum to disarrayed rock blocks from inside to outside (Fig. 3.10), and the farthest outer stratum of disarrayed rock blocks of the toppled rock mass is in identical pattern of rock deposition as formed by the landslide.

(2) *Deep creep deformation*: The front edge of the Huangtupo landslide (previously on the riverfront) is adjacent to the core of the Guandukou syncline; and the terrain is of smooth slope and simple structure, thru observing from the river in the west of Huangtupo. The structure of terrain within the Huangtupo landslide area is complicated, for instance, a reverse or knee-type asymmetric fold is found here and there
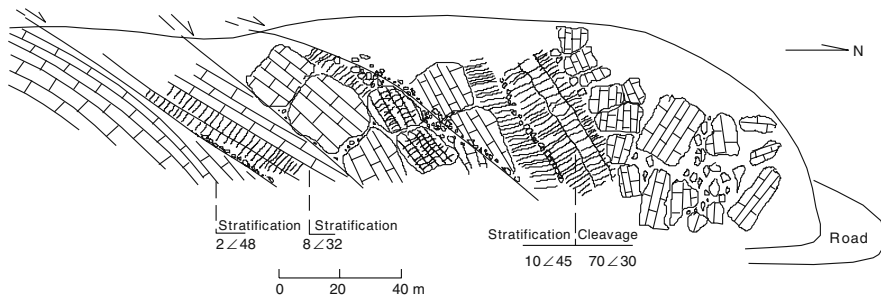
Fig. 3.10 Toppling deformation in the west side of the Huangtupo landslide

(Fig. 3.11), and the fold hinge is near the east–west direction, with axial plane facing the Yangtze River. In addition, smooth shearing slippage is common (Fig. 3.12). The direction of shearing slippage in the upper part is westward.

The deep gully (Sandaogou) of the inner Huangtupo landslide is found to be of loose surface stratum in many places, revealing the deformed rock mass in the deep area. Figure 3.13 shows one of the sections of Sandaogou, T_2b^2 formed fuchsia rock blocks deposit onto T_2b^3 muddy pelmicrite, one reverse fold with intact pattern develops under the interface, and it represents the kinematic property of the upper layer downward along the slope. Fissures develop in the fold, a universal characteristics of fold with a slope of creep deformation. The cleavage still runs in an
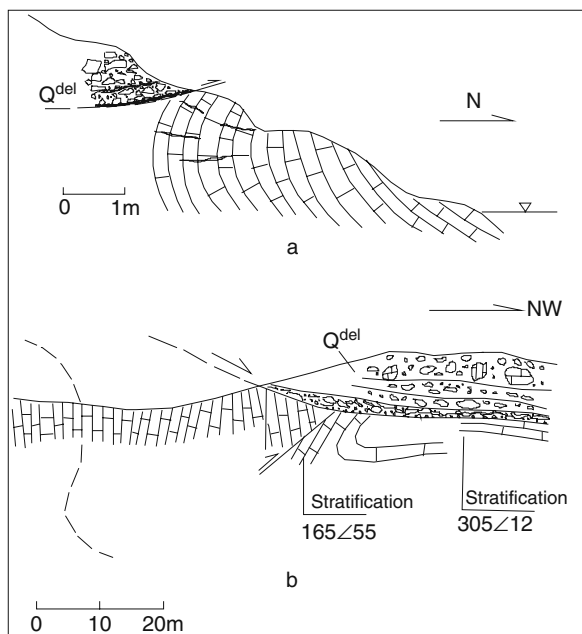
Fig. 3.11 Occurrences of slippage and fold in the front edge of the Huangtupo landslide
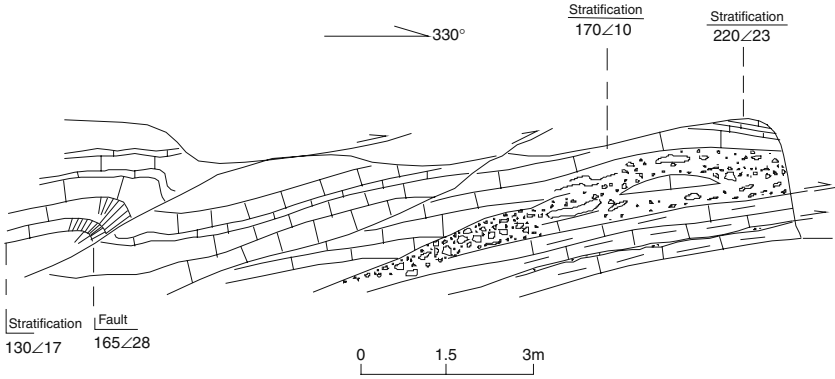
Fig. 3.12 Occurrences of asymmetric fold and shear slippage in the front edge (previously the riverfront) of the Huangtupo landslide

east–west direction, consistent to that of local cleavage, indicating that the fold rock is still part of the bedrock.

According to the fold and shearing slippage as well as the reflected kinematics property, the following characteristics can be concluded: (1) Distribution only in the front edge of the Huangtupo landslide and of loosely consolidated deposition underneath; (2) Small-size fold in terms of outcrop dimension, and the axial plane inclines downward the dip slope, just opposite to the secondary fold, produced coincidently with the longitudinal fold structure in early Guandukou; (3) The terrain fold is an outcome of creep deformation due to long-term gravity effects on the slope rock, which is inconformity to rock blocks produced by rapid deformation
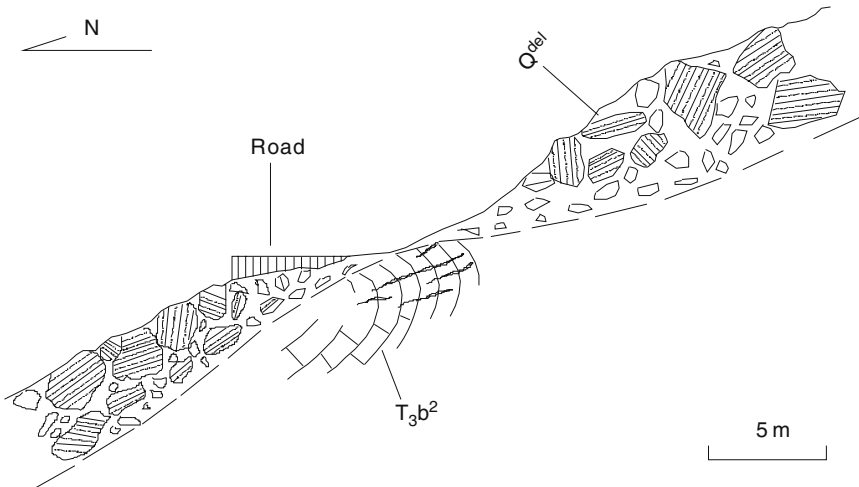
Fig. 3.13 Asymmetric fold and shearing slippage of Sandaogou of the Huangtupo landslide

of the landslide; fold turn generally goes with fissure development, which is different from the fold generated by structural stress action; (4) The movement direction of the upper area of shearing sliding plane faces the dip slope, still opposite to the bedrock landslide caused by the Guangdukou longitudinal fold structure. These characteristics demonstrate that the folds are neither the cause of formation nor the outcome of landsliding; rather, they are results of long-term creep deformation due to gravity. It can be concluded as per the deformation property of the Huangtupo landslide that the deformation is not the cause of formation of local stratum due to limits within Huangtupo domain, and that the deformation is not the outcome of landsliding because of the gradual transition relation of the deformed section and the bedrock. Also the deformation is an outcome of long-term gravity action on the slope.

Landslide

The top stratum of the Huangtupo landslide is composed of fuchsia stone blocks (T_2b^2) of the 2nd section of the Badong formation, merging onto the 3rd section (T_2b^3), with the interfacing pattern distributing in the form of insole in some NE20° as well as longitudinal length of 1100 m and width of 400–500 Mc (Fig. 3.14). The border in the front edge of T_2b^2 fuchsia stone blocks runs some 800 m to the north more than that of stratum border of T_2b^3/T_2b^2; it is obvious that this is the cause of the deposition of the landslide due to the "over-coverage" of such a large area and long distance.

(1) *Pattern of physiognomy of the Huangtupo landslide*: Two levels of platforms develop within Huangtupo. The 1st one has an elevation of 285–310 m, upon which the 1st Badong Senior High School is located, trending EW, 350 m in length and more than 100 m in width, trending SN. The 2nd platform has an elevation of 430–455 m, the Badong Substation and Badong Bus Transportation Co., Ltd are located on top of this platform, and it trends EW with a length of 370 m and an SN-trending width of 150 m. A reverse landform appears in the local section of this platform. The pattern of physiognomy of the platform is sharply in contrast to the straight slope on both sides (EW) of the Huangtupo landslide and difficult to compare with the elevation of the jump stratum, which is probably formed as a result of the landslide; due to variation of slope angle of the landslide's underside, the landslide reflects a corresponding transformation of ground pattern. The elevation is some 600 m in the rear edge of the landslide, with a dimly distinguishable pattern of sliding wall, which is generally an east–west arc physiognomy.

The slope angle is 40–45°, consistent to that of the terrain of fuchsia muddy siltstone of the 2nd section of the Badong formation (T_2b^2). This pattern of physiognomy is not limited to landslides of small size.

(2) *Section structure of the Huangtupo landslide*: The electrical method mapping is completed for the front edge of the Huangtupo landslide by the Badong formation research team from China University of Geosciences in 1997. A better
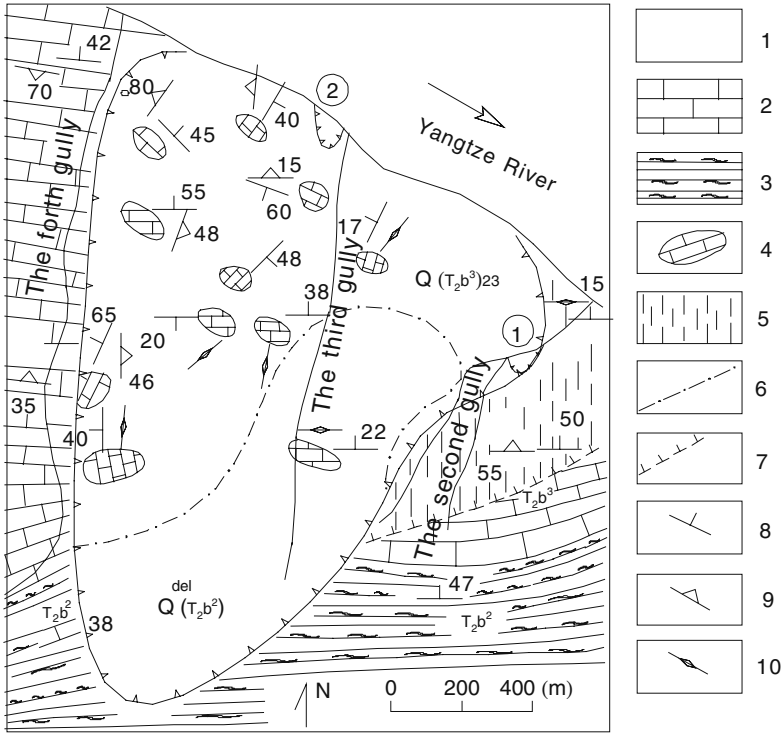
Fig. 3.14 Geological map of the Huangtupo landslide. 1 – The muddy pelmicrite of the 3rd section of the Badong formation; 2 – the muddy siltstone and silty mudstone of the 2nd section of the Badong formation; 3 – the outcrop of loose deposition of stone block (the terrain pattern and cleavage pattern marked alongside); 4 – toppling deformation area; 5 – landslide border; 6 – front border of small size landslide of Huangtupo; 7 – transition border of toppling and bedrock; 8 – terrain pattern; 9 – cleavage attitude; 10 – perpendicular cleavage; Circle 1: Erdaogou landslide; Circle 2: landslide on the west side of Sandaogou

understanding of the geological structure of the front section of the Huangtupo landslide is obtained by the analysis of resistance ratio section. Figure 3.15 (above) shows resistance ratio section of the Huangtupo landslide, and the ratio is obtained thru certain processing of resistance, reflecting the relative value of resistance and eliminating error caused by landform; Fig. 3.15 shows geological explanation as per the resistance ratio section.

(3) *Characteristics of landslide zone development*: Based on observations along the river, the front edge of the Huangtupo landslide and the landslide shear zone between the Erdaogou and Sidaogou are dimly distinguishable, and the following is description of characteristics obtained from two observation points:

Observation point 1: The riverfront 300 m in the east of Sidaogou has an elevation of some 80 m, where a breccia zone with a thickness of 2–3 m develops. The size of the breccias is mixed, ranging from 50 cm to 1–20 cm in terms of size of granules.
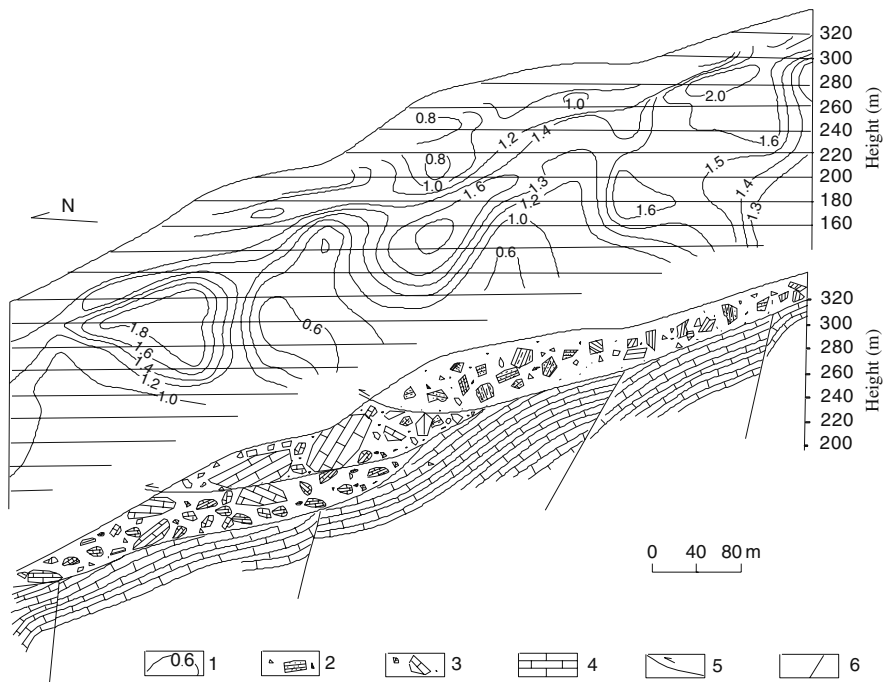
Fig. 3.15 Resistance ratio section (*above*) and geological explanation (*below*) of the Huangtupo landslide. 1 – ratio contour; 2 – stone blocks composed by muddy siltstone and silty mudstone of the 2nd section of the Badong formation; 3 – stone blocks of muddy pelmicrite of the 3rd section of the Badong formation; 4 – pelmicrite; 5 – sliding plane; 6 – fault

The breccias are subject to strong pressure, with individual ones in the form of shredded cabbage as a result of strong pressure and friction as well as released stress, which rebounds and causes surface peeling. The breccias are in the form of calcareous half cementation. The pattern of the breccias zone is $168°\angle36°$, with the underlying terrain reverses; as per the conclusion of the pattern variation, the upper terrain of breccias zone slides horizontally northward (Figs. 3.16a and 3.17).

Observation point 2: The breccias zone 200 m to the west of Erdaogou has a thickness of 1–1.5 m, smoothly inclines northwest ($305°\angle12°$) and is composed of light yellow grey muddy gravel primarily in the form of roundness with manor edges and corners, as well as polished and scraped on the surface (Figs. 3.18, 3.19 and 3.20). The breccias are of various sizes and generally of several centimeters, and the percentage of breccias and mud is 25–65%. The top stratum of breccias zone is composed of fracture rock mass and cracked rock mass, and the cleavage pattern ($220°\angle22°$) is inconsistent with the direction of local cleavage. The bottom stratum is T_2b^3 stratum subject to strong deformation, and reverse fold and pressing fault (Fig. 3.16b), etc., develop. This zone of strong deformation is an outcome of primary creep deformation.

Fig. 3.16 Section of shearing outlet of the Huangtupo landslide. a – 300 m to the east of Sidaogou; b – 200 m to the west of Erdaogou
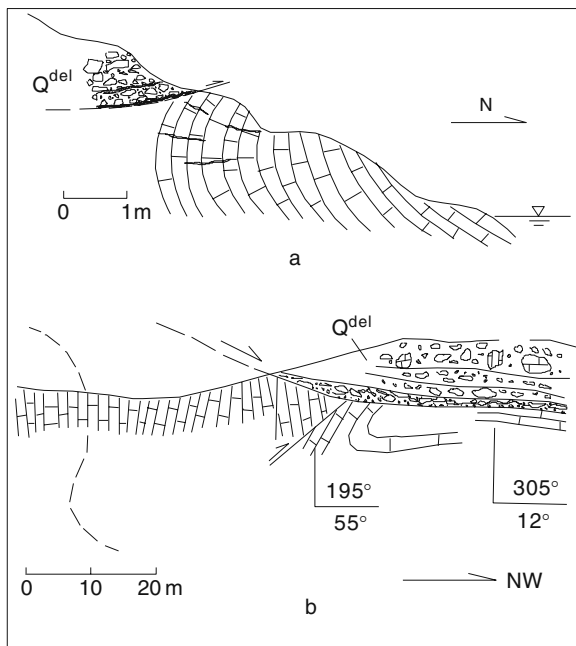
It is demonstrated from various angles that the Huangtupo landslide experiences sliding on the basis of primary creep deformation, including the front edge of the landslide. The rock mass in the Huangtupo landslide is fragmented; although rock masses of large size remained, displacement, staggering, and rotation occurred together, causing discontinuity of patterns of structure planes and lines among rock masses.

Fig. 3.17 Breccias at the shearing outlet in the front edge of the Huangtupo landslide, a shredded cabbage pattern occurs as a result of strong pressure, in the riverfront, 300 m to the east of Sidaogou

Fig. 3.18 Landslide zone in the front flank of the Huangtupo landslide, in the riverfront, 200 m to the west of Erdaogou

Observation point 3: TP3 adit reveals the sliding plane and shows clearly the contact relation between the sliding body and the sliding bedding, as well as the basic property of the sliding zone (Fig. 3.21).

The breccias or muddy breccias zone of large size in the front edge of the Huangtupo landslide (riverfront) is compatible to the loose deposition zone, certainly the outcome of the shearing outlet. Nevertheless, Huangtupo landslide is not formed overnight; instead, it is an outcome of multiple stages, characterized by loss of stability.

Fig. 3.19 Rounding and polish of breccias in the front flank landslide of the Huangtupo landslide, on the riverfront, 200 m to the west of Erdaogou
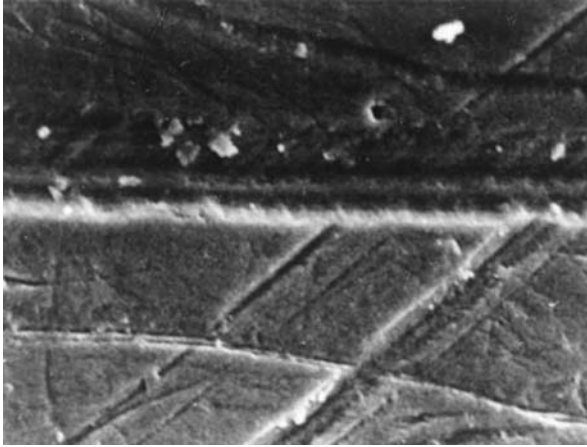
Fig. 3.20 Surface scraping of breccias in the front flank landslide of the Huangtupo landslide, on the riverfront, 200 m to the west of Erdaogou

Fig. 3.21 Characteristics of the outcrop of the sliding zone
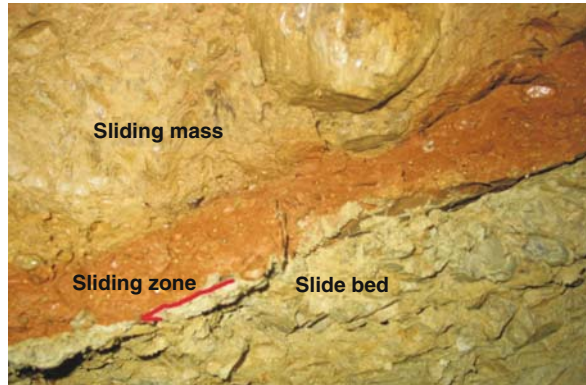
Subsequent Reform of Landslide

The Huangtupo body with long-term slope deformation and sliding mass consists mainly of muddy stone blocks, and then it was subjected to reconstruction of tens of and even hundreds of thousands of years' weathering and denudation up until the present pattern.

On June 10, 1995, a landslide occurred on the top stratum of Erdaoqiao, with the landslide plane in the form of a sector in terms of longitudinal length of 100 m, maximum width of 90 m, thickness of 5–13 m, and volume of $6.7 \times 10^4 \text{m}^3$. The landslide body slid toward Erdaogou from the east side, NW of Erdaogou; the landslide occurs in the deposition of stone blocks composed of T_2b^3. The direct trigger of this landslide was loading of solid waste and life water in the rear edge. The landslide occurred on the edge of the east side of the Huangtupo landslide; it was not caused by movement of the Huangtupo landslide, but by local reconstruction (Fig. 3.22).
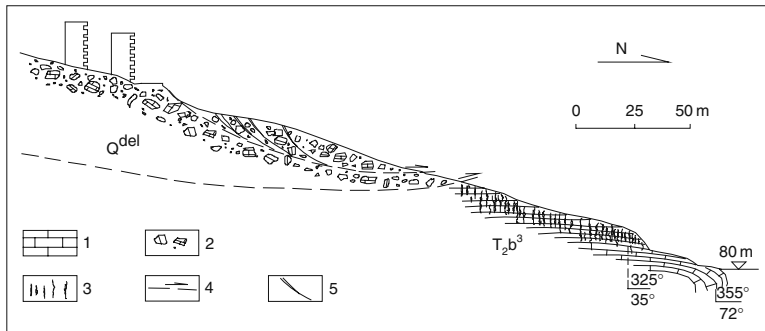
1. Pelmicrite; 2. Stone blocks deposition of landslide; 3. Cleavage; 4. Sliding plane; 5. Tension fissure

Fig. 3.22 Profile of Erdaogou landslides. 1 – Pelmicrite; 2 – stone blocks deposition of landslide; 3 – cleavage; 4 – sliding plane; 5 – tension fissure

On October 29, 1995, a landslide occurred in the west side of the Sidaogou outlet, which was in the form of a long sector with length of some 200 m, maximum width of around 100 m, and volume approximately of 20×10^4 m^3. The rear edge of the landslide had an elevation of some 150 m, sliding NE into the Yangtze River. The direct trigger of the landslide was rainfall and the fluctuation of water level of the Yangtze River. The landslide occurred in the stone block deposition of the Huangtupo landslide, identical to that of Erdaogou landslide in terms of an outcome of subsequent reconstruction of the Huangtupo landslide.

The occurrences of minor landslides in the Huangtupo area are reactivations of the ancient Huangtupo landslide. The stone blocks, forming the deposition of the Huangtupo landslide, are the physical preconditions contributing to the later, minor landslides due to their loose structure; in like manner, the river was flowing and washing, and gully washing produced steep landform, which led to powerful movement of landslides. Rainfall, fluctuation of water level of the Yangtze River, and possible earthquakes are direct triggers of landslides.

Landslide Evolution Pattern

According to conclusions provided through study of the formation and the evolution of the Huangtupo landslide, we can draw the chart of landslide evolution pattern, as shown in Fig. 3.23.

The 1st phase (a), slope development, river washes downward and causes formation of the Huangtupo slope;

The 2nd phase (b), deformation of the slope due to long-term action of gravity, the river washes out, in a continuous, downward motion , the front edge of the slope is hollowed, with toppling deformation in the shallow section. The surface rock mass disperses and rolls out along with the occurrence of loosely consolidated deposition; the shear strength concentration zone in the deep slope forms and develops and causes creep deformation;
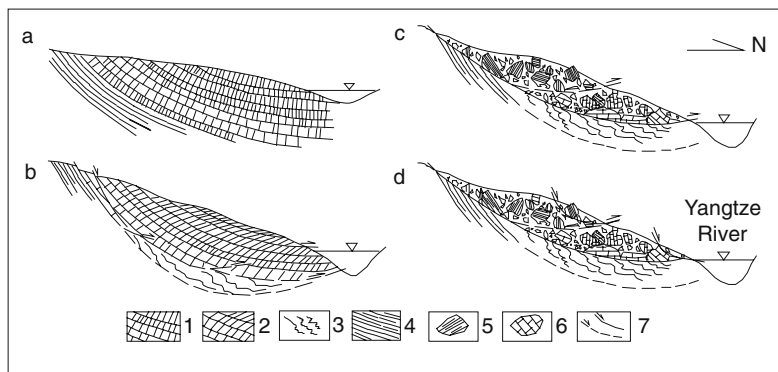
1. Cleaved muddy pelmicrite; 2. Toppled and deformed cleaved muddy pelmicrite; 3. Creep landslide zone; 4. Muddy siltstone; 5. Stone block deposition; 6. Landslide plane

Fig. 3.23 Slope deformation and landslide pattern of the Huangtupo landslide. 1 – Cleaved muddy pelmicrite; 2 – toppled and deformed cleaved muddy pelmicrite; 3 – creep landslide zone; 4 – muddy siltstone; 5 – stone block deposition; 6 – landslide plane

The 3rd phase (c), landslide phase, when the river washes out continuously downward, due to the long-term deformation which develops to certain extent, and some creep sliding deformation planes intersect and lead to a large-size landslide;

The 4th phase (d), reconstruction phase, when local reconstruction of the landslide occurs as a result of variation of external condition and on the basis of large-size landslide.

Conclusions

(1) The strata of the Badong formation are distributed widely in the Three Gorges reservoir area, where it tends to form large-size landslides and deep loosely consolidated geological body; hence it is a typical slide-prone stratum.

(2) The strata of the Badong formation in the Three Gorges reservoir area can be divided into five sections, and the lithology combinations are characterized by sandwich of soft and hard strata. Spatially, the lithology and lithological combinations are characterized by unique law of variation.

(3) The strata of the Badong formation are characterized by rich variation, an outcome of long-term slope deformation as well as all-important evidence for understanding the triggers and mechanism of landslide formation.

(4) The Huangtupo landslide is representative of the development of the Badong formation, along which the major deformation and destruction are important evidences in studying division of landslide development phases, landslide formation mechanism, landslide subsequent reconstruction, and landslide evolution pattern.

References

Carey SW (1953) The rheid concept in geotectonics. Geol. Soc. Aust. J., 1: 67–117

Fu ZR, Cai XL (1996) Tectonics of Epimetamorphic Rock Region. Geological Publishing House, Beijing, 21–32

Savage WZ, Varnes DJ (1987) Mechanics of gravitational spreading of steep-sided ridges ("Sackung"). Eng. Geol., 35: 31–36

Wu YF (1996) Huangtupo landslide and its geological background. In: Cui ZQ, Deng QL (eds.) Paper Collection on Geotechnical Engineering. China University of Geosciences Press, Wuhan, pp. 93–97

Zischinsky U (1966) On the deformation of high slopes. Proc. 1st Cong. Int. Soc. Rock Mech. 2: 179–185

Zong LX, Yin YP, Tang C (1996) Geological study on the new Badong County site in the Three Gorge Reservoir area planned to move. In Paper Collection of the Institute of Environment & Geology, Ministry of Geology and Mineral Resources. Geological Publishing House, Beijing, 1: 41–53

Chapter 4
Distribution of Dangerous Rockmasses on the High Steep Slopes in the Three Gorges Area

Xuanming Peng, Lide Chen, Bolin Huang, and Zhoufeng Chen

Abstract The locality features of high steep slope and dangerous rockmass in the section of a 63 km-long valley in the Great Three Gorges area are described by authors on the basis of the site investigation and geological mapping result of many field surveys. There are 12 high, steep dangerous rockmasses in the area which are described, as is the monitoring situation. The high and steep slope in the valley section is controlled by stratum lithology and locality feature, and hazard of dangerous monomer rock is mainly subject to the lithology and fracture combination, along with human activity.

Keywords Valley section · Three Gorges · High steep slope · Dangerous rockmass · Local features

Introduction

The study site is located in the middle reaches of Yangtze River, the section of the Great Three Gorges between Fengjie county and Yichang city, on the junction area of the mountain chain which includes Dabashan Mountain, Wushan Mountain, and Jingshan Mountain, where the level II cascade of the three great geological cascades in China is located. From the west to the east, the Yangtze River valley is deep and forms a typical middle mountain and gorge valley morphology. The overall mountain chain grows higher toward the near transmeridional, but parts of it go toward the southeast, which is almost parallel to the direction of regional tectonic line. When the river cut the bevel or transverse tectonic line, the resulting valleys there are bevel-oriented or transverse-oriented. The crest elevation is between 1,000 and 2,000 m, and the relative height is between 800 and 1,500 m. The terrain flattens somewhat around Xiling Gorge in the lower reaches with the relative height of about 300–1,000 m. The valley in the Yangtze River area is rather narrow, and the slope

X. Peng (✉)
Yichang Center of China Geological Survey, Yichang, 443003, China

there is steep; generally the main river is wide, at between 150 and 300 m, and the narrowest section is only a little more than 90 m. The bank slope angle is primarily between 35 and 55 degrees, but some are 75 degrees.

This area is one of the places where the geologic hazard occurs frequently. In order to support the construction of the Three Gorges Project, the Ministry of Land and Resources of China carried out geo-hazard investigations at a mapped scale of 1:100000 in 19 counties in the area, and at three different times geological hazard treatment was applied. The related engineering prevention works or the monitoring pre-warning works for the sea routes that could have been blocked were applied, for the bank slope that could possibly constitute a threat to passing ships. Along with the impounding of the Three Gorge reservoir, the navigation condition in Three Gorges area improved greatly and there will be 3–6 ships passing each minute. The threat to ships by rockfall or collapsed rock happens from time to time, which will bring more risk to navigation. Currently, the China Geological Survey performed an investigation on high steep bank and slopes as well as the dangerous rock, which will be helpful in providing the relational basis for the operating safely and for pre-warning of dangerous rock and falling stone as they affect sea routes.

Geological Background for High Steep Bank Slopes and Dangerous Rockmasses in the Three Gorges River Valley

Basic Features of Rock and Soil

In accordance with the formation, tectonic type and physical mechanics nature, the rock and soil can be divided into four construction types and eight engineering geological rock groups (Yin 2005).

(1) *Magmatite and metamorphic rock construction type*: This includes two types of hard block type: magmatite and harder strip or block schist. The former is composed of granite, diorite in Silurian Period, and is distributed in the anticline core section of Huangling. The new rock is hard and has good completeness; the latter is composed of cluster schist, gneiss, magmatite in Proterozoic Kongling and are distributed in the anticline contour of Huangling.

(2) *Clastic rock construction type*: This type is mainly distributed in the section of Fengjie and Zigui basin in this area, and it can be divided into approximately three rock groups, i.e., (a) hard and thick sandstone group. It is mainly composed of thick-thickest feldspathic sandstone, quartz sandstone, conglomerate, and siltstone, with sparse amounts of mudstone, shale, and thin coal beds. All of them are distributed in each anticline core section, East of Chongqing, i.e., it is late Triassic Xujiahe and Jurassic Shaximiao Formation, Penglaizhen Formation, together with the middle Devonian and Sinian Nantuo Formation and Liantuo Formation distributed east of the Three Gorges; (b) the soft and hard sandstone and

claystone interbedding rock group. It is mainly composed of thick-thickest lamellar feldspathic sandstone, quartz sandstone, siltstone and other mudstone, and shale that are of different thicknesses and shows an interlayering type. It is also associated with the Lower Jurassic which contains marlite, bioclastic limestone, and a thin coal seam, etc., which are distributed in Zigui basin, but primarily in Jurassic strata; (c) The rock group with the soft and weak claystone as the main body: it is mainly composed of thick-thickest (block) mudstone, sand mudstone, and strip shale, with medium-thick lamellar sandstone, gypsic horizon, and coal seam, all of which is distributed in the syncline wing of eastern Sichuan and the syncline contour of Zigui.

(3) *Carbonate rock construction type*: Mainly distributed in the gorges east of Fengjie, it can be divided into two engineering rock groups as per the features of lithology combination. They are (1) the rock group with the hard carbonate as the main layer. It is mainly composed of most strata of the middle or low Triassic, Permian, Carboniferous, Ordovician, Cambrian period, and upper Silurian period, with shale and thin seams contained within. Since the carbonate rock in this group is hard and intact, making the slope relatively stable, it forms the steep Yangtze River Three Gorges, the Daning-he Small Three Gorges, and other valleys. Some deformation is mainly under the control of a soft and weak interlayer; (2) This is the lamellar and nubby carbonate rock and clastic rock interlayering rock group with a soft and hard layer. It is mainly composed of Triassic Badong Formation (or Leikoupo Formation), and Permian strata (except Changxing Formation), Carboniferous, Devonian, and Cambrian and are mainly the lamellar limestone, dolostone, mudstone, and sandstone, with coal beds, bauxite, hematite, phosphorite layer, and others. The rock in this group constitutes the stability of the bank and slope, is mainly under the control of the weak layer, and the interface of the soft and hard layer. Most of the rock in this group forms dangerous rockfall and landslides.

(4) *Loose ground group*: It is mainly characterized by the deposition of eluvium, alluvial, and colluvial materials, which are scattered along the floodplain, terrace, and slope. Because of the weak strength and non-cementation, this material can move along the top side of the underlying rock under external force.

Basic Features of the Weak Structural Plane of Rock and Soil

In view of the failure condition of rockfall or landslide, the weak interlayer and weak structural plane play a very obvious role in rockmasses, especially in hard and massive rockmasses. The soft layer (plane) in this area is mainly composed of the following types, i.e., (1) the weak interlayer in the rock system with coal seam. Taking the dangerous rockmass in Lianziya as a typical example, the dangerous rockmass at the top is the Qixia Limestone, but Liangshan coal measure strata underlies it. Cal excavation (including the bauxite), which makes up a layer of the

dangerous rockmass, is being heavily mined and eliminated. The upper Permian Longtan Formation, upper Triassic Xujiahe Formation, and low Jurassic Xiangxi Formation belong to this type. The coal seam, or carbonaceous shale, shale or mudstone, bauxitic claystone and others contained, which belongs to the weaker layer, forms multiple weak interlayers. Not only does this constitute a sliding plane but also the soft bedding causes the slope on the top to be deformed. (2) The weak interlayer in the thick and thickest carbonate rock. The dangerous rockmass in Lianziya in Three Gorges is the typical structure of the rockmass. In the Qixia Limestone, there are multiple layers of thin carbonaceous shale or shale occurring frequently, all of which constitute a key structural plane to cause the thick limestone to be deformed. (3) The mud interlayer in clastic rock layer. It can be seen in the mudstone of the Jurassic period. The basic formation condition is that the mineral in the claystone constitutes the medium-hydrophilic montmorillonite, constituting a high content, as well as being located in the belt where there exists a strong influence for structural change (such as the syncline axial region and lifting origin, or the anticline leaning origin), the fault movement (slip), and fractured broken belt formed under the force of discontinuity; and by the force of water, the claystone mud with the high content of broken hydrophilic mineral was changed into sub-clay. (4) The structural interlayer plane of clastic rock type: the structural interlayer plane in this rock group is mainly divided into three types as per the contact relationship of different lithology, i.e., sandstone–sandstone, mudstone–mudstone, sandstone–mudstone. (5) The structural interlayer plane of carbonate rock type. It includes the structural interlayer plane of limestone–limestone, marlite–marlite, limestone–marlite and so on. Its intensity reduces in turns, and the intensity of the new structural plane is less than the old one. (6) The structural plane of the middle layer in coal strata: It includes the interface between coal seam, carbonaceous shale, shale, bauxite, and other weak terrain, limestone, and sandstone; especially when they constitute the bottom layer and downside slope, the hard rock on the top can fall or slide down along them.

Features of Rockmass Structural Plane

The formation of risk-prone rockmass and the structural plane of rockmass has a close relationship (Xiao & Yang 1999). In order to analyze the relationship between dangerous rockmass, high steep slope and structural plane, the authors made a statistical comparison based on the structural planes of 7794 joint fissures in 150 river sections gathered in the dangerous rock and high steep slope zone, i.e., Qutang Gorge and Wu Gorge, and found that the advantageous structural plane is distributed parallel to or crossed with the tectonic line (Yichang Centre of China Geological Survey 2001). The X joint grows, and the unloading fissure keeps trending after the structure, and thus, the structural joint grows. Under an advantageous free face condition, these structural planes blend with the surface fracture or landslip layer and will be inclined to form dangerous rockmasses in the high and steep slopes and banks of the reservoir area (Fig. 4.1).
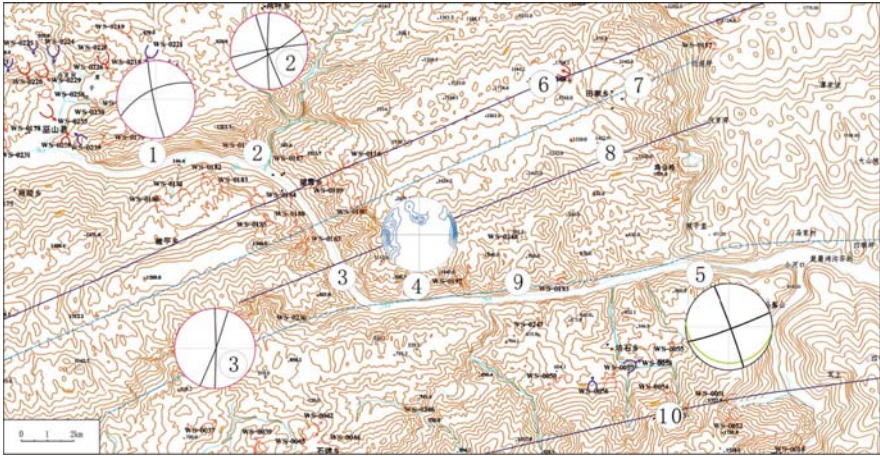
Fig. 4.1 The relationship between the formation of the structural plane in the Wu Gorge section in the Three Gorges reservoir area and the distribution of key dangerous rockmass and the regional geological tectonic line. 1 – Stereographic projection of the structural plane of upper Wu Gorge; 2 – stereographic projection and structural planes of Hengshixi DRM; 3 – stereographic projection and structural planes of Jianchuandong DRM; 4 – apices isopycnic drawing and structural planes of Jiandaofeng rockfall 5 – stereographic projection and structural planes of Huangyanwo DRM; 6 – Hengshixi anticline; 7 – Chuanjianxia syncline; 8 – Shengnufeng anticline; 9 – Guandoukou-Shengnuxi syncline; 10 – Maozishan anticline

Distribution Features of Dangerous Rockmasses in the Three Gorges Reservoir Area

Profiles of Dangerous Rockmasses

In 1999, the geological hazard pre-warning engineering project "Geological hazard survey and construction of monitoring and pre-warning system in Three Gorges Region" under Chinese Land and Resource Survey program was executed. Under the organization of Geological Environment Bureau of China Ministry of Land and Resource Department as well as China Geological Survey, a wide geological survey (1: 100000 in mapped scale) was made in the 19 counties (districts) in the Three Gorges reservoir area with a total area of 54,175 km² covered by China Geological Environment Survey Academy as the pioneer. Through the investigation, a total of 5,706 hazard sites were found and recorded for the investigation, among which there are 3,830 sites for landslide, 67%; 549 sites for rockfall, 9.6%; 90 sites for debris flow, is 1.6% (Fig. 4.1). Most of them are small geological hazards and the recorded number is 3,658, 64.11% of the total number; 93 large geological hazard sites, which is 1.6% of the total number of geological hazard sites.

From Sandouping, the site where the Three Gorges dam built, to Chongqing city, there are a total of 214 landslide and rockfall sites along the banks of the Yangtze River, existing on a length of roughly 600 km. It covers over 50 km², and the total

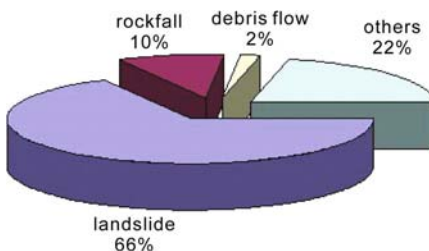**Fig. 4.2** Pie graph of geo-hazard quantity in Three Gorges reservoir area

rockfall
10%

debris flow
2%

others
22%

landslide
66%

Unit: m³

$V = 100*10^4-500*10^4$
$V = 500*10^4-1000*10^4$
$V = 1000*10^4-3000*10^4$
$V = 3000*10^4-5000*10^4$
$V >5000*10^4$

$V = 50*10^4-100*10^4$

$V < 50*10^4$
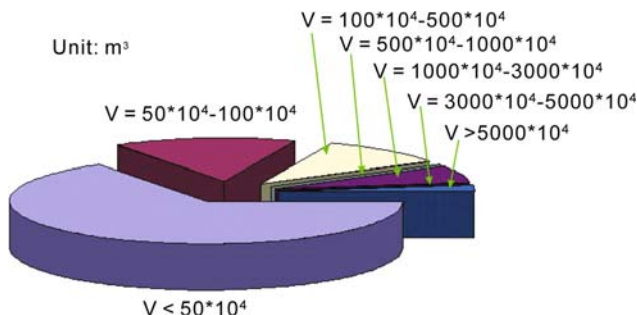
Fig. 4.3 Statistical pie graph of rockfall scale on both banks of the Yangtze River

volume of landslide and rockfall is 1,352 million m^3, among which the landslide is found in 47 places with a volume of 117 million m^3, is 21.96% of the total amount, and is 8.6% of the overall volume. All these rockfalls are mainly distributed on the high and steep slope on both banks and are mostly centered in the three valleys known as Xiling Gorge, Wu Gorge, and Qutang Gorge; meanwhile, the rockfall scale is mainly medium and small; those of less than 1 million m^3 are in 38 places and are 80.8% of the total number of rockfall sites (Figs. 4.2 and 4.3).

Description of the Key Dangerous Rockmass

The main purpose of the current investigation is aimed at the dangerous rockmass in the tributary stream and 1st level branch stream in the Yangtze River. This rockmass could pose a threat to passing ships when the Three Gorges Reservoir is impounded. Through the investigation, the key dangerous rockmass was mapped at the scale of 1:2000 (Fig. 4.4). This chapter will not describe the Lianziya dangerous rockmass which has already been described in detail by predecessors and has already had an efficient engineering treatment.

The special geological condition brings up the topic of the Lianziya dangerous rockmass, which is well known as it is on the opposite bank the Xintan landslide, located in the Xiling Gorge area. Meanwhile, there are plenty of dangerous rockmasses distributed, that are of different size. After an overall investigation in 2006

Fig. 4.4   Regional map showing the locality of the important dangerous rockmasses in the Great Three Gorges River valley

and 2007, the authors will give a brief introduction for 12 important dangerous rockmasses (Fig. 4.1), for example, Jianchuandong, that are evaluated by the investigation (outlined in this text), but as mentioned, the Lianziya dangerous rockmass will not be covered here.

Currently, China Geological Survey has already placed the important dangerous rockmass in this area into the special monitoring system, and the related monitoring and study work is still being carried out.

Fengxiangxia Dangerous Rockmass in Qutang Gorge

The Fengxiangxia dangerous rockmass is located in the SE wing of Qiyaoshan anticline in Qutang Gorges, which is also in the NW wing in the closed Qidaomou syncline. The dangerous rockmass consists of hard dolostone and limestone of Triassic Jialingjiang Formation, which dips toward SW a little. The dangerous rockmass is 120 m long, 5–10 m wide, and 10–30 m high, with a volume of almost 1,2000 m^3. The reach of the Yangtze River is separated transversely into the Qidaomen anticline and the Fengxiangxia syncline respectively from the NW to the SE, which two belong to the NW wing of Qiyaoshan anticline, with steep cliff stand at both banks. The Fengxiangxia dangerous rockmass is located on the north bank, which is dominated by a bottom weak dip angle interlayer (Fig. 4.5) and Qidaogou gulch on the east side, developed with a long and large fissure in the steep dip angle in the northeast direction, and thus forms a creep-tense mode dangerous rockmass (Zhang 1997). As to the unsteady feature of which is a threat to the Yangtze River sea route, it is worthy of making a further study.

Hengshixi Dangerous Rockmass in Wu Gorge

The Hengshixi dangerous rockmass in Wu Gorge is located on the right bank of the entrance of Hengshixi brook at the north bank of Wu Gorge, is configured in the northwest wing of Hengshixi anticline, and consists of M1# dangerous rockmass on the top and M2# dangerous rockmass at the bottom (Fig. 4.6).

M1# dangerous rockmass consists of hard limestone of Permian Qixia Formation. The dangerous rockmass is located in the middle of a ridge-shaped chine
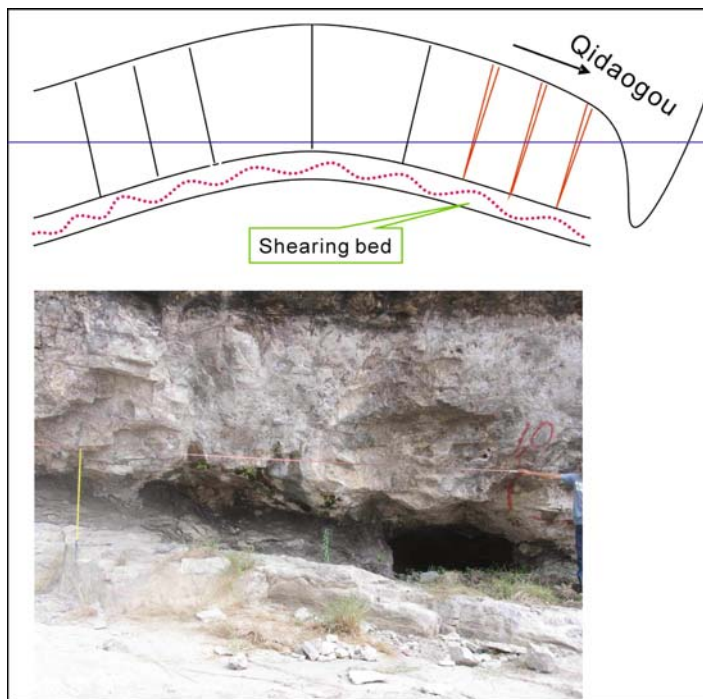
Fig. 4.5 Creep-tense mode of dangerous rockmass in Fengxiangxia Gorge and its underlying large cutting belt between layers (the scale in figure is 1.5 m)

formed by the Yangtze River and Hengshixi brook, three sides of which are free faces. The rear contour features tensile and jointed breakage, with a long, large through joint forming inside, which cuts through the dangerous rockmass and causes it to be broken. The M1# dangerous rockmass is 27.7 m long, 11.2 m wide, 76.8 m high and is 23,700 m^3 in total volume. Due to the effects of excavating coal in previous years, the coal-bearing Permian Ma'an Formation underneath the Qixia Formation deforms severely, which gives the rockmass formation an external-oriented, reverse and open breakage. In accordance with investigation, it is found that the root of the dangerous rockmass has already formed a subsiding pit with a depth of 16 m, which can be seen at the toe of the dangerous rockmass (Fig. 4.7).

The M2# dangerous rockmass is composed of the Silurian Shamao Formation sandstone, limestone and weak sand shale underneath, and the near rock layer is generally toward the NW with an angle between 25° and 35°. The rockmass is broken, and it is broken structurally. Due to the effects of cutting the slope to build a simple road, the right side of the dangerous rockmass had already collapsed during this process, and a triangular free face was formed. Meanwhile, the localities toward the east and Hengshixi Brook are also free faces. The rear of the dangerous rockmass is a beveled formation with the sheared breakage of Hengshixi Brook (or almost parallel), and it is controlled by the underlying rockmass that contains the

Fig. 4.6 The Hengshixi
dangerous rockmass

broken structure and the shearing joint. The M2# dangerous rockmass is 25 m long, 12 m wide, 117 m high, and is 31,800 m³ in total volume. Currently the dangerous rockmass is creeping and will constitute a huge thread to the coal mine wharf and vessels in the surrounding area, so a further study on its formation origins is necessary in order to make an evaluation of its stability, and subsequent reasonable disposal plan for the possibility of problems.

Tongxincun Dangerous Rockmass in Wangxia Village, Wu Gorges

The Tongxincun dangerous rockmass in Wangxia village is located in the left bank of the Yangtze River in Wushan county in the Great three Gorges area, and it is 11 km away from the new county site of Wushan county. The dangerous rockmass is in the core section of the Hengshixi anticline, where the stratum is flat with an angle of 340° ∠ 5°; the slope body is composed of Permian Gufeng Formation (Pg), Longtan Formation (Plt), and Wujiaping Formation (Pw). The lithology of Pg is black lamina shale, lamina argillite, and lamina dolostone; Plt is grey thick shale, lamina sandstone with coal contained within, and the Pw is grey dark lamina silicon limestone and lamina shale. The flat section is composed of mainly shale, whereas

Fig. 4.7 Longitudinal section plan of actual measuring project geology for Hengshixi dangerous rockmass (M1#). (1) Subsiding pit; (2) siltstone; (3) quartz sandstone; (4) shale; (5) limestone; (6) coal bed
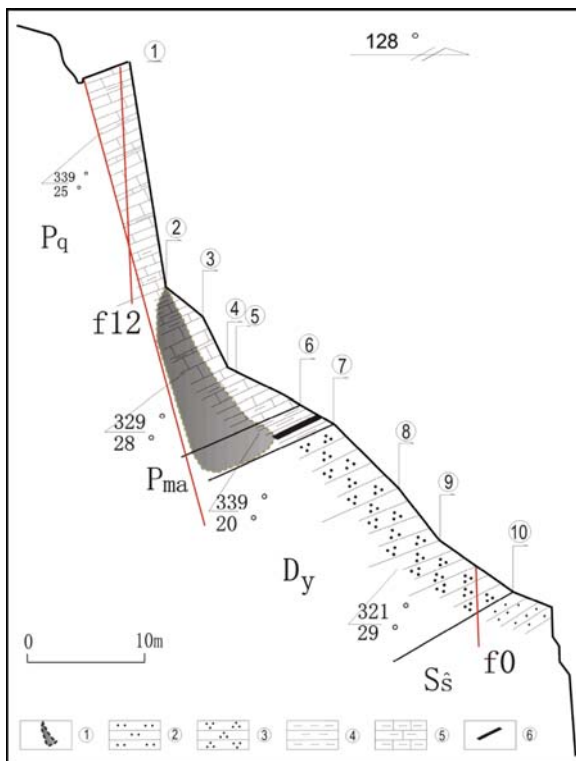
the steep section is mainly composed of the mixed layer of argillite and limestone. The K2 coal bed (Plt coal bed) in the slope body has already been excavated; it is located at the bottom of Pw, black, with glossy metal and lineation, and is distributed in a strip type. It has a shell-shaped breaking edge, crisp, but less hard and it is easy to become pulverized. The coal layer has top and bottom layers, the top layer is about 0.3–0.5 m thick, the bottom layer is about 0.3–0.8 m, and the middle interlayer is the shale with a thickness around 0.4–0.8 m. The coal mine is designed for a one-time excavation, and a wooden column is used to support the lane; the top plate to excavate coal is the thick lamination limestone, each layer is around 8.6 m thick; the motherboard is the bauxite with the thickness between 0.8 and 2.0 m.

This dangerous rockmass is located on a slope with an elevation of between 1,100 and 1,250 m, the slope root is a flat slope within its 30 m, the slope gradient is 30°, but the top is almost a 90° cliff. In the last 10 days of July, 1999, the dangerous rockmass in this slope happened to deform severely. There are six large fractures that exist in the slope, and a dangerous rockmass cluster with the dimensions of 230 m in length, 50 m in width, and 115 m high was formed, and its total volume is about 1.32 million m^3. The fracture in the free face of the rockmass widened about 20 cm in 1 week, and the dangerous rockmass that is separated from the mother rock is around 8.6 m long, 15 m wide, and 75 m high with a total volume of 1,000 m^3

Fig. 4.8 Tongxincun
dangerous rockmass

Fig. 4.9 Subsiding pit on the
top of the dangerous
rockmass

(Fig. 4.8). There are subsiding pits at the top that have a diameter of roughly 10 m
(Fig. 4.9). After collecting statistics on the fracture in the cliffs of several rockmass,
it was found that two groups of advantageous joints grow inside the rockmass, i.e.,
90–100° ∠ 80–85°, 165–174° ∠ 75–82°. The two groups of joints are vertical with
each other and form the boundaries of steep cliffs and dangerous rockmasses. Its
damage mechanism is the subsiding-bevel lifting mechanism together with human
excavation activities. This dangerous rockmass constitutes a huge threat to the local
residents, the mineral company, and the sea route.

Liaojiaping Dangerous Rockmass in Wangxia Village, Wu Gorge

Located on the left bank of Wu Gorge, Yangtze River in Wushan county, Liaojiaping
slope is about 11 km away from the new county site of Wushan county. It is in the

Fig. 4.10 Liaojiaping
dangerous rocks group

core of Hengshixi anticline. On the east side of the Liaojiaping slope, there is gutter-like topography, and in the west, it is a gulch formed by Laoshucuo fault, so that it forms a protruding ridge (Fig. 4.10) with three free-face sides around it. From the bottom to the top of the slope, the composition is sandstone, siltstone, and mudstone of Silurian Shamao Formation (Ss), quartz sandstone of Devonian Yuntaiguan Formation (Dy), and silicon dolomitic limestone of Carbonic Dapu Formation (Cd), in which the siltstone and mudstone of Silurian Shamao Formation (Ss) and Devonian siltstone (Dy) are weakly interbedded. Under the constraint of lithology, the slope looks like a cascade as a whole, because of the influence of "plough type" (the top is steep, but the bottom is flat) Laoshucuo fault, the attitude of the Silurian Shamao Formation (Ss) at the bottom is still $340° \angle 30°$, but normally $130° \angle 15°$ for the terrain on the top, whereas the overall attitude is $130° \angle 5°$ for the steep rockmass where the terrain is flat.

Liaojiaping slope has seven layers of weak terrain from the slope top to the root, i.e., four layers of Ss mudstone, argillaceous siltstone, and three layers of Dy siltstone interlayer. The average thickness of the interlayer with an elevation over 400 m is 1–2 m, most of which are siltstone, mudstone; the S2 s mudstone, and the argillaceous siltstone in the lowest section is the thickest weak terrain in the slope and is about 200 m thick. In the micro-terrain, because of the existence of the seven soft layers, seven cascading cliffs, and a six-level narrow platform and long flat coastal line is formed (Fig. 4.11).

There are two groups of large or long fractures that occur in the steep slope of Liaojiaping. One group is parallel to the fracture with a high dip angle toward the NNW part of the Yangtze River. Its attitude is $72° \angle 85°$, is polygonal linear, is coarse, and is the widest one, about 20 m. Most of them are filled already, and the filling which is mostly clay and gravel has an average distance of 10 m, the average trace length is 15 m; the other group is parallel to the fracture with the high dip angle SW of the bird's nest rock gulch, the attitude is $10° \angle 85°$, it is straight linear, coarse, the average distance is 1 m, and the average trace length is 5 m; the
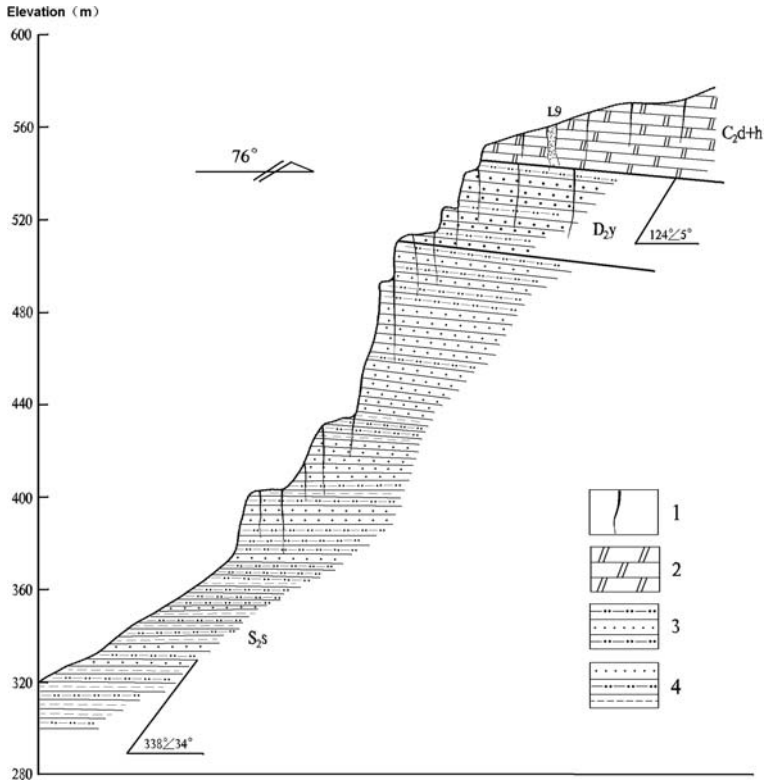
Fig. 4.11 Section plane of Liaojiaping slope 1 – fissures; 2 – dolomite; 3 – sandstone; 4 – siltstone mudstone

fracture that has a large width and long history is filled already. Since the lithology is the same under the free face condition, the two groups of fractures have equal effect in the dangerous rockmass. The vertical fracture in the two groups cut each other, and then form plenty of rock stacks in the cliff and isolate the dangerous rockmass, whereas the weak interlay forms the foundation for the rock stack and dangerous rockmass. The damage mode is toppling (Hoek & Bray 1981). The 30 m rear rockmass structure in the slope body of Liaojiaping is correspondingly intact, and the large fracture grows less, making the total volume of the broken dangerous rockmass about 397,000 m^3. The dangerous rockmass in Liaojiaping constitutes a big threat to the local residents and to the sea route.

Jianchuandong Dangerous Rockmass in Wu Gorge

The Jianchuandong dangerous rockmass located on the left bank of the Yangtze River in Wu Gorges is 12 km away from Wushan county and is at the root of the west side of well-known Fairy Mountain in Wu Gorge, 200 m in the upper reaches,

opposite Qingshi. Since 2006, the authors found and recognized the dangerous rock-mass after an investigation was made on the high and steep slope section in the Three Gorge area, and after that, the issue was of concern by all parties.

The Jianchuandong dangerous rockmass is distributed in the area of the asymmetric "V-shape" valley, and the river in this section is narrow, about 400–500 m wide, the relative elevation difference is 900 m, and the overall slope is around 55°. The morphology of the left bank features three sidesteps of cascading alternating steep cliffs and accompanying flat slope. The surface of the three sidesteps is composed of the Fairy Mountain anticline core section of Daye Formation, Section 3 siliceous limestone with firestone core and Section 4 dolomite or breccia of Jialingjiang group in Triassic Jialingjiang Formation. The steep slope between the 3 sidesteps is mainly composed of Jialingjiang Formation at the bottom part of Section 1 to Section 3, and Section 4 is composed of breccia of Jialingjiang Formation. The 1st sidestep forms the Jianchuandong dangerous rockmass, the 2nd one forms the cliff and slope terrain of Fairy Mountain, and the 3rd one is the flat roof of the slope top. The valley-side slope forms several gulches, among which, the one on the NW side of dangerous rockmass in Jianchuandong can only gather rain in a certain season, and the one on the SE side has perennial running water in the rainy season.

The dangerous rockmass cliff is composed of Section 4 limestone of Triassic Daye Formation, with the Jialingjiang Formation lying above the dangerous rock-mass. The overall Section 4 of the Daye Formation is the hard thick limestone with thin limestone contained within occasionally. Though the joint cracks in the east of the dangerous rockmass are well formed, the joint cracks enlarge and grow far less than the surrounding rockmass.

For the regional tectonics, the section between Hengshixi Brook and Qingshi forms the Hengshixi anticline, Chuanjianxia closed reverse syncline, the Fairy Mountain anticline, and Guandukou-Shengnuxi syncline from the north to the south. The overall fault does not expand, but only the Laoshucuo fault developed in SE wing of Hengshixi anticline in the area of Wangxia (Fig. 4.12). Among this area, the stratum reversed on the NW wing of the Hengshixi anticline and the NW wing of the Chuanjianxia syncline. The SE wing was formed as Silurian stratum in the core of the Hengshixi anticline extends incompletely under the influence of the Laoshucuo fault. The direction of the regional tectonic line is NE15–20°, and in this section, the Yangtze River forms a right angle roughly parallel with the discontinuity line.

Tectonically, the dangerous rockmass in Jianchuandong is located at the turning part of the core section in the SE wing of the Fairy Mountain anticline. The core section in the Fairy Mountain anticline is flat in general and features the joint developed in the whole.

The boundary of the Jianchuandong dangerous rockmass has obvious features and looks like a bevel triangle, where the head is heavier than the root. The elevation of the cliff top in the dangerous rockmass is 267 m, the base elevation is 153 m, the dangerous rockmass is 114 m high, 45 m wide in the shoulder section, but only 14 m wide at the base section. The overall volume of the dangerous rockmass is around 60,000 m^3. The center elevation is 220 m, and it forms a height difference of 45–75 m as the river has an elevation varying from 145 to 175 m. The SE side

Fig. 4.12 Geological sketch of the nearby Jianchuandong dangerous rockmass. (1) – Hengshixi syncline; (2) – Chuanjianxia anticline; (3) – Shengnufeng syncline; (4) – Guandoukou-Shengnuxi anticline; (5) – Laoshucuo fault. I – Hengshixi DRM; II – SZGYP DRM; III – Wangxia DRM; IV – Jianchuandong DRM; V – Jiandaofeng rockfall
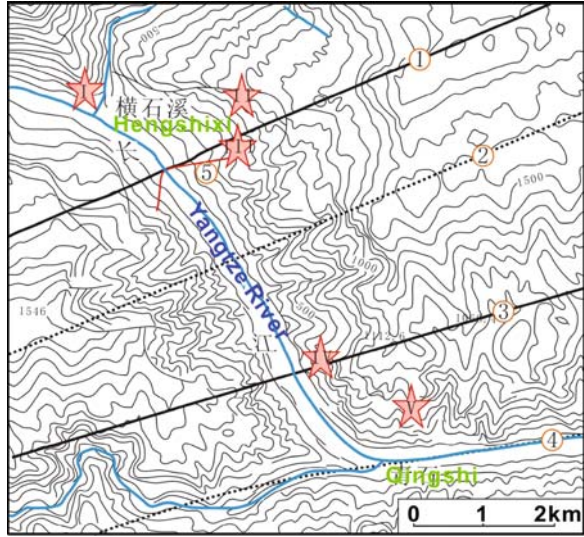
shoulder section of the dangerous rockmass or above occurs after the layer and the joint cracks to form a slope in a cascading shape; the SE side contour underneath the shoulder section of dangerous rockmass is a wide unloading fracture (Fig. 4.10, L1), which makes the dangerous rockmass separate from the SE side of the mountain; the NW side of the dangerous rockmass in Jianchuandong is a vertical steep cliff (Fig. 4.13).

There are some remains of isolated rock stacks at the SW side at the root of the dangerous rockmass. In view of the evolution of the slope, it can be judged that
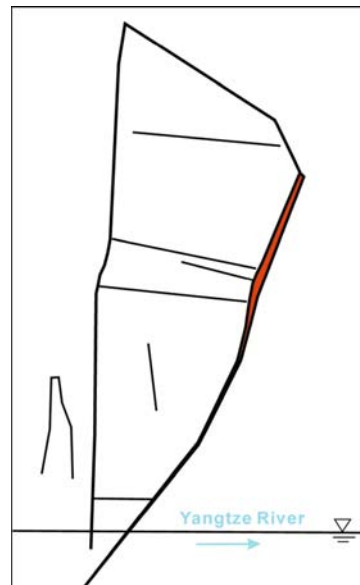
Fig. 4.13   3D sketch of JCD dangerous rockmass

the rock stack is the remaining material after the dangerous rockmass collapsed. At present, the remains are 24 m high, and the fracture, with a width of 3–5 m, is between the Jianchuandong dangerous rockmass which separates them. When the Three Gorges reservoir impounds water to the water level of 175 m, the base of Jianchuandong dangerous rockmass will be in the various (145–175 m) water levels of the Three Gorges reservoir, and its stability will be possibly influenced along by the change in water level.

The dangerous rockmass on the NW and SW side features free faces. The rockmass also features a free face toward the Yangtze River on the SW side, the free face on the NW side features a gulch, and two free faces constitute a vertical steep cliff. The boundary on the SE side of the dangerous rockmass is the unloading fracture (L1) developed under the condition of discontinuity joint. It looks like the top is wider than the bottom due to weathering, some of which are filled with gravel, or looks like the breakage with the dissolved or remained gravel (Fig. 4.14). From the top to the bottom, it narrows to 153 m elevation. The opening of the L1 fracture in
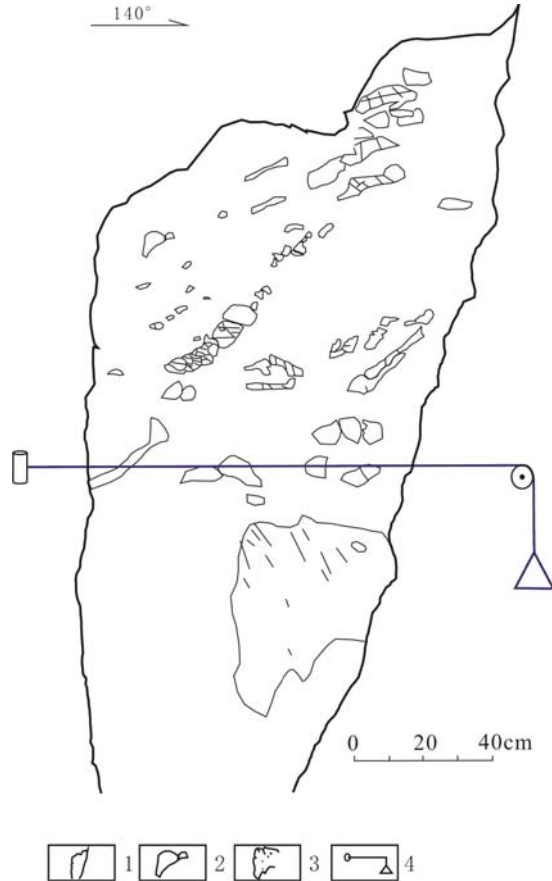
Fig. 4.14 Fracture packing of 2# extensive sense.
1 – fracture shape, 2 – stone fragment, 3 – the scratch on the earth surface after splitting fragment, 4 – extensive sense

the SE side of the dangerous rockmass becomes narrow from the top to the bottom, which shows that the deformation damage of Jianchuandong dangerous rockmass has an accumulated deformation feature, and the accumulated deformation process is still going on. The fracture in the rear contour of the dangerous cliff body extends with the attitude of $242° \angle 86°$.

The slope and bank where the dangerous Jianchuandong rockmass lies is the transverse cascading structure with flat dip angle. Under the background where the discontinuity joint grows, the unloading fracture in the rockmass of the slope and bank extends quietly, and forms the base of all contours and deformation features of the dangerous rockmass. However, the dangerous rockmass has a good completeness, the cut fracture inside does not expo at all except for the surface breakage, and the one in the middle and bottom. The top expands a little. This feature has a tiny possibility to influence its stability and affects the existence of the dangerous rockmass. However, at the outside of dangerous rockmass, especially the east side of L1# fracture in the lower reaches, the through and large fracture expands quietly, i.e., 1.5 crannies per meter. Additionally, on the right shoulder section of the dangerous rockmass, the isolated dangerous stone separates and forms, and by the cut of discontinuity, the surface grows, which results in a possibility of collapse. The distribution of these isolated dangerous stones and its stability constitutes a certain threat to sea shipping, so some necessary preventative actions need to be taken to remove the hazard.

There are some thoroughfares (lane) at the base of dangerous rockmass, and they were caused by manual excavation, previously. In the process of investigation, the project team traveled 11 m along existed lane (Fig. 4.15). The lane lies underneath the dangerous rockmass, and it can be observed that the L1 fracture wedge extends out to the top plate of the lane. However the rockmass inside the lane, same as the surrounding rockmass in the underlying base of dangerous rockmass, the joint cracks that is vertical to Yangtze River expand quietly with an opening of between 5 and 30 cm and is filled with yellow clay. On the clay and interface of the surrounding
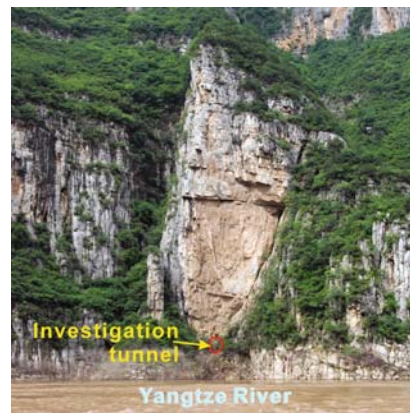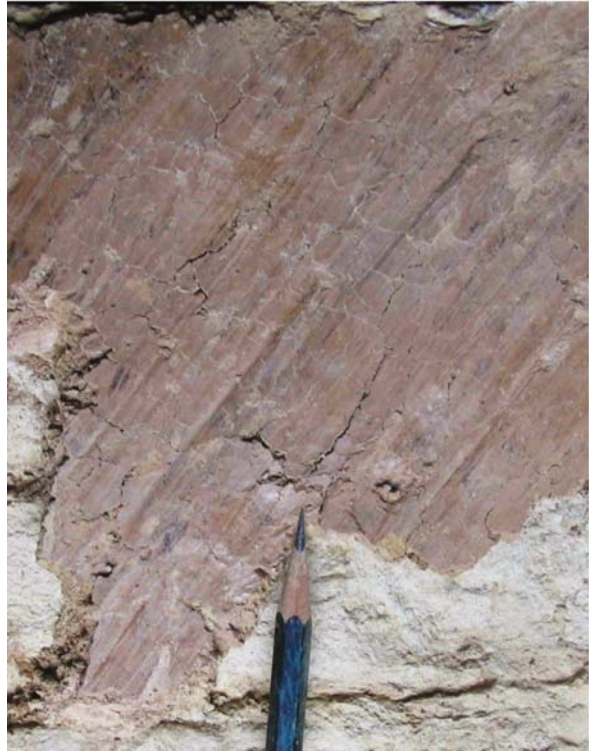

Fig. 4.15 The JCD dangerous rockmass photo

Fig. 4.16 The scratch on the earth of the lane (the direction of scratch is toward the Yangtze River and downward)

rock, slickenside and a scraped surface can be observed (Fig. 4.16), showing that the dangerous rockmass is displaced along the fracture.

Currently, the investigation and study of the dangerous rockmass has just begun, and the dangerous rockmass there has already been put into the monitoring system for severely deformed dangerous rockmasses on high, steep slopes and banks in the reservoir area. The 1st stage of installation for deformation monitoring network for the dangerous rockmass has already been completed in a preliminary manner.

Jiandaofeng Rockfall in Wu Gorge

In accordance with the key deformation and instability features and high steep slopes and banks focused on by the investigation in 2006, the authors made a non-scheduled wide patrol, and found that sections between Jiandaofeng and Kongming-bei of top mountain on the left Yangtze River bank in Qingshi section, Wu Gorge, happened to collapse along the high and steep bank and slope of discontinuity from time to time, though it was less in volume, normally between 0.1 and 1.0 m³, but the height difference of the failure site is more than 400 m, with huge energy, and thus it constitutes a huge threat to ships. It was also found that two landslips happened in the area of Jiandaofeng Mountain in July, 2007. The collapsed section looks like
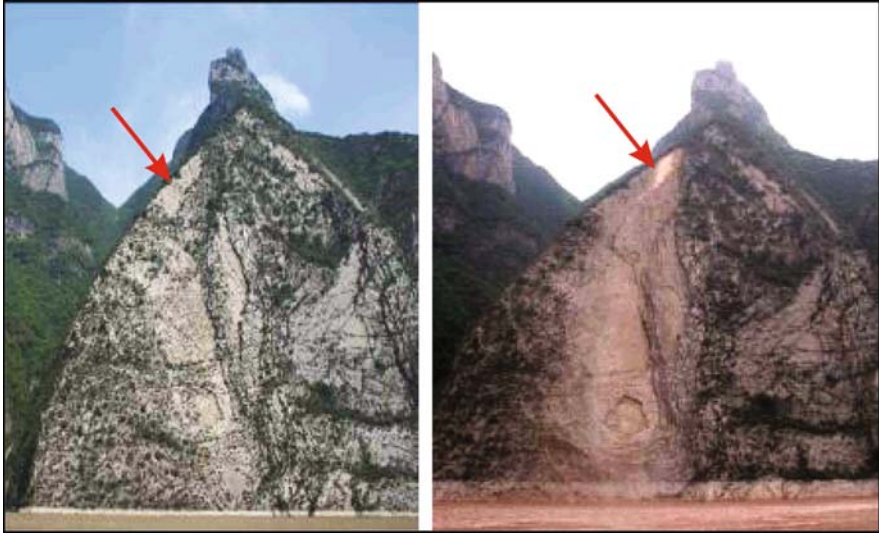
Fig. 4.17 Comparison of the situation before and after the rockfall occurred in Jiandaofeng area in Wu Gorge in 2007. **Left**: Before rockfall (taken in 2006); **Right**: After rockfall (taken in 2007)

a plate, 20 m long from the east to the west, 0.35 m wide, 80 m high, with a total volume of 560 m^3 (Fig. 4.17).

In accordance with the interview with witnesses and ships personnel, there were no ships around within an area of 500 m when it collapsed on July 3rd. The falling stone produced a huge amount of soot, and on July 23rd, a second landslip happened at the same site, but luckily the falling stone did not hit any vessels even though there was a passenger ship moving toward the upper reaches. The ship was close to the cliff, at 50 m in the lower reaches, and the passenger ship had more than 50 passengers. The falling stones boundary is the unsteady joints along the Section X (red and blue lines in Fig. 4.18). (1) and (2) are the vestiges left by the landslip that happened on July 3rd and 23rd, 2007 respectively.

Huangyanwo Dangerous Rockmass in Wu Gorge

The Huangyanwo dangerous rockmass is located on the south bank of Tieguanxia, Wu Gorge, 12 km below the reaches of Fairy Mountain. The river at Tieguanxia is narrow, about 200 m wide, and the steep cliff is 100 m high, roughly formed by the Section 3 limestone of Triassic Jialingjiang Formation at both banks. The slope top is the flat slope formed by the section 4 dolomitic limestone and landslip breccia of Triassic Jialingjiang Formation.

The area of Tieguanxia where Huangyanwo exists is the main tectonic body with a direction of EW and overlapping tectonic section with a direction of near SN, and it constitutes the terrain of steep bank and slope at both banks or conversely, the structural bank and slope.
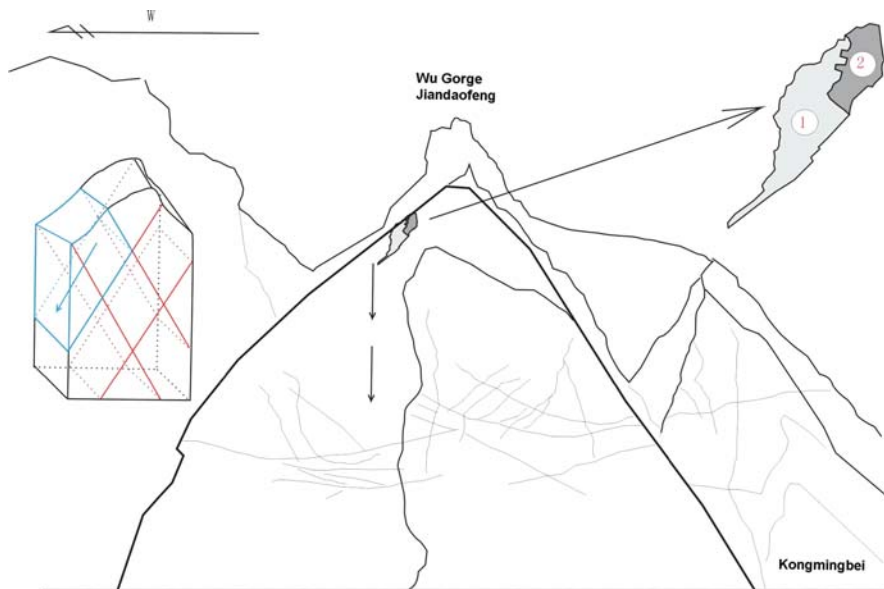
Fig. 4.18 Trace and collapsing mechanism of rockfall occurred at the top of the triangular surface of Jiandaofeng

The fracture in the cliff at 400 m in this section extends extensively, the vertical, through and large fracture of two groups and horizontal terrain surface cuts the rockmass into single and thin erect wall shape (Figs. 4.19 and 4.20), and there are three places where the top hangs in the air since the below rockmass collapsed. These single and thin "rock walls" will possibly collapse or fall down. Additionally, the river in this section is narrow, all of which makes ships terrified.

Shangpingtuo Landslide and Houzibao Dangerous Rockmass in the Front of Wu Gorge

The Shangpingtuo landslide and Houzibao dangerous rockmass is located on the right bank of Lianzixi Brook, 3 km away from the west side of Badong county. Tectonically, it is located in the north wing of the Nanmuyuan anticline, is composed of limestone with firestone strip of Permian Wujiaping Formation, and underlies weak terrain of coal-bearing Longtan Formation and silicalite, mudstone of Permian Gufeng Formation, and the vertical fracture extends in a parallel manner to the Yangtze River. It is very susceptible to failure. Since the previous coal excavation weakens the lower part, if the Three Gorges reservoir impounds water, the resultant large empty area in the bottom of the mountain will be submerged, and the stability of the dangerous rockmass will be worsened further, as deformation becomes more active. The rear fracture of the dangerous rockmass in Houzibao trends throughout, and the underlying coal measure strata in Permian System and coal cave has

Fig. 4.19 An isolated
dangerous rockmass in
Huangyanwo

already been submerged. As a result, the possibility for deformation and failure will be increased when the project is disadvantageous, such as when the water level in the reservoir descends.

The dangerous rockmass is composed of the layer movement zone and other lamination limestone with weak, interbedded, and soft rock in coal seams located below, and thus the structure is hard at the top, but soft at the bottom. The SW steep cliff in the landslip forms a fracture. In accordance with the investigation, the west side of the steep cliff of the dangerous rockmass has 14 fractures with a width of 10 cm and length of 80 m or more within a scope of 200 m long. These fractures with steep dip angle joints and a beveled slope cut the laminated limestone into block structures, of the chain type. The dangerous rockmass in Houzibao in the fore part of the cliff has free faces in the north and west sides (Fig. 4.21), the rear fracture T_1 has an opening of 3.8 m, the depth of cutting reaches to the roof of the bottom coal strata; the fracture at the rear contour is distributed into multiple crannies vertically, and the contour condition of the landslip displacement has formed already.

Fig. 4.20 The dominate discontinuity in Huangyanwo area. The red plane with steep dip angle is a joint plane, the red plane with gentle dip angle is the layer surface, and the black one with steep dip angle is the free face
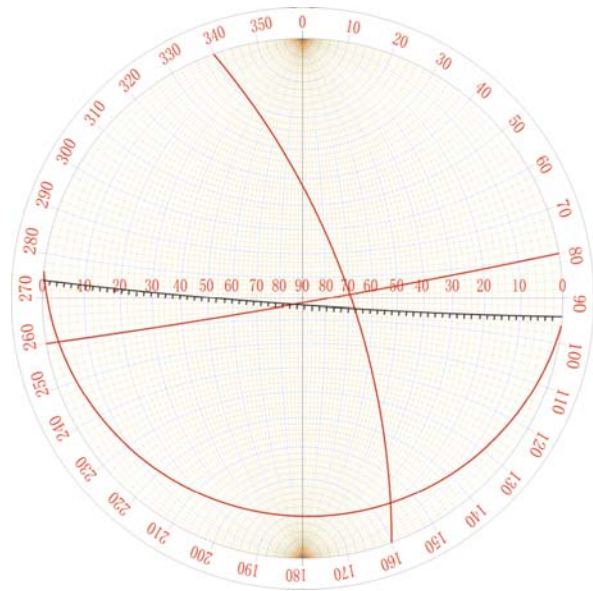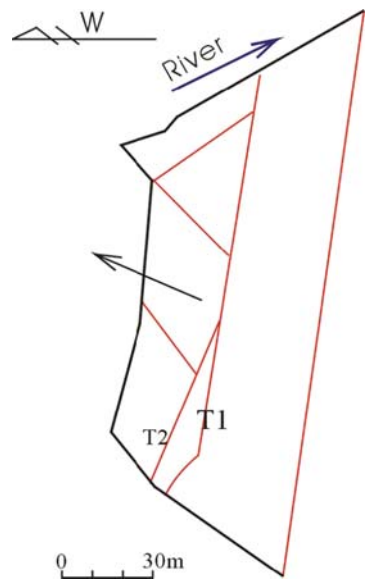

Fig. 4.21 Fissure distribution of the dangerous rockmass at a 150 m elevation level

The plane shape of the dangerous rockmass in a 150 m height level is similar to a rectangle with a length of 82 m and a thickness of 32 m roughly. The section plane consists of a 2-sidestep structure, 180 m tall, the top is narrow, but the bottom is wide. The top is thick, around 8.5 m, the bottom around 34 m. In the 3-dimensional

Fig. 4.22 Engineering geology section of the dangerous rockmass
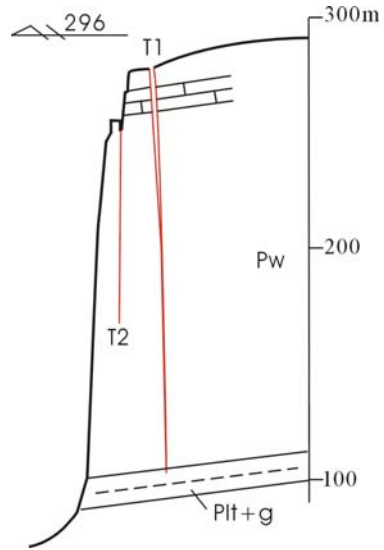
view, it looks like a ridge-table type column, with a total volume of 460,000 m³. The main body of the dangerous rockmass is composed of nodular limestone; it forms a layered shear zone at a height level of 160 m and 260 m, and the coal-bearing Longtan Formation and shale of Gufeng Formation, with a structure of hard top and weak bottom. The front edge of the soft rock is submerged in the river (Fig. 4.22). The attitude of rocks is 9–15° ∠16–25°, forming an angle of 15°–30° with slope direction, the slope structure is a cataclinal-inclined slope, and the apparent dip of terrain is 4°–6°53′. The dangerous rockmass in Houzibao is 174.3 m high, 33.9 m thick at the bottom, and the height thickness ratio (H/b) is 5.14. The inner friction angle of the movement layer zone is 19–28°, the inner friction angle of roof in the coal measure strata is 24° roughly.

Suozishan Dangerous Rockmass in Xiling Gorge

The Suozishan dangerous rockmass is located on the right bank of the Yangtze River and is 1.5 km away from the entrance of Xiangxi River. The stratum is limestone in the middle-thin layer (average thickness is 10 cm) of Jialingjiang group in the Triassic Period; the average distance of the joints is 1.3 m. The locality is in the anticline at the west wing of Huangling; joints are located within the east wing of the Zigui basin. In the east side, there is the NNE-trending Jiuwanxi rupture at 15 km in length, and the stratum is the monocline structure, the layer attitude being 314° ∠31°.

Its average slope angle is 70°, the boundary of the east side is a fracture with an attitude of 110° ∠80°, the boundary of the west side is a fracture with an attitude of 100° ∠80°, all of which form a small gulch. The dangerous rockmass is 80 m

long, 15–20 m wide roughly, now it is higher about 100 m than water surface; the
whole height is around 200 m before the impoundment of water, and it looks like
a shuttle attached to the mountain (Figs. 4.23 and 4.24). In view of the reflection
of local fishermen, the rear boundary opens 3 m. The projection drawing of the
structure level (Fig. 4.25) shows that there are plenty of advantageous attitudes in
the rockmass, as the rockmass there is broken. Most of the cut crannies are ones with
an attitude of 80° ∠80° (nearly parallel to the joint of Yangtze River), 178° ∠70°
(nearly vertical to layer mechanism), and 314° ∠31°, and the blocks that are cut are
of $1 \times 1 \times 0.7$ m^3 in size Though most of the dangerous rockmass will be submerged
by water after impoundment, the gravel and ground swell caused by loss of stability
cannot be ignored.

Baituo Dangerous Rockmass in Xiling Gorge

The Baituo dangerous rockmass is located on the left bank of the Yangtze River
and is 2.5 km away from the entrance of Xiangxi River. Over the stratum, it is
the core section with a thick limestone strip of Permian Wujiaping Formation, with
shale contained intermittently. Below the stratum, is the thick limestone of Permian

Fig. 4.24 Side schematic of Suozishan Mountain
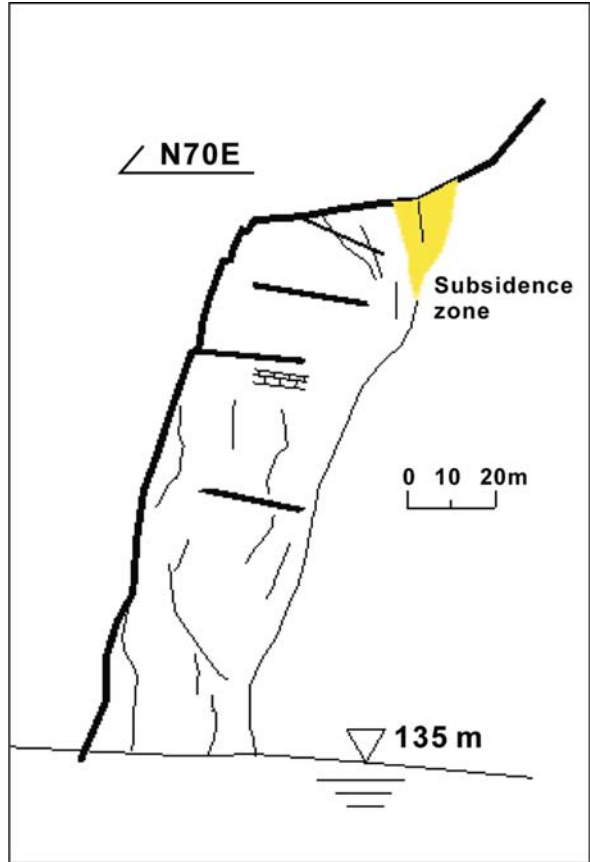
Maokou Formation and Gufeng Formation, lying in waves, of a coarse nature. The average distance of large joints is 5 m, and the average distance of small joints is 2 m; the rockmass has a rather complete structure and is a thick broken block structure (Fig. 4.26). The locality is the anticline at the west wing of Huangling, and it is jointed with the east wing of Zigui basin. In the east side, there is the NNE-trending Jiuwanxi rupture at 8 km, the near side is the Xintan landslip, and the opposite side is the Lianziya dangerous rockmass. The stratum is a monocline structure, and the lay attitude is 305° ∠30°.

The dangerous rockmass is 550 m long, the slope is 100 m high roughly, and its free face is 210° with a slope angle of 80°. At its NW side, the monocline bedding slope is the borderline, the vegetation at the borderline grows, the borderline's SE side is a large fracture, with an attitude of 100° ∠65°. Inside the dangerous rockmass, joints extend with roughly vertical bedding, the advantageous structural side is the one with an attitude of 150° ∠65° (Fig. 4.27). The blocks are normally large, and its movement side or bottom is the bedding. Since the large joints that are parallel

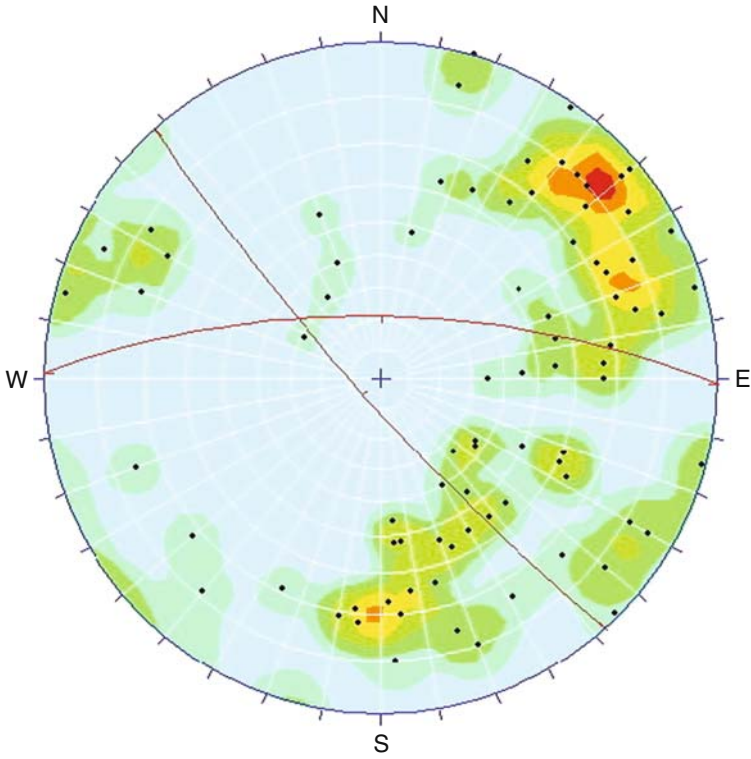**Fig. 4.25** Density map of joint poles of Suozishan Mountain

Fig. 4.26 Photograph of the front of the Baituo dangerous rockmass
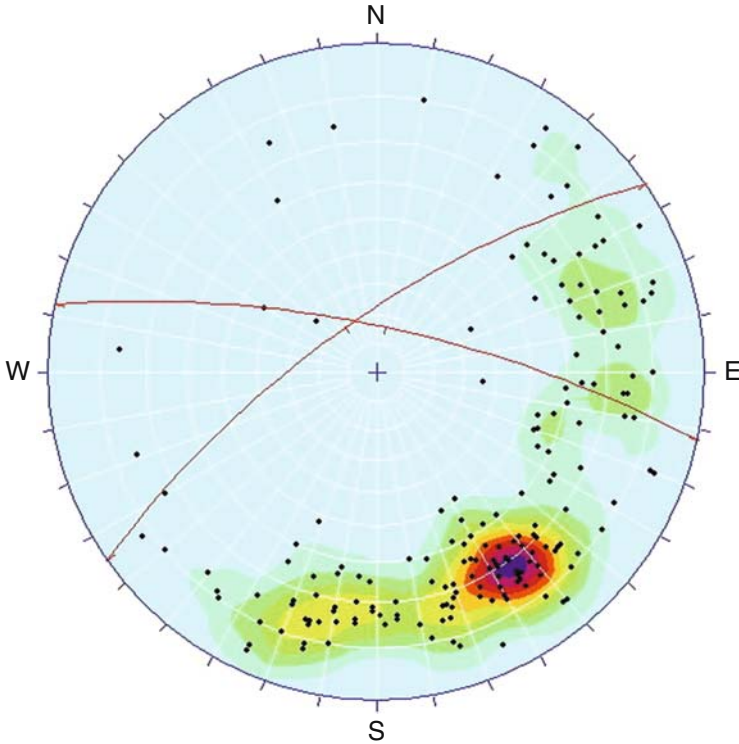
Fig. 4.27 Density map of joint poles of the Baituo dangerous rockmass

to Yangtze River are inactive, the inside cut borderline in the dangerous rockmass is not clear, and it needs an evaluation to determine its stability in the future.

The Wentianjian Dangerous Rockmass in Xiling Gorge

The Wentianjian dangerous rockmass is located on the right bank of the Yangtze River and is 1.5 km away from the entrance of Jiuwanxi Brook. Over the stratum is limestone in the middle layer with shale of Cambrian Tianheban Formation, and below it is the middle-thin limestone, of shale contained within the Cambrian Shipai Formation (Figs. 4.28 and 4.29). The rockmass upside is rather complete, but the downside is rather broken. The average distance of joints is 0.8 m, some of which are in suspension. The geological characteristics of the dangerous rockmass are typical, with the top harder than the bottom. The locality is the anticline west wing of Huangling. In the W side, there is the NNE -trending Jiuwanxi Brook rupture at 1.5 km; the stratum is a monocline structure, and the lay attitude is $270° \angle 20°$.

The dangerous rockmass there has been cut into an isolated rockmass. The dangerous rockmass there is 100 m high roughly, about 2–5 m thick, 50 m long approximately, and the foundation is the broken Shipai group limestone with shale within.

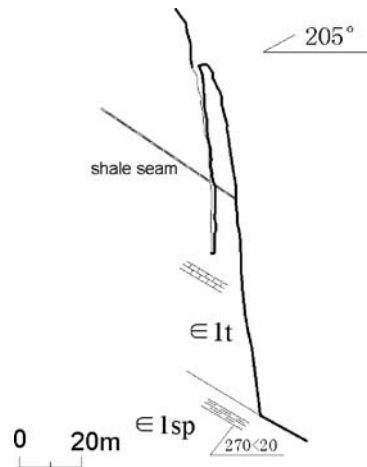**Fig. 4.28** The Wentianjian
dangerous rockmass

Fig. 4.29 Sketch of the
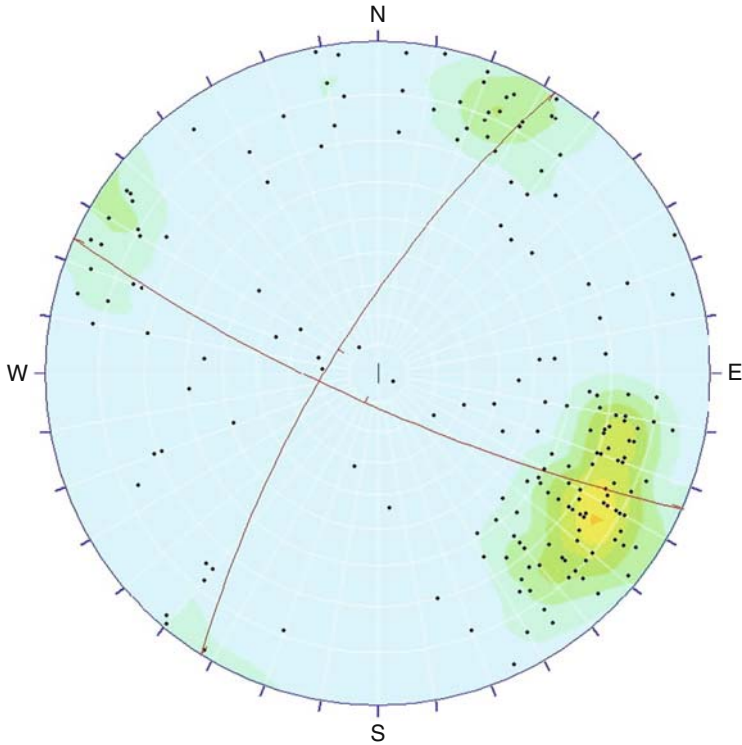Wentianjian dangerous
rockmass

Fig. 4.30 Density map of joint poles of the Wentianjian dangerous rockmass

Its cut borderline is $140° \angle 70°$ and $25° \angle 85°$, respectively. The two groups consti-
tute an advantageous structural plane of the dangerous rockmass (Fig. 4.30); there
is one group of shale inside the dangerous rockmass at the top, and it is weath-
ered heavily, so it produces a large influence on the stability of the dangerous rock-
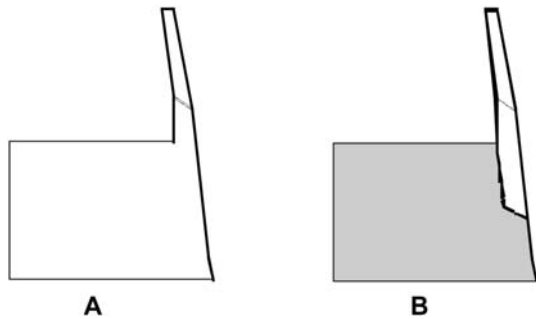mass. After a preliminary analysis, two damage modes can be found. One is that the

Fig. 4.31 Possible failure
model of the Wentianjian
dangerous rockmass

rockmass bends from the middle shale (see "A" in Fig. 4.31) and the other is that the fracture at the bottom of the dangerous rockmass keeps opening, and finally it falls down from the fracture downside, see "B" in Fig. 4.31. The dangerous rockmass is a well-known landscape in the tributary stream of the Yangtze River, i.e., "Wentianjian," but it brings a huge threat to the sea routes.

The Jiuwanxi Dangerous Rockmass at the Entrance of Jiuwanxi Brook, Xiling Gorge

The dangerous rockmass at the entrance of Jiuwanxi Brook is located at 700 m of the left bank of Yangtze River where Jiuwanxi Brook enters. Over the stratum, is the thick limestone and dolostone of Cambrian Shilongdong Formation. The rockmass is broken, some of which extends in a transverse drape (Fig. 4.32). The average distance of joints is 0.7 m, but it is rare for them to be cut into blocks. The overall attitude of the strata is $290° \angle 30°$ with the bedding in a waves shape, but also coarse in nature.

The dangerous rockmass is 70 m long, 5 m thick, and 50 m high, approximately, with three sides being cut, and the attitude of borderline is $120° \angle 70°$, $60° \angle 70°$. The two groups are the advantageous structural planes of rockmass (Fig. 4.33). The rockmass is 80 m higher than the river surface, and it constitutes a huge threat to the tourists who are traveling in the Jiuwanxi Brook and a hazard to the ships that go across.

Fig. 4.32 The Jiuwanxi dangerous rockmass

Conclusions

Through the investigations, the following conclusions are obtained.

(1) After making the related improvements and monitoring the landslips along both banks that possibly block the sea routes, causing a safety threat to passing ships,
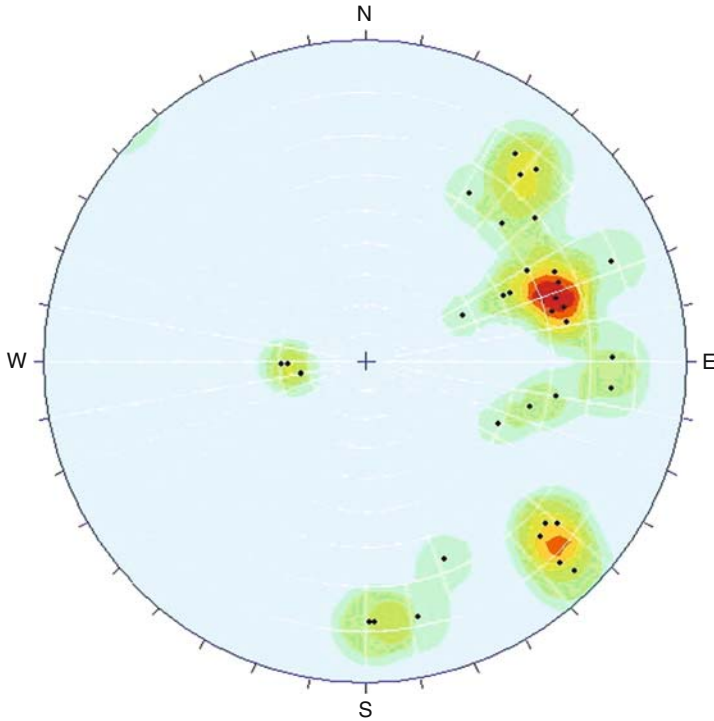
Fig. 4.33 Density map of joint poles of the Jiuwanxi dangerous rockmass

the one that is the greatest geological hazard to the safety of sea routes is the landslip and falling stone;

(2) Through the investigation of the dangerous rockmasses at both banks of the sea route from Yichang to Fengjie, it can be clearly seen that the space distribution situation of the dangerous rockmasses constitutes a direct threat to passing ships;

(3) The high and steep slope in the river section is mainly controlled by stratum lithology and structure, and the distribution of dangerous rockmasses and damage is mainly under the influence of lithology combinations, structural plane, coal excavation, construction of road wharfs, and other human activities;

(4) After mapping the dangerous rockmass at a 1:2000 scale, the borderline condition and geological structure of dangerous rockmass can be clearly seen, and this lays a solid foundation for evaluating the stability of dangerous rockmasses and other related conditions.

References

Hoek E, Bray JW (1981) Rock Slope Engineering. Taylor & Francis, p. 358

Xiao SF, Yang SB (1999) Rockmass Mechanics. Geological Publishing House, Beijing

Yin YP (2005) Human-cutting slope structure and failure pattern at the Three Gorges reservoir. Journal of Engineering Geology 13(2):145–154

Zhang ZY, Wang ST, Wang LS (1997) Principle of Engineering Geology Analysis. Geological Publishing House, Beijing, pp. 351–352

Chapter 5
An Evaluation Study of Bank Collapse Prediction in the Three Gorges Reservoir Area

Qiang Xu, Minggao Tang, and Runqiu Huang

Abstract When the impoundment of the Three Gorges reservoir reaches a water level of 175 m, the reservoir banks along the main river course and its tributaries will have a total length of 5,311 km. Among them, the rock banks are 213 km, and the banks of unconsolidated soil and rock mixture are 249 km. Bank collapse is one of the main engineering geological problems in the Three Gorges reservoir area. In this chapter, using an extensive amount of data on bank collapse obtained through geological investigation, field measurement of the bank collapse parameters, and simulation analysis, we systematically explored the bank collapse types, parameters, and bank collapse prediction methodology. In the Three Gorges reservoir area, the typical bank collapses are wash and abrasion, toe-erosion collapse, rock break-off and slides, and landslide. The evolutionary processes, the distribution features, and the corresponding geological conditions of these bank collapse types are analyzed as well. Eigenvalue angles of the rock and soil masses, including underwater deposit eigenvalue angle θ, wash–abrasion eigenvalue angle α, and steady above-water eigenvalue angle β, are fully discussed in the chapter. Based on the exploration of the correlation between bank collapse prediction parameter and the composition of the rock and soil mass and the correlation between mechanical features and the hydrodynamic conditions in the reservoir, an innovative prediction method that is adaptive to mountain–river reservoirs like Three Gorges reservoir area, Bank-Slope Structure Prediction Method (BSSPM), is proposed. The analogical study of three water storage reservoirs for many years, a comparison of the predicted results with that of the actual happenings, shows that BSSPM has a good adaptation for bank collapse prediction of mountain–river reservoirs.

Keywords Three Gorges reservoir · Mountain–river · Reservoir bank collapse prediction · Bank-Slope Structure Prediction Method (BSSPM) · Bank collapse types · Bank collapse prediction parameter

Q. Xu (✉)
State Key Laboratory of Geo-hazard Prevention and Geo-environment Protection
(Chengdu University of Technology), Chengdu 610059, China
e-mail: xuqiang_68@126.com

Introduction

The Three Gorges reservoir is the biggest hydropower station so far in the world. When the reservoir capacity reaches a water level of 175 m, the total bank length will be 5,311 km. Among them, 213 km are rock mass areas and 249 km are unconsolidated soil and rock mixture deposit areas (Zhang et al. 1994; Zhang et al. 1998). The studies of bank collapse in the Three Gorges reservoir area mainly located on those bank slopes near towns and cities. The bank length along the slopes of 133 towns and cities, and the slopes of the enterprises outside these towns and cities, is 462.17 km, about 8.7% of the total length. The densely engineered reservoir banks of towns and cities, being unconsolidated soil mixture with different causes of formation-landsides, collapse, Wushan loess, slope wash deposits, river terrace deposits, etc., occupy 55.53% of the total length, among which 77.8 km (19.5%) are landslide slope and deformed banks, both with poor stability; 52.3 km (13.1%) are proluvial banks with high stability; 311.5 km (67.4%) are riverward bank slopes mainly made of weak rocks – mud rock, shale rock, marlstone rock, etc., and bedrock of weak rock interlayers, with potential instability. When the water storage is completed, the stability of the reservoir banks is not only related to the safety of people's lives and their properties on both sides of the reservoir area but also concerned with social and political stability. It is therefore of urgency and necessity to make an evaluation study of the bank collapse prediction in the Three Gorges reservoir area so as to provide a scientific basis for bank collapse measures of prevention and treatment.

The traditional evaluation method of predicting reservoir bank collapse applies to reservoirs on the plain. For example, Караушев 1958, etc., put forward basic algorithmic methods and graphical solutions for the prediction of bank collapse margin, after doing researches on reservoir bank collapses. An array of reservoir bank collapse prediction cases have proved that the Three Gorges reservoir, a mountain–river reservoir, is so different from reservoirs with homogeneous banks on plains in terms of slope structure, slope compositions, etc. (The Research Group of Bank Collapse of Guanting Reservoir 1958), that the traditional evaluation method becomes inadequate in the timely prediction of bank collapses in Three Gorges reservoir area. A new evaluation method of bank collapse prediction is consequently needed to meet the requirements in the mountain–river reservoir of Three Gorges.

The evaluation of mountain–river reservoir bank collapses mainly involves the study of bank collapse types, bank collapse parameters, and bank collapse prediction methodology, on which many researches have been conducted.

In terms of bank collapse type, bank rebuilding has been categorized into bank scour, whole slip, and rock mass collapse by Zhang et al. (2002), after analyzing the characteristics of the bank collapses at Fengjie in Three Gorges reservoir area. Yin (2004) and Tang (2003) also made simple taxonomic studies of reservoir bank collapses. The fact, however, is that this research, on account of limitations of their studies of only a certain stretch of banks on a specific length of the bank slope within the Three Gorges reservoir area, is not adequate for the bank collapse predictions for the whole area.

In terms of bank collapse prediction method, Wang et al. (2000), after investigating bank collapses of tens of reservoirs for nearly 10 years, proposed a "Two-Section Method" and successfully applied it to the predictions of bank collapses on the Waiyang–Fuzhou Railway Line. The "Two-Section Method" worked quite well when it was applied to mountain–valley reservoirs in Southern China. Its application in Three Gorges reservoir, though, turned out to be quite inadequate. Xu (2003) has also explored bank collapse and constructively raised arguments about the modification of the graphical method of bank collapse prediction in red rock areas on the basis of his research on redbed river valley slopes in Sichuan Basin. Ma et al. (2002) and Fan et al. (2002) recommended "the analogy method with stable slide shape" in light of the principles of the analogy in engineering geology, by which the prediction is more accurate and valid in that the stable side shape is in collocation with different engineering slopes, and rock mass properties have been fully taken into consideration.

Few explorations at present, however, have been done upon the prediction parameter of mountain–river reservoir bank collapse, and reference value in this respect is very limited. Bank collapse, a complicated process of geological history, is subject to many factors, e.g., regional structure, topographical features, lithologic characters of the stratum, bank slope structure, physical–mechanical property of the rock mass, ground water and surface water, the dynamic action inside the reservoir, vegetation, and human activities. These elements are indicators of the difficulties in extracting and obtaining the prediction parameters and especially the causes for mountain–river reservoir bank collapse.

This chapter is a systematic research of bank collapse types, bank collapse parameters, and bank collapse prediction method in Three Gorges reservoir area, involving a great quantity of investigation data obtained by means of site geological investigation, field measurement of the bank collapse parameter, and simulation analysis.

Bank Collapse Types in the Three Gorges Reservoir Area

Bank collapses of mountain–river reservoirs are often characterized by several types of bank deformation and destruction and the corresponding variant evolution models and processes due to differences in terms of the bank slope's topography and geomorphology, structure, material composition, self-stability, dynamic condition of reservoir water, etc. Table 5.1a–d is a summation of the bank collapse types and

Table 5.1a Evolutionary processes of bank collapse types in Three Gorges reservoir area: Wash and abrasion

Bank collapse types	Diagram
Wash and abrasion	

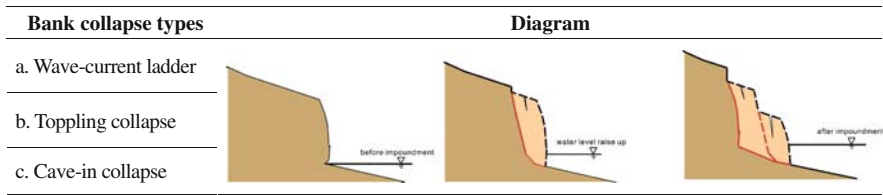**Table 5.1b** Evolutionary processes of bank collapse types in Three Gorges reservoir area: Toe-erosion collapse

Bank collapse types	Diagram
a. Wave-current ladder	
b. Toppling collapse	
c. Cave-in collapse	

Table 5.1c Evolutionary processes of bank collapse types in Three Gorges reservoir area: Rock break-off and slides

Bank collapse types	Diagram
a. Block break-off and rock slides	
b. Soft-toe collapse	
c. Mudstone recess	
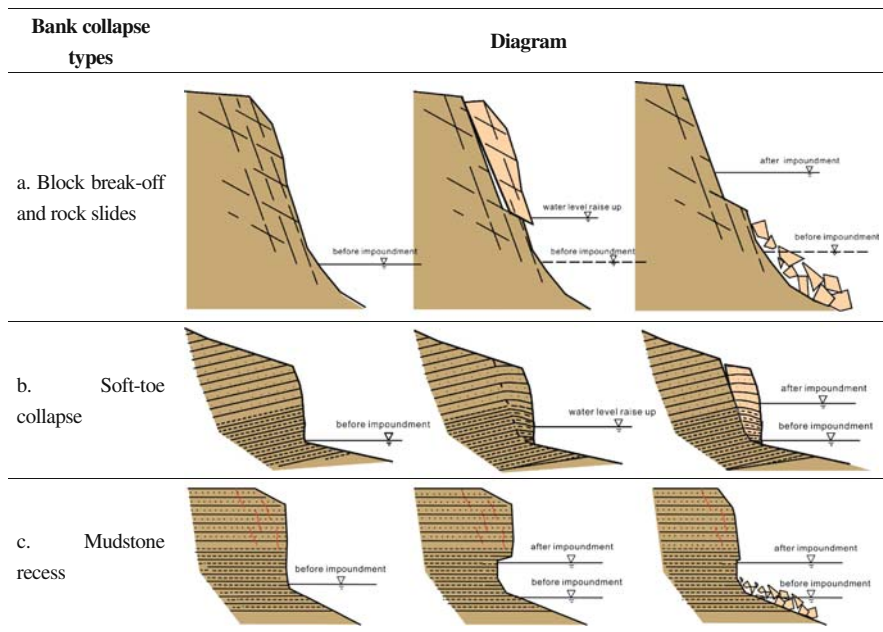
their evolution diagrams based on adequate investigations of the geological conditions generating bank collapses in the Three Gorges reservoir area.

Wash and Abrasion

Wash and abrasion refers to the reservoir bank condition of slow recession caused by the wash and erosion of external agencies like current and wave movement inside the reservoir (Tang et al. 2006a; 2006b). This type of bank collapse, with general distribution in Three Gorges reservoir area, mainly originates in bank slopes of gentle incline, intensely weathered granite sand slopes and an intensely weathered redbed belt (Table 5.1a). The reservoir bank reformation is slow and lasting, and the reformation scale is limited. Figure 5.1 is a case in point.

Table 5.1d   Evolutionary processes of bank collapse types in the Three Gorges reservoir area: Landslide

Bank collapse types		Diagram
Ancient landslide revivification		
Surficial slip of the thick loose deposit	a. Landslide deposit	
	b. Slope eluvial deposit	
	c. Proluvial deposit	
	d. Artificial spoil	
Sliding along the bed -deposit interface		
Bed rock sliding along the weak accordant layer		

Toe-Erosion Collapse

Toe-erosion collapse refers to a type of bank destruction and reformation caused by the collapsing and the removing of off-balance substances from the upper slope as a result of the softening and eroding of the earth toe of the lower slope by the reservoir water. This type of bank collapse, characterized by its greater vertical displacement than the horizontal, its direct correlation with the weight of the earth block, is widely distributed in the Three Gorges reservoir area, and consequently occupies a great proportion of the total bank collapse length (Table 5.1b). Toe-erosion collapse

Fig. 5.1 Wash and abrasion collapse

usually occurs on the fairly slanting slopes (with gradient 30°–60° and fairly good stability) composed of thick sandy soil, silty soil, and silty clay (Wushan's loess-like soil) (Fig. 5.2).

Toe-erosion collapse can be further classified as wave-current ladder, toppling collapse, and cave-in.

(1) *Wave-current ladder*: This type of bank collapse is obviously corresponding to the wash height and assumes gentle ladder destruction as the water edge erosion of the soil on the slope moves its way downward when the water level drops step by step.

(2) *Toppling collapse*: With the action of water scouring, side erosion, undercutting the bank toe and the formation of recesses, and subsequent action of slope weight and the exuding of underground water, the bank slope falls or topples down in a strip or cone manner. The causative factors are as follows: (a) The

Fig. 5.2 Toe-erosion collapses (Huang et al. 2005)

slope soil is not solid in terms of anti-scouring. (b)Water scouring is more powerful than the slop's anti-scouring when the stream action works directly on the slope. Toppling collapse generally fall into two categories – falling and toppling. The vertical movement of the falling or toppling is greater than its horizontal movement. Toppling collapse is characteristic of a fast rate of collapse, great recession scale, wide distribution, high frequency, unexpected occurrence, and formation of strips in most cases, and cones in rare conditions. In the Three Gorges reservoir area, it is the most frequent type of toe-erosion collapses.

(3) *Cave-in collapse*: The collapse is caused by the holes under the bank slope or partial depression, and the slope soil, as a result of the interaction of self-weight, hydrostatic and hydrodynamic pressure by groundwater, moves from ambient space to the center of the hole.

Rock Break-Off and Slides

Rock break-off and rock slides derive from the steep rock slope composed of joint fissures which may cause direct instability, with the action of external agencies like the scouring by the reservoir current and wind-driven waves. This type of bank collapse often unexpectedly occurs inside the intensely weathered rock belt with intensive unloading fissures (Table 5.1c). Figure 5.3 is typical example. In the Three Gorges reservoir area, rock break-off and slides are classified in terms of slope structure as the following three items.

(1) *Block break-off and slides*: When the instability-generating joint fissures exist inside the rock slope, the rock blocks collapse as a result of the loss of strength of the fissures and the action of external agencies like reservoir current and wind-driven waves.

Fig. 5.3 Rock break-off and slides

(2) *Soft-toe collapse*: When the dip rock slope is structured inside as hard in the upper part and soft in the bottom, the foundation support (the bed of the slope) is most likely to be destabilized by erosion. As long as the destabilization happens, through the action of weight leading to the slope's compression or even crack in tension, the upper part of the slope will collapse. The strike of the attitude of the rock bed and the included angle between the slope strikes is not equivalent; some slope strikes intersect their terrain strikes' included angle at a big angle. But generally speaking, the rock stratum is introversive with dip angles less than $15°$. The upper part of this kind of slope is usually made of solid sandstone, and its lower part close to the bank, soft purple-red mudstone, which is subject to disintegration or destabilized. Through the long-term action of the gravitational field of the upper thick layer of sandstone, the destabilized bottom is compressed or deformed. In addition, sets of high dip angles inside the thick sandstone further contribute to sectional collapses along the high dip angles' structural planes.

(3) Mudstone recess inside the almost-horizontal inter-bedding sand-mud bank slope, recesses 1–2 m deep in the purple-red sandstone subject to weathering and disintegration, is often cut by the waves of the reservoir. The upper sandstone, therefore, sticks out as a cantilever structure. Considering the normal existence of almost vertical fissures inside, the upper solid sandstone, through the action of gravity, produces tension cracks in and along these fissures and it partially collapses. This is the common case in the redbed bank slope of the Yangtze River, often producing gently retrogressive bank collapse.

Landslide

Landslide is a kind of reservoir bank reformation through sliding of the entire rock–soil mass in the direction of a void as a result of the action of reservoir currents, rainfall, and other causative factors after the storing of water. To be more specific, landslide, commonly caused by the rise and fall of the reservoir level in mountain–river reservoirs, is a cumulative deformation through long-term and wide-ranging gentle destruction. This type of deformation is apt to happen along the unstable slope and especially along the slope that is sensitive to a hydrodynamic field (Table 5.1d). In terms of different slope structure, landslides are further classified into the following four categories in the Gorges reservoir area.

(1) *Ancient landslide revivification*: Reactivation of old landslides after the water storing, the formerly stable or almost stable sliding slope reactivates or a partial slide or collapse, through the action of the reservoir storing, is generated.

(2) *Surficial slip of the thick loose deposit*: Sliding of the plane layer of the thick loose deposit the superficial part of some stable or almost stable thick accumulations with different causes-collapse and slide deposit, slope wash deposit, proluvial deposit, artificial storing, etc. creep downward and become deformed, or the front edge partially slides.

(3) *Sliding along the bed–deposit interface*: When the deposit is not thick and the bed-deposit depth of the bed-deposit interface is not high, the accumulation, under the influence of reservoir storing, moves as a whole, downward along the bed-deposit plane.

(4) *Bed rock sliding along the weak accordant layer*: If there exists weak interlayers, e.g., sandstone–mudstone interbedding, argillized interlayer between limestone and marlite strata – inside, the accordant bed rock with moderate angle dip or moderately low angle dip, the weak layers, through the immersion after storage, is destabilized so that the shearing resistance is greatly reduced, and the holistic landslide along the weak layer occurs. In particular, it is to deserve attention that when the upper part of the accordant slope is precipitous and the lower part inclined to slide, according to the principle of effective stress, the gently slanting toe of the slope, though with original friction, will slide as a whole, as a result of the reduction of its skid resistance through the immersion. The Qianjiangping Landslide in Zigui County of Hubei Province in July of 2003 and the world famous Vajont Landslide in Italy are representative of this type.

The investigation statistics of sections of the bank slopes in the Three Gorges reservoir area show that the length of wash and abrasion type is 31.74% of the investigated total length, break-off and slide 51.15% of the total, and landslide 17.11% of the total (Table 5.2).

The Prediction Parameter in Three Gorges Reservoir Area

Eigenvalue of the Bank Collapse Prediction Parameter

The investigations reveal that wash and abrasion type and toe-erosion collapse often bear evidence indicated by the following three eigenvalue angles:

(1) Underwater deposition eigenvalue angle (θ) refers to the stable slope angle formed through sandbank accumulation at the site of underwater shoal of the washed and eroded loose soil from the banks by reservoir water.

(2) Wash–abrasion eigenvalue angle (α) refers to the steady eigenvalue angle of the rock and soil mass on the slope within the normal range of water level in the Three Gorges reservoir area – the backed-up water level is 145–175 m.

(3) Steady above-water eigenvalue angle (β) refers to the steady eigenvalue angle of the rock and soil mass above the design highest level-backed-up water level 175 m in the Three Gorges reservoir area through the action of external agencies.

Sampling Investigation of Bank Collapse Prediction Parameter

Bank collapse prediction research is supposed to be done prior to the reservoir storage. Based upon large amount of practice, two sampling investigation methods of the bank collapse prediction parameter are presented.

Table 5.2 Length statistics of different bank collapse types in the Three Gorges reservoir area

Geographical position (boroughs and counties)	Wash and abrasion (m)	Collapse, break-off and slides (m)	Landslide (m)
Yunyang	12210	14080	6440
Wushan	3370	3880	900
Badong	6820	1250	2930
Zigui	7790	14151	3850
Xingshan	1750	1900	550
Yiling	0	3140	0
Wanzhou	37990	17715	2825
Fengjie	9070	600	750
Zhongxian	2178	19068	5290
Changshou	2016	13000	1346
Wulong	2872	4909	2396
Fengdu	5070	32098	804
Fuling	6009	45900	612
Shizhu	0	2271	4291
Kaixian	6055	21284	38651
Yubei	4800	4000	0
Banan	3220	4880	0
Nan'an	3220	1380	410
Jiangbei	5320	4620	0
Yuzhong	2400	2420	0
Jiulongpo	3700	1300	0
Dadukou	3060	0	0
Shapingba	2310	2240	450
Beibei	3290	1580	1670
Jiangjin	3350	4530	180
Total length of each type (m)	137870	222196	74345
Percentage (%)	31.74	51.15	17.11

(1) *Longitudinal analogy*: In the reservoir area, mean lower water level in the natural river course, river's flooding range, and mean flood level correspond to the lowest design level, the reservoir's water level range (the regulated level range), the highest design level when the reservoir is filled with water. To fulfill the spot measurement of bank collapse parameter along a section of banks, we first measure the steady eigenvalue angles of different rock and soil masses in the three range belts – the belt below the mean lower water level of the existing natural river course, the river's flooding belt, and the belt above the mean flooding level. Statistics is then applied to obtain the taxonomies of the rock and soil masses and their eigenvalue angles, which are further applied to analogical inference of the eigenvalue of the bank collapse prediction parameter under the condition that the reservoir be filled – underwater deposition eigenvalue angle (θ), wash–abrasion eigenvalue angle (α), and steady above-water eigenvalue angle (β).

(2) *Cross-direction analogy*: The bank collapse prediction parameter of the reservoir before the impoundment is obtained via investigating the long-term impounded reservoirs that have similar conditions. The steady eigenvalue

angles of different rock and soil masses in the three range belts after the reservoirs' storage are as follows: The belt below the lowest design level, the reservoir's water level range (the regulated level range), and the range belt above the highest design level are directly obtained, and these steady eigenvalue angles are analogically applied to the calculation of the eigenvalue of bank collapse prediction parameters in the reservoir to be explored.

Statistics of the Eigenvalue of Bank Collapse Prediction Parameter in the Three Gorges Reservoir Area

The eigenvalue of bank collapse prediction parameters of different rock and soil masses in the Three Gorges reservoir area is obtained after a great amount of spot investigation and classification of the quaternary-system loosely consolidated deposit bank slopes and the intensely weathered belt of the redbed slopes that are liable to collapse (Table 5.3).

Bank Collapse Prediction Parameter of the Alluvial–Proluvial Bank Slope

Alluvial–proluvial soil slopes are widely distributed in the Three Gorges reservoir area. This kind of slope, with a dualistic structure of upper thickness and lower thinness in most cases, is mainly exposed along the branch river gulch and terraces along the main river and well developed along the wide and gentle river valley. It is essentially composed of alluvial silty clay, silty soil, sand–gravel soil, pebble and gravel soil, etc. Its eigenvalue angles of bank collapse prediction parameter under normal circumstances are steady under water eigenvalue angle 8–13°, wash–abrasion eigenvalue angle 10–14°, and steady above-water eigenvalue angle 18–26°.

Bank Collapse Prediction Parameter of the Residual Soil Slope and Landslide Accumulation Slope

Residual soil slopes and landslide accumulation slopes, better-developed along the banks from Wanzhou down to lower reaches than the rest banks along the river, are mainly distributed along banks of great gradient, with compositions of dilapidated and residual soil, gravity accumulation of gravel soil, clay, and silty clay. The eigenvalue of the bank collapse prediction parameter along these slopes is, under normal circumstances, steady; underwater eigenvalue angles are from 13° to 15°, wash–abrasion eigenvalue angles are from 14° to 17°, and steady above-water eigenvalue angles are from 25° to 30°.

Bank Collapse Prediction Parameter of the Wushan Loess-Like Soil and the Intensely Whole Weathered Granite Belt

Wushan loess-like soil (silty clay) and the intensely whole-weathered granite belt in the Three Gorges reservoir area are two types of quaternary-period loosely

Table 5.3 Statistics of the classification of the eigenvalue of bank collapse prediction parameters in Three Gorges reservoir area (Xu et al. 2007)

Stratum no.	Rock and soil types		Underwater deposition eigenvalue angle θ (°)			Wash–abrasion eigenvalue angle α (°)			Above water steady eigenvalue angle β (°)		
			Aver.	Min.	Max.	Aver.	Min.	Max.	Aver.	Min.	Max.
Q^{al+pl}	Cohesive clay	Clay	13	8	17	14	10	19	26	20	34
		Silty clay									
	Silty	Silt	11.5	5	16	13	7	18	22	18	27
	Silt and sand	Silt and sand	10	4	15	12	5	18	20	18	26
	Sandy soil	Fine sand	8	3	12	10	4	16	18	16	25
	Pebble and gravel	Pebble and gravel	9.2	4	14	11.5	6	16	22	17	28
Q^{el+dl}	Gravelly soil	Gravelly clay	13	9	18	14	10	19	25	21	31
Q^{col+dl}		Gravel and soil	13	9	18	15	11	20	26	22	32
Q^{del}		Rock blocks and soil	14	10	19	17	13	22	30	25	34
Q^{ml}	Refills	Artificial refills	14.6	9	22	16.8	11	24	27	18	35
J_{2S} J_{1-2Z}	Redbeds Intensively weathered layer	Intensively weathered mudstone	16	14	19	18	16	21	31	23	35
T_{2b}		Intensively weathered sandstone	17	14	19	19	16	21	32	23	35

consolidated accumulation with relative particularity. Wushan loess-like soil is mainly distributed along the banks around Wushan, with also exposures in Fengjie, Yunyang, Fengdu, and Fuling. In the ordinary course of events, its steady under-water eigenvalue angles are from 10° to 12°, wash–abrasion eigenvalue angles are from 12° to 15°, and steady above-water eigenvalue angles are from 20° to 30°. The intensely whole weathered granite belt is mainly distributed along sections of banks close to the dam, namely sections of the banks along Yiling and Zigui. In normal cases, the steady underwater eigenvalue angles are from 10° to 12°. Wash–abrasion eigenvalue angles are from 13° to 18°. Steady above-water eigenvalue angles are from 20° to 45°.

Bank Collapse Prediction Parameter of Redbed Slope

The redbed slopes in the Three Gorges reservoir area are characteristic for their lithological weakness, poor weather resistance, and easy disintegration in immersion. Through the destabilization of immersion, the redbed slope is liable to collapse and recess. The redbed slopes in the area, however, are widely distributed in Badong, Fengjie, Yunyang, Wanzhou, Kaixian, Shizhu, Zhongxian, Fengdou, Fuling, Changshou, and the urban area of Chongqing (the reservoir postlude) and the area around Chongqing. Redbed bank collapse often happens along the intensely weathered banks. In normal cases, the steady underwater eigenvalue angle of the intensely weathered redbed bank is 16°, the wash–abrasion eigenvalue angle 20°, and steady above-water eigenvalue angle 35°.

Evaluation of Bank Collapse Predictions in the Three Gorges Reservoir Area

In the Three Gorges reservoir area, the bank slope structure is varied and complicated. The application of traditional bank collapse prediction method has been proven to be unreasonable and is sometimes far beyond the actual situation. In this part of our chapter, Bank-Slope Structure Prediction Method (BSSPM) is presented on the basis of geological spot investigation of several hundred bank sections in the Three Gorges reservoir area, on the combination of bank collapse types, bank collapse parameters, and the analyses of the practical bank collapse regions of Three Gorges reservoir and of the reservoirs that have been analogically studied.

The main principle of BSSPM is based on the features of mountain–river reservoirs, according to different bank slope structures and bank collapse types, using different prediction models to prediction. Bank collapse is forecasted in accordance with different petro-fabric underwater deposit eigenvalue angles, wash–abrasion eigenvalue angles, steady above-water eigenvalue angles, the lowest design level, and the highest design level. BSSPM, a method of analogical illustration, is of great adaptability and versatility.

Classified Illustration in Terms of BSSPM

Illustration of Wash–Abrasion and Toe-Erosion Collapse

Figure 5.4 illustrates the bank collapse that happens on the thick accumulative bank slope. η_1 and η_n refer to the underwater deposit eigenvalue angle of differently composed formations; α_1 and α_n are the wash–abrasion eigenvalue angles; β_1 and β_n are the steady above-water eigenvalue angles; A, B, and C are the points of intersection of the water level and reservoir bank reformation line. D is the intersection of reservoir bank reformation line and the form line. E is the intersection of the highest design level and the form line. L, M, and N are intersections of the boundaries of differently composed formations and reservoir bank reformation line, and S is the reservoir bank reformation width.

Figure 5.4 is explained as follows: With the intersection of static water level and the bank slope as the starting point, lines are in turn drawn in accordance with the inclination angles – the differently composed formations' eigenvalue angles η_1, η_2, ..., η_n. When one of these lines is extended to intersect the lowest design level at B, B also serves as the starting point to draw lines in turn in accordance with differently composed formations' inclination angles – wash abrasion eigenvalue angle α_1, α_2, ..., α_n. When one of these stretch lines intersects the highest design level at C, C once more serves as the starting point to draw lines in turn, in accordance with differently composed formations' inclination angles-above water, steady eigenvalue angle β_1, β_2, ..., β_n. When one of these extended lines intersects the form line of the bank slope at D, we can get the mean horizontal distance between D and E – the predicted bank collapse width S.

According to the prediction idea discussed above, a bank collapse illustration of thin accumulative bank slope with subterranean rock–soil mixture bank slope (including its terrace) and redbed bank slope are presented in Table 5.4.
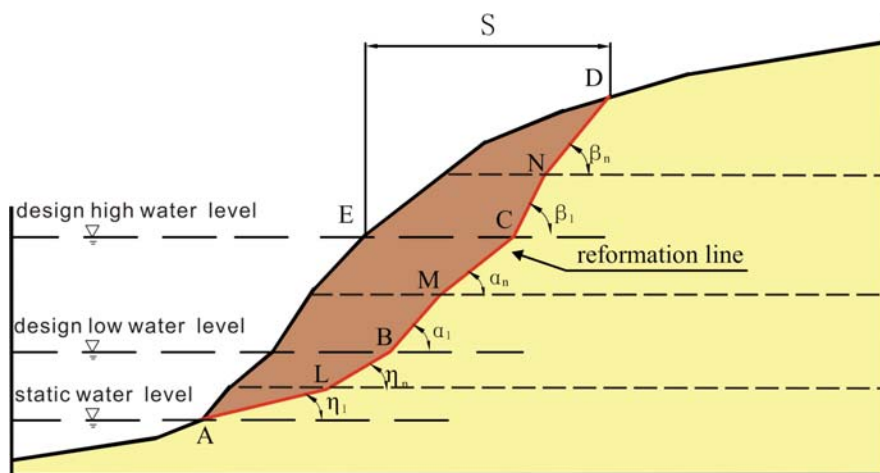

Fig. 5.4 Thick accumulative bank slope's bank collapse width in terms of BSSPM

Table 5.4a   Classified bank collapse prediction in terms of BSSPM: For a fresh bedrock–deposit interface

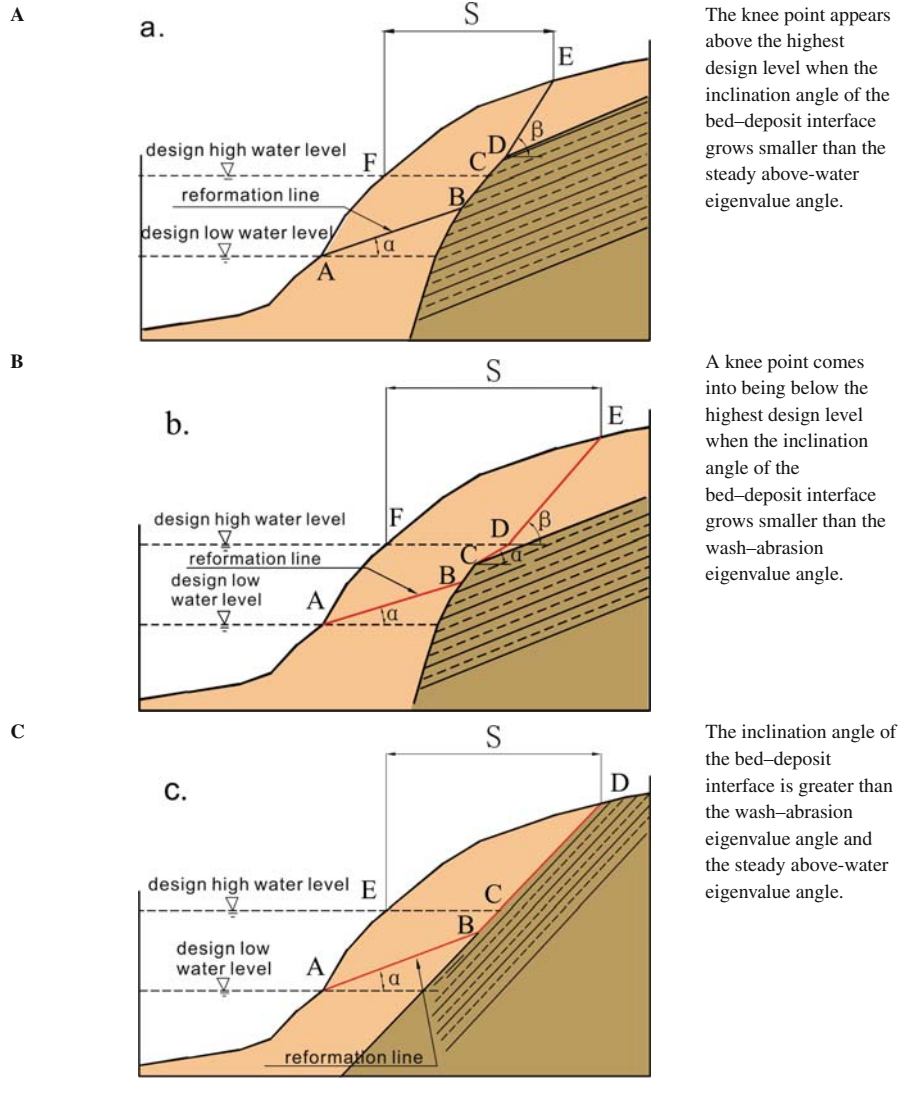| Features of the structure	The prediction line of the bank collapse intersects the bed–deposit interface and the underlying stratum is not weathered.

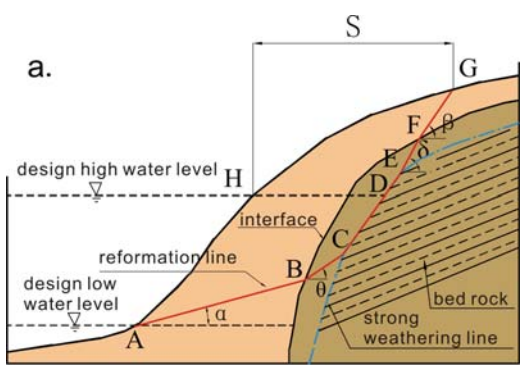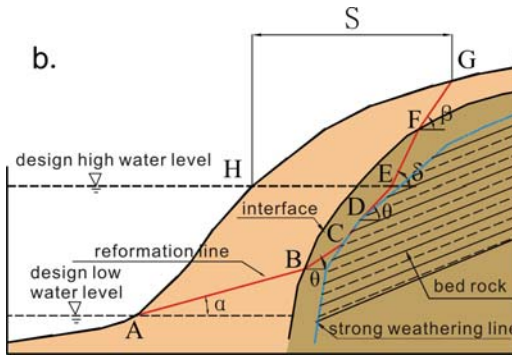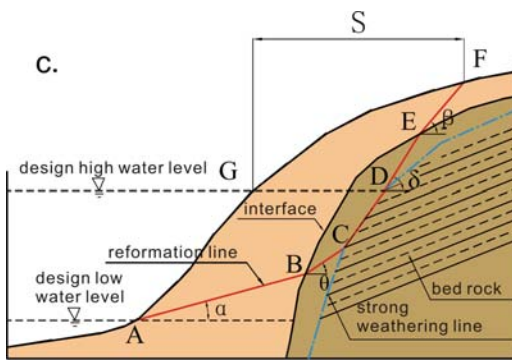| A		The knee point appears above the highest design level when the inclination angle of the bed–deposit interface grows smaller than the steady above-water eigenvalue angle.
B		A knee point comes into being below the highest design level when the inclination angle of the bed–deposit interface grows smaller than the wash–abrasion eigenvalue angle.
C		The inclination angle of the bed–deposit interface is greater than the wash–abrasion eigenvalue angle and the steady above-water eigenvalue angle.

Table 5.4a (continued)

Features of the structure	The prediction line of the bank collapse intersects the bed–deposit interface and the underlying stratum is not weathered.
Illustrations	With the intersection A of the lowest design level and the bank slope as the starting point, below the highest design level, the bank collapse prediction line is drawn according to the inclination angle – the wash–abrasion eigenvalue angle α, the deposit layer. Above the highest design level, the bank collapse prediction line is drawn according to the inclination angle – the steady above-water eigenvalue angle β of the slope deposit. When the bank collapse prediction line meets the bed –deposit interface, the bank collapse prediction line is in agreement with the bed –deposit interface until inclination angle of the bed–deposit interface grows smaller than the steady above-water eigenvalue angle (a) or smaller than the wash–abrasion eigenvalue angle (b) at a certain point at which the bank collapse prediction line is drawn according to the steady above-water eigenvalue angle or the wash–abrasion eigenvalue angle of the deposit layer at the corresponding place. When the inclination angle of the bed–deposit interface remains greater than the wash–abrasion eigenvalue angle and the steady above-water eigenvalue angle, the bank collapse prediction line goes up to the top of the slope along the bed–deposit interface (c). The predicted bank collapse width S equals the horizontal distance from the intersection point of the last bank collapse prediction line and the crest of the slope to the corresponding point of the elevation of the starting point of the steady above-water bank slope line.
Notes	If there are two or more than two types of substance in the target bank slope accumulation, the prediction method of thick accumulative bank slope is supposed to be taken into the synthetic analysis.

Table 5.4b Classified bank collapse prediction in terms of BSSPM: For weathered bedrock–deposit interface

Features of the structure	The prediction line of the bank collapse intersects the bed–deposit interface and the underlying stratum is intensely weathered.

A		
		The knee point appears above the highest design level when the inclination angle at the borderline of the intensely weathered underlying bed rock grows smaller than the steady above-water eigenvalue angle of the intensely weathered rock stratum.

Table 5.4b (continued)

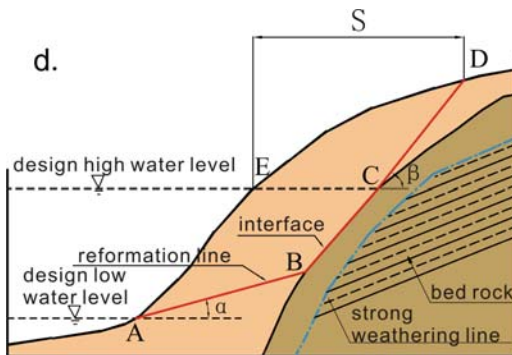| Features of the structure	The prediction line of the bank collapse intersects the bed–deposit interface and the underlying stratum is intensely weathered.

| B | | The knee point appears below the highest design level when the inclination angle of the borderline of the intensely weathered underlying bed rock is smaller than the steady above-water eigenvalue angle of the intensely weathered rock stratum. |

| C | | The inclination angle of the intensely weathered underlying bed rock is greater than the wash–abrasion eigenvalue angle of the intensely weathered rock stratum below the highest design level but smaller than the steady above-water eigenvalue angle of the intensely weathered rock stratum of the highest design level. |

| D | | The inclination angle of the underlying bed–deposit interface below the highest design level is smaller than the wash–abrasion eigenvalue angle of the intensely weathered rock stratum but greater than the wash–abrasion eigenvalue angle of the slope deposit. |

Table 5.4b   (continued)

Features of the structure	The prediction line of the bank collapse intersects the bed–deposit interface and the underlying stratum is intensely weathered.
Illustrations	With the intersection *A* of the lowest design level and the bank slope as the starting point, below the highest design level, the bank collapse prediction line is drawn according to the inclination angle – the wash–abrasion eigenvalue angle α of the slope deposit, and above the highest design level, the bank collapse prediction line is drawn according to the inclination angle – the steady above-water eigenvalue angle β of the slope deposit. When the bank collapse prediction line meets the bed–deposit interface, and inside the bed rock there exists intensely weathered strata with varied thickness, the bank collapse prediction line is drawn according to the inclination angle – the wash–abrasion eigenvalue angle θ or the steady above-water eigenvalue angle δ of each of the intensely weathered rock stratum until the line stops where the last weathered stratum ends. Then the bank collapse prediction line goes along the intensely weathered rock stratum till the inclination angle of the intensely weather rock stratum grows smaller than the steady above-water eigenvalue angle (a, c) or the wash–abrasion eigenvalue angle (b) at the corresponding point of the intensely weather stratum. When the bank collapse prediction line goes once again to the bed–deposit interface, it is goes in accordance with the steady above-water eigenvalue angle β or the wash–abrasion eigenvalue angle α of the slope deposit. If the inclination angle of the bed–deposit interface keeps smaller than the wash–abrasion eigenvalue angle and the steady above-water eigenvalue angle of the intensely weathered rock stratum (d), the bank collapse prediction line goes along the bed–deposit interface till it reaches the crest of the slope or the knee point where the steady above-water eigenvalue angle or the wash–abrasion eigenvalue angle of the slope substance becomes greater than the inclination angle of the bed–deposit interface. The bank collapse prediction line further goes in accordance with the predicted eigenvalue angle of the slope substance till it intersects the crest of slope. The predicted bank collapse width *S* equals the horizontal distance from the intersection point of the last bank collapse prediction line and the crest of the slope to the corresponding point of the elevation of the starting point of the steady above-water bank slope line.
Notes	1. If the bank collapse types a, b, c, and d overlap, an integrated approach involving all corresponding prediction methods is due to be applied. 2. If there are two or more than two types of substance in the bank slope accumulation, the prediction method of thick accumulative bank slope is to be taken into the synthetic analysis.

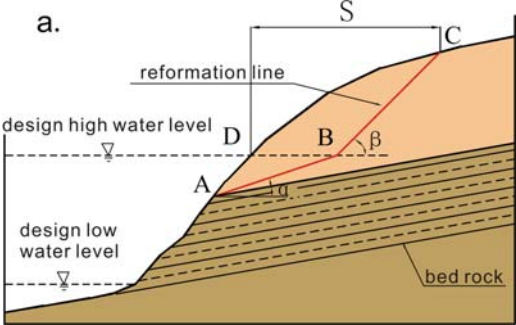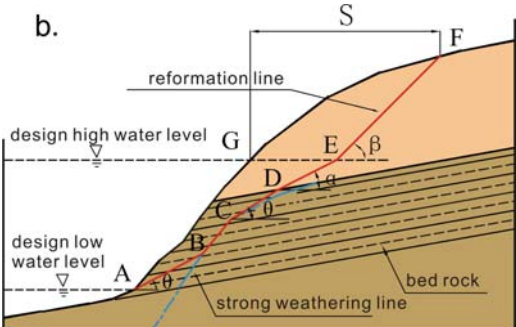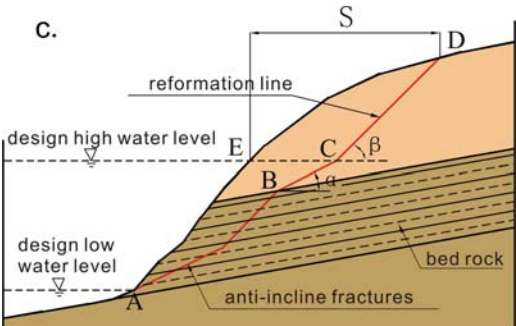**Table 5.4c** Bank collapse prediction in terms of BSSPM: For rock–soil mixture bank slope (including the terrace)

Features of the structure	Rock–soil mixture bank slope (including the terrace)	
A		The rock stratum is not broken and extroversive fissures are not developed.
B		The rock stratum is to a great extent weathered, and the inclination angle of the borderline of intense weathering is greater than the wash–abrasion eigenvalue angle of the intensely weathered rock stratum.
C		The rock stratum is broken, and the extroversive fissures are well developed.

Table 5.4c   (continued)

Features of the structure	Rock–soil mixture bank slope (including the terrace)
Illustrations	If the rock stratum is not broken (a), below the highest design level, the bank collapse prediction line is drawn according to the inclination angle – the wash–abrasion eigenvalue angle α of the bank slope deposit above the bedrock, and above the highest design level, the bank collapse prediction line is drawn according to the inclination angle – the steady above-water eigenvalue angle β of the slope deposit. When there exists in the bedrock intensely weathered rock strata with certain thickness (b), the line is drawn inside the bed rock according to the inclination angle – the wash–abrasion eigenvalue angle θ of the intensely weathered rock stratum until it reaches the borderline. The line then goes along the borderline until the inclination angle of the intensely weathered rock stratum borderline becomes smaller than the wash–abrasion eigenvalue angle at the corresponding point of the intensely weathered rock stratum. The bank collapse prediction line further goes in accordance with the wash–abrasion eigenvalue angle of the intensely weathered stratum, the wash–abrasion eigenvalue angle and the steady above-water eigenvalue angle of the slope deposit above the bedrock. If there are accordant extroversive run-through fissure sets(c) inside the bedrock strata, the bank collapse prediction line inside the bedrock drawn along the fissure set line, the bank collapse prediction line of the slope above the bedrock is the same as the above-mentioned. The predicted bank collapse width S equals the horizontal distance from the intersection of the last bank collapse prediction line and the crest of the slope to the corresponding point of the elevation of the starting point of the steady above-water bank slope line.
Notes	1. If there are two or more than two types of substance in the slope above the roof of the bed rock, refer to the synthetic prediction method of thick accumulative bank slope.
	2. If the accordant rock bank is weathered to a great extent, and there are well-developed extroversive fissure sets, bank collapse types b and c are supposed to be taken into consideration so that the most correlative type is found as the main prediction foundation omite after a comparative study.
	3. If on the highest design level there is still bedrock stratum, the bank collapse prediction is omitted.

Table 5.4d   Bank collapse prediction in terms of BSSPM: For Redbed bank slope (intensely weathered)
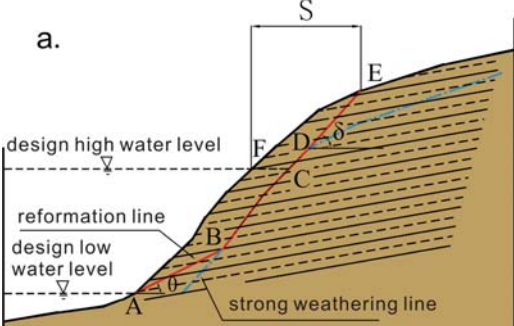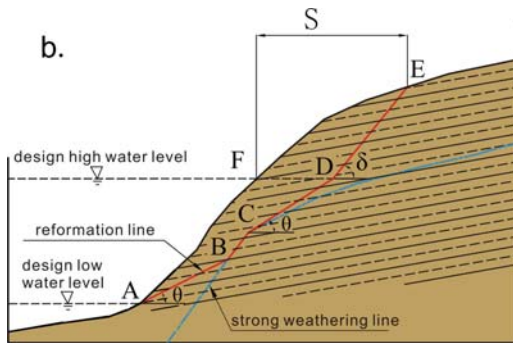
Features of the structure	Redbed bank slope (intensely weathered)

A

The knee point appears above the highest design level when the inclination angle of the borderline of intense weathering grows smaller than the steady above-water eigenvalue angle of the intensely weathered rock stratum.

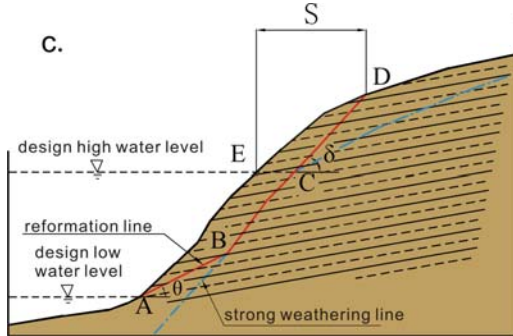**Table 5.4d**   (continued)

Features of the structure	Redbed bank slope (intensely weathered)

B		The knee point appears below the highest design level when the inclination angle of the borderline of intense weathering grows smaller than the wash–abrasion eigenvalue angle of the intensely weathered rock stratum.
C.		The inclination angle of the borderline of intense weathering is greater than the wash–abrasion eigenvalue angle of the intensely weathered rock stratum below the highest design level but smaller than the steady above-water eigenvalue angle at the highest design level.
Illustrations	If there is an intensely weathered stratum with certain thickness in the redbed bank slope, the intersection of the lowest design level and bank slope serves as the starting point A. Below the highest design level, the bank collapse prediction line is drawn according to the inclination angle – the wash–abrasion eigenvalue angle θ of the intensely weathered redbed stratum, and above the highest design level, the bank collapse prediction line is drawn according to the inclination angle – the steady above-water eigenvalue angle δ of the intensely weathered stratum. When the bank collapse prediction line reaches the borderline of the intensely weathered stratum, it goes along the borderline until the inclination angle of the borderline grows smaller than the wash–abrasion eigenvalue angle θ (b) or the steady above-water eigenvalue angle δ (a, c) at the corresponding point of the intensely weathered stratum. The bank collapse prediction line further goes in accordance with the predicted eigenvalue angle of the intensely weathered redbed stratum. The predicted bank collapse width S equals the horizontal distance from the intersection of the last bank collapse prediction line and the crest of the slope to the corresponding point of the elevation of the starting point of the steady above-water bank slope line.	
Notes	(1) Reference to the prediction method of thick accumulative bank slope is necessary in the case of the banks along the Yichang–Badong in Hubei, Wanzhou, Fengjie, Yunyang, and other places in Chongqing if the lowest design level after reservoir storage is higher than the low water level before the reservoir filling. (2) If there are two or more than two types of substances in the slope above the water level, the prediction method of the accumulative bank slope is to be applied.	

Bank Collapse Prediction of Landslide

The traditional broken line model is not suitable for the research of landslide bank collapse in terms of its application principle and the deformation mechanism. The traditional bank collapse prediction method often leads to results too far from the actual bank collapse situation. In fact, landslide bank collapse is essentially a problem of stream-caused landslides. The prediction of bank collapse width, actually, is to define the landslide scope, especially the posterior border of the slide. It is more feasible to use limit equilibrium analysis method or numerical simulation means, both employed to find the potential sliding plane which is further used to define the bank collapse width. The research, however, is actually slope (landslide) stability analysis, which has deviated from the normally defined bank collapse prediction.

Attention Points on the Application of BSSPM

(1) Accurate and reasonable geological models should be established before the bank collapse prediction is applied.

(2) When two or more structural patterns overlap along the bank slope, their corresponding bank structure prediction methods should be integrated.

(3) The definition of eigenvalue angles follows the steps – first, the investigation and definition of the statistical values of underwater steady eigenvalue angle (shoal accumulation eigenvalue angle), wash–abrasion eigenvalue angle, and steady above-water eigenvalue angle of the target bank slope having different compositions. Secondly, statistical values are applied to the research of bank collapse prediction. Statistical value, here, is used to mean the average obtained via great amount of spot measurements of the three eigenvalue angles around the target section plane of the corresponding bank slopes, with having different composition.

(4) The borderline of the intensely weathered bed rock refers to the borderline between the intensely weathered rock stratum and the moderately weathered rock stratum. The research of bank collapse prediction has been done only within the intensely weathered belt in most cases.

(5) In the case of wash–abrasion bank collapse, due to the long process of the bank collapse evolution, the bank collapse prediction borderline cannot simply be regarded as the potential sliding plane, and the limit equilibrium method cannot be used just as well to analyze the stability of the bank slope so that the bank slope protection works are designed. The reason is that wash–abrasion bank collapse and landslide bank collapse are different in terms of evolutionary processes and mechanical mechanism, so the two cannot be confused with each other.

(6) In the case of rock–soil mixture bank slopes, if the highest design level is still located on the bed rock, it is not necessary to do the research on bank collapse prediction.

(7) For the rock bank slopes, prediction researches are only done on the redbed slope and bank slopes with abnormally developed joint fissures within the water level range, or bank slopes with intensely weathered depth within the water level range.

Application of BSSPM

Application of BSSPM in the Analogical Prediction of Reservoir Bank Collapse

In order to test the validity and reliability of BSSPM in application, Ertan reservoir on Yalong River, Baozhusi reservoir on Bailongjiang River, and Gongzui reservoir on Dadu River, which have similarities to mountain–river reservoirs after years of water storage, are analogically studied in term of bank collapse. The comparative study of prediction results and the practical bank collapse widths are shown in Table 5.5.

Table 5.5 Comparison of the predicted width and the real bank collapse width in similar reservoirs

Reservoirs for comparison	Bank collapse sites	Bank collapse types	Slope structure	Predicted width S (m)	
				BSSPM	Physical circumstances at present
Ertan	Matoutian	Toe-erosion collapse	Soil slope	42	35
	Daniuwan	Toe-erosion collapse	Soil slope	15	12
	Bawangshan	Landsip	Rock and soil mixture slope	8.2	6.8
Baozhusi	Huangniliang	Wash and abrasion	Soil slope	17	13
Gongzui	Zhusihe Section	Wash and abrasion	Soil slope	2.6	0.5
	Gonghe Station terrace	Wash and abrasion	Soil slope	10.6	8
	Fishing sandbar	Wash and abrasion	Rock and soil mixture slope	0.8	0.8

Table 5.5 shows that the predicted results obtained by BSSPM are very close to the practical survey except that the predicted width is generally slightly larger than the usual width which refers to the reformed width after gaining balance through the long-term action of the reservoir water.

The Application of BSSPM to the Bank Collapse Prediction in Three Gorges Reservoir Area

BSSPM is employed to forecast bank collapses along several hundred sections of representative bank slopes in the Three Gorges reservoir area. With the employment of remote sensing technology, the factual bank collapses are monitored after the first

Table 5.6 Comparison of the predicted bank collapse width and real bank collapse width in Three Gorges reservoir area

Monitor region	Bank collapse types	Collapse sites	Monitor result via remote sensing			Result via bank slope structure prediction method	
			Bank collapse length (m)	Bank collapse width (m)	Height of posterior edge (m)	139 m bank collapse width (m)	Height of posterior edge (m)
Slope close to the bank	Wenchangge	Wash and abrasion	8	16	145	20.5	148
	Shawan	Landslide	40	20	151	23	155
Badong	Upper par of Ljiawan	Landslide	50	30	150	32	150
	Jiaojiawuchang	Landslide	15	13	145	15	148
Fengjie	Xinfangzi	Landslide	120	100	190	110	195
	Wulipu	Wash and abrasion	20	10	142	15	145
	Zhujiahuayuan	Toe-erosion collapse	40	15	145	15	145
	Chengjiawan	Landslide	20	30	146	35	150
	Wanjiazui	Toe-erosion collapse	80	20	143	25	150

storage up to the 139 m level, in the Three Gorges reservoir area. Table 5.6 shows the real bank collapses after the storage level reaches 139 m in the Three Gorges reservoir area and the predicted results obtained by BSSPM.

Table 5.6 shows that the predicted results via BSSPM and the actual bank reformations after the first storage level are very close in terms of their scale, and the former is just a little bit greater than the latter. Because of the gradualness of bank collapse evolution, it is reasonable that the bank collapse width is shorter than the predicted width. The prediction by means of BSSPM, therefore, matches the bank collapse occurrences in the Three Gorges reservoir area, and BSSPM, with satisfactory adaptability and reliability, can be applied to bank collapse forecasting for such mountain–river reservoirs as the Three Gorges reservoir.

Conclusions

This chapter, on the base of plenty of exploration data of bank collapse in the Three Gorges reservoir area through geological investigations, field measurement of the bank collapse parameters, physical simulation indoors, theoretical analysis, and other comprehensive means, has systematically explored the bank collapse types, bank collapse parameters, and bank collapse prediction method. Three conceptions can be concluded.

(1) The representative bank collapse types in the Three Gorges reservoir area are wash and abrasion, toe-erosion collapse (wave-current ladder, toppling collapse, and cave-in), rock break-off and slides (block break-off and slides, soft-toe collapse, and mudstone recess), and landslide (reactivation of old landslides, sliding of the plane layer of the thick loose deposits, sliding along the bed–deposit interface, and bedrock slide along the accordant weak layer). The evolutionary processes, distribution features, and corresponding geological conditions of these bank collapse types are explored as well.

(2) After much spot investigation and measurement of the bank collapse parameters along the representative bank sections in the Three Gorges reservoir area, several bank-collapse-related eigenvalue angles of the rock and soil masses, including underwater deposit eigenvalue angle θ, wash–abrasion eigenvalue angle α, and steady above-water eigenvalue angle β, are discussed in the chapter. Through statistical analysis, regularity relationship between bank collapse prediction parameters eigenvalue and the composition and mechanical features of the rock and soil mass, the hydrodynamic conditions in the reservoir have been acquired.

(3) Bank-Slope Structure Prediction Method is put forward by the authors of this chapter to deal with bank collapse prediction of such mountain–river reservoirs as the Three Gorges reservoir with complicated slope structure, compositional substances, and dynamic conditions. Bank-Slope Structure Prediction Method is designed in accordance with the characteristics of mountain–river reservoirs, with different prediction models to deal with different slope types,

slope structures, and bank collapse types. Bank collapses are forecasted via the calculation of underwater deposit eigenvalue angle, wash–abrasion eigenvalue angle, steady above-water eigenvalue angle of the varied petro-fabric formations, and through the prediction of the highest design level and the lowest design level. The application of Bank-Slope Structure Prediction Method to the bank collapse investigation of Ertan reservoir, Baozhusi reservoir, and Gongzui reservoir sufficiently supports the argument that Bank-Slope Structure Prediction Method applies well to the bank collapse prediction of mountain–river reservoirs analogous to the Three Gorges reservoir.

On account of many factors, bank collapse prediction, like the prediction of earthquakes and landslides, requires systematic research. To achieve breakthroughs in the prediction range of the bank collapse, more fundamental and further research is still needed in terms of influencing and representation factors affecting slope stability.

References

Fan YC, Zhang YY, Hu XW (2002) Prediction method and evaluation for reformation of reservoir bank. *Sichuan Water Power*, 21(4): 69–83 (in Chinese)

Huang RQ, Xu Q, Li YS (2005) *An Evaluation Study of the Bank Collapse Types, Bank Collapse Prediction Parameter, and the Prediction Area*. Chengdu: Chengdu University of Technology (in Chinese)

Ma SZi, Jia HB, Tang HM (2002) Analogy method with stable side shape to predict reservoir side rebuilding of rock shore. *Earth Science-Journal of China University of Geosciences*, 27(2): 231–234 (in Chinese)

Tang HM (2003) A study on reservoir bank collapse and its engineering prevention in the Three Gorges project. *Journal of Ezhou University*, 10(4): 1–6 (in Chinese)

Tang MG, Xu Q, Huang RQ (2006a) Types of typical bank slope collapses on the three gorges reservoir. *Journal of Engineering Geology*, 14(2): 172–177 (in Chinese)

Tang MG, Xu Q, Huang RQ (2006b) Study on the forecasting parameters of the bank collapse and the influence factors in the Yangtze Three Gorges project region, China. *Journal of Chengdu University of Technology (Science of Technology Edition)*, 33(5): 460–464 (in Chinese)

The Research Group of Bank Collapse of Guanting Reservoir (1958) *A Study of Reservoir Bank Collapse.* Beijing: China Water Publishing House (in Chinese)

Wang YM, Tang JH, Ling JM (2000) Study on prediction method for reservoir bank caving. *Chinese Journal of Geotechnical Engineering*, 22(5): 569–571 (in Chinese)

Xu RC (2003) *Red Stratum and Dam*. Wuhan: China University of Geosciences Press (in Chinese)

Xu Q, Liu TX, Tang MG (2007) A new method of reservoir bank-collapse prediction in the Three Gorges reservoir-River bank structure method. *Hydrogeology & Engineering Geology*, 34(3): 110–115 (in Chinese)

Yin YP (2004) *Prevention Study on Big Geology Hazards of New Settlement Address of Three Gorges*. Beijing: Geological Press (in Chinese)

Zhang QH, Ding XL, Zhang J (2002) A Study of slope rebuilding of Fengjie stream segment after the Three Gorges project reservoir impoundment. *Chinese Journal of Rock Mechanics and Engineering*, 21(7): 1007–1012 (in Chinese)

Zhang XG, Li ZY, Zheng DH (1998) *Specialized Engineering Geology*. Beijing: Geological Press, pp. 236–241 (in Chinese)

Zhang ZY, Wang ST, Wang LS (1994) *Analyzing Theory of Engineering Geology*. Beijing: Geological Press (in Chinese)

Караушев AB (1958) *Rivers and Reservoir Dynamics*. Beijing: China Water Publishing House (Chinese translation by Cheng CG)

Chapter 6
Distribution Features of Landslides in Three Gorges Area and the Contribution of Basic Factors

Jianping Qiao and Meng Wang

Distribution Features of Landslides

The research area in this chapter is the Three Gorges area from Yunyang to Wushan county, which is about 100 km long and 40 km wide and covers some 4,000 km^2 in total. Forty percent of landslides in the Three Gorges area happened in this region, and 205 landslides have been recorded with relatively complete data. Factors such as the stratum, structure and shape of the slope are the main environmental factors that predispose failure conditions for landslides in this region. These factors are referred to in this chapter as "root factors" (Qiaq et al. 2003) (Figs. 6.1 and 6.2).

Landslides and Lithology

The area has a full strata exposure, while Fengjie county divides the area into two parts: the west and the east. The western part is mainly sandstones and sand–mud interbeds formed of red clastic rocks in Jurassic of Mesozoic, with only a few out-croppings of limestone from the Triassic along the Jialing River, while the eastern part is mainly carbonate strata from the Paleozoic and the Mesozoic, with interbeds of red clastic rocks and coal. The outcroppings in this region range from pre-Sinian to the Jurassic (with only the strata from the upper Silurian of the Paleozoic, the lower Devonian and the upper Carbonic missing). The developments of landslides and collapses in all the strata vary.

Landslides and Environment

From the landslide-generating locations of landslides in this region, we can see that the majority of them are closely connected with syncline structures. When folds

J. Qiao (✉)
Key Laboratory of Geo-surface Process and Mountain Hazards, Institute of Mountain Hazards and Environment, Chinese Academy of Science, Chengdu 610041, China
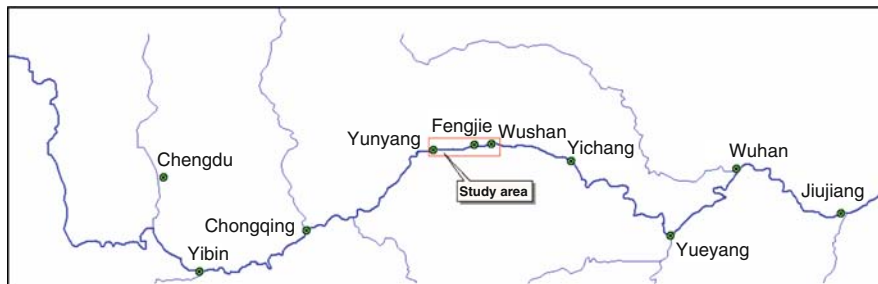
Fig. 6.1 Location of the study region on the Yangtze River
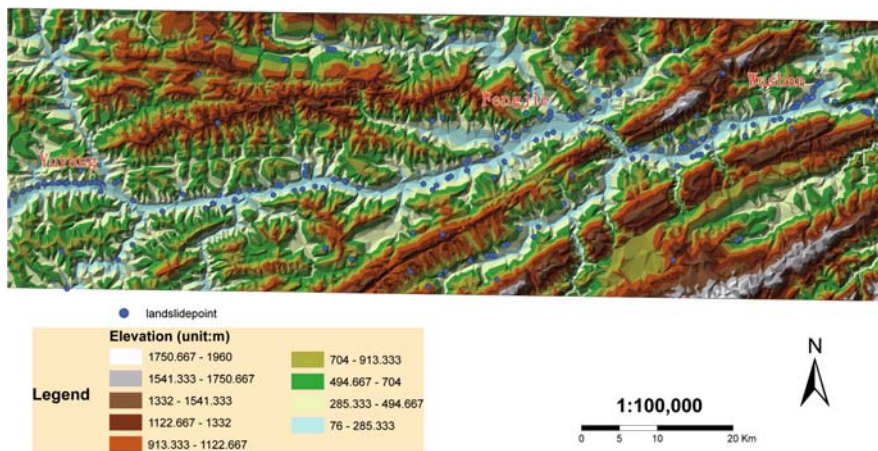

Fig. 6.2 Topography and distributions of landslides

develop, the stratum that forms the landslide is at the transitional zone and is characteristic of being steeper in the upper part and gentle in the lower part and also of a certain inclination (about 20°). On the other hand, the cross fractures on the narrow anticline control the distributions of the secondary ravines, which are very much developed. So when the edge of the valley, the stratum production, the lithology condition and the structural terrain occur together, the sliding surface, namely the stratum mentioned above, is vulnerable to failure by a comparatively weak surface. Thus facing the river and under gravity, the upper part of the stratum cannot remain intact and it slides down.

Landslides and Landforms

Fengjie county divides the Three Gorges area into two parts with striking differences in terrain and formation lithology. To the west of Fengjie county is a medium and low mountainous area and an open valley, which is mainly composed of red

clastic sedimentary from the Triassic and Jurassic, and the terrain is strictly controlled by geological structure. The anticline forms the mountain and the syncline forms the valley, which accordingly makes up a medium and low mountainous area with a "narrow range" but a "wide valley." East of Fengjie and far off to Yichang city, features are mainly made up of metamorphic assemblage in Algonkian, carbonates and clastic rocks in Sinian and lower Proterozoic. Daba Mountain and Wushan Mountain are features located in this region, forming an erosion geomorphology with mainly medium and low mountains and valleys.

Characteristics of Landslide Hazards

According to the investigations from 1984 to 1990 made by Chengdu Institute of Mountain Hazards and Environment (CAS), the river banks from the Three Gorges Dam to Chongqing city (to the west of the dam) have experienced a total of 214 recorded landslides and collapses, the combined mass of which amounts to 13.52×10^8 m^3, among which 47 collapses produced 1.173×10^8 m^3 in volume and 167 landslides 12.35×10^8 m^3. Collapses and landslides accounted for 21.96% and 78.04% of the total number with 8.6% and 91.4% of the total mass respectively (Table 6.1). On average, there were 0.36 landslides and a mass of 225.32×10^4 m^3 per km^2.

Table 6.1 shows that the main types of damages in this region were mainly landslides, which could be categorized into seven levels based on scale differences (Table 6.2).

Table 6.2 shows that collapse and landslides are the main characteristics of the damage on the banks and valleys in this area along the Yangtze River. Wanzhou county functions as a divide. Only a few landslides and collapses occurred to the west of Wanzhou, and their volumes are comparatively small, while on the east are commonly large and giant landslides and collapses, with large volumes of mass and high frequency of occurrence. The west part is 317 km long, accounting for 52.8% of the total reach, within which only four giant landslides and collapses with a total volume of 1.05×10^8 m^3 have happened. On average there is one large or giant

Table 6.1 Statistics of landslides and collapses

| Region | Length of the valley (km) | Landslides | | Collapses | | Total | | Percentage of landslides | |
		Number (times)	Volume ($\times 10^8$ m^3)	Number (times)	Volume ($\times 10^8$ m^3)	Total number (times)	Total volume ($\times 10^8$ m^3)	Number (%)	Volume (%)
Chongqing to Three Gorges Dam	600	167	12.35	47	1.173	214	13.52	78.04	91.4

Table 6.2 Statistics of landslides and collapses on the seven levels

Region	Length of the valley (km)	Type	Unit	Scale range (×10⁴ m³)							Total
				<50	50–99	100–500	501–1000	1001–3000	3001–5000	>5000	
Chongqing to Three Gorges Dam	600	Collapse	Times	31.00	7	5	0	3	0	1	47
			Volume	290.50	492	1250	0	3700	0	6000	1.173×10^8 m³
		Landslide	Times	93.00	13	21	8	20	5	7	167
			Volume	1138.20	893	4330	5950	38150	21500	51500	12.35×10^8 m³

Table 6.3 Distributions of landslides and collapses over 1000×10^4 m^3 for areas on both sides of Wanzhou (from Three Gorges area Landslide Headquarter of the Ministry of Land and Resources, 2003)

Item	The west part (on the west of Wanzhou)	The east part (on the east of Wanzhou)
Length of the valley (km)	317.00	283.00
Percentage in the total reach (%)	52.80	47.20
Landslide and collapse (times)	4.00	7.00
Each landslide for average length along the total reach (km/time)	79.25	40.43
Volume ($\times 10^8$ m^3)	1.04	0.97
Volume every km (10^4 m^3/km)	32.81	34.44

landslide or collapse every 79.25 km, and 32.81×10^4 m^3 of deposits per kilometer. The east part is 283 km long, taking up 47.2% of the total, within which seven large and giant landslides and collapses have occurred, producing 0.97×10^8 m^3 of deposits, which means that there should be one large or giant landslide or collapse every 40.43 m^3 and 34.44×10^4 m^3 of deposits per kilometer (Table 6.3).

From the statistics (2001) by Chengdu Institute of Mountain Hazards and Environment (CAS), we can see that among the 205 typical landslides in this region (from Yunyang county to Wushan county), 24 (11.7%) are over 1000×10^4 m^3 in volume. Ten happened in Yunyang, 11 in Fengjie, 3 in Wushan, totaling 62209.8×10^4 m^3 in volume (Table 6.4).

Root Factors of Landslides

Factors such as stratum lithology, gradient, height difference, aspect, slope shape are the decisive internal characteristics that can cause landslides (here triggering factors are not considered). External factors cannot easily trigger landslides without

Table 6.4 Statistics of landslides on different scales occurring in the area between Yunyang and Wushan

Region	Unit	Range interval ($\times 10^4$ m^3)					
		<1	1–10	10–100	100–1000	>1000	Total
Yunyang	Time	24	2	21	7	10	64
	Volume $\times 10^4$ (m^3)	0.1153	15	945	1662	28028.8	30650.9153
Fengjie	Time	19	16	26	12	11	84
	Volume $\times 10^4$ (m^3)	0.07	106.5	1300.5	3783	27481	32671.07
Wushan	Time	25	1	17	11	3	57
	Volume $\times 10^4$ (m^3)	0.145	5.6	618.1	4645.59	6700	11969.435
Total	Time	68	19	64	30	24	205
	Volume $\times 10^4$ (m^3)	0.3303	127.1	2863.6	10090.9	62209.8	75291.4203

these internal characteristics being present, and their parameters and attributes can be obtained through surface investigation and GIS (Dong & Wong 1987; Darevskii & Romanov 1994; Aleotti 1999). Each root factor makes different function to landslide processes, and "contribution rates" are used here to represent different effects on the development of landslides. "Contribution rates" are a measureable determination of to what extent, in terms of a comparative percentage, these contributing features are each responsible for landslide occurrence. Practically, the contribution rate of the root factor has gained a weighted application. The part from Yunyang to Wushan has been densely distributed with numerous dangerous landslides that account for 40% of the total in the whole area. The inventory database of the landslides from Chengdu Institute of Mountain Hazards and Environment has stored the data and a distribution map of these 205 landslides within a region of 100 km long and 40 km wide; all these landslides occurred after 1970s. In each document, root factors of the landslide process can be found. GIS was used to make a 1:200,000 geological map (processed protectively) and a 1:50,000 digitally processed topography with related vectors, to supplement some missing information in the database and to establish an environmental information graph. A total of 7,440,000 sampling grids (covering an actual area of 4,650 km^2) are formed after the topography is processed with a 25×25m grid. Thus the precision of the information graph has a high level of accuracy, and the analytical data of the root factors are up to quantitative standard, making the research results more reliable.

Inversion of Root Factors

The inversion of root factors approach is to first assess the data for the 205 landslides from the CDMI database and find out the interrelation between the landslides and the root factors. At this point determine the type of factors and establish a corresponding calculating standard. Finally, examine the effects of these root factors as to the development of landslides. The interrelation is as follows:

$$\sum f(U_1, U_2 \cdots U_i) \rightarrow \sum f'(U_1', U_2' \cdots U_i') \tag{6.1}$$

In this formula, f is the relation between the landslide and the root factor, U_1, $U_2 \cdots U_i$ the root factors, f' the relation between environment and root factors and $U_1', U_2' \cdots U_i'$ environmental root factors.

Determining the Root Factors of Landslides

From the writer's extended research experience about landslides in the Three Gorges area and some results gained by other scholars of the same research field (e.g. Wu et al. 2004; Liu 2003; Tang et al. 2004; Zhu 2004; Zhu et al. 2004; Liu & Ni 2005), we can see that the inner conditions forming the landslides are closely related to factors

such as stratum lithology, gradient, slope shape, height difference, aspect, which can be obtained through field investigation and various graphs and data. If the triggering factors and the inner structure of the slope are not considered and the five factors influencing the development of landslides are defined as the root factors, the set U_i in formula (6.1) can be represented as follows:

$$U_i \in (U_1, U_2, U_3, U_4, U_5) \tag{6.2}$$

In this formula, U_1 is lithology, U_2 slope grade, U_3 slope shape, U_4 height difference and U_5 aspect.

Statistics of Environmental Root Factors

We can build a graph of information layers about these five environmental root factors according to the root factors (U_i) that affect landslides using the ArcGIS software system, then add the set (U_i') of environmental root factors to formula (6.1), which can be represented as follows:

$$U'_i \in (U'_1, U'_2, U'_3, U'_4, U'_5)$$

In this formula, U'_1 is stratum, U'_2 gradient, U'_3 slope shape, U'_4 height difference and U'_5 aspect. In the graph of five digitalized layers, 7,440,000 grids are built and sampled, and 37,000,000 environmental root factors are obtained (Fig. 6.3), which can be used as the basic information for the statistical analysis about the contribution rate.
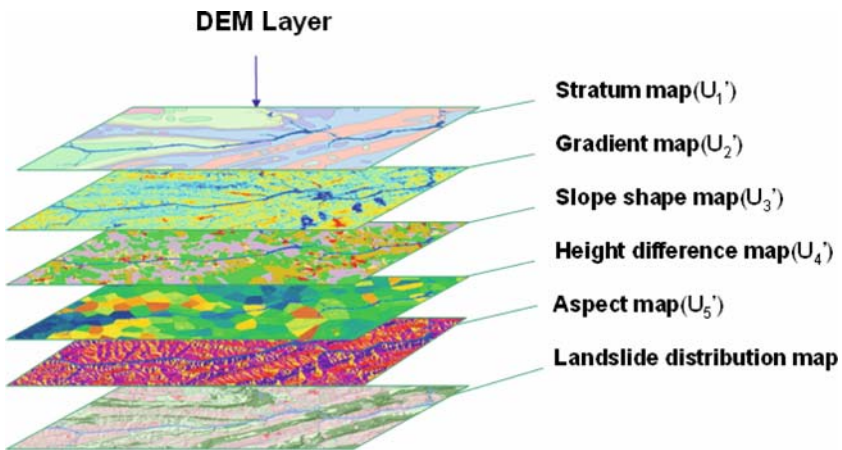
Fig. 6.3 The topography of environmental root factors

The Contribution Rates of Root Factors to Landslides

Contribution rate is an approach to analyzing the influence of root factors on landslides, which is meant to get a quatitative evaluation of each factor's impact on the development of a landslide. By calculating the contribution rate, a easy mathematical method borrowed from economics, we can visualize the rule of root factors' impact on the development of landslides (Fig. 6.4).

Contribution Index

After establishing the inverse relation between the root factors of landslide and environmental root factors, S_i, as the evaluation index, is chosen to get the following formula that shows the environmental factors' impact on the development of landslides:

$$U_1'' = U_1'(S_i) = U_1'(S_1, S_2, S_3)$$
$$\vdots \tag{6.3}$$
$$U_5'' = U_5'(S_i) = U_5'(S_5, S_5, S_5)$$

In this formula, S_1 stands for the area of landslides with U_1', S_2 for the number of landslides within U_1', S_3 for the mass of the landslides occurred within U_1', and U_2', U_3', U_4', U_5' repeat the formula in the same way. The three evaluation indexes S_1, S_2
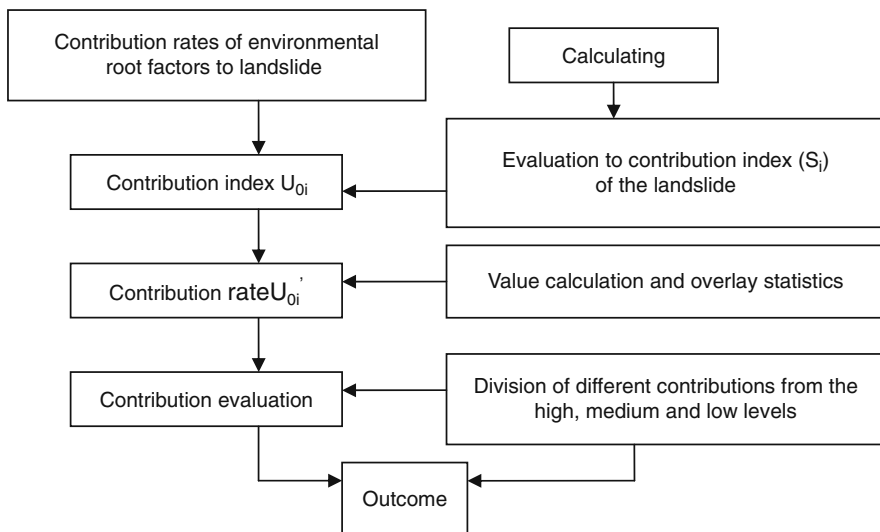
Fig. 6.4 Evaluation sequence for the environmental root factors

and S_3 are used to calculate the environmental root factors' contribution index to the development of landslides:

$$U_{oi} = U_i''/M = (U_1'', U_2'', U_3'', U_4'', U_5'')/M \qquad (6.4)$$

In this formula, U_{oi} stands for the contribution index, U_i'' the set of valued factors, $U_1'' \cdots U_5''$ valued factors, M the sum of evaluation index ($M=3$ namely S_1, S_2, S_3). When formula (6.4) is extended, a calculating relation of the five factors' contribution index can be expressed as follows:

$$U_{o1} = U''_1/M = U_1'(S_1, S_2, S_3)/M$$
$$\vdots \qquad (6.5)$$
$$U_{o5} = U''_5/M = U_5'(S_1, S_2, S_3)/M$$

In this formula, U_{o1} stands for the contribution index of lithology, U_{o2} for that of slope grade, U_{o3} for that of slope shape, U_{o4} for that of height difference and U_{o5} for that of aspect. A contribution index only represents a calculating numerical interval of the root factor, but it cannot sufficiently show the degree of impact on the development of landslides.

Contribution Rate

Contribution rate is a standard to figure out the degree of a certain factor's influence, and it can be used to evaluate environmental root factors' influence on landslides. The approach is to figure out the five environmental root factors' respective impact on the landslide in a certain area, and the contribution rate can be represented as follows:

$$U_{oi}''(\%) = U_{oi}/\sum U_{oi} \times 100\% \qquad (6.6)$$

In this formula, U_{oi}' stands for contribution rate. If formula (6.6) is substituted with formula (6.4) and (6.5), then the calculation formula of the five root factors' contribution rate can be expressed as follows:

$$U_{o1}'(\%) = \frac{U_1'(S_1,S_2,S_3)/M}{\sum U_1'(S_1,S_2,S_3)/M}$$
$$\vdots \qquad (6.7)$$
$$U_{o5}'(\%) = \frac{U_5'(S_1,S_2,S_3)/M}{\sum U_5'(S_1,S_2,S_3)/M}$$

Using formula (6.7), we can work out these five root factors' contribution rates.

The Contribution Rates of Strata (ρ_i)

The Contribution of the Strata's Areas (ρ_1)

There are 22 strata in this region, and the proportion of each stratum will show its possible contribution rate on the landslide (Fig. 6.5).

In this diagram, ten strata respectively account for more than 2% of the total number. Here, their area S is greater than or equals to 100 km^2, accounting for 94.658% of the total area, and they are the prominent strata lithology in this region.

(1) The Jurassic strata

> J_2s – Upper Shaximiao Formation Group: mudstone, quartz sandstone, siltstone
>
> J_3p – Penglai Group: mudstone, quartz sandstone
>
> J_3s – Suining Group: quartz sandstone, siltstone, mudstone
>
> J_1z – Zhenzhuchong Group: quartz sandstone, siltstone, shale, rock with coal hold between at the bottom
>
> J_2xs – Lower Shaximiao Formation Group: mudstone, shale
>
> J_2x – Xintiangou Group: mudstone, sandstone

(2) The Triassic strata

> T_2b – Badong Group: limestone, shale, rock with clay at the bottom
>
> T_1j – Jialingjiang Group: limestone, brecciaous limestone, dolomite, occasionally plaster holds between
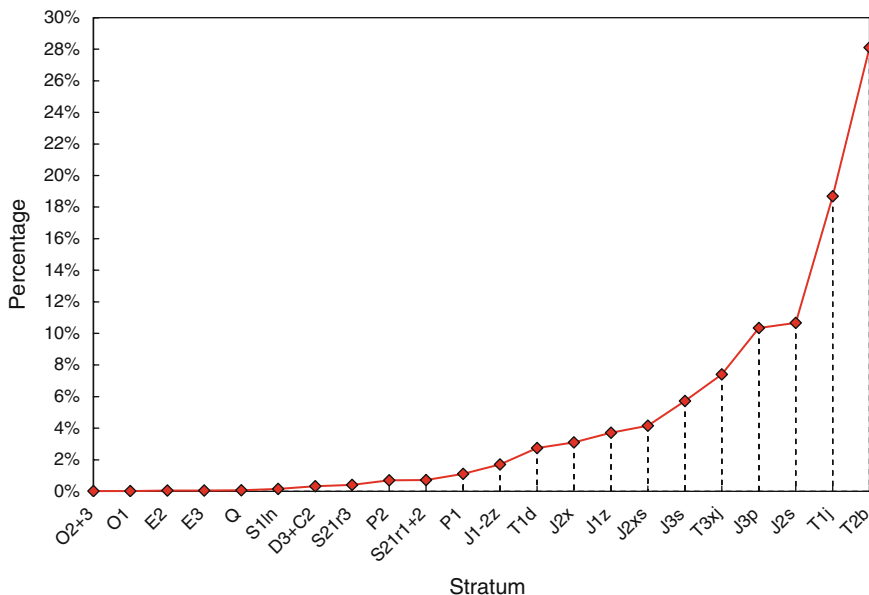
Fig. 6.5 A diagram showing the distribution of each stratum's area as a percentage of total

T_3xj – Xujiahe Group: lithic sandstone, siltstone, shale, coal
T_1d – Daye Group: limestone

The Contribution to the Number of Landslides (ρ_2)

Among the 22 strata in this region, 8 types have never experienced landslides. Hence they are considered to have no contributions to landslides. Another four kinds, namely D_3+C_2, Sz_1r_3, P_2 and P_1, are apt to suffer landslides, but they comprise a very small part of the area, which does not make significant contributions to landslides in this region. These 12 kinds account for only 5.342% of the total area of the studied region, so they should not be considered in the evaluation. Thus the rest 10 are the prominent kinds, and if the contribution rate of each is recorded (Fig. 6.6), the sensitivity of each stratum to the number of landslides can be analyzed.
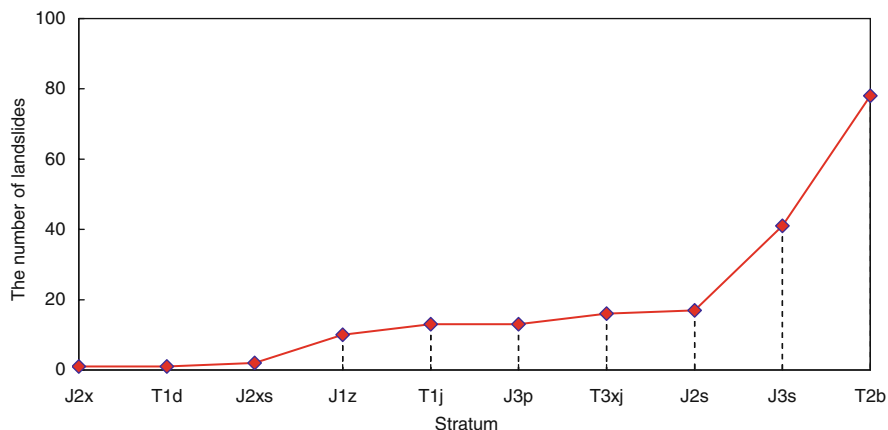
Fig. 6.6   Graph showing the number of landslides distributed in each type of strata

The Contribution to the Scales of Landslides (ρ_3)

Generally, the contribution of a certain stratum to the mass of the landslide shows the scale of the landslide and the possible damage, and it is a key factor in the analysis of possible dangers. Evidently, there can be special cases. For instance, landslides in towns may be small in scale, but due to the dense population, the damage is apparently far greater in the countryside. A case in point is the landslide that happened in Wushan. The mass of the landslide is only 100,000 m^3, but the damage was far greater than a landslide with a mass dozens of times or even hundreds of times larger in the countryside, which was because of the dense population in the town. Here, in order to avoid complicating the problem, we will only discuss the distributions
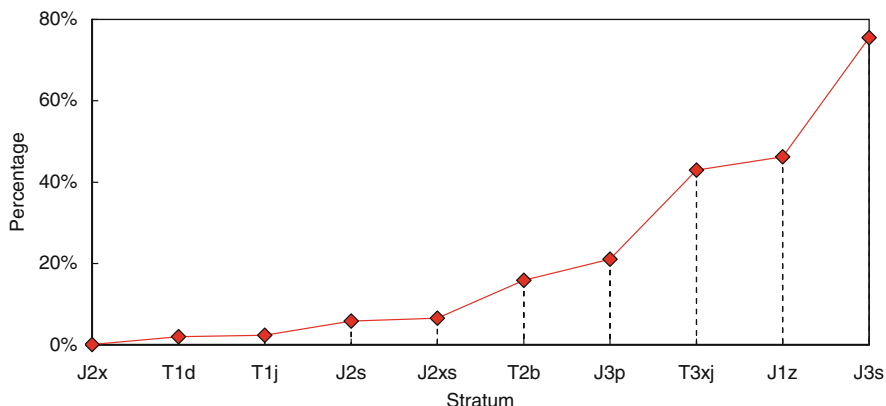
Fig. 6.7 The relation between the mass of the landslide and the stratum's area

of the landslides and will not refer to the type of landslides for the moment. The greater volume a stratum contributes to a landslide, the more large landslides will develop within this stratum (Fig. 6.7)

Calculating the Contribution Rates

Giving Values

When the contribution types of the strata are given different figures (10, 9, ... 2, 1), then Table 6.5 can be represented as follows:

In Table 6.5 the principle of giving values is that for a different contribution type and the more the contribution a stratum makes to the landslide, the larger the figure will be, and vice versa. A certain kind of stratum shows different results for different contribution types, so the values of different contribution types vary. Applying the actual contribution value directly still works. For instance, we can take the contribution values in Tables 6.6, 6.7, and 6.8 for calculation.

Table 6.5 Given values to contribution types of landslide-prone strata

Contribution type	Giving values to strata
ρ_1	$(T_2b)_1 (T_1j)_1 (J_2s)_1 (J_3p)_1 (T_3xj)_1 (J_3s)_1 (J_2xs)_1 (J_1z)_1 (J_2x)_1 (T_1d)_1$ 10 9 8 7 6 5 4 3 2 1
ρ_2	$(J_3s)_2 (T_2b)_2 (J_1z)_2 (T_3xj)_2 (J_2s)_2 (J_3p)_2 (T_1j)_2 (J_2xs)_2 (T_1d)_2 (J_2x)_2$ 10 9 8 7 6 5 4 3 2 1
ρ_3	$(J_3s)_3 (J_1z)_3 (T_3xj)_3 (J_3p)_3 (T_2b)_3 (J_2xs)_3 (J_2s)_3 (T_1j)_3 (T_1d)_3 (J_2xs)_3$ 10 9 8 7 6 5 4 3 2 1

Table 6.6   Evaluations of the strata's contribution degrees

Classifications of strata (ρ)	Contribution rate U'_{01} (%)	Contribution degree
T_2b	16.4	$D_0(\rho)_1$ (high)
J_3s	15.3	
T_3xj	13.1	
J_1z	11.7	$D_0(\rho)_2$ (medium)
J_3p	11.7	
J_2s	10.4	
T_1j	9.0	
J_2xs	6.7	$D_0(\rho)_3$ (low)
T_1d	3.1	
J_2x	2.6	

Table 6.7   Evaluations of the contribution rates of height differences

Classifications of height differences (h_i)	Contribution rate U'_{04} (%)	Contribution degree
$h_6=600$ m	10.70	$H_0(h)_1$ (high)
$h_7=700$ m	10.24	
$h_8=800$ m	9.84	
$h_5=500$ m	9.58	
$h_9=900$ m	8.73	
$h_{10}=1000$ m	7.61	
$h_{13}=1300$ m	6.76	$H_0(h)_2$ (medium)
$h_{11}=1100$ m	6.30	
$h_4=400$ m	5.64	
$h_{14}=1400$ m	5.44	
$h_{12}=1200$ m	4.13	
$h_3=300$ m	3.67	$H_0(h)_3$ (low)
$h_{16}=1600$ m	3.28	
$h_{15}=1500$ m	3.02	
$h_{17}=1700$ m	2.16	
$h_2=200$ m	2.16	
$h_1=100$ m	0.65	

Table 6.8   Evaluations of the slope shapes' contribution rates

Classifications of slope shapes (Π_i)	Contribution rate U'_{03} (%)	Contribution degree
χ	36.9	$F_0(\Pi)_1$ (high)
δ	23.69	$F_0(\Pi)_2$ (medium)
β	21.94	
α	11.44	$F_0(\Pi)_3$ (low)
–	6.75	

Superimposing Counting

By using sum-average arithmetic method and superimposing the contribution values (ρ_1, ρ_2, ρ_3) of a certain stratum as described in Fig. 6.4, we can get the following comprehensive contribution index:

$$
\begin{aligned}
\rho_i &= \frac{1}{N} \sum_1^3 \rho_i \\
&= \frac{1}{N} \left[(\rho)_1 + (\rho)_2 + (\rho)_3 \right]
\end{aligned}
\tag{6.8}
$$

In this formula, ρ is the contribution index of the stratum, N is the index total ($N=3$). Formula (6.8) can be used to derive the contribution index of each stratum.

Analysis of Contribution Rates

By calculating the contribution index, we can see the stratum's influence on the development of the landslide, while the degree of influence can be evaluated through contribution rate D_0:

$$
D_0(\rho)_i = \frac{D(\rho)}{M} (i = 1 - 3)
\tag{6.9}
$$

In this formula, $D_0(\rho)$ is the contribution rate of the strata, $D(\rho)$ is the contribution index, and M is the sum of the contribution indexes of the ten strata ($M = \sum_1^{10} D(\rho)_i$). We can visualize the contribution effect of the strata by using formula [9] to calculate the contribution rate of each stratum (Fig. 6.8).
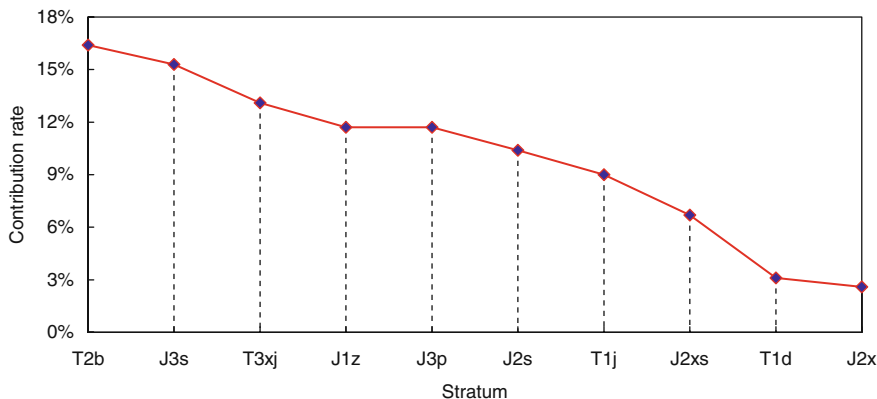
Fig. 6.8 Analysis of the contribution rates of the landslide-prone strata

The contribution rate will be graded in order to analyze each stratum's contribution degree to the development of the landslide. The contribution degree can be represented by grading the contribution rates in geometric progression intervals to three levels, namely high, medium and low:

$$d = \frac{D_0\left(\rho\right)_{\max} - D_0\left(\rho\right)_{\min}}{3} \tag{6.10}$$

Substituting formula (6.8) for the index of contribution rate in Fig. 6.5, we can figure out the result, namely $d=4.6$.

The three levels of intervals are

$$x_1 = (a_1 - a_2)$$
$$x_2 = (a_2 - a_3) \tag{6.11}$$
$$x_3 = (a_3 - a_4)$$

In this formula, x_1 stands for the interval of high contribution degree, x_2 for that of medium and x_3 for that of low.

a stands for the range of the interval, among which $a_1 = D_0(\rho)_{\max}$, $a_2 = a_1 - d$, $a_3 = D_0(\rho)_{\min} + d$ and $a_4 = D_0(\rho)_{\min}$. Substituting formula (6.11) for the index of contribution rate $D_0(\rho)$, we can get the result: $x_1 = (16.4–11.8)$, $x_2 = (11.8–7.2)$, $x_3 = (7.2–2.6)$. After the above calculation, we can get the strata's contribution effects to the landslides in this region (Table 6.6).

The contribution rates of the other four landslide factors can be figured out in the same way that has been used to obtain the contribution rate of the stratum factor.

The Contributions of Height Differences (h_i)

The elevation of Three Gorges area ranges from 100 to 1700 m above sea level. By using the DEM, the height difference between slope crown and slope toe can be got and ranges from 0 to 1700 m. The area can be divided into 17 levels of slopes with 100 m difference for each. The contribution rates of the height differences to the landslides in this region can be obtained the same way as mentioned above.

The Contribution Rate of Slope Shape (Π_i)

The five typical slope shapes in the Three Gorges area are the main shapes that develop the landslides (Fig. 6.9). Using DEM and classifying the whole area into five slope shapes, we can obtain the contribution rates of the slope shapes to the landslides with the same method mentioned above (Table 6.8).

| I Concave slope | II Upper concave and under convex slope | III Straight slope | IV Convex slope | V Upper convex and under concave slope |
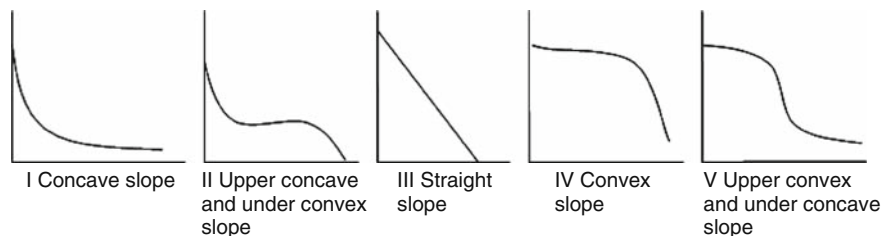
Fig. 6.9 Longitudinal diagram of the typical slopes in the area

The Contribution Rate of Slope Grade (α_i)

Low mountains and valleys are the main landforms around the Three Gorges area. By using DEM, the whole area can be classified into nine levels according to different slope grades (Table 6.9), and we can figure out the slope grades' contribution rates to the landslides with the same method mentioned above (Wu & Qiao 2005) (Table 6.10).

The Contribution Rate of Aspect (β_i)

Aspect is the direction of the slope's free face. Generally there are many directional aspects, namely south, north, east, west slope, northeast, southeast, northwest and southwest slope accordingly. Using DEM, we can classify the aspects in the area into

Table 6.9 Comparisons of slope grade classifications

								Unit: (degrees)
α_1	α_2	α_3	α_4	α_5	α_6	α_7	α_8	α_9
<10	10–20	20–30	30–40	40–50	50–60	60–70	70–80	>80

Table 6.10 Evaluations of the slope grades' contribution rates

Classifications of slope grades (α_i)	Contribution rate U'_{02} (%)	Contribution degree
(20°–30°)	18.49	$P_0(\alpha)_1$ (high)
(30°–40°)	18.49	
(40°–50°)	15.59	
(10°–20°)	13.36	$P_0(\alpha)_2$ (medium)
(50°–60°)	11.14	
(60°–70°)	8.24	$P_0(\alpha)_3$ (low)
(<10°)	5.12	
(>80°)	5.12	
(70°–80°)	4.45	

Table 6.11 Comparisons of aspect classifications

N	NE	E	SE	S	SW	W	NW
0–22.5, 337.5–360	22.5–67.5	67.5–112.5	112.5–157.5	157.5–202.5	202.5–247.5	247.5–292.5	292.5–337.5

Table 6.12 Evaluations of the aspects' contribution rates

Classification of aspect (β_i)	Contribution rate U'_{05} (%)	Contribution degree
157.5°–202.5° (S)	19.33	$A_0(\beta)_1$ (high)
112.5°–157.5° (SE)	16.22	
202.5°–247.5° (SW)	12.67	$A_0(\beta)_2$ (medium)
292.5°–337.5° (NW)	11.78	
0°–22.5° (N)	9.56	$A_0(\beta)_3$ (low)
247.5°–292.5° (W)	8.89	
67.5°–112.5° (E)	8.82	
22.5°–67.5° (NE)	6.67	
337.5°–360° (N)	6.67	

eight kinds for every other 45° (Table 6.11) and can obtain the slope's contribution rate to the landslide with the same way mentioned above (Table 6.12).

Comprehensive Evaluations and Weights of the Root Factors' Contribution Rates

Evaluations of Contribution Rates

The evaluations of different contribution rates can be gained through analyzing the five root factors' contribution rates to the development of the landslides in the area (Table 6.13, Fig.6.10). These evaluations of the contribution rates suggest that height difference, gradient and stratum make the greatest contributions to the development of landslides. The terrain condition and stratum in the area are favorable to the development of landslides, so the effective free face and vulnerable sliding stratum are the main internal conditions that predispose the development of landslides.

The Switch of Contribution Rate and Weight

The above results can be used to regionalize landslide risks. A most important index in regionalizing the landslide risks is the weight of the developmental factors, while the weight of contributions can be obtained by switching the contribution rates. Contribution rate itself has represented the root factor's influence on the landslide,

Table 6.13 Classifications of root factors' contribution rates

Contribution degree \ Root factor	Stratum (ρ_i)	Slope grade (degrees) (αi)	Slope shape (Πi)	Height difference (m) (h_i)	Aspect (degrees) (β_i)
High	T_2b J_3s T_3xj	20–50	IV	600–1000	157.5–202.5 112.5–157.5
Medium	J_1z J_3p J_2s T_1j	10–20 50–80	V III	1100–1400 400	202.5–247.5 292.5–337.5
Low	J_2xs T_1d J_2x	>80 <10	II I	100–300 1600–1700	0–22.5 247.5–292.5 67.5–112.5 22.5–67.5 337.5–360
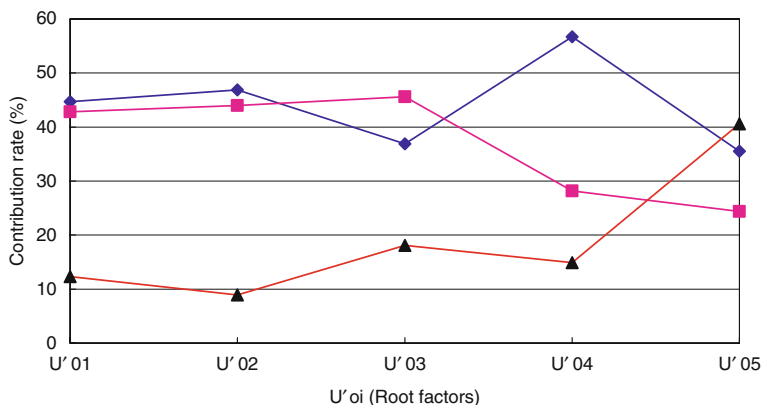
Fig. 6.10 Distributions of root factors' contribution rates

so the weight used in regionalizing the risks in fact is the root factor's contribution rate. Using contribution rate is a new approach for deriving the weight of the factors. Hence, after the contribution rates are decided, they can be changed to weight by normalizing and averaging them as shown in Table 6.13 and processing the probability of the factors. Solving the problem by switching the contribution rate and weight is widely used in economics and is also an international approach, and it is a mature statistical method for indexes, such as, main-element analysis, contribution rate of factor variance. All these factors have been developed into mature calculation software (SPSS), which can be a reference in the study of factors' weight in landslides. Influences from subjective factors can be avoided when contribution rate

Fig. 6.11 Calculation flow chart of contribution weight
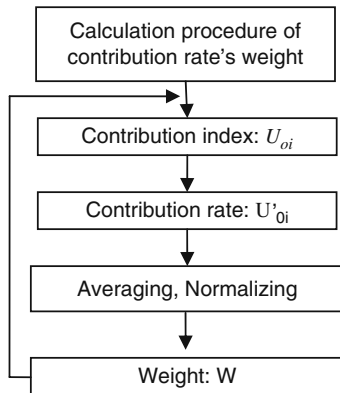
is used to obtain the weight. This method is called the root factor's contribution weight (Fig. 6.11) and is quite simple and easy to calculate.

How to switch contribution rate and weight:

(1) Self-weight (inner weight values of factors)

$$W_i = U_i / \Sigma U_i (i = 1 - 3) \tag{6.12}$$

In this formula, W_i is the factor's self-weight, and U_i is the contribution rate of the factor ($U_i = U'_{0i}/m$, U'_{0i} is the contribution rate of a factor in different regions, and m is the sum of factors in different contribution range).

(2) Mutual weight (weight values for the factors)

$$W'_j = U'_j / \Sigma U'_j (j = 1 - n) \tag{6.13}$$

In this formula, W'_j stands for the factor's mutual weight, U'_j for contribution rates of factors ($U'_j = \Sigma U'_{0ij}$, and U'_{0ij} is the contribution rate of each factor). The factors' self-weights and mutual weights can be obtained (Tables 6.14 and 6.15) by substituting formula (6.12) and (6.13) for the contribution rates in Tables 6.6, 6.7, 6.8, 6.10, and 6.12.

Table 6.14 Self-weights of root factors

Root factor / Weight value	Stratum (ρ_i)	Slope grade (degrees) (αi)	Slope shape (Πi)	Height difference (m) (h_i)	Aspect (degrees) (β_i)
High	0.50	0.49	0.54	0.54	0.47
Medium	0.36	0.35	0.33	0.32	0.32
Low	0.13	0.16	0.13	0.14	0.21

Table 6.15 Mutual weights of root factors

Stratum (ρ_i)	Slope grade (degrees) (α_i)	Slope shape (Π_i)	Height difference (m) (h_i)	Aspect (degrees) (β_i)
0.20	0.23	0.16	0.25	0.16

Contribution weight is of great significance in evaluating the risks of a landslide, and the weight values in Tables 6.14 and 6.15 have been employed by the author in the study of regionalizing the risks of landslides in Three Gorges area on Yangtze River.

References

Aleotti P (1999) Landslide hazard assessment: summary review and new perspectives. *Bulletin of Engineering Environment* 58:21–44

Darevskii VE, Romanov AM (1994) Calculation of landslide danger and maximum landslide pressure by the variation method. *Soil Mechanics & Foundation Engineering* 31(2): 79–80

Dong WM, Wong FS (1987) Fuzzy Weighted Averages and implementation of the Extension Principle. *Fuzzy Sets and Systems* 21:183–199

Fan YX, Luo Y, Chen QS (2001) Establishment of weight about vulnerability indexes of hazard bearing body. *Journal of Catastrophology* 16(1):85–87

Guzzetti F (2000) Lsndslide fatalities and evaluation of landslide risk in Italy. *Engineering Geology* 58:89–107

Liu RZ, Ni JR (2005) Landslide and rock fall hazard zonation in China. *Journal of Basic Science and Engineering* 13(1):13–22

Liu Y (2003) Risk analysis and zoning of geological hazards (chiefly landslide, rock fall and debris flow) in China. *The Chinese Journal of Geological Hazard and Control* 14(1): 95–99

Qiao JP, Zhu AX, Chen YB, Wang RX (2003) A 3D visible evaluation of landslide risk degree under integration of GIS and artificial intelligence. *Science in China Ser. E Technological Sciences* 46(Supp.):142–147

Tang HM, Lin XS, Chen HK, Tang F (2004) Risk zoning assessment of geological disaster in Wanzhou area, Chongqing City. *The Chinese Journal of Geological Hazard and Control* 15(3):1–4

Wu CY, Qiao JP (2005) A study of the contribution ratio of slope orientation to landslide development along the banks from Yunyang to Wushan in Three Gorges Reservoir Area. *Journal of Sichuan University (Engineering)* 37(4):25–29

Wu SR, Jin YM, Shi JS, Zhang YS, Han JL, He F, Dong C (2004) A primary study on landslide warning criterion An example from the reservoir region of the Three Gorges. *Journal of Jiling University (Earth Science Edition)* 34(4):596–600

Zhu AX (2004) Mapping Landslide susceptibility in the Three Gorges area, China using GIS, expert knowledge and fuzzy logic. *GIS and Remote Sensing in Hydrology, Water Resources and Environment (Proceedings of ICGRHWE held at the Three Gorges Dam, China, September 2003)*. IAHS Publ. 289:385–391

Zhu LF, Wu XC, Ying KL (2004) Risk zonation of landslide in China based on information content model. *Journal of Earth Science and Environment* 26(3):52–55

Chapter 7
Discussion on Land Use Based on Landslide Management in Three Gorges Reservoir Areas

Xuanming Peng, Xiao Lin, and Bolin Huang

Abstract   On the basis of the analysis of historic landslide hazard impacts to local society and economy, disaster land status quo, and features in the Three Gorges area several technological methods, structural measures, and social and ecological mitigation measures have been implemented for the Xintan landslide disaster. The Xintan landslide is a typical landslide in the area and is used as an example for the general treatment methods of landslide reclamation and engineering in the Three Gorges Reservoir area. These methodologies can be applied in land treatment projects which are about to be put into place in other areas on a large scale. These methods have great potential to significantly ease the tension between people and land issues, will help to promote the successful outcome of the construction of the Three Gorges Project, and will solve the migration and settlement problems of the displaced people who have become migrants, as a result of being relocated from their lands. These methods can solve the sustainable development problems of the social economy in the Three Gorges Reservoir areas.

Keywords   Landslide disaster · Disaster land · Land treatment · Land use · Mode investigation · Mitigation · Reclamation

Introduction

As indicated in the history of the Three Gorges areas, the landslide disasters were and are serious, some of which directly resulted in the transfer of the county political and economic centers to other areas. The landslides had a double impact on the ancient culture in the areas. And along with the migration and construction activity of the migrants, the construction of the Three Gorges Project and its reservoir areas has caused a great amount of land exploitation and new land-use patterns based on the landslide reclamation during the first, second, and third phase of the geographic

X. Peng (✉)
Yichang Geology and Mineral ResearchInstitute, Ministry of Land and Resources,
P.R.C., Yichang443003, China

disaster prevention and control work. This work has achieved many positive results in expanding the urban and agricultural land and has facilitated the ecological recovery of the land destroyed in the landslide disaster (Peng 2004, Yin 2004).

There are many successful experiences in transforming, reclaiming, and controlling the landslide and expanding the urban and rural lands. Landslides have occurred in Xiakou village in Xingshan County, Hubei; the Huangtupo landslide in Badong County, and the landslide at the Xiufeng temple in Wushan. These examples can be considered to be the typical models for managing and reclaiming the landslide sites and expanding the utility of urban lands. In this chapter, the author discusses the interactive relationship between the landslide disasters in the Three Gorges Reservoir areas, the societal aspects of land management, and the ecological recovery for land destroyed in landslide disasters. Taking for example the prevention and control of the landslide disaster in Zigui County, the first county in the Three Gorges Reservoir areas, as the primary example, decisions have been made based on a number of considerations. There has been research and inquiry as to the people's knowledge about landslide disasters and the scientific prevention and control of these disasters within the constraints of the socioeconomic situations as well as the mutual restraints between human activities and landslides. It can be demonstrated that the land treatment measures for the landslides have resulted in a win–win outcome of alleviating and inhibiting the disasters and expanding the living spaces for human beings. The implemented land reclamation and development for the land destroyed in the landslide can also be used as examples to summarize an effective development and utilization mode for the agricultural and forestry lands. The implementation and promotion of these measures will have great significance in easing the tension between people and lands, as it will promote the success and lessen the impacts associated with the construction of the Three Gorges Project. This will be accomplished by providing tools and methodologies for the living, farming, and construction activities of the displaced migrants and will solve the sustainable development problems of the social economy in the Three Gorges Reservoir areas.

The Effect of the Landslide Disasters on the Three Gorges Reservoir Areas

The Historical Landslide Management Situations

The historical landslide management situations in Zigui County, Zigui, indicates that it was a place where the geological disasters of landslides, collapses, and debris flow have always occurred, with landslides being the primary hazard. Landslides caused great harm to shipping on the Yangtze River and impacted the lives as well as the property of the local residents. According to the historical documents such as those found in the County Records and Local Records, there were as many as 18 destructive landslides that occurred in Xintan.

In the year 1370, Zhu Yuanzhang sent troops to occupy Guizhou and moved the Zigui County seat from Danyang to Changning, the city of the Chu Emperor. According to the "Guizhou Records," on the rainy day of May 20, the intercalary (leap year) date of Jiajing 40 year (1561), the city of the Chu Emperor and thousands of the official offices as well as the residential houses of the local people were destroyed, which caused the Zigui County Seat to be moved back to the town of Guizhou. The Badong County, described in the "Come to Sichuan" written by Luyou in Southern Song Dynasty, used to be situated in the north coast and then it moved to the southern coast as a result of the big landslide that occurred in the county of the north coast. These kinds of landslides which caused the whole county to relocate resulted in a devastating blow to the social and economic structures at that time. As such, these situations were common in the history of the Three Gorges.

After the founding of the People's Republic of China, several landslides have occurred in Xintan. In particular, the big landslide that occurred in the year 1985 destroyed the whole town of Xintan, which shocked the world. On July 13, 2003, a landslide occurred in Qianjiangping, destroying the metallic silicon factory, the shale brickyard plant, and a total of four plants in the town of Shazhenxi were wholly destroyed. Damage of this type to a town located in the county's mountainous areas meant the destruction of the industrial base of the town. It also destroyed the farmland covering an area of $71.7\,hm^2$, which had a great impact on agriculture. The landslide changed the entire industrial and agricultural economy of the town to a great extent, and it was difficult to recover.

The landslide would cause a recession in terms of agricultural production. Once a landslide occurs, the residents inhabiting the landslide areas would lose their natural flat and rich land. They can only farm a short distance up the sloping land, as it is steep, barren, and subject to soil erosion, which results in a drop of the agricultural production, influencing the lives of the farmers by making agricultural and forestry economic structures even more fragile. Some farmers left their homeland because of the landslides, which had a heavy impact on the local society, resulting in serious social problems.

However, not all landslides are destructive, in some regional areas the landslides have some positive effects. For example, in the Ming and Qing dynasties, due to the hindrance of shipping, Xintan and Xinglong became the commodity collection and distribution centers as well as the transit port in the upper part of the Yangtze River. As a result, the local residents of Lingtan, Fangtan, and Jiaotan had more living and commercial activities. With reference to the "Guizhou Records," from the Qianlong of the Qing Dynasty, the transit and commercial trades were prosperous among the incoming and outgoing vessels, and the rich ship owners, together with the merchants, have built the characteristic Xintan residence houses along the south and north coast of Xintan. The great Xintan landslide, occurred on June 12, 1985 and totally destroyed the flagstone alley of Qing Dynasty in the north coast and the traditional residence houses, which reflects the double impacts on the social and economic activities, brought by the landslide disasters. Also, the flat areas created by the landslide are often good places for the residents to live in.

The Present Growth of the Geographic Disaster Areas in Zigui County

In accordance with the field surveys as well as historical information for the Xiangxi River basin and the town of Shazhenxi summarized by the authors, there are 566 various geological hazard points in Zigui County, of which 514 are landslide points, 35 are collapse points, 3 are debris-flow points, 11 are ground subsidence points, and 3 are earth cracks, with a total area of $57{,}737{,}400\,\mathrm{m}^2$, constituting 2.4% of the land area of the county. The total volume is $1{,}220{,}000{,}000\,\mathrm{m}^3$. The landslides constitute 90% of the total geological disaster points, covering 2.3% of the land area of the county with a volume of $1{,}159{,}198{,}200\,\mathrm{m}^3$. The landslides occur in 14 towns of the county and are particularly numerous in the towns of Shuitianba, Guizhou, Shazhenxi, Guojiaba, and Lianghekou (Table 7.1). The geological disasters have caused great losses to the county, as shown in Table 7.2.

Table 7.1 Landslide disaster statistics for various towns of Zigui County

Town name	Number landslides	Area of land-slides ($10^4\,\mathrm{m}^2$)	Volume of land-slides ($10^4\,\mathrm{m}^3$)	Percentage of the national territory occupied	Distribution frequency
Maoping	5	17.47	233.81	0.1	0.024
Guizhou	66	975.49	34951.11	7.6	0.516
Qu Yuan	13	176.0	5222.0	0.8	0.060
Shuitianba	95	966.53	19067.52	4.3	0.424
Xietan	28	240.39	3005.85	1.7	0.193
Shazhenxi	70	1508.33	34003.25	8.0	0.372
Lianghekou	49	215.82	2568.91	0.8	0.182
Meijiahe	35	216.49	1667.17	2.5	0.398
Mopin	15	95.02	549.47	0.7	0.106
Wenhua	25	129.03	1191.77	0.9	0.170
Guojiaba	48	307.01	4316.48	1.6	0.257
Zhoupin	20	151.61	1691.49	1.1	0.149
Zhilan	13	104.44	1425.2	0.9	0.111
Yanglinqiao	32	351.11	6385.79	1.5	0.136
Total	514	5454.74	115,919.82	32.5	2.949

The Forced Conversion of Land-Use Types

The stress conversion of the land utilization is the replacement and turnover process of the various land utilization methods in the different regional areas within a certain period of time. The basic driving forces for the conversion of the land-use types are the external functions of the human activities and the evolution of the development of natural ecological systems. The former one is a direct, short-term, and self-driven obligatory process while the latter is an indirect, long-term,

Table 7.2 Loss statistics of the great geological disasters in 1997–2003 for Zigui County

Year	Landslides	Total volume (10^4 m^3)	Rooms destroyed	Agricultural land destroyed (hm^2)	Economic loss (10^4 RMB)	Casualties	People
1998	8	1300	889	13.73	1000	None	409F 1327
1999	7	618.6	420	None	672	None	66F 913
2000	13	707.7	3300	26.7	319	Three injured	None
2001	18	3833.5	None	None	7050	None	245F 1424
2002	87	332	None	None	1900	2D, 2I	1169F 4825
2003	71	44034	404	71.7	25233	24D, 5I	479F 7562

D: died; I: Injured; F: Family

and spontaneous succession process. The total land area to be submerged after the Three Gorges Reservoir impoundment to a water level of 175 m will reach up to 55,400 m^2, which will cause increased weight and volume, creating a large impact to land use in the Three Gorges Reservoir areas, which will in turn create a great impact on the livelihood of the urban and rural residents, as well as the agricultural and forestry economy (Liu Yan-sui 2001). Population migrations result in an increasing demand for urban construction sites, resulting in a sharp reduction of the per capita land area. This kind of impact makes human concerns the primary issues which tend to surpass the natural evolving forces. This causes a rapid conversion of the land-use types in the Three Gorges Reservoir areas, which attempt to mitigate the basic living problems of the residents there. On the other hand, the changes and pressures have provided an opportunity for the reorganization and more effective utilization of the land resources. Establishing new land-use patterns which not only apply to the ecological principles but also provide sustained development is a task of great importance to the millions of migrants.

Zigui, next to the Three Gorges Dam, is the county with the highest water-level rise and the greatest extent of submerging of land. According to statistics, the comprehensive submergence index of the county is 10% of that of the Three Gorges Reservoir areas and 50% of that of Hubei Province. With reference to the highest water level of 175 m designed for the Three Gorges Project, the areas to be submerged will cover 11 towns and 154 villages, which constitute 5.9% of the national territory land. The people in the submergence areas number 67,000, which constitute 16% of the total population. There are 208 km of county-level roads, 56 ports, a length of 311.4 km of electric transportation lines, 18 hydropower stations, and a length of 353.4 km of communication lines. The original Zigui County and towns of Xiangxi, Xintan, Guojiaba, and Shazhenxi along the Yangtze riverbanks which are more economically developed will be submerged. As the town of Xiangxi has been

removed, other towns absorb the new migrants to establish a new migrant town in the back of the old town.

The amount of cultivated lands destroyed in landslide disasters per year is about 45.3 hm^2 in Zigui County. Dating from the years 2003 to 2009 during which the construction will be finished, the loss of the cultivated lands will be about 317.3 hm^2, constituting 1.4% of the total cultivated land loss. Although the proportion is relatively small, and can be looked at as a "soft loss" which is the return of farmland to the forest, the "hard loss" of the cultivated lands destroyed in the landslide disasters are impossible to recoup. It is estimated that the cultivated lands destroyed in the landslide disasters constitute 5% of the actual loss of the cultivated lands, and the land in the disaster areas have been cultivated for quite a long time and have a mature fertility. It is of great significance to try and recover or re-exploit those kinds of cultivated lands destroyed in the landslide disasters.

With the forecast of "the general plan for the land use in Zigui County" in the year 2010, the amount of the new lands cultivated by the new migrants could reach 4935.6 hm^2, and the total areas of the cultivated lands could reach 18261.3 hm^2, recovering up to half of the original lands. However, the population has increased to 428,000, and the cultivated lands per capita are as low as 0.043 hm^2, which is 0.044 hm^2 lower than the minimal acceptable amount specified by the nation. It shows that the cultivated lands cannot sustain the whole population, and only expanding the environment and population capacity of Zigui County can solve the problem.

There is development potential in the land destroyed in the landslide disasters, from the standpoint of expanding the environment and population capacity. First, the landslide would stay stable for a relatively long period of time after it has released much of its energy and its deposits result in more flat or gently sloping fields. Second, many ancient sloping fields have been cultivated for quite a long time and have a high soil maturity. These situations have a potential to increase the unit output. Therefore, it is necessary to adjust the amount and structure of the land destroyed in the landslide disasters through reclamation and land treatment and to substantially increase not only the cultivated lands but also the output, meeting the demand for expanding the environment and population capacity.

Research on the Development and Utilization of the Land Destroyed in the Landslide Disasters

Engineering Technical Methods for the Land Treatment

The prevention and control projects of the slide land are the premise and foundation for the treatment, development, and utilization of the land. The development and utilization of the slide land should be based on the effective project control. Often, development with the intent to make the population more prosperous would affect

the design and construction of the treatment project. The development of the slide land is associated with the preliminary prevention and control tasks.

At present, the landslide control engineering for urban land use adopts the measurements of anti-slide piles, enhanced drainage, load reduction, back pressure, pre-stressed anchorage, and other improvements (National Territory Resources Department of People's Republic of China 2000). As for the availability of land for the urban migrants, the density of population is large and the degree of intensive activity is high. Thus, there is a great demand for safety. Once the landslide mitigation measures are destroyed again, the losses would be quite enormous. Therefore, the investment will be larger, the construction standard will be higher, and the periodic monitoring period on engineered and mitigated landslides by technological means would be longer.

Developing the agricultural land is to mainly solve the structure and layout problems of land use. The population density and economic intensity are relatively less impacting than that of urban land. Along with the limited investment, the safety standard is somewhat less.

The project's technological design for land destroyed in the landslide includes soil and water loss design, field project design, and traffic and road design. The following goals are to be achieved through the implementation of the technological measurements: preventing soil erosion, improving the natural environment and cultivated land quality and output, reducing the poverty rate, enhancing production and development, and improving people's quality of life.

Example of Analysis: Treatment, Development, and Utilization of Land in Xintan Which Was Destroyed in the Landslide

There are about 20 years since the landslide, which impacted the original town of Xintan, and it has been submerged under the reservoir water to a depth of 135 m. The landslide residual body will be covered by the natural vegetation, and the terraced geomorphologic formations which were formed by the landslide is almost the same as Maojiayuan's gentle sloping fields, and the scarp of the Jiangjiapo landslide is visible. At a distance of 1.5 km downstream is Qu Yuan, a new town for the migrants, and these new residents around the landslide now belong to the Yangtze village, town of Qu Yuan.

Since the situation is stabilized on the Xintan landslide residual body and due to the elimination of original urban functions, no project treatment actions were adopted to stop the sliding of the landslide. The treatment goal of land destroyed in the landslide is designated as field reclamation and land recovery. On the one hand, the local residents return and resume some agriculture activities spontaneously; the local government also has organized a project to change the cultivation of the slopes by means of slope terracing. They have also repaired some necessary water facilities. On the other hand, along with the start of the third stage of the Three Gorges Project, the resettlement pressure of latter settled migrants is getting larger and larger, and

thus, it is imperative to expand the cultivated land area. Now the Xintan landslide is developing and the "Qu Yuan–Xintan land reclamation and treatment project" is finished. The investment of the city level is 315,700 RMB and the increased cultivated land is 6.66 hm^2.

The lots with the most potential for land development in the landslide area are mainly located on the platform of the Sanyougou sloping field and the Maojiayuan sloping field as well as the platform of Jiangjiapo; the area between Jiangjiapo sloping field and Guangjiaya still has rockfall accumulation that is not suitable for development. The main aspect of the reclamation project is engineering, by changing the slope surface to terraces supported with corresponding irrigation, and road projects in this field.

1. The project of changing the slope surface to terraces: The development areas are the slope of Sanyougou with a slope of 15°, the Mao courtyard with a slope of 15–25°, and the platform of the Jiangjiapo slope. These areas are the major land development projects for mitigating landslides, and the area is designed to be level terraces. Level terraces distribute along the contour lines, according to the terrain, adding fill material to contour the lower formations of the slope. Terrace ridges are composed of walls of block stone which is limestone, 1.2–1.4 m high with a thickness of 0.7–0.8 m; the formed terrace is (800–120) × (2–4) m^2 filled with materials of block stone and soil from the landslide. The surface is covered by a yellow soil layer 20- to 30-cm thick, and to add fertile soil as a cultivation layer, the cover soil of Jiangjiapo slope's terrace is excavated from the residues of arable land which is 175 m beneath the water level. The height difference of the terraces after completion is about 1.5 m.

2. Field road projects: The road is composed of the field road and the farming road, the former is used to transport agricultural products, and the latter is used to farm in the fields. The highway is 300 m above the landslide, and it connects the town of Qu Yuan and Lepingli that is the hometown of Qu Yuan, including the Huangyan tunnels which are excavated, and it is also a natural field road. Below the 300-m level there will be construction of a new gravel road with vertical drains and dry walls of retaining soil located on both sides. The farming road is stone-class terrace which is orthogonal in shape, with terrace widths of 1–1.5 m, which will allow for uniform distribution in the terraced area.

3. Irrigation projects: The main characteristic of the Xintan landslide land is an area of collapse that allows for large quantities of infiltration from rainfall and poor drainage conditions of groundwater, so people also design the irrigation system for the terraced areas. The system is mainly along the high-ridge line of Gaojialing and consists of three cylindrical reservoirs which are 3–3.5 m high, with a diameter of 2.5–3.5 m. Through water diversion, the water is collected from the platform of the Jiangjiapo slope and links up with the three reservoirs to meet the higher elevation terraces' irrigation requirements. As Xintan has abundant rainfall except in the dry season, there is no construction of a drainage system. The farmers use their own ways of irrigation and diversion.

   The Xintan landslide land is being developed mainly as agricultural land. The development follows the principle of "adjust measures to local conditions, ecological protection, and sustainable development." Where possible, apply agricultural science and technology planning and design, taking into account the ecological environment. This approach mainly includes planning and design of planting, technical design, and ecological agriculture protection design.

   After the treatment the primary benefit is planting, the new 6.6 hm^2 dry fields of the landslide area are mainly for the cultivation of maize, potatoes, and citrus gardens. The soil between the height of 200 and 300 m has a higher fertility and more corn should be planted, as well as other kinds of economically beneficial crops. The surfaces of the terrace above 300 m are mainly the former landslide soil of poor fertility or this cover is a thin layer of external fill soil. As such, the water retention of the soil is relatively poor, so potatoes are cultivated. The section with high groundwater, the Sanyougou ditch area of Maojiayuan, was designated for orange gardens, and the levels of terraces of Jiangjiapo slope can be interplanted with oranges, pears, loquat, Chinese chestnut, and other economical and fruit-bearing orchards.
   The aim of agricultural technology design is to improve the fertility of the soil

(1) By providing a deep layer of soil. As the layer for cultivation is thin and in poor fertility condition, the soil should be deeply turned year by year and given more organic and chemical fertilizers. Some sections of the Jiangjiapo slope can use ash fertilizer which remains after the burning of reeds or grasses.
(2) By rotation. Plant some kinds of legumes that have nitrogen nodules, such as rapeseed and straw, thus improving soil structure and fertility. Also, it is advised that local abundant labor be used to develop manual weeding and increase green manure.

   The design of ecological protection is mainly for the protection of terraced fields. The first step is to protect the natural vegetation on the residual body. The primary ecological design is to set up the easement zone of the Yangtze River and forests for the conservation of water supply. Introduce two kinds of aquatic plants lower than 175 m from Lake Strand zones and plant Yangtze River easement zone between 175 and 200 m in height. Select well-developed and fast-growing tree species such as *Metasequoia*, the roots of which are effective in reducing surface runoff, which prevent soil and water loss to the front edge of the slide land. These trees also help to prevent large-scale bank collapse. Plant a coniferous forest in the areas at the height of 700–800 m between Huangyan and Guangjiaya, which can not only maintain wellspring sand to avoid water and soil loss but also separate the rock fall area in Guangjiaya from the lower terraced area. This will guarantee the safety of crops and orange gardens. In the terraced area, grow plants with strong root systems, such as Chinese chestnut, to protect the terrace stability.
   In addition, in order to cooperate with agricultural production and utilize the idle labor of the village in Yangtze River, two pig farms and breeding bases are set up in two places, 250 m away from Sanyougou and 500 m away from Jiangjiapo

slope. The tunnel at Huangyan will soon be opened to traffic, so that the problem of outgoing transportation of agricultural goods can be solved.

After improving the design, the Xintan landslide has caused great changes in the land-use pattern; and this new land structure utilization tends to be rational. The increased cultivated land is 6.6 hm^2 in area, after the project has been implemented, accounting for 71.5% of the whole area in the project district. The forest land covers an area of 0.37 hm^2, accounting for 4.0%; the traffic land accounts for 4.4%; and the water areas are 2.2% (Table 7.3).

Through the agricultural ecology design, the terraced fields are the central production area, the forests and fruit gardens are located around these fields as protective belts, and an ecological land-use protection and means of production have been implemented. With the establishment of the pig farms, the interrelationship between the inner elements of this system is much closer to that of the stereotypical type of agriculture and is much improved: potatoes and maize which are planted in terraced fields are used for feeding the pigs as well as meeting the peasant's life needs. The cistern provides the water source for pig farming throughout the year; the excrement and urine of the pigs is good organic fertilizer for increasing the production of crops and citrus orchards in the garden. And it can also improve the soil structure and increase fertility at a rapid rate; the sale of pigs offers more capital for the peasants, which makes the terraced fields turn from low yield into progressively high yield. As long as the development of these elements is balanced, the whole land system will be active year by year, more investments will be offered by the people, and the productivity of the land will increase. Along with the opening of the Huangyan tunnel, the most remote areas of the town of Qu Yuan and Guizhou in Zigui County will connect to the town of Maoping. The land development of the Xintan landslide has three kinds of benefits: economic, social, and ecological.

(1) Economic benefits: The project investment is 315,700 RMB, but the annual agriculture income has increased to 331,600 RMB, the average increased income per person is up to 218 RMB, and in subtracting 2 years of the cost, the investment can be returned. The citrus growers can have good incomes only after 4 years; the output is about 37,500 kg/hm^2 and the average income is 52,500 RMB.

(2) Social benefits: The social benefits of Xintan landslide land development are outstanding. First, the amount of the cultivated land per person has risen from

Table 7.3 The utilization type balance of Xintan landslide land development (unit $=$ hm^2)

Project	Before development	After development	Increased land
Cultivated land		6.6	
Abandoned garden	2.36		1.74
Forestry land		0.37	
Land for transportation		0.47	
Water area		0.2	
Unused land	6.87	1.65	4.86

0.107 to 0.08 hm^2 and this has attracted the displaced migrants from the Yangtze River to join in the projects of construction, terrace cultivation, and pig-raising markets. Thus, the peasant's income has increased and social stability is maintained. Second, the scattered inhabitants moved to the Shidaling to work for a living, which can conserve not only the living spaces but also the capital construction cost so that a unified electricity supply, water supply, and postal communication can be implemented and the urbanized and living levels of the peasants will be improved. In addition, the newly structured agricultural ecosystem can improve the production of the land at a constant rate through rational operation and can offer a long-term economic growth source, resulting in sustainable development of the migrant's economics and social situation.

(3) Ecological benefits: (a) Transformation of the land destroyed in the landslide disasters into the terraced slopes. The establishment of the slope easement and the pig farms forms an organic agriculture ecosystem through which the production can be increased yearly, which compensates for the land destroyed in the landslides. (b) Effective increase of the vegetation cover, which will be good for conserving water and preventing the land from erosion and orienting the evolution of the ecosystem in an improved way. (c) Fully make use of the system to produce the organic fertilizers and green fertilizers to improve the soil structure, increase the soil fertility, and reduce the amount of the fertilizer and pesticides used, which reduces the pollution to the soil and water environment of the Yangtze River.

Research on the Mode

The effects of the Three Gorges Reservoir impounding are impacting not only the construction of the new city for the migrants but also the living and sustainable development of the farmers who have lost their lands. At present the immigration policies of the nation greatly support the urban population and the agricultural population that have been urbanized; however, compensation is less to the farmers.

The nation's compensation can only meet the temporary needs, and the farmers cannot lose their lands. The only way to solve the problem is to explore and make available more agricultural lands. There are many advantageous factors in the land development and treatment after the landslide. Although the amount of the cultivated lands reclaimed is not much, the social and ecological significances are remarkable.

The "protection–production" agricultural ecosystem established through the development of the landslide in Xintan has become the typical example for the agricultural lands destroyed in the landslide disasters, and it is the success of this role model in the Three Gorges Reservoir areas that has been demonstrated. On the one hand it increases the income and the living standards of the people, and on the other hand it promotes the recognition for protecting the ecosystem of the people in the Three Gorges Reservoir areas, encouraging them to develop in a sustainable way (Fig. 7.1).
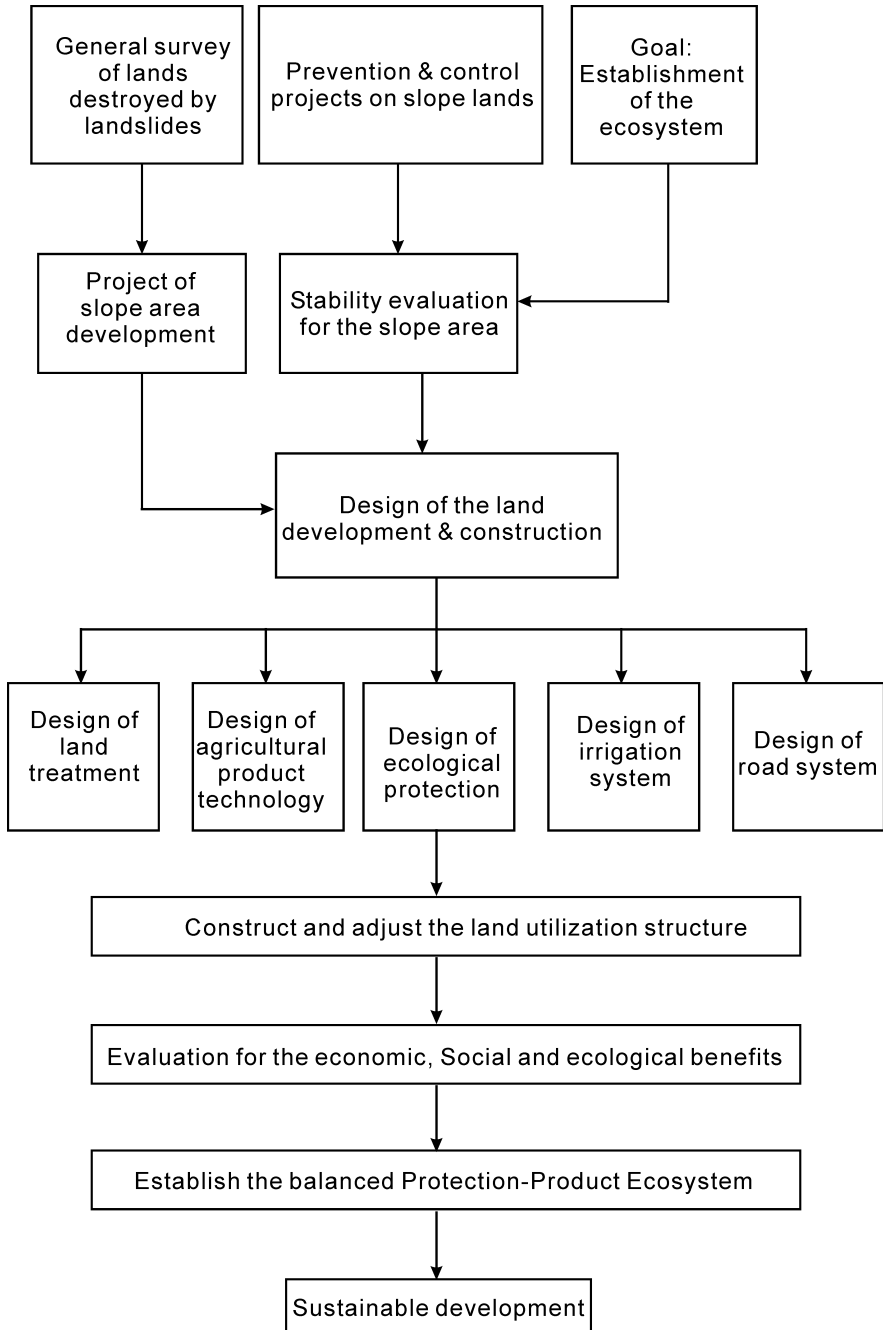
Fig. 7.1 The treatment and reclamation procedures of the land destroyed in the landslide

Landslides and the surrounding environment are very fragile, so apart from the development of land to establish good land-use policies, the ecological benefits should also be taken into account. Generally speaking, improving land-use mining capacity is reasonably effective, and ecological factors are one of the evaluation indicators. As part of the whole ecosystem of the Three Gorges, regardless of their size and development purposes, landslides are being reclaimed and modified for the complete ecological restoration and reconstruction of landslide sites.

On July 13, 2003, a large landslide occurred in Qianjiangping of Shazhenxi town, resulting in 14 deaths and 10 missing. Landslide in the Upper Triassic Shazhenxi group muddy siltstone is a bedrock landslide. The landslide has a longitudinal length of 1,200 m, a frontal width of 850 m, the largest thickness of 30 m, and a longitudinal volume of about 200 million m^3; the front shear exposure of the landslide is about 100 m high, and the back edge or scarp is 450 m high in elevation. The landslide has a horizontal displacement of about 200 m and an approximately 100 m vertical drop. The bedrock in the front of the landslide ran out to the opposite shore of the Qinggan-he River supinely, depositing silt and debris in the river bed to a height of halfway up the opposite mountainside. This material formed a landslide dam, which blocked the Qinggan-he River.

Although the slide is different from the new landslides in physical properties, it has something in common in the land development. (a) After landslide occurs, the mass comes to rest, and the landslide has been at rest so long that it still has higher stability even if it is not modified. (b) After the landslide, the overall slope is gentle and does not require further modifications if the slope is more than 25°. Returning farmland to forest is suitable for the design of farmland infrastructure. (c) There are multi-level platforms on a landslide, the original vegetation and farming layer is better preserved, and the residual highway is evenly distributed. People simply fill in cracks in the road which can be used for access. Industrial plants in the central part of the landslides have a high ratio of hardening wasteland, suitable for the establishment of agricultural and sideline production and processing bases. These are the favorable factors of agricultural land improvement and development in Qianjiangping landslide. Because of the impact of dredging rivers, the slip of surface soil is very prominent. It is no longer suitable for the construction of housing on the landslides. Through the development of agriculture and forestry economics, a partial solution to the problem of surviving during and after the disaster has produced the greatest economic and social significance.

As far as the sloping fields on which the engineering treatments have been implemented are concerned, there are many cases for developing the agricultural lands. For example, the Pengjiacao sloping field with a volume of 922,000 m^3 and the Wang Yanling sloping field with a volume of 8,000 m^3 are situated in the town of Xia Kou and Xingshan and are sloping fields of middle and small scale, respectively. Both of them are slump accumulation sloping fields, and the engineering methods should include building a circular gutter around the sloping fields and an anti-sliding pile or anti-sliding retaining wall at a height of 210–220 m on the middle and lower parts of the sloping fields. In addition, establishing a stone bulkhead or similar structure on the emerging slope or front part of the sloping fields is an effective measure.

After these measures are put in place, cultivate economical plants such as corn and sweet potatoes or use oranges such as those planted on the terraced fields in the sloping areas to solve the land problems of the 40 farmers inhabiting the sloping fields. Such cases are similar to the technical charts listed in Fig. 7.1.

Conclusions

On the basis of the brief summary of the impacts to the social economy in the Three Gorges Reservoir areas caused by the landslide disasters and through the analysis of the present situation of the land destroyed in the landslide in Zigui County in the Three Gorges Reservoir areas, as well as the case analysis for the typical examples of the treatment of the slide land in Xintan, the following are the conclusions:

(1) Throughout history, the landslide disasters have caused great impact on the economy and society of the counties in the Three Gorges Reservoir areas. Along with the increasing demand of the Three Gorges Project for the reservoir water and the urban and rural construction lands, the cultivated land per capita was reduced sharply, and combined with the effects of the geological disasters, the relationship between people and land will be overwhelmingly intensified.

(2) Many sloping fields have been cultivated for quite a long time and have a high soil maturity. Adjusting the amount and structure of the land destroyed in the landslide disasters through reclamation, land treatment, and other measures substantially increase not only the amount of cultivated lands but also the productivity, meeting the demand for expanding the environment and population capacity.

(3) The engineering technical methods for the treatment of the sloping fields can be used for the treatment of the land destroyed in the landslide. However, the first goal of the land treatment is to prevent soil erosion and improve the soil quality.

(4) As the sloping fields and the ecosystem of the peripheral areas are fragile, it is necessary to establish a "prevention–production" agricultural ecosystem on the land destroyed in the landslide disasters to achieve maximum social, economic, and ecological benefits.

(5) The development and utilization methods of the land treatment for the Xintan landslide are a positive value and should be promoted where possible in the Three Gorges Reservoir areas.

References

National Territory Resources Department of People's Republic of China (2000) The Standard of the Land Development and Treatment. Chinese Human Affairs Publishing House, Beijing.

Peng XM (2004) The analysis of the stability and treatment of the sloping fields of Longwang temple in the Three Gorges Reservoir areas. Journals of the Ocean University of China (Natural Science Edition) 34(2): 289–296.

Yin YP (2004) The Research on the Significant Geological Disasters and the Preventing and Controlling in the New Sites Established by the Migrants in the Three Gorges Reservoir Areas. Geological Press, Beijing.

Part II
Case Studies for Typical Landslides

Chapter 8
Mechanism for the Rapid Motion of the Reactivated Qianjiangping Landslide in Three Gorges Dam Reservoir, China

Fawu Wang, Yeming Zhang, Zhitao Huo, and Xuanming Peng

Abstract The first impoundment of the Three Gorges Dam reservoir in China started from a water-surface elevation of 95 m on June 1, 2003 and reached 135 m on June 15, 2003. Shortly after the water level reached 135 m, many slopes began to deform and some landslides occurred. The Qianjiangping landslide is the largest one; it occurred on the early morning of July 14, 2003, and caused great loss of lives and property. Field investigation revealed that although failure occurred after the reservoir reached 135 m, the stability of the slope was already reduced by pre-existing, sheared bedding planes. To study the mechanism of the rapid motion of this reactivated landslide, two soil samples were taken from a yellow clay layer and a black silt layer in the sliding zone and a series of ring shear tests were conducted on the samples. One series of ring shear tests simulates the creep deformation behavior, while the other series simulates different shear rates. Conclusions drawn from analysis of the ring shear tests indicate that the mechanism of the rapid motion of the reactivated landslide was caused by the rate effect of the black silt layer during the motion phase after the creep failure. The yellow clay layer did not play any important role in the rapid motion in the 2003 event.

Keywords Landslide · Rapid motion · Ring shear tests · Clay · Silt · Water–soil interaction · Rate effect

Introduction

The Three Gorges Dam construction on the Yangtze River in China is the largest hydroelectricity project in the world. The dam site is located at Sandouping village near Maoping, the capital of Zigui County, Hubei Province. The designed final dam height is 185 m, the final length 2309.5 m, and the designed final highest water

F. Wang (✉)
Research Centre on Landslides, Disaster Prevention Research Institute, Kyoto University, Gokasho, Uji, Kyoto 611-0011, Japan
e-mail: wangfw@landslide.dpri.kyoto-u.ac.jp

level 175 m. When dam construction is finished, the Three Gorges Reservoir will reach Chongqing city, about 660 km upstream from the dam. The first impoundment started from 95 m on June 1, 2003, and reached 135 m on June 15, 2003. Shortly after the water reached 135 m, many slopes began to deform and some landslides occurred.

In the early morning, at 00:20 on July 14, 2003, the Qianjiangping landslide occurred at Shazhenxi town (Fig. 8.1) beside Qinggan-he River, a tributary of the Yangtze. The Qianjiangping landslide was located on the western side of Qinggan-he River. On the opposite side of the river is the main street of Shazhenxi. The distance from the landslide to the junction of the Qinggan-he River with the Yangtze is about 3 km, and the distance along the Yangtze River from the junction to the Three Gorges Dam is about 50 km (the direct distance is about 40 km).

There was some loss of life and serious economic damage caused by the Qianjiangping landslide. It destroyed 346 houses and 70 ha of fields and rice paddy. Four factories on the lower part of the slope near Qinggan-he River (a brick factory, a metal and silica factory, a chemical fertilizer factory, and a food factory) were seriously damaged. Direct economic losses were about 7 million USD, and it reduced the asset value at Qianjiangping by 40%. Most of the workers became unemployed. In addition, 3 km of provincial roads and 20.5 km of electricity lines were cut. Twenty-two boats and ships were damaged and sunk in Qinggan-he River and the Yangtze River. Although a warning was given by the local government based on precursory deformation of the slope 2 h before the final failure, 13 people on the slope and 11 fishermen on boats in the nearby area were killed. The main reason for the deaths on the slope was that the people did not imagine that the landslide area would be so large and believed their houses would be safe, because there was no ground deformation around them before the final failure of the slope. For the deaths on the river, the reason was just that it was not predicted that the landslide could

Fig. 8.1 Location map of the Qianjiangping landslide in the Three Gorges Reservoir area, Hubei Province, China

Fig. 8.2 View of the Qianjiangping landslide from the upstream side of Qinggan-he River (taken by F.W. Wang, March 15, 2004)

move so rapidly. It was the wave caused by the rapid sliding that killed the fishermen on their boats. A water trace left on the red bridge (shown in Fig. 8.2) detected after the landslide indicated that the highest level of the wave was about 30 m above the water level of 135 m.

Features of the Landslide

Figures 8.2 and 8.3 are photographs of the landslide taken from the upstream side and front of the landslide, respectively. The landslide had a tongue-shaped plan, with a length of 1,200 m and a width of 1,000 m. It moved about 250 m in the main sliding direction of S45°E. The average thickness of the sliding mass was about 20 m, thinner in the upper part and thicker at the lower part. The total volume was estimated to be more than 20 million m^3. The elevation of the main scarp was 450 m, and the elevation of the Qinggan-he River water level was 135 m when the

Fig. 8.3 Front-on view of the Qianjiangping landslide (taken by Y.M. Zhang, July 15, 2003)

Fig. 8.4 View of the
unrotated trees on the sliding
mass in the middle of the
Qianjiangping landslide

landslide occurred. The landslide release surface was along a bedding plane in the
bedrock (Fig. 8.2). Factory buildings on the sliding mass still remained standing
after sliding for about 250 m (Fig. 8.3). However, because serious cracks developed
in the buildings, they could not be used again and were demolished and the building
materials were recycled (compare with Fig. 8.2). Standing trees on the sliding mass
in the middle of the landslide (Fig. 8.4) indicate that the angle of the sliding surface
remained constant and no rotation occurred. The exposed sliding surface at the upper
part was very planar and subparallel to the sandstone bedrock strata (Fig. 8.5). All
of these phenomena show that the sliding mass slid along a planar sliding surface.
When the sliding mass entered Qinggan-he River, the dip direction of the strata was
changed to N45°W, which is opposite to the original dip direction of S45°E. The
dip angle is about 5° in the bed of Qinggan-he River (Fig. 8.6). The deposits at

Fig. 8.5 The exposed planar
sliding surface, which is also
a sandstone bedding plane
(there is a damaged rice
paddy in front of the person)

Fig. 8.6 View of the reversed dip direction of the sandstone beside Qinggan-he River (taken by F.W. Wang, March 16, 2004)

the distal landslide margin contain white gravel with clasts up to 100 mm or so in diameter. The dip angle of the sandstone bedding at the distal margin is steeper than 30° (Fig. 8.7).

Figure 8.8 is a topographic map of the Qianjiangping landslide prepared after the 2003 event (modified from Wu et al. 2006). The water level of the Qinggan-he River changed from 95 to 135 m when the first impoundment of the Three Gorges Dam reservoir was conducted. The Qinggan-he River made a big curve in front of the Qianjiangping slope, and erosion by the river at the toe of the slope probably had a negative effect on the stability of the slope. The highest elevation of the main scarp is about 420 m. The landslide has a tongue-like shape in plan view, with a length of 1,200 m and a width of 1,000 m. It moved about 250 m in the main sliding direction

Fig. 8.7 Gravels displaced from the bed of Qinggan-he River and deposited in the toe of the landslide deposit (*circled* in photograph). Note that the sandstone dip direction is reversed and the dip angle has become steeper compared with Figs. 8.4 and 8.5)

Fig. 8.8 Topography of the
Qianjiangping landslide after
the 2003 sliding event
(modified from Wu et al.
2006)

Topography of the Qianjiangping landslide after the 2003 sliding event

------ Boundary of the main sliding area in 2003 event
—— Boundary of pre-exisiting landslide
☐HT Horizontal investigation tunnel
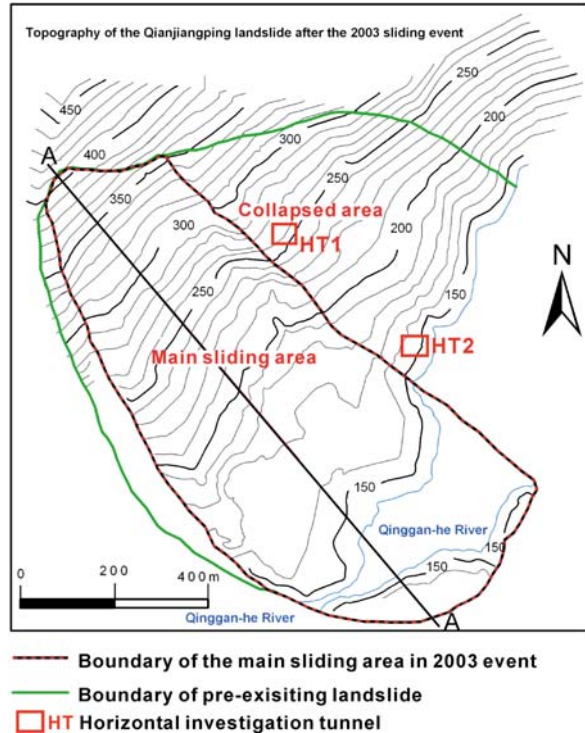
of S45°E. The average thickness of the sliding mass was about 26 m, thinner in the
upper part and thicker at the lower part. The total volume was estimated to be more
than 20 million m^3.

Based on the sliding distance of the 2003 event, the Qianjiangping landslide was
divided into two areas: the main sliding area and the collapsed area. There was
no obvious difference between the two areas before the 2003 event. However, they
became quite different after the 2003 event. In the main sliding area, the sliding
plane was exposed at the main scarp, and the toe slid into the Qinggan-he River,
damming the river flow. The collapsed area was just drawn down by the movement
of the main sliding area. Many cracks were found in the collapsed area, but its
sliding distance was very limited in the 2003 event. According to an analysis of
the topographic features of the two areas, it is believed that the two areas moved
together for a very long period before the 2003 event and that their sliding planes
should be the same surface or should have exhibited very similar behavior.

Generally, reactivated landslides cannot move at high velocities, because the
material in the sliding zone was previously crushed to clay and little excess pore
pressure can be generated during the later landslide motion. However, the Qianjiang-
ping landslide showed a behavior that was different from this scenario. To clarify
the mechanism of this high-velocity reactivated landslide, more detailed analyses

were conducted on the materials taken from the sliding zone of the Qianjiangping landslide, including grain size distribution, clay mineral components, and mechanical properties. As a typical dip-slope landslide, it attracts investigations by many landslide researchers (Wang and Yang 2005; Cao et al. 2007; Yin and Peng 2007).

In order to investigate the sliding zone of the 2003 landslide in more detail, two horizontal investigation tunnels (HT1 and HT2) were excavated by China Three Gorges University in the collapsed area to check the properties of the sliding zone as they existed before the 2003 event. The locations of the two tunnels are plotted in Fig. 8.8.

Figure 8.9 is a longitudinal section of the main sliding block of the Qianjiangping landslide. The bedrock in the landslide area is feldspathic quartz sandstone, fine sandstone with carbonaceous siltstone, siltstone with mudstone, and silty mudstone of the Lower Jurassic Niejiashan formation ($J_{1-2}n$). The dip direction of the strata is reversed near the Qinggan-he River. The average slope angle of the slide plane in the upper part is 24°. An energy line connecting the top and toe of the sliding mass is inclined at 10°, which is the apparent friction angle of the landslide. The 10° value indicates a highly mobile landslide.
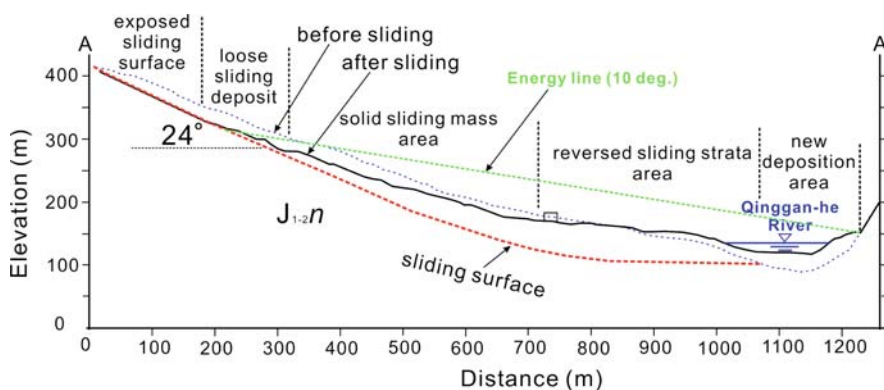
Fig. 8.9 Central longitudinal section of the Qianjiangping landslide

Scratches on the Failure Surface

Figure 8.10 shows a sequence of two photographs of scratches on the sliding surface at the upper part of the landslide. Figure 8.10a shows the original situation, while in Fig. 8.10b a slice of sandstone has been stripped away from the plane to reveal more scratches. This shows that the scratches were present beneath the landslide sliding surface before the landslide occurred. The scratch strike direction is S15°W (red arrow). The sliding direction (S45°E) of the July 2003 event (blue arrow) is also shown by the water dribble trace in Fig. 8.10b. The angle between the sliding direction and the scratches is about 60°. Comparison of the two photographs shows that the scratches were not formed by the event of July 2003. They must have
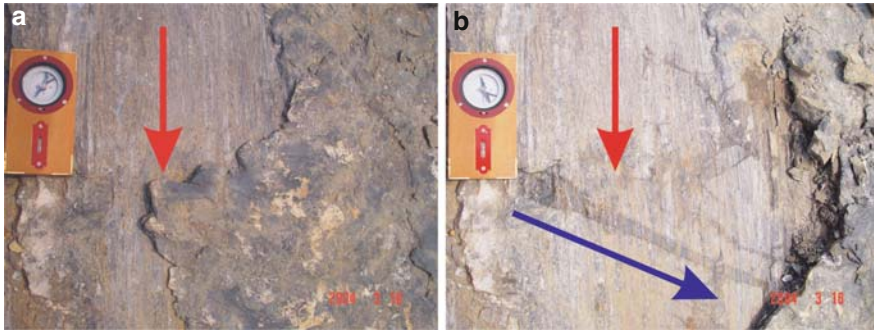
Fig. 8.10 A pair of photographs at the same site showing the pre-existing scratches that underlie the sliding surface of the July 2003 event (*blue arrow* shows the sliding direction, *red arrows* show the strike direction of the pre-existing scratches). The scratches are inferred to be slickensides formed by bedding-plane shear during folding of the rocks in the Cretaceous period

formed earlier, probably in a much older geological event, because calcite vein-stone is widely distributed along them. This site lies between the Zigui syncline and Baifulai-Liulaiguan anticline that were folded during the Cretaceous period (Wang et al. 2002) and so the scratches can be interpreted as slickensides along bedding-plane shears.

Possible Triggering Factors and Sliding Mechanism

The high water level within the landslide toe caused by impounding of the Three Gorges Reservoir was naturally considered to be the trigger. Impoundment started from June 1, 2003, and the reservoir water level reached 135 m on June 15, 2003. The first cracks due to the slope deformation, however, were observed on October 22, 2002, near the present main scarp. This means that the slope was in a critical state even before impoundment of the reservoir. With the slope in such a critical state, failure probably was triggered by the direct reduction in normal load within the toe of the slope caused by the rising water level.

According to local people, sandstone and mudstone were exposed in the Qinggan-he River bank before the reservoir was impounded. The dip angle of the sliding surface, which is also a bedding plane, was measured as $32°$ at the upper part. Zhang et al. (2004) observed two sets of large transversal cracks crossing the upper and middle parts of the slope. Although some rice paddies were located on the upper part of the landslide (Fig. 8.3), the associated high water table from irrigation should have been kept perched by the impervious weathered mudstone. The rice paddy was started 10 years ago, and a pond for water supply was built near the paddy. So, for landslide stability analysis, the boundary conditions for the landslide are very clear. There was little volume of landslide in the uppermost part. The right lateral boundary was open and so had no friction to resist sliding. As shown in Fig. 8.10, the sliding surface was along a pre-existing structural shear plane.
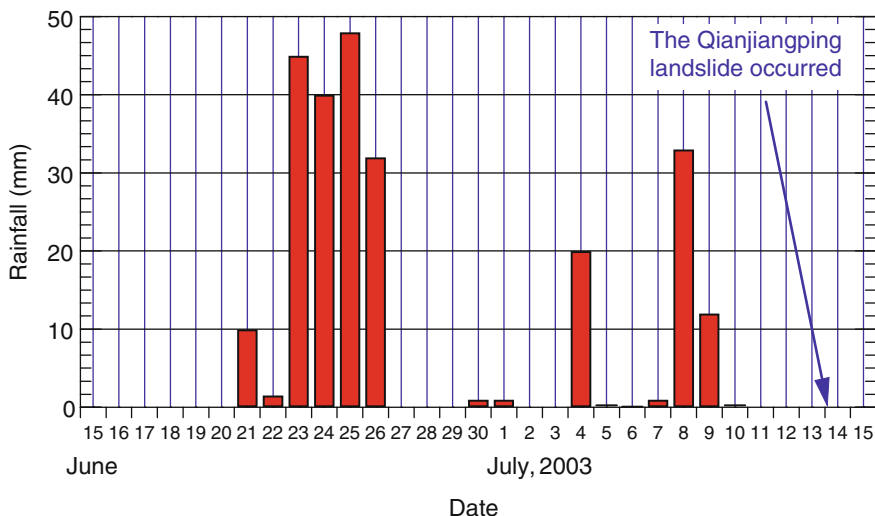
Fig. 8.11   Precipitation data monitored in Yichang city, 70 km from the landslide

Precipitation is monitored in Yichang city (Fig. 8.1), about 70 km from the land-slide site. Intense rain from June 21 to June 26 and rain from July 4 to July 9, 2003 (Fig. 8.11) may have saturated the sliding mass and increased its unit weight. However, considering the high permeability of the slickensided sandstone and the transverse cracks crossing the sliding mass, it is not likely that high pore pressure would have resulted.

The landslide toe had been eroded by the Qinggan-he River long ago and offered little resistance to sliding. Only the left lateral boundary offered side friction and tension resistance from the neighboring rock mass. For such a huge landslide, the mechanical model can be simplified as a two-dimensional longitudinal section as shown in Fig. 8.12a. The situation of the landslide after failure is sketched in Fig. 8.12b.
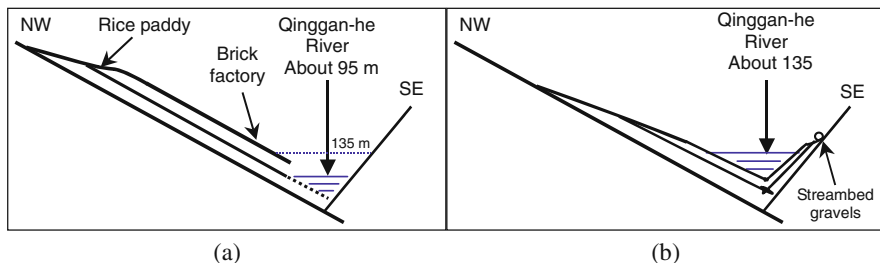
Fig. 8.12   (**a**) Structural model of the Qianjiangping slope and (**b**) a sketch of the landslide after failure

With the slope in a critical state (Fig. 8.12a), an increase in water level in the river would decrease the effective normal stress in the toe of the slope, and the shear resistance would decrease at the same time. These changes in the mechanical balance resulted in the slope failure.

For additional factors contributing to the failure, some attention should be paid to the factories on the lower slope before the landslide occurred. The brick factory had been quarrying mudstone in the lower part of the slope as raw material for brick making from 1997. Some 2–3 million bricks (each about $250 \times 120 \times 50$ mm^3) had been produced during the 6 years. Such removal of mass from the toe of a landslide is a very dangerous action that leads to slope instability (but the presence of the landslide was unrecognized by experts until the cracks appeared in 2002).

When the existence of the widely distributed scratches on the sliding surface is considered, it is easy to assume that the shear strength between the sliding mass and the sliding surface was at residual strength. If this assumption were true, the rapid, long-runout sliding would be difficult to explain, because a rapid loss of shear strength is necessary to achieve the high rate of acceleration. As mentioned previously, the scratches probably were formed in the Cretaceous period, and the beds on either side of the scratched surface were bonded together with calcite cement. After the occurrence of the landslide, Zhang et al. (2004) observed crushed crystalline calcite, some 20–30 mm thick, widely distributed on the exposed sliding surface on the upper part of the landslide. Figure 8.13 shows a sample of the calcite. Generally, failure of crystalline calcite is characterized by brittle fracture. After a certain small distance of shearing, the cement bonding would have been destroyed. The quick loss of adhesion of the crystalline calcite could be the main reason for the rapid landslide acceleration after the initial failure of the slope.

We have to mention that the above estimation was made after the first investigation on the Qianjiangping landslide (Wang et al. 2004). Later, after many times field investigation, especially after horizontal tunnels were excavated in the landslide site, we got some new findings presented in the following section (Wang et al. 2008).

Fig. 8.13 Photograph of a crystalline calcite sample taken from the sliding surface at the upper part (The *white color* is crystalline calcite)

Experimental Study on the Rapid Sliding Mechanism of the Reactivated Landslide

Sampling the Sliding Planes

Observation and sampling were conducted in tunnel HT1. Figure 8.14 shows two photographs taken in the tunnel that face the sliding direction and show the sliding zone. In the investigation tunnel, two layers were observed in the sliding zone. The upper layer is a black clay layer with calcite blocks, while the lower layer is yellow clay. Both layers were water saturated with a thickness of 200 mm and were in a plastic state.

In situ observations reveal that the yellow clay layer may be the old sliding plane because the percentage of fine-grained particles was higher in the yellow layer than in the black layer. It is likely that the black layer formed in the 2003 event. Numerous
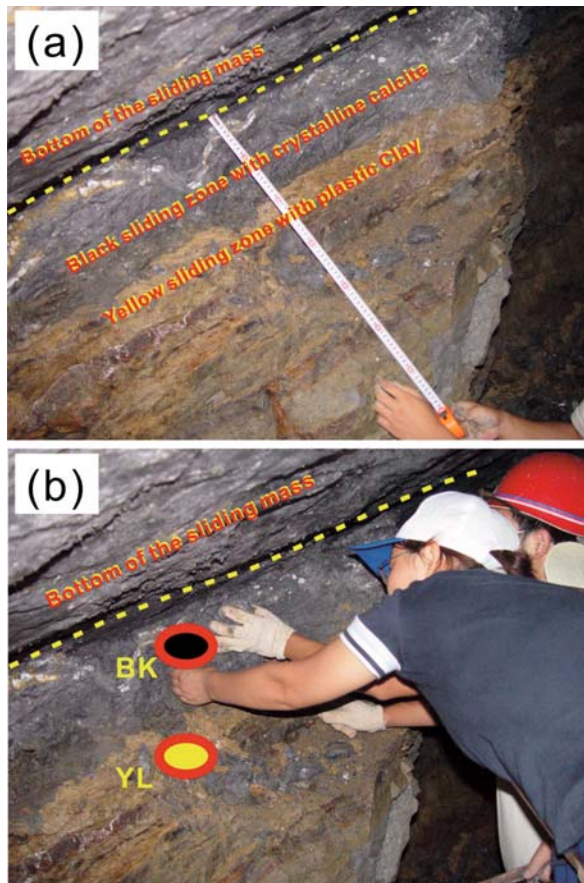
Fig. 8.14 Photograph of the sliding zone in a horizontal investigation tunnel. (**a**) Under the bottom of the sliding mass, the sliding zone can be observed to consist of two layers. The *upper layer* is *black* and includes crystallized calcite, and the *lower layer* is *yellow plastic clay* with a high water content. (**b**) Sampling from the black silt (BK sample) and yellow clay (YL sample) layers of the sliding zone

small blocks of crushed calcite were found in the black layer. It is reasonable to consider that the black clay layer was derived from the original black mudstone during the recent sliding. For laboratory tests, soil samples were taken from the two layers and named as the black sample (BK sample) and the yellow sample (YL sample).

Soil Properties

To clarify the basic properties of the two samples, grain size analyses, Atterberg limit measurements, and X-ray diffraction analyses were conducted on the two samples. Figure 8.15 shows the grain size distributions (Fig. 8.15a) and soil classification (Fig. 8.15b) of the two samples. It is clear that the YL sample has more fine particles than the BK sample. In the I_p–W_L chart, the YL sample is classified as CL (clay with a low liquid limit), while the BK sample BK is classified as ML (silt with a low liquid limit).
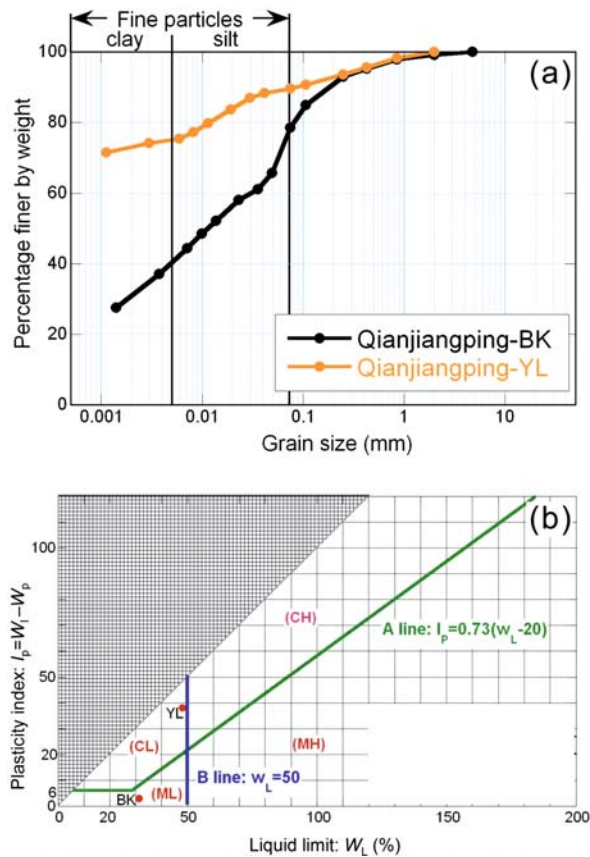
Fig. 8.15 Properties of the samples taken from the slide zone. (**a**) Grain size distribution of the samples. (**b**) Soil classification in the I_p–W_L chart. The black silt sample is labeled BK, and the yellow clay sample is labeled YL
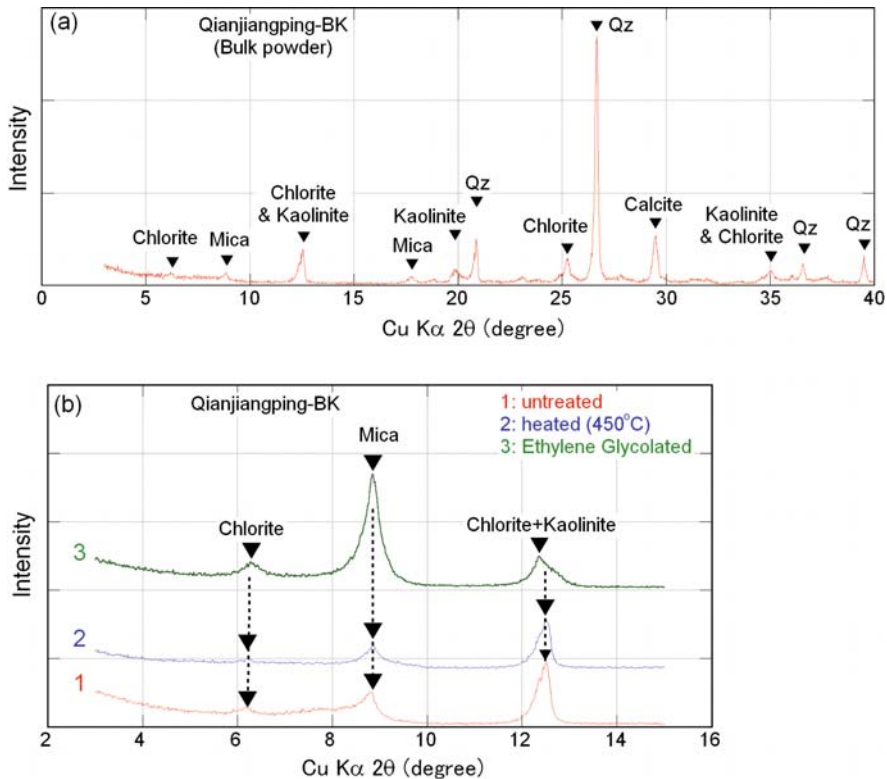
Fig. 8.16   X-ray diffraction pattern for the black silt sample (BK sample)

Figures 8.16 and 8.17 show the X-ray diffraction patterns of the BK sample and the YL sample, respectively. Figures 8.16a and 8.17a show the results for bulk powders of the two samples. Figures 8.16b and 8.17b show the results in the range from 3 to 15° for heating treatment to 450°C and treatment with ethylene glycol (Yoshimura 2001). Comparison of the BL sample (Fig. 8.16) with the YL sample (Fig. 8.17) indicates the following tendencies:

(1) There is no chlorite in the YL sample.
(2) There is no calcite in the YL sample.
(3) Chlorite–vermiculite appears as a weathering product in the YL sample.

From these results, it can be determined that the BK sample and the YL sample have the same rock source and that the YL sample is more maturely weathered than the BK sample. Through long-period shearing, grain crushing could occur in the sliding zone. As the result, the silt would become too clay. Moreover, oxidization due to groundwater flow by the water–soil interaction through the sliding zone changed the soil color from black to yellow.
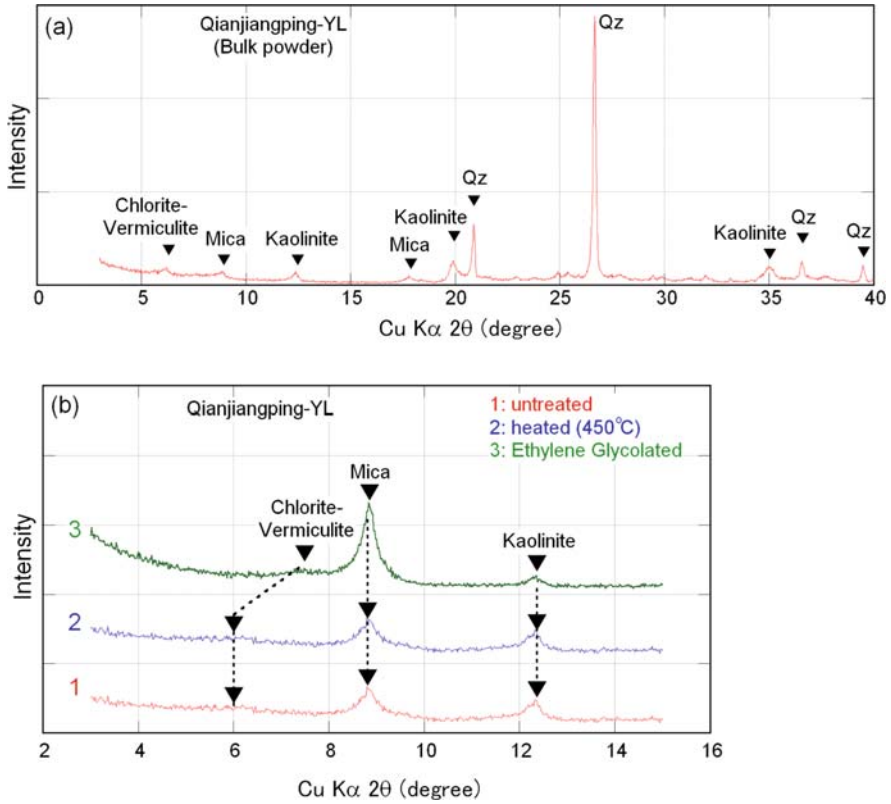
Fig. 8.17 X-ray diffraction pattern for the yellow clay sample (YL sample)

Ring Shear Tests to Simulate the Sliding Process

Ring shear apparatus DPRI-5 was employed to simulate the sliding process of the Qianjiangping landslide. In the 1980s, a series of ring shear apparatus was developed in the Disaster Prevention Research Institute (DPRI), Kyoto University, Japan (Sassa 1994; Sassa et al. 2003). The ring shear apparatus DPRI-5 is one of the series with an outer ring that is 180 mm in diameter and an inner ring that is 120 mm in diameter. Shear torque tests and shear velocity tests can be conducted with the DPRI-5. It is also possible to conduct undrained shearing tests to simulate rapid sliding in undrained (water-saturated) materials.

In this study, two series of ring shear tests were conducted. One series uses shear torque tests to simulate the landslide sliding process and the other uses shear velocity tests to examine the effect of shear velocity in mobilizing the shear resistance.

Shear Torque Test to Simulate the Sliding Process

The Qianjiangping landslide has a slope angle of 24° in the exposed sliding surface at main scarp and an average thickness of 26 m. These parameters were used to determine the initial normal stress acting on the soil element in the sliding zone (assuming the unit weight of the sliding mass is 18 kN/m^3). To simulate the sliding process in the sliding zone after failure, the test was designed as given below.

First, consolidate the sample normally with the initial normal stress and then apply part of the initial shear stress gradually under drained conditions. Thereafter, change the shear box to the undrained condition and increase the shear stress until failure occurs. Through this process, the after-failure processes of a rapid landslide can be simulated.

The tests were conducted on the BK sample and YL sample with the following procedure:

(1) Set the oven-dried soil sample into the shear box using the air deposition method.
(2) Saturate the sample with CO_2 gas and deaired water.
(3) Consolidate the fully saturated sample with the initial normal stress of 388 kPa.
(4) Apply the shear stress of 141 kPa at 1.2 kPa/min to avoid excess pore water pressure generation under natural drained conditions with the drainage valve open.
(5) Increase the shear stress further to make the soil specimen fail under undrained conditions at the rate of 0.28 kPa/min and measure the shear resistance mobilized during the shearing process.

The test results for the BK sample and the YL sample are shown in Figs. 8.18 and 8.19; they indicate that the two samples behaved differently. For the BK sample, shear resistance decreased quickly when the sample failed at a low residual shear resistance. Meanwhile, for the YL sample, shear resistance showed only a very small decrease and recovered quickly to the post-failure value.

The mobilized friction angles of the BK sample and the YL sample, which are defined as the inverse tangential function of the ratio of mobilized shear resistance to the total normal stress, are shown in Fig. 8.20. For the YL sample, after failure, the mobilized friction angle stayed at about 20°. Using the 24° slope angle of the sliding plane, a factor of safety (FoS) of 0.82 is obtained, which indicates that the slope will move along the yellow layer. For the BK sample, the mobilized friction angle was 26.5° at first, showing a greater shear resistance to the sliding when the slope angle was 24°. Because the black layer is between the rigid sliding block and the soft yellow layer (see Fig. 8.14), shear displacement would be caused by the sliding that occurred along the yellow layer. After the shear displacement reached about 2,000 mm, the mobilized friction angle started to decrease; and when the shear displacement reached 2,600 mm, the mobilized friction angle decreased suddenly from 25 to 12°. Considering that the slope angle of the energy line of the Qianjiangping
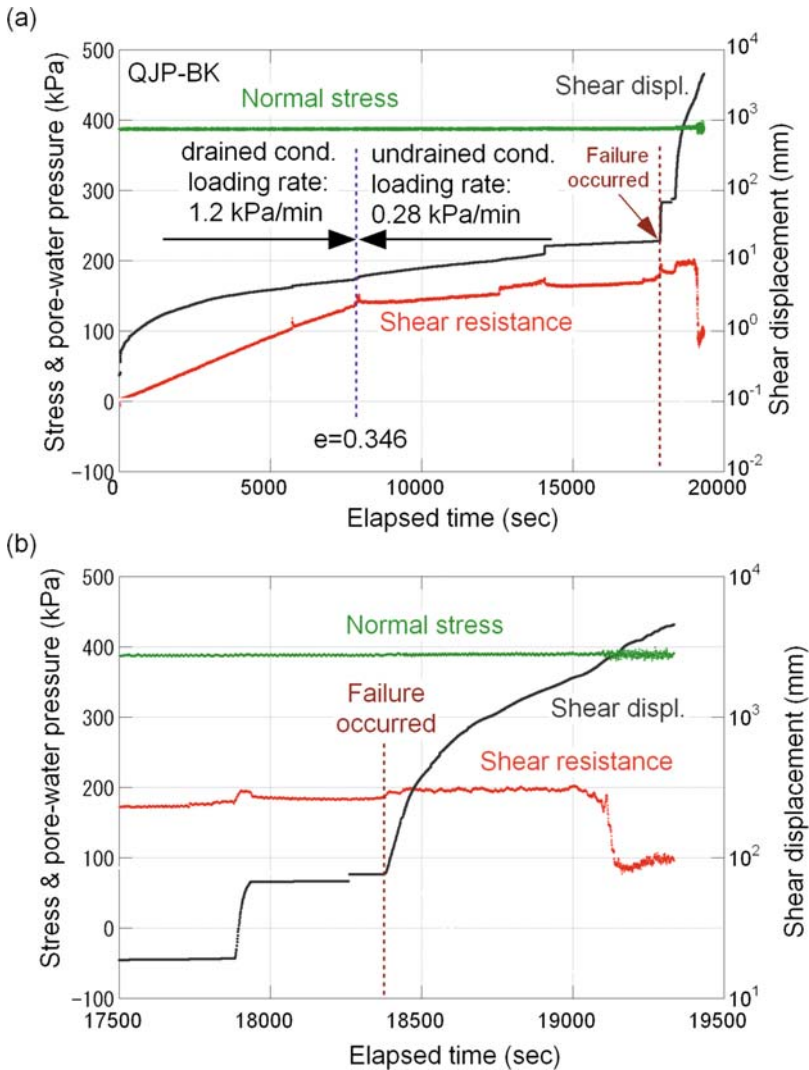
Fig. 8.18 Shear torque ring test results for the black silt sample (BK sample) from the Qianjiangping landslide. (**a**) Time series data for the whole test. (**b**) Close-up of the data near failure

landslide is about 10°, the mobilized 12° friction angle suggests the main sliding may have occurred along the black silt layer. The decrease of the mobilized friction angle may be due to excess pore pressure generation caused by grain crushing of the black silt layer during the shearing. This phenomenon was comprehensively studied by Sassa (Sassa et al. 1996, 2004) and his colleagues (Wang et al. 2000, 2002; Fukuoka et al. 2004) with undrained ring shear tests on sandy soils. Through this study of the Qianjiangping landslide, it is reasonable to estimate that excess
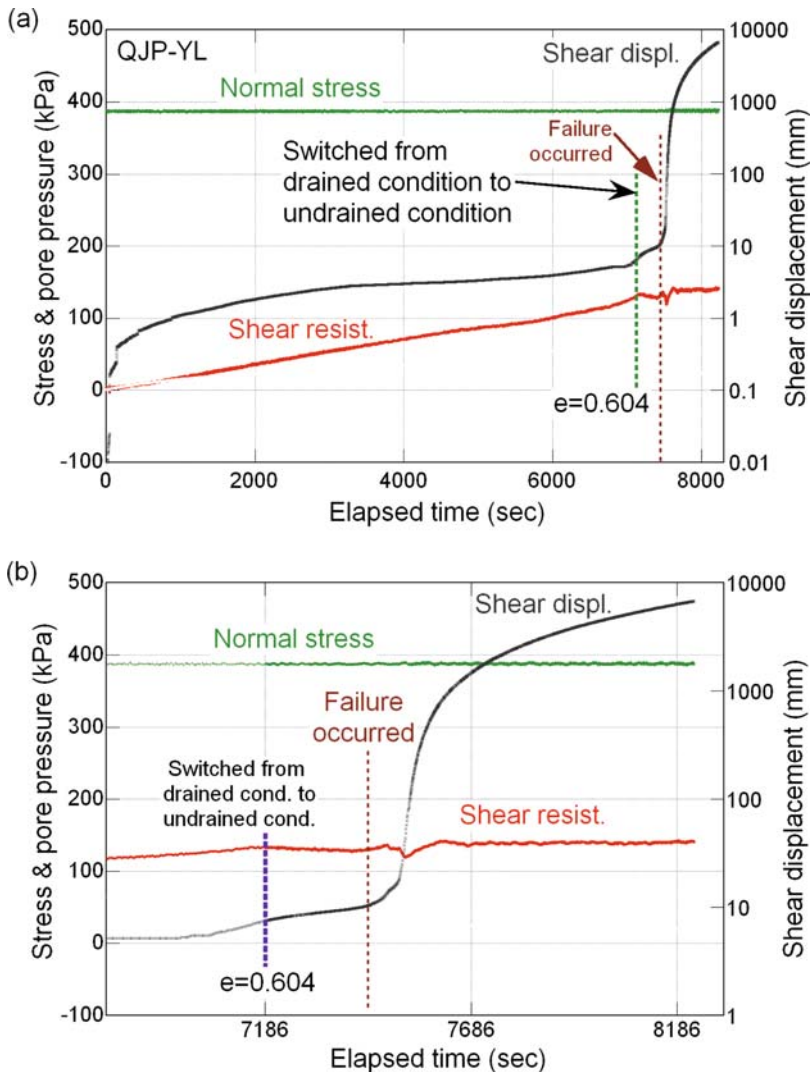
Fig. 8.19 Shear torque ring test results for the yellow clay sample (YL sample) from the Qianjiangping landslide. (**a**) Time series data for the whole test. (**b**) Close-up of the data near failure

pore pressure generation was caused by grain crushing of the black silt layer, which eventually will become a yellow clay layer.

Shear Velocity-Controlling Test to Simulate the Sliding Process

The purpose of this test series is to investigate the rate effect on the shear resistance. Rate effect is a phenomenon where the shear resistance of some soils becomes

Fig. 8.20 Mobilized friction
angle from the creep
simulation test for the black
silt sample (**a**) and the yellow
clay sample (**b**) from the
Qianjiangping landslide
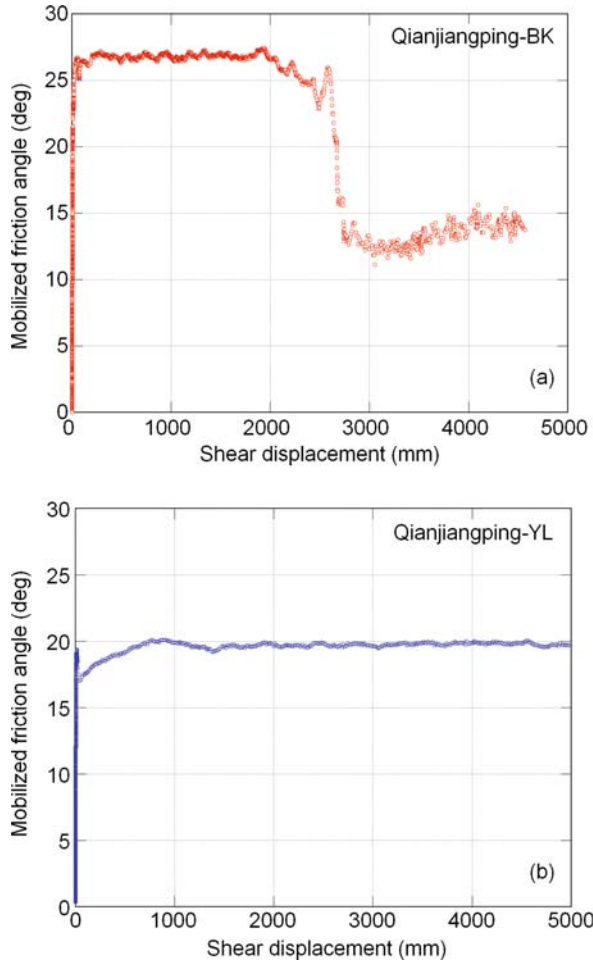
smaller when the shear velocity becomes higher; while for other soils, their shear
resistance becomes larger or remains constant (Tika et al. 1996; Saito et al. 2007).
In this series, tests were conducted using the following procedure:

(1) Prepare the saturated sample with the same procedure as described previously.
(2) Consolidate the sample at 200 kPa.
(3) Shear the sample with different shear velocities under the undrained condition
    and measure the shear resistance.

Figure 8.21 shows the relationship of the mobilized shear resistance with shear
displacement of the two samples at different shear velocities. It is clear that for the
BK sample, the shear resistance does not depend on the shear velocity when the
shearing velocity is small (Fig. 8.21a). At shear velocities of 0.01 and 1 mm/s, the
shear resistance did not show any obvious change, whereas at a shear velocity of

Fig. 8.21 The relationship between mobilized shear resistance and shear displacement at different shear velocities in the shear velocity ring test. Results for the black silt sample (**a**) and the yellow clay sample (**b**) from the Qianjiangping landslide
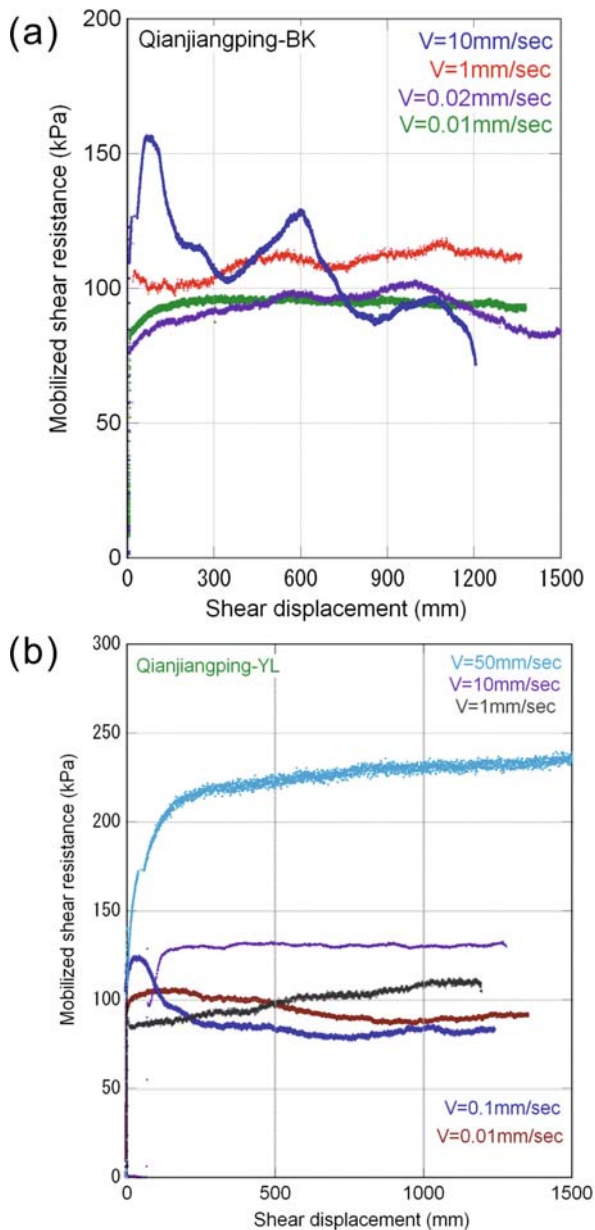
10 mm/s, the shear resistance became smaller than those produced at lower velocities when the shear displacement exceeded 750 mm. This result would mean that for the BK sample, shear resistance became lower when movement occurred at high velocity, while, for the YL sample, the mobilized shear resistance became higher at higher shear velocity (Fig. 8.21b).

Fig. 8.22 The relationship
between mobilized shear
resistance and shear velocity
for the black silt sample
(**a**) and the yellow clay
sample (**b**) from the
Qianjiangping landslide
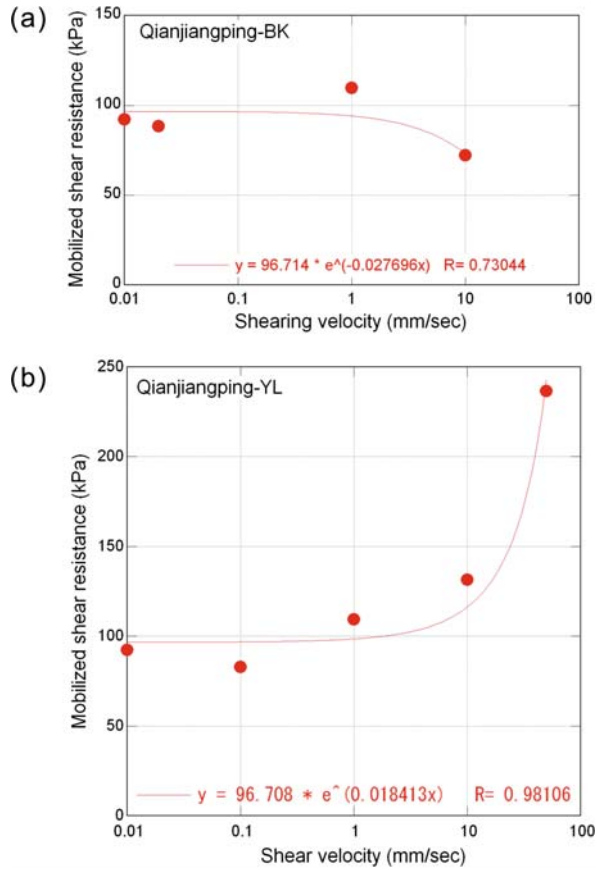
Figure 8.22 was obtained by plotting the mobilized shear resistance with shearing velocity for the two samples. Through comparison of the results, differences in the change of mobilized shear resistance with shear velocity can be examined. For the BK sample, the shear resistance became slightly smaller when the shear velocity increased, while for the YL sample, the shear resistance became much greater when the shear velocity increased. For the YL sample, the shear resistance shows a positive relationship with the shear velocity. When the shear velocity becomes higher, the shear resistance becomes higher.

Discussion and Conclusions

A detailed field investigation was made of the Qianjiangping landslide that occurred after the first impoundment of the Three Gorges Reservoir. The mechanisms of the landslide, especially the factors affecting slope failure, were studied, and reasons for the rapid and long distance movement of the landslide were considered. Based on fieldwork and analyses, the following conclusions were reached:

(1) The Qianjiangping landslide is a reactivated landslide with dip structure. The sliding surface was along a pre-existing structural plane of weakness (a bedding-plane shear).

(2) Quarrying of mudstone for brick manufacture from the toe of the slope and intense rainfall before the landslide put the slope in a critical state. This is not to assign blame for the landslide on the operators of the brick factory. Although quarrying of rock from the toe of a landslide is not good practice, there was no information to indicate that it was bad practice until the landslide was recognized. Prior to the cracks appearing, there appears to have been no reason to expect that the slope was unstable and hence little reason to exercise caution.

(3) The high water level in the Qinggan-he River through impoundment of the reservoir was the trigger for the landslide occurrence.

(4) The mechanism of the Qianjiangping landslide can be interpreted from the two series of ring shear tests. The motion of this landslide could be controlled by the black layer and the yellow layer. During the first phase of landsliding, the sliding mass should move along the yellow layer. Because the black layer lies on the yellow layer, shearing deformation should also occur in the black layer. After shearing proceeded for a large distance and the shear velocity reached a certain value, the main sliding plane shifted to the black layer because the shear resistance in the yellow layer became greater than that in the black layer. With the sudden decrease of the shear resistance in the black layer, rapid motion occurred in this reactivated landslide.

(5) Because the landslide has a tectonic background, and there are many similar slopes in the nearby area, detailed evaluations for those slopes are very important for the future stability of the Three Gorges Reservoir when it is raised to its final operating level.

This research has very important significance for landslide disaster prevention and mitigation. Although reactivated landslides generally move with low sliding velocity, they can shift to rapid motion when the soil near the existing sliding plane has the tendency toward a negative rate effect. When landslides have moved for a certain distance, the decrease in shear resistance of the newly developed sliding plane could make the landslide move rapidly.

References

Cao L, Luo XQ, Cheng SG (2007) Research on similar material of physical model for Qianjiangping landslide. Journal of China Three Gorges University (Natural Sciences Edition), 29(1): 37–39 (in Chinese with English abstract)

Fukuoka H, Wang G, Sassa K, Wang FW, Matsumoto T (2004) Earthquake-induced rapid long-traveling flow phenomenon: May 2003 Tsukidate landslide in Japan. Landslides: Journal of the International Consortium on Landslides, 1(2): 151–155

Saito R, Sassa K, Fukuoka H (2007) Effects of shear rate on the internal friction angle of silica sand and bentonite mixture samples. Journal of the Japan Landslide Society, 44(1): 33–38 (in Japanese with English abstract)

Sassa K (1994) Development of a new cyclic loading ring-shear apparatus to study earthquake-induced-landslides. Report for Grain-in-Aid for Developmental Scientific Research by the Ministry of Education, Science and Culture, Japan (Project No. 03556021), 106 pp

Sassa K, Fukuoka H, Scarascia-Mugnozza G, Evans S (1996) Earthquake-Induced Landslides; Distribution, Motion and Mechanisms. Special Issue of Soils and Foundations, pp. 53–64

Sassa K, Fukuoka H, Wang G, Ishikawa N (2004) Undrained dynamic-loading ring-shear apparatus and its application to landslide dynamics. Landslides, 1(1): 9–17

Sassa K, Wang G, Fukuoka, H (2003) Performing undrained shear tests on saturated sands in a new intelligent type of ring-shear apparatus. Geotechnical Test Journal, 26(3): 257–265

Tika TE, Vaughan PR, Lemos LJ (1996) Fast shearing of pre-existing shear zones in soil. Geotechnique, 46(2): 197–233

Wang FW, Sassa K, Fukuoka H (2000) Geotechnical simulation test for the Nikawa landslide induced by 1995.1.17 Hyogoken-Nambu earthquake. Soils and Foundations, 40(1): 35–46

Wang FW, Zhang YM, Huo ZT, Matsumoto T, Huang BL (2004) The July 14, 2003 Qianjiangping landslide, Three Gorges Reservoir, China. Landslides, 1(2): 157–162

Wang FW, Zhang YM, Huo ZT, Peng XM, Wang SM, Yamasaki S (2008) Mechanism for the rapid motion of the Qianjiangping landslide during reactivation by the first impoundment of the Three Gorges Dam Reservoir, China. Landslides, 5(4): 379–386

Wang, XF, Chen, XH, Zhang RJ (2002) Protection of geological remains in the Yangtze Gorges area, China with the study of the Archean-Mesozoic multiple stratigraphic subdivision and sea-level change. Geological Publishing House, Beijing, 341 pp (in Chinese)

Wang ZH, Yang RH (2005) The activity characteristics and movement style of Qianjiangping Landslide in the Three Gorges Reservoir region. The Chinese Journal of Geological Hazard and Control, 15(3): 5–8 (in Chinese with English abstract)

Wu AQ, Ding XL, Li HZ, Chen SH, Shi GH (2006) Numerical simulation of startup and whole failure process of Qianjiangping landslide using discontinuous deformation analysis method. Chinese Journal of Rock Mechanics and Engineering, 25(7): 1297–1303 (in Chinese with English abstract)

Yin YP, Peng XM (2007) Failure mechanism on Qianjiangping landslide in the Three Gorges Reservoir region. Chinese Hydrogeology and Engineering Geology, 51(3): 49–52 (in Chinese with English abstract)

Yoshimura, T. (Eds.) (2001) Clay Minerals and Alteration. Geology Series 32, the Association for Geological Collaboration in Japan, Tokyo, 294 pp (in Japanese)

Zhang YM, Liu GR, Chang H, Huang BL, Pan W (2004) Analysis of Qianjiangping landslide structure in Three Gorges reservoir area and revelation. Yangtze River, 49(9): 61–64 (in Chinese)

Chapter 9
Evaluation of the Roles of Reservoir Impoundment and Rainfall for the Qianjiangping Landslide in Zigui County, Three Gorges Area

Baoping Wen, Jian Shen, and Jianmin Tan

Abstract The Qianjiangping landslide occurred following the first impoundment of the Three Gorges reservoir and a prolonged rainfall. To evaluate the quantitative effects of the reservoir impoundment and rainfall on the landslide, a sensitive analysis was performed with particular consideration to the landslide's unique characteristics and the seven parameters susceptible to the interactions between the landslide's materials and water from the two sources. These parameters include unit weight of the landslide's material, groundwater level above the slip zone, shear strength components of the upper and lower sections of the landslide's slip zone, and uplift pressure of the reservoir water. Results of this study show that the factor of safety (FS) of the landslide was the most sensitive to the cohesion of shear strength of the slip zone's lower section, and the least sensitive to groundwater level above the slip zone. It is found that the effect of shear strength reduction of the slip zone's lower section was the most crucial in the landslide's initiation. The landslide resulted from the combined influences of the reservoir impoundment and rainfall. The role of the reservoir impoundment in the landslide was dominant with a contribution percentage about 61.3%, whereas rainfall may have been the factor triggering the landslide.

Keywords Qianjiangping landslide · Rise of reservoir water level · Prolonged rainfall · Sensitive analysis

Introduction

The sudden occurrence of the Qianjiangping landslide in Zigui county, the Three Gorges area, at 0:20 AM, July 14, 2003 not only caused 24 casualties and huge economic losses but also drew great attention from both the public and researchers. This landslide took place 43 days after the impoundment of the Three Gorges reservoir, and a prolonged rainfall of 162.7 mm during the period between June 21, 2003

B. Wen (✉)
China University of Geosciences (Beijing), Beijing 100083, China

and July 11, 2003. Apparently, both the reservoir impoundment and the prolonged rainfall must have played important roles in the occurrence of this landslide. A number of researchers, e.g., Dai et al. (2004), Wang et al. (2004), Yang et al. (2006), believed that this landslide's occurrence was largely due to shear strength reduction of a pre-existing weak zone along a bedding plane of shale that was saturated by groundwater from both the reservoir impoundment and rainfall. Liu et al. (2005) argued that the influence of the reservoir impoundment on the landslide became significant only after the rise of the reservoir water level was greater than 15 m. Yin and Peng (2007) thought that the influence of rainfall on the landslide was greater than the reservoir impoundment because the shear strength of the landslide's slip zone had little change, as it was a pre-existing shear zone. Xiao et al. (2007) presented a result that the reservoir impoundment had a greater effect on the landslide's occurrence than rainfall. Obviously, there has been an argument about the relative importance of the reservoir impoundment and rainfall in the landslide's occurrence among researchers, and few studies show insightful understanding about the quantitative roles of the two effects on the landslide in terms of the interactions between the landslide's materials and water from the two sources.

It has been well recognized that water within a landslide decreases its stability in several ways as a result of a series of complex physical, chemical, and mechanical interactions between the landslide's materials and water. The most common processes include increasing unit weight of the landslide's materials, pore-water pressure at the slip zone, and seepage force within the landslide; reducing shear strength of its slip zone, etc. Thus, an in-depth understanding of water influence on a landslide should consider changes in all of the processes above. Certainly, decrease of a landslide's stability due to water influence mentioned is site-specific, because there is a great variation in landslide characteristics and nature of the water occurring within the landslides. For the Qianjiangping landslide, the reservoir impoundment mainly influenced its lower part, while rainfall infiltration should have mainly influenced its upper part above the reservoir water level. In this chapter, quantitative roles of the reservoir impoundment and rainfall in the Qianjiangping landslide were evaluated on the basis of a sensitive analysis of the factor of safety (FS) of the landslide with a series of parameters susceptible to the interactions between the landslide's materials and water from the two sources. Selection of the parameters was focused on the unique characteristics of the Qianjiangping landslide and nature of water from the two sources.

Site Description

The Qianjiangping landslide is located on the left bank of the Qingganhe River, one of the tributaries of the Yangtze River, where water level rose from 95 m above sea level (A.S.L) to 135 m after impoundment of the Three Gorges reservoir. At 0:20 AM, July 13, 2003, the slope of the river bank, about 20,000,000 m³ in volume, rapidly slipped down about 200 m in less than 5 min and blocked the

Fig. 9.1 Simplified plan of the Qianjiangping landslide (from Wang et al. 2008)
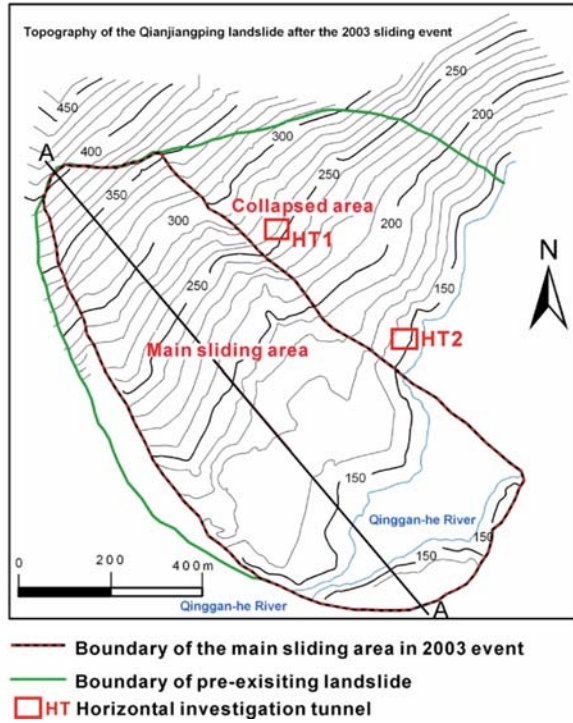
Qingganhe River, forming a landslide dam (Figs. 9.1 and 9.2). Field investigation post-landsliding found that the main scarp of the landslide was along the bedding plane of shale of early and middle Jurassic in age, and that the toe of its slip surface was located near the floodplain of the Qingganhe River, where the elevation was about 100–110 m A.S.L.
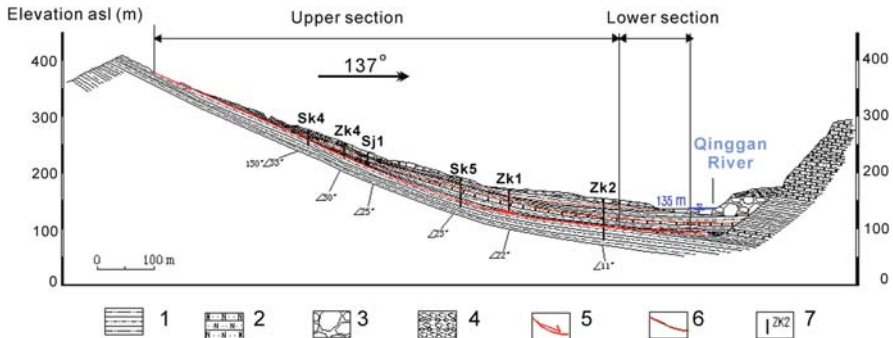
Fig. 9.2 Main cross section through the Qianjiangping landslide.
1: Silty mudstone + clayey siltstone; 2: Sandstone; 3: Colluvium; 4: Alluvium; 5: Main slip zone; 6: Sub-slip zone; 7: Borehole and its number (Please note that SJ1 denotes a deep shaft)

The landslide material was composed of loose to very loose colluvium, and highly fractured sandstone, siltstone, and mudstone of early and middle Jurassic age. The thickness of the colluvium was about 5–15 m, and that of the highly fractured classical rocks was 20–45 m. Field investigation and deep shaft results revealed that the sequence of the fractured classical rocks experienced no change compared with the intact bedrock, showing that their bedding planes had a dip of 32–15° downward and about parallel to the slope. In situ measurement using an in situ bulk density test showed that unit weight of the landslide's material varied, with a range of 16.05–22.57 kN/m^3 with an average value of 17.58 kN/m^3.

Eight boreholes and two deep shafts disclosed that the landslide had a main slip zone and two to three sub-zones. The sub-zones were found to be the pre-existing tectonic shear zones developed along bedding planes of mudstone and siltstone. Prominently, the main slip zone consisted of two distinctive sections characterized by their occurrences and locations: the upper and lower sections (Fig. 9.2).

The upper section of the main slip zone, containing a striated and slickensided surface, was seen to develop along the bedding plane of the dark gray shale interbedded by the mudstone and sandstone. Occurrence of this section of the slip zone was found to be consistent with its underlying bedrock, showing an "L" shape occurrence with dip angle 32° at the main scarp and 15° near the middle part of the slope. Wen (2008) found that this part of the slip zone was a pre-existing shear zone that resulted from tectonic shearing and argillation of shale due to progressive weathering. The slip zone, about 5–10 cm thick, very soft and very wet, was composed of dark gray clayey soil with some limestone and calcite fragments. Particle size analysis showed that the clay content of the slip zone varied from 22% to 39%, and its gravel content was 20% to 35%. It is noteworthy that major part of the slip zone was above the reservoir water level when first impoundment of the reservoir reached the water level of 135 m A.S.L.

The lower section of the slip zone occurred sub-horizontally and slightly inward to the slope. This section of the slip zone was found to be a newly formed shear zone across the bedding plane of mudstone, as a result of landsliding. The slip zone was about 100–120 m long, being much shorter than the upper section, which was 600–650 m long. Materials of the slip zone consisted of dark reddish clayey soils with mudstone fragments. Different from the upper section of the slip zone, this part of the slip zone was fully immersed by the reservoir water when first impoundment of the reservoir reached the water level of 135 m A.S.L.

Additionally, boring revealed that the bedrock immediately under the main slip zone, about 1–2 m thick, was very fractured, while the bedrock deeper was slightly fractured, indicating that the bedrock immediately below the slip zone was much more permeable.

Shear strength of the landslide's main slip zone was examined in laboratory (Table 9.1). Shear strength components of the undisturbed samples from the upper section of the slip zone under their natural and saturated states were determined using the direct shear test, and those of the samples collected from slightly weathered mudstone near the lower section of the slip zone, under their naturally dry and saturated states, were measured using triaxial test.

Table 9.1 Shear strength components of the Qianjiangping landslide's main slip zone

	Saturated		Unsaturated	
Slip zone	Cohesion (kPa)	Internal friction angle (°)	Cohesion (kPa)	Internal friction angle ϕ (°)
Upper section	72.51	13.54	114	16.66
Lower section	112.8	20.8	1500	33.1

Analysis Methods

To compare quantitative effects of the reservoir impoundment and rainfall on the Qianjiangping landslide, a sensitive analysis was performed considering interrelationships between the factor of safety (FS) of the landslide and a series of parameters susceptible to the interactions between the landslide's materials and water from the two sources. The FS of the landslide was computed based on two-dimensional limit equilibrium model (2DLEA) using the Janbu method, one of the most popular methods for the landslides with non-circular slip surfaces. The 2DLEA was implemented using the software SLOPE/W developed by GEO-SLOPE International. The 1-1 cross section through the toe and crown of the landslide was used for computation (Fig. 9.2).

Based on characteristics of the Qianjiangping landslide, the parameters changed due to the reservoir impoundment and rainfall should have include unit weight of landslide materials, cohesion and internal friction angle of the slip zone, pore-water pressure at the slip zone due to rise of groundwater above the slip zone, and uplift pressure of the reservoir water when it saturated the fractured bedrocks underlying the slip zone. As mentioned above, the Qianjiangping landslide main slip zone was made up of two distinct sections: the upper section along a pre-existing shear zone within shale and the lower section across a bedding plane of mudstone. Apparently, the shear strength of the two sections operated during landsliding should be the residual strength of the pre-existing shear zone interbedded by shale, and the peak strength of mudstone, respectively. Accordingly, values of the seven parameters of the landslide were changed following the reservoir impoundment and rainfall.

To evaluate sensitivity of the FS of the landslide to the seven parameters, and the quantitative effects of the reservoir impoundment and rainfall on the Qianjiangping landslide, sensitive index (SI) and effect index (EI) were introduced in this study

$$\text{SI} = (\eta_1/\eta_2) \times 100\% \tag{9.1}$$

where $\eta_1 = |\Delta\text{Fs}| \times 100\%/\text{Fs}_0$, $\eta_2 = |\Delta X_i| \times 100\%(X_{i\,\max} - X_{i\,\min})$. η_1, η_2 represent the variation ratio of the FS of a landslide and a parameter, respectively. ΔX_i is variation of the parameter X_i, $X_{i\,\max}$ $X_{i\,\min}$ represent its maximum and minimum values Fs_0 is the initial value of FS of a landslide, ΔFs is the variation of FS resulted from ΔX_i:

$$\text{EI} = \Delta \text{Fs}_{\max, Xi} \times 100\% / \Sigma \Delta \text{Fs}_{\max, Xi} \tag{9.2}$$

where $\Delta \text{Fs}_{\max, Xi}$ is the maximum variation of FS when change of parameter X_i reaches its maximum value.

As mentioned before, the landslide took place 43 days after impoundment of the Three Gorges reservoir and a prolonged rainfall during the period between June 21, 2003 and July 11, 2003. This gives three indications: (a) groundwater within the landslide from both the reservoir water and rainfall had fully interacted with the landslide materials before landsliding; (b) influence of the reservoir impoundment on the landslide took place earlier than the rainfall; (c) and the landslide remained stable after the reservoir impoundment and before rainfall. Therefore, the initial state of the landslide for the sensitive analysis in this study was designated to be the moment when the reservoir water level reached 135 m A.S.L., the design water level of the Three Gorges reservoir's impoundment. Accordingly, initial values of the seven parameters aforementioned were as follows: (a) zero for both pore-water pressure at the slip zone above the reservoir water level and uplift pressure of the reservoir water; (b) natural and saturated unit weight of the landslide materials for those above and below the reservoir water level, respectively; (c) the residual shear strength components of the clay seam within the shale at its natural (unsaturated) state for the upper section of the slip zone; and (d) the peak shear strength components of the mudstone at its natural dry state for the lower section of the slip zone.

Assuming rainfall before landsliding fully infiltrated into the landslide and caused the rise of the groundwater table above the slip zone above the reservoir water table, the upper section of the slip zone, primarily, caused an increase in pore-water pressure at the slip zone. Thus, rainfall of 162.7 mm before landsliding caused a maximum rise of groundwater table of 16.3 cm, and as a result, a maximum increase of pore-water pressure. Given that the reservoir water gradually infiltrated into the fractured bedrock immediately below the slip zone following the reservoir impoundment, when the water in Qingganhe River rose from 95 to 135 m A.S.L, the uplift pressure of reservoir water reached its maximum value of 400 kPa. Because pore-water pressure resulted from rainfall infiltration directly corresponding to the rise of groundwater level above the slip zone, this parameter was represented using

Table 9.2 Parameters for the sensitive analysis

Parameters (X_i)	Range
Unit weight of the materials above the reservoir water level (X_1)	17.6–23.6 kN/m³
Cohesion of the slip zone's upper section (X_2)	114–72.5 kPa
Internal friction angle of slip zone's upper section (X_3)	16.7–13.5°
Groundwater level above the slip zone (X_4)	0–16.3 cm
Cohesion of the slip zone's lower section (X_5)	1500–112 kPa
Internal friction angle of slip zone's lower section (X_6)	33.1–20.8°
Uplift pressure due to reservoir impoundment (X_7)	0–400 kPa

rise of groundwater level in this study. Moreover, shear strength components of most of the upper section and all of the lower section of the landslide's slip zone reached their lowest values when they were saturated by rainfall and the reservoir water, respectively. Ranges of these parameters for the sensitive analysis are given in Table 9.2.

Results and Discussion

Computation yielded an FS of 2.43 when the landslide was at its initial state. When the parameters changed from their initial values following the reservoir impoundment and rainfall, the FS of the landslide linearly decreases (Figs. 9.3–9.7). However, decrease of the FS with change of each parameter varies greatly due to difference in both range of each parameter and effects of the reservoir impoundment and rainfall on the landslide. For the parameters to have the same unit, specifically shear strength components of the upper and lower sections of the slip zone, it seems that the FS is more sensitive to shear strength components of the upper section than those of the lower section in terms of unit variation of these counterpart parameters
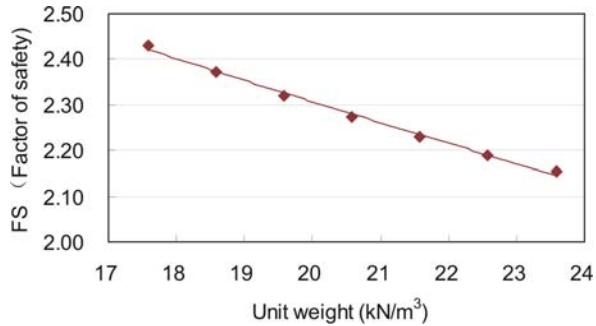
Fig. 9.3 Correlation between FS and unit of weight of the landslide's material
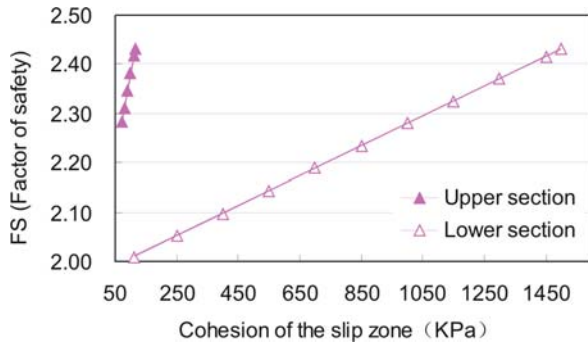
Fig. 9.4 Correlations between the FS and cohesions of the landslide's slip zone

Fig. 9.5 Correlations
between FS and internal
friction angles of the
landslide's slip zone
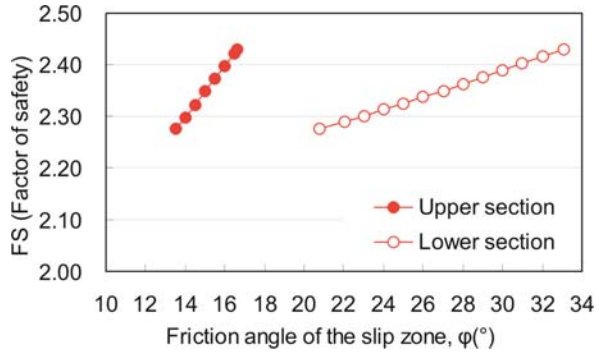
Fig. 9.6 Correlations
between FS and groundwater
level above the landslide's
slip zone
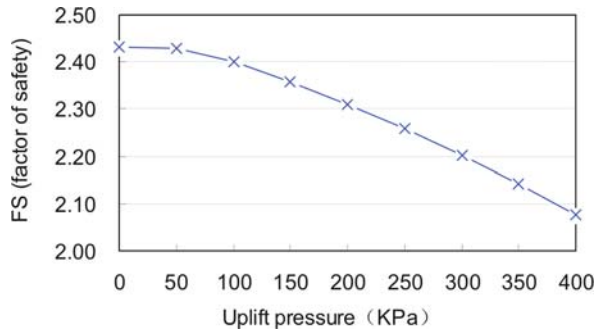
(Figs. 9.3 and 9.4). But, this may not represent the real situation because variation range of each pair of the parameter was very different during development of the landslide. In addition, note that the FS of the landslide showed no change when uplift pressure was less than 50 kPa, corresponding to the reservoir water level below 100 m A.S.L. This is because the toe of the landslide's slip surface was above 100 m A.S.L.

Fig. 9.7 Correlations
between FS and uplift
pressure of the reservoir
water
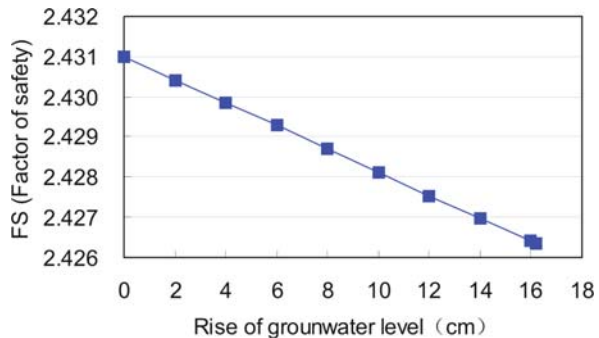
Sensitivity of the FS to the Parameters Within the Reservoir Impoundment and Rainfall

Figure 9.8 shows the correlations between the variation ratios of FS and those of the seven parameters after the reservoir impoundment and rainfall. Apparently, the slope of each correlation curve represents a sensitive index (EI) of FS to each parameter as defined in this chapter, which considers both each parameter's variation range and its correlation with FS. It is clearly seen that in the range of these parameters, the FS of the landslide was the most sensitive to cohesion of the lower section of the slip zone, followed by uplift pressure, unit weight of the landslide material, internal friction angles of the upper and lower sections of the slip zone, and cohesion of the upper section of the slip zone. The FS of the landslide was the least sensitive to groundwater level above the slip zone. When change of these parameters reached their maximum or minimum values, ratio of maximum decrease of the corresponding FS also demonstrates a similar trend (Fig. 9.9).

Consistent with FS sensitivity to each parameter, effects of these parameters' change on the landslide's stability exhibit a very similar order in terms of effect index (EI) as defined in this chapter (Fig. 9.9): (a) EI of the cohesion of the lower section of the slip zone was the greatest (27.8%) and EI of the groundwater level above the slip zone was the least (0.3%). EI of other five parameters on the landslide were relatively moderate, specifically, 38.1% for shear strength components of the lower section of the slip zone, 23.3% for the uplift pressure, 20.1% for the shear strength components of the upper sections of the slip zone, and 18.3% for
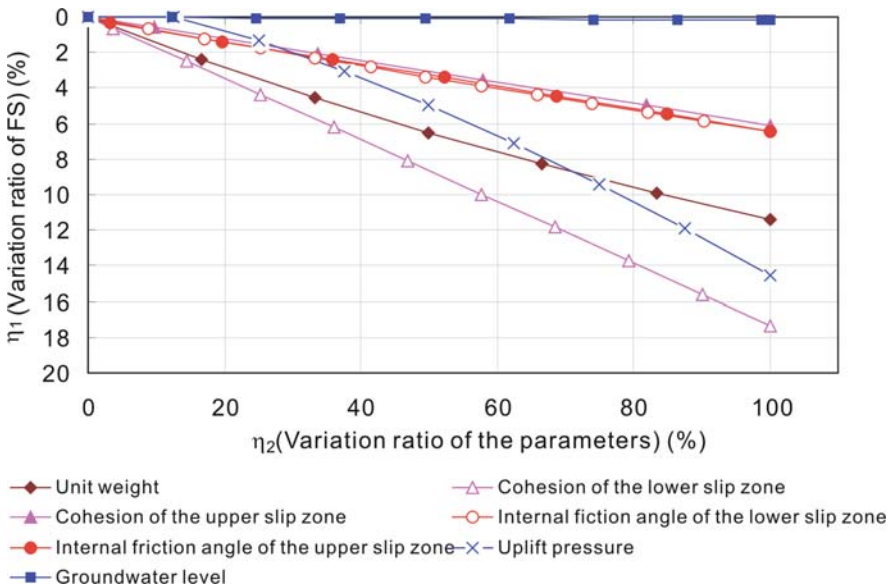
Fig. 9.8 Correlations between ratio of the FS variation and that of the parameters
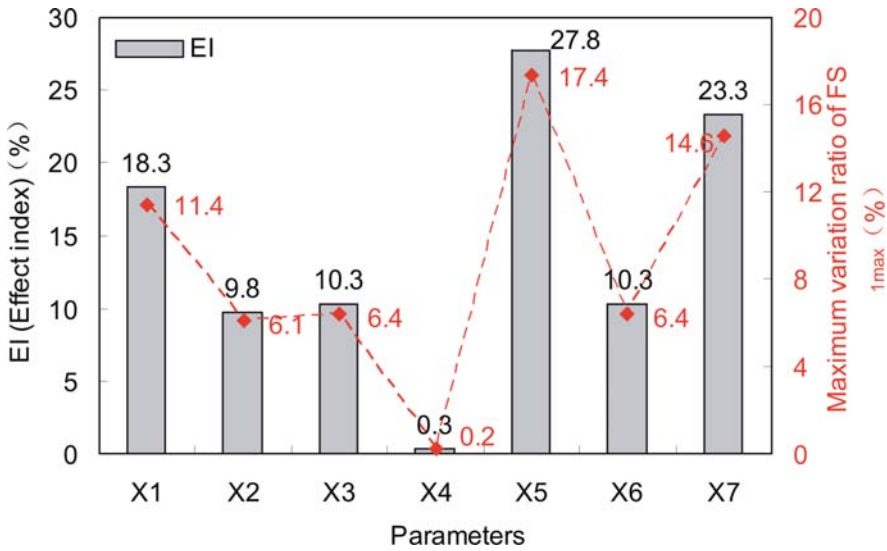
Fig. 9.9 Variation of the maximum ratio of FS and EI of the parameters (denotations of the parameters X_1–X_7 are shown in Table 9.2)

unit weight of the landslide's material. These results suggest that reduction of shear strength of the lower section of the slip zone, particularly reduction of its cohesion component, was the most significant for the landslide occurrence, next were loading of uplift pressure of the reservoir water, reduction of shear strength of the upper section of slip zone, and increase of unit weight of the landslide's materials above the reservoir water level. The rise of groundwater level above the slip zone, i.e., increase of pore-water pressure at the slip zone, seems to be insignificant to occurrence of the landslide. Both reduction of shear strength of the landslide's slip zone and loading of the uplift pressure of the reservoir water resulted in the decrease of shear resistance of the landslide, particularly shear resistance of the lower section of its slip zone, which was the most crucial for the landslide's occurrence. On the other hand, increase of unit weight of the landslide's material led to an increase of driving force of the landslide. As a consequence, a combination of these effects resulted in sudden occurrence of the landslide. Nature of occurrence and the materials of the landslide's slip zone suggest that shear strength reduction of the lower section of the slip zone should be largely the result of water weakening the mudstone by water saturation and hydrolysis during and after the reservoir impoundment, and that shear strength reduction of the upper section of the slip zone was mainly attributed to decrease of soil suction when it was saturated by infiltrated rainfall.

Quantitative Roles of the Reservoir Impoundment and Rainfall in Occurrence of the Landslide

As mentioned before, for the Qianjiangping landslide, the following changes were largely initiated by infiltration of rainfall: increase of unit weight of the landslide's

materials, decrease of shear strength of the upper section of the slip zone, and rise of groundwater table above the slip zone, while these changes resulted from the reservoir impoundment: shear strength reduction of the lower section of the slip zone and loading of uplift pressure of the reservoir water. Figures 9.3–9.7 show that the FS of the landslide was still greater than 1, and even greater than 2 if each parameter reached its maximum or minimum values individually, i.e., the worst situation for the landslide's stability. This gives the indication that the landslide was stable. When all the parameters reached their maximum or minimum values simultaneously, the FS of the landslide was reduced to 0.95 from 2.43, suggesting failure of the landslide. The latter situation was actually more close to reality, as it happened on the landslide. Hence, the landslide's occurrence must have been the consequence of the combined effects of both the reservoir impoundment and rainfall. Consequently, for the landslide, effect indices (EI) of the parameters susceptible to the reservoir impoundment and rainfall were 61.3% and 38.7%, respectively, giving a clear indication that the reservoir impoundment played a much more important role in the landslide's occurrence than rainfall. Rainfall may have acted as a triggering factor.

It should be mentioned that the rise of water level of the Three Gorges reservoir to the level of 135 m A.S.L. during its first impoundment must have taken some days, rather finished in a moment. Change of the parameters susceptible to the reservoir impoundment must have taken place before the water level reached 135 m A.S.L. Therefore, the assumption for computation made in this chapter may not fully represent the real situation. Nevertheless, the computation results based on the assumption are of great significance for evaluation of roles of the reservoir impoundment and rainfall, and for understanding their effects on the landslide.

Conclusions

Impoundment of the Three Gorges reservoir and rainfall resulted in changes of a series of parameters for the Qianjiangping landslide susceptible to the interactions between the landslide's materials and water from the two sources. These parameters are as follows: unit weight of the landslide's materials, groundwater level above the slip zone, shear strength components of the slip zone's upper and lower sections, and uplift pressure of reservoir water. Sensitive analysis shows that the FS of the Qianjiangping landslide was the most sensitive to cohesion of the lower section of the landslide's slip zone, followed by uplift pressure, internal friction angles of the upper and lower sections of the slip zone, cohesion of the upper section of the slip zone, and unit weight of the landslide materials. The FS of the landslide was the least for groundwater level above the slip zone. These results suggest that weakening of the slip zone's lower section by the reservoir water contributed the most to the landslide's occurrence. These results further confirmed that the Qianjiangping landslide resulted from combined influences of the reservoir impoundment and rainfall. However, the reservoir impoundment played a more important role than rainfall. The latter may have behaved as a triggering factor.

References

Dai FC, Deng JH, Tham LG, Law KT, Lee CF (2004) A large landslide in Zigui County, Three Gorges area. Canadian Geotechnical Journal 41(6): 1233–1240

Liu CH, Chen CX, Feng XT (2005) A slope failure due to rise of water level of the Three Gorges reservoir. Rock and Soil Mechanics 26(5): 668–703 (in Chinese)

Wang FW, Zhang YM, Huo ZT, Matsumoto T, Huang BL (2004) The July 14, 2003 Qianjiangping landslide, Three Gorges Reservoir, China. Landslides 1(2): 157–162

Wang FW, Zhang YM, Huo ZY, Peng XM, Wang SM, Yamasaki S (2008) Mechanism for the rapid motion of the Qianjiangping landslide during reactivation by the first impoundment of the Three Gorges Dam reservoir, China. Landslides 5(4): 379–386

Wen BP (2008) Technical report: Characteristics of the slip zones of Qianjiangping landslide and weak zones within the slope adjacent to the landslide (in Chinese)

Xiao SR, Liu DF, Hu ZY (2007) Geo-mechanical model of the Qianjiangping landslide in the Three Gorges area. Rock and Soil Mechanics 28(7): 1459–1464 (in Chinese)

Yang WM, Wu SR, Shi SJ, Pan F (2006) Mechanism of the Qianjiangping landslide in Zigui county, Hubei Province. Coal Mining Engineering 4: 57–59 (in Chinese)

Yin YP, Peng XM (2007) Analysis of mechanism of the Qianjiangping landslide. Hydrogeology and Engineering Geology 3: 51–53 (in Chinese)

Chapter 10
Unsaturated Creep Test and Modeling of Soils from the Sliding Zone of the Qianjiangping Landslide in the Three Gorges Area, China

Shimei Wang and Qingjie Yin

Abstract Water is the most sensitive factor affecting the mechanical characteristics of rock and soil mass. The increase in the water ratio of unsaturated soil mass reduces both instantaneous strength and long-term strength of soils and changes the soil's creep property. In view of the close correlation of rock and soil mass with water action and effects over time, this chapter presents the concept of "unsaturated soil creep" based on the theories of unsaturated soil mechanics and creep soil mechanics. An unsaturated soil creep triaxial apparatus has been researched and developed based on the basic principles used in the application of unsaturated soil triaxial apparatus and triaxial creep apparatus. The law of the impact of matrix suction on the creep characteristics of the soil mass in the Qianjiangping landslide in the Three Gorges area has been applied, and an unsaturated soil creep model that can reflect the impact of matrix suction has been established through tests using the apparatus. The research result has facilitated a new approach for analyzing the long-term strength and deformation of unsaturated soils and predicting the long-term stability of the landslide under the action of reservoir water fluctuation or rainfall.

Introduction

The landslide soil mass fluctuates between a saturated state and an unsaturated state under the condition of rainfall infiltration and reservoir water level variation. Rainfall or reservoir impoundment results in stability reduction, deformation increase, or failure of the landslide, which does not always occur at once but happens over a period of time (Yang et al. 2007a; Riemer 1992) in most cases. How to test the

S. Wang (✉)
Key Laboratory of Geological Hazards on Three Gorges Reservoir
Area of Education Ministry, China Three Gorges University, Yichang 443002, China
e-mail: wwsm3044@yahoo.com.cn

rheological property of landslide soil mass under water action has become an important subject on the study of the deformation process and long-term stability of landslides under the action of rainfall and reservoir water impoundment.

The unsaturated soil mechanics theory (Fredlund & Rahardjo 1993) has found an application in the mechanism of landslide generation triggered by rainfall and reservoir water impoundment. The analysis of stability has revealed the mechanism (Rahardjo et al. 2001; Krahn et al. 1989; Huang & Qi 2002) of the impact of matrix suction on the deformation and stability of landslides; however, the time effect has not been taken into account, so the rheological process of gradual change of the deformation and stability of landslides with time under water action has not been investigated, and the landslide generation time cannot be predicted. The rheological theory of soils has accommodated the time effect (Wang et al. 2004; Han et al. 2001; Yang et al. 2007) of deformation and destruction in the prediction of the deformation and stability of landslides, but the instruments and test methods used in rheological tests all cannot control matrix suction. As a result, the law and mechanism of the impact of water on the rheological property of landslides cannot be studied and evaluated quantitatively, and the rheological model that can reflect water impact cannot be established.

In view of the close correlation of rock and soil mass with water action and the time effect, the authors suggest that the unsaturated creep law of landslide soil mass be studied by controlling matrix suction. This can be facilitated by devising and presenting an apparatus design scheme and entrusting a manufacturer with a trial manufacture of the first domestic unsaturated soil triaxial creep apparatus that can control matrix suction. Unsaturated creep tests of landslide soil mass are conducted, the unsaturated rheological property of landslide soil mass under water action is studied, and the rheological model of unsaturated soils that can reflect matrix suction is established by using the unsaturated soil triaxial creep apparatus that can control matrix suction. Results are obtained by combining the theories of the unsaturated soil mechanics and rheological soil mechanics with experiments taking the typical landslide in the Three Gorges area as the research object.

The study has presented a new theoretical basis for analyzing the long-term strength and deformation of unsaturated soils and predicting the long-term stability of landslides under the action of reservoir water impoundment and rainfall and thus is of much theoretical significance and application value.

Unsaturated Soil Creep Apparatus

Design Concept

The gas in an unsaturated soil mass will generate matrix suction. Matrix suction can be expressed by the difference $(u_a - u_w)$ between pore air pressure and pore water pressure. The matrix suction in unsaturated soils is difficult to measure and control, so the matrix suction in the unsaturated soil triaxial apparatus is used (Fredlund & Rahardjo 1993) by controlling pore air pressure and pore water pressure. The

authors suggest that the principle and technology of controlling matrix suction in the unsaturated soil triaxial apparatus are transplanted in conventional triaxial creep apparatus, i.e., the loading system of the conventional triaxial creep apparatus and the air pressure control system of the unsaturated soil triaxial apparatus are organically integrated into the same test system, so that the unsaturated soil triaxial creep apparatus that can control matrix suction is developed.

The Structure of the Unsaturated Soil Creep Apparatus

Based on the design concept, the first unsaturated soil creep apparatus was made by a Chinese company, which can control matrix suction. The apparatus structure includes (1) confining pressure control system, (2) pore air pressure control system, (3) pore water pressure control system, (4) axial pressure system, (5) pressure chamber, (6) measurement and data acquisition system, and so on (Figs. 10.1 and 10.2). The axial pressure system and confining pressure control system of the unsaturated soil creep apparatus are the same as those of the conventional triaxial creep apparatus, whereas the pore air pressure control system and pore water pressure control system of the unsaturated soil creep apparatus are different from those of the conventional triaxial creep apparatus. The technical principle of the unsaturated soil creep apparatus is as follows: there is a ceramic plate of high air entry value at the test sample bottom, and it enables the water in the test sample to pass but not the air in the test sample, thus achieving the purpose of controlling both pore air pressure and pore water pressure. The technical indexes of the apparatus are the test sample
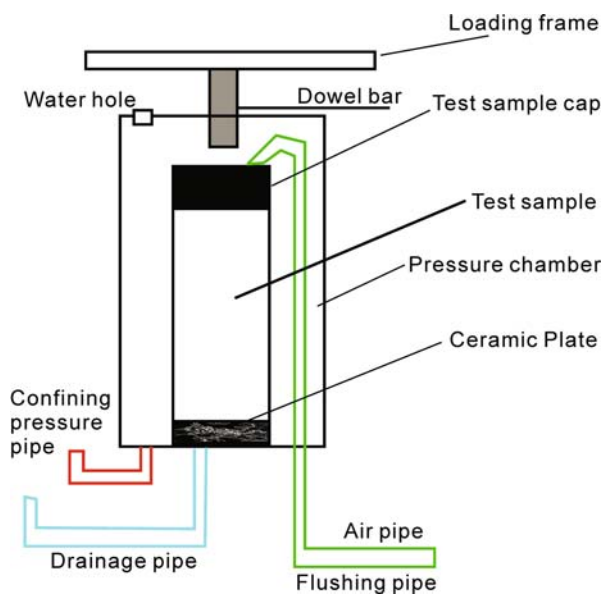
Fig. 10.1 Schematic of unsaturated soil creep apparatus structure

Fig. 10.2 Photograph of unsaturated soil creep apparatus

size $\Phi = 6.18$ cm $\times$ 12.5 cm; the confining pressure $\sigma_3 = 0$–600 kPa; the pore water pressure $u_w = -30$–600 kPa; the pore air pressure $u_a = 0$–600 kPa; the axial force $F = 6$ kN; the axial deformation $\Delta L = 0$–25 mm; the externally measured volume variation of the test sample $\Delta V = 0$–50 cm^3.

Testing Method

The matrix suction needs to be controlled during the whole process of the test, so the unsaturated soil triaxial creep test is much more complex than the conventional soil creep test. Through repeated tests and research, the following test procedure and method are generalized:

(1) Test sample preparation: The preparation method is the same as that for the conventional triaxial creep test.
(2) Saturation of the ceramic plate (conducted before test sample loading):

    (1) Close each valve of the pressure chamber, fill the pressure chamber with air-free water, and open the drainage valve below the ceramic plate until much water flows out of the drainage valve.
    (2) Wash the air bubbles accumulated below the ceramic plate several times repeatedly until there is confirmation of no air bubbles. At this point, saturation of the ceramic plate is completed.

(3) Test sample loading: The loading method is the same as that for the conventional triaxial creep test.
(4) Consolidation test for controlling matrix suction:

    (1) Close the drainage valve, exert 5 kPa confining pressure σ_3 on the pressure chamber, and record corresponding numerical value after test sample deformation and drainage becomes stable.
    (2) Synchronously and slowly exert the overall confining pressure σ_3 and pore air pressure u_a to the predetermined net confining pressure $(\sigma_3 - u_a)$ for drainage and consolidation of the test sample until deformation and water discharge reach the stability criterion. The stability criterion: the volume

variation is no more than 0.01 cm^3 within consecutive 2 h, and the duration is no less than 48 h. When consolidation is completed, the pore water pressure u_w is in proximity to zero and the matrix suction $(u_a - u_w)$ is equal to the pore air pressure u_a.

(3) The ceramic plate bottom surface is washed once every 8–10 h during the consolidation test to remove air bubbles and to eliminate the impact of air bubbles on consolidation drainage effects.

(5) Triaxial shear creep test (staged loading method) for controlling matrix suction and net confining pressure:

   (1) Calculation of the staged load increment: Calculate the peak strength τ_f based on the unsaturated soil strength formula. Loads are applied for the creep test in n stages, and then $1/n$ of the peak strength is set as the increment of the load of each stage, i.e., $\Delta F = \tau_f / n$.

   (2) Successively exert shear loads for shearing as per ΔF, $2\Delta F$, and $3\Delta F$. The creep stability criterion under the shear load action of each stage: the total amount of deformation is less than 0.005 mm within $1d$ continuously or continuous observation of 30–60 h is performed during constant speed flowing.

   (3) The ceramic plate bottom is washed to remove air bubbles once every 8–10 h during shearing.

   (4) After completing the test, save data; remove the test sample; measure the water content in the upper, lower, and middle parts; clean the ceramic plate surface using air-free water; and saturate the ceramic plate again for use in the next test.

Some Important Items That Need Attention

(1) The overall confining pressure σ_3 shall be kept to exceed the air pressure u_a in the whole process of exerting the overall confining pressure σ_3 and pore air pressure u_a to prevent the overall confining pressure σ_3 from being less than the air pressure u_a and thus causing expansion of soil samples and bulging and even destruction of outer layer rubber membrane of soil samples.

(2) During back-pressure saturation of the ceramic plate or soil samples, the exerted back pressure cannot be overly high (the difference between the back pressure and the air pressure is no more than 50 kPa in general) to prevent the ceramic plate from being jacked up or damaged because the pressure in the lower part is higher than that in the upper part.

(3) The discharge pipeline at the bottom of the pressure chamber shall be washed periodically (e.g., every 8 h) and frequently in the whole process of the test. During the unsaturated test and test sample drainage, part gas will be mixed with water and discharged out of the ceramic plate at the test sample bottom and enter the discharge pipeline at the bottom; when the gas in the discharge pipeline is increased, water discharge from the test sample will be affected, and thus the test sample consolidation effect will be affected.

Unsaturated Creep Test of Slip Soils in the Qianjiangping Landslide

Test Soil Samples

The Qianjiangping landslide is located at Qianjiangping Village on the left bank of the Qinggan-he River, a branch of the Yangtze River, Zigui County, Hubei Province, in Three Gorges area. The Qianjiangping landslide is a large bedrock landslide formed in the Three Gorges area shortly after the Three Gorges Reservoir water level was raised to 135 m, with a total volume of approximately 2400×10^4 m^3. The test soil samples are collected from the slip soils in the Qianjiangping landslide and pass through a sieve of 2 mm in diameter to make remolded test samples. The physical property indexes and strength parameters from lab tests are presented in Table 10.1.

Table 10.1 Conventional physical and mechanical property indexes of slip soils in the Qianjiangping landslide

Water content (%)	Volume weight (kN/m^3)	Specific gravity	Liquid limit (%)	Plastic limit (%)	Plastic limit index (%)	Cohesive force (kPa)	Internal friction angle (°)	Internal friction angle of unsaturated soil (°)
18.9	21.1	2.65	34.7	16.4	15.8	9.335	18.2	15

Unsaturated Soil Shear Creep Loading Test

The loading mode uses the loading method, i.e., a creep shear test for a new test sample is conducted again for the load of the next stage after shear creep stabilization or damage occurs under the action of the load of each stage. The consolidation drainage shear creep test method is used.

The test scheme is as follows: the unsaturated soil creep test where different matrix suctions are exerted respectively under the condition of fixed net confining pressure and fixed shear stress level. The loading scheme is as follows: the net confining pressure $\sigma_3' = (\sigma_3 - \sigma_a) = 100$ kPa; the shear stress level $D_r = (\sigma_1 - \sigma_3)/(\sigma_1 - \sigma_3)f = 0.5$; the matrix suction is exerted sequentially as per $u_a = 100, 150, 200,$ and 300 kPa.

The main failure stress σ_{1f} can be calculated as follows based on Fredlund's unsaturated soil strength theory:

$$\sigma_{1f} = \left[(\sigma_3 - u_a) + 2c \frac{\cos \phi'}{1 + \sin \phi'} \right] \frac{1 + \sin \phi'}{1 - \sin \phi'} + u_a$$

Table 10.2   Unsaturated soil creep test loading scheme

Net confining pressure $\sigma_3^{\prime}$ (kPa)	Matrix suction u_a (kPa)	$(\sigma_1 - \sigma_3)_f$ (kPa)	$0.5\,(\sigma_1 - \sigma_3)_f$ (kPa)
$\sigma_3^{\prime} = 100$ kPa	100	315.30	157.65
	150	347.33	173.66
	200	386.35	193.17
	300	456.445	228.22

where $c = c' + (u_a - u_w)\tan \phi^b$; c' and ϕ' are the effective cohesive force and effective internal friction angle of slip soils, respectively; and ϕ^b is the internal friction angle of the unsaturated soil related to matrix suction. See Table 10.2 for loading details.

Test Procedure

(1) Test sample preparation: Prepare a remolded test sample as per the water content and density corresponding with the consolidation pressure level of 25 kPa.

(2) Consolidation: The test sample is consolidated in the triaxial creep apparatus using the staged loading mode, and the loading ratio is set at 1, i.e., net confining pressure is exerted sequentially as per 25, 50, and 100 kPa for saturated consolidation. The confining pressure of the next stage is exerted after consolidation stabilization of the confining pressure of each stage; after consolidation is completed under the confining pressure of 100 kPa, and the matrix suction of the first stage can be exerted. Exert air pressure and the confining pressure increment based on the exerted matrix suction.

(3) Exert deviatoric stress: The once-through loading method is used to exert deviatoric stress, i.e., the counterweight equivalent to $0.5\,(\sigma_1 - \sigma_3)_f$ is exerted on the test sample at a time.

(4) Observation of deformation and pore water pressure: The sampling intervals can be adjusted in the stage of exerting deviator stress with lasting time, i.e., the sampling interval is 5 s within 1 min; 30 s within 1–10 min; 5 min within 10 min–1 h; 60 min within 1–24 h; 4 h after 24 h. The total duration of creep observation is 7–15 days.

(5) Repeat steps (1)–(4) for the creep test of matrix suction of the next stage until completion of all planned tests.

Creep Test Result

The creep curves (Fig. 10.3) and isochronous curves (Fig. 10.4) of the unsaturated creep test of slip soils in the Qianjiangping landslide are plotted based on the original creep test data.
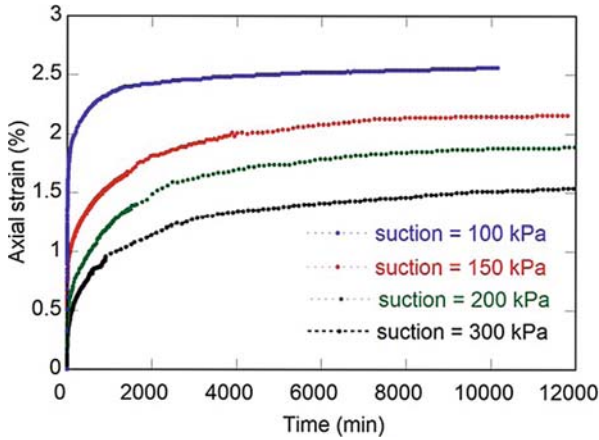
Fig. 10.3 Unsaturated soil creep curves under the condition of 100 kPa net confining pressure and the stress level of 0.5
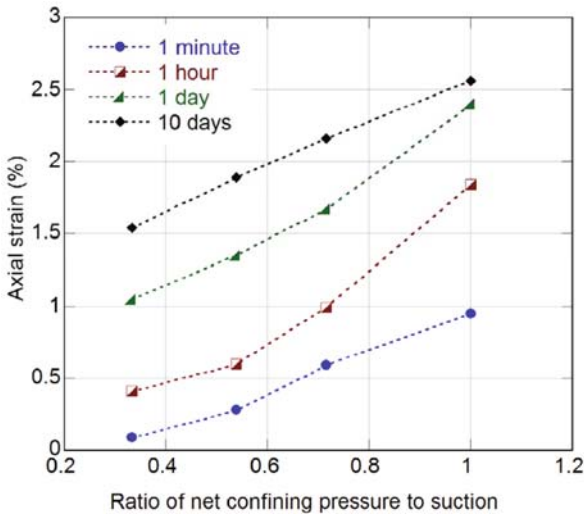
Fig. 10.4 Unsaturated creep isochronous curves of slip soils in the Qianjiangping landslide

Unsaturated Creep Modeling of Slip Soils in the Qianjiangping Landslide

Modeling Concept

Based on the unsaturated creep test result (Figs. 10.3 and 10.4 in the section "Creep Test Result") of slip soils in the Qianjiangping landslide, such creep law has been obtained as follows: (1) creep strain is increased with time increase and decreased

with matrix suction increase; (2) creep strain shall be increased with increase in the ratio of the net confining pressure to matrix suction under the condition of fixed creep time. It can be known from this that creep strain shall be of functional relation with the three variables such as time, stress, and matrix suction, and thus the model can be presented as in the following expression:

$$\varepsilon = f_1(t) f_2 \left(\frac{\sigma_3'}{u_a} D_r \right) \tag{10.1}$$

where $f_1(t)$ is time function and $f_2 \left(\frac{\sigma_3'}{u_a} D_r \right)$ is stress function. The specific expression of $f_1(t)$ and $f_2 \left(\frac{\sigma_3'}{u_a} D_r \right)$ in the unsaturated creep model of slip soils in the Qianjiangping landslide is derived as follows based on the analysis and processing of the test data.

Creep Strain–Time Relation

Based on the original data of creep test, take the logarithm of creep strain and time t and plot the creep strain–time double logarithmic curve, as shown in Fig. 10.5. It can be seen that the double logarithmic relation of creep strain with time is approximate to linear relation. It can be seen from this that the creep strain–time relation function can be expressed in the following power function: $f_1(t) = (\frac{t}{t_r})^n$.

It can also be found from Fig. 10.5 that the straight slope n of the double logarithmic relation of creep strain with time is decreased with suction increase, and then the points of the slope with the ratio (σ_3'/u_a) of the net confining pressure to matrix suction are plotted in Fig. 10.6. It can be found that the relation of the slope with the ratio is also approximate to linear relation and can be expressed as follows: $n = k \frac{\sigma_3'}{u_a} + C$.
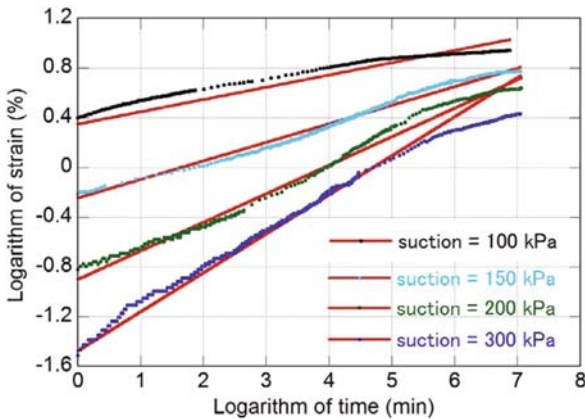
Fig. 10.5   The net confining pressure is 100 kPa and the stress level is 0.5. From the strain–time double logarithmic curve, it can be known that strain is of a power exponent relation with time
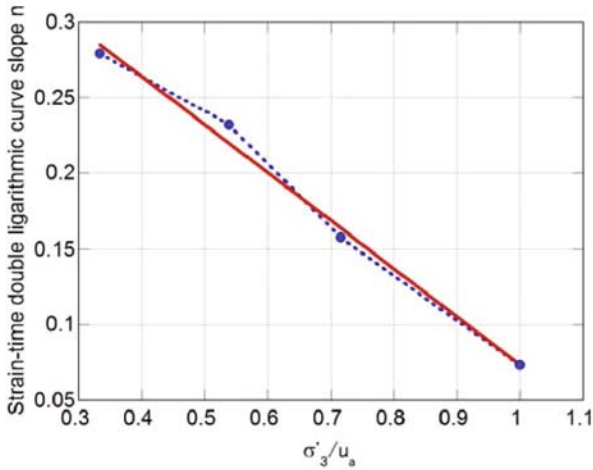
Fig. 10.6 The relation curve of the slope n with (σ'_3/u_a) in the strain–time double logarithmic curve

Then the functional relation of creep strain with time expressed in power function is obtained as follows:

$$f_1(t) = \left(\frac{t}{t_r}\right)^{k\frac{\sigma'_3}{u_a}+C} \tag{10.2}$$

Where t_r is reference time, and here $t_r = 10$ min is used as the reference time (because it is found that the linear relation of $\ln \varepsilon - \ln t$ is insufficiently ideal when t_r is set at 1 min).

Creep Strain–Stress Relation

The stress level D_r in the test scheme is a fixed value; therefore, only the functional relation of creep stain with matrix suction is analyzed here. It can be seen from Fig. 10.5 that the intercept R of the $\ln \varepsilon - \ln t$ straight line is decreased with matrix suction increase, and the points of the intercept R with the ratio (σ'_3/u_a) of the net confining pressure to matrix suction are plotted in Fig. 10.7. It can be found that the relation of the intercept R with the ratio is also approximate to linear relation and can be expressed as follows:

$$R = \alpha D_r \frac{\sigma'_3}{u_a} + d \tag{10.3}$$

where α and d are parameters.
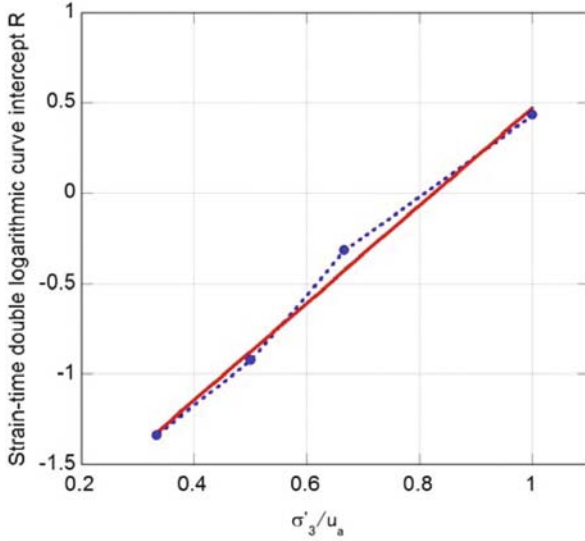
Fig. 10.7   The relation curve of the intercept R with $D_r \sigma'_3 / u_a$ in strain–time double logarithmic curve

Creep Strain–Time–Stress Relation

The double logarithmic straight line of creep strain with time in Fig. 10.5 is expressed in the following equation:

$$\ln \varepsilon = R + n \ \ln \left(\frac{t}{t_r} \right) \tag{10.4}$$

where $R = \alpha D_r \frac{\sigma'_3}{u_a} + d$ is the intercept of the straight line and $n = k \frac{\sigma'_3}{u_a} + C$ is its slope. Set $d = \ln B_r$ and substitute R, n, and D in Eq. (10.4) to obtain

$$\ln \varepsilon = \ln B_r + \alpha D_r \frac{\sigma'_3}{u_a} + n \ln \left(\frac{t}{t_r} \right). \tag{10.5}$$

Convert Eq. (10.5) to obtain the following creep model equation:

$$\varepsilon = B_r \exp \left(\alpha \frac{\sigma'_3}{u_a} D_r \right) \left(\frac{t}{t_r} \right)^n \tag{10.6}$$

where B_r, α, and n are model parameters; D_r is shear stress level; and t_r is reference time and is set at 10 min here.

Determination of the Model Parameters

First, the slope n and intercept R of the straight line are calculated based on the double logarithmic straight line $\ln \varepsilon - \ln t$ (Fig. 10.5) of creep strain with time; then the relational straight lines of the slope n with σ_3'/u_a (Fig. 10.6) and the intercept R with $\sigma_3'/u_a D_r$ (Fig. 10.7) are plotted. The model parameters k and C are calculated based on the slope and intercept of the straight line in Fig. 10.6, and further the parameter n is calculated. The parameters α and d are calculated from the slope and intercept of the straight line in Fig. 10.7, and further B_r is calculated from d. All parameters such as B_r, α, and n in the model thus can be obtained. The unsaturated creep model parameters of slip soils in the Qianjiangping landslide that are obtained from this test are presented in Table 10.3. Substitute the model parameters in Table 10.3 in Eq. (10.6) and then obtain the specific expression of the unsaturated creep model equation of slip soils in the Qianjiangping landslide as follows:

$$\varepsilon = 0.0051 \exp\left(2.7582 \frac{\sigma_3'}{u_a} D_r\right) \left(\frac{t}{10}\right)^{-0.3141 \frac{\sigma_3'}{u_a} + 0.3816}. \tag{10.7}$$

The symbols in Eq. (10.7) are the same as those in Eq. (10.6).

Table 10.3 Unsaturated soil model equation parameters (net confining pressure of 100 kPa, shear stress level of 0.5) in Qianjiangping landslide

Matrix suction (kPa)	B_r	α	K	C
100	0.0051	2.7582	−0.3141	0.3816
150				
200				
300				

Model Verification

Substitute the exerted confining pressure $= 100$ kPa, shear stress level $= 0.5$, matrix suction $u_a = 100, 150, 200,$ and 300 kPa, , , and in creep model equation (10.7), respectively. The creep curves obtained from the creep model equation and the creep data acquired from the test are jointly plotted in Fig. 10.8 for comparison. It can be known from the comparison that the tendency of the creep curves obtained from the creep model equation is basically consistent with that of the creep data acquired from the test, indicating that the creep model can better reflect the unsaturated creep characteristics of slip soils in the Qianjiangping landslide. However, it can also be found that the creep mode is a good fit with the test curves in the initial stages of the curves, whereas as time increases, the model curves are somewhat deviated from the test curves, indicating the model curves are raised when compared with the test curves. This indicates that the unsaturated soil creep model established in this chapter can simulate only the unsaturated creep characteristics of slip soils in
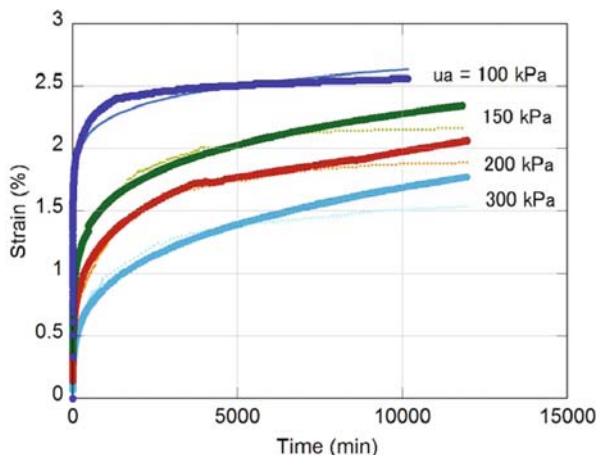
Fig. 10.8 Comparison between test curve and calculated curve of creep test of non-saturated soil of Qianjiangping slide (Note: the *straight line* is the test curve, and the *bold line* is the creep model curve.)

the Qianjiangping landslide in the early stages of creep, and if the desire is to simulate all creep characteristics of unsaturated soils, the creep model must be further improved and perfected.

Conclusions

The test and theoretical investigation of unsaturated creep characteristics of slip soils have been conducted, as presented in this chapter based on the modern unsaturated soil mechanics and test method and basic theory on the conventional soil creep mechanics. The unsaturated soil creep triaxial apparatus that can control matrix suction has been developed. Unsaturated soil creep tests of slip soils in the Qianjiangping landslide have been conducted using the apparatus. The test result reflects the law of the increase of the unsaturated soil creep amount with matrix suction decrease, thus revealing the internal mechanism that rainfall or reservoir water level rise may result in an increase in landslide creep deformation and even destabilization. Through data processing and development of the equation, the unsaturated soil creep model equation that can reflect the impact of matrix suction has been established. The comparison of the model curves with the test curves indicates that the established creep model equation can better simulate the unsaturated soil creep characteristics. The research findings of this chapter are of certain new conception in both test method and theory. The research findings have presented a new theoretical basis for analyzing the long-term strength and deformation of unsaturated soils and predicting the long-term stability of landslides under the action of reservoir water impoundment and rainfall and thus are of much theoretical significance and application value.

Both test apparatus and operation methods for the unsaturated soil creep test are more complex than those for the conventional creep test, and the period of the unsaturated soil creep test is longer than that of the conventional creep test; therefore, the test data acquired in this chapter are very limited. The unsaturated soil creep model established on the basis of the limited test data still requires more tests for verification and consecutive improvement, so that it tends to be more perfect and applicable.

References

Fredlund DG, Rahardjo H (1993) Soil Mechanics for Unsaturated Soils. Wiley-IEEE, 517 pp

Han AG, Nie DX, Ren GM, Han KL (2001) Research on shear rheological property of slip soils in large landslides. Journal of Engineering Geology 9(4): 345–348

Huang RQ, Qi GQ (2002) The effect of unsaturated percolation matrix suction on side slope stability. Journal of Engineering Geology 10(4): 343–348

Krahn J, Fredlund DG, Klassen MJ (1989) Effects of soil suction on slope stability at North Hill. Canadian Geotechnical Journal 26: 269–278

Rahardjo H, Li XW, Toll DG, Leong EC (2001) The effect of antecedent rainfall on slope stability. Geotechnical and Geological Engineering 19(3):371–399

Riemer W (1992) Landslide and reservoir (keynote paper). In: Proceedings of the 6th International Symposium on Landslides, Christchurch, pp. 1373–2004

Wang C, Liu HW, Xu Q (2004) Improved Mesri creep model of slip soils in Xietan Landslide in Three Gorges area. Journal of Southwest Jiaotong University 39(1): 15–19

Yang CH, Wang YY, Li JG (2007a) Experimental investigation of the effect of water ratio on rock creep law. Journal of China Coal Society 32(7): 695–699

Yang WM, Xu RC, Wu SR et al. (2007b) Creep Deformation and Stability of Maoping Landslide of Geheyan Reservoir of the Qingjiang River in Western Hubei Province. Geological Bulletin 26(3): 313–320

Chapter 11
Monitoring on Shuping Landslide in the Three Gorges Dam Reservoir, China

Fawu Wang, Yeming Zhang, Zhitao Huo, and Xuanming Peng

Abstract   The Shuping landslide was reactivated by the initial impoundment of the Three Gorges Dam Reservoir, China, in June 2003. For the purposes of landslide disaster mitigation in the reservoir area and identification of landslide movement and deformation caused by reservoir level changes, a monitoring system mainly consisting of drum-style extensometers was installed in the eastern part of the Shuping landslide. Systematical monitoring was started in August 2004 with installation of 13 extensometers above the waterline after the initial impoundment. In August 2006, 11 more drum-style extensometers were installed above the high waterline (175 m), and 5 flexible extensometers were installed along a longitudinal section in the elongation to low waterline. In August 2007, three more drum-style extensometers were installed to make the whole monitoring line connected. In this chapter, the monitoring results from August 2004 to May 2008 are presented, and the deforming of the Shuping landslide caused by both reservoir level changes and rainfall is examined.

Keywords   Landslide · Monitoring · Displacement · Reservoir level change · Rainfall

Introduction

The Three Gorges Dam in China is the largest hydropower project in the world. The dam site is located near Maoping town, Zigui County, Hubei Province (Fig. 11.1). The main body of the dam, which is 181 m high and 2,310 m long, was finished by the end of 2006, and the reservoir level will reach a maximum of 175 m in 2009, allowing for full electric power capacity.

When the dam was partially completed, water impoundment was started in the reservoir to produce power and control flooding downstream. The first

———————————————

F. Wang (✉)
Research Centre on Landslides, Disaster Prevention Research Institute, Kyoto University
Gokasho, Uji, Kyoto 611-0011, Japan
e-mail: wangfw@landslide.dpri.kyoto-u.ac.jp
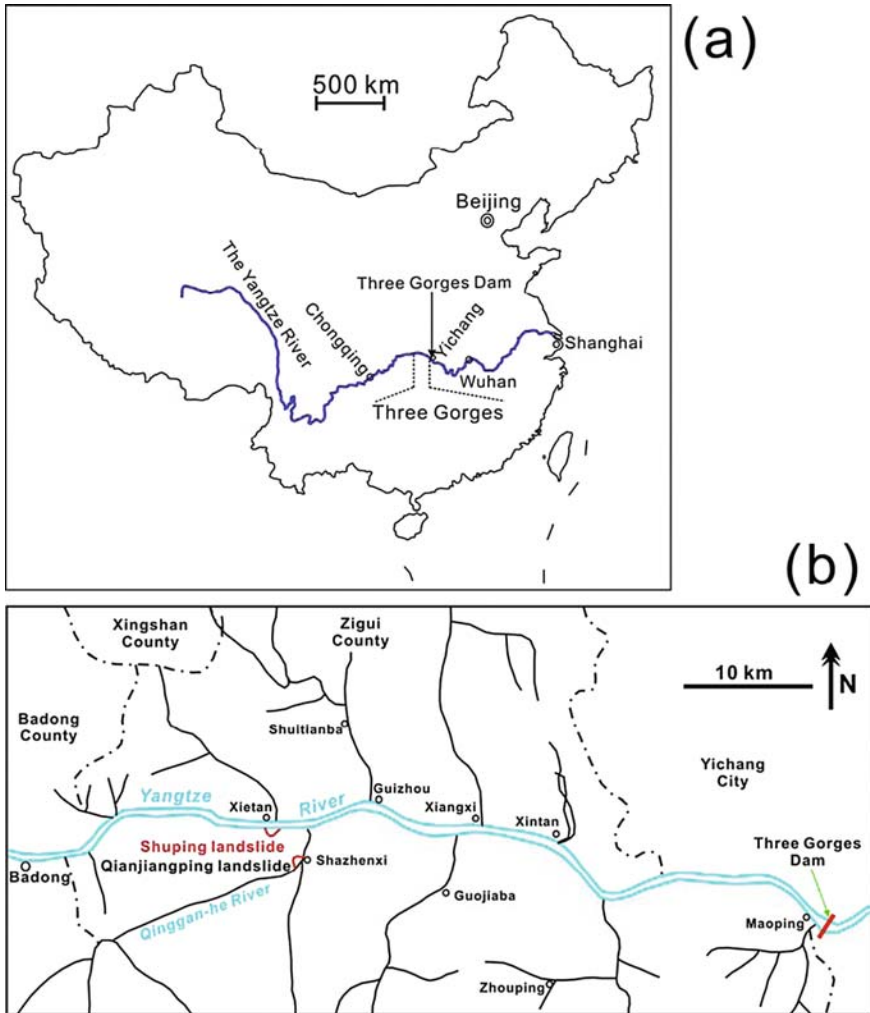
Fig. 11.1 Location map of the Three Gorges Dam and the Shuping landslide in China

impoundment was achieved on June 1, 2003. In 15 days, the reservoir level was increased from 95 to 135 m. Coincident with the impoundment, landslides occurred along the edge of the reservoir. Some of the landslides moved for long distances. In addition, some ancient landslides were reactivated and are currently causing ground deformation. One landslide in the Qianjiangping area of Shazhenxi town (Fig. 11.1b) moved rapidly and killed 24 people. Eleven people were killed directly by the sliding mass, and another 13 people were killed by landslide-induced seiches in the Qinggan-he River, a tributary of the Yangtze River (Wang et al. 2004, 2007). In the Shuping area, which is along the south bank of the Yangtze River, just 3 km from the Qianjiangping landslide, a large ancient landslide was reactivated during

the first impoundment and caused ground deformation as the reservoir level changed (Wang et al. 2008).

In this chapter, we discuss the movement and deformation of the Shuping landslide, based mostly on the results of extensometer measurements since 2004.

Description of the Shuping Landslide

The Shuping landslide is located on the right bank of the Yangtze River, about 3 km northwest of Shazhenxi town, Zigui County, Hubei Province. The landslide is about 60 km upstream of the Three Gorges Dam site (Fig. 11.1b). Preconstruction landslide investigations for the purpose of the Three Gorges Dam identified the Shuping landslide as an ancient slide (Chen et al. 1997). The landslide area is underlain by sandy mudstone and muddy sandstone of the Triassic Badong formation (T_2b). In the Three Gorges area, many landslides occurred in this unit (Wen et al. 2004). Figure 11.2 is a photograph of the Shuping landslide, taken from the opposite bank of the Yangtze River. The landslide extends into the Yangtze River and a valley divides the landslide into two blocks designated as eastern Block-1 and western Block-2.

Figure 11.3 is the plan of the Shuping landslide, which lies between elevation 65 and 400 m with a width of about 650 m. Boreholes indicate that the landslide is between 40 and 70 m thick, and the landslide volume is about 20 million m^3. The average slope of the landslide ranges from 22° in the upper part to 35° in the lower part.

According to the local inhabitants, cracks appeared in the roads and houses on the slope as soon as the first impoundment was finished on June 15, 2003. Figure 11.4 shows a crack at the right boundary of Block-1 in an outcrop on a local road. Red, clay-rich landslide debris on the right side of the photograph is displaced against gray sandy mudstone and muddy siltstone of Triassic Badong formation (T_2b).

Fig. 11.2 A photograph of the Shuping landslide facing the main stream of the Yangtze River (taken from the opposite bank, facing south)
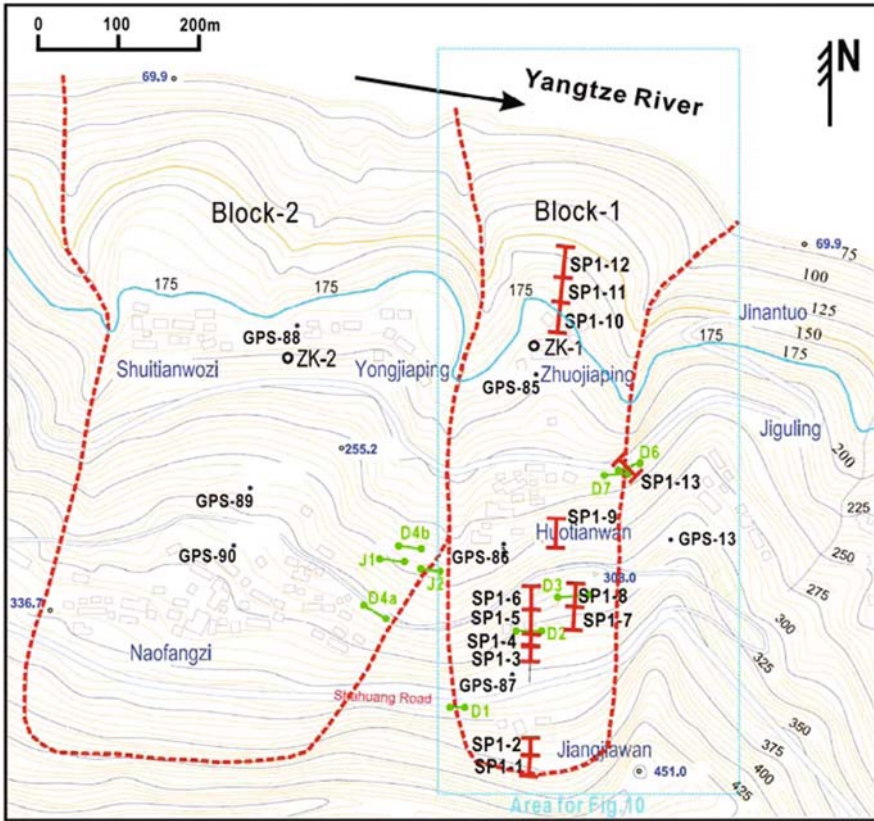
Fig. 11.3 Plan of the Shuping landslide (the locations of the extensometers shown in this map are those installed in 2004)

The reservoir level was kept nearly constant at 135 m for a long period after the first impoundment. Muddy water was observed coming out of the toe of Block-1 on January 5, 2004, and again on February 8, 2004. Since March 2004, the water near the toe has remained muddy. Figure 11.5 shows the muddy water at the toe in April 2004. The muddy water may be due to groundwater flow along the active slide surface. On the nights of January 25, 2004, and February 8, 2004, local inhabitants reported loud noises from the deep within the slope.

Figure 11.6 shows the cracks along the Shahuang Road in the upper part of the slide in July 2007. The road was paved in April 2007. The cracks reached about 10 cm in width in 3 months.

To monitor the movement of the Shuping landslide, the Chinese Ministry of Land and Resource installed six Global Positioning System (GPS) stations along the longitudinal axis of Block-1 and Block-2 (GPS-85 to GPS-90 in Fig. 11.3) and surveyed monthly. Figure 11.7 shows the first 6 months of movement data after the installation. In Block-1, more displacement occurred at the toe (GPS-85) and in the middle
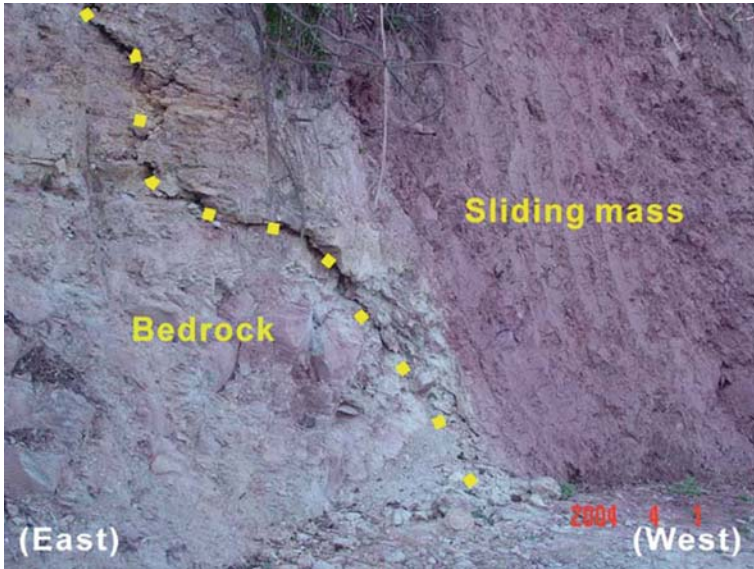
Fig. 11.4 Crack at the right boundary of Block-1 outcropped at a local roadside
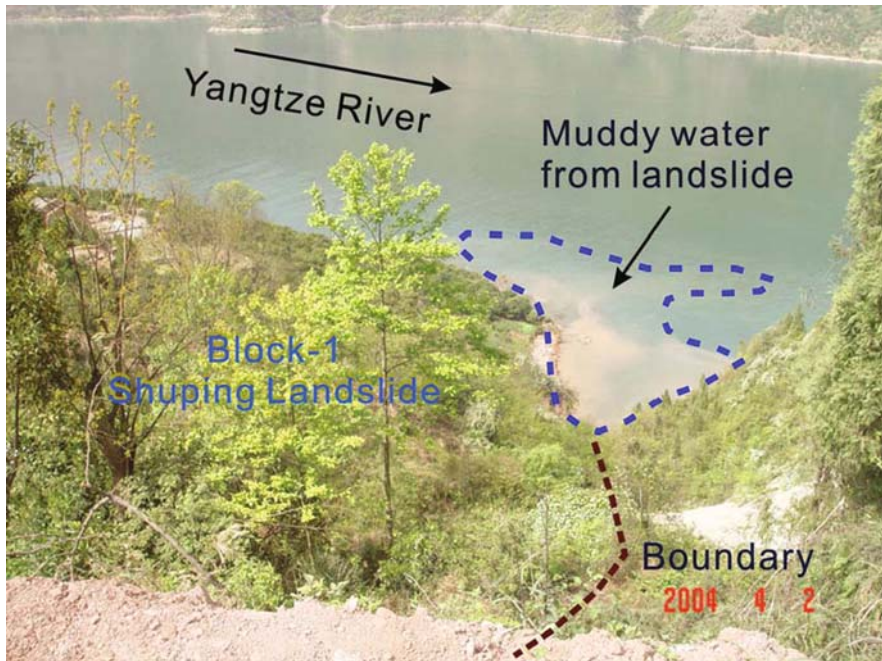
Fig. 11.5 The phenomenon of muddy water coming from Block-1 of the landslide (photo taken on April 2, 2004)
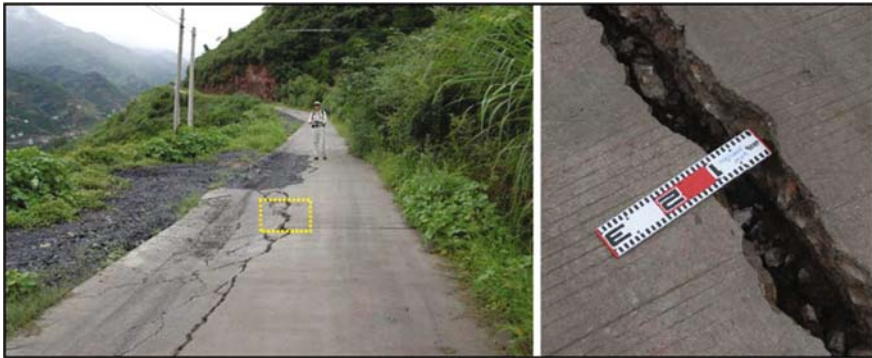
Fig. 11.6 Failure situation of the Shuping landslide at the Shahuang Road (photos taken on July 13, 2007)

of the slide (GPS-86) than in the upper part (GPS-87). In Block-2, more displacement occurred in the toe (GPS-88) than in the upslope parts of the slide (GPS-89 and GPS-90).

In China, local inhabitants are trained to recognize landslide deformation and report it to local officials. The local government may then have appropriate experts conduct detailed investigations. In the Shuping area, the inhabitants were requested to measure cracks three times per day. Figure 11.8 shows the crack monitoring
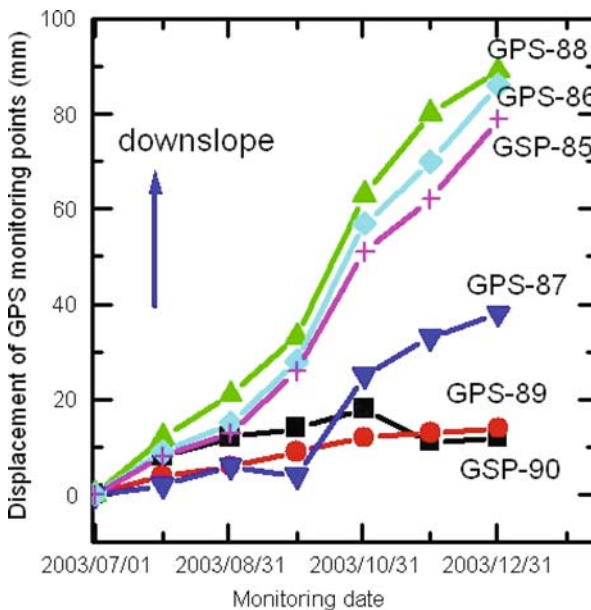
Fig. 11.7 GPS monitoring results on the Shuping landslide by Chinese Ministry of Land and Resource (measured by Geo-Hazard Mitigation Research Institute, China Three Gorges University)
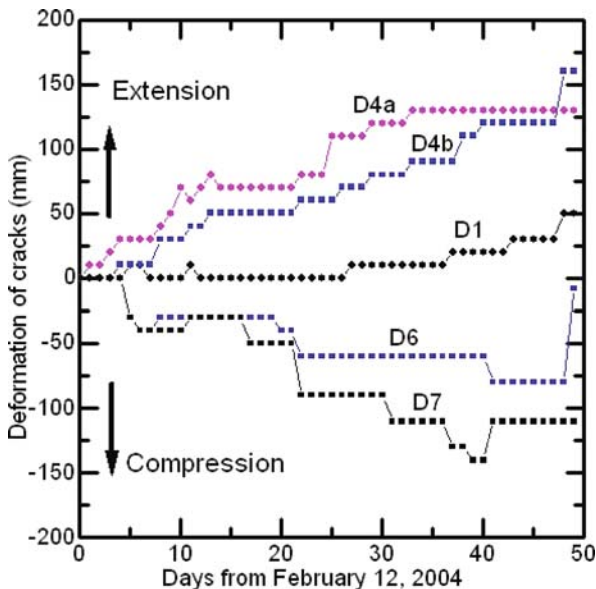
Fig. 11.8 Crack monitoring results on the Shuping landslide by the local residents (Zhang et al. 2004)

results for 50 days in early 2004. A maximum of 150 mm of both stretching and shortening occurred during the monitoring period (Zhang et al. 2004).

Based on the data, evacuation instructions were issued to the 163 families, a total of 580 people, to move out of the slide area. By May 2004, the relocation of the inhabitants of the Shuping landslide to other stable areas was finished.

Landslide Geometry

Estimation of the landslide geometry is critical to risk analysis. To determine the depth of the sliding surface (surface of rupture), a borehole was drilled in the lower part of Block-1 at ZK-1 (see Fig. 11.3 for the location) in December 2004. In the borehole, the groundwater table was about 8.8 m deep, and the surface of the rupture zone, which consisted of silty clay with gravel, was at a depth between 66.7 and 75.9 m. Slickensides were numerous in the zone (Wang et al. 2005).

Extensometers Monitoring Results

Part 1: August 2004–July 2006

In April 2004, we installed the first two drum-style extensometers in the Shuping landslide across two ground cracks, one at the east boundary crossing the crack

shown in Fig. 11.4 and the other in the centerline of Block-1. Zhang et al. (2004) summarized the results of the initial movement monitoring.

In August 2004, 11 additional extensometers were installed nearly along the centerline of Block-1 (the locations are shown in Fig. 11.3). Extensometers SP1-1 and SP1-2 were installed near the main scarp of the landslide. Extensometers SP1-3 through SP1-9 were installed between the Shahuang Road and a local agriculture road (Fig. 11.3). One of these, SP1-5, crossed a continuous crack. Extensometers SP1-10 through SP1-12 were installed near the toe and the Yangtze River. Extensometers SP1-13 was located along the east boundary of Block-1. In addition, warning alarms were connected to extensometers SP1-5 and SP1-13. The alarms were set to a trigger when the displacement rate exceeds 2 mm/h. The maximum measurable displacement of each extensometer is 500 mm. To measure both stretching and shortening, the target of the extensometer was adjusted to the middle of the drum. The extensometer and standing pile were connected by a super invar line that was protected by a vinyl pipe. The measurements were recorded on both paper and a flash memory card. Data collection was conducted once a month, and at each time, the target was adjusted in order to ensure successful monitoring during the following month.

Figure 11.9 shows the monitoring results from the extensometers for the 2 years between August 2004 and July 2006. Rainfall near the landslide and the water level in the Three Gorges Reservoir (measured upstream of the dam by the China Yangtze River Three Gorges Project Development Company) are also shown. No stretching was detected across the main scarp of the landslide (SP1-1 and
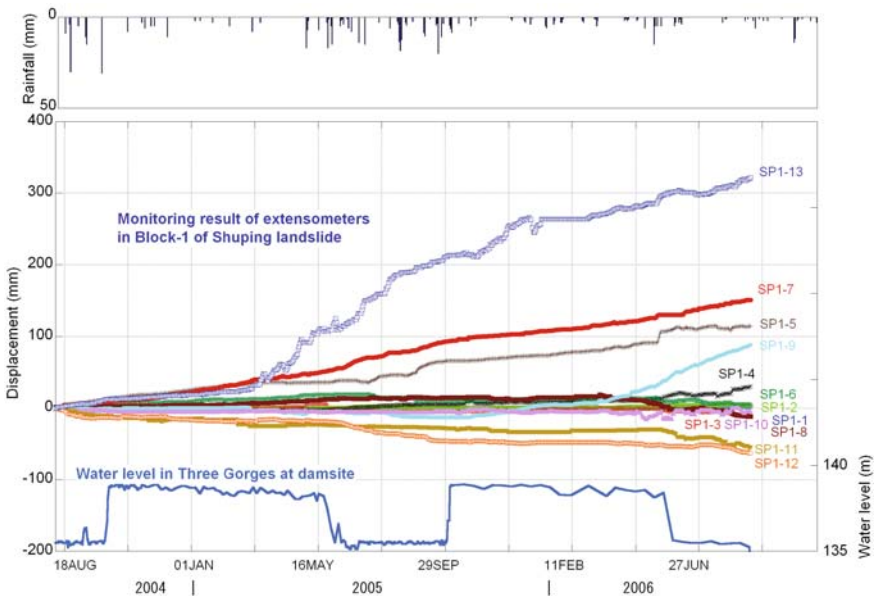
Fig. 11.9 Monitoring results with the drum extensometers for the period from August 2004 to August 2006 in Block-1 of the Shuping landslide. Rainfall for the period and the water level in the Three Gorges Reservoir are also shown

SP1-2), but stretching occurred in the middle of the slide (SP1-5, SP1-7, SP1-9, and SP1-13), and shortening occurred near the toe (SP1-11 and SP1-12). The monitored results correspond to observed ground deformation, including ground cracks, at least qualitatively. Deformation (and landslide movement) occurred synchronously with water-level fluctuations in the reservoir. Notably, the landslide was active when the reservoir level decreases. Locally, such as at SP1-5, the rate of movement increased during the period of rainfall (in the wet season). Thus, movement of the Shuping landslide appears to occur in response to both reservoir level changes and rainfall.

Part 2: August 2006–July 2007

In July and August 2006, an additional 11 extensometers were added to the monitoring system. As a result, a total of 22 extensometers were located in a nearly continuous line along the centerline of Block-1 above 220 m in elevation. In addition, two extensometers were located along the east boundary of the slide. However, our inability to place extensometers across the Shahuang Road and the local agriculture road resulted in two gaps in the monitoring line (Fig. 11.10). In the area near the high waterline, five flexible extensometers consisting of stiff carbon fiber rods connected to an extensometer transducer were installed to monitor the displacement (Fig. 11.11).

Figure 11.12 shows the monitoring results of the drum extensometers installed along the centerline and the east boundary of Block-1, changes in the reservoir level, and the daily rainfall at Xietan town (see Fig. 11.1b for location) measured by Zigui County Meteorological Observatory, Hubei Provincial Meteorological Bureau. Xietan is a small town on the opposite bank across from the Shuping landslide. Because the rainfall gauge is only about 1 km from the Shuping landslide, the data provide a reasonable estimate of the rainfall at the slide.

In Fig. 11.12a, the monitoring results from areas with the greatest deformation (stretching or shortening) are shown. The most stretching (about 240 mm) occurred at three extensometers, i.e., extensometer SP1-N-5 in the upper part of the slide and the two extensometers (SP1-N-23 and SP1-N-24) along the east boundary. At extensometer SP1-N-7 in the upper part of the slide a period of stretching was followed by a period of shortening. About 85 and 60 mm of shortening occurred at extensometers SP1-N-15 and SP1-N-11, respectively.

The remainder of the extensometers recorded smaller deformations (Fig. 11.12b, c, and d). In general, shortening deformation was more common than stretching in the upper half of the landslide. Continuous stretching was recorded at only three extensometers (SP1-N-4, SP1-N-12, and SP1-N-19) (Fig. 11.12b, c, and d), whereas shortening was recorded at most of the other extensometers.

Most of the movement occurred during a period when the water level in the Three Gorges Reservoir is lowered to prevent flooding in the wet (monsoon) season in the region. We speculate that the movement occurred as a result of the increased precipitation during the wet season, but the effect of the declining reservoir level on landslide stability requires additional consideration. Our monitoring results suggest

Fig. 11.10 Location of the extensometers installed in August 2006 in Block-1 of the Shuping landslide (the area of this figure is shown in Fig. 11.3)
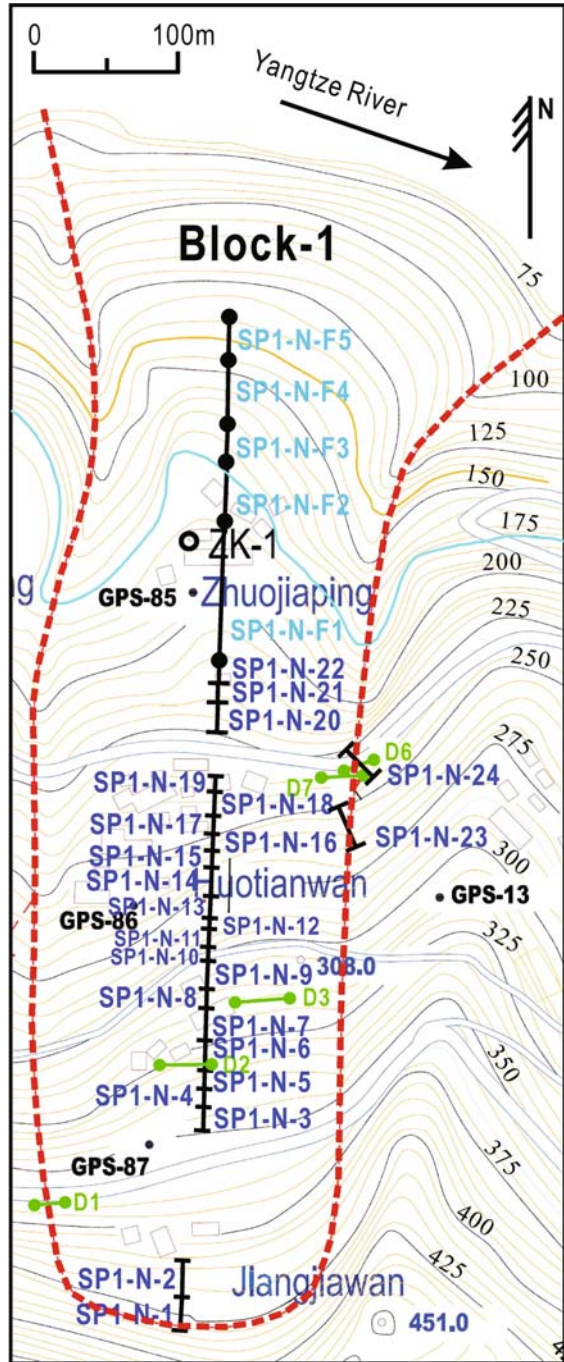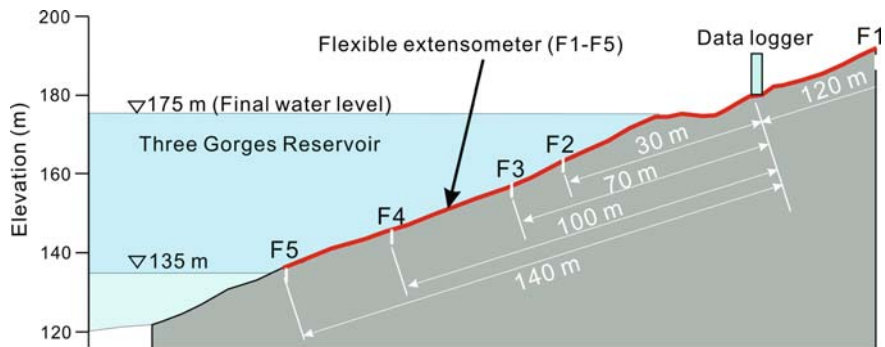
Fig. 11.11 Schematic showing the installation concept of flexible extensometers in the area affected by the changing water level at the toe part of the Shuping landslide, Block-1

that landslide stability is not increased during the period of lower reservoir levels, which has significant implications for landslide disaster mitigation.

Figure 11.13 shows that some of the deformation in the lowermost part of the landslide below the high waterlines coincides with the impoundment in October 2006. Additional deformation occurred during a period of gradually declining reservoir level, which began in February 2007 during the wet season.

Part 3: August 2007–May 2007

In August 2007, with three additional extensometers, a continuous monitoring system passing Shahuang Road and the local road was completed. During this work, maintenance and adjustment of the drum-style extensometers were conducted. The positions of some extensometers were changed to cross obvious cracks and make the monitoring system better. Figure 11.14 shows the modified extensometer line. As a result, a total of 24 extensometers were located in the line along the centerline of Block-1 above 220 m in elevation. In addition, two extensometers (M-25 and M-26) were located along the east boundary of the slide. The five flexible extensometers were kept in the area near the high waterline.

Figure 11.15 shows the monitoring result from August 2007 to May 2008. It is shown that the displacement of the Shuping landslide became active (1) when water level increased rapidly from 145 to 156 m in October 2007; (2) during the rainfall period around April. Also, the whole tendency is that the displacement gradually accumulated when the water level decreased from 156 to 148 m.

Longitudinal Deformation Model

Based on the monitoring results and field observations, we developed longitudinal deformation models of the Shuping landslide. Figure 11.16 shows the slope
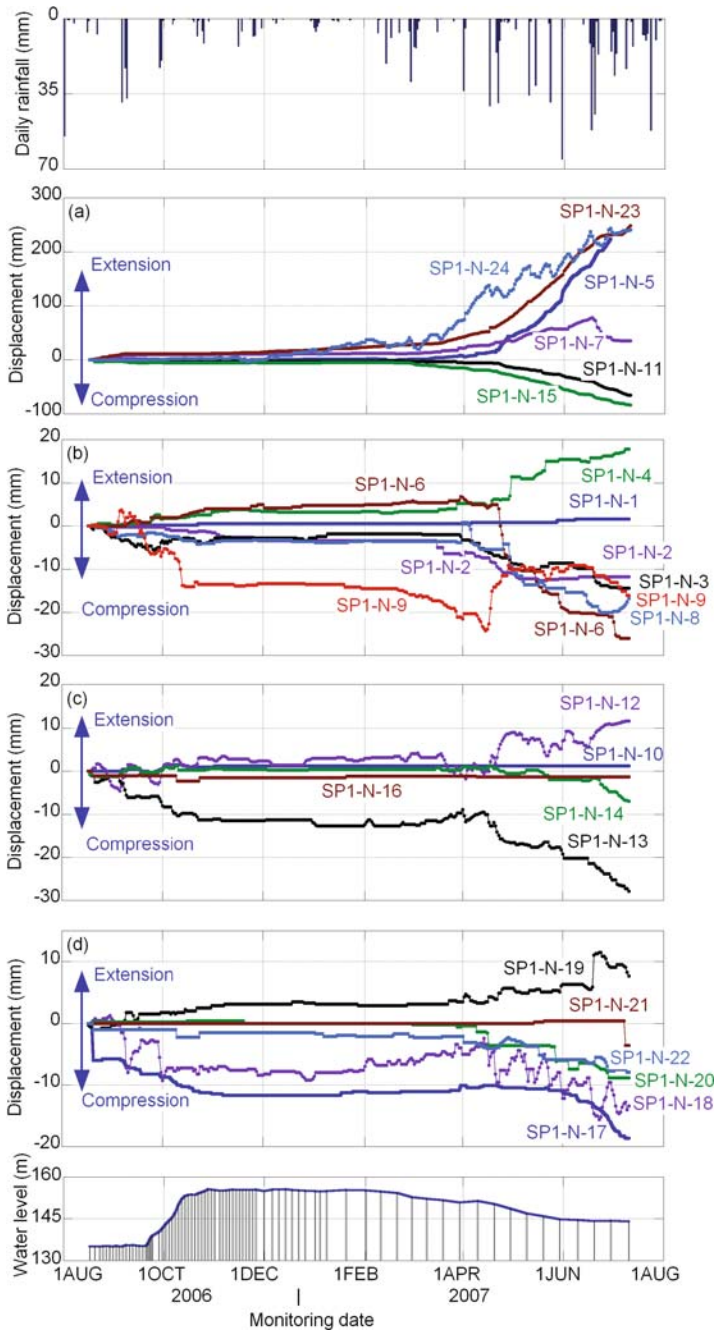
Fig. 11.12 The monitoring results of the drum-style extensometers in Block-1 of the Shuping landslide in the period from August 2006 to July 2007, the changing water level in the Three Gorges Dam Reservoir, and local rainfall data
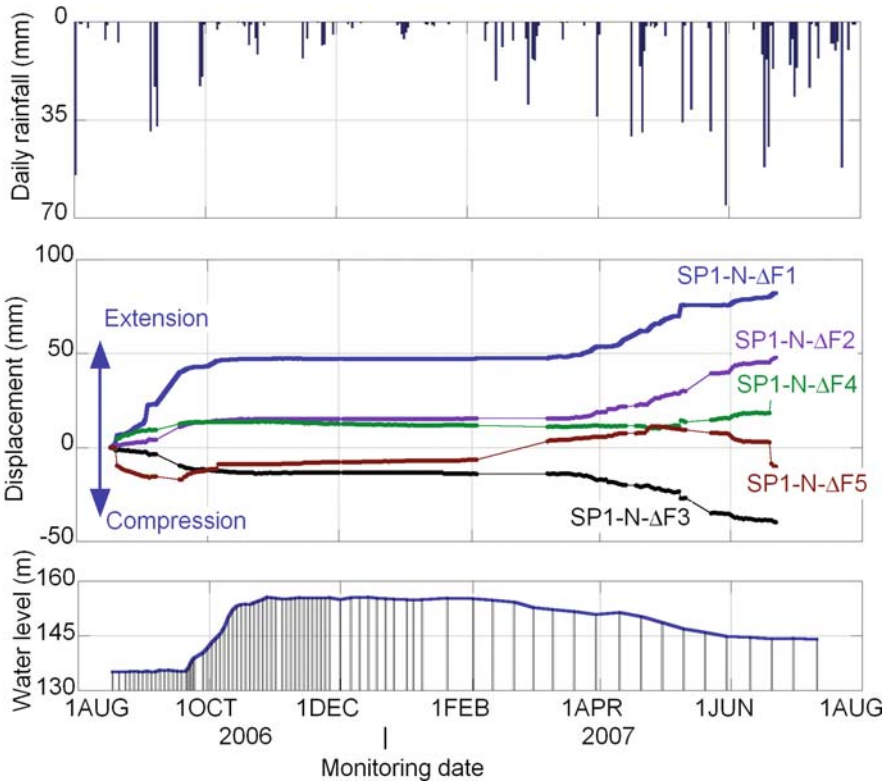
Fig. 11.13 The monitoring results of the flexible extensometers at the toe part of Block-1 of the Shuping landslide in the period from August 2006 to July 2007 and the comparison with the water level changing in the Three Gorges Dam Reservoir

deformation based on the first 2 years of monitoring from August 2004 to July 2006. Because of gaps in the instrumentation, the deformation model is not continuous or complete. Stretching occurred in the upper part of the slide near Shahuang Road, and shortening occurred in the lower slide near ZK-1. Figure 11.9 shows more stretching occurred near the Shahuang Road than shortening that occurred near the toe. However, the initial GPS monitoring indicated that the greatest displacements initially occurred in the lower part of the slide (Figs. 11.3 and 11.7). Thus, during the initial impoundment, the lower part of the slide moved most.

Figure 11.17 shows our longitudinal deformation model of Block-1 based on the monitoring results from August 2006 to July 2007. The *solid line* under the slope surface represents the displacement in that period. Lines tilted toward the river indicate stretching and those tilted upslope indicate shortening. The estimated landslide geometry is shown using *dotted lines*. An inclinometer in borehole ZK-1 indicates that the depth of the surface of rupture is about 45 m.

Fig. 11.15 Monitoring results with the continuous monitoring line from August 2007 to May 2008
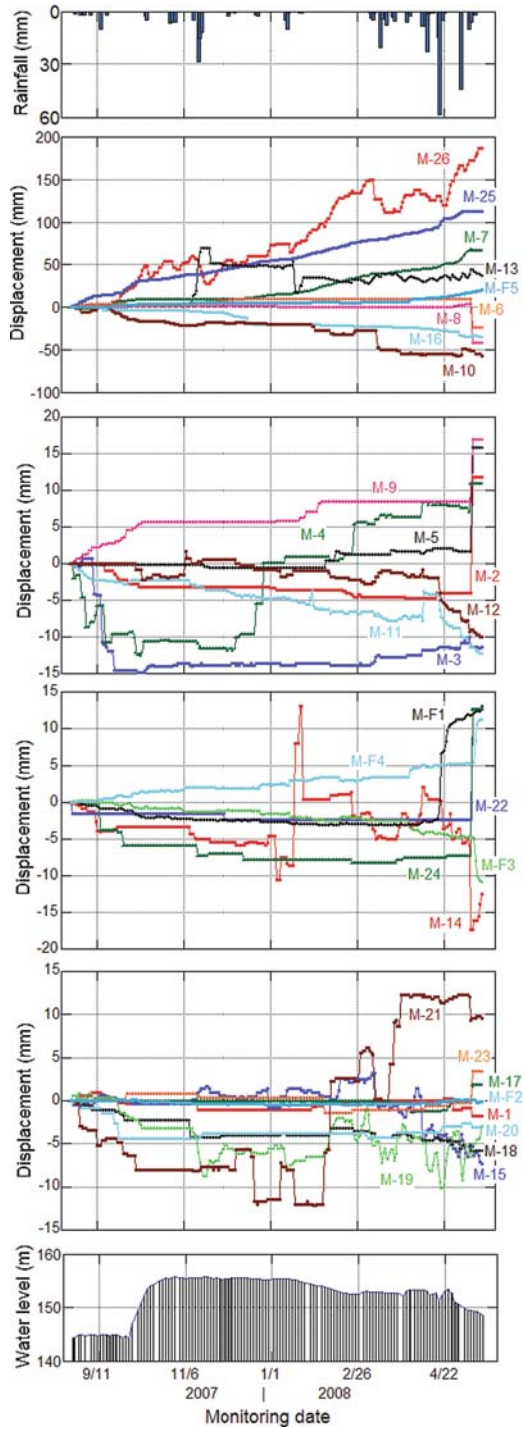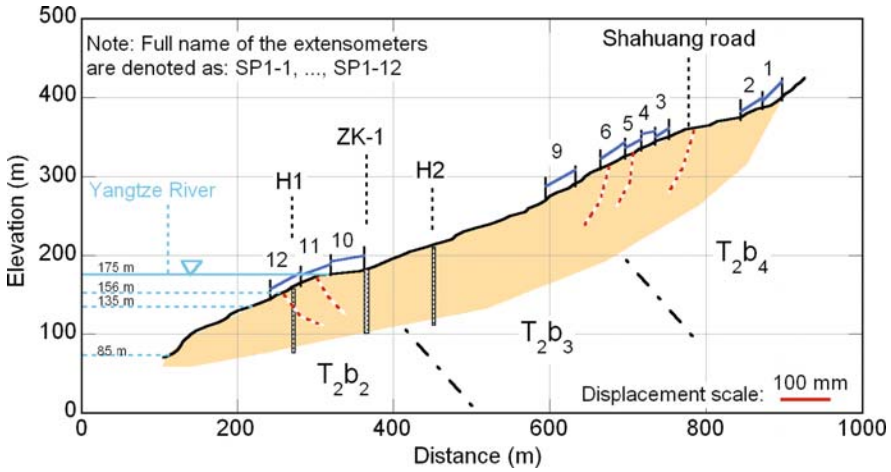
Fig. 11.16 Estimated deforming style of Block-1 of the Shuping landslide based on the monitoring results from August 2004 to July 2006 and the surveying results on the cracks distributing in the slope surface
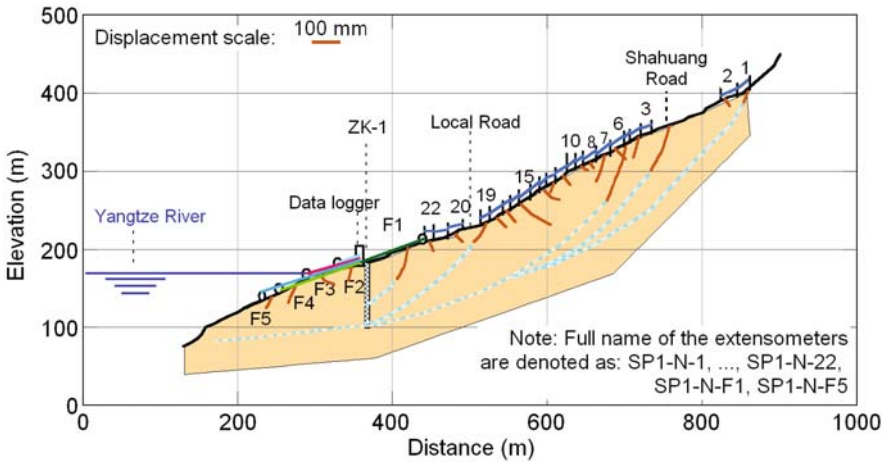

Fig. 11.17 Estimated deforming style of Block-1 of the Shuping landslide based on extensometer monitoring from August 2006 to July 2007

Conclusions

Based on extensometer measurements over a 3-year period, we conclude the following:

(1) Movement of the Shuping landslide corresponds to water level changes in the Three Gorges Reservoir. Interestingly, movement also occurs during periods of declining reservoir level.

(2) Comparison of displacement and deformation data over a 4-year period suggests increasingly complex deformation of Block-1 of the Shuping landslide. Areas of intermixed shortening and stretching occur currently on the slide.

(3) Movement of the landslide occurred during the wet season when reservoir level is lowered for flooding control. Thus, movement monitoring of this landslide is critical even during periods of low reservoir level.

References

Chen D.J., Xue G.F., Xu F.X. 1997. *Study on the Engineering Geology Properties in Three Gorges*. Hubei Scientific Press, Wuhan, 294p.

Wang F.W., Zhang Y.M., Huo Z.T., Matsumoto T., Huang B.L. 2004. The July 14, 2003 Qianjiangping Landslide, Three Gorges Reservoir, China. *Landslides*, 1(2): 157–162.

Wang F.W., Wang G., Sassa K., Takeuchi A., Araiba K., Zhang Y.M., Peng X.M. 2005. Displacement monitoring and physical exploration on the Shuping Landslide reactivated by impoundment of the Three Gorge Reservoir, China. In *Landslides – Risk Analysis and Sustainable Disaster Management*. Springer Verlag, Berlin, Germany, pp. 313–319.

Wang F.W., Sassa K., Zhang Z.Y., Huo Z.T. 2007. Mechanism of the rapid motion of Qianjiangping landslide induced by water level change in the Three Gorges dam reservoir, China. In *Proc. First North American Landslide Conference, Vail, Colorado, June 2007*, pp. 1648–1655.

Wang F.W., Zhang Y.M., Huo Z.T., Peng X.M., Araiba K., Wang G.H. 2008. Movement of the Shuping landslide in the first four years after the initial impoundment of the Three Gorges Dam Reservoir, China. *Landslides*, 5(3): 321–330.

Wen B.P., Wang S.J., Wang E.Z., Zhang J.M. 2004. Characteristics of rapid giant landslides in China. *Landslides*, 1(4): 247–261.

Zhang Y.M., Peng X.M., Wang F.W., Huo Z.T., Huang B.L. 2004. Current status and challenge of landslide monitoring in Three-Gorge Reservoir area, China. In *Proc. Symposium on Application of Real-time Information in Disaster Management, Japan Society of Civil Engineers, 25 June 2004, Tokyo*, pp. 165–170.

Chapter 12
The Anlesi Landslide in Wanzhou, China: Characteristics and Mechanism of a Gentle Dip Landslide

Wenxing Jian, Zhijian Wang, and Kunlong Yin

Abstract Many gentle dip landslides have taken place in Wanzhou, located in the Three Gorges Reservoir area. In order to study the mechanism of the gentle dip landslides, the authors selected the Anlesi landslide as a typical gentle dip landslide to study in detail. Field investigations show that the slip zones of the Anlesi landslide formed from a white mudstone in Jurassic red strata by compressive stress. The X-ray diffraction and infrared ray analysis reveal that the main mineral components of the slip zone are composed of montmorillonite, illite, feldspar, and quartz. A set of tests were conducted on the slip zone specimens to obtain the physicomechanical characteristics. Test results show that the slip zone soils are silty clay, of medium swelling potential, as shear strength becomes very low once the slip zone attracts water to saturation.

The main factors contributing to the gentle dip landslide mechanism are incompetent beds, recent tectonic activities, and intensive rainfall. Several stable, continuous, and thick incompetent beds exist in Jurassic red strata in Wanzhou. The integrity of incompetent beds was compromised under tectonic stress. The recent tectonic activities caused shear failure along the incompetent beds and joints in the sandstone. With the effect of intensive rainfall, water permeates to the incompetent beds along tectonic fissures, resulting in swelling of the soil material and high hydrostatic pressure in fissures of the strata. Therefore, the slopes are prone to slide along the incompetent beds.

Creep tests have been conducted to study the rheological properties of slip zone soils of the Anlesi landslide. The stages of creep attenuation and even rapid creep can be seen clearly from the creep curves. The rheological properties of the slip zone soils have nonlinear characteristics, and the nonlinear Burgers model formula was obtained successfully. FLAC3D software was used to simulate the Anlesi landslide in Jurassic red strata in Wanzhou city. The simulation results show that the stress, displacement, and plastic area change with varying creep time. The maximum displacement at X-direction reaches 7.59 m after a 200-year creep. Therefore, the Anlesi slope failed completely indicated by the rheology effect of Jurassic red strata.

W. Jian (✉)
Faculty of Engineering, China University of Geosciences, Wuhan 430074, China
e-mail: wxjian@cug.edu.cn; wxjian0506@yahoo.com

Introduction

In order to build and utilize the Three Gorges Dam safely, much work has been done to investigate landslides in the Three Gorges Reservoir area. Five groups of landslides, the Taibaiyan landslides, Anlesi landslides, Caojiezi landslides, Pipaping landslides, and Diaoyanping landslides, were discovered in Wanzhou which is located in the middle bank area of the Three Gorges Reservoir (Fig. 12.1). Statistical data show that the total area of the landslides in Wanzhou is about 9.27×10^6 m^2 and the total volume is about 2.35×10^8 m^3 (Nanjiang team of Sichuan Geology and Mineral Bureau 1987). These landslides can be divided into two types: gentle dip rock landslides and soil deposit landslides. The dip of the slip surfaces of the gentle dip rock landslides are about 3–6° and most of the soil deposit landslides took place at the toe of the gentle dip rock landslides.

The formation mechanism of the gentle dip rock landslides in Wanzhou is not clear. Many experts and scholars have researched the formation mechanism of these landslides. Collected geological site exploration material and laboratory data of some landslides in Wanzhou were analyzed in detail. The results show that these landslides have multistage platforms and approximately horizontal sliding surfaces (Liu et al. 2002). The properties of sliding deposits and the characteristics of shear failure surfaces of the Heping Square landslide in the same area have been studied in detail. The conclusion reveals that the Heping Square landslide is not a gentle dip
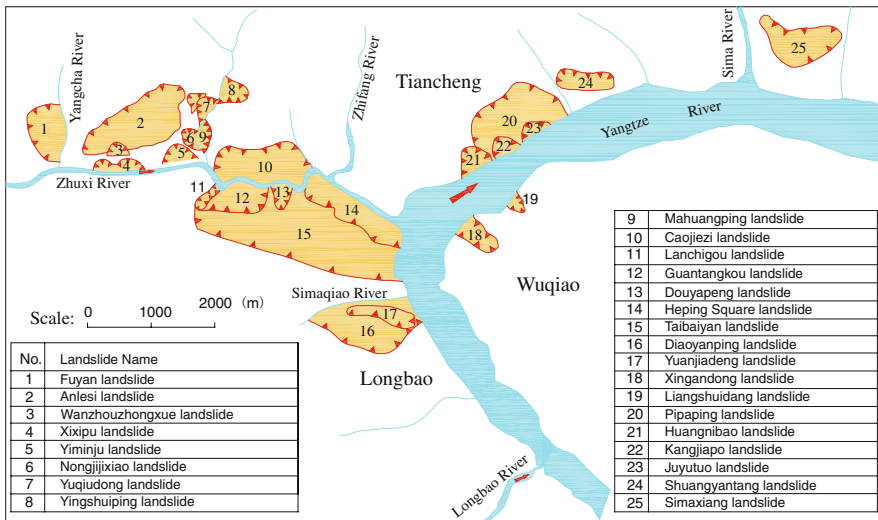

Fig. 12.1 Landslide distribution in Wanzhou in the Three Gorges Reservoir area

bedrock landslide, but a loose mixed accumulation that includes colluvial, residual, and alluvial deposits found at the intersection of the Yangtze River and the Zhuxi River (Sun et al. 2002a,b). The Douyapeng landslide was triggered mainly by loading, foot excavation, and water due to human activities (Qiao 1994; Peng and Li 1995; Qu and Yang 1998). Research reveals that the landslides in Wanzhou are a group of retrogressive landslides occurring in gentle dip red Jurassic strata, and the main triggering mechanisms are intensive rainfall, incompetent beds, and cracks near the crest of the slopes (Wu and Li 1994). Another study shows that the landslides occurred along the approximately horizontal dipping Jurassic red strata. The dip of the sliding surfaces of the landslides is very gentle or near horizontal, and the horizontal and vertical sliding displacements are small. The main controlling factor of the landslides is the montmorillonite mudstone in red strata, and the primary triggering factor is earthquake (Tang 1997). Research on the huge loose deposits at the two banks of the Zhuxi River demonstrates that the soil deposit landslide formed from rock-drop accumulation (Chen et al. 2004). In brief, there are two viewpoints on the formation mechanism of the gentle dip landslides in Wanzhou. One opinion considers that the gentle dip landslides formed along the Jurassic red incompetent strata. Another view is that the gentle dip landslides in Wanzhou mainly formed from the loose deposits.

A lot of research has also been done on similar landslides in other places. The Tiantaixiang landslide took place in Tiantai Village, Xuanhua County, Sichuan Province, on September 9, 2004. The dip of its slip surface is only about 5–7°. It is noted that groundwater was responsible for pushing the landslide body, splitting rock, and intensifying the slope sliding along with the factor of heavy rainfalls (Huang et al. 2005). The Minguochang landslide took place in Jian village, Tiefeng, Wanzhou, at 11:25 on September 5, 2004. This landslide slipped along a Jurassic carbonaceous shale stratum. The formation mechanism of the landslide could be described as follows: (1) The geological structures, i.e., the dip of strata, were in the same direction as that of the slope, and the slope-forming strata made up of Jurassic clastic rocks were the dominant geological factors causing the landslide. (2) Erosion of the Yangjia River and the construction activities were important external causes of the landslide. (3) Rainstorm precipitation was the triggering factor for the landslide (Jian et al. 2005a; Jian et al. 2007). The Qianjiangping landslide took place in Shazhenxi, Zigui County, of Three Gorges Reservoir on July 13, 2003. Research shows that the landslide slipped along a carbonaceous shale stratum surface and was triggered by heavy rainfall. At the same time, water-level rise of the Qinggan River and man-made excavation at the site accelerated the occurrence to some degree (Zhang et al. 2004; Liao et al. 2005).

The research on the mechanism of gentle dip landslide mentioned above is mainly based on the physical and mechanical properties and the structural deformation of red beds. However, few studies have been done on the mechanism of gentle dip rock landslides from creeping behavior to sliding of the red beds which is triggered by heavy rainfall. The authors used the Anlesi landslide as an example to study the mechanism of the gentle dip landslides in the red beds changing from creeping to sliding.

Geological Backgrounds

The landslides are located in the middle of the Wanzhou syncline (Fig. 12.2). The syncline trends ENE. The strata near the axial surface of the syncline are very gentle, and some of the strata are near horizontal. The strata are made up of Jurassic Shaximiao formation (J_{2s}^2–J_{2s}^3), Suining formation, and the Quaternary formation. The Shaximiao formation is composed of red mudstone, sandy mudstone, siltstone, and grey feldspar sandstone. The Suining formation is composed of brown mudstone, siltstone, and sandstone. The Quaternary formation is made up of alluvial, residual, and colluvial deposits.

The Jurassic layers contain three groups of joints as follows: (1) The strike of group one is NWW, the dip direction is NNE, and the dip is 77–80° (with north as zero azimuth). (2) The strike of group two is NE, the dip direction is SE, and the dip is 70–85°. (3) The strike of group three is NEE, the dip direction is SSE, and the dip is 65–80°. These three group joints develop well in both sandstone and mudstone. The scale of the joints is huge in sandstone, and the length can reach several hundred meters. Conversely, the scale of the joints is small in mudstone, but the number is greater than that in the sandstone.
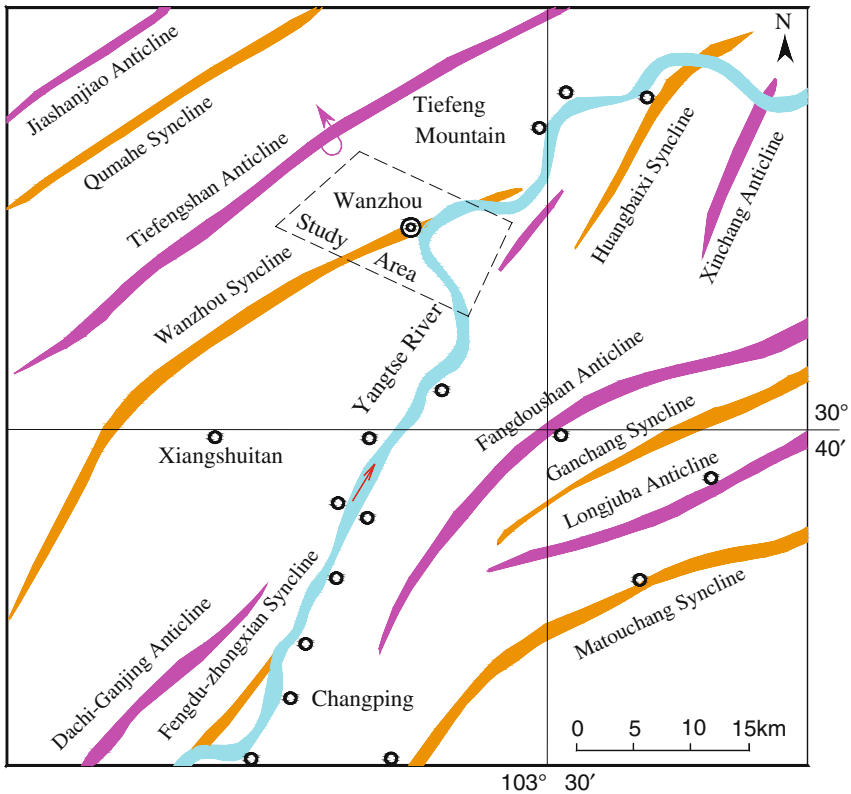

Fig. 12.2 The geological structure map of the Wanzhou area

Characteristics of Anlesi Landslide

The Anlesi landslide is located on the NNW limb of the Wanzhou syncline which trends NEE. The exposed strata are mainly red Jurassic Shaximiao formation (J_{2s}), and the lithologies are a series of purple-red mudstone, silty mudstone, muddy siltstone, and grey feldspar sandstone. The Anlesi landslide is about 600 m in length (sliding direction), 2,100 m in width, $10\,1 \times 10^4$ m^2 in area, and 2486×10^4 m^3 in volume (Fig. 12.3). The bedrocks are composed of siltstone and some mudstone with the dip direction about $150°$ and dip about $4–5°$. The depth of the sliding surface ranges from 10 to 40 m, and even reaches 48 m near the head (Cui 1993). The sliding surface is basically parallel to the layers of bedrock (Fig. 12.4a and b). The catchment area of the landslide is large, and several pools are located on the grooved fracturing zone on the head. Several large-scale, loose deposit landslides exist at the
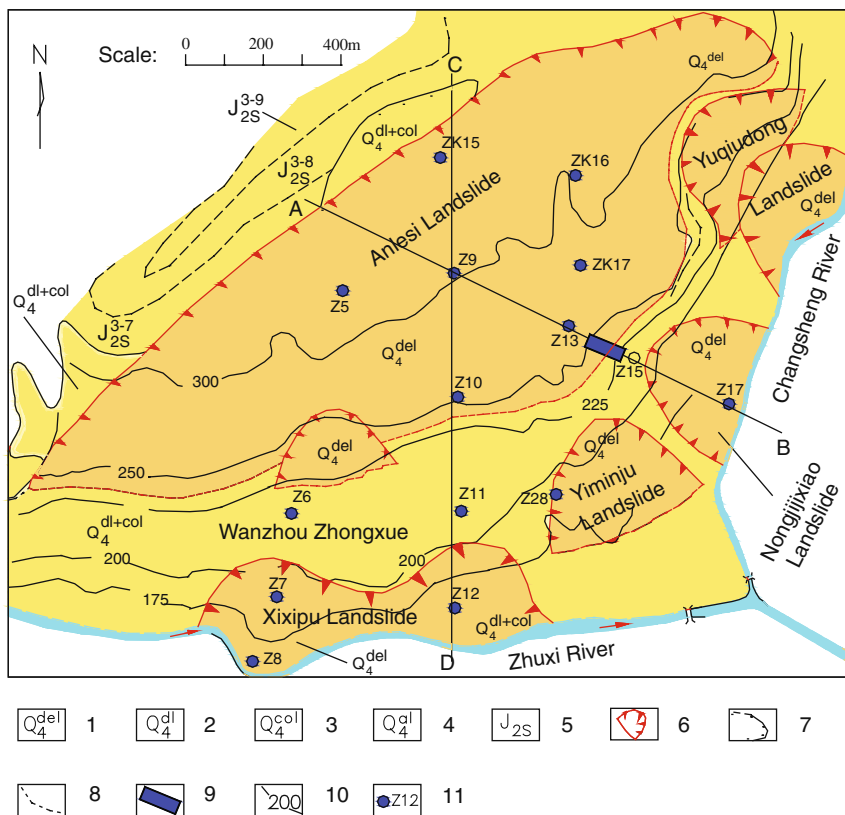

Fig. 12.3 Geological map of the Anlesi landslide. 1 – Displaced material by landslide movement; 2 – Residual deposits; 3 – Colluvial deposits; 4 – Alluvial deposits; 5 – Jurassic Shaximiao formation (J_{2s}); 6 – Landslide boundary; 7 – Unconformity; 8 – Layer boundary; 9 – Test trench; 10 – Contour; 11 – Borehole and its number
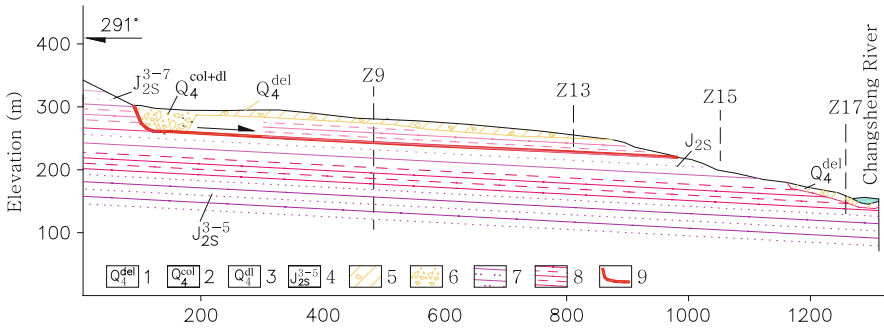
Fig. 12.4a A–B geological profile of the Anlesi landslide. 1 – Displaced material by landslide movement; 2 – Colluvial deposits; 3 – Residual deposits; 4 – Jurassic Shaximiao formation; 5 – Clay with a few gravels; 6 – Gravels and boulders; 7 – Sandstone; 8 – Mudstone; 9 – Slip surface
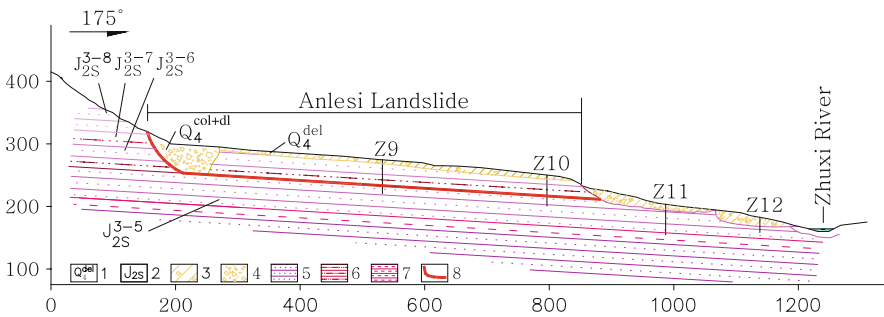

Fig. 12.4b C–D geological profile of the Anlesi landslide. 1 – Landslide deposits; 2 – Jurassic Shaximiao formation (J_{2s}); 3 – Clay with a few gravels; 4 – Gravels and boulders; 5 – Sandstone; 6 – Siltstone; 7 – Mudstone; 8 – Slip surface

Anlesi landslide foot such as the XixiPu, Yiminju, Nongjijixiao, and Yuqiaodong deposits (Jian et al. 2005b).

Macroscopic Geological Features of Slip Zones

In order to evaluate the characteristics of the slip zone of the Anlesi landslide, field investigation was done in detail along the toe of the surface of rupture, and a long trench was dug between borings Z13 and Z15 (Fig. 12.3). Two layers of slip zones were exposed (Fig. 12.5) in the trench. The first slip zone (Y1) was at the bottom of the profile, about 229 m in altitude. The material in the slip zone is made up of white clay and gravels. The largest grain size of the gravels is about 5 cm, generally in the range 0.5–1.0 cm. The thickness of the slip zone is about 20–35 cm. The overlying rock is sandstone and the underlying rock is silty mudstone (Fig. 12.5a). The sliding surface can be seen clearly at the bottom of the white clay (Fig. 12.6), and the sliding
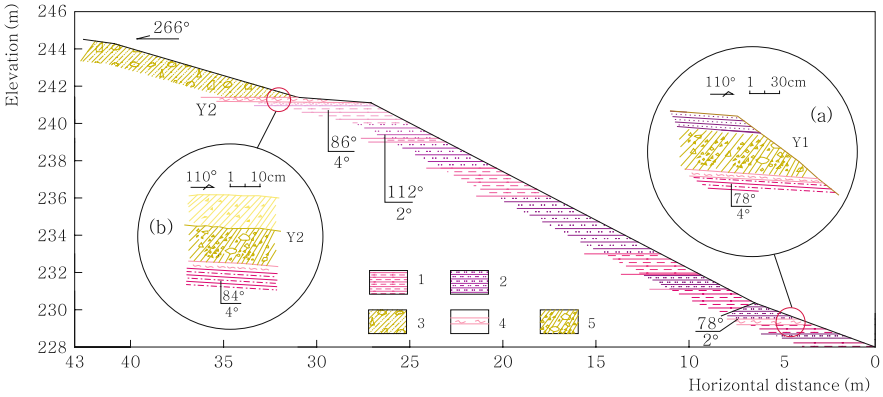
Fig. 12.5 Geological profile of the slip zones of the Anlesi landslide in the excavated trench. 1 – Mudstone; 2 – Sandstone; 3 – Silty clay with crushed stone; 4 – Slip zone; 5 – White clay with breccias (the slip zone soil of Y1 and Y2)

direction shown by striations is 100°. The second slip zone (Y2) is at the top of the profile, about 241 m in altitude. The slip zone is composed of grey white clay and gravels with 10–15 cm in thickness. The grey white clay has great stickiness and high water content. The gravels are mainly made of white mudstone. The shape of the gravels is subangular or angular. The grain size of the gravels is generally about 0.5–2.0 cm in diameter, the largest up to 3 cm and the smallest may be less than 0.1 cm. The overlying soil is Quaternary yellow clay, and the underlying rock is silty mudstone (Fig. 12.5b). The sliding surface and striations can be seen clearly at the bottom of the white clay (Fig. 12.7), and the direction of the striations is 102°. These macroscopic features indicate that the two layers of slip zones formed from white mudstones by the effect of the tectonic compressive stress.

Fig. 12.6 The slip surface of Y1 slip zone

Fig. 12.7 The striations of Y2 slip zone of the Anlesi landslide (the sliding direction is 102°)

The Mineral Components of the Slip Zones of the Anlesi Landslide

X-Ray Diffraction Analysis

The X-ray diffraction was carried out at the test center of China University of Geosciences with the X-ray diffraction instrument D/MAX – 3A made by a Japanese company. The test conditions are as follows: Cu target, Kα beam, Ni filter, 30 kV voltage, 30 mA electric current, the scanning velocity 6°/min, at the temperature 22°C, and the humidity 56%. The result shows that the mineral components of Y1 sliding surface of the Anlesi landslide are made of 85% montmorillonite, 5% illite, 5% quartz, and 5% feldspar (Fig. 8), and the mineral components of Y1 slip zone are made of 75% montmorillonite, 10% illite, 5% quartz, and 10% feldspar. The mineral components of Y2 sliding surface of Anlesi landslide are made of 65% montmorillonite, 15% illite, 15% feldspar, and 5% quartz; and the mineral components of Y2 slip zone are 65% montmorillonite, 5% illite, 20% feldspar, and 10% quartz.
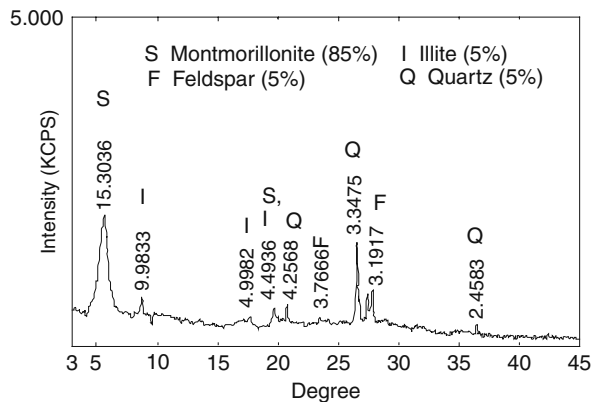

Fig. 12.8 X-ray diffraction chart of Y1 sliding surface

Infrared Ray Analysis

Infrared (IR) ray analysis was carried out at the test center of China University of Geosciences with the Fourier transform infrared ray instrument MAGNA-IR550 made by Nicolet Company in the United States. The infrared ray analysis indicates that there is a large amount of montmorillonite because of the appearance of medium-intensity OH zone in 3620 cm^{-1} and the wide and gentle H_2O zone in 3400 cm^{-1}, and no typical region of kaolinite in 3700 cm^{-1} (Fig. 12.9). The main mineral components displayed from the IR analysis are basically consistent with the results of the X-ray diffraction analysis. From the analysis, it can be concluded that the mineral components of slip zones of the Anlesi landslide are almost the same with that of incompetent beds in Jurassic red strata located in Wanzhou (Jian et al. 2005c).
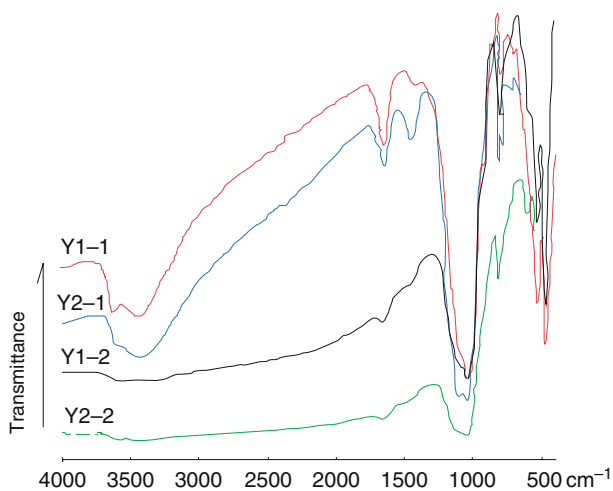

Fig. 12.9   Infrared ray analysis of slip zones Y1 and Y2

The Microcosmic Structure Features of Slip Zone

The technology of the scanning electron microscope is a very effective means of accessing information about soil structure (Xiong et al. 2007). With this technology, the microcosmic structure features of the slip zone soils were studied in detail, including features of striations in slip zones, directional crystal structures, forms of minerals, and so on. The test equipment is an environmental scanning electron microscope of Quanta 200.

Features of Striations

Observations with the scanning electron microscope on the Y1 and Y2 slip zones reveal that striations concentrate mainly in the sliding surfaces. These striations are
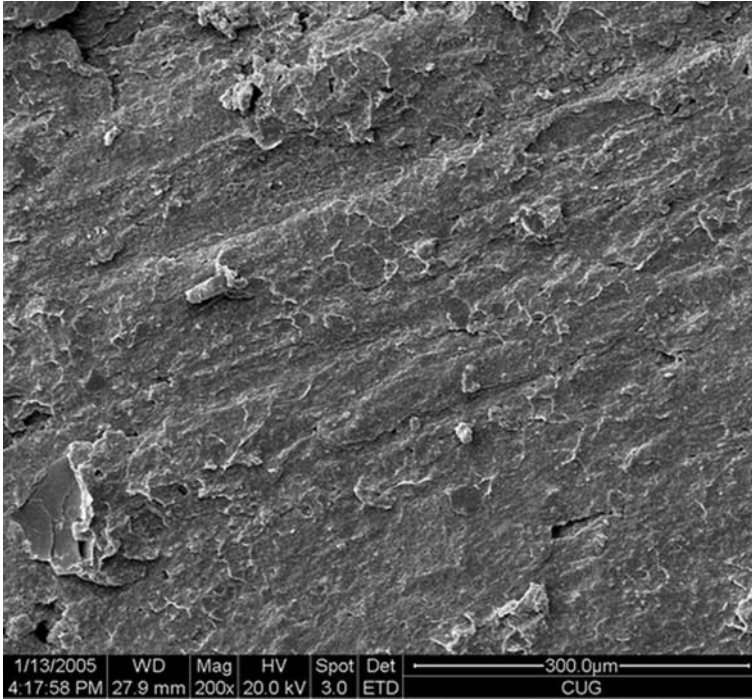
Fig. 12.10 The microstriations of Y1 sliding surface

smooth, straight, and have good extension (Fig. 12.10). It was noticed that the striations on the surfaces of the slip zones have periodicity. Three different periods of striations were found and the angles between the previous two periods and the latest one are about 30° and 50°, respectively. The striations formed earlier were cut off by the later ones.

Features of Mineral Directional Crystal Structure

The scanning electron microscopic analysis shows that the shapes of the clay mineral crystals are mainly sheet (Fig. 12.11) with a few long strip (Fig. 12.12). The minerals in the slip zones are mainly composed of montmorillonite. Some of the minerals in the slip zones are directional to some extent. From the direction perpendicular to the observed sliding direction, the minerals obviously have directional layer characteristics, and the oriented sheet minerals in the slip zones are approximately parallel to sliding surfaces (Fig. 12.13). From the direction parallel to the observed sliding direction, the direction of the oriented minerals and the most recent sliding direction has an angle of about 30°. It indicates that the slip zones of the Anlesi landslide were compressed and had slid many times. The former sliding direction was about 130°.
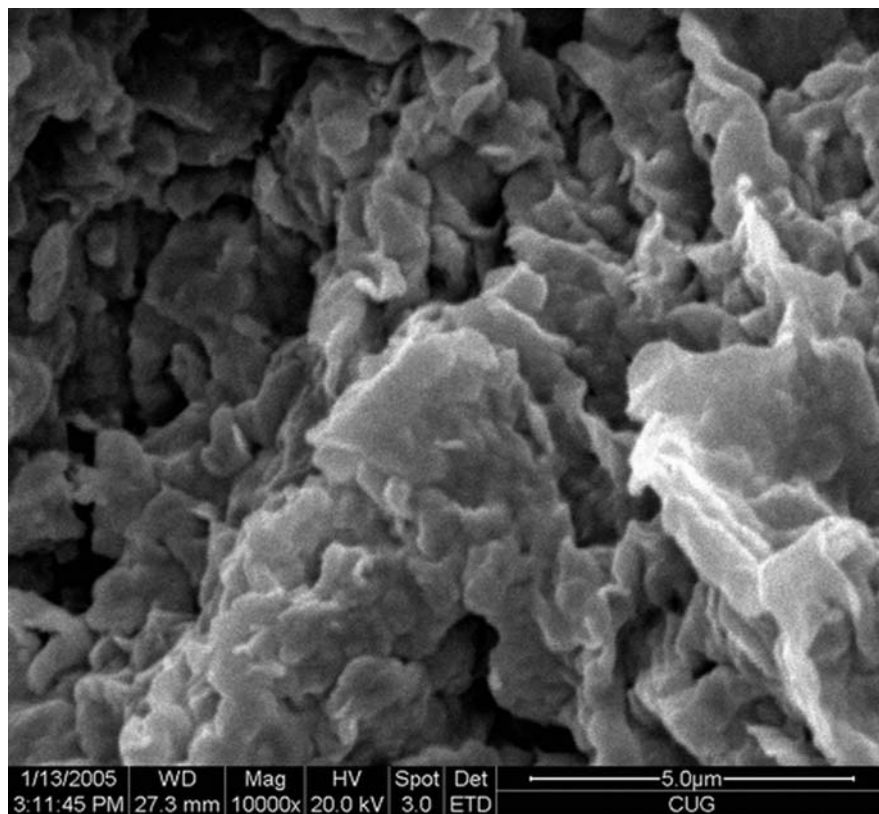
Fig. 12.11 The sheet crystal structure of the clay mineral of Y1 slip zone

Physical Properties of Slip Zones

A group of experiments were conducted to obtain the grain size distribution, the liquid and plastic limits, the maximum dry density, the optimum water content, and shear strength of slip zones of the Anlesi landslide. The samples were obtained from Y1 and Y2 slip zones exposed in the trench shown in Fig. 12.5. The experiments were carried out strictly in accordance with the Standard for Soil Test Method (GB/T 50123 1999).

Grain Size

Sieve and hydrometer analyses were used to obtain the grain size distribution of the slip zones. The results show that sands comprise 1.9%, silts 72.3%, clays 25.8% in Y1 slip zone; and sands comprise 26.2%, silts 31.8%, clays 42.2% in Y2 slip zone. Therefore, both the slip zone soils are classified as silty clay.
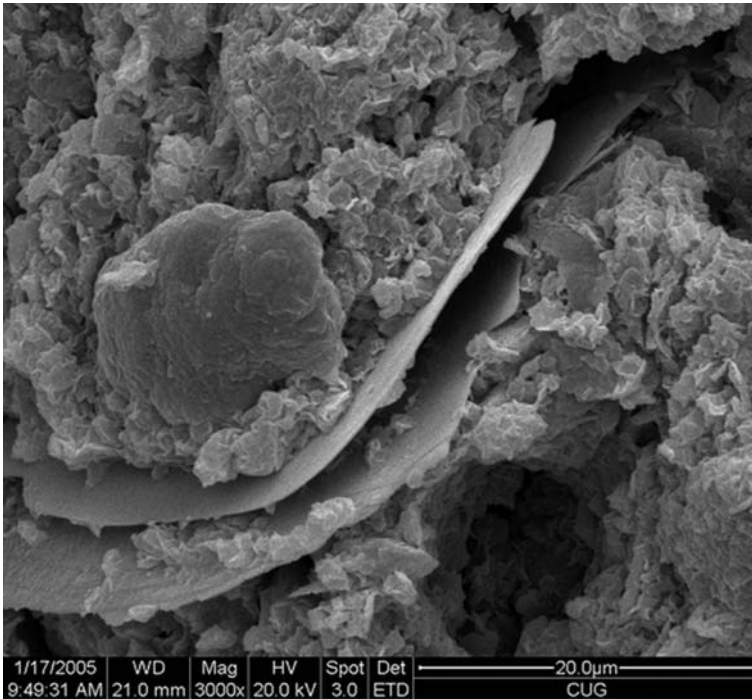
Fig. 12.12 Long-strip structure of the clay mineral of Y1 slip zone

Maximum Dry Density and Optimum Water Content

The method of standard Proctor compaction was used to measure the maximum dry density and the optimum water content of the slip zones. The maximum dry density of Y1 slip zone is 27.3% and the optimum water content is 1.453 g cm^{-3}; those of Y2 slip zone are 20.8% and 1.574 g cm^{-3}, respectively (Fig. 12.14).

Liquid and Plastic Limit

The method of rolling and twisting was used to measure the plastic limit, and penetrating cone liquid limit device was used to measure the liquid limit of the slip zones. For Y1 slip zone, the plastic limit is 29.3%, liquid limit is 43.2%, and plastic index is 14. For Y2 slip zone, the plastic limit is 20.1%, liquid limit is 34.1%, and plastic index is 14. According to the liquid plastic limit of the slip zones, it can be determined that both of the two slip zone soils are silty clay.

Swelling Potential

The free swelling test was used to measure free swelling potential. Result shows that the free swelling potential of Y1 slip zone is 87.5% and that of Y2 slip zone
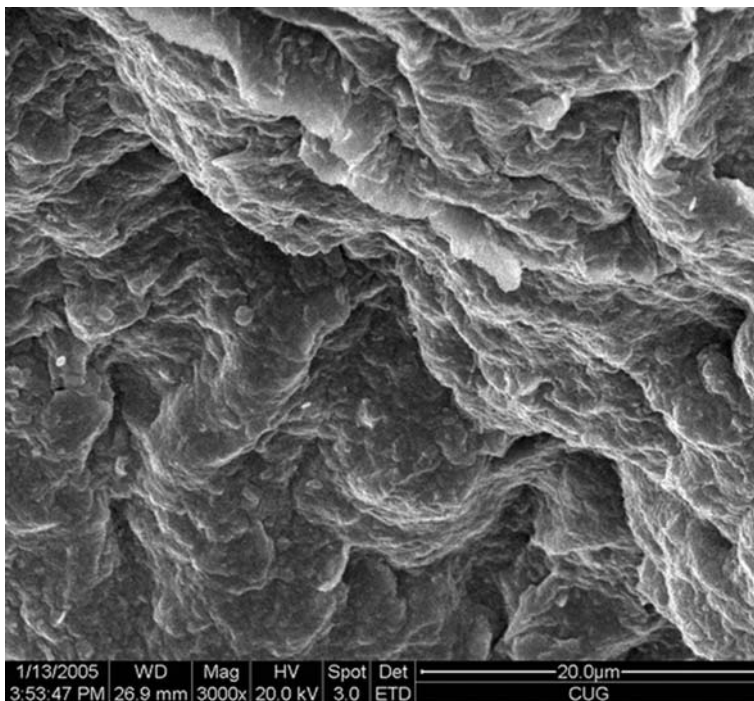
Fig. 12.13 Directional crystal structures of the clay minerals of Y1 slip zone

is 57.0%. Therefore, Y1 slip zone is a medium-swelling clay and Y2 slip zone is a low-swelling clay. Swelling potential of Y1 and Y2 slip zone soils under various confining pressure was discussed in detail in the book *Formation Mechanism and Prevention Methods of Landslide Sliding Along Horizontal Strata* (Yin et al. 2007).
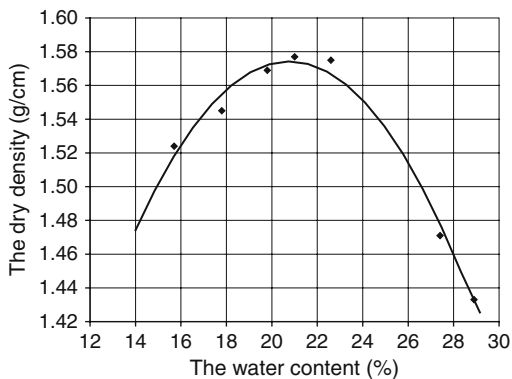

Fig. 12.14 Standard Proctor compaction curves for Y2 slip zone

Shear Strengths

Direct shear tests were conducted on the specimens of Y1 and Y2 slip zones in three different conditions: (1) specimens prepared under liquid limit condition, and then cut with a ring shear to annular specimens; (2) specimens compacted with standard proctor compacter under optimum water content, and then saturated with vacuum; and (3) specimens prepared by a shear ring with undisturbed samples and saturated by capillary. Slow consolidated shear tests were conducted on the specimens with the rate of 0.02 mm/min. The test results show that the shear strength of undisturbed samples is close to the shear strength of samples prepared under the liquid limit condition and the value is relatively low. However, the shear strength of specimens prepared by compaction is higher (Table 12.1). In order to study the relationship between the swelling potential and the shear strength, quick shear tests were carried out under the following three conditions: (1) specimens confined around side, the top side, and bottom side; (2) specimens confined around side and bottom side; and (3) specimens confined only around side. Specimens were seated in specimen molds under the three conditions mentioned above and saturated by capillary. Test results are shown in Table 12.2 and illustrate that the values of shear strength parameters c and ϕ reduced rapidly with the slip zone soil swelling potential changing from a natural condition to complete swelling. It is very similar to the shear strength properties of expansive soil in the roadbed (Zhang & Jiang 2001).

Table 12.1 Direct shear test conditions and results of Y2 slip zone

Test condition (slow consolidated shear test)	c (kPa)	ϕ (°)
Sample prepared under liquid limit	6.3	16.7
Prepared by compaction and saturated by vacuum	10.2	25.1
Undisturbed samples saturated by capillary	5.9	13.5

Table 12.2 Quick shear test results of Y1 and Y2 slip zones under various conditions

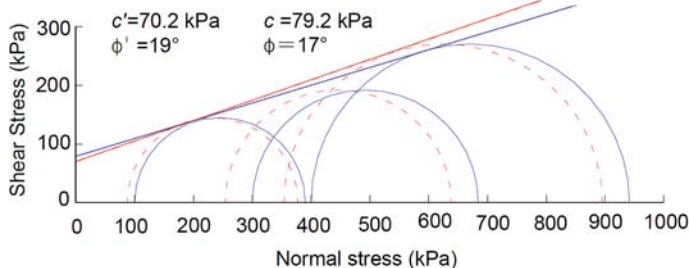| Slip zone	Confined condition	Water content (%)	Density (g cm^{-3})	Shear strength parameter	
Y1	(1)	34.45	2.02	c (kPa)	21.2
				ϕ (°)	10.3
	(2)	40.68	1.97	c (kPa)	14.2
				ϕ (°)	8.2
	(3)	45.73	1.91	c (kPa)	2.6
				ϕ (°)	2.6
Y2	(1)	24.01	1.80	c (kPa)	22.4
				ϕ (°)	13.2
	(2)	28.07	1.77	c (kPa)	13.2
				ϕ (°)	10.0
	(3)	32.97	1.73	c (kPa)	1.6
				ϕ (°)	1.9

Fig. 12.15 Mohr circles at failure and Mohr envelopes for both total and effective stresses of Y1 slip zone soil

Triaxial consolidated undrained tests were performed on Y1 and Y2 slip zone soils with standard triaxial device. Specimens of slip zone soils were prepared by compaction with optimum water content and saturated by vacuum in a pressure cell. The confining pressure is 100, 200, 300, and 400 kPa, respectively. The test results are shown in Fig. 12.15. The total shear strength parameters c and ϕ are 79.2 kPa and 17.0°, respectively, and those of effective stress are 70.2 kPa and 19.0°, respectively.

Comparing the shear strength parameters of the slip zone soil obtained above with parameters used in the designs of landslide prevention in Wanzhou (Luo et al. 2005), it can be found that (1) the shear strength parameters obtained in slow shear tests and triaxial tests are larger than those used in designs; (2) the shear strength parameters obtained in quick shear tests for the complete swelling samples are smaller than those used in designs; (3) the shear strength parameters obtained in quick shear tests for partly swelling samples are basically consistent with those used in designs.

Factors Contributing to the Gentle Dip Landslides

Incompetent Beds

Several stable, continuous, and thick incompetent beds exist in Jurassic red strata in Wanzhou. Most gentle dip landslides slipped along incompetent beds. In order to reveal the mechanism of the gentle dip landslides, it is very necessary to study the properties of the incompetent beds. Several tests were conducted on the specimens of the incompetent beds to obtain the mineral components and the physical properties (Jian et al. 2005c). The results show that the main mineral components and properties of the incompetent beds are almost the same as the slip zone soils of the Anlesi landslide, and the incompetent beds are medium swelling potential silty clay. In order to discuss the contribution of incompetent beds to the gentle dip landslide mechanism, the distribution, the fabric, and the shear strength of the incompetent beds were investigated and presented as follows.

Distribution of Incompetent Beds

Strata exposed at Wanzhou are mainly the Shaximiao group and the Suining group of the Jurassic series. Their lithology is a set of very thick purple-red sandstone, grey feldspar–quartz sandstone, purple-red pelitic siltstone, silty mudstone, and mudstone. There exist several stable, continuous, and thick incompetent beds in this set of strata. These incompetent beds can be classified into two kinds: (1) Grey, stable, continuous, thick montmorillonite mudstone with a thickness of 3–80 cm, and even thinner than 1 cm. The main features of the incompetent beds are a high content of montmorillonite, water expansion, softening, and low shear strength. (2) Purple-red mudstone which occur mainly on layer surfaces of the purple-red mudstone formed from the shear deformation of the purple-red mudstones. The thickness is about 1–10 cm and the main ingredient is illite.

Fabric and Structure of Incompetent Beds

The study area is located at the core of the Wanzhou syncline (Fig. 12.2). Strongly squeezed by the tectonic stress in the SN and NWW–SSE direction, great shear displacement took place between the layers. The J_{2s} strata are stable, nearly horizontal in the Wanzhou area. Shear joints are well developed in the strata, and small-scale shearing surfaces (Fig. 12.16) in incompetent beds can be seen in the field. The scanning electron micrographs show that the grey white incompetent beds located 276.2 m high at the north side of Shalong Road, Sanwan pool (Fig. 12.17), are mainly composed of montmorillonite, illite, quartz, feldspar, and so on and in which exist
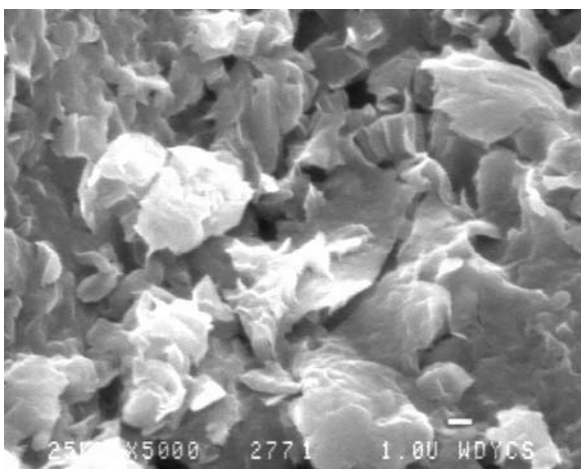

Fig. 12.16 A shear surface in an incompetent bed near Jianchayuan, Wanzhou

Fig. 12.17 An incompetent
bed at the north side of
Shalong Road, Sanwan pool,
Wanzhou

Fig. 12.18 Sheet crystals of
clay mineral of an
incompetent bed

a large amount of sheet crystals (Fig. 12.18), many microfissures and micropores,
a few microgrid fissures, and directional crystal structures. The phenomenon above
shows that the Jurassic incompetent beds in Wanzhou were acted upon by a set of
compressive tectonic forces, and shearing failures occurred in some of the incompe-
tent beds. Therefore, the shearing strength of the incompetent beds became greatly
weakened.

Shear Strength of Incompetent Beds

The shear strength of incompetent beds was tested in unsaturated (natural) and sat-
urated states with consolidated quick direct shear tests and consolidated drained
direct shear tests. The specimens were compacted under optimum water content

Table 12.3 Conditions and results of direct shear tests

Conditions	Methods	Results
Unsaturated	Consolidated drained direct shear test	$c = 23.31$ kPa, $\phi = 21.8^{\circ}$
	Consolidated quick direct shear test	$c = 18.80$ kPa, $\phi = 24.6^{\circ}$
Saturated	Consolidated drained direct shear test	$c = 14.52$ kPa, $\phi = 24.1^{\circ}$
	Consolidated quick direct shear test	$c = 40.08$ kPa, $\phi = 18.2^{\circ}$

with the standard proctor compactor. (1) Preparation for unsaturated specimens: the specimens are saturated by capillarity for 48 h. (2) Preparation for saturated specimens: the specimens are saturated by vacuum. The speed of consolidated quick direct shear tests is about 0.8 mm/min, and the consolidated drained direct shear tests is about 0.02 mm/min with the vertical stress 100, 200, 300, and 400 kPa, respectively. The test conditions and results are shown in Table 12.3. It is obvious that the shear strength parameters of remolded specimens under the saturated condition are considerably smaller than those under the unsaturated condition. Therefore, it can be concluded that the shear strength will drop greatly, once the incompetent beds attract water to saturation.

The triaxial consolidated undrained tests were performed with standard triaxial apparatus. Preparation of the specimens: (1) preparation of unsaturated specimens: the specimens were compacted under optimum water content, then saturated by capillarity for 48 h; (2) preparation of saturated specimens: specimens were compacted under optimum water content and saturated under pressure head in pressure chamber. The cell pressure is 100, 200, 300, and 400 kPa, respectively. The test conditions and test results are shown in Table 12.4. It is obvious that the shear strength parameters of remolded specimens under saturated conditions are approximately only half of the shear strength parameters under unsaturated conditions. Under consolidated undrained conditions, the total shear strength parameters are $c = 27$ kPa, $\phi = 17.0^{\circ}$ and the effective shear strength parameters are $c' = 19$ kPa, $\phi' = 23.0^{\circ}$.

Table 12.4 Conditions and results of triaxial tests

Conditions	Methods	Results
Saturated	Unconsolidated undrained	$c = 29.0$ kPa
	Consolidated undrained	$c = 27.0$ kPa, $\phi = 17.0^{\circ}$
		$c' = 19.0$ kPa, $\phi' = 23.0^{\circ}$
Unsaturated	Unconsolidated undrained	$c = 60.3$ kPa

Contributions of Incompetent Beds to Landslide Formation

Under the tectonic stress and unloading effect, the shear displacement occurred along incompetent beds and tectonic fissures perpendicular to the layer surfaces formed in the beds. Therefore, the integrity of the incompetent beds was broken. Underground water permeates to incompetent beds along the tectonic fissures and results in two effects on incompetent beds. One effect is that the shear strength of

the incompetent beds decreased greatly due to the montmorillonite swelling after absorbing water. The other effect is that great hydrostatic pressure occurs. Under the two kinds of effects and other loads, the strata creep along the incompetent bed layers, resulting in sliding. A lot of research has been done on the formation mechanism of the Taibaiyan landslides, the Anlesi landslides, the Caojiezi landslides, the Pipaping landslides, and the Diaoyanping landslides in Wanzhou. It is considered that the five group landslides took place along incompetent bed layers, and the loose mixed deposits at the foot of the five groups of landslides are formed from residual, colluvial, and alluvial deposits (Yin et al. 2007). The deformation and failure of cut slopes in gentle dip red strata was studied, and the results show that the deformation and failure occurring along gentle dip red beds was very common (Cheng et al. 2004). Research on landslides occurring in cretaceous red beds shows that landslides are prone to take place along red bed layers (Yuan & Ni 2004). The facts mentioned above indicate that incompetent beds are prone to become sliding surfaces for gentle dip rock landslides under some special conditions.

Latest Tectonic Activities

The Earth's crust rose intermittently for several times after the Tertiary Period in the eastern Sichuan Province (Tan & Bao 1991; Gao 1992). A plantation surface and several river terraces formed due to the tectonic activities. When the Earth's crust rose, the mountains were cut down by the erosion of the Yangtze River. As a consequence, the stress field of bank slopes changes, the sloping sides of the bank valley became unstable, and debris begins to slide into the river. According to the results of the topography analysis and the absolute age of the gentle dip landslides, the landslide formation time is correlative to the river terrace time. The absolute age of the Anlesi landslide is about 315–384 thousand years (Yang 1988), corresponding to the formation time of terrace 4. Therefore, the formation of the gentle dip landslides in Wanzhou correlates with the latest tectonic activities.

Intensive Rainfall

Wanzhou is located in the middle latitude zone, which experiences tropical weather. According to the statistics of the Sanxia Weather Department, Wanzhou is the center of abundant precipitation in the Three Gorges Reservoir. The rainy season begins in March and ends in September. Annual rainfall is about 1253 mm. It was recorded that the greatest continuous rainfall reached 488.7 mm, the most 3-day continuing rainfall reached 388.6 mm, and the most rainfall in 1 day was 243.3 mm. Rainstorms often occur from May to September (Cui 1993). The gentle dip landslides slip along the red incompetent beds. With the effect of rainfall, water permeates to incompetent beds along the tectonic fissures and makes incompetent beds swell. Thus, the shear strength of incompetent beds decreases greatly, and great hydrostatic pressure occurs in the fissures. As mentioned in the "Introduction" section,

three typical gentle dip landslides – the Tiantaixiang landslide (Huang et al. 2005), the Minguochang landslide (Jian et al. 2005a; Jian et al. 2007), and the Qianjiangping landslide – were triggered by heavy rainfall (Zhang et al. 2004; Liao et al. 2005). Therefore, the slopes are prone to slide with the effect of rainfall.

Creep Properties of the Slip Zones of the Anlesi Landslide

Slip zones are the main factors that control the gentle dip landslides in Wanzhou. The properties and the shear strengths of slip zone soils are very important parameters in analyzing the deformation mechanism and evaluating the slope stability. In order to explore the mechanism of the gentle dip landslides, the creep experiments of slip zone soils of the Anlesi landslide have been done to establish the rheological formula of the slip soils in this section.

Test Facilities

The facility used in the creep test is the SR-6 triaxial creep instrument produced in Liyang city, Jiangsu Province. Cell pressure is provided by vacuum, and deviator stress is provided by gravity. Therefore, the pressures are very stable during testing. The data of cell pressure, pore pressure, drainage volume, and deformation can be obtained automatically from the facility system.

Test Procedure

The Anlesi landslide is a typical gentle dip landslide forming in red clastic rocks. In order to study the rheological deformation characteristics, remolded specimens were used in test with the disturbed soils obtained from Y1 and Y2 slip zones. Water is added to the slip zone soils until water content reaches the liquid limit, and the soils were thoroughly mixed with water. The specimens were trimmed to be cylindrical with diameter of 60 mm and height of 120 mm. The specimens were put to a saturation instrument to saturate with vacuum until the B value is greater than 0.95. Then the specimens were mounted to the chamber of SR-6 triaxial creep instrument to consolidate. The cell pressure for the consolidation is 100, 200, 300, and 400 kPa, respectively. The average consolidation time is about 2–3 days based on the speed of pore pressure dissipates. Considering the state of the slip zone soils, drainage-consolidated triaxial creep tests were performed.

Step loading was used in the test. The time for each step loading was determined by the deformation rate. When the total deformation is less than 0.01 mm within 3 days, the next step loading was applied. The step loading continues until the specimen fails. The data were automatically obtained with the automated data acquisition system.

Test Results

Boltzmann superposition method was used to deal with the data of creep tests of Y1 and Y2 slip zones due to the step loading being used in the test. Figures 12.19–12.22 show the creep curves of the Y1 slip zone under various cell pressures. The time length of each step loading is about 11000–26000 min, where the D stands for deviator stress and the D_r stands for the normalized deviator stress with maximum deviator stress. The definition is as follows:
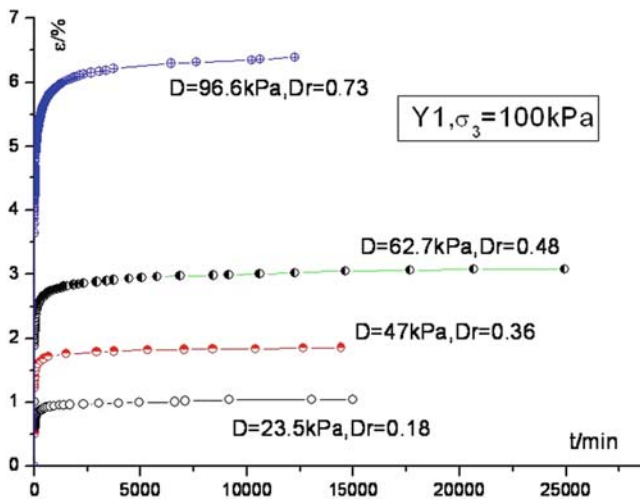

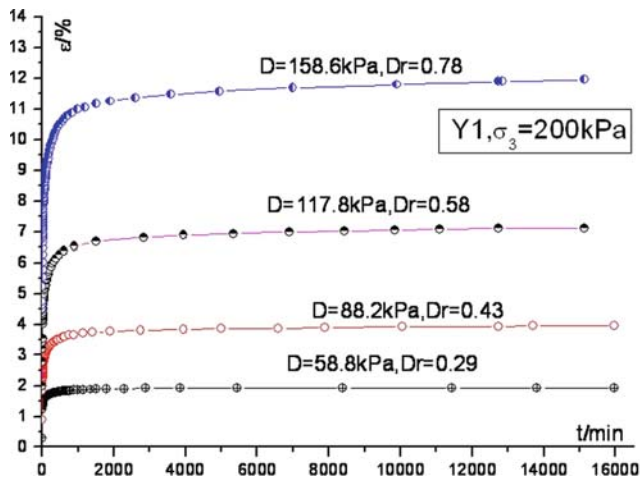**Fig. 12.19**   The creep curve of Y1 slip zone soil under 100 kPa cell pressure

Fig. 12.20   The creep curve of Y1 slip zone soil under 200 kPa cell pressure
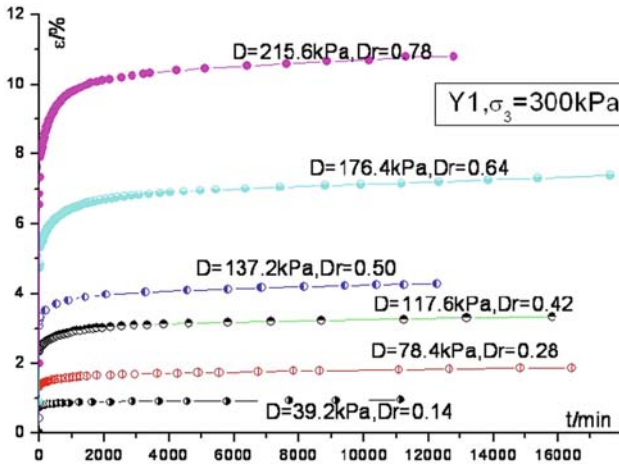
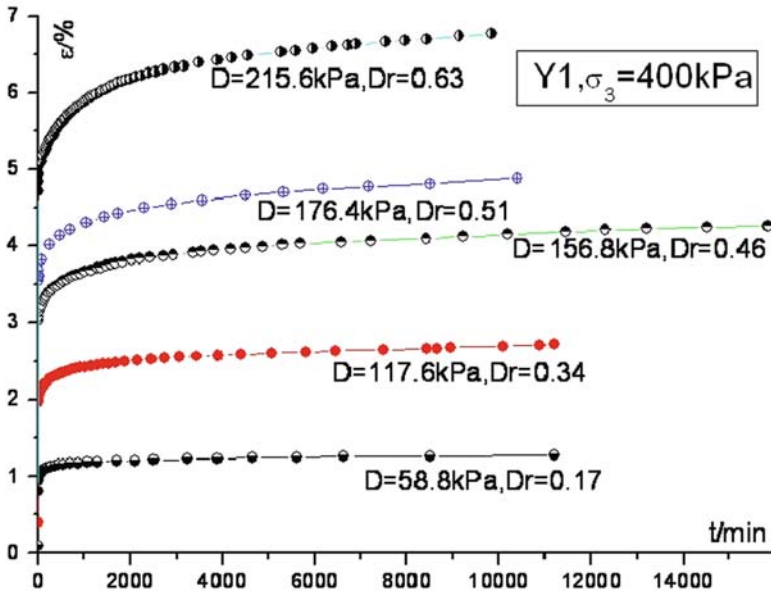**Fig. 12.21** The creep curve of Y1 slip zone soil under 300 kPa cell pressure

Fig. 12.22 The creep curve of Y1 slip zone soil under 400 kPa cell pressure

$$D_{\mathrm{r}} = D/D_{\max} = (\sigma_1 - \sigma_3)/(\sigma_1 - \sigma_3)_f. \tag{12.1}$$

The maximum D_{r} is about 0.90 and the minimum is about 0.18. The first stage of creep attenuation and the second stage of even rapid creep can be seen clearly from the creep curves. Nevertheless, the third stage of accelerating creep cannot be observed from the curves. The same results of the Y2 slip zone soils were obtained from the test.

Burgers Rheological Model of Slip Zone Soils

Based on the data obtained from the creep tests, several theoretical models including Burgers model, Singh–Mitchell nonlinear creep model, and Mesri model were used to describe the creep properties (Wang 2008). In order to analyze the creep properties clearly, the model parameters and results of Burgers model were demonstrated.

The Burgers Model Parameters

The method to determine the Burgers model parameters according to the creep curves obtained from the creep tests was introduced and illustrated in detail in Chap. 4 in Wang's Ph.D. dissertation (Wang 2008). The Burgers model parameters of Y1 slip zone soil were listed in Table 12.5, where the K, G_1, η_1, G_2, and η_2 are the Burgers model parameters. K stands for the bulk deformation under static water pressure, G_1 stands for the instant deformation under action of shear stress, G_2 stands for the total deformation of the creep attenuation stage under action of shear stress, η_1 stands for the strain rate of the even rapid creep stage under the action of shear stress, and η_2 stands for the attenuation rate of the creep attenuation stage.

    The characteristics of Burgers model parameters are as follows. (1) The Burgers model parameters of Y1 slip zone are almost the same as those of Y2 slip zone. (2) The K value increases with the increase of cell pressure (Fig. 12.23). The K value decreases exponentially with the increase of deviator stress under a fixed cell pressure. (3) The η_1 decreases with the D_r increase (Fig. 12.24). Thus, the η_1 decreases with the deviator stress increase. (4) D/G_2 shows the deformation size of the first stage of creep attenuation. D/G_2 accelerating increases with the normalized deviator stress increases (Fig. 12.25), and it can be expressed as $D/G_2 = 3.192\text{e-}6 - 3.751\text{e-}6 \times D_r + 10.36\text{e-}4 \times D_r{}^2$. (5) G_2/η_2 shows the rate of the first stage of creep attenuation (Fig. 12.26). The value can be expressed as $G_2/\eta_2 = 0.0076 - 0.0194 \times D_r + 0.0158 \times D_r^2$. The G_2/η_2 has the minimum value, when $D_r = 0.5$.

The Nonlinear Burgers Model

Based on the linear rheological model theory, the model parameters have no correlation with stress conditions. However, the results obtained from the tests show that the Burgers model parameters have been affected by both deviator stress and cell pressure. Therefore, the rheological properties of the slip zone soils have nonlinear characteristics. Suppose the mechanical parameters have a correlation with the stress condition, the nonlinear Burgers model formula is as follows:

$$\begin{cases} e_{ij}(t) = \left\{ \frac{\Delta(t)}{2G_1} + \frac{t}{2\eta_1} + \frac{1}{2G_2}\left[1 - \exp\left(-\frac{G_2}{\eta_2}t\right)\right]\right\} * ds_{ij} \\ e(t) = \frac{\Delta(t)}{3K} * d\sigma \end{cases} \qquad (12.2)$$

where $K = K(\sigma)$, $G_1 = G_1(\sigma)$, $\eta_1 = \eta_1(\sigma)$, $G_2 = G_2(\sigma)$, $\eta_2 = \eta_2(\sigma)$, i.e., the model parameters are connected with the stress. According to the relationship

Table 12.5 The Burgers model parameters of Y1 slip zone soil

Sample number	Cell pressure (kPa)	D (kPa)	D_r	K (Pa)	G1 (Pa)	G2 (Pa)	η_1 (Pa.min)	η_2 (Pa.min)
Y1-1-11#	100	23.5	0.18	7.01E+06	3.08E+06	3.84E+06	1.30E+11	1.67E+09
		47	0.36	6.53E+06	2.88E+06	2.37E+06	3.12E+11	1.17E+09
		62.7	0.48	4.05E+06	1.72E+06	2.31E+06	1.60E+11	1.87E+09
		96.6	0.73	2.13E+06	1.51E+06	1.76E+06	9.83E+10	4.64E+08
Y1-2-12#	200	58.8	0.29	8.22E+06	4.13E+06	3.96E+06	2.66E+11	8.87E+08
		88.2	0.43	6.25E+06	2.11E+06	2.52E+06	2.06E+11	1.01E+09
		117.8	0.58	3.21E+06	1.77E+06	1.82E+06	1.71E+11	7.67E+08
		158.6	0.78	2.22E+06	1.13E+06	1.86E+06	1.66E+11	1.82E+08
Y1-5-21#	300	39.2	0.14	1.86E+07	1.03E+07	7.06E+06	1.96E+11	1.86E+09
		78.4	0.29	1.23E+07	6.85E+06	6.93E+06	1.92E+11	3.16E+09
		117.6	0.43	8.25E+06	4.11E+06	5.41E+06	2.21E+11	3.17E+09
		137.2	0.50	6.84E+06	3.56E+06	4.47E+06	1.87E+11	2.68E+09
		176.4	0.64	4.23E+06	2.42E+06	4.09E+06	1.52E+11	3.22E+09
		215.6	0.79	3.48E+06	1.76E+06	2.87E+06	1.51E+11	1.79E+09
Y1-5-11#	400	58.8	0.17	1.85E+07	1.03E+07	8.10E+06	2.21E+11	2.36E+09
		117.6	0.34	1.11E+07	5.79E+06	8.14E+06	1.77E+11	2.95E+09
		156.8	0.46	8.27E+06	4.72E+06	5.51E+06	1.97E+11	3.22E+09
		176.4	0.51	7.11E+06	3.74E+06	7.85E+06	1.43E+11	5.96E+09
		215.6	0.63	6.55E+06	3.03E+06	5.30E+06	1.01E+11	3.36E+09

Fig. 12.23 Relationship between K and D_r
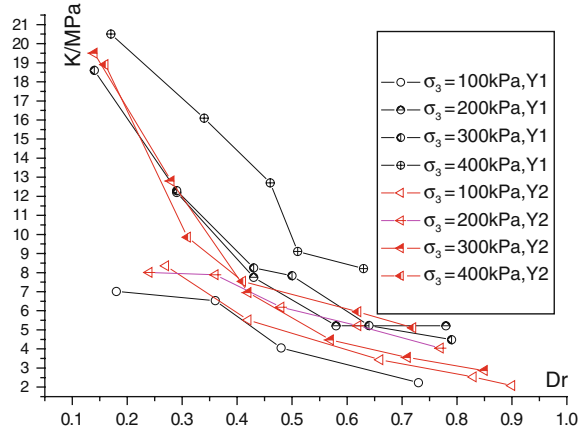
Fig. 12.24 The relationship between η_1 and D_r

$$\eta_1 = 2.506E11 - 1.215E11 Dr$$

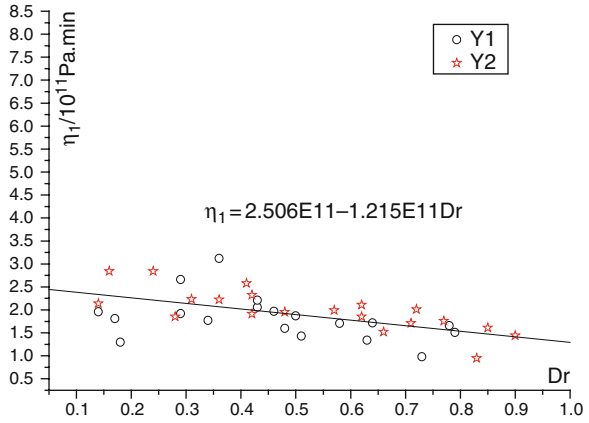$$Y = 3.192E\text{-}6 - 3.751E\text{-}6 * X + 1.036E\text{-}4 * X^2$$

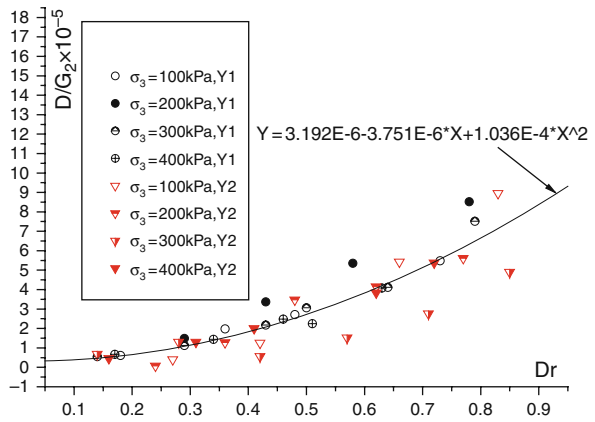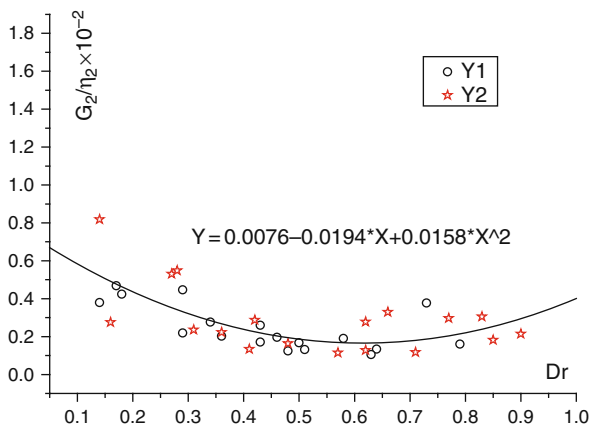**Fig. 12.25** The relationship between D/G_2 and D_r

Fig. 12.26 The relationship between G_2/η_2 and D_r

between the model parameters and D_r mentioned above, the formulas $G_2 = G_2(\sigma)$, $\eta_1 = \eta_1(\sigma)$, $\eta_2 = \eta_2(\sigma)$ can be expressed as follows:

$$\eta_1 = A_1 + B_1 D_r, \quad A_1 = 2.506 \times 10^{11}, \ B_1 = -1.215 \times 10^{11} \tag{12.3}$$

$$\frac{1}{G_2} = (A_2 + B_2 D_r + C_2 D_r^2)/D, \quad A_2 = 3.192 \times 10^{-6}, \ B_2 = -3.751 \times 10^{-6},$$
$$C_2 = 1.036 \times 10^{-4} \tag{12.4}$$

$$\frac{G_2}{\eta_2} = A_3 + B_3 D_r + C_3 D_r^2, \quad A_3 = 0.0076, \ B_3 = -0.0194, \ C_3 = 0.0158. \tag{12.5}$$

The K and G_1 reveal the properties of the instant stress of soil and can be calculated with the convection of E, μ, and G_2. The E and μ can be obtained by the compression tests. According to the Duncan–Chang model (Duncan and Chang, 1970)

$$E = K_a p_a \left(\frac{\sigma_3}{p_a}\right)^n [1 - \frac{R_f(\sigma_1 - \sigma_3)(1 - \sin\phi)}{2c\cos\phi + 2\sigma_3 \sin\phi}]^2 \tag{12.6}$$

$$B = K_b P_a \left(\frac{\sigma_3}{p_a}\right)^m \tag{12.7}$$

$$B = \frac{E}{3(1 - 2\mu)} \tag{12.8}$$

where $c, \phi, K_a, K_b, m, n, R_f$ are the parameters of Duncan–Chang model. The parameters of $K = K(\sigma), G_1 = G_1(\sigma), \eta_1 = \eta_1(\sigma), G_2 = G_2(\sigma), \eta_2 = \eta_2(\sigma)$ can be obtained through formula (12.3) to formula (12.8). Put all those parameters to formula (12.2), a three-dimensional nonlinear Burgers model can be obtained successfully.

Numerical Simulation of the Anlesi Landslide

Geological Model

In order to analyze the formation mechanism of the Anlesi landslide, numerical modeling of the landslide has been done from the viewpoint of the rheological properties of rock and soil. It is supposed that the topography of the Anlesi slope before sliding is similar to that after sliding. Based on the geological conditions of the Anlesi landslide, a geological profile before the slope sliding has recovered (Fig. 12.27). From the bottom to the top of the profile, seven layers exist.

Layer 1: the J_{2s}^{3-5}, mainly made up of feldspar–quartz sandstones;
Layer 2: the Y1 incompetent bed, the average thickness is about 0.3 m;
Layer 3: pelitic siltstone, the average thickness is about 10 m and it is in the middle of Y1 and Y2 incompetent beds;
Layer 4: the Y2 incompetent bed, the average thickness is about 0.3 m;
Layer 5: feldspar–quartz sandstone above the Y2 incompetent bed, the thickness is about 10–25 m;
Layer 6: the J_{2s}^{3-6}, J_{2s}^{3-7}, J_{2s}^{3-8} layers, located at the head of the landslide, mainly composed of feldspar–quartz sandstone; and
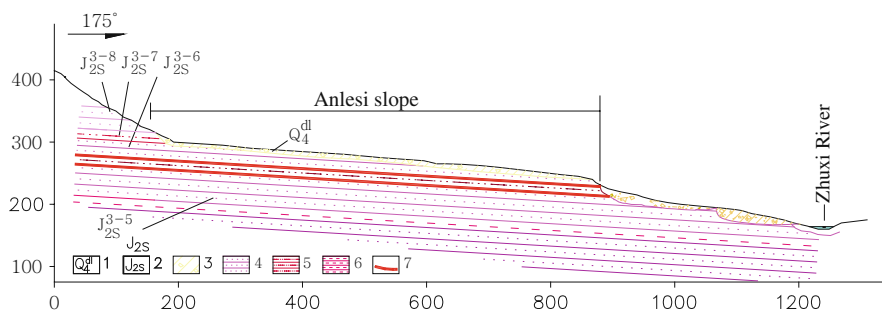Layer 7: residual and colluvial deposits above layer 5, the thickness is about 5–10 m.

Fig. 12.27 Recovered geological profile of the Anlesi slope before failure. 1 – Residual deposits; 2 – Jurassic Shaximiao formation; 3 – Clay with a few gravels; 4 – Sandstone; 5 – Siltstone; 6 – Mudstone; 7 – Incompetent beds

Meshes for Numerical Modeling

Based on the geological model, a two-dimensional numerical simulation was conducted on the Anlesi slope with FALC^{3D} software to analyze the stress and deformation of the slope before failure. In order to decrease the error, the range of the slope is much greater than that of the landslide. The coordinates for the model is
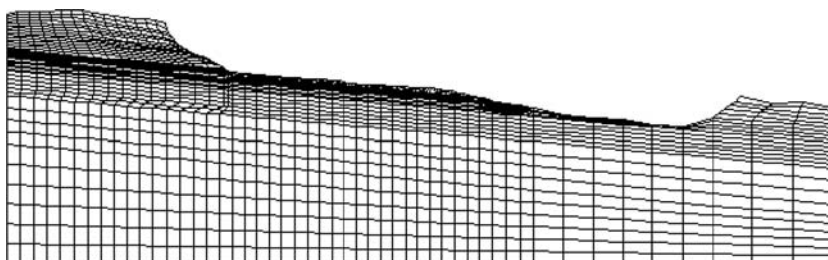
Fig. 12.28 Meshes for the Anlesi landslide numerical modeling

X (0, 2500), Y(–260, 490), and the coordinates of the landslide is X (640, 1540), Y (220, 310). There are 2691 elements and 5906 nodes. Figure 12.28 shows the two-dimensional meshes which generate for the numerical modeling.

Numerical Simulation Considering the Elastic–Plastic Properties of Rock and Soil

The properties of the materials occurring in the profile are shown in Table 12.6. Those parameters are mainly obtained from the experiments and other research (Wang 2008). The parameters of residual and colluvial deposits including layer 7 in the geological profile were obtained from the experiments of the reconnaissance on landslides in Wanzhou. The uniaxial tensile strength of feldspar–quartz sandstone including layers 1, 5, and 6 was calculated from the following formula:

$$\frac{S_c}{\sigma_t} = \frac{2}{[1 - \frac{\sqrt{2}}{2}\sqrt{(1 + tg^2\phi)(1 - \sin\phi)}](1 - \sin\phi)}$$

where S_c is uniaxial compressive strength, σ_t is uniaxial tensile strength.

The results show that principal stress is compressive in the slope (Fig. 12.29), and only at the head of the slope tensile stress occurs (Fig. 12.30). Under the elastic–plastic condition, the vertical displacement is about 20 cm, and the horizontal displacement is about 2 cm. The whole slope is in the elastic condition. Figure 12.31 shows the horizontal displacement of the Anlesi slope before the sliding. Therefore, the Anlesi slope is stable considering the elastic–plastic properties of rock and soil.

Numerical Simulation Considering the Rheological Properties of Rock and Soil

The creep properties of the materials occurring in the profile are shown in Table 12.7. Those parameters are mainly obtained from the experiments and from some research (Wang 2008; Wang et al. 2008). Because the thick and stable

Table 12.6 Elastic – plastic properties of rock and soil of the Anlesi slope

| Material	Location	Density (kg/m^3)	Cohesion(Pa)	Friction angles (°)	Bulk modulus (Pa)	Shear modulus (Pa)	Uniaxial compressive strength (Pa)
Colluvial and residual deposits	Layer 7	2100	2.00E+05	31.0	2.44E+08	1.03E+08	1.00E+04
Feldspar–quartz sandstone	Layers 1, 5, and 6	2479	6.63E+06	59.6	4.57E+10	3.68E+09	1.61E+06
Incompetent bed	Layers 2 and 4	2550	3.20E+04	26.8	1.30E+08	3.60E+07	3.00E+04
Pelitic siltstone	Layer 3	2503	3.64E+06	41.0	3.30E+09	1.59E+09	8.00E+05
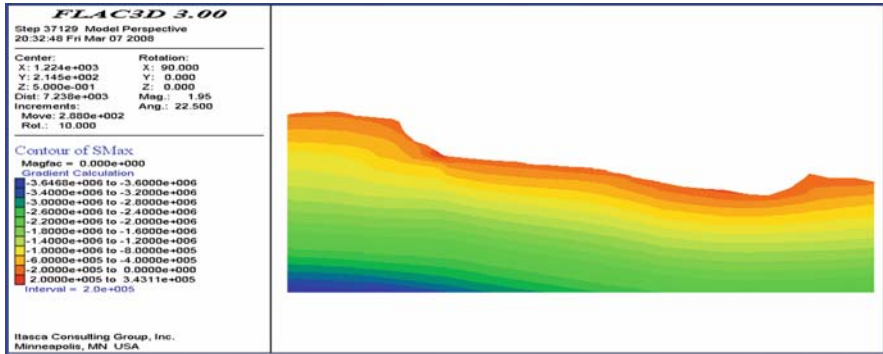
Fig. 12.29 The contours of principal stress at the Anlesi slope
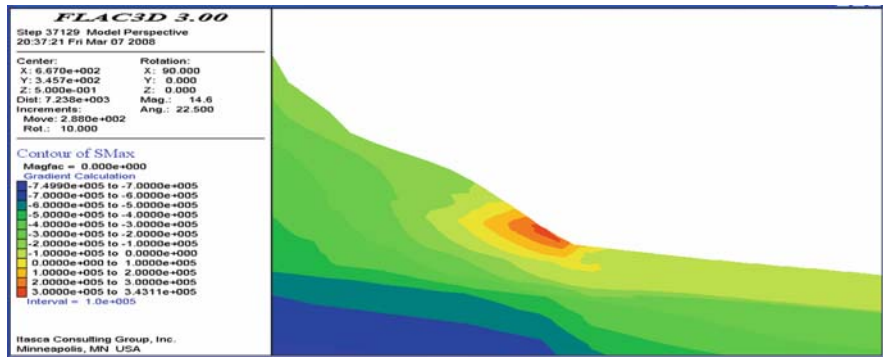

Fig. 12.30 The contours of principal stress at the head of the Anlesi slope
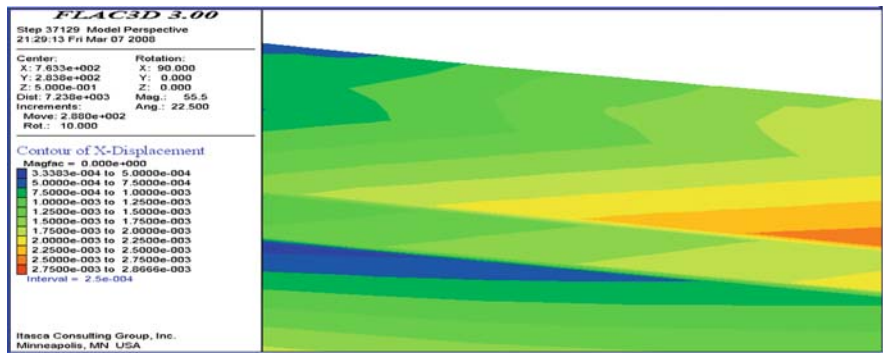

Fig. 12.31 The contours of horizontal displacement of the Anlesi slope near the incompetent beds

Table 12.7 Creep properties of rock and soil of the Anlesi slope

Material	Location	Cohesion (Pa)	Friction angle (°)	Bulk modulus /Pa	σ_t (Pa)	η_1 (Pas)	η_2 (Pas)	G_1 (Pa)	G_2 (Pa)
Colluvial and residual deposits	Layer 7	2.00E+05	31.0	2.44E+08	1.00E+04	1.00E+14	2.00E+12	1.10E+08	1.65E+09
Feldspar–quartz sandstone	Layers 1, 5, and 6	6.63E+06	59.6	4.57E+10	1.44E+06	1.51E+16	7.92E+14	1.62E+09	2.33E+10
Incompetent bed (Y2)	Layer 4	2.35E+04	15.2	1.30E+08	3.00E+04	1.55E+13	3.50E+11	3.98E+06	7.82E+06
Pelitic siltstone	Layer 3	3.64E+06	41.0	3.30E+09	8.00E+05	1.44E+15	7.20E+13	1.62E+09	2.33E+10
Incompetent bed (Y1)	Layer 2	2.30E+04	16.4	1.30E+08	3.00E+04	1.18E+13	1.93E+11	4.72E+06	5.51E+06

incompetent beds have become mud under the tectonic effect, the creep parameters of Y1 and Y2 incompetent beds before sliding is considered the same as that of the slip zone soils. Therefore, the creep parameters of Burgers rheological model for the two incompetent beds are obtained from the creep experiments on the slip zone soils. Because the Burgers model can describe both stress creep and stress relaxation, the civic model was used to simulate the rheological properties of Anlesi landslide with FLAC3D software.

The average depth of incompetent beds of Anlesi landslide is about 20–30 m. The average vertical stress is about 500 kPa, the consolidation stress is about 400 kPa, and the deviator stress is about 140–180 kPa. Therefore, the cell pressure of about 400 kPa and the deviator stress of about 156 kPa were used for calculating the parameters of slip zone soils.

The viscous coefficient of the pelitic siltstone which is between Y1 incompetent bed and Y2 incompetent bed was obtained from the research on the bank slope stability during the "7.5" period. The parameters of residual and colluvial deposits were obtained from experiences.

The two-dimensional creep calculation began from elastic–plastic equilibrium, and the maximum creep time is 200 years. The rules of the distribution and time change of stress, displacement, and plastic area were discussed here. Considering the rheological properties of rock and soil, the principal stress is compressive in most part of the slope after 10-year creep (Fig. 12.32). Only at the steep head does tensile stress concentrate. Compared with the elastic–plastic model, the area of the tensile stress is larger, the maximum tensile stress is bigger and reaches to 440 kPa. The stress on half of the slope is tensive after 20-year creep. There exist two areas of the slope where the tensile stress concentrates. One area is located at the main scarp of the slope and the other is at the head of the slope (Fig. 12.33). The maximum tensile stress is about 744 kPa. The stress on the whole slope is tensive after 50-year creep. The maximum tensile stress is located at the sandstone at the head of the slope and it is about 940 kPa (Fig. 12.34). At the surface of residual and colluvial deposits, the stress is still in compressive condition. Under 3 m, the stress becomes tensive,
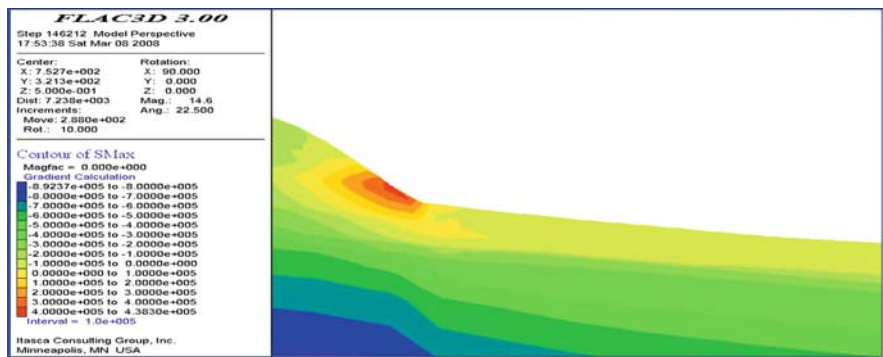

Fig. 12.32 The distribution of principal stress after 10-year creep in the Anlesi slope
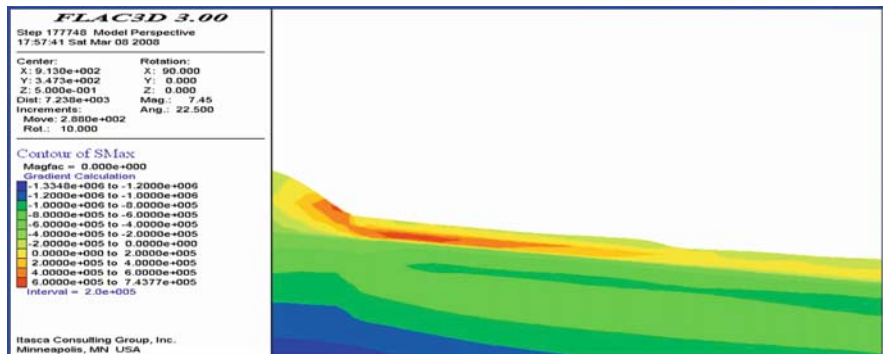
Fig. 12.33 The distribution of principal stress after 20-year creep in the Anlesi slope

and the value is about 0–50 kPa. The displacement of the slope changes with the creep time varying. The displacement of the slope sliding along incompetent beds is visible after 5-year creep. The displacement at the foot of the slope is greater than that at the head of the slope (Fig. 12.35). The displacement increases with the creep time becoming longer. The maximum displacement at X-direction reaches 7.59 m after 200-year creep (Figs. 12.36 and 12.37). Figure 12.38 shows the relationship between the surface displacement and time. A linear relationship can be seen from the figure. The direction of the sliding is parallel to the layer beds.

The slope is under the elastic condition after 5-year creep except for the Y1 and Y2 slip zones where the partial shear failure occurs (Fig. 12.39). Partial shear failure occurs at the main scarp after 10-year creeping, and the tensile failure occurs in the feldspar–quartz sandstone at the head of the slope. The tensile failure place occurs in the feldspar–quartz at the head of the slope after 50-year creeping (Fig. 12.40). The tensile stress area extends to the ground after 100 years of creeping (Figs. 12.41 and 12.42). The plastic area extends to the ground and the feldspar–quartz is separated from the bed rock at the head of the slope, and the whole slope fails completely.
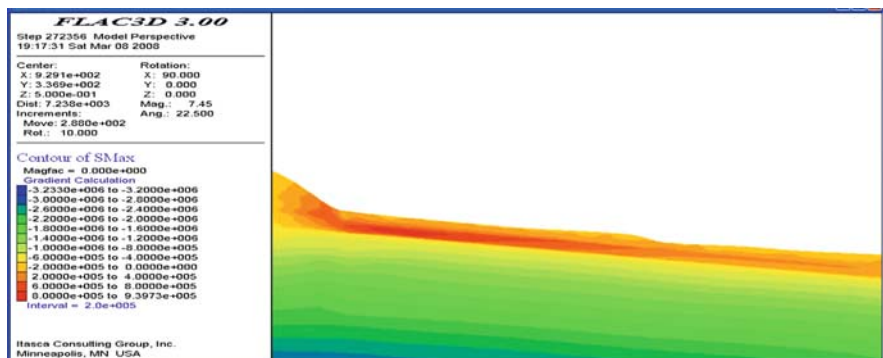
Fig. 12.34 The distribution of principal stress after 50-year creep in the Anlesi slope
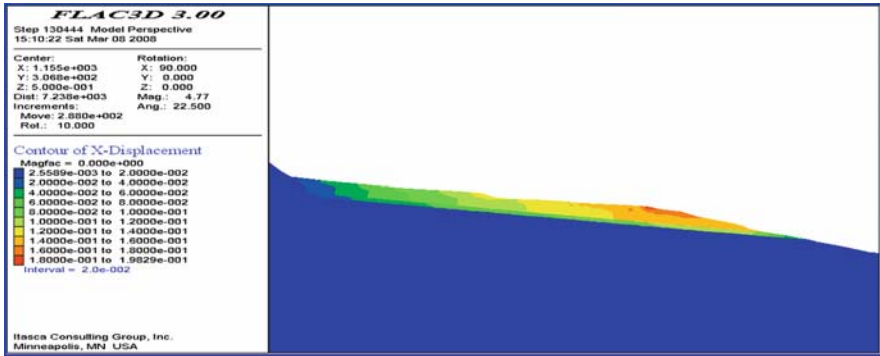
Fig. 12.35 The displacement in the *X*-direction after 5-year creep in the Anlesi slope
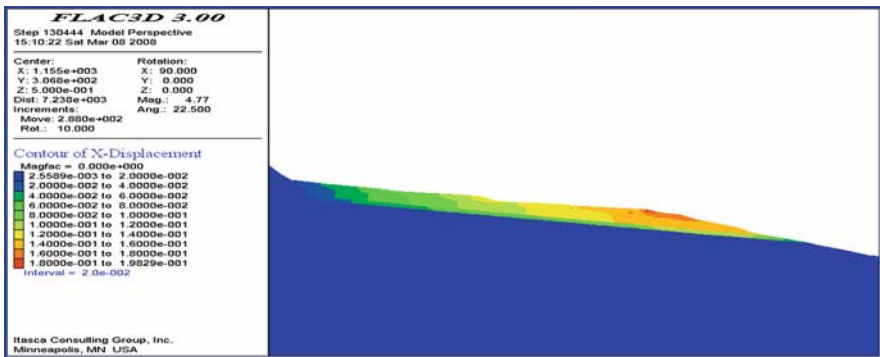
Fig. 12.36 The displacement in the *X*-direction after 50-year creep in the Anlesi slope

Fig. 12.37 The displacement in the *X*-direction after 200-year creep in the Anlesi slope

Fig. 12.38 The displacement of Anlesi slope versus time change
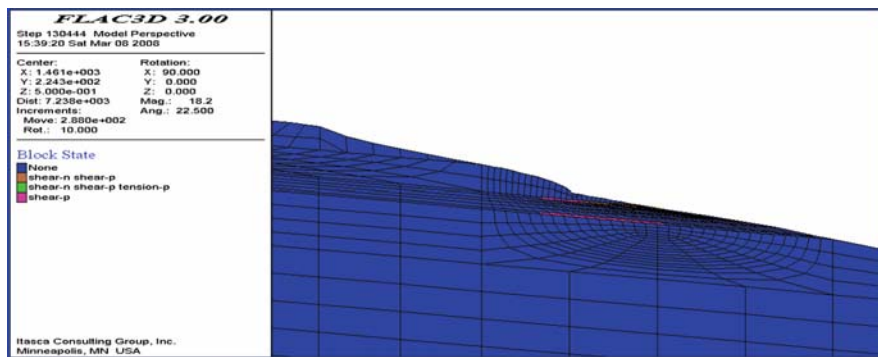
Fig. 12.39 Plastic deformation of incompetent beds at the slope toe after 5-year creep at Anlesi slope
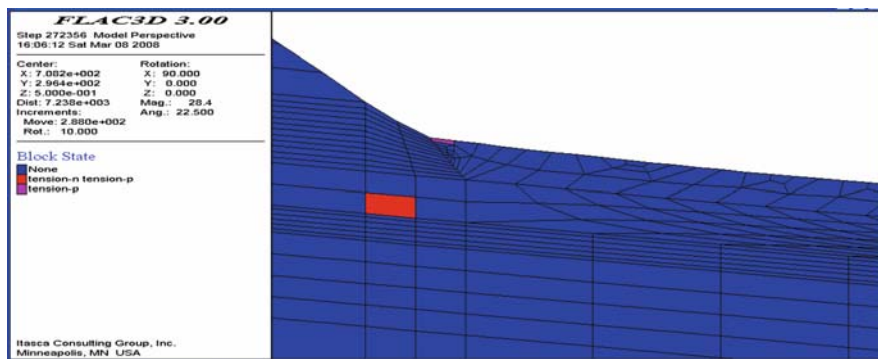
Fig. 12.40 Tensile failure of sandstone at the head of the slope after 50-year creep in the Anlesi slope
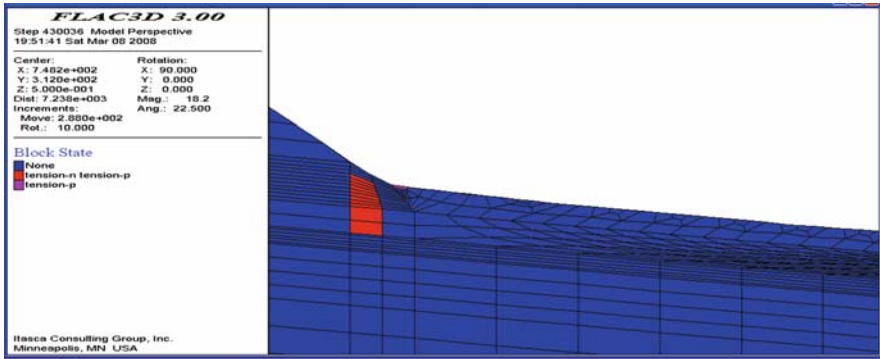
Fig. 12.41 Tensile failure of sandstone at the head of the slope after 100-year creep in the Anlesi slope

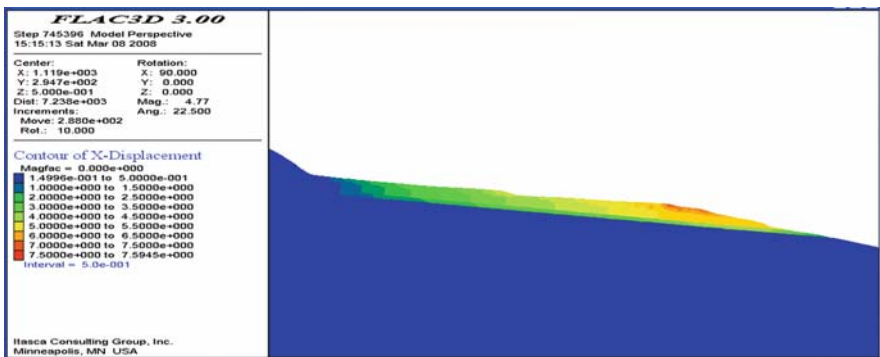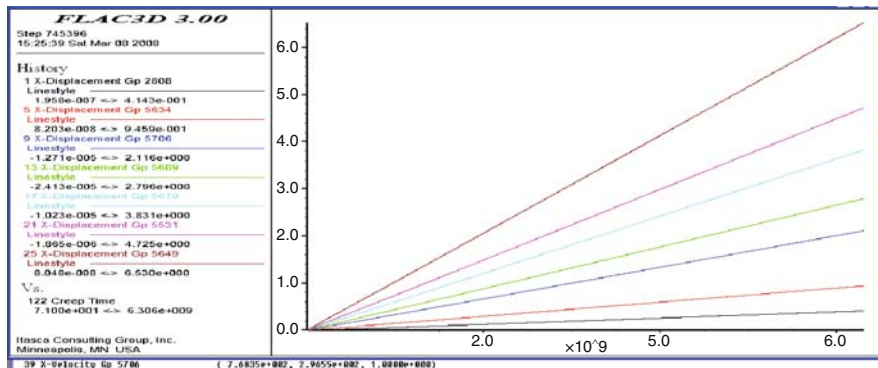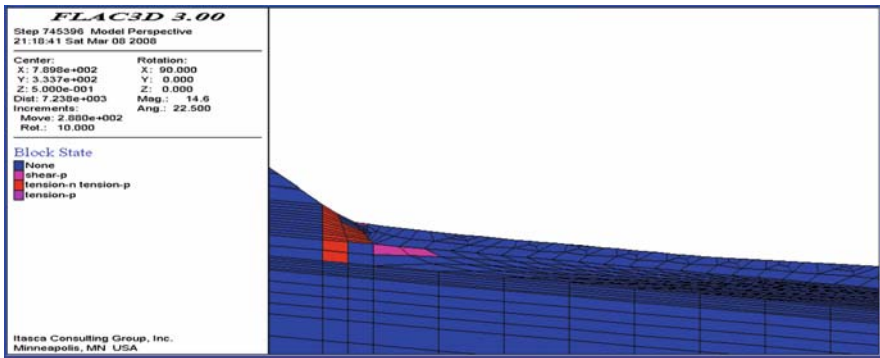**Fig. 12.42** Tensile failure of sandstone at the head of the slope after 200-year creep in the Anlesi slope

Conclusions

(1) The Anlesi landslide is a typical gentle dip rock landslide in Wanzhou in the Three Gorges Reservoir area. The slip zones of the Anlesi landslide formed from a white mudstone in Jurassic red strata by compressive stress. The main mineral components of the slip zones are composed of montmorillonite, illite, feldspar, and quartz. The slip zones are potential medium-swelling silty clay, and shear strength becomes very low once the slip zone attracts water to saturation.

(2) The main factors contributing to the gentle dip landslides are incompetent beds, recent tectonic activities, and intensive rainfall. First, the integrity of incompetent beds was broken under tectonic stress. Then, the latest tectonic activities cause shear failure along the incompetent beds and joints in the sandstone. With the effect of intensive rainfall, water permeates to the incompetent beds along tectonic fissures, resulting in swelling in the incompetent beds and high

hydrostatic pressure in fissures of the strata. As a result, the slopes are prone to slide along the incompetent beds.

(3) Creep test results prove that the stages of creep attenuation and even rapid creep can be seen clearly from the creep curves. The parameters of the Burgers model have been affected by deviator stress and cell pressure. The rheological properties of the slip zone soils have nonlinear characteristics, and the nonlinear Burgers model formula was obtained successfully.

(4) The simulation results show that the stress, displacement, and plastic area of the Anlesi slope changes with varying creep time. The maximum displacement at X-direction reaches 7.59 m after 200-year creep. Therefore, the formation mechanism of Anlesi landslide can be illustrated from the viewpoint of rheological properties of Jurassic red beds.

References

Chen XC, Huang JB, Yuan YX (2004) Structural characteristics of rock drop accumulation and transformation type of slopes failure. The Chinese Journal of Geological Hazard and Control 15(1): 5–10 (in Chinese)

Cheng Q, Zhou YJ, Huang SB (2004) Distortion and failure character of excavation slope in approximate level red beds. Soil and Rock Mechanics 25(8): 1311–1314 (in Chinese)

Cui ZQ (1993) An introduction on safety evaluation of the Three Gorges Reservoir shores. Wuhan: Bureau of Geotechnique of Changjiang Water Resources Commission, pp. 92–131 (in Chinese)

Duncan JM, Chang CY (1970) Nonlinear analysis of stress and strain in soils. Journal of the soil Mechanics and Foundations Division, ASCE, 96(5): 1629–1653

Gao SJ (1992) Stress field and earthquake of earth crust in Three Gorges reservoir of Yangtse river. Beijing: Geology publishing company, pp. 18–31 (in Chinese)

Huang RQ, Zhao SJ, Song XB (2005) The formation and mechanism analysis of tiantai landslide, Xuanhua county, Sichuan province. Hydrogeology & Engineering Geology 32(1): 13–15 (in Chinese)

Jian WX, Cheng CJ, Yin KL (2007) Primary investigation of characteristics and formation mechanism of Minguochang landslide. 1st North American Landslide Conference, June 3–8, 2007. Vail Marriott Mountain Resort & Spa, Vail, Colorado, USA, pp. 1628–1636

Jian WX, Yin KL, Yan TJ (2005a) Characteristics and formation mechanism of Minguochang landslide in Wanzhou District. The Chinese Journal of Geological Hazard and Control 16(4): 20–23 (in Chinese)

Jian WX, Yin KL, Zheng L (2005b) Formation mechanism and slide prevention methods of soil deposits at the toe of Anlesi landslide in Wanzhou. Earth Science-Journal of China University of Geosciences 30(4): 487–492 (in Chinese)

Jian WX, Yin KL, Ma CQ (2005c) Characteristics of incompetent beds in Jurassic red clastic rocks in Wanzhou. Rock and Soil Mechanics 26(6): 901–905 (in Chinese)

Liao QL, Li X, Lee S, et al. (2005) Occurrence, geology and geomorphy characteristics and origin of Qingjiangping landslide in Three Gorges Reservoir area and study on ancient landslide criterion. Chinese Journal of Rock Mechanics and Engineering 24(17): 3146–3153 (in Chinese)

Liu HX, Wang XB, Wang YP (2002) Landslide features and stability analysis of horizontally bedded rock mass in the TGP reservoir area. Yangtze River 33(5): 18–20 (in Chinese)

Luo C, Yin KL, Chen LX (2005) Probability distribution fitting and optimization of shear strength parameters in sliding zone along horizontal-stratum landslides in Wanzhou City. Chinese Journal of Rock Mechanics and Engineering 24(9): 1588–1593 (in Chinese)

Nanjiang team of Sichuan Geology and Mineral Bureau (1987) Geotechnical Exploration Report of Wanzhou Landslides in the Three Gorge Reservoir (in Chinese)

Peng XF, Li YS (1995) Characteristic of Douyapeng landslide, Wanxian county and it's control. The Chinese Journal of Geological Hazard and Control 6(1): 68–73 (in Chinese)

Qiao JP (1994) Douyapeng landslide in Wanxian city, Sichuan province. Mountain Research 12(4): 213–218 (in Chinese)

Qu SQ, Yang CY (1998) Effect of underground water on the stability of douyapeng landslide in Wanxian, Chongging. Journal of Chongqing Jiao Tong Institute 17(3): 106–111 (in Chinese)

Standard of People's republic of China (1999) GB/T50123, Standard for soil method (in Chinese)

Sun YZ, Su AJ, Wang JH (2002a) Characteristics of shear failure surfaces of Heping square landslide. Yangtze River 33(6): 15–16 (in Chinese)

Sun YZ, Zhang QX, Wang YP (2002b) Substance characteristics and significance of accumulation of Heping Square landslide of Wanzhou in the Three Gorges Reservoir region. Hubei Geology & Mineral Resources 16(4): 25–27 (in Chinese)

Tan ZD, Bao JS (1991) Evaluation of Earth Crust Stability and Prediction of Earthquakes Triggered by Reservoir in Three Gorges Reservoir of Yangtse River. Beijing: Geology publishing company, pp. 25–28 (in Chinese)

Tang DK (1997) Application of engineering geology system on stability analysis of landslides in Wanxian. Ren Min Chang Jiang 28(1): 33–36 (in Chinese)

Wang ZJ (2008) Rheological Experimental Study and Mechanism Research on Gentle Dipped Landslides of Jurassic Red Strata in WanZhou City. Ph.D. dissertation of China University of Geosciences, pp. 74–103 (in Chinese)

Wang ZJ, Yin KL, Jian WX (2008) Experimental study on rheological behaviors of Wanzhou red strata in Three Gorges Reservoir area. Chinese Journal of Rock Mechanics and Engineering 27(4): 840–847 (in Chinese)

Wu SM, Li RG (1994) Numerical simulation on formation mechanism of Wanxian landslide groups. Hydrogeology & Engineering Geology 21(6): 17–21 (in Chinese)

Xiong CR, Tang HM, Liu BC (2007) Using SEM photos to gain the pore structural parameters of soil samples. Earth Science-Journal of China University of Geosciences 32(3): 415–419 (in Chinese)

Yang MD (1988) Origin and evolution of Three Gorges of Yangtse river. Journal of Nanjing University 24(3): 466–473 (in Chinese)

Yin KL, Jian WX, Wang Y, et al. (2007) Formation Mechanism and Prevention Methods of Landslide Sliding Alone Horizontal Strata in Wanzhou. Wuhan: The publishing House of China University of Geosciences (Wuhan), pp. 39–64 (in Chinese)

Yuan CH, Ni J (2004) Treatment and characters of red sandstone landslides in expressways. Soil and Rock Mechanics 25(5): 745–748 (in Chinese)

Zhang JX, Jiang SH (2001) A brief discussion on properties of swell soil and stability of foundation in Dangyang-Yichang speedway. Earth Science-Journal of China University of Geosciences 26(4): 424–428 (in Chinese)

Zhang YM, Liu GR, Chang H (2004) Geological analysis of Qiangjiangping landslide in Three Gorges Reservoir. Yangtze River 35(9): 24–26 (in Chinese)

Chapter 13
Preliminary Study on Mud-Rock Flows Channel of the Bailuxi River, Wuxi County, China

Lide Chen, Zhoufeng Chen, and Xuanming Peng

Abstract   The Bailuxi River is located in the mountainside of Dabashan Mountain and to the west side of the watershed of the Daninghe River and the Duhe River. It is at the southeast edge of an area of heavy rainfall in the centre of the Qinba mountainous region. For reasons of its climatic environment and the existence of a sufficient supply of sediments and large reserves of such in the river reaches, the human engineering and economic activity have become more and more intensive, resulting in an increase in hazardous environmental and geological conditions for mud-rock flows to occur in the Bailuxi River. Since the mud-rock flows there constitutes a direct threat to the inhabitants' life and property safety in Bailu Town and its bank downriver of the Daninghe River, attention and concern for the hazardous condition are necessary. Through investigation, it has been found that the mud-rock flow channel of the Bailuxi River consists of the main mud-rock flow channel and its branches, the Yangjiawan branch of the mud-rock flow channel being the largest, the most dangerous, and potentially the most damaging one. The branch channel is a frequent mud-rock flow channel at a small scale, but during certain conditions, a large mud-rock flow at a considerably large scale could possibly occur. The primary channel flow of a large-sized scale is of low frequency and it is only triggered by large-sized mud-rock flows occurring in the branch channels. The deposit in the area of Bailu is the accumulation of the mud-rock flows that have erupted previously.

Keywords   Bailuxi River · Mud-rock flows · Stability

Introduction

Bailuxi River is the primary branch of the left bank of the Daninghe River at Bailu Town, Wuxi County. The T-shaped Bailu Town is distributed along the entrance of the Bailuxi River and the left bank of the Daninghe River. The fan-shaped mud-rock

L. Chen (✉)
Yichang Center of the China Geological Survey, Yichang 443003, China
e-mail: brianchenlide@yahoo.con.cn

flow deposits at the east side of Bailu Town are densely inhabited as it is as flat as a pancake, and the land there is easy to cultivate and it is a convenient transportation corridor. Zhushaping Village, Daping Village, Houping Village, Erping Village and other villages as well as Bailu Town are located around the interior channel and the channel entrance areas. A high-level road, Wuxi-Shiyan road (shortened to "Wushi Road" hereinafter) that is newly built, crosses the mud-rock flow channel area (Chen et al. 2007).

The mud-rock flow hazard of the Bailuxi River is not taken seriously by the local government, inhabitants or the "Wushi Road" project construction department. Some sections of Wushi Road and its bridges are built in the Yangjiawan branch channel, where the Houping villager committee building and the charity house for the old people are located. These facilities, which are threatened directly by the mud-rock flows from the branch channel, have been recently built on the mud-rock flow tongue-shaped deposit of the Yangjiawan branch channel. Although the fact that homes were damaged by the mud-rock flow that erupted over 170 years before and the knowledge has been known through succeeding generations, the inhabitants there are not concerned, since no large-sized mud-rock flow has erupted in more than a century. Some villagers even built their houses on the potentially unstable, direct flow channel of a mud-rock flow. In the downstream area of the Daninghe River, from the section of Bailu Town, there are thousands of inhabitants who live along the left bank by the road, and as this area has a greater density for inhabitants in Wuxi County. Therefore, the investigation and analysis on the Bailuxi mud-rock flow channel as well as the forecast for the possible dangers caused by the future mud-rock flow relates directly to the life, properties and safety of local and down-river inhabitants and traffic-flow among these areas is at significant risk.

The Bailuxi River mud-rock flow channel is approximately 4 km away from the rear section of the Jiandaoxia reservoir that is planned for construction. We made relevant investigations for the Bailuxi River mud-rock flow channel to evaluate the adverse affects that could be caused by a Bailuxi River mud-rock flow into the reservoir and onto the Shenjiping (or Tanmu) pump station which is a part of the Daninghe River Water Increase Project for the Centerline of South–North Water Transfer Project. However, given the limited initial scope and depth of the project, the investigation at this time is only to forecast and evaluate qualitatively the danger of the mud-rock flow channel using the geological genesis mechanism analysis method.

Physical Geography, Geology and Geomorphology Background

Physical Geography

Located in the area of Wuxi County, Chongqing City, the Bailuxi River originates from the west side of the Dabashan Mountain watershed at the joint boundary of Chongqing and Hubei province (Fig. 13.1). The river drainage area reaches in a west-eastern direction, is 7.50 km long from the east to the west, 7.0 km wide from
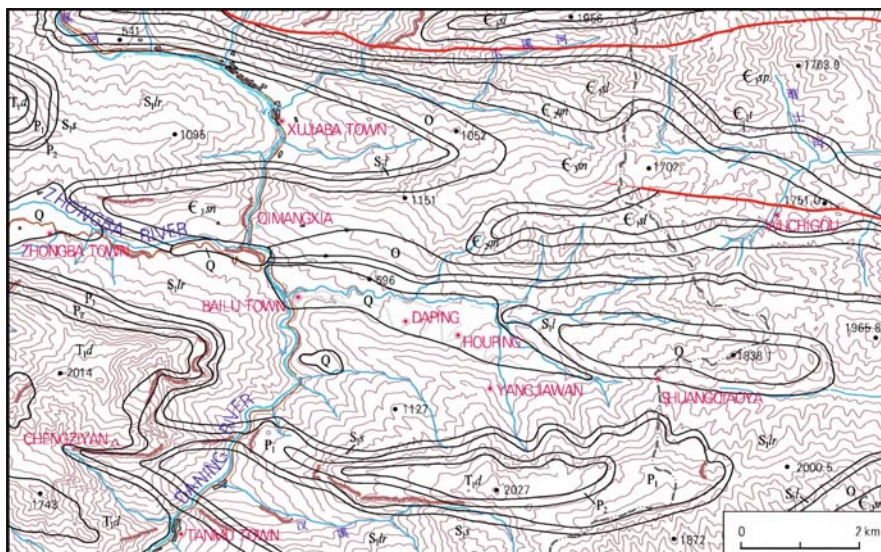
Fig. 13.1 Regional geologic and topographic map of mud-rock flows channel of the Bailuxi River (For the abbreviations refer to Appendix A, Stratigraphic Column in Three Gorges Area (modified from Yin 2004).)

the south to the north in its upper reaches, but 1 km wide in its lower reaches. It is similar in shape to, and looks like a funnel. The overall descent of the river is 1,300 m (1,700–1,400 m), the average falling gradient of the riverbed is 198.7‰ and the catchment area is 29.2 km². The average height above sea level of the watershed in the river reach is 2,200 m, the highest altitude is 2,314.4 m, the elevation at the opening of the channel is 366 m and the maximum height difference is 1,948.4 m.

The Bailuxi River is located in the middle latitudes region and belongs to a sub-tropical zone characterized by a warm, wet monsoon climatic region. The climate there frequently changes and the weather which is errant in spring features moist heat in summer, clear autumns and dry, cool winters. Due to the Qinling Mountain and Dabashan Mountain, the climate in the river reach is volatile and wet, with abundant rainfall. According to Wuxi County's weather station's statistics information, the average air temperature is 17.91 centigrade and its average annual rainfall is 1,097.6 m, and the upper reaches' average annual rainfall is 1,333 mm in the region of the Daninghe River, which is located in the southeast edge of the Qingba rainstorm centre. The rainstorm season is primarily in the summer for the months of July, August and September.

Geomorphology

The dendritic drainage of the Bailuxi River is funnel-shaped; it originates from the Duanshuwan in the east. At the right bank of the Bailuxi River, there are three branch
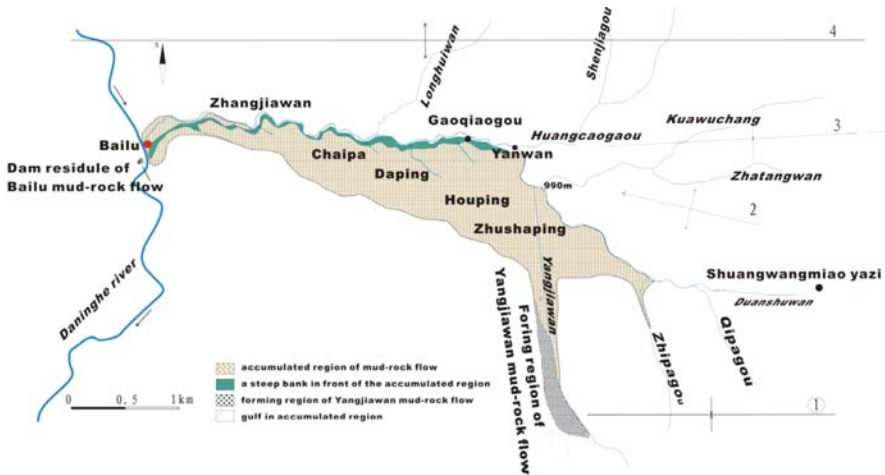
Fig. 13.2 Map showing the plane of the Bailuxi mud-rock flow. 1 – Chenziyan syncline; 2 – Shuangqiaoya anticline; 3 – Wuchigou syncline; 4 – Qimangxia anticline

channels from the top to the bottom, i.e. Zhatangwan, Huangcaoguo, Longhuiwan, while the branch channels of the left bank are Qipawan, Zhipawan and Yangjiawan from the top to the bottom in a natural bend (Fig. 13.2).

The area where the branch channel of the right bank of the Bailuxi River flows across is distributed Cambrian, Ordovician and lesser amount of Silurian strata. The channel bed material is mainly conveyed away through water flow annually, which provides limited solid rock fragment material to the mud-rock flow of the main channel, but compensates the water source for it. The geomorphology and geological characteristics of the left bank branch channel of the Bailuxi River makes the channel branch conducive to mud-rock flows, especially the Yangjiawan mud-rock flow. The Yangjiawan is the left bank branch of the Bailuxi River, where there is a narrow channel valley and a precipitous slope; it flows slightly northwards for 3.6 km, where it is 1.2 km distant from the mountain exit to the mud-rock flow deposit downstream. The total fall of the Yangjiawan branch channel is 1,200 m, the average gradient is 333‰ and the drainage basin area is 2.9 km^2.

Lithology

The rock in the surveyed area is distributed east-westwards, where there are exposures of the stratum of Cambrian limestone, Ordovician limestone and Silurian clastic rock (named Luoreping Formation). Permian limestone is interspersed with coal bed and Triassic limestone (named Daye Formation) and others from the north to the south, located in a natural bend.

The Silurian clastic rock in the Shuangqiaoya anticline wing section spreading to the west has been greatly deformed under pressure; the shape of rock layer is rather steep, and in some cases are overhanging cliffs. The broken rock is inclined to effloresce and an inverted relief formed accordingly. It forms a valley in the anticline area and forms a mountain in the syncline area, which provides ideal environmental geological conditions for the unstable physical geology phenomena in the river reach, which are falls, landslide, water and soil loss and so on; whereas the erratic distribution of weathered and etched Silurian stratum in both banks and the upper reach of Bailuxi River provides the setting and sufficient material source for the initiation of mud-rock flows.

The Cambrian, Ordovician, Permian and Triassic Period strata that are shown in the river reach is hard dolomite and limestone, is weathered slowly, but forms high and steep cliffs in general, which are inclined to fall and form landslides, while triggering other unstable geological phenomena.

Tectonics

The middle and upper reaches of the Daninghe River is located in the arc structural pressured belt of south Dabashan Mountain, consisting of a series of near east-western and compact arc drapes and fault block clusters. The drapes spread from the near west-east to slightly south to form an arc, all of which are asymmetry. The rock layer is mostly steep, of which some are overhanging, and the folds become closer and closer as it trends to the north. The relief is also reversed with syncline mountain and anticline valley, and the recent tectonic movement of the area is characterized by intermittent uplift.

The Qimangxia anticline is located on the north side of the Bailuxi River and trends west-eastwards (with the dolomite and limestone of upper Cambrian Sanyoudong Formations). In the corners and in both wing sections is the Ordovician (O) limestone intercalated with clastic and Silurian (S) clastic rock. The north extension of the Qimangxia anticline is almost upright, but the south wing is of medium obliquity to the south. At the east end of the Bailuxi River is the Shuangqiaoya anticline which plunges westwards with the Ordovician at the core, but the stratum in the south section is reverse. North of the Shuangqiaoya anticline, the Wuchiguo syncline occurs with the Silurian at the core. The Wuchiguo syncline is becoming narrow in the west direction, but widening in the east.

South of the Shuangqiaoya anticline is the Chengziyan syncline with the Permian and Triassic strata at the core. The Chengziyan syncline is surrounded by the Silurian- and Permian-age material together with the Triassic Daye Formation, whereas the Silurian and Permian strata constitute a sharp-edge drape. The Triassic stratum constitutes the core of the syncline which has a flat occurrence. The typical constitution between the Permian and Triassic systems is the prostration phenomena, the inferior folds developed inside the Silurian with north northeasterly

and northeast-trending cracks and joints that are well developed, and the rock are broken and easily to be weathered.

Vegetation, Cultivation and Human Activity

The forest vegetation in the river reach of the Bailuxi River is sparse in coverage. In the area of the watershed of the east side in the upper reach, the vegetation cover over the areas where the Silurian clastic rock is located is damaged completely, whereas the Silurian system at both sides in the north and south of the river reach has sparse shrubbery and the base rock is mostly exposed. The slope formed by the Silurian system and the deposit remains in the upper reach of Yangjiawan branch channel is farmland, where the bushes are thinly scattered. The vegetation in the area of limestone stratum grows more densely among the cliff and steep wall formed by the Permian, in comparison with the Triassic limestone in the upper reach of Yangjiawan Branch River, where there is less forest.

Recently, the human activity in the Bailuxi River area reach is increasing. The Wushi high-level road that is being built across the mud-rock flow channel crosses the watershed of Dabashan Mountain. The main structure of the road is located in the slope on the left bank of the Bailuxi River; the waste slag caused by cutting the slope to build the road is piled mostly in the big and small channels. Since all of this can be washed away, there will be no opportunity for a mud-rock flow to occur. Some sections of the in-building road goes across the Bailu mud-rock flow deposit, especially where it extends over the Yangjiawan branch channel and Duanshuwan branch channel in the upper reach of the Bailuxi River. Not enough attention has been paid as to its vulnerability, i.e. first, some road and bridge location changes have been made, which causes a fairly large economic loss; second, the newly built bridge was not considered a factor in the issue of whether it is a problem for the mud-rock flow, and the protection requirement, and the location of a pier, was not adequately considered when it was chosen. It is not built in the channel, which is rather dangerous if mountainous flood and mud-rock flow erupts.

Distribution and Growth Features of Mud-Rock Flow

The features of the physical geography and geological character of the left bank branch channel of the Bailuxi River are determined to be the branch channel for which the conditions for mud-rock flow occur and increase in size. Actually, the Duanshuwan branch, the upper reach of the Bailuxi River and the Qipawa, Zhipawan and Yangjiawan, on the left bank branch channels, are the mud-rock flow channels that are hazardous. The Yangjiawan is the biggest and the most dangerous and destructive one. The general features of the deposit in many cross-sections of the mud-rock flow have multiple stratum indicating that the branch channels are the highest frequency mud-rock flow channels (although individually, are small in scale), but under certain conditions, a considerably larger scale mud-rock flow can

possibly erupt. The main channels are of the lowest frequency, each possibly occurring every 100 to 200 years which can become increasingly hazardous by the addition of the branch channels' large-sized mud-rock flows. The accumulated mud-rock flow deposits in the area east of Bailu Town are the combination of the mud-rock flows erupted previously.

The mud-rock flows erupted from branch channels deposited at Zhushanping, Houping and Daping at the east side of Bailu Town. The fan-shaped deposition area of mud-rock flow forms an irregular triangle spreading from the east to the west. It ends at the middle and lower reaches of Bailuxi River, at the north side, at the upper reach of the Bailuxi River, and the place from Duanshuwan to Huangcao channel, opening in the northeast. At the south side, it is separated completely by the precipitous slope formed by the obvious geological boundary and the Silurian stratum, then forms a splaying channel with shallow cuts along the boundary. The deposit is brushed and etched frequently by the water flow of the Bailuxi River at its north side. The front side forms a precipitous ridge with different heights from 10 to 60 m at the left bank of the Bailuxi River and from the upper to the lower reaches.

The area of the opening of the Bailuxi River, where Bailu Town is located, and the place of Erping at the east side is the accumulation region of the mud-rock flows of the Bailuxi River main channel. It has been found in field investigation that a mud-rock flow erupted once before in the main channels, and today we can see in the field that there is a triangular-shaped dam remnant once formed by the Bailuxi mud-rock flow still standing on the right bank of the Daninghe River with its top at

Fig. 13.3 Triangular-shaped dam residual once formed by the Bailuxi mud-rock flow stands on the right bank of the Daninghe River. *Arrow* indicates the top which is about 25 m above the water

about 25 m above the water. The remnants of the Daninghe River dam can be seen (Fig. 13.3). It was formed by the mud-rock flows erupting in the main channel. It can be presumed that the mud-rock flow was rather considerable in size.

Analysis of the Yangjiawan Branch Channel Mud-Rock Flow

The Bailuxi River mud-rock flow consisted of the branch channel mud-rock flow and the main channel mud-rock flow, among which, the Yangjiawan is a branch channel that erupts mud-rock flow in a large scale of the most damaging capacity. It has distinct features for the formation area, flow area and deposit area for mud-rock flow. Nowadays, the local villagers are still in dread of the damage caused by the previous mud-rock flow; it remains mysterious to them to a certain degree.

The Mud-Rock Flow of the Yangjiawan Branch Channel

According to the investigation, a large-scale mud-rock flow erupted once before in Yangjiawan in 1834. The mud-rock flow damaged tens of houses built over the original deposit and then flowed towards the northwest direction along the Houping, Daping direction after scouring out the channel opening of Yangjiawan, and then damaged more tens of houses there, and submerged rice fields around Daping. After the mud-rock flow occurred, the mud flowed over the local villagers' wooden wall, which was as tall as an average person. It was found by the investigation that the eruption frequency of mud-rock flows in the Yangjiawan is 8–10 years, all of which were at a small scale. These small-scale mud-rock flows are mostly limited by channel size, when it enters into the Bailuxi River. The river valley becomes suddenly wider and the water amount increases too. The mud-rock flow materials will be then transported to the Daninghe River via the wide Bailuxi River, or this material will be moved to the lower reach, which is the Daninghe River, by means of water flow, and no subsequent damage will occur.

In the area around the mountain exit of the Yangjiawan branch channel, the right bank of the branch channel is a tongue-shaped mud-rock flow deposit with a width of almost 200 m, and it is 5–10 m higher than the normal water level of the Yangjiawan branch, which is now the deposit in the natural quarry, used for building road and houses for local people. For years, there has never been any large-sized flood or mud-rock flow that can reach these places. However, in view of the deposit composite and structure, the tongue-shaped deposit is a part of the moving and accumulated area of the Yangjiawan branch mud-rock flow. But since flat land for construction is in shortage in the mountainous area, the local inhabitants built the Villager Committee building and charity house for the old, on the tongue-shaped deposit. These two brick and concrete structures were built in 2004. The newly built Wushi high-level road goes across the mountain exit of the Yangjiawan channel valley after its original construction plan was changed. The bridge is at a higher level, 2–4 m over the riverbed, and the span of the bridge is 15 m. The bridge piers are located inside

Fig. 13.4 View of Yangjiawan River mud-rock flow region

the deposit, among which the right bank piers are located in the channel bed, which prevents the Yangjiawan branch channel from releasing floodwaters. All these structures are under a direct threat of a Yangjiawan mud-rock flow (Fig. 13.4).

Formation Area of Yangjiawan Branch Channel Mud-Rock Flow

The water system in the upper reach of the Yangjiawan River resembles the shape of tree branches. The watershed of the river reach is 1,954.7 m and its maximum height above sea level is 2,027.3 m. The elevation of the channel opening is 790 m, and thus the height difference between the maximum elevation and the channel opening elevation is 1,230 m. The area in the upper reach of the Yangjiawan River is the reverse landform formed by the Chengziyan syncline, which features a characteristic "soft at bottom but hard on the top" slope structure. The bottom layer features weak rock of Silurian clastic rock stratum and Permian Period with weak coal stratum at the base on top of the Silurian. The hard Permian and Triassic limestones at the top comprise most of the steep slope and they form a high and steep cliff; whereas the Silurian clastic rock and the Permian coal stratum at the bottom are inclined to be weathered and eroded, which make the top steep cliff subject to failure, as it is not adequately supported by the underlying weak layers. This loss of support can potentially cause landslides to occur, and this landslide material provides the source of the Yangjiawan mud-rock flows, which are primarily composed of weathered Silurian material.

The deposit in the upper reach of the Yangjiawan River is the solid material source of branch channel mud-rock flows. Under the steep slope area that is formed by the left bank in the upper reach of the Yangjiawan River (composed of Permian

and Triassic limestones), there is a large-sized clastic rock and soil deposit, its source being the weathered remaining deposit and the landslide deposit on the upper section of the slope. The deposit spreads along the Yangjiawan channel valley in an elongated, strip-like shape. It is at a large scale at the left bank with a length of 1,500 m, a width of 0–250 m (150 m on average), a height of 20–60 m (for the front ridge) and volume of 650,000 m^3. In comparison, the right bank is rather less. The deposit is eroded frequently by the water from the Yangjiawan channel valley, which caused the deposit to easily lose its basic stability. The front section of the deposit forms steep cliffs at a different height, and as it is short in the lower reach but high in the upper reach, some of the material occasionally falls. Under normal conditions, the fallen deposit will be moved to the lower reaches of the channel valley along with the water flow. Since the front ridge of deposit in the upper reach is steep, it is cut by multiple gullies (see Fig. 13.2).

The Movement and Accumulation Region of the Yangjiawan River Channel Mud-Rock Flow

The total length of the Yangjiawan mud-rock flow is 12 km, and the transaction of the channel valley is U-shaped. At both banks, the accumulative platform is at 1–3 level; the initiation area in the upper reach is 8 km long, where a complete first level accumulative platform is established. The fall distance differential between the top of the accumulative platform and the slope base is maximal; it reaches a height of 30–40 m. The deposit of the accumulative platform is composed of material containing mud and broken stone or broken stone and soil with block stone. The riverbed at the slope base is eroded frequently by water, where mostly clean broken stone with block stone are distributed. The rear edge of the accumulative platform is mostly the steep 50–80° limestone, characterized by a rocky slope or cliff. The slope angle of the side slope of the accumulative platform is uniformly 40–60°.

The movement area is 4 km long, whereas the height of accumulative platform at both sides is descending, in general. The height difference of 3–5 m is between this platform and the location of the Villager's Committee building in Houping village. However, since it is located in the lower reach of the Yangjiawan River, the water erosion is very intensive; but the side slope of the accumulative land is still steep as well with frequent slides still developing.

The middle and lower reaches of the Yangjiawan River is U-shaped, and the channel bed is 21–30 m wide. The steep ridge at both sides is 15–18 m high, almost upright. The channel is straight, and a 180 (‰) comparative decrease. The deposit there has clear stratum. One exposed section shows the structure of the Yangjiawan mud-rock flow which previously occurred (Fig. 13.5). It has six layers with a thickness of 0.9–2.5 m for each one. Tithe very bottom layer does not show at all, and the most top layer is very thin because of the rebuilding work that has occurred since. The composition and structure of the clastic rock and soil at each layer is very similar, and the change along the vertical direction between each layer is not clear. The soil composite is 30–40% approximately, most of the clastic rock is limestone, but the less-weathered Silurian clastic rock debris is less evident comparatively, is

Fig. 13.5 Part of the section showing the structure of the Yangjiawan mud-rock flow deposits. Each layer was made up of a thinner coarse layer and a normal one (the man is about 1.7 m tall)

mostly 3–10 cm in diameter and is about 60–70% of the broken stone material, with poor textual maturity. Some of these are greater than 1 m in diameter and the broken stone appears to be a "rubble wrapped by mud" phenomena (Fig. 13.6).
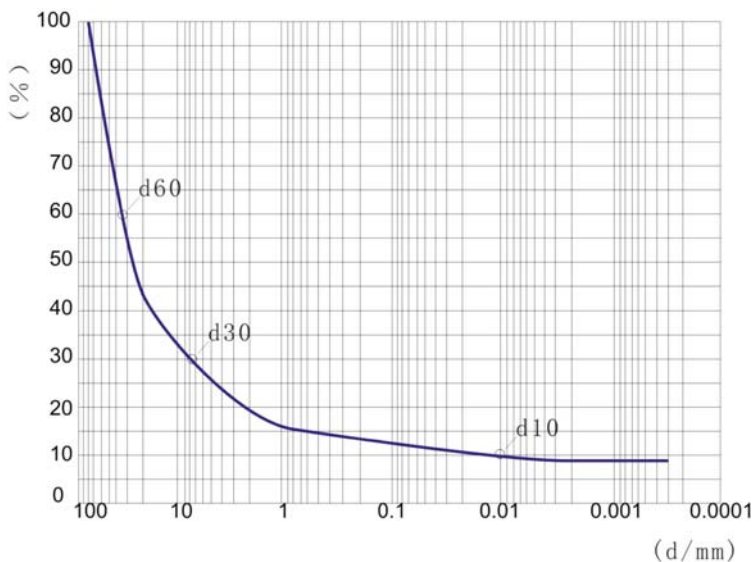

Fig. 13.6 Grain-size accumulation curve of the Yangjiawan mud-rock flow deposits (d/mm means the grain size in diameter and the unit is mm)

Fig. 13.7 Farmers rice paddy buried by the mud-rock flow that occurred historically

The farmland soil is 24–50 cm thick and spotty in its distribution. It exists over the section and is used for various activities. The soil layer is of a light brown color externally and is black on the interior (Fig. 13.7).

Two villages exist in the area from the mountain exit of the Yangjiawan channel to the west-north. These two villages, Houping and Daping, are located where the gravel is spread entirely over the farmland. The natural slope angle is 10–11° and spreads from the east to the west for 4 km in length to form a bevelled triangle (Fig. 13.8). The area at the north–south section of the mountain exit of the Yangjiawan River is widest, at about 1 km, and then becomes narrower and narrower to the exit of the Bailuxi River to about 200 m. There are several gullies over the slope of mud-rock flow deposit where Daping and Houping villages exist, all of them cut into a V-shaped channel facing the west-north section at the steep ridges at the front side of the deposit, there is a shallow and wide U-shaped gully inside the deposit, and its depth is between 2 and 4 m, with a width between 10 and 20 m.

Evaluation of the Probability of a Yangjiawan Branch Channel Mud-Rock Flow

The root cause of the Yangjiawan branch channel mud-rock flow is the formation and rainstorm-type channel valley mud-rock flow.

Investigations have shown that the massive landslide deposit in the area under the steep slope in the upper reach of the Yangjiawan channel valley is the source of material that would add to a high-velocity mud-rock flow in the Yangjiawan branch

Fig. 13.8 Triangle-shaped accumulated area of the mud-rock flow of the upper branch valley of the Bailuxi River at the confluence with the Yangjiawan. It is the biggest and the most dangerous mud-rock flow region

channel. The stability of the source deposit is the key factor which dictates the hazard. Undoubtedly, the Yangjiawan source material not only bursts into the mud-rock flow in a frequent and small scale, but under certain conditions, it is completely possible that a mud-rock flow can become a large-sized event. Meanwhile, the clastic solid material accumulates with time and the danger of the eruption of new mud-rock flow increases, proportionately. Since the human engineering and economic activity in the vulnerable area becomes more frequent than at any previous time, it can be forecasted that the damaging capacity of mud-rock flows will be more and more serious. Under a full capacity water condition, there is a possibility that a mud-rock flow at a large scale can occur in the source material located in the upper reach of the Yangjiawan.

Analysis on the Possibility for the Bailuxi Main Channel to Burst into a Mud-Rock Flow

The reach of the Bailuxi River looks and acts like a funnel, and the water system in the upper reach is a network of waterways resembling the shape and configuration of tree branches. The branch channel at the right bank provides limited clastic solid material to a mud-rock flow in the main channel, however, when the main channel erupts in a mud-rock flow event, the right bank branch channel can provide a rich water source, and this is a key factor in causing the main channel to erupt into a mud-rock flow. The left bank branch channel is the mud-rock flow channel and is

especially likely to initiate a mud-rock flow in the Yangjiawan River. The outburst of mud-rock flow in the branch channel directly causes the main channel rock flow eruption, in most cases.

The source material area of mud-rock flows in the main channel of the Bailuxi River does include not only the material source area of branch channel mud-rock flow, but also the accumulated material and deposits of branch channel mud-rock flow events. The massive mud-rock flow compound deposits and the source area of mud-rock flow in branch channels in the area of Zhushaping, Daping and Houping (at the east side of Bailu Town) constitute the main solid erosional material source when mud-rock flows erupt in the main channel. The maximum extension area of the main channel mud-rock flow is somewhat short when compared with the longer area in the upper reach of the Bailuxi River. The area is in the entrance of the Bailuxi River, Bailu Town and Erping at the east side which is the depositing area of the main channel mud-rock flow. Currently in the area of Bailu Town, the remnants of the dam formed by the mud-rock flow eruption at the right bank of Daninghe River shows the massive scale of mud-rock flows when the main channel erupts. Though the damage caused by the mud-rock flow cannot be recognized from the current record, the loss that can be caused by the possible re-eruption of the similar mud-rock flow and the disaster derived accordingly cannot be underestimated.

The geological condition of substance source area consists of the geological features of the branch channel material source area and that of the mud-rock flow deposit of the branch channel. The geological features of the branch channel material source area will not be given in detail here. A simple description for the geological features of the mud-rock flow deposit in the area around Daping and Houping is given as follows: The mud-rock flow deposit in the left bank of the upper reaches of the Bailuxi River at the towns of Daping and Houping is flat as a whole, the slope height difference being about 500 m. Several wide and shallow gullies exist on the surface. The mud-rock flow deposit is the sole flat land in the mountainous valley. The main river section which is the Bailuxi River in the expansion area of the main mud-rock flow channel formed from the north side to the west and east is an anisomerous V-shaped riverbed configuration with a 20°–30° slope at the right bank, which is comparatively flat. Most of these areas show the Silurian clastic rock; at the left bank, most areas are steep slopes of 50°, and erosion is taking place generally into the cliff, where the geology is steep, and was formed by a solid mud-rock flow deposit with a height difference between 20 and 60 m for the bank slopes (Fig. 13.9). The average height is approximately 40 m. Under the action of side erosion of the Bailuxi River, the steep ridges at the front part of the left bank deposit become a kind of landslide at a different level at the edge where water seeped out. Wushi Road original construction plans had to be changed because of its proximity to the landslide near the deposit. All these landslide deposits will be moved to the Daninghe River by the flow of water after it goes into the main channel of the Bailuxi River, which would not result in any damage to the lower reach of the Bailuxi River.

The initiation region of the main channel mud-rock flow includes the initiation and accumulation regions of the branch channel mud-rock flows.

Fig. 13.9 High steep slope on the lower part of the left bank of the Bailuxi River

Under full maximum water conditions, including side erosion by the Bailuxi River floodwaters, the mud-rock flow deposit in the area around Daping and Houping at the east side of Bailu Town will possibly provide continuous clastic solid substance to the mud-rock flow erupted in the main channel, and it would cause the small-scale liquid mud flow beginning in the upper reach or branch channel to evolve into a sticky mud-rock flow at a more dangerous larger scale.

The increasing amount of human construction and economic activity in the river area increases the possibility for the mud-rock flow to occur. For instance, the Wushi Road construction produced plenty of loose construction waste slag, and as a result, a material source is formed on both sides of the river. The cut-slope of the road caused the two sides of the inner gully to fail, and the new landslide deposit provides new source material to add to the mud-rock flow. All these loosened deposits are an important factor as rainstorms can trigger mud-rock flows and swell the size of the mud-rock flows.

The movement region of the mud-rock flow channel of the Bailuxi River contains the solid material compensating for the area that distributes in the area where it originates from Daping village to the east, ends at the exit of the Bailuxi River in the west and is adjacent to Bailu Town near the bank of the Daninghe River. The boundary in the north is the Bailuxi River and the Liangshuigou River is the boundary to the south. The channel length at the north side is 4 km with an area of 3.3×10^6 m^2, the composite of clastic solid substance is the soil aggregate with an average thickness of 40 m and 1.3×10^8 m^3 for reserves; if the amount is 20% of clastic solid substance that will compose the mud-rock flow directly, the total amount will be around 2.6×10^6 m^3.

The falling gradient of the lower reach of the Bailuxi River is small; the curved river valley is an anisomerous U shape for both sides with a width of 50–100 m. At the left bank, a steep ridge formed at the front part of the mud-rock flow deposit where some slides developed; whereas in the right bank, there is a stable flat slope

without landslide-susceptible geology. The frequent water flow only affects the narrow river way, and rice fields are grown in the land on both sides of the river way. There is one waterfall, 4 m tall, in the ditch gully located in the middle reach of the Bailuxi River, which cuts through Ordovician limestone. At the left side of the waterfall, there is a larger channel for water to penetrate through it, and some water flow in the upper reach drains through the penetration channel.

The Bailuxi River is an old mud-rock flow channel, but since the Daninghe River, a trunk stream, brings quantities of mud and sand, the deposit fanning area at the gully opening is washed away completely by the water at the interval of mud-rock flows, and there is only the fan-shaped deposit remaining on the surface.

The left bank of the Daninghe River where it joins with the Bailuxi River, where Bailu Town is located, is also the deposition area for the main mud-rock flow channel. At both sides of the Daninghe River, it can be seen that remnants of the dam that was formed by the mud-rock flow in the main channel remain, and the remnants can be more clearly seen from the right bank. Opposite to Bailu Town, a triangle buttress-shaped deposit remains upright at the right bank of the Daninghe River (Fig. 13.5), which is higher than the water surface by about 25 m. The surface area of the deposit is 200 m^2. The dam remnants at the right bank are opposite to the mud-rock flow deposit at the left bank of the Daninghe River, but constitute a part of the whole. Based on field observation, the deposit at the left bank and the dam remnants form a natural slope angle of about 101. The deposit is of soil aggregate where the mud content is about 40%. The rock aggregate is mainly limestone, but has little Silurian clastic rock. Most of the broken gravels are of a size of 3–20 cm, which is 50% of the total, but the large boulder content is much less.

According to the field investigation, an analysis is made by considering the structure of the deposit at both banks. The dam remnant, which was formed by the mud-rock flow and which blocked the river, is the only direct proof that the mud-rock flow rapidly erupted at a large scale in the Bailuxi River. Though the time was not recorded, it was definitely earlier than or in 1834.

Mud-rock flow at a small scale is rather frequent in the area around Bailu, and it also demands as much attention and concern as the hazard in the main channel.

When a small-scale mud-rock flow erupting in the branch channel enters into the Daninghe River, it would not cause any damage, because the riverbed of the Daninghe River is wide and allows for a great amount of the water flow to pass, moving with it, the clastic solid substance to the lower reach, via the annual flow of water. However, for the area with a dense population concentration, a small-scale mud-rock flow will still threaten the safety of the road and the inhabitants of Bailu Town.

The danger of mud-rock flow in a large scale cannot be ignored. The Bailuxi River is the ideal environmental and geological setting for the eruption of mud-rock flows at a large scale. The area around the Bailuxi River with its steep ridge at the front part of the mud-rock flow deposits can easily lose its stability. The estimated potential seismic intensity in this area is No. 7 level. Additionally, the area in the mountainside of Dabashan Mountain, which is the watershed of the Daninghe River and the Duhe River, is a regional centre area for rainstorms. The clastic solid

material located in the river reach is sufficiently large with a continuous reserve of materials. All other conditions being present, the eruption of a mud-rock flow is likely, when there is a rainstorm or long-duration rain or earthquake event. If the left bank branch channel of the Yangjiawan River erupts its own mud-rock flow, it is possible that a new eruption of mud-rock flow in the main channel of the Bailuxi River will occur, causing a direct threat to the life and property of the inhabitants who live in Bailu Town and in the deposit area in the river reaches of the Bailu River.

Hazard Analysis of the Bailuxi River Mud-Rock Flow and the Resulting Countermeasures

As the Yangjiawan River branch channel has the largest potential for both size of an event and damage in the Bailuxi River reach, the mud-rock flow erupting there will not only threaten the life and property safety of the inhabitants who live in Daping and Houping, as well as the main traffic line, but the more serious issue is that it will trigger a mud-rock flow in the main channel at a larger scale. Once the flow material blocks the flow of the Daninghe River (by means of the formation of a natural dam as was previously experienced) the entire Town of Bailu may be submerged completely. The subordinate damage caused by any natural crack in the dam or surrounding embankments can possibly result in flooding, which is a huge threat to the safety of the inhabitants who live in the area of both banks. Therefore, a clear understanding and recognition of the potential damage that would be caused by a possible mud-rock flow erupting, first in the branch channel and then the main channel of the Yangjiawan River and other branches, should be undertaken.

In view of the special condition in the river reach of the Bailuxi River, the main prevention activity must be to stabilize the source material.

The control of the stability of the material source area includes the recognition that the mitigation work should include the source area of the branch channel mud-rock flow and also the area of the main channel rock flow. In view of the significance of the Yangjiawan mud-rock flow along the whole river reach, the prevention for the mud-rock flow in the Bailuxi River and the prevention for the mud-rock flow in the branch channel in the Yangjiawan River must take priority. Especially important is the prevention and control of the unstable, loose, massive and clastic rock deposit on the massive dam in the upper reach. It is a significant integral part of the task to stabilize the material source of mud-rock flows in the branch channel. The control measures must include mainly revegetation, with the appropriate construction measures as support.

In the area of the left bank in the lower reach of the Bailuxi River (at Daping and Bailu Town), the mud-rock flow deposit of the branch channel is steep in the front part, where there are the unstable geological phenomena such as small-scale slides. It is suitable to take certain engineering measures to stabilize the source material to protect the slope. The construction of retaining walls may prevent shallow landslides and the slide deposits on both sides of the channel valley if it is solidly built on the

loose bank and slope. Meanwhile, measures must be taken to improve the recognition of the hazard by inhabitants, throughout the whole river valley. The land for construction, especially for the local inhabitants to build houses on, must be evaluated for exposure to hazard and perhaps the land in the flow path should have regulations for building. Since the mud-rock flow in the Bailuxi River is of such a large scale, its potential flow must be managed comprehensively along the whole river reach. In the water-converging area of the branch channel, the biological prevention measures must be taken so as to improve the percentage of vegetation coverage. In the formation and region of the movement, especially for the dangerous slope, the engineering measures should be used so as to prevent mud and sand in the channel valley from migrating towards the lower reaches. Obstructing sand dams and/or valley dams is necessary. At the opening of the Bailuxi River and the terminus of the deposit field, some kind of diversion dike should be considered, whereas the high and steep edge or slope formed by the mud-rock flow deposits at the channel opening at Bailu Town should be reinforced to prevent the mud-rock flow.

Reference

Chen LD, Chen ZF, Li XB, Jin WQ, Peng XM (2007) Primary research on Bailuxi debris flow in Wuxi, Chongqing. Geology and Mineral Resources of South China, 2: 54–61.

Yin YP (2004) Major Geological Hazards and the Prevention on Relocation Sites of the Three Gorges Reservoir, the Yangtze River. Geological Publishing House, Beijing (in Chinese).

Chapter 14
Stability Assessment and Stabilizing Approaches for the Majiagou Landslide, Undergoing the Effects of Water Level Fluctuation in the Three Gorges Reservoir Area

Tonglu Li, Changliang Zhang, Ping Xu, and Ping Li

Abstract The Majiagou landslide is located on the left side of the Zhaxi-he River, a tributary of the Yangtze River. There is a large old landslide there originally, on which three secondary landslides were formed. The Majiagou landslide is one of the secondary ones. After the water level of the Three Gorges Reservoir rose from 95 to 135 m in June 2003, the Majiagou landslide occurred including a 20 m- long, 3–5 cm wide, (locally 10 cm-wide) fissure at its back that occurred in a time-frame of 3 months. The implication is that the reservoir impounding reactivated the landslide. The slide mass of the Majiagou landslide is composed of a thin layer of silty clay on the top with low permeability and a thick layer of angular pebbles as the main portion beneath the silt clay which has high permeability. The rate of water level fluctuation is between 0.6 and 4.0 m/d with regard to the altitude between 145 and 175 m in the reservoir during its normal operational state. Under these conditions, the FEM method was applied to simulate the groundwater changes in the slide mass, coinciding with the reservoir water level fluctuation. The results suggest that the groundwater level almost changes with the reservoir water level simultaneously within the slide mass, which means that the groundwater gradient is very gentle. Therefore, the effect of the reservoir water level fluctuation on the landslide stability is mainly by the action of buoyant force. Without considering dam failure, the seepage force is so little as to be negligible. The stability of the landslide in cases of different water levels is then calculated using the Morgenstern-Price method, and the results show that the factors of safety decrease with the water level rise. As the water level increases to 165 m, the factors of safety are at the minimum value, increasing with the water level rise. The minimum value reflects that the landslide is in a critical state, so stabilizing design was applied using stabilizing piles as well as a water drainage system. The project was completed in early 2006, and the water level has risen to 156 m in October 2006. Monitoring data illustrated that there is no further deformation of the landslide and the stabilizing piles, so the stabilizing work is effective.

T. Li (✉)
Department of Geological Engineering, Chang'an University,
Xi'an, Shaanxi Province, China 710054
e-mail: dcdgx08@chd.edu.cn

Introduction

The Majiagou landslide is located on the left side, 2.1 km up to the outlet of
the Zhaxi-he River, a tributary of the Yangtze River. The geographical posi-
tion is $31°01'08''$–$31°01'17''$ north latitude, $110°41'48''$–$110°42'10''$ east longitude,
and administratively, belongs to Group 8, Penjiapo Village, Guizhou Town, Zigui
County, Hubei Province, China (Fig. 14.1). It is one of the secondary landslides
which occurred on a large old landslide. A 20 m long, 3–5 cm wide (locally 10 cm
wide fissure) developed on the back of the landslide in the 3 months as the water
level of the Three Gorges Reservoir rising from 95 to 135 m. After that, the fis-
sure stabilized, with no further opening. This situation indicates that the landslide
is sensitive to the water level change. If the water level changes again, there is the
possibility of reactivation. There are civilians and farmland as well as an economic
forest on the landslide. The census and economic investigation suggested that 47
families including 132 persons are living on the landslide and 320 Mu of farmland
and orange forest on it are the critical economic base of the villages. The oranges
there are the well-known local products. In 1996, the vice-chairman of the nation at
the time, Jintao Hu visited Penjiapo village, located on the landslide to encourage
the orange planting (Fig. 14.2). It is estimated that if the landslide fails, it would
cause losses of 34,220 thousands Yuan RMB due to direct effects, and 14,390 Yuan
RMB in indirect losses, and deaths and injuries could not be prevented. Thus, the
deformation of the landslide attracted the attention of the government officials and

Fig. 14.1   Location of Majiagou landslide

related specialists. They ordered an investigation and the application of control measures, as needed. The front of the landslide is saturated under water as the water level of the Three Gorges Reservoir changes between 145 and 175 m with 30 m in fluctuation. The key problem is the effect of the water level changes on the landslide stability. The worst case scenario for the landslide stability affected by the water level change should be considered and as the base for stabilizing.

The effect of water level change on landslide stability is related to the material components and permeability of the slide mass and the shape of the slide zone as well as the rate and the extent of the water level fluctuation. The authors had carried out the whole process of the landslide investigation and stabilizing design. By field investigation and exploration, the engineering geological features of the landslide were clarified; the physical–mechanical parameters and the permeability of the slip mass, slip zone and the slip bed were tested in lab and in situ. The two-dimensional unstable flow model of FEM method was used to simulate the regularities of the groundwater level change affected by the reservoir water level. The Morgenstern–Price method was applied to calculate the landslide stability in combination with the results of water level simulation to achieve the correlation between the water levels and the factors of safety. The worst case was used to assess the landslide stability and design for the stabilizing plan. The plan was completed in early 2006, and the water level rose to 156 m in October 2006. Monitoring data illustrated that there is no further deformation of the landslide and the stabilizing piles, so the stabilizing work is effective.

Engineering Geologic Characteristics of the Majiagou Landslide

The Geologic Background of the Landslide

Around the landslide outcrops the Suining group, which stratigraphically is Upper Jurassic series composed of grey feldspar quartz sandstone and silty mudstone,

which is interbedded. The bedrock has the attitude of 270–290° in dip direction and of 5–30° in dip angle, close to the major orientation of the landslide movement. The Majiagou landslide is located in the front side of a large old landslide. The large landslide is a bedrock slide slipping along the rock bedding and covers all the left side of the lower part of the Majiagou Brook which is a tributary of the Zhaxi-he River. It is located on the left bank, and the slide mass distributes in the elevation between 130 and 300 m. It covers an area of 5 km² and has a size of up to 2 billion m³. A large reversed platform, takes up an area of about 1.5 km² and is formed on the top of the slide, on which a small dam was built to store water (Figs. 14.3 and 14.4). The slide mass of the large landslide is mostly composed of large sandstone blocks filled with detritus of purplish red mudstone. A 3–5 m thick layer of brown-red clay containing rock blocks covers the top of the slide mass, which is a residual and diluvia deposit and may have been deposited after the landslide formed, and therefore it can be concluded that the old landslide happened at least before the Holocene.

In the front side of the old landslide, under the margin of the top platform, three secondary landslides developed. Two of these secondary landslides on the upper reach of the Majiagou Brook lie above the water level of the Three Gorges Reservoir, and their toe areas are obstructed by the opposite slope of the right side of the Majiagou Brook, with no space for further slippage. As a result, it is empirically recognized that these secondary landslides are of a stable state and have experienced no disturbance. The Majiagou landslide is the one on the outlet of the Majiagou Brook and the front part of it extended into Zhaxi-he River. In 2003, the Three Gorges Reservoir impounded water up to 135 m in elevation, and then a long fissure appeared in the back of the slide. If the slide fails, not only will it bring great damage to local residents and properties but also the wave it creates will run into the Yangtze River along the Zhaxi-he River to threaten the safety of navigation.
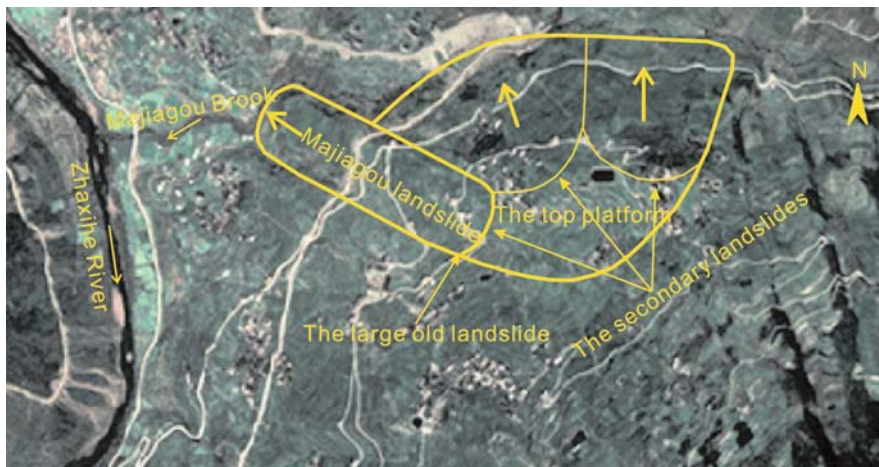
Fig. 14.3 Satellite image of the Majiagou landslide
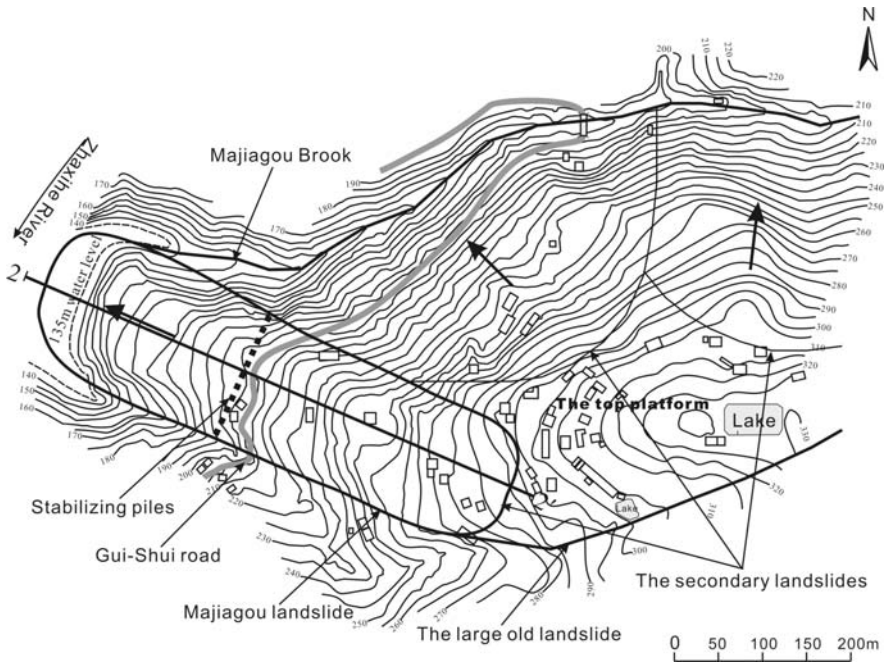
Fig. 14.4 The plan map of the Majiagou landslide

The Geomorphic Form of the Landslide

The Majiagou landslide has a long-narrow tongue-shaped form in plane view, with a movement direction of 290° NWW. The south and north sides of the landslide are bordered by the two brooks and the back is bordered by the new formed fissure. The elevation of the front and the back is 130 and 280 m, respectively, with a height difference of 150 m (Fig. 14.5). The landslide has a gradient of 20–25° on the surface,
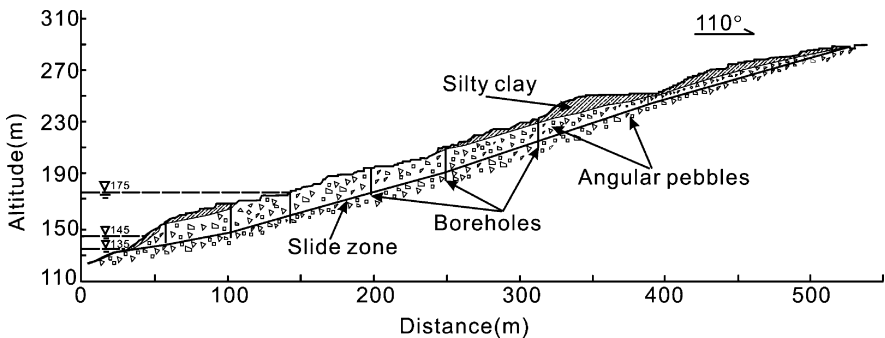
Fig. 14.5 The main section of the Majiagou landslide

a width of 150 m, and a length of 538 m. The front portion has submerged into the Zhaxi-he River whose water level is 135 m at the time. Because of wave erosion, a 30–45 m high scarp has formed above the water table. The mean gradient of the slide surface is 18°. According to the results of the boreholes on the landslide, the slide mass has the thickness of between 17.5 and 8.9 and 13.2 m on an average, has the surface area of 9.68×10^4 m^2 in plan, and has a size of 127.8×10^4 m^3.

The Material Components of the Landslide

The landslide mass is composed of two types of materials. The top 3–5 m is a layer of residual silty clay containing rock blocks. The ratio of rock blocks to soil is between 6:4 and 7:3. The silty clay is brown red, wet, and plastic to hard plastic. The components of the contained rock blocks are composed of feldspar quartz sandstones, shale and siltstones, silty mudstones, etc. The size of the blocks is generally 0.5–5 cm, the maximum ones up to 20 cm in diameter and in angular shape. The main portion of the slide mass lying under the silty clay is full of angular pebbles and composed of large sandstone blocks filled with weathered mudstone detritus. Some of the detritus has broken into a state that is like soil, with a ratio of rock blocks to soil of from 8:2 to 9:1, with a high proportion of rock blocks. This layer has a thickness of 8–11 m, of which the size of rock blocks is generally 1–2 m, with the largest up to 7–8 m. The rock blocks contained are of angular or sub-angular shape, in a filling of soil. The landslide is of a loose structure and high water permeability.

The slide zone revealed by boreholes is composed of muddy shale and crushed sandstone including a small amount of sandstone pieces. The slide zone appears purple and grey in color, saturated and soft plastic in state. It can also be observed in the investigation pits in the southwest front, and the investigation draft in the central part of the slide, there occurs a film of crushed muddy materials containing polished faces and slickensides. The thickness of the slide zone is 0.5–0.8 m. There is a layer of perched water within the slide zone. The perched water can be observed in the draft as overflow, in the boreholes as hanging water, and in the east side as down springs. Because the material of the slide mass and the slide bed are similar, the perched water is an important indicator of the slide zone.

The material of the slide-bed is also angular pebbles, similar to that of the slide mass. The main components are the sandstone rock blocks filled with the weathered mudstone detritus and fine soil. All the boreholes on the landslide did not reveal intact bedrock, which means the old landslide is a large one with a deep slide zone, and the Majiagou landslide is only a little shallow part at its front, reactivated by the reservoir water.

The Hydrogeological Characteristics of the Landslide

The surface water system related to the landslide is that of the Zaxihe River in front, the Majiagou brook in the east side and another little brook in the west side. The two brooks have permanent water flows which cut down below the slip zone of

the landslide in their downstream reach, so the brooks have no essential effect on the landslide stability. However, the Zhaxihe River has a prominent effect on the landslide as its water level changes with the reservoir.

The grounder water in the landslide is mainly the perched pore water on the slide zone which flows out as springs.

Based on the permeability tests on the ground surface and in the boreholes, the silt clay on the top portion of the slip mass has the permeability coefficient of 1.38×10^{-5} cm/s, being a weak permeability; while the angular pebbles below the silt clay has that of 1.52–0.006 cm/s, being of a high permeability. The slip zone has the permeability equivalent to the silt clay which is a relatively water-tight layer. The slip bed has the permeability equivalent to the angular pebbles with high permeability. All the boreholes did not reveal a phreatic level in the landslide.

The landslide is in the Three Gorges rainstorm district where there is frequent rainfall. The monthly mean precipitation by years is 1066.92 mm, and the maximum annual precipitation is 430.6 mm (1963), while the minimum is 733 mm (1966). The rainfall is concentrated from April to October, and monthly mean precipitation is 87.2–147.2 mm in these periods; from May to September it is over 130 mm, which is 67.2% of the total precipitation in a year. The rain season is popular in storm rain and long-term rains, which generally occur in spring and autumn. The groundwater is supplied by penetration of rain water. Because of annual rainfalls, the silt clays of the slide mass and the slip zone are annually saturated, but the angular pebbles have high permeability because of their more and large porosities. With the rainfall occurring, the slip mass and the slip bed usually experience pore water penetrating down instantaneously which is obstructed by the relative water-tight slip zone to form perched water. The phreatic level is deep seated; therefore, the reservoir impounding may have little influence on the water content of the slip zone, but can affect the water dynamic conditions.

Physical and Mechanical Properties of the Soil of the Landslide

The physical and mechanical properties including natural density and saturated density of the slide mass, the shear strength of the slide zone, and the permeability of the slide mass, the slide zone, and the slide bed need to be determined for the landslide stability assessment.

Density of the Slide Mass

As the soil contains too many irregular rock blocks, it cannot be sampled by the ring cut; therefore, the natural density and saturated density of the slide mass are obtained by in situ test.

The process is to excavate a cubic pit of about 50 cm × 50 cm × 50 cm in size and to weigh the soil being cut package by package during excavation. As the pit is completed, its bottom and walls are covered with thin watertight film, as it is filled up with water, the water volume is gauged bucket by bucket. The natural density is

Table 14.1 The test results of the densities of the slide mass

Soil type	Test number	Location	Natural density (kN/m^3)	Saturated density (kN/m^3)
Silty clay	R06	TC02	20.66	21.47
	R03	TC11	23.02	23.59
	R05	TC18	19.40	19.80
	average		21.0	21.6
Angular pebbles	R04	TC01	20.80	21.40
	R02	TC04	21.54	22.29
	R07	TC05	21.54	22.56
	R01	TC15	21.94	22.99
	R08	TC16	21.98	22.85
	average		21.60	22.40

equal to the quotient of the cumulative soil weight to the cumulative water volume. For measuring the saturated density, water is allowed to penetrate to the area tested to make the soil fully saturated. The next operation is the same as that mentioned above. Using this method, the results of the soil densities were achieved and are shown in Table 14.1.

As shown, the difference between the natural density and the saturated density is small, which indicates that the soil of the slide mass is close to a naturally saturated state. The silty clay on the top layer contains irregular rock blocks and fragments, so the deviation of the density is very high. But this layer is relatively thin; as a result, it has little effect on the stability assessment.

Shear Strength of the Slide Zone

Shear strength of the slide zone is based on a laboratory shear test with the soil samples collected in the investigation pits. The laboratory test result statistics are shown in Table 14.2.

Because the samples contain more or less fragments, both c and φ have high variation. We chose the parameter for calculation mainly based on residual values and our experiences regarding the landslides in this area.

Table 14.2 Statistics of the saturated direct shearing test results for the slide zone

Strength indexes	Peak strength		Residual strength	
	φ/°	c/kPa	φ/°	c/kPa
Count	6	6	6	6
Range	5.2–30.0	6.8–21.0	2.7–25.0	5.1–18.5
average	14.6	18.0	12.4	13.4
Standard deviation	7.6	8.6	5.7	5.8
Coefficient of variation	0.52	0.48	0.46	0.43

Permeability of the Soils of the Landslide

To determine the permeability of the soils in the landslide, six groups of water injection tests were completed in the boreholes. The material of the landslide can be recognized as two main types of silty clay and angular pebbles, so water injection tests were done, one group in the former and five groups in the latter, respectively. The results are shown in Table 14.3.

It is indicated that the silty clay has a permeability coefficient of 1.38×10^{-5} cm/s, which is a weak permeable soil, while the angular pebbles has that of 1.52–6.00×10^{-3} cm/s, which is a strong permeable soil.

Table 14.3   Water injection test results of the soils on the landslide

Number	Borehole number	Test depth	Soil type	Permeability coefficient	
				(cm/s)	(m/d)
1	ZK2	10.0–10.3	Angular pebbles (Fragments)	0.025	21.60
2	ZK4	0.5–0.67	Silty clay	1.38×10^{-5}	1.19×10^{-2}
3	ZK6	10.4–10.6	Angular pebbles (weathering mudstone)	0.006	5.18
4	ZK10	4.3–4.5	Angular pebbles (Rock blocks)	0.064	55.30
5	ZK1	6.4–6.6	Angular pebbles (Rock blocks)	1.520	1313.28
6	ZK11	6.1–6.3	Angular pebbles (Rock blocks)	0.500	432.00

Effect on the Ground Water by the Reservoir Water Level Fluctuation

The groundwater level in the landslide changes correspondingly with the reservoir water level fluctuation, and therefore movement of the groundwater level impacts the stability of the landslide. Generally the change of groundwater rate falls behind that of the reservoir water level. The dynamic process is related to the soil permeability of the landslide and the rate of the reservoir water level change. Here, we first study the effect of soil permeability and the rate of the water level change on the groundwater. The problem can be generalized as a two-dimensional unsteady flow model. Owing to the high water content of the landslide soil, the unsaturated soil characteristics are not considered, and the permeability is assumed to be homogeneous. The basic equation for seepage flow is expressed as

$$k \left(\frac{\partial^2 H}{\partial x^2} + \frac{\partial^2 H}{\partial y^2} \right) = m_w \gamma_w \frac{\partial H}{\partial t} - Q \tag{14.1}$$

where H is the total water head, k is permeability coefficient, Q is flow quantity, m_v is flow-resistant coefficients, and γ_w is water unit weight.

It is difficult to deduce the analytical solution of Eq. (14.1), therefore the finite element method is applied to simulate the groundwater heads for different of reservoir water levels. From the results, the zero water head line is recognized as the phreatic line. The stabilities of the landslide in different reservoir water levels are calculated with the phriatic lines. The meshes of the finite element model on the main section of the Majiagou landslide are shown in Fig. 14.6.

The parameters of the soil permeability and the reservoir water level change need to be selected. In all the cases, it is usually the worst conditions combinations which are taken for simulation. Thus for the permeability, the lowest, and for the rate of water level change, the highest should be available. As shown in Table 14.3, the permeability coefficient is taken as 10^{-5} cm/s.

The water level adjustment schedule of the Three Gorges Reservoir in its normal operational state is as follows (GDGH 2004a). From the beginning to the end of May, the water level in front of the dam drops from 175 to 155 m with the rate of less than 1 m/d, average 0.67 m/d; from 1 to 10 June, water level drops from 155 to 145 m with the rate of 1.0 m/d. The threshold limit for water level is 145 m which is maintained to prevent flooding during the flood season which extends from the middle of June to the end of September. If the flood occurs once per 5, 20, 100 and 1,000 years, the water level would rise to 147.2, 157.5, 166.7 and 175.0 m, respectively. After a flood peak, the reservoir water level in front of the dam drops rapidly to about 145 m, the threshold limit level for preparing for another flood. The rising rate of the water level is up to 3–4 m/d as the 100 and 1,000 years flood occurrence during flood season. The water level rises from 145 to 175 m during the beginning of September to the end of October, and a 175 m level is maintained until the beginning of the next May. The water level in front of the Three Gorges Dam fluctuates between 145 and 175 m, for a range of 30 m (Fig. 14.7). The schedule for the reservoir normal water level management is shown in Fig. 14.6. It is shown that the rate of water level change is between 0.6 and 4.0 m/d, so the highest rate of 4.0 m/d is used for simulation.
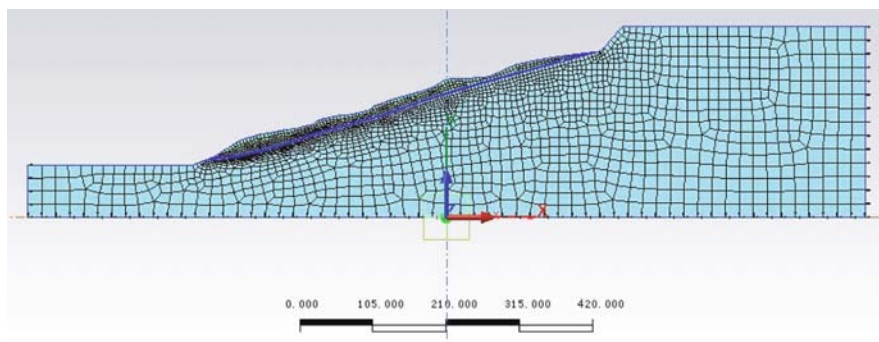

0. 000   105. 000   210. 000   315. 000   420. 000

Fig. 14. 6 The meshes of the model on the main section for groundwater simulation
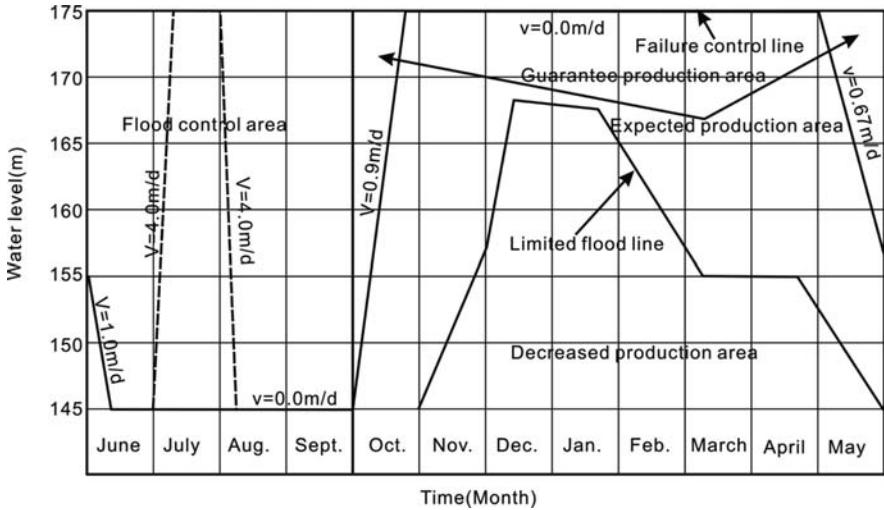
Fig. 14.7 The water level management schedule of the Three Gorges reservoir in a normal operational state

It is now supposed that the model is homogenous in permeability and the permeability coefficient is 10^{-5} cm/s and the rate of water level change is 4 m/d. First, the water level of the reservoir starts from 145 m to simulate the water rising process. At the moment, the groundwater level is horizontal. The water level rising from 145 to 175 m requires 7.5 days, so the simulated phreatic levels are given by the intervals of one day and the last half day which are equivalent to the reservoir water level intervals of 4 m and the last 2 m. Then the initial water level of the reservoir starts from 175 m to simulate the draw-down process. The groundwater level is horizontal at the beginning, too. The simulated phreatic levels are given by the intervals of the first half day and one day, which are equivalent to the reservoir water level intervals of the first 2 and 4 m in the after. Figure 14.8 (a) and (b) shows the simulated results where the reservoir water level just rises to 175 from 145 m and drops down to 145 from 175 m, respectively. Figure 14.9 shows all the simulated phreatic lines up and down.

It is shown that the groundwater level rises with the reservoir water level synchronously, but the phreatic line tends to dip to the inner of the slope, the higher the reservoir water level, the greater the gradient. The highest gradient presents at the reservoir water level occurs at the 175 m level. To each phreatic line, the groundwater level is gentle outside, while it becomes steeper to the inner side, as shown in Fig. 14.8(a). The phreatic line becomes flat when the reservoir water level keeps static at 175 m.

On the contrary, with the reservoir water falling, the groundwater level draws down synchronously either. The phreatic line inclines to the outer of the slope, the lower the reservoir water level, the higher the gradient. The highest gradient appears at the reservoir water level just getting at 145 m. To each phreatic line,
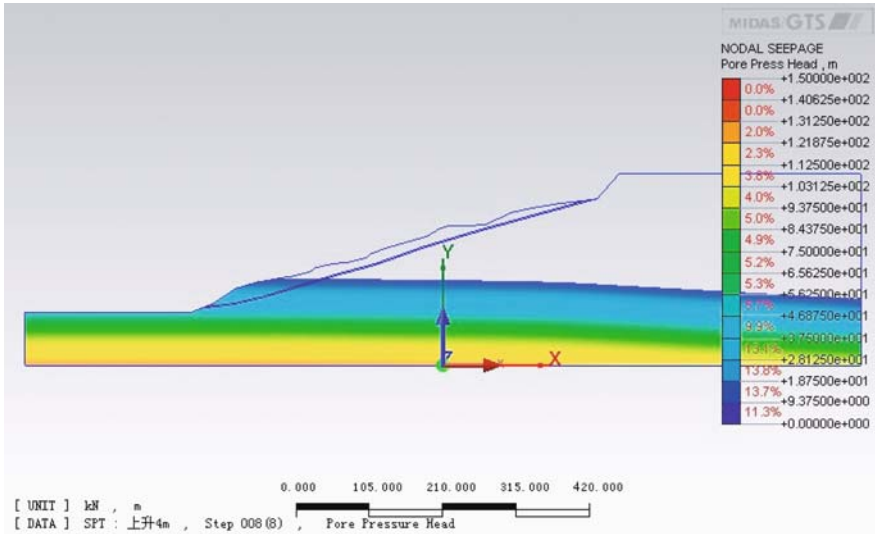
(a) For $k = 10^{-5}$ cm/s, $v = 4$ m/d up rising
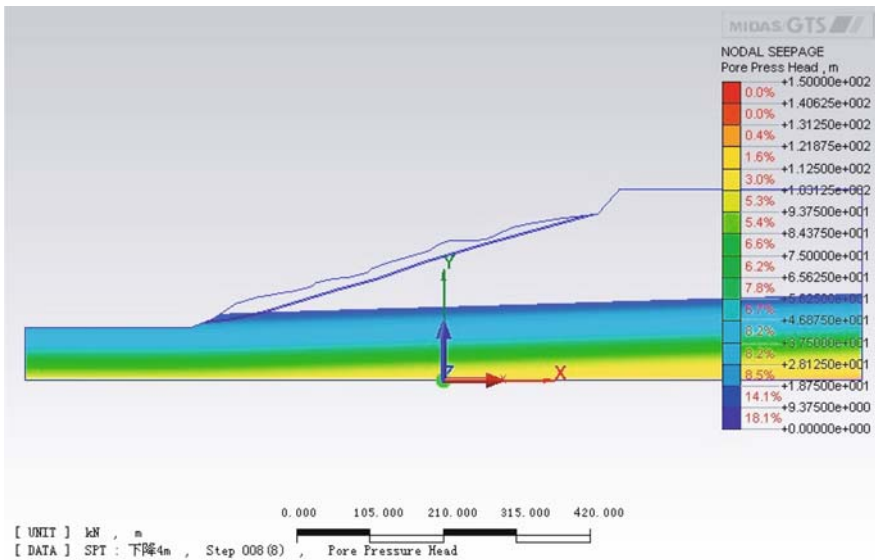
(b) For $k = 10^{-5}$ cm/s, $v = 4$ m/d drown down

Fig. 14.8 The simulated results of the reservoir water level effect on groundwater

the groundwater level is gentle outside, while becomes steeper to the inner side, as shown in the Fig. 14.8(b). When the reservoir water level stays steadily at 145 m, the phreatic line becomes flat.

Figure 14.8 shows that, in all cases, for both rising and falling of the reservoir water level, the phreatic line in the range of the slide mass is very flat, and even the
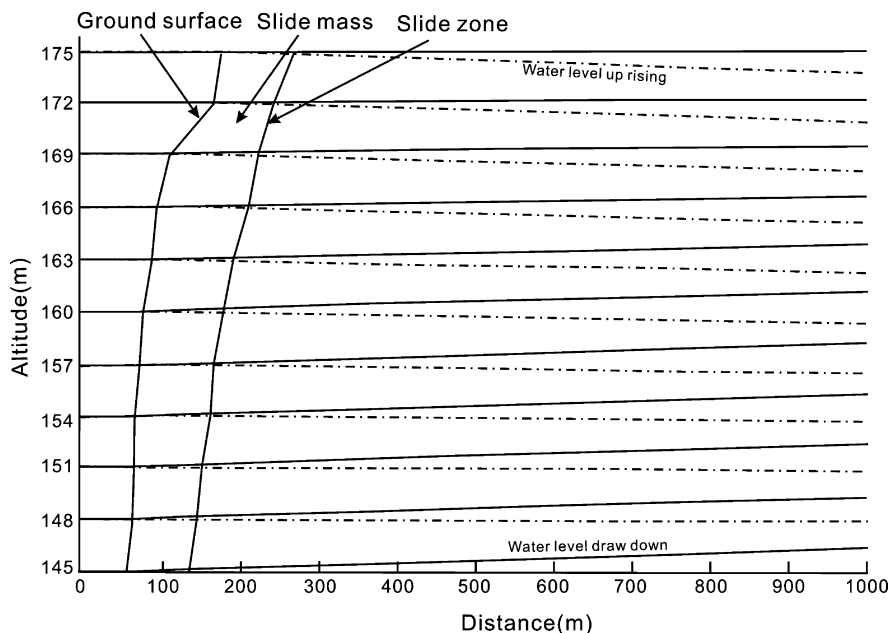
Fig. 14.9   The simulation results of the water level, up and down movement for $k=10^{-5}$ cm/s, $v=4$ m/d.

lines for rising and falling are overlapped. Thus the hydraulic gradient is as little as that of the seepage force and may be negligible.

The simulated cases above are in the worst conditions, for other possible combined conditions, such as larger in permeability coefficient and slower in the water level change, it is easy to recognize that the phreatic line must be gentler than that in the above simulation.

Therefore, the simulated results show that the effect of the reservoir water level on the groundwater of the landslide is mainly due to the fluctuation of the phreatic level, so the action of the groundwater on the slide mass is mainly the buoyant force rather than the seepage force.

Stability Assessment of the Landslide Undergoing the Reservoir Water Level Change

Based on the test results and the experience with the materials of the landslide, the parameters applied in the stability calculation are accepted as follows:

The density of the slide mass:

Natural unit weight:

The silty clay is 21.0 kN/m^3, the angular pebbles is 21.6 kN/m^3

Saturated unit weight:

The silty clay is 21.6 kN/m^3, the angular pebbles is 22.4 kN/m^3
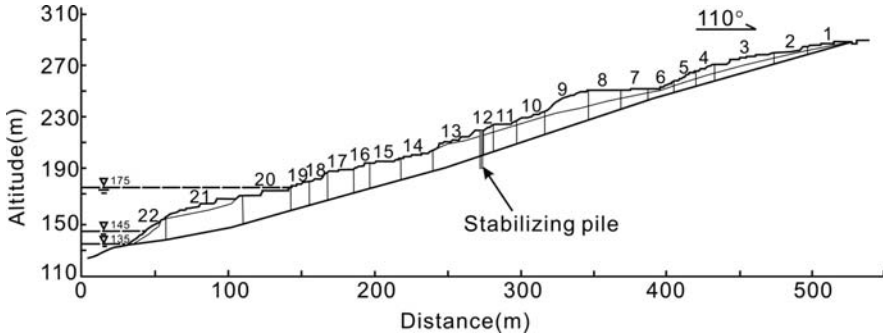
Fig. 14.10 Slices for the stability calculation

The shear strength parameters of the slide zone in effective stress value are

$$c = 10 \text{ kPa}, \varphi = 14°$$

The Morgenstern–Price method (Morgenstern and Price 1965), a more perfect method at present to consider both the force equilibrium and the moment equilibrium, is applied. Under the coordinate system in Fig. 14.10, the force equilibrium and the moment equilibrium are expressed as Eqs. (14.2) and (14.3), respectively.

$$\left(1 - \frac{dy}{dx}\frac{tg\phi'}{F}\right)\frac{dE}{dx} - \left(\frac{dy}{dx} + \frac{tg\phi'}{F}\right)\frac{dX}{dx}$$
$$= -\left(\frac{dy}{dx} + \frac{tg\phi'}{F}\right)\frac{dW}{dx} - \frac{c' - utg\phi'}{F}\left[1 + \left(\frac{dy}{dx}\right)^2\right] \tag{14.2}$$

$$X = y\frac{dE}{dx} - \frac{d(Ey_E)}{dx} \tag{14.3}$$

where E is the horizontal thrust force between the slices, X is the vertical shear force between the slices, c' is the effective cohesion, φ' is the effective friction angle, y is the function of the slide surface, y_E is the function of the horizontal force position, and u is the pore water pressure.

The method assumes

$$X = \lambda f(x)E$$

where λ is a constant and $f(x)$ is a given function.

And let

$$y = Ax + B$$
$$\frac{dW}{dx} = px + q$$
$$f(x) = kx + m.$$

Since

$$\frac{dy}{dx} = A$$

$$X = \lambda(kx + m)E$$

$$\frac{dX}{dx} = \lambda k E + \lambda(kx + m)\frac{dE}{dx} \tag{14.4}$$

Then, Eq. (14.2) becomes

$$\left[-\lambda k \left(A + \frac{tg\phi'}{F} \right) x + 1 - A\frac{tg\phi'}{F} - \lambda m \left(A + \frac{tg\phi'}{F} \right) \right] \frac{dE}{dx} - \lambda k \left(A + \frac{tg\phi'}{F} \right) E$$
$$= - p \left(A + \frac{tg\phi'}{F} \right) x - (1 + A^2)\frac{c' - utg\phi'}{F} - q \left(A + \frac{tg\phi'}{F} \right)$$

Let

$$K = -\lambda k \left(A + \frac{tg\phi'}{F} \right)$$

$$L = 1 - A\frac{tg\phi'}{F} - \lambda m \left(A + \frac{tg\phi'}{F} \right)$$

$$N = -p \left(A + \frac{tg\phi'}{F} \right)$$

$$P = -(1 + A^2)\frac{c' - utg\phi'}{F} - q \left(A + \frac{tg\phi'}{F} \right)$$

Thus

$$\left(Kx + L \right)\frac{dE}{dx} + KE = Nx + P \tag{14.5}$$

This equation is available in the domain $[x_i, x_{i+1}]$, the boundary conditions are

$$E(x_i) = E_i$$
$$E(x_{i+1}) = E_{i+1}$$

The solution of Eq. (14.5) is

$$E(x) = \frac{1}{(Kx+L)}\left(\frac{1}{2}Nx^2 + Px + C\right) \qquad (14.6)$$

where C is a constant.

The x in the above equations can be defined as in local coordinate. Taking the left boundary of each slice as the origin of x axis, then $C = E_i L$ when $x = 0$, so

$$E_x = \frac{1}{(Kx+L)}\left(E_{i-1}L + \frac{1}{2}Nx^2 + Px\right). \qquad (14.7)$$

The Eq. (14.3) can be changed as the follow:

$$d[E(y_E - y)] = \left(-X - E\frac{dy}{dx}\right)dx.$$

After integrating the above equation, we can get

$$M_x = M_{i-1} - \int_0^x \left(X + E\frac{dz}{dx}\right)dx.$$

Replace X and E in Eqs. (14.4) and (14.6), we have

$$M_x = M_{i-1} - \int_0^x \frac{\lambda x/Kx + (\lambda m + A)/K}{x + L/K}\left(E_i L + \frac{1}{2}Nx^2 + Px\right)dx$$

Let

$$G = -\lambda k/K$$
$$H = -(\lambda m + A)/K$$
$$W = L/K.$$

Then

$$M_x = M_{i-1} + \int_0^x \frac{Gx + H}{x + W}\left(E_{i-1}L + \frac{1}{2}Nx^2 + Px\right)dx$$

And

$$M_x = M_{i-1} + \int_0^x \frac{1}{x+W}\left[\frac{1}{2}GNx^3 + (GP + \frac{1}{2}HN)x^2 \right.$$
$$\left. + (GLE_{i-1} + HP)x + HLE_{i-1}\right]dx.$$

Let

$$R1 = HLE_{i-1}$$

$$G1 = \int_0^x \frac{1}{x+W} dx = \ln|(x+W)/W|$$

$$R2 = GLE_{i-1} + HP$$

$$G2 = \int_0^x \frac{x}{x+W} dt = x - WG1$$

$$R3 = GP + \frac{1}{2} HN$$

$$G3 = \int_0^x \frac{x^2}{x+W} dx = \frac{1}{2}x^2 - WG2$$

$$R4 = \frac{1}{2} GN$$

$$G4 = \int_0^x \frac{x^3}{x+W} dt = \frac{1}{3}x^3 - WG3$$

Then, we have

$$M_x = M_{i-1} + (R1G1 + R2G2 + R3G3 + R4G4) \tag{14.8}$$

We change Eqs. (14.7) and (14.8) to differential form. Suppose Δx is the width of a slice, the term x in Eqs. (14.7) and (14.8) can be replaced by Δx, thus

$$E_i = \frac{1}{(K\Delta x + L)}(E_{i-1}L + \frac{1}{2}N\Delta x^2 + P\Delta x) \tag{14.9}$$

$$M_i = M_{i-1} + (R1G1 + R2G2 + R3G3 + R4G4) \tag{14.10}$$

Equations (14.9) and (14.10) are the explicit expression of the Morgenstern–Price method, which include two unknown variables F and λ (Guoliang Lei 1988, 1998). The boundary conditions for solution are $E_0 = 0$, $M_0 = 0$; $E_n = 0$ $M_n = 0$. First, to give $E_0 = 0$, $M_0 = 0$, then to calculate $E_i = 0$ and $M_i = 0$ one by one, at last, we get the values of E_n and M_n. Adjust F and λ to make $E_n = 0$ $M_n = 0$. Then, the converged factor of safety F and the corresponding λ are achieved. This procedure can be carried out on Excel Spreadsheet.

According to the simulated results of the phreatic levels, the effect of the reservoir on the landslide is by the buoyant force which is equivalent to the resultant forces of all boundary pore water pressures around the slice, and the seepage force can be neglected. Thus, in order to simplify the calculation, we just use effective density instead of saturated density for the slide mass under water and the pore water pressure in related equation would not be considered yet.

The slices of the main section are shown in Fig. 14.10. The factors of safety are calculated in the cases where the reservoir water levels are 130, 135, 140, 145, 150,

Table 14.4 Results of the stability calculation

Water level (m)	λ	F
130	0.3180	1.03200
135	0.3107	1.03180
140	0.3126	1.02730
145	0.3141	1.02190
150	0.3154	1.01490
155	0.3165	1.00850
160	0.3172	1.00490
165	0.3173	1.00487
170	0.3171	1.00810
175	0.3169	1.01280
Totally submerged	0.3147	1.13480

155, 160, 165, 170, and 175 m, respectively. The whole landslide is above the water level when the reservoir water level is at 130 m. The calculated results are shown in Table 14.4. The correlation between the reservoir water level and the factor of safety is also shown in Fig. 14.11.

As the reservoir water level is 135 m, just a little part of the landslide is submerged in water, so the factor of safety in this case is very close to that in the case where the landslide is above water. As the reservoir water level changes between 135 and 160 m, the factor of safety of the landslide decreases with the water level rising. As the water level rises from 160 to 175 m, the factor of safety increases. The result is contradictory to the general assumption that the stability of a landslide decreases with more sliding mass submerged. As we examine the structure of the slide surface, it may be easy to understand. Generally, the slide surface of a landslide
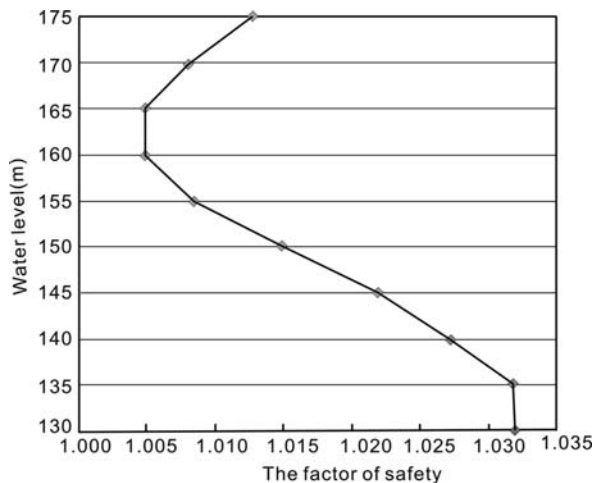

Fig. 14.11 Correlation between the reservoir water level and the factor of safety

has two portions. The lower is a resistant portion which is gentler, while the upper slide portion is steeper. The factor of safety decreases as the resistant portion is submerged because the up resistant force decreases more than the down thrust force, while it increases as the slide portion is submerged because the down thrust force decreases more than the resistant force.

In all the cases, the stability of the landslide is assessed to consider the worst condition, and thus the factor of safety of this landslide should be taken as the lowest value, 1.0046.

Before impounding, the factor of safety is 1.0320. The landslide is close to critical state at this time. As the reservoir water level rose to 135 m, the factor of safety decreased to 1.0318. Though a little reduction, the stability of the landslide deteriorates, causing a tensile fissure on the back of the landslide, this means that the landslide has begun a creep deformation. The landslide experienced a new equilibrium state through deformation. The back tensile crack did not develop as the reservoir water level was kept at 135 m. But the balance may be broken and the landslide may get to the critical state, even slipping, with the rising of the water level. Therefore, the stabilizing work has been done before the reservoir water level rises in the next period.

Stabilizing Work and the Efficiency

The assessment results show that when the reservoir water level rises to 165 m, the factor of safety of the Majiagou landslide would be 1.0046. It is of a critical state. In order to guarantee the safety of the civilians and other facilities on the landslide, the stabilizing work is essential.

All the protected objects on the landslide lie above the Guishui road (Figs. 14.3 and 14.4). The possible approaches such as unloading the top and overloading the foot cannot be accepted according to the situation of the landslide. Anchoring is also not available because the soil of the slide bed is loose. Therefore, the stabilizing piles and necessary drainage system are the few suitable ways that can be considered.

The position of the stabilizing piles should be at the level of the GuiShui road, thus, it can protect the road and the protected objects above the road.

The horizontal forces acting on the piles is the resultant force of the down thrust force on the up side of the piles and the up resistant force on the down side of the piles, which can be calculated by Morgenstern–Prince method. The design factor of safety should be adopted when calculating the down thrust force and the minimal factor of safety should be adopted when calculating the up resistant force. The force acting on the piles is expressed as follow (Li et al. 2006):

$$\Delta E_i = B\left[E_i(\lambda, F_{des}) - E_i(\lambda, F_{min})\right] \tag{14.11}$$

where ΔE_i is the force acting on the pile plugging in the ith down side of slice, $E_i(\lambda, F_{min})$ is the down thrust force acting on the pile, $E_i(\lambda, F_{min})$ is the up resistant force acting on the *pile*, F_{min} is the minimal factor of safety of the landslide, F_{des} is
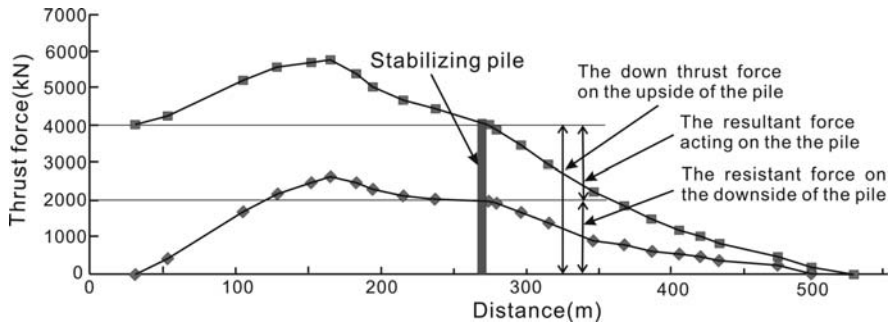
Fig. 14.12 The line of the pushing force of this landslide

the design factor of safety of the landslide, and B is the space between the stabilizing piles.

According to the related mitigation work criterions for the landslides in the Three George Area (GDGH, 2004b), the design factor of safety F_{des} of this landslide is taken as 1.150, the minimal safety factor F_{min} is 1.0046, the space of the piles is taken as 5 m, and then calculated for the line of the thrust forces of this landslide as shown in Fig. 14.12. The stabilizing piles lie in the down side of the 12th slice, and the force acting on the each pile is

$$\Delta E_{12} = 5 \times (3,870 - 1,906) = 9,820 \, kN.$$

Therefore, 20 reinforced concrete stabilizing piles were set in the landslide. The plan section of the pile is 2×3 m, the space between piles is 5 m, the length of all the piles is 22 m, and the length extending in the slide bed is 8 m. The piles were made

Fig. 14.13 Inner forces of the stabilizing pile

of C30 concrete and φ32 steel bars. The shearing force and the moment distribution along the pile are shown in Fig. 14.13.

Besides the stabilizing piles, surface drainage systems were designed to decrease penetration of the surface water and to reduce the risk to the piles. After the piles were completed in early 2006, the reservoir water level rose to 156 m in October 2006, and throughout the 2 years of observation up un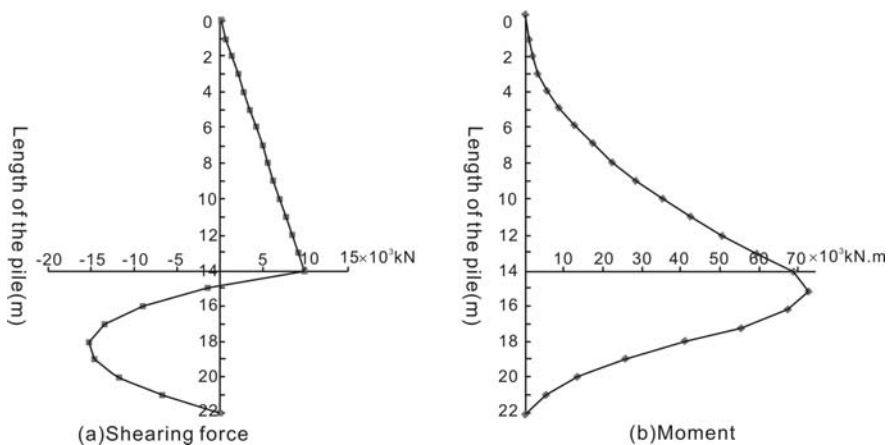til now, the landslide has not experienced apparent deformation, and it reflects that the stabilizing work is effective.

Conclusions

1. The Majiagou landslide is a secondary slide mass in the front of a large old landslide. It is reactivated by impounding of the Three Gorges Reservoir, which means that the landslide has been close to the natural critical state, and is sensitive to the reservoir water rise. Therefore, investigation and stabilizing are necessary for the safety of the civilians and the facilities on the landslide.
2. The simulated results by the finite element method show that the underground water in the slide mass changes with the reservoir water level simultaneously, in a normal operational state, and the hydraulic gradient is small, so the action of the reservoir water level fluctuation on the landslide is by the buoyant force, and the seepage force may be negligible.
3. The calculated results of the landslide stability by Morgenstern–Price method suggest that the stability of the landslide decreases with rising of the reservoir water level, and the factor of safety goes to the minimum value when the reservoir water level rises to 165 m. After that, the stability increases with the rising of the reservoir water level.
4. The stabilizing piles and the necessary drainage system had been applied to mitigate the landslide. After the project was finished, and throughout 2 years of monitoring, it is proven that the landslide has not experienced apparent deformation and the stabilizing project is effective.

References

Lei GL (1988) A suggestion for calculation of stabilizing pile. Proceedings of Landslide Research, Edition 6. China Railway Press, pp. 39–48
Lei GL (1998) Calculation of the interaction between multi-rows stabilizing piles and landslide. Proceedings of Landslide Research, Edition 13. China Railway Press, pp. 65–72
Li TL, Zhao C, Fu YK (2006) Analysis of several concepts about calculation of landslide stability and the thrust force. Chinese Journal of Engineering Geology (Supplement issue), 291–296

Morgenstern NR, Price VE (1965) The analysis of the stability of general slip surfaces. Geotechnique 15(1):79–93

The Guidance Department for the Geological Hazard Mitigation in the Three Gorges Reservoir Area (GDGH) (2004a) The Technical Demands for Engineering Geological Survey of the Third Period Geological Hazard Mitigation in the Three Gorges Reservoir Area

The Guidance Department for the Geological Hazard Mitigation in the Three Gorges Reservoir Area (GDGH) (2004b) The Technical Demands for Design of the Third Period Geological Hazard Mitigation in the Three Gorges Reservoir Area

Chapter 15
Mass Rock Creep and Landsliding on the Huangtupo Slope in the Reservoir Area of the Three Gorges Project, Yangtze River, China

Qinglu Deng and Xueping Wang

Abstract   The Huangtupo slope is one of the most noted large-scale slopes with geologic hazards that cause problems related to the residential safety of immigrants in the reservoir area of the Three Gorges Project, Yangtze River, China. The gravitational process, blended with tectonic deformation, large-scale covering of loose debris, and long-term surficial mass movement, complicates the Huangtupo slope and gives rise to a lack of consensus on the slope nature and stability. Characterization of the structural geometry of the slope deformation and reconstruction of its development history are believed to be pivotal in understanding what has happened and what will happen to the slope. Based on a thorough field investigation combined with an electrical resistivity survey, a three-stage model involving mass rock creep–primary landsliding–partial reactivation is proposed. The first stage follows the incision of the Yangtze River along the axes of the Guandukou syncline, when Huangtupo experienced long-term gravitational deformation referred to as 'mass rock creep'. Mass rock creep in the Huangtupo slope can be classified as two basic processes: toppling and deep-seated creep. Toppling mainly occurs on the exterior part of the slope and is characterized by inclination, sliding, and segmentation of brittle deformation of cleavage rocks. Deep-seated creep occurs predominantly in the interior part of the slope and brittle–ductile flow folding accompanying low-angle shearing is its representative deformation. A primary, large-scale landslide occurred in the second stage as a subsequence of previous mass rock creep. The landslide was ca. 4×107 m^3 in volume with elevations of 640 m a.s.l. at the head and of 80 m a.s.l. at the foot. Significant evidence for the landslide is the variation of attitudes of structural foliation and lineation among outcrops in the slope. The last stage began subsequent to the original sliding; surficial and partial reactivation on the Huangtupo landslide plays a leading role in this stage. Two sliding events in this area in 1995 were ascribed to the partial reactivation mainly due to rainfall, water level fluctuation of the Yangtze River, as well as human activity. It was

Q. Deng (✉)
Faculty of Engineering Geology, China University of Geosciences, Wuhan 430074, China
e-mail: dengqinglu@263.net

suggested that analogous failures in 1995 would continue on the Huangtupo land-slide and become even more frequent under the combined effect of human activity and reservoir filling.

Keywords China · Landslide · Mass rock creep · Three Gorges Project

Introduction

The Three Gorges Project is a huge project. A dam, 175 m high and 2335 m long, is being constructed in Sandouping, 40 km above the Gezhouba Dam, Yichang City (see Fig. 15.1). The reservoir will cover an area of 1084 km^2 and have a capacity of 39.3 billion m^3, and migrant resettlement is the chief constituent of the project. There are 847,500 people to be moved and resettled from ten county capital towns and three cities involved in movement. Ensuring that such a large population lives and works peacefully and contentedly in their new homes is crucial to the Three Gorges Project as a whole.

The county-seat town of Badong, situated on the southern shore of the transition between the Xiling and Wu Gorges of the Yangtze River, is one of the towns that needed to be moved. The Huangtupo slope was selected as the site of the new county-seat town of Badong early in 1982 because of the construction of the Gezhouba Dam in Yichang. The Three Gorges Project has accelerated the development of new Badong and a new and modern town has been developed.

Unfortunately, it was noted during the geological investigations involved in the construction of the Three Gorges Project on the Yangtze River that the Huangtupo slope might be a large-scale landslide (Zhong et al. 1992). This is seemingly confirmed by two sliding events that took place at Huangtupo in 1995. From then on,
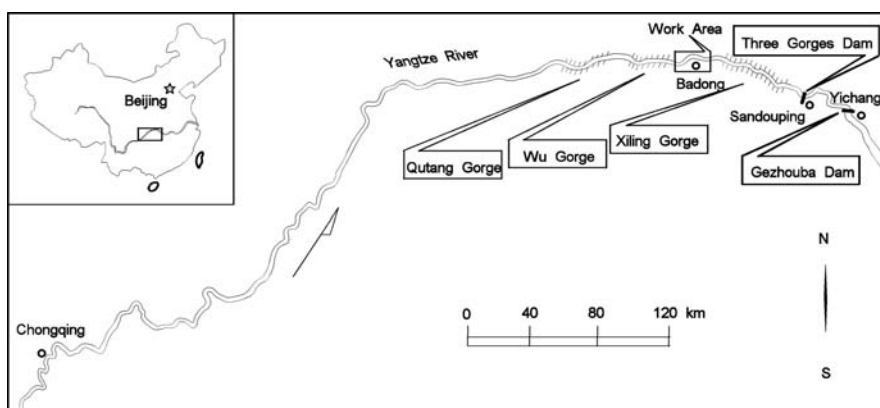

Fig. 15.1 Regional map of the Three Gorges Project showing location of the dam site

engineering geologists and the Chinese government have been solicitous about the future of Badung on the Huangtupo slope.

Obviously a better understanding of the nature of the slope is of critical importance in determining the fate of Badong: to continue to develop or to relocate it again. Although investigations have recently been carried out on the Huangtupo slope, uncertainty remains concerning its characteristics. For example, is it an old and large-scale landslide? What is the relationship between the failures in 1995 and the old landslide? Could the slope problems be solved by appropriate mitigation measures?

The slope is large in dimension with an area of ca. 1.6 km^2 and complex in deformation, which makes it difficult to be well-understood by limited engineering investigations. In addition, in previous studies, much attention has been paid to the short-term stability analysis and assessment, whereas the origin and the development of the deformed slope are largely ignored.

In order to comprehensively understand the Huangtupo slope, we have undertaken studies focusing on the rock deformation in the slope. In this chapter, the deformational structures are described and the mass movement process of the slope is discussed. On the basis of the research, a three-stage model is proposed for the evolution of the Huangtupo slope.

Geological Setting

Most of the Huangtupo slope is covered with loose debris with an average thickness of 40–50 m. However, basement rock can be observed in two deeply cut ravines. Rocks in and near Huangtupo consist of the second and the third members of the Badong group of the Middle Triassic Period (Fig. 15.2). The second member located in the upper part of the slope is a purplish-red pelite alternating with pelitic siltstone. The third member, situated in the middle and lower parts of the slope, is a gray pelitic limestone with a khaki weathering surface interlayer with grayish green calcareous pelite. According to observations of thin sections and chemical analyses, the second member is made up mainly of clay minerals with an average carbonate content of ca. 5–10%. In contrast with the second member, carbonate is the main component in the third member, which contains 25–35% clay minerals.

Huangtupo is situated on the south limb of the Guandukou syncline. The bedding dips downslope at a moderate angle in the middle and upper parts of the slope; in the lower part of the slope, where it is closer to the axes of the Guandukou syncline the dip becomes more gentle. Axial cleavages trending E–W with a steep dip are intensively developed. The cleavage spacing is 1–2 cm or less in the medium to thin beds of pelitic limestone of the third member of the Badong group. These cleavages are characterized by the cleavage planes lined with grayish green, phyllitic films with thicknesses 0.5–2 mm. As is noted in the following discussion, the cleavages as discontinuous planes play an important role in the deformation and failure of the Huangtupo slope.
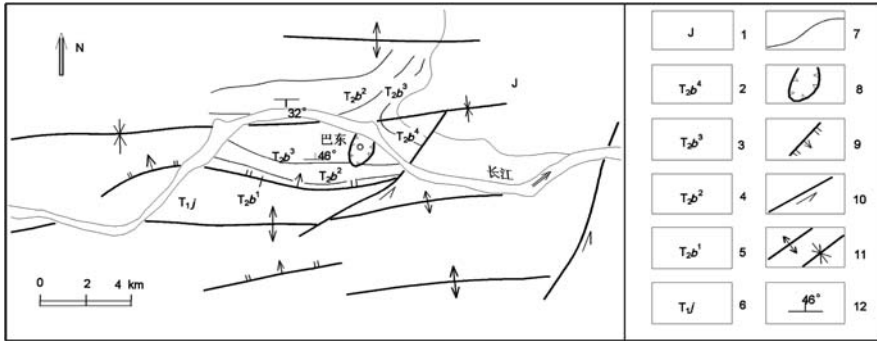
Fig. 15.2 Geographic schematic geological map of Badong. 1 – Jurassic (clastic deposits); 2 – the fourth member of the Middle Triassic Badong group (purplish-red pelite and pelitic siltstone); 3 – the third member of the Badong group (gray pelitic limestone); 4 – the second member of the Badong group (purplish-red pelite and pelitic siltstone); 5 – the first member of the Badong group (gray pelitic limestone); 6 – the Jialingjiang group of the lower Triassic (limestone); 7 – boundary between members of the Badong group; 8 – Huangtupo landslide; 9 – faults; *arrows* in direction of dip; *hachures* indicating the downthrown block; 10 – sinistral strike–slip faults; 11 – folds, anticline on the left and syncline on the right; and 12 – bedding attitude

Mass Rock Creep

Brief Introduction of Mass Rock Creep

The concept of mass rock creep is used following Chigira (1992) to define deformation of rock slopes that deform slowly and gradually under the force of gravity. Mass rock creep of a slope can form complex structures including folds, faults, numerous fractures, and even loose debris near the ground surface. The appearance of such debris accumulation is similar to that formed by a landslide, but the process is distinct from landsliding because it lacks a well-defined master sliding surface, a catastrophic failure process, and a long-distance displacement. The existence of a transitional relation between the deformational and the stationary parts in a deformed slope is generally another character of mass rock creep.

This kind of deformation of slope rocks belongs to long-term gravitational deformation (Chigira 1992). Generally, long-term gravitational slope deformation of a large slope differs in style and behavior between deep and shallow parts (Mencl 1968). Plastic or viscous deformation can occur at depth in a gravitationally unstable slope; flow folds characterized by asymmetric and overturned geometry and shear faults are its representative structures. Brittle deformation develops in the upper part of such a slope; toppling, segmentation, and rotation of rock segments relative to each other are the common phenomena of the deformation. The former has been described with various terms such as depth creep (Ter-Stepanian 1966), sackungen ('sagging', Zischinsky 1966), deep-seated continuous creep (Hutchinson 1968), deep-seated creep (Nemcok 1972) and rock-flow (Varnes 1978). It is also included

in the conception of mass rock creep (Chigira 1992, 1994). These terms can be categorized as two groups: creep and flow. Varnes (1978) used 'rock-flow' because the term 'creep' may be confused with creep in material science. However, Chigira (1992) commented that 'rock-flow' might be confused with rock-flow in a deeper part of the Earth′s crust. Because the term 'creep' is more widely used in documents in relation to slope deformation and slope, creep has consistent aspects on deformational mechanism and behavior compared with that in material science and so creep (deep-seated creep) is adopted in this chapter. Brittle long-term deformation at the shallow upper part of the slope failure mainly originates from toppling. Thus, toppling is used here. In this chapter, long-term slope deformation is referred to as mass rock creep following Chigira (1992), but the integrity of deep-seated creep and toppling in a deformation slope is emphasized.

Mass Rock Creep at Huangtupo

Intense deformation consisting of toppling and deep-seated creep is visible at and near the Huangtupo slope.

Toppling

At the eastern edge of the Huangtupo slope, an intensively deformed zone is as much as hundreds of meters wide (Fig. 15.3): this zone has been described as the influenced or 'pulled' zone of the preexisting Huangtupo landslide (BGCWR 1994). It is characterized by the toppling of rock that has undergone intense axial cleaving (Figs. 15.4 and 15.5). The cleavage slices were rotated and toppled downslope. Shearing along these cleavages without a visible opening can be observed. The bedding of the toppled rock mass is well preserved, while sliding often happens along the bedding planes.

From the characteristics of toppling in this area we can infer that cleavage toppling can induce bedding-plane slipping (see Fig. 15.6). Because no voids formed along cleavages during cleavage sliding due to toppling, the toppled beds will be increased in length. The increase in length of the toppled bed must be accommodated by bedding sliding (partial sliding) between the toppled and non-toppled beds. Based on the measured data (see Fig. 15.6(a)), it can be estimated that the accumulated sliding displacement is 0.55 m in a 100-m long bed. Figure 15.6(c and d) indicates that the displacement of the surface bed increases in proportion to the number of toppled layers. Given a slope with 100 beds of each 100 m long, which toppled just like the measured bed, the accumulated displacement will reach 55 m. Thus, toppling can induce remarkable displacement; this is a possible reason that toppling rock masses are often accompanied by downslope sliding, as illustrated in Fig. 15.7.

In contrast to the eastern edge of the Huangtupo slope, where bedding planes are well preserved in the deformed rock mass (see Figs. 15.4 and 15.5), an outcrop to the west of the Huangtupo slope shows that the bedded rock in the outer part of
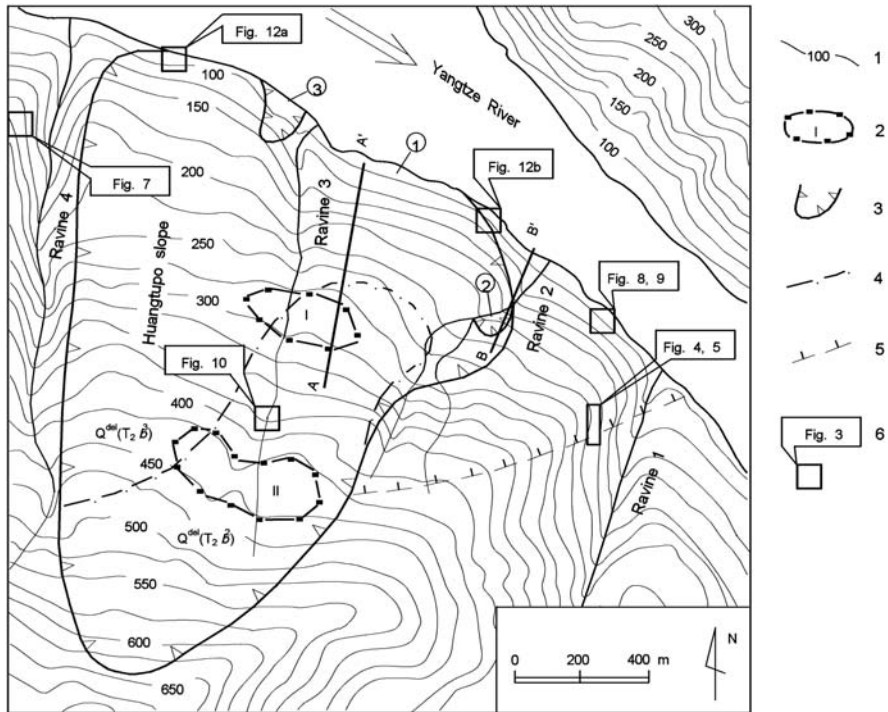
Fig. 15.3 Landform of the Huangtupo slope and observation locations shown in the text. 1 – contours with interval of 25 m; 2 – terrace; 3 – landslide. □ the main landslide of the Huangtupo, □ Erdaogou landslide, □ Sandaogou landslide; 4 – boundary of landslide debris accumulations (Q^{del}) between origins of T_2b^2 and T_2b^3; 5 – southeastern boundary of mass rock creep; 6 – observation location and corresponding figure in the text

the slope has been fractured into blocks and debris (Fig. 15.7), which appears to be similar to landslide debris. However, a transitional relation from miscellaneous debris accumulation to bedrock can be observed in this material indicating that it has not undergone substantial downslope movement.
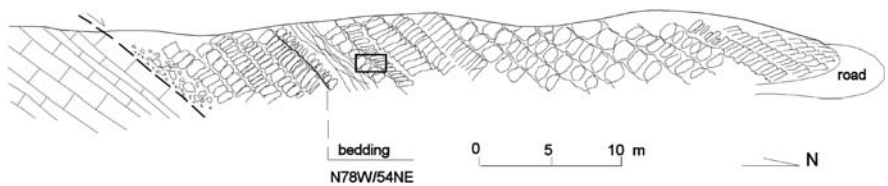
Fig. 15.4 Cross-section showing toppling deposits resulting from cleavage in the pelitic limestone (the third member of the Badong group) at the east edge of the Huangtupo slope. The *square* is the position described in Fig. 15.5

Fig. 15.5 Beds with development of cleavage and toppling of cleavage slices, a detail of Fig. 15.4. Right is to the north
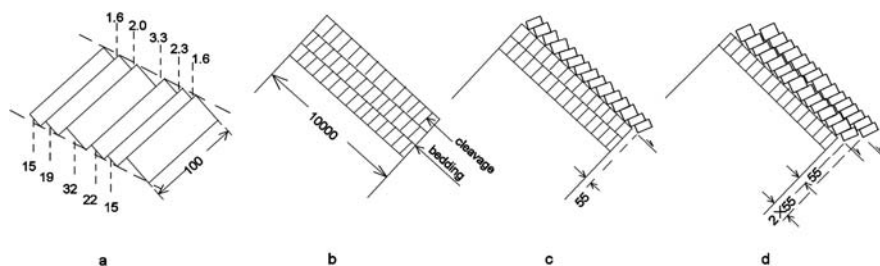
Fig. 15.6 Toppled rock slices and associated developing models at the east edge of the Huangtupo slope. (**a**) Toppled rock slices as measured in situ, *numbers on top* indicating the slipping displacement along cleavages (in centimeters), *numbers on the bottom* showing the width of slices (in centimeters) and the *numbers on the right* showing the lengths of slices (in centimeters); (**b**)–(**d**) Models for cleavage-toppling process at the east edge of the Huangtupo slope: (**b**) in-place beds with developed cleavages of the slope across 100 m long; (**c**) beginning with cleavage toppling in the top bed, accompanied with a dislocation of 0.55 m at its front edge; (**d**) toppling development toward deeper slope: a model indicates toppling involves the top two beds with each dislocation of 0.55 m; measurements are in centimeters
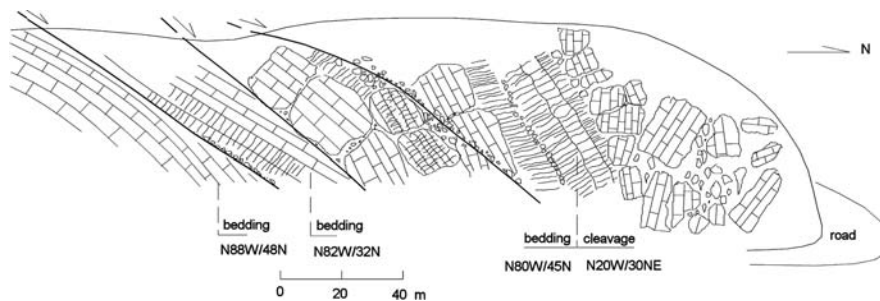
Fig. 15.7 Toppling west to the Huangtupo slope. Toppled rock slices are accompanied by bedding sliding surfaces, and there is a transitional relation of deformation between the outer and the inner parts of the toppling slope

Deep-Seated Creep

Near the axes of the Guandukou syncline, the bedding dips gently and the structure
is simple except within the Huangtupo slope. Along the bank of the Yangtze River
at Huangtupo, overturned and asymmetric knee-like folds and lower angle faults
dipping into the slope are commonly developed (see Figs. 15.8, 15.9, 15.10 and
15.12). Fold axes are sub-horizontal and their direction is E–W; axial surfaces dip
into the slope. The asymmetric folds indicate that the rock mass has undergone
movement to the north (downslope).

The Huangtupo slope is deeply cut by several ravines, where shear faults and
asymmetric folds also can be observed. Figure 15.10 shows a fold in ravine 3. This
fold lies just beneath the debris accumulation on the Huangtupo slope and half of it
was taken off by the preexisting Huangtupo landslide; however, the asymmetric and
overturned shape of the fold can be inferred from the remnant part.
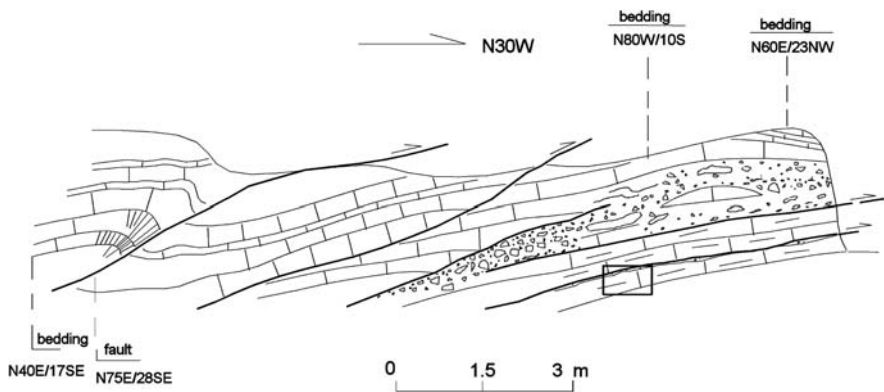
Fig. 15.8   Gentle sliding surfaces and accompanied asymmetric folds at the front edge of the
Huangtupo slope. Movement directions of the overburden blocks are to the north. The *square*
indicates the position shown in Fig. 15.9

Fig. 15.9   A detail of Fig.
15.8, showing a sliding
surface (in the *upper part* of
the photograph) accompanied
by asymmetric and
overturned folds beneath the
surface. The right is to the
north

north.
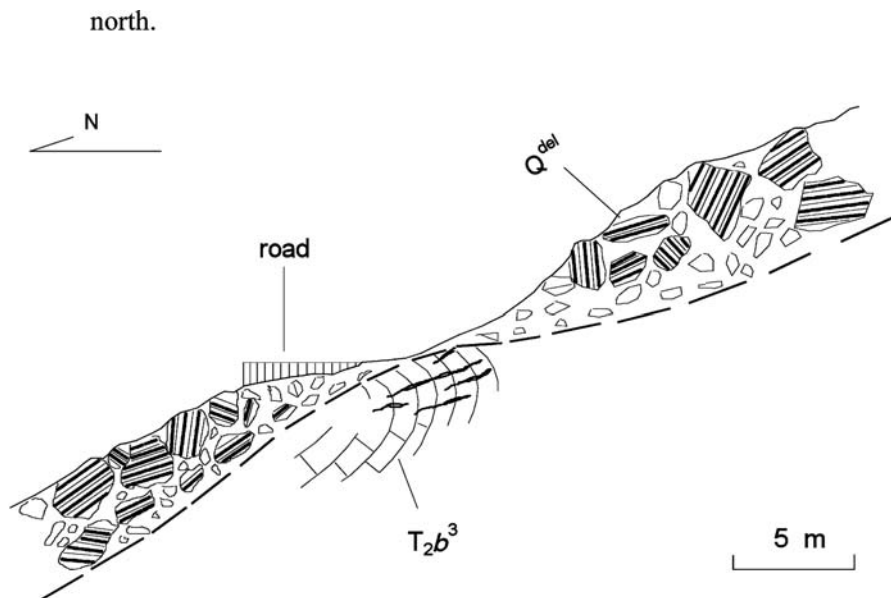
Fig. 15.10   A reversed fold beneath the Huangtupo debris accumulation in the upper reach of ravine 3. Q^{del} is the debris accumulation; T_2b^3 is the third member of the Badong group; *black lines* in the axial part of the fold indicate openings (cracks)

The features of these types of folds, sliding surfaces, and their kinematics are summarized as follows:

1. They are only found in the basement rocks beneath the Huangtupo debris accumulation along the front of the Huangtupo slope and in deeply cut ravines.
2. The folds are asymmetric, which indicates downslope movement. These folds can be distinguished from those of tectonic origin which is characterized by the movement that is independent of the local topography (as can be seen at or near Huangtupo), where the interlayer folds induced by the folding of the Guandukou syncline have upslope movement.
3. Openings of various widths are common in these folds, especially in the axial parts, which is not characteristic for folds of tectonic origin (without openings).
4. The sliding surfaces are sub-parallel to the slope surface on the middle and upper parts of the Huangtupo slope, and become more gentle and even dipping toward the slope in the lower part, which appears to be listric as a whole. The slipping direction is toward the river and is in contrast with that of interlayer gliding induced by the folding of the Guandukou syncline.

Landslide at Huangtupo

There is a region in the middle to upper parts of the Huangtupo slope where purplish-red debris accumulation originating from T_2b^2 overlies the khaki material from T_2b^3, the surface of which is shaped like the sole of a shoe; it is 1100 m long

and 500 m wide (Fig. 15.11). The boundary between T_2b^3 and T_2b^2 protrudes 800 m northward. There is no doubt that the long-distance overlay of debris was made by rock-mass sliding. But, from this landslide, to infer that the Huangtupo slope involves only a relatively small landslide is misguided (e.g., Zhong et al. 1992). Realistically, some features of the Huangtupo slope, such as landform, surface geological architecture, the anomaly of electrical resistivity and the presence of a sliding zone, indicate the Huangtupo landslide may be much larger than that postulated here.

Landform

There are two terraces on the Huangtupo slope. The lower one is 350 m long and 100 m wide at an elevation of 285–310 m a.s.l. (terrace I in Fig. 15.3); the upper is 370 m long and 150 m wide at an elevation of 430–455 m a.s.l. (terrace II in Fig. 15.3). A gentle backslope appears in the front of the terrace II. Because of its terraces, the surface of the Huangtupo slope is distinct from other slopes along the river. These terraces cannot be river terraces because they are not continuous in elevations. The origin of the terraces on the Huangtupo slope is probably from old landsliding. The variation in ground surface may be a reflection of attitude change of the surface of sliding on bedrock. Fujita et al. (1975) and Chigira (1984) pointed out that landslide topography is controlled by bedrock geology to a great extent.

This topographic texture is not limited to the relatively small landslide (the area of purplish-red debris from T_2b^2) and differs from that outside Huangtupo; it suggests that the Huangtupo slope as a whole is an old landslide.

Surface Geological Texture

Rock exposures are broadly dispersed in the area of the khaki, loose debris accumulation (from T_2b^3) at Huangtupo (Fig. 15.11). They have been taken for 'outcrops of bedrock' and have been used to demonstrate that Huangtupo is not a landslide as a whole (CUG; HEGTH and Zhong). In fact, these 'outcrops' are relatively large-scale rock blocks that have been broken apart and rotated in relation to each other. The evidence for this action is as follows:

1. Every 'outcrop' is of small extent, generally with a surface area of only several tens of square meters.
2. Bedding attitudes among 'outcrops' vary greatly, even though some 'outcrops' are spaced only tens of meters apart.
3. Cleavage strikes of individual outcrops also differ, in contrast with those in the bedrock (stationary part) outside Huangtupo, where cleavages trend E–W.

These blocks might be due to the mass rock creep, but such sizes of blocks are not likely to have been made by cleavage toppling. If, in addition, these blocks are caused by a deep-seated creep, there should be a transitional relationship between
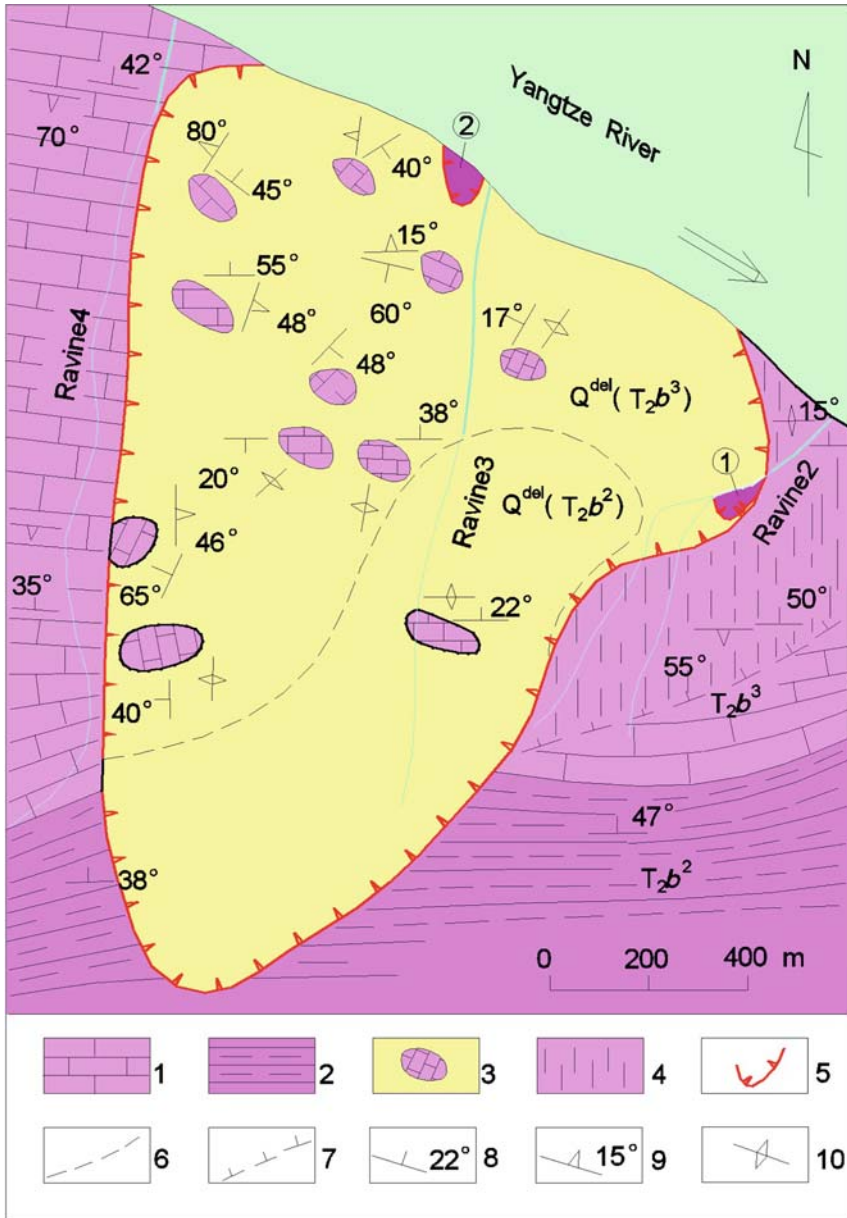
Fig. 15.11 Engineering geological map of the Huangtupo slope. 1 – pelitic limestone; 2 – pelite alternating with pelitic siltstone; 3 – rock exposure in debris accumulation (attitudes of cleavage and bedding in each exposure are shown nearby); 4 – zone of mass rock creep; 5 – landslide boundary; 6 – boundary between the purplish-red debris accumulation originated from T_2b^2 and the khaki materials from T_2b^3; 7 – southeastern boundary of mass rock creep; 8 – attitude of bedding; 9 – attitude of cleavage; 10 – subvertical cleavage; Erdaogou landslide; Sandaogou landslide

them and their neighbors. However, no transitional zone exists. Therefore, landsliding is the most possible cause.

Sliding Zone

A zone of sliding can be identified at the lower edge of the Huangtupo slope along the bank of the Yangtze River and in the deeply cut ravines at Huangtupo. Two representative outcrops can be described as follows:

- Outcrop 1 is located on the riverbank at an elevation of 80 m a.s.l. and 300 m east to the ravine 4 (Fig. 15.12(a)). A breccia zone 2–3 m thick has developed along this zone. Rubble in the breccia is characterized by polished slickenside surfaces, flattened shapes, and heterogeneous fragment sizes, ranging from millimeters to decimeters. The breccia is semi-cemented by carbonate. The breccia zone has a gentle dip in the direction 168°. Beneath the brecciated zone, the rock mass shows intense folding and faulting. The features of the folds, such as asymmetry and development of fractures in their axial parts, are consistent with the characteristics of the deep-seated creep.
- Outcrop 2, situated on the riverbank west to the ravine 2, presents a shear zone with a thickness of 1–1.5 m and a dip of 12° in the direction 305° (Fig. 15.12(b)). This shear zone consists of rubble of pelitic limestone and of pulverized gouge; the rubble is ca. 25–65% of the zone. Subangular rubble with slickenside surfaces occurs in varying sizes. The overburden rock mass has been fractured into fragments; cleavage attitudes of these fragments have been changed in comparison with the in-place E–W trending axial cleavages; the measured cleavage runs N50°W. Faults and overturned folds can be seen underneath the zone; these faults and folds are considered to be deep-seated creeps.

Sliding zones in different locations at the lower edge of the Huangtupo slope can be traced as a single zone. This zone extends along the lower edge of the loose debris accumulation on the Huangtupo slope. This sliding zone is also exposed in ravines 2 and 3 (also reported by Wu 1996). The sliding zone in the upper reach of the ravine 3 is presented in Fig. 15.10. This zone consists of breccia with slicken-sided and flattened rubble. Its overburden debris comes from T_2b^2; a long-distance (over 400 m) movement must have taken place for the debris from the T_2b^2 source to the present place (see Fig. 15.11). An overturn fold developed underneath the zone; this deformation has been described as a deep-seated creep. Cleavages in the deformed rock mass underneath the zone maintain extending E–W, coinciding with the strikes of regional axial-plane cleavages, which indicates the deformed rock mass may be the bedrock of the old Huangtupo landslide.

This zone forms the boundary between the loose debris accumulation (above) and the deformed rock mass (beneath). In this manner, this zone differs from those formed in the preceding long-term deformation and it constitutes a primary sliding surface of the old Huangtupo landslide.
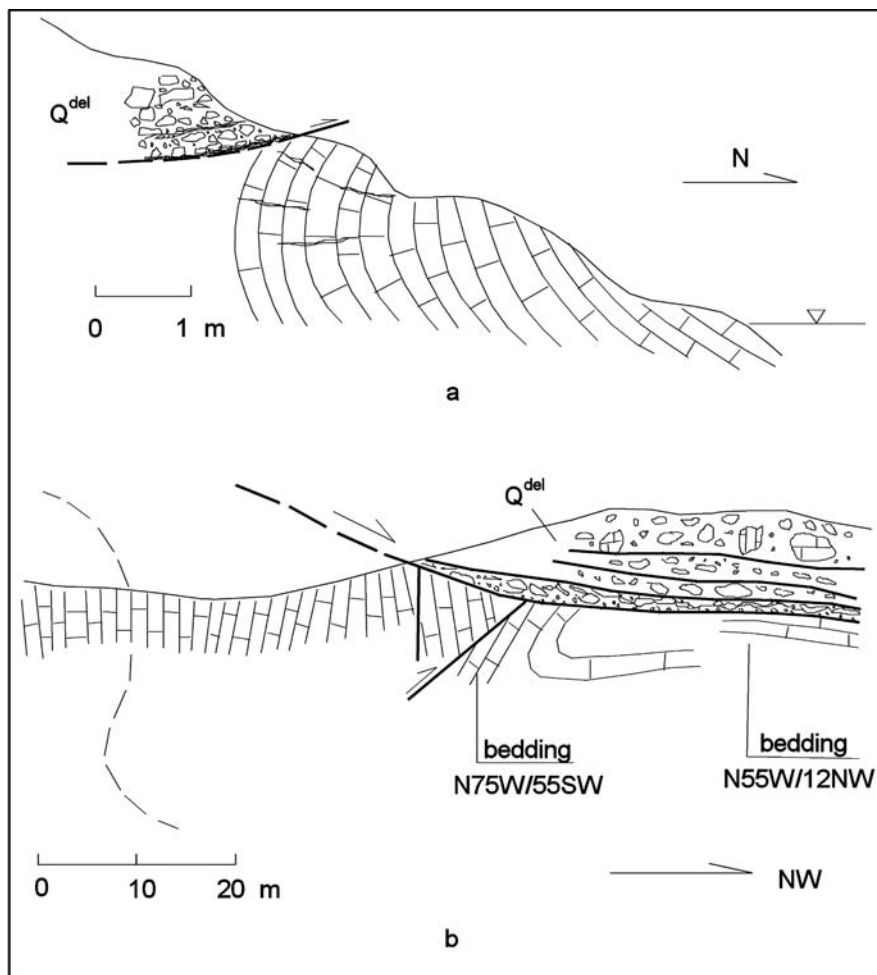
Fig. 15.12 Sliding zones at the front edge of the Huangtupo landslide. Locations 300 m to the east of ravine 4 (**a**) and 200 m to the west of ravine 2 (**b**). Overburden is landslide debris accumulation. The part beneath the sliding zone is strongly deformed; it is considered to be a deep-seated creep

Electrical Resistivity Constraints for Landslide Geometry

Drill-hole exploration has revealed clearly that the upper part of the Huangtupo slope is a landslide. It was seen from these boreholes that the purplish-red debris from T_2b^2 overlies the rock mass of T_2b^3; a distinct sliding surface developed between these two materials. Some holes were also drilled in the middle to the lower parts of the Huangtupo slope, but they did not provide decisive data to allow a unanimous opinion on the geology of the slope among researchers (BGCWR and HEGTH). The large scale of the Huangtupo slope, long-term gravitational mass rock

creep, preexisting deformation of tectonic origin, and debris covering complicate the slope. To aid understanding of the special geometry of the slope deformation of the Huangtupo slope, an electrical resistivity survey was conducted at the middle to the lower parts of the Huangtupo slope by the China University of Geosciences, Wuhan, in 1997 (the senior author of this chapter participated in the work). The combined sounding-profiling measurements using two- and three-electrode arrays have been used in the resistivity survey. Figure 15.13(a) presents ratio profiling curves obtained by the ratio processing from apparent resistivity data (Wang et al. 1988). The ratio processing, that is, the so-called gradient transformation introduced by Karous and Pernu (1985), is applied to remove interference and to provide better presentation of resistivity changes. This processing method is an aid to the resistivity interpretation. In general, a ratio profile can more accurately reflect subsurface resistivity distribution. Significant information can be obtained from the ratio profile:

1. A zone of relatively low ratio values exists in the slope at a depth of 40–50 m. This zone stretches continually and coincides with the base of the landslide as delineated by drilling in the upper part of the slope (above elevation of 250 m a.s.l.). It can be deduced that the lower ratio value zone shows the sliding surface of the landslide. Besides, the zone extends to the front part of the Huangtupo slope although it is relatively faint and shows signs of branching toward the slope surface. The zone with lower ratio value in the lower part of the slope can be interpreted as a sliding surface or an aquifer. It is not likely to form an aquifer in T_2b^3 consisting of pelitic limestone with high permeability and component homogeneity on the whole, as revealed by drilling in this area. Thus, this zone of low resistivity is probably a sliding surface at the bottom of the old Huangtupo
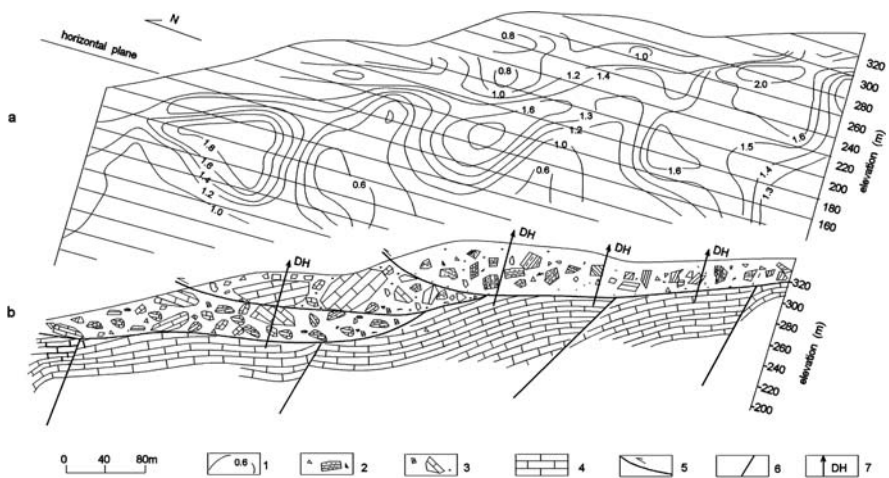

Fig. 15.13 Ratio profile of resistivity (**a**) and its geological interpretation (**b**). 1 – ratio contour of resistivity; 2 – prehistoric landslide debris accumulation originated from T_2b^2; 3 – prehistoric landslide debris accumulation originated from T_2b^3; 4 – limestone of T_2b^3; 5 – sliding surface; 6 – fault; 7 – borehole

landslide. Based on experiments, Dewhurst et al. (1996) pointed out that a sliding surface might result in permeability anisotropy. The sliding surface at the bottom of the Huangtupo landslide may act as an impermeable barrier, which can give rise to water retention at this surface and an associated low-value anomaly of resistivity.

2. The high-value anomaly of resistivity beneath that zone is due to the bedrock of pelitic limestone of T_2b^3, in which some high-angle faults can be interpreted from the ratio contours. These faults do not extend up into the low resistivity zone and the overburden rock mass.

3. The shapes of the ratio contours are incongruous between above and beneath the low-value zone; they have linear shapes with lower ratio curves above the low-value zone and are ring-like with higher ratio curves beneath that zone.

The information available from electrical resistivity is in conformance with the assumption that there is a sliding zone beneath the Huangtupo slope. This zone is not only in the upper part, but also extends into the middle and the lower parts of the slope. Combining the results of the ratio profile of resistivity and the drill-hole exploration in this area, we constructed the interpreted cross-section (Fig. 15.13(b)).

Shallow Process on the Surface of the Preexisting Huangtupo Landslide

Two smaller landslides, Erdaogou and Sandaogou, occurred on the surface of the Huangtupo slide in 1995 (see Fig. 15.11). One of these landslides, which was 90 m wide, 100 m long, 5–13 m thick, and had a volume of 6.7×10^4 m^3, slid on the right slope of the ravine 2 on June 10 (Erdaogou landslide, see Figs. 15.14 and 15.15). It occurred as a reactivation of a small part of the preexisting Huangtupo landslide. The debris accumulation, which originated from T_2b^3, supplied the material for the sliding. Municipal waste and drainage at the back of the landslide were the direct triggering forces. Though this recent slide occurred on the surface of the Huangtupo landslide, there is no evidence to relate it to possible reactivation of the entire landslide. Instead, the process represented only local modification of the Huangtupo landslide mainly due to human activities.

On October 29 in the same year, another relatively small landslide, 100 m wide, 200 m long, and ca. 20×10^4 m^3 in volume, took place west of ravine 3 (Sandaogou landslide). It moved toward the Yangtze River in a north-northeast direction. Rainfall and change of water level of the Yangtze River are two main triggering factors (Yu and Wu 1996). As was the case of the first small landslide described above, this slide also developed on the surface of the Huangtupo landslide and was a result of reactivation of a part of the main slide.

Other secondary slides have probably taken place on the Huangtupo landslide. Some armchair-shaped landslide surface, distinct or obscure, can be identified. Similar slope failures will probably continue, because favorable conditions for reactivation still exist, and may be even more frequent and widespread due to the settlement construction, land mismanagement, and reservoir filling.

Fig. 15.14 Erdaogou landslide occurred on June 10, 1995. Note it developed in the debris accumulation. View is from the northwest

Numerous fractures have formed on the Huangtupo slope (Fig. 15.16). These fractures cluster mainly in three regions: two are in the vicinity of the recent slides in ravine 2 (Erdaogou landslide) and west of ravine 3 (Sandaogou landslide), respectively, where fractures are probably the products of the sliding or the preceding deformation, and of the further deformation of the slides. The other fracture area is
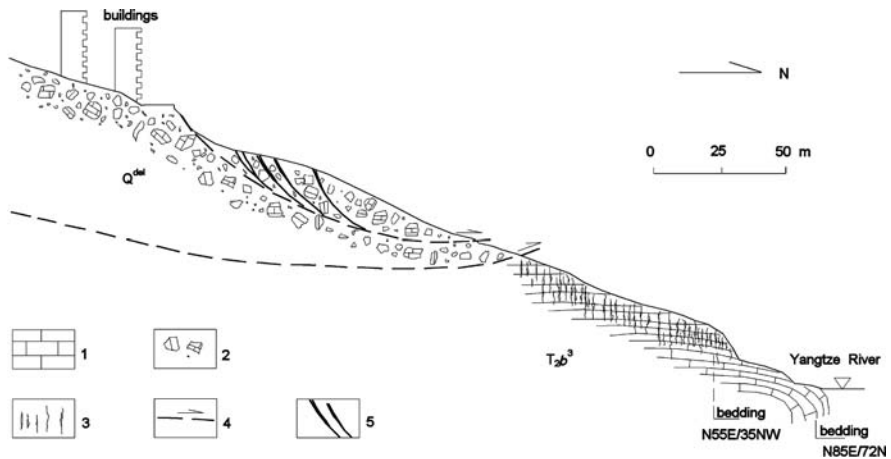
Fig. 15.15 Cross-section along ravine 2, showing the relationship between the zone of mass rock creep (T_2b^3), prehistoric landslide debris accumulation (Q^{del}) and secondary landslides. 1 – pelitic limestone of T_2b^3; 2 – landslide debris accumulation (Q^{del}); 3 – cleavages; 4 – sliding surface; 5 – ground fracture
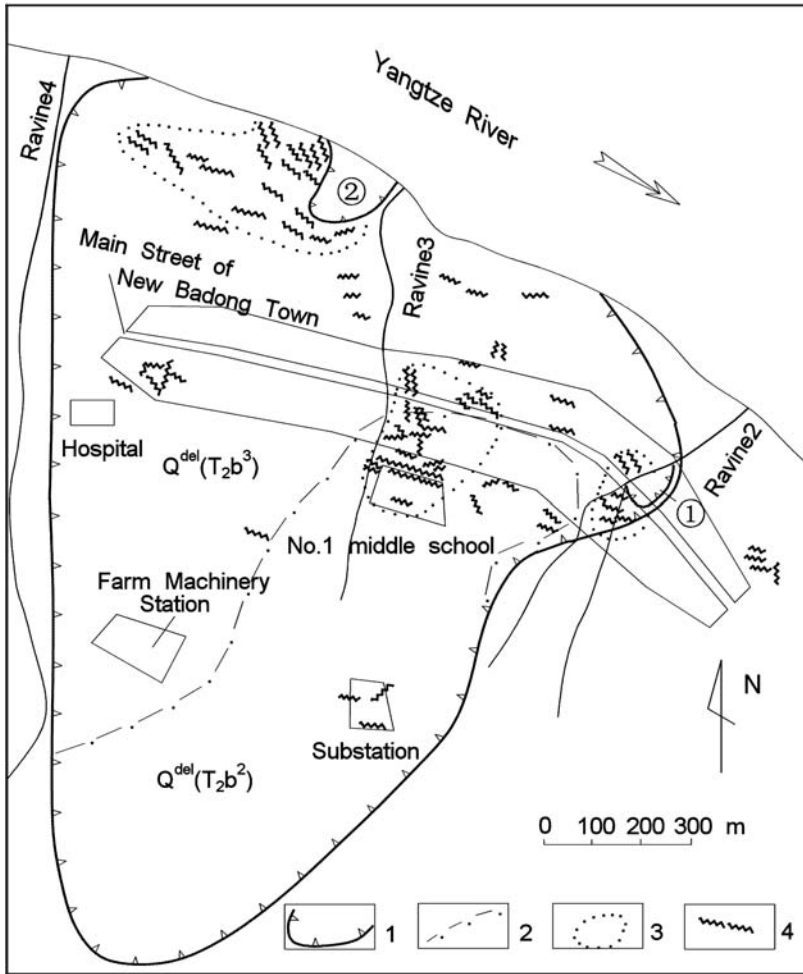
Fig. 15.16 Distribution of recent fractures on the Huangtupo slope. 1 – boundary of landslide; 2 – boundary of landslide debris accumulations (Q^{del}) between origins of T_2b^2 and T_2b^3; 3 – region of intensive fractures; 4 – fracture; ① Erdaogou landslide; ② Sandaogou landslide

in the center of the Huangtupo slope. It threatens to cause a new problem, where >30 fractures with varying directions, maximum lengths of as much as 100 m, and maximum crack openings of >5 cm, have been developed.

Summary and Discussion

Figure 15.17 presents a scheme showing the development of the deformation of the Huangtupo slope.
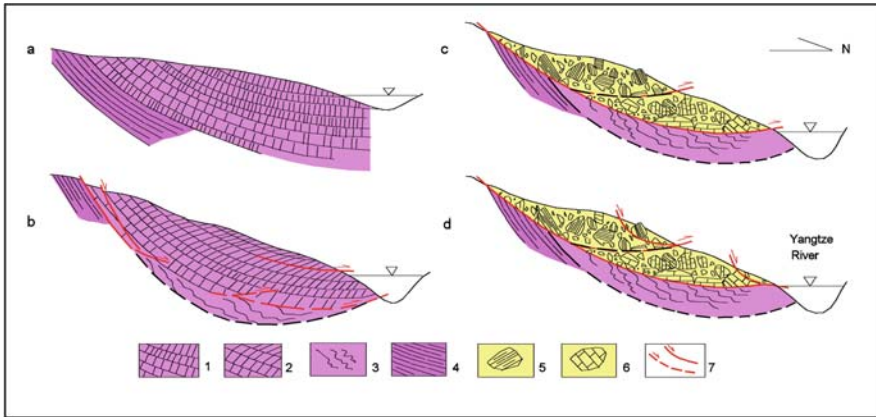
Fig. 15.17 Development scheme of deformation of Huangtupo slope. (**a**) Predeformation stage of the Huangtupo slope; (**b**) long-term gravitational mass rock creep; (**c**) prehistoric landslide; (**d**) secondary landslide. 1 – pelitic limestone (T_2b^3) with intense cleavage; 2 – toppled pelitic limestone; 3 – deep-seated creep zone; 4 – pelite alternating with pelitic siltstone (T_2b^2); 5 – debris originated from T_2b^2; 6 – debris from T_2b^3; 7 – sliding surface

Beginning with the river cutting along the axes of the Guandukou syncline (Fig. 15.17(a)), the Huangtupo slope as a dip slope emerged eventually, evolving into a gravitationally unstable state. Over a long period, the slope was stable enough to stop it sliding entirely until it was deformed by means of toppling and deep-seated creep [Fig. 15.17(b)].

Intense deformations at and near the Huangtupo slope have also been recognized by some researchers (e.g., Yuan and Jiang 1992; Wu 1996), but it was surmised to be the product of landsliding. It was suggested that the deformation to the east of the Huangtupo slope was the result of dragging by the Huangtupo landslide and that the deformation in front of the Huangtupo slope was a landslide-induced compressional structure. If soil or soft rock were the constituents of the slope, this explanation would be feasible. However, this slope deformation has occurred mainly in hard rock.

The folds beneath and around the debris accumulation described above are due to brittle–ductile deformation in a brittle–ductile setting or to viscous creep, both of which are a relatively long-term processes. The debris, in contrast, could be formed rapidly in a brittle setting. These two types of deformation differ in formative setting and process. They could not appear at the same time under the same conditions. This means that the folds cannot be a product of the Huangtupo landslide activity. Conversely, these folds are characterized by development of cracks at their axial parts and by geometrical asymmetry that indicates mass movement in a downslope direction. Thus, these folds can be distinguished from those of tectonic origin; in this case, folds of possible tectonic origin in the vicinity of the Huangtupo slope are the secondary folds of the Guandukou syncline, which are smooth at axes and show geometrical asymmetry indicating apparent mass movement toward the upslope.

For the above reasons, we describe the fold deformation in the Huangtupo slope as a deep-seated creep, a process occurring in the depths of the slope due to gravity.

Toppling was distributed across the upper part of the Huangtupo slope. Its deformational classification lies between the deep-seated creep and brittle segmentation of the rock. Toppling, which can induce downslope sliding activity, might be one of the driving forces for the folding of in situ materials in front of a slope; in this manner, the toppling can be related to the creep. Based on this recognition, toppling can be considered as a constituent part of mass rock creep.

The model of mass rock creep for the Huangtupo slope is formally similar to the distributed shear model postulated for Sackung by Mencl (1968) (introduced and discussed by Dramis and Sorriso-Valvo 1994). Mencl′s model also divides long-term slope deformation ('Sackung') into two parts: viscous deformation in an interior part (ductile zone) and shearing on discrete surfaces in exterior part (brittle zone). But the structural pattern differs between these two models, especially in the shallow part.

Mass rock creep gradually weakens the strength and reduced continuity of rock mass, by which favorable conditions existed for sliding of the entire Huangtupo slope, until sliding did occur (Fig. 15.17(c)). At Huangtupo, there still is a dispute as to whether or not the landslide material continues to the foot of the slope. However, the variation in attitude of bedding planes and cleavages among the exposures on the Huangtupo slope strongly supports the idea that there has been a landslide in that area. Interpretation of the resistivity profiles and recognition of the sliding zone are also in agreement with the view that there is landslide material at the foot of the slope. Perhaps the entire landslide is not a simple one, but is a composite with multiple sliding zones that formed at several stages, as shown in a geological section interpreted from a resistivity profile (Fig. 15.13(b)).

Several thermoluminescence and electron-spin resonance ages have been reported for the Huangtupo landslide, ranging from 11×10^4 to 40×10^4 years BP (Cui and Zhong). Because the long-term deformation that preceded the landslide was not recognized until recently, some reported ages (specially the older ones) may represent the age of preceding creep deformation. Thus, it seems that the actual age of occurrence of the Huangtupo landslide has not been well determined thus far. The obscure landslide topography, deeply incised ravines, and height (ca. 80 m above the riverbed) indicate that the Huangtupo landslide is fairly old; an age of 100,000 years, or even older, seems acceptable.

Subsequent to the primary sliding, the Huangtupo landslide has experienced long-term dismantling (Fig. 15.17(d)). A common process in this stage is the surficial and partial reactivation on the main landslide for adaptation to the local change of slope gradient. The recent failures of Erdaogou and Sandaogou are two such processes.

Presently, the Huangtupo slope as a whole is stable or quasi-stable. New deformation (fractures) is only occurring locally. As can be seen along the foot of the Huangtupo slope, the sliding zone of the main landslide has been partially cemented by carbonate, which makes it more competent than the overlying accumulation of loose debris. Since the development of the deeply cut ravines, the main Huangtupo

landslide is no longer one entity and the failure possibility of the main Huangtupo slope as a whole has been reduced. Thus, the geological conditions are favorable for the development of partial failure instead of reactivation of the entire Huangtupo landslide.

Stability assessments conducted by various researchers using several methods of analysis, including the finite element and Sarma methods (Sarma 1979), show that the Huangtupo landslide as a whole is stable under natural conditions, but is likely to reactivate (at least partially) if subjected to reservoir filling and/or earthquake shocking, as well as to poor land management. Instability is most apt to occur whenever two or more causes act simultaneously (Deng 1998; He and WCU).

Surface failure, such as the sliding that occurred in 1995, will continue because the influencing factors as noted earlier continue to exist. The most vulnerable parts of the slope are in the middle and front of the slope, which are directly affected by human activity and reservoir filling.

Mass rock creep, large-scale landsliding, and relatively minor surface failures constitute a complex process of deformation and failure of the Huangtupo slope. Mass rock creep can reduce rock mass quality and can establish material and deformational conditions that render the slope susceptible to subsequent landsliding. Many engineering geological problems encountered in the population resettlement practices in the reservoir area of the Three Gorges Project may be related to the gravitational mass rock creep. Thus, to clarify this type of slope deformation is especially significant to the resettlement work of the Three Gorges Project.

Slope control at this scale will be difficult and expensive. Prevention and avoidance are the best mitigation measures. If possible, it would be wise to permanently evacuate inhabitants from the Huangtupo slope.

Conclusion

1. The Huangtupo slope has experienced three deformational stages: gravitational mass rock creep, primary large-scale landsliding, and subsequent failure of small parts of the primary landslide.
2. Mass rock creep at Huangtupo has two components: toppling and deep-seated creep. Toppling has developed by rotation and inclination of rock slices bounded by cleavages and by shearing along these cleavages. Deep-seated creep formed shearing zones and folds. The shearing zones are sub-parallel to bedding surface; the folds are characterized by asymmetry and development of openings (cracks) at their axes; both kinds of deformation indicate a mass movement downslope. Toppling by cleavage can induce bedding shearing, by which it is inferred that deep-seated creep is related to the toppling.
3. The preexisting Huangtupo landslide occurred as a result of the mass rock creep. The evidence for the landslide includes varying attitudes of bedding planes and of cleavages in block exposures within debris accumulation, continuously

extending and surface-parallel zones of low resistivity anomaly, and a sliding zone that coincides with the boundary between the debris accumulation and the deformed rock mass. This landslide involves the entire Huangtupo slope; the foot reaches the riverbank at an elevation of ca. 80 m a.s.l.

4. The two smaller slides that occurred on the Huangtupo slope in 1995 are the products of partial reactivation of the preexisting landslide. Similar local reactivation will be expected to continue and may become even more common as a result of human activity and reservoir filling.

References

Bureau of Geotechnique of Changjiang Water Resources Commission (BGCWRC) (1994) Geology Investigation of New Sites for Badong Towns and Villages. Research Report, BGCWRC, Wuhan, China, pp 17–69 (in Chinese)

Chigira M (1984) Mass rock creep of crystalline schist (Part 1) – the relationship between geological structures and landslide topographies in the Sambagawa terrane in the Kanto mountainous land. J. Jpn. Soc. Eng. Geol. 25: 32–44

Chigira M (1992) Long-term gravitational deformation of rocks by mass rock creep. Eng. Geol. 32: 157–184

Chigira M (1994) Deep-seated rockslide-avalanches preceded by mass rock creep of sedimentary rocks in the Akaishi Mountains, Central Japan. Eng. Geol. 38: 221–230

China University of Geosciences (CUG) (1997) Research on Slope Stability and Control Measures in the Front of the Huangtupo Slope in Badong Town. Research Report, CUG, Wuhan, China, pp 8–16 (in Chinese)

Deng QL (1998) The Tectonic and Stability Study of the New Badong Town Slope in the Reservoir Area of the Three Gorges Project on the Yangtze River. Ph.D. Thesis, China University of Geosciences, Wuhan, China, pp 85–97 (in Chinese)

Dewhurst DN, Brown KM, Clennell MB, Westbrook GK (1996) A comparison of the fabric and permeability anisotropy of consolidated and sheared silty clay. Eng. Geol. 42: 253–267

Dramis F, Sorriso-Valvo M (1994) Deep-seated gravitational slope deformation, related landslides and tectonics. Eng. Geol. 38: 231–243

Fujita T, Hirano M, Hada S (1975) The structural control of landslides in the Kawai area, Tokushima prefecture, Shikoku. J. Jpn. Soc. Landslide 13: 25–36

Hutchinson JN (1968) Mass movement. In: Fairbridge, RW (ed) Encyclopedia Geomorphology. Reinhold, New York, pp 688–696

Karous M, Pernu TK (1985) Combined sounding-profiling resistivity measurements with the three-electrode arrays. Geophys. Prospecting 33: 447–459

Mencl V (1968) Plastizitatslehre und das wirklike Verhalten von Gebirgsmassen. Felsmech. Ing. Geol. (Suppl.) IV: 1–8

Nemcok A (1972) Gravitational slope deformation in high mountains. Proc. 24th Int. Geol. Congr. Montreal Sect. 13: 132–141

Sarma SK (1979) Stability analysis of embankments and slopes. Geotech. Eng. Div. 105(GT12): 1512–1514

Ter-Stepanian G (1966) Types of depth creep of slopes in rock masses. Proc. 1st Congr. Int. Soc. Rock Mech. 2: 71–79

Varnes DJ (1978) Slope movement types and processes. In: Landslides Analysis and Control. Special Report 176, National Academy of Science, Transportation Research Board, Washington, DC, pp 11–13

Wang XT, Sun RG, Qu ZF (1988) Ratioing technique in interpretation of combined profile. J. Changchun Univ. Earth Sci. 18(1): 81–88

Wuhan Communication University (WCU), Geotechnique Bureau of Changjiang Water Resources Commission (GBCWRC) (1997) Computer Intelligent Imitation System for the Landslides of Huangtupo and Zhaoshuling of Badong in the Reservoir Area of the Three Gorges Project. Research Report, WCU and GBCWRC, Wuhan, China (in Chinese)

Wu YF (1996) Huangtupo landslide and its geological problems. In: Cui ZQ, Deng QL (eds) Geotechnical Engineering. China University of Goesciences Press, Wuhan, China, pp 93–97 (in Chinese with English abstract)

Yu XW, Wu YF (1996) Sandaogou landslide in Badong town in the Three Gorges of the Yangtze River. J. Eng. Geol. 4(1): 1–7 (in Chinese)

Yuan DW, Jiang BH (1992) Preliminary study on landslides in the area of the new Badong town. Proceedings Symposium on Stability Analysis of Nature Slope and on the Slope Deformation of Mount Huaying Sichuan Province, China, Seismologic Publishing House, Beijing, China, pp 236–238

Zhong LX, Yin YP, Tang C (1992) Environmental geology research on the new site of the Badong town in the reservoir area of the Three Gorges Project. In: Environment Institute (ed) Collection of Papers of Environmental Geology vol. 1. Geology Press, Beijing, China, pp 41–53 (in Chinese)

Zischinsky U (1966) On the deformation of high slopes. Proc. 1st Congr. Int. Soc. Rock Mechanics 2: 179–185

Chapter 16
Study on the Possible Failure Mode and Mechanism of the Xietan Landslide When Exposed to Water Level Fluctuation

Zhenhua Zhang, Xianqi Luo, and Jian Wu

Abstract   Hydrogeological conditions of bank slopes in the Three Gorges Reservoir will change greatly due to the fluctuation of water level in the reservoir, which will affect the stability of the bank slopes. The probable failure mode and mechanism of the Xietan landslide is presented using a physical model in order to test varying conditions of water level fluctuation. The result will give insight as to the failure modes and mechanisms of landslides that have engineering geological conditions similar to those of the Xietan landslide.

Keywords   Xietan landslide · Three Gorges Reservoir · Model test Failure mode and mechanism

Introduction

Hydrogeological conditions of bank slopes in the Three Gorges Reservoir will change with the reservoir impoundment, which will affect the stability of the bank slopes. For example, after reaching the 135 m water level impoundment of Three Gorges Reservoir and discontinuous rainfall from June 21 to July 11, 2003, the Qianjiangping slope failed, resulting in 1,200 people becoming homeless, 14 deaths, and 10 people missing until the morning of July 20 (Li 2003; Headquarter of the Three Gorges Reservoir Geological Hazards Control in the Ministry of Land and Resources 2003). In order to explore the Xietan landslide failure mode and mechanism due to water level fluctuation of reservoir impoundment and operation, a physical model test is taken to study the failure mechanism of this landslide, which will give information about the failure mode and mechanism of the landslides that have engineering geological conditions similar to those of the landslide.

Z. Zhang (✉)
Key Laboratory of Geological Hazards on Three Gorges Reservoir Area, Ministry of Education, China Three Gorges University, Yichang 443002, China
e-mail: zenithzhang@sina.com

Introduction to the Xietan Landslide

This landslide lies in Xietan Town, Zigui County, Hubei Province, China, located on the left bank of Yangtze River and is 48 km away from the Three Gorges Dam. The location of the landslide is shown in Fig. 16.1. The landslide takes on a long tongue-like shape, the front part of the landslide is broad, and the back part is narrow (Fig. 16.2). The elevation of the landslide is 60–380 m from the top to the bottom, the length in longitudinal direction is 780 m, the widths of the rear and front parts are 140 and 460 m, respectively, the thickness of the front half part of the landslide is about 45 m and that of the back half part is about 20 m. The volume of the landslide is 894×10^4 m^3. There are three terraces that developed on the landslide. The sliding mass of the landslide is composed of four layers which are slope wash, debris, slipping zone and bed rock from top to bottom. The thickness of the slope wash is from 0.5 to 4.4 m and the slope wash is composed of silty clay with reduced and block stone. The average thickness of the debris is 30 m, the greatest thickness is 45 m, and the debris is composed of reduced and block stony soil with ratios of soil to stone that are different in different parts. The thickness of the slip zone soil is 0.7–2.7 m, which is mainly composed of reduced stony soil. The structure of the debris is not compacted, and the cementation condition of the debris material is poor, which will cause the structure of the debris to be broken when the debris meets reservoir water. The photograph of the landslide is shown in Fig. 16.3.

Fig. 16.1 Location of the landslide

Fluctuation of Reservoir Water Level

The landslide has been exposed to the 135 and 156 m water level impoundment of the Three Gorges Reservoir, as the reservoir water level reached 135 m on June 15, 2003 (Li 2003) and 156 m on October 27, 2006 (China Three Gorges Project Corporation 2006; Luo et al. 2007). The process of 135 and 156 m water level
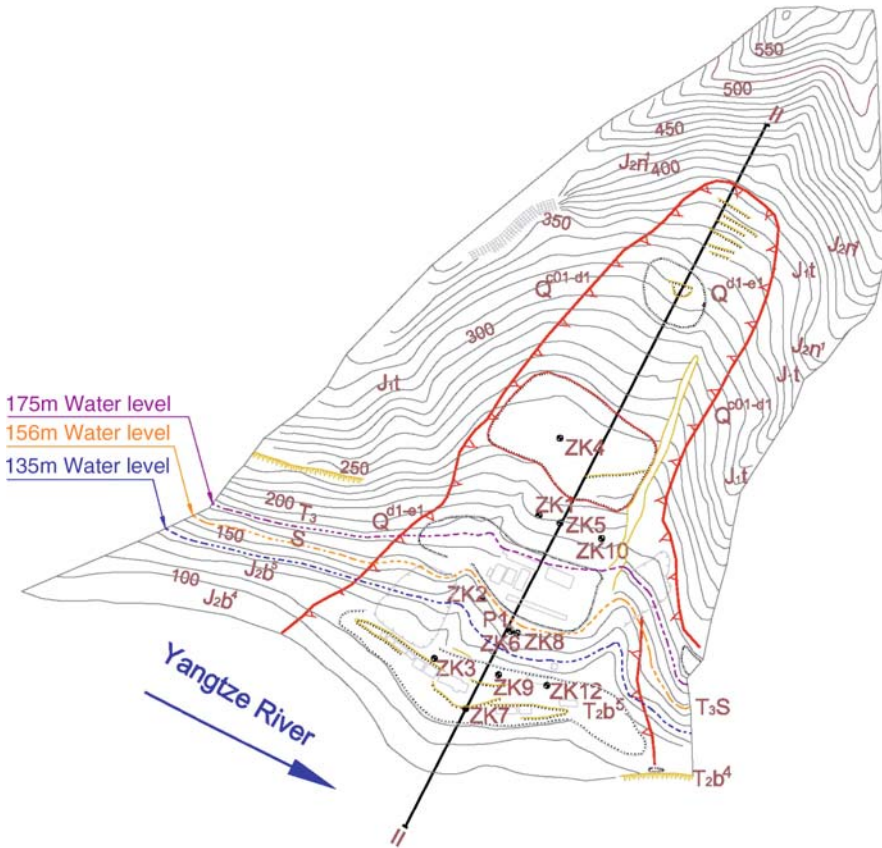
Fig. 16.2 Geological plane sketch of the landslide

impoundment is shown in Figs. 16.4 and 16.5. The reservoir water level will rise to 175 m in 2009, and the fluctuation of reservoir water level during the course of subsequent operation of the reservoir is shown in Fig. 16.6 (Yangtze River Water Resource Commission 1992). The landslide will be exposed to the 175 m water level impoundment in 2009 and the fluctuation of reservoir water level during the course of the operation of the reservoir.

Physical Model Test

Apparatus for the Model Test

The test system is composed of a flume, a lifting apparatus, and a series of water supply apparatus for simulating the fluctuation of reservoir water level. The dimension
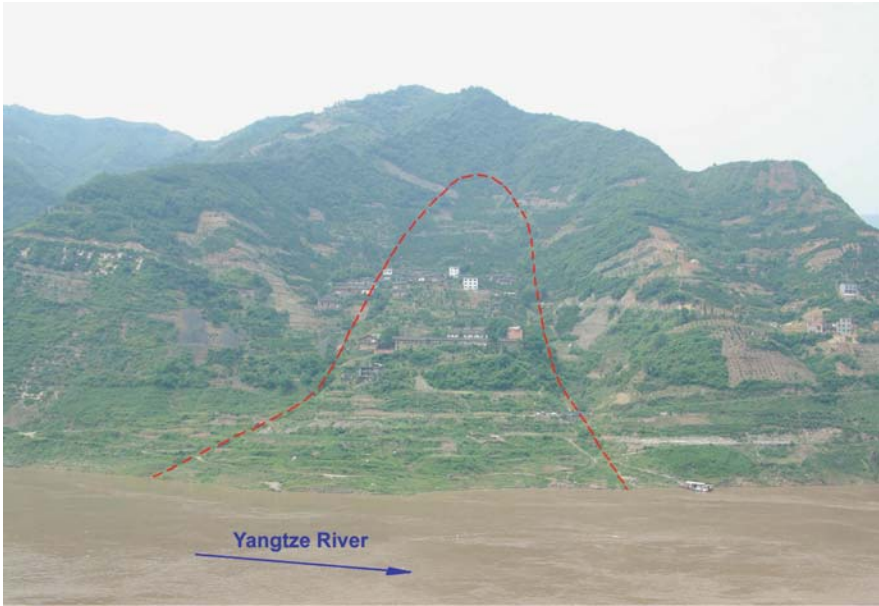
Fig. 16.3 Photograph of the landslide
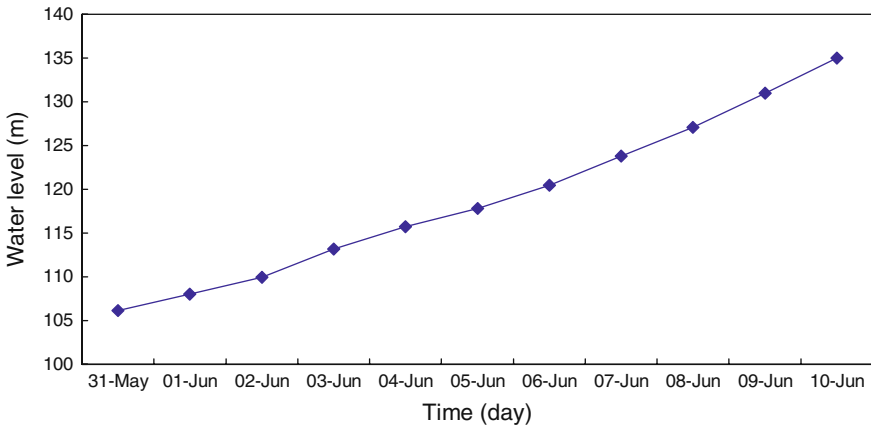
Fig. 16.4 The process of the 135 m water level impoundment of the Three Gorges Reservoir

of the flume is $150 \times 15 \times 100$ cm^3 (length $\times$ width $\times$ height), and the sketch and picture of test system are shown in Figs. 16.7 and 16.8, respectively. The water supply apparatus simulating reservoir water level is composed of an upstream water tank located in the back edge of the slope and the downstream water tank in the front of the slope. Stable supplement of water for the back edge of the slope is obtained through the upstream water tank at the back of the slope, and the fluctuation of water level is simulated by adjusting the supplemental water obtained through the
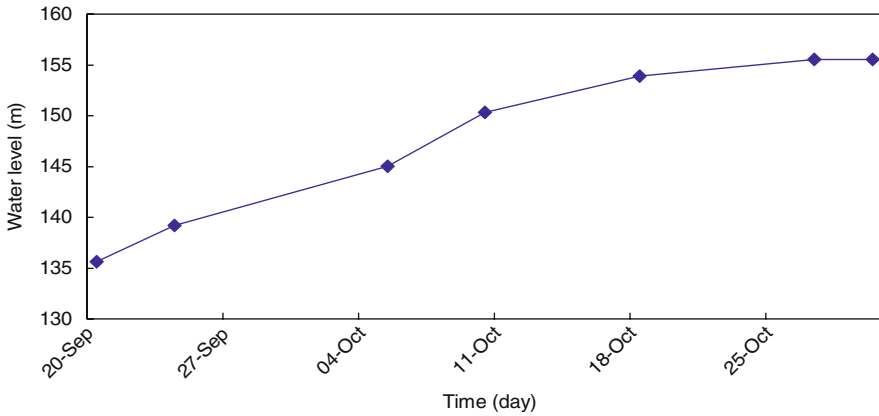
Fig. 16.5   The process of the 156 m water level impoundment of the Three Gorges Reservoir
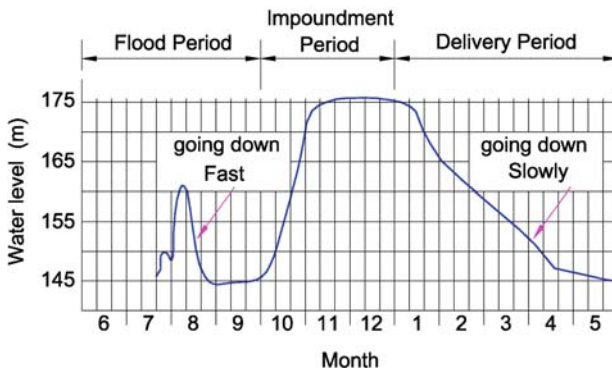
Fig. 16.6   The fluctuation of reservoir water level during the course of the reservoir operation

downstream water tank. Lifting and turning of the model flume can be accomplished through a fixed hinge and a jacking apparatus in the bottom of the model flume; the maximum turn angle was 20°. The failure tests of slopes with different inclinations can be conducted in the flume. At the bottom of the model flume, there are five piezometric tubes in order to measure the underground water table in the slopes and to drain water in the flume, as well.

Section Plane Selection for the Model Test

According to the report on geologic investigations of the landslide, the main sliding direction is in accordance to a II-II section plane (shown in Fig. 16.2). Therefore, a II-II section plane was chosen for the plane stress model test for the landslide in order to study the failure mechanism of the landslide under the condition of the fluctuation of reservoir water level. The II-II section plane is shown in Fig. 16.9.
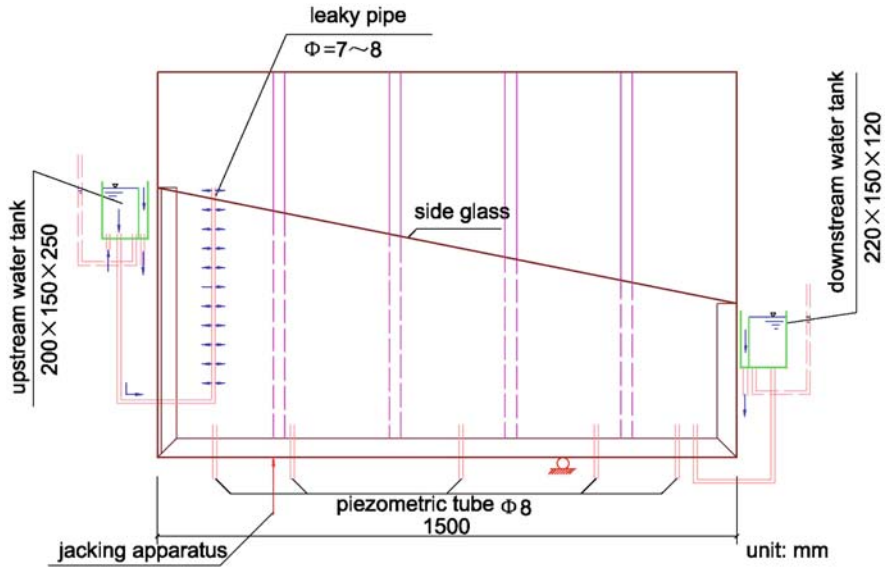
Fig. 16.7 Sketch of the test system

Fig. 16.8 Photograph of the test system

Preparation of Similarity Materials for the Model Test

Formulation of Similarity Material of the Model Test

According to similarity law, the geometric similarity ratio of model and prototype is 1:530. As a result, the angle of the slope of the sliding surface was 16.1°, and the total length of the slipping surface was 155 cm. The value of the cohesion and friction angle of the sliding surface material of the model should meet the
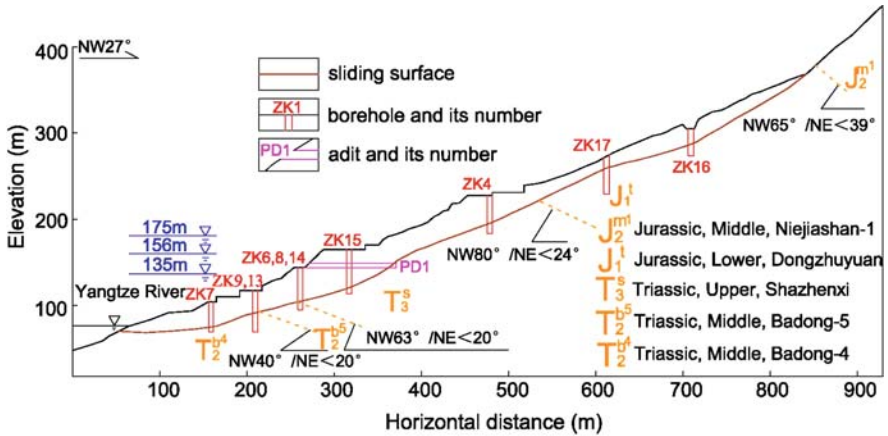
Fig. 16.9 The II-II section plane sketch of the landslide

requirements of similarity law. Four sliding surface materials—double-layered plastic film, flint-glazed plastic film, soap daub, and artificially mixed material containing talc powder—were compared and tested. Artificially mixed material containing talc powder was chosen as the sliding surface material for its value of cohesion and the friction angle being very close to that satisfying similarity law and also as it has the added quality of being waterproof.

Slide mass material was determined using similarity material tests. The mass material was filled and compacted in laminate, and the mass weight was about 45 kg (mass material is the mixture of sand and clay with different proportion). Table 16.1 shows the physical properties of the slide mass.

Table 16.1 Physical properties of the slide mass for physical modeling

Composition	Compact bulk density (g/cm^3)	Apparent density (g/cm^2)	Porosity (%)	Water content (%)	Remark
20% sand + 80% clay	1.8	2.60	30.8	15.0	Fine sand <2.0 mm

Simulation of Fluctuation of Reservoir Water Level

Stable water supply from the upstream water tank at the back of the landslide model was used to simulate the groundwater of the landslide, and the supply altitude of its prototype was 315.35 m. The fluctuation of reservoir water level is obtained from the water pool where the water level is controlled by the downstream water tank at the front of the landslide. The fluctuation of reservoir water level is caused by the reservoir impoundment and operation that is indicated by the progression of 135,

156, and 175 m impoundment levels which also occur during reservoir operations as mentioned above. According to the similarity law, a geometric similarity ratio of 1:530 of model and prototype was used to determine the fluctuation of reservoir water level for the physical model. The relationship between the time of the model test and the prototype is as follows. The formulation is according to that of similarity law:

$$t_m = \sqrt{t_p}$$

where t_m is the time of physical model and t_p is the time of prototype.

Model Test Phenomenon and Its Analysis

When the upper osmotic valve is turned on, the failure process of the landslide under conditions of groundwater seepage and fluctuation of reservoir water level is described as follows.

Upstream water flowed through a leaky pipe and into the soil layer of the slide mass, and when the seepage and saturation line moved gradually to the front part of the slide mass, the water supply was stopped. During the course of the 135-m water level impoundment, the lateral crack appeared at the surface of the soil layer in the front of the landslide. The cracks developed gradually and then arc collapses occurred in the front of the landslide. This kind of arc collapse of the soil layer in front of the landslide appeared one by one. When the water level rose to 135 m and remained at that level until the time when reservoir water level began to rise to 156 m, five collapses occurred. When the water level rose to 156 m and remained at that level until the time when the reservoir water level began rising to 175 m, seven additional collapses occurred. When the water level rose to 175 m and remained at that level until the time when the reservoir water level started fluctuating, as shown in Fig. 16.6, there were five more collapses. The development of the failure process of the landslide is shown in Fig. 16.10 and demonstrated in Fig. 16.11.

Failure Mode and Mechanism of the Landslide

In the light of results of above tests and analysis, the initiation point of deformation and failure of the landslide was in the front of the landslide during the course of reservoir water level impoundment. A small part collapsed at first, which caused a free face for the back part of the slide mass.

When the reservoir level continued to rise, a new collapse occurred, and with the reservoir water level still continuing to rise, the slide mass slid part by part from the front to the back (shown in Fig. 16.9), until at last, the whole slide mass failed. The failure phenomenon of the landslide after the 135 m water level impoundment is shown in Fig. 16.12.

a) top view   b) elevation view
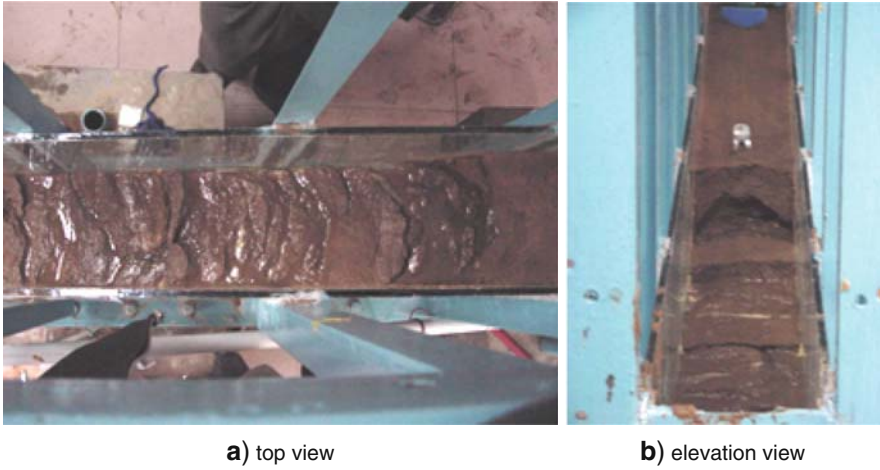
Fig. 16.10   Slide mass sliding, part by part, from the front to the back
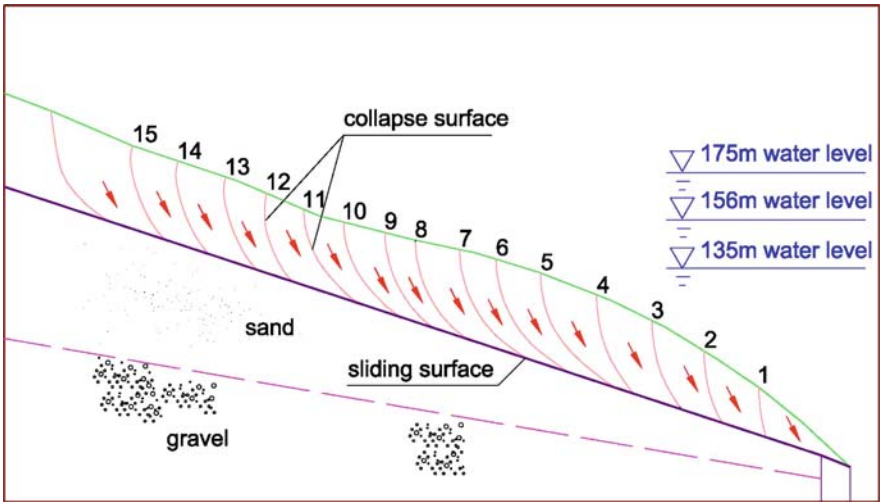
Fig. 16.11   The development of the failure process

During the course of impoundment of the Three Gorges Reservoir, the ground water table in the foreside of the slope increased with the reservoir water level (shown in Fig. 16.13), and the pore water pressure of the front part of the slide mass which was under the reservoir water level increased, causing the soil structure under the ground water table to fail. Meanwhile, the shear strength of this part of the slide mass near the reservoir water level decreased, which made the slide mass near the reservoir water level to collapse (shown in Fig. 16.11). Because of the different

Fig. 16.12 Partial collapse of the landslide after the 135 m water level impoundment
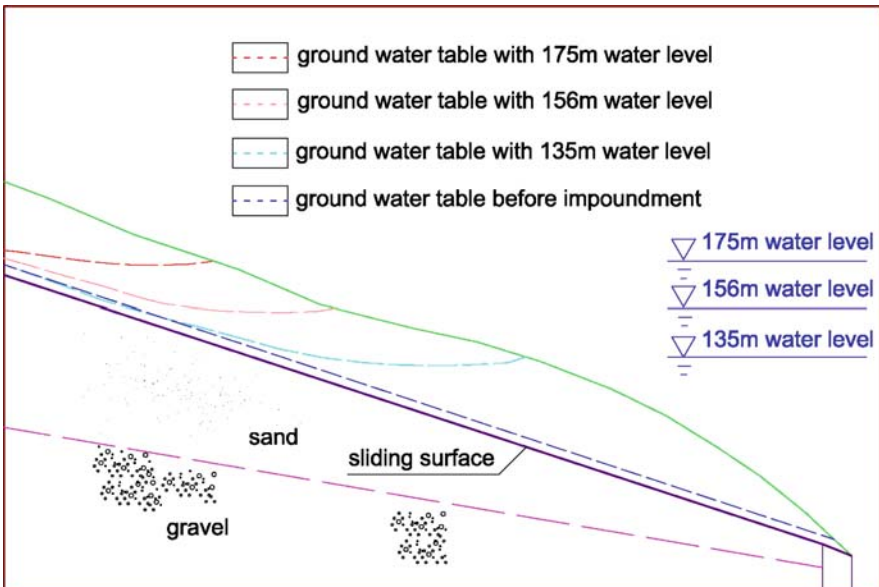
Fig. 16.13 Ground water tables with different reservoir water level after the seepage field stabilized

cohesion and friction angle between the soil of the slide mass under the reservoir water level and that above the reservoir water level, and the value of cohesion and friction angle of former greater than that of latter, the shear strength of the former is greater than that of the latter. As a result, the collapses only happened near and above the reservoir water level and the collapse surfaces take on an arc which are steep near the former and gently inclined near the latter.

Exploration of the Failure Modes of Other Landslides Similar to the Landslide

The failure mode of the landslide is attributed to three factors: the first one is fluctuation of reservoir level, the second one is the composition of the slide mass which is debris and easily broken when they are exposed to the reservoir water, and the third one is that the slip surface is gently inclined and regular. If these factors apply to other old landslides in the Three Gorges Reservoir area, the failure modes of the landslides should be that of mass sliding, part by part, from the front to the back.

References

China Three Gorges Project Corporation (2006) Successful implementation of the goal of 156 m water level impoundment of Three Gorges Reservoir. Large Dam and Safety, 5:68
Headquarter of the Three Gorges Reservoir Geological Hazards Control in the Ministry of Land and Resources (2003) Qianjiangping landslide of Zigui County, in Hubei Province. The Chinese Journal of Geological Hazard and Control, 14(3):139
Li XG (2003) 135 m-water level impoundment log of the Three Gorges reservoir. China Three Gorges Construction, 6:57
Luo XY, Hua XJ, Zhao B (2007) Analysis of water surface gradient variation in Three Gorges Reservoir Area during the course of 156 m water level impoundment. Science and Technology Information, 33:663
Yangtze River Water Resource Commission (1992) Report of Conceptual Design of Yangtze River Three Gorges Multi-purpose Project. Wuhan, China

Chapter 17
A Study of the 1985 Xintan Landslide in Xiling Gorge, Three Gorges Area, China

Guofu Xue

Abstract   The Xintan landslide occurred on June 12, 1985 on the left bank of the Yangtze River, 27 km upstream from the Three-Gorge Dam. It has a large volume of about 20 million m^3 and totally destroyed the Xintan Town. Detailed geological investigation has been conducted since 1968, and a precise monitoring system was established in 1977, so that the early warning was issued before the 1985 event. In this chapter, the geological condition, monitoring data of the landslide deformation used for early warning are presented, with an analysis of the mechanism of the large-scale landslide.

Keywords   Survey · Monitoring · Creeping · Mechanism · Landslide

Introduction

In the early morning of June 12, 1985, a large-scale landslide took place on the left bank of the Yangtze River, 27 km upstream from the planned Three-Gorge Dam. Involving a volume of about 20 million m^3 of sliding mass, it totally destroyed an ancient town, Xintan, which previously had a population of 1371 (Fig. 17.1).

Detailed geological investigation at the site has been conducted since 1968. A precise monitoring system was set up in 1977 and early warning was given before the 1985 event so that all of the 1371 local inhabitants moved away in an orderly manner without suffering any casualties. Both banks of the Yangtze River around Xintan have been unstable sections throughout history. There have been two large-scale landslides described in the historical record which took place in 1031 and 1542 and interrupted the traffic through the Yangtze River waterway. The landslide originated in the colluvial and diluvial deposits on the slope. It has attracted great attention due to its critical location and enormous volume, the threat to the only waterway connecting Sichuan and Hubei provinces, and the possible effect to the construction

G. Xue (✉)
Three Gorges Exploration and Research Institute, Yangtze River Hydraulic Management Committee, China
e-mail: shingtonxue@126.com
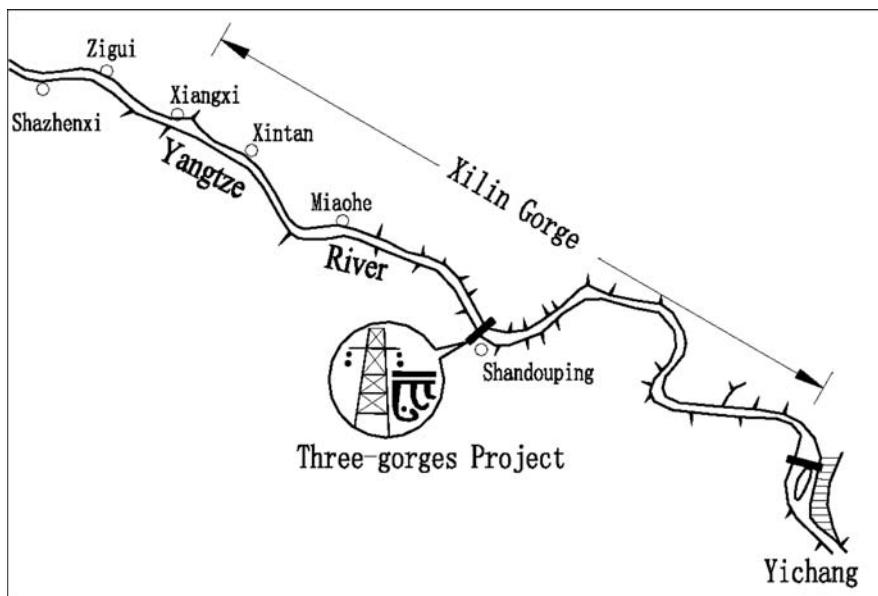
Fig. 17.1 Location of Xintan landslide

and operation of the Three Gorges Project downstream that will be the largest dam and hydropower station in the world. Since 1968, a detailed geological survey of the slope was carried out, including geological mapping on the scale of 1:2000, and which included information from 9 boreholes and 16 exploration pits. A deformation monitoring system composed of four collimation lines was set up at the end of 1977 and eight monitoring survey points and a triangulation network were added in July 1984. Such enormous works laid a solid foundation for the short- to mid-range forecast of the landslide activities. Immediately after the landslide, a comprehensive investigation and research program was conducted using aerial photographic mapping (Fig. 17.2), infrared scanning imaging, topographic surveys, geological surveys, geophysical prospecting, drilling, shaft and trench excavation, reset of the surface deformation monitoring system, and setting up underground monitoring systems such as inverted plumb lines in shafts, inclinometers, and piezometers in boreholes. The intensity and scope of the research work and the success in forecasting the Xintan landslide is one of the most notable accomplishments worldwide, for landslide hazard mitigation (Edil and Schultz 1983; Fookes et al. 1985; Sauer 1984).

Natural Settings and the Geological Structure of the Xintan Slope

The Xintan region is within a rainstorm area of the western Hubei Province. The annual mean precipitation of the area is around 1100 mm. The rainy season is from May to September and the torrential rain is usually concentrated in June and July.

before sliding   after sliding
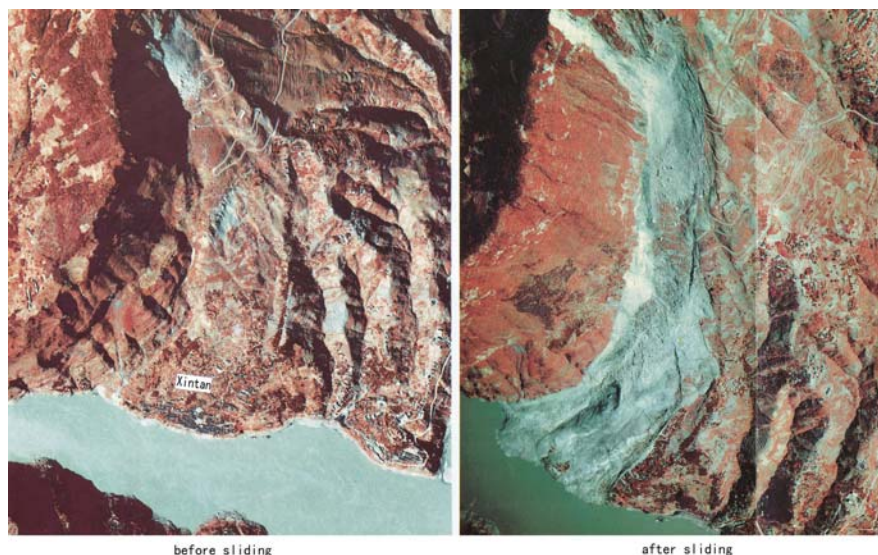
Fig. 17.2 Infrared aerial images of Xintan landslide area (From Ministry of Geology and Mineral Resources, PRC)

The recent maximum rainfall in this area during a 5-day period occurred at Xinshan County 40 km away from Xintan landslide area and the maximum 12 h record is 545 mm which took place 60 km away.

The pattern of the crust movement of the Three Gorges region is of massive and intermittent uplift with a magnitude of 1700–2000 m since the latter part of the Yanshan Movement, which results in the landform of high mountains cut by deep valleys which provide favorable topographic conditions for slope movement, such as rockfall, avalanche, and landslide.

The bedrock outcropped at Xintan successively from east to west is Silurian shale and sandstone, Devonian quartz-sandstone, carboniferous limestone with coal seams, striking N10–30E, i.e., roughly perpendicular to the Yangtze River. It dips NW, i.e., the upstream at angles of 25–38 degrees (Fig. 17.3). In the course of down-cutting of the Yangtze River, the bank of the soft Silurian shale and sandstone being more sensitive to erosion was shaped into a trough-type slope of a gentle angle while the section formed by the firm Devonian–Permian limestone and sandstone was shaped into a cliff of 300–450 m in height to the west of Xintan.

Being divided mainly by two sets of joints and with underlying incompetent shale and coal seams, the cliff retrogresses unceasingly due to the frequent rock-falling under the long-term action of de-stressing, settlement, solution, gravity, and weathering.

The great volume of colluvium deposited in the trough-type slope of the shale to form the Jiangjiapo–Xintan slope was the material base of the giant landslide. The accumulation slope stretching along S–N was roughly 2 km long, narrower in the north portion (300–500 m wide) and wider in the south portion (1100 m wide along the riverside line), with total area of 1.1 km². The elevation at its back fringe was
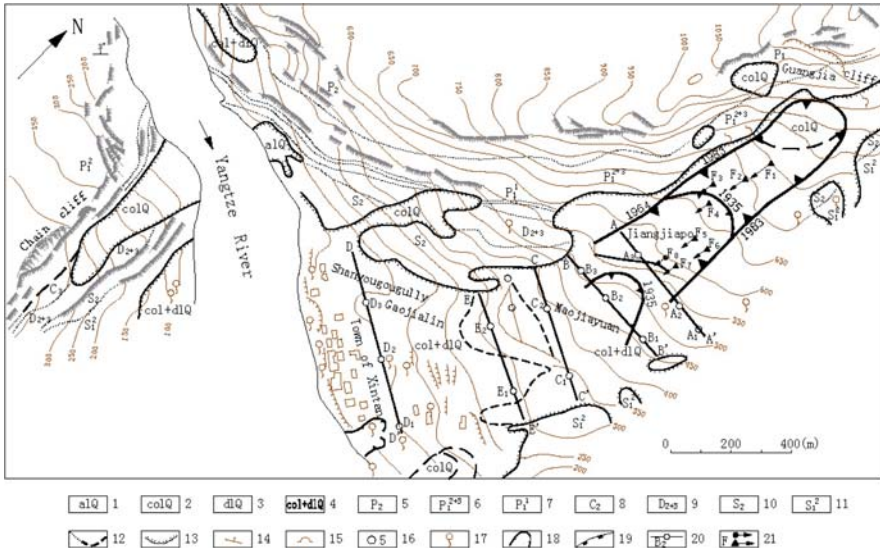
Fig. 17.3 Geological map of Xintan slope. 1 – Quaternary alluvium; 2 – colluvium; 3 – slope wash; 4 – colluvium and slope wash; 5 – upper Permian limestone; 6 – Qixia–Maokou limestone, Permian; 7 – Ma'anshan coal seam, Permian; 8 – carboniferous limestone; 9 –Devonian sandstone; 10 – Silurian sandstone and shale; 11 – Luoreping shale, Silurian; 12 – lithological contact; 13 – contact line between quaternary and bedrock; 14 – attitude of stratum; 15 – coal-mine opening; 16 – borehole with number; 17 – gravity spring; 18 – old landslide; 19 – crack and the year it occurred; 20 – collimation line with code; 21 – horizontal displacement of survey point

900 m and 65 m at the shoreline. The average 86 m at its greatest height, increased from east to west. The total volume of the accumulations was over 30 million m^3. There were two transverse steps at the middle part of the slope (Figs. 17.3 and 17.4). One was the front step of the Jiangjiapo slope, being at elevation of 500–560 m, a height of 40–60 m, in the direction of N30E and at a slope angle of 50–60 degrees. The entire slope was divided by the step into two parts: upper section (Jiangjiapo slope) and lower section (Xintan slope). Another was the front step of the Maojiayuan flat being at an elevation of 270–330 m, in a direction of N75E and about the same height and slope angle as the former. It subdivided the Xintan slope into the Maojiayuan flat and the down-step gentle slope. Xintan Town was situated on the lower slope close to the shoreline. A gully named Sanyougou developed along the foot of the western cliff, acting as a main drainage system for both surface and underground water flow. The accumulations, based on their geneses, could be classified as the following: (1) colluvium comprised the back talus and the 20–30 m of the surficial portion of the Jiangjiapo slope and consisted of limestone blocks and debris which were loose, without sorting and with clay less than 5% in volume; (2) colluvium-slope wash made up the 10–40 m of bottom portion of the Jiangjiapo slope and was relatively dense, composed of debris and boulders of mainly limestone, locally purple-red sandstone, and shale, with a rather high content of clay (which may form lens).
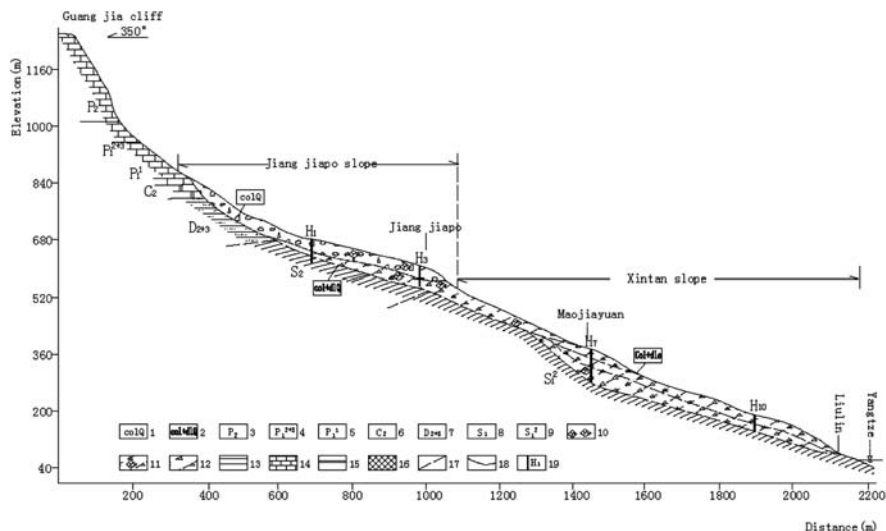
Fig. 17.4 Longitudinal geological section of the slope. 1 – Quaternary colluvium; 2 – colluvium and slope wash; 3 – upper Permian; 4 – Qixia–Maokou formation, lower Permian; 5 – Ma'anshan formation, lower Permian; 6 – Huanglong formation, middle carboniferous; 7 – upper-middle Devonian; 8 – Shamao formation, lower Silurian; 9 – Luoreping formation, lower Silurian; 10 – limestone blocks; 11 – limestone block-debris with soil; 12 – limestone–sandstone debris with soil; 13 – shale; 14 – limestone; 15 – coal seam; 16 – sandstone; 17 – lithological contact; 18 – speculative slip plane; 19 – borehole with number

The two types of accumulations above which formed the Jiangjiapo slope had a volume of about 13 million m³; (3) slope wash and colluvium was distributed at Maojiayuan flat and the area between the former and Gaojialing ridge, composed of a high content of clay debris of mainly Devonian quartz-sandstone, Silurian sandstone, and a small amount of Permian limestone. Locally, clay occurred in the form of lenticular layers; (4) mixed accumulations of alluvium and colluvium, distributed around the Gaojialing ridge and the town of Xintan and composed of mainly sub-angular limestone debris and rubble with alluvial gravel, cobble, and lenticular clayey seams, were dense, as they were 10–30 m thick. The third and fourth types, 19 million m³ in volume, made up the Xintan slope.

On the whole, there was a tendency that the density of the accumulations and clay content increased and the porosity and permeability decreased from surface to bottom and from the back fringe to the front of the slope.

The source of the underground water was mainly rainfall, and partially the surface and underground water of the western cliff. The colluvium of the surficial portion of Jiangjiapo slope and the back talus was highly permeable and there was no water storage in it. Due to the higher content of clay and lower permeability in the Xintan slope and the bottom portion of Jiangjiapo slope, the groundwater table fluctuated much over time. There were several groups of permanent springs at the mouth of the Sanyougou gully, in the middle part of Xintan town and Liulin. The

discharge of a single spring was 0.01–0.2 l/s in the dry season and 0.7–2 l/s in the rainy season.

In summary, the Jiangjiapo–Xintan slope possessed the external characteristics and internal causes for landslide occurrence. In fact, it was an unstable slope comprised of a series of ancient multistep landslides with different scales which reactivated repeatedly through history.

In the last decades, the rockfalls in volumes of tens of thousands of cubic meters took place many times from the western cliff. A large-scale landslide occurred on July 3, 1935 when Xintan Town was in the famous "357" rainstorm area. At that time, the 7-day heavy storm resulted in 1.5 million m^3 of accumulation at the front part of the Jiangjiapo slope and 200,000 m^3 of overburden at the Liulin village near the river slipped down and 20 or more houses of the village were pushed into the Yangtze River.

Features and Mechanism of the Landslide

Developing Process of the Landslide

The Xintan landslide resulted from the long-term deformation of the colluvium and slope wash of the upper section (Jiangjiapo slope) of the entire slope. The progress of the deformation could be divided into two stages.

Upslope-Stepwise Progressive Deformation Stage (Before the Rainy Season of 1983)

In 1935, at the front part of Jiangjiapo slope, a landslide, as described above, took place and probably failed to the surface of bedrock. In 1962, a tension crack 270 m long appeared upslope from the main scarp of the landslide above and separated an unstable part 200,000 d m^3 in volume from the slope. After the rainy season of 1964, a 450 m long side crack trending S–N was formed on the western part of the slope. After the rainy season of 1982, the intermittent longitudinal cracks and corresponding feather cracks originated on both side of Jiangjiapo slope and remarkable tension cracks were found in the back fringe. The development processes of the local landslide and cracks show that the release of the accumulated energy of the slope and the deformation progress was going on upslope, in a stepwise, progressive deformation. This stage could be further divided into three periods (Figs. 17.5 and 17.8):

a. Creep period (before August 1979). From November 1977 when the monitoring survey system was put into effect at the end of this period, the total horizontal displacements of survey points A_3 and B_3 at the front part of Jiangjiapo slope were 110 and 126.4 mm, respectively, and their mean monthly displacements

Fig. 17.5 Curves show the accumulative horizontal displacements of the survey points
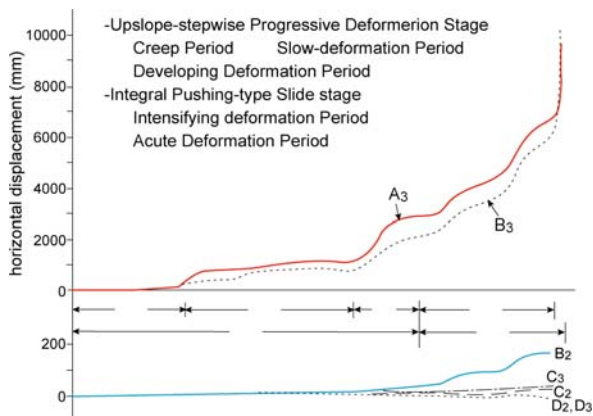
were 5.5 and 6.3 mm. The data above shows that the deformation of this period was gentle and rather uniform. The slope deformation did not respond to rainfall.

b. Slow deformation period (August 1979–before rainy season 1982). In this period, the total horizontal displacements of A_3 and B_3 reached 1088 and 848.4 mm, respectively, and the mean monthly displacements were 17.8 and 13.1 mm. The monthly displacements of A_3 and B_3 sharply increased, becoming 336.3 and 152.1 mm, respectively, at the greatest point.

c. Developing deformation period (rainy season 1982–April 1983). In this period, the total horizontal displacements of A_3 and B_3 were 2768 and 2086.6 mm, respectively, and the mean monthly displacements were 129 and 95.3 mm. The monthly displacements of A_3 and B_3 in the rainy season further increased, reaching 525.6 and 207 mm, respectively.

Integral Pushing-Type Slide Stage (May 1983–Major Landsliding in 1985)

After the rainy season in 1982, the cracks on both sides of Jiangjiapo slope, which had disconnected, extended quickly and remarkable tension cracks further developed in the back fringe, which indicated that the boundary conditions for an integral sliding reached the maximum. The survey results of the nine monitoring points F_1–F_3, A_3 that were distributed on Jiangjiapo slope (Fig. 17.3) showed that the total horizontal displacements of each point decreased from 6.9 m (F_1 at back part of the slope) to 2.7 m (A_3 at front part) gradually from July 2, 1984 to May 15, 1985, which indicated that the deformation pattern of the slope was shifted from upslope-stepwise progressive stage to the integral pushing-type sliding stage (Fig. 17.5). It could be further divided into two periods according to the characteristics of deformation:

a. Intensifying deformation period (May 1983–the middle of May 1985). In this period, the cracks on both sides and at the back fringe of Jiangjiapo slope further extended and were connected, forming an integral curved tension boundary. At

the front step, small-scale slipping took place from time to time, i.e., 1200 m^3 of slope material to the west of A_3 slid down with gushing mud and water. The total horizontal displacement of A_3 was 5374 mm, and the mean monthly displacement was 108 mm. The maximum monthly displacements of A_3 and B_3 reached 476.5 and 499.1 mm, respectively.

b. Acute deformation period (middle of May–June 12, 1985). From May 14 to June 11, the horizontal displacements of A_3 and B_3 were as great as 8.8 and 13.7 m, respectively. From the beginning of June, a series of indications of an impending large-scale landslide appeared on Jiangjiapo slope. Until June 9, the ground surface at the back fringe slipped down to a height difference of 13.5 m. There was some rock rolling and small-scale landsliding that took place frequently at the front step.

The ground surface downslope from the step, at elevation 380–400 m, was becoming wet and bulging. At 4:15:00 h, a landslide involving 600,000–700,000 m^3 of slope material at an elevation of 360–520 m in the Sanyougou gully occurred. On June 11, the slope continued slumping quickly along the curved tension boundary crack on both sides, where more tension cracks occurred.

The ground at elevation 380–400 m was further shearing and bulging, showing characteristics of exposed slip plane. The 1 day horizontal displacements of A_2 and B_3 reached 6.1 and 3 m, respectively. The large-scale landslide on Jiangjiapo slope which had been brewing for a long time was at a critical moment.

In contrast, the lower slope, Xintan slope had been in stable condition before the major sliding. Since 1977, all survey points on the collimation lines C, D, and E on the slope except for points C_2 and C_3, that were close to the front steep of Jiangjiapo slope and slightly displaced had little displacement (Fig. 17.3).

The Course of the Landslide

At about 3:45:00 h, June 12, 1985 (based on a seismogram the time and duration of the failure lasted from 3:51:58 to 3:56:05 h, i.e., for 00:4:07 h). Following a roaring sound, millions of cubic meters of accumulations bounded by the curved tension crack of Jiangjiapo slope slipped down en masse along the surface of bedrock, causing the mass (a volume of 2.8 million m^3 at Maojiayuan flat) to move southward and shear out at an elevation of around 380 m (Fig. 17.6). As soon as the mass at Maojiayuan flat was sheared off and 2.8 million m^3 of mass slid away from the flat, the sliding of the 11 million m^3 of mass speeded up as result of the loss of resistant body. Comparing the topographic maps surveyed before and after the landslide indicates that a total of 4.8 million m^3 of mass moved away from the slope above the elevation of 380 m, i.e., from the place above the slip plane. Most of it slid off at the place below elevation of 630 m or so and rushed down along Sanyougou gully in the form of a debris flow, partly flowing into the river water and forming the largest slip tongue and generating the highest surge of water during this event. In the course of
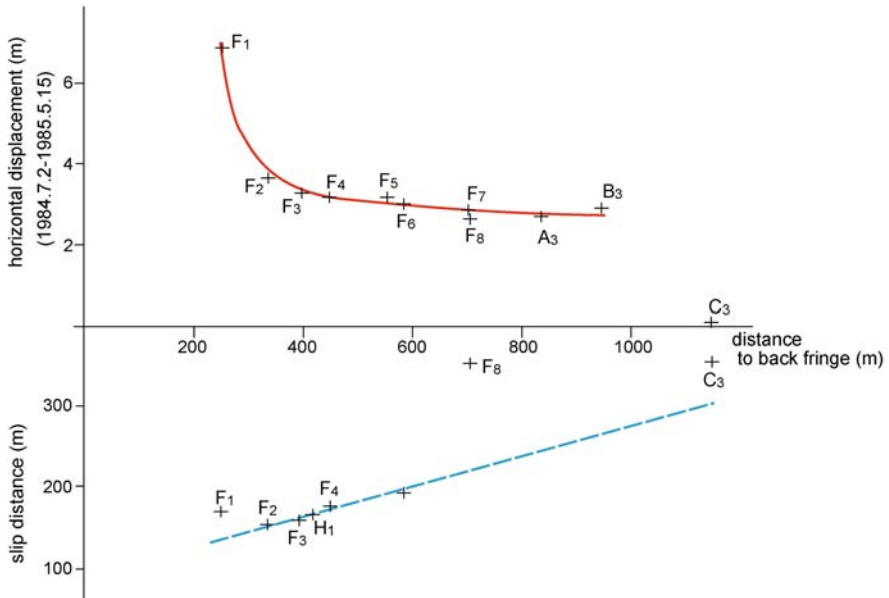
Fig. 17.6 The displacements of reference marks before and after the slide

movement, the sliding mass cut off part of the bedrock of the western cliff, widened and partially cut down Sanyougou gully. Another portion of the sliding mass (about 1.7 million m^3) being pushed off from Maojiayuan flat moved southward and then distributed on Gaojialing ridge and the narrow area to the east of the ridge. Comparing the locations of the survey monuments before and after the landsliding shows that the horizontal displacements of Jiangjiapo slope increased from 100 m or so at the back part to 200 m or so at the front part (Fig. 17.7). Though the ground surface has experienced long-distance displacement and there are a great amount of cracks
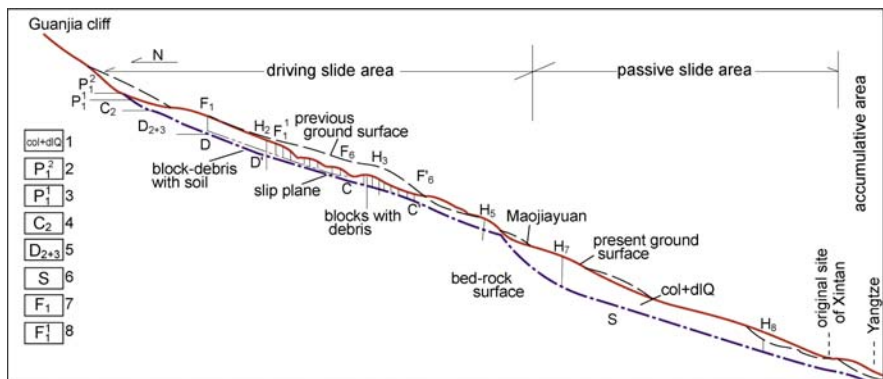
Fig. 17.7 Longitudinal geological section of Xintan landslide

and scars existing there, the vegetation and surface features remain intact, which shows the character of integral slip.

Under the pounding, loading, and dragging effects of the debris flow from Jiangjiapo slope, the lower slope, i.e., the Xintan slope which had been in stable situation was disturbed in different degrees and depth and became divided into three parts with different features:

(1) Maojiayuan flat and Gaojialing ridge – Relatively Stable Zone (IIa). Gaojialing ridge kept its original topography, being about 70–120 m wide and 10–50 m higher than the ground on both sides and extending in S–N direction. Northward, it is connected with Maojiayuan flat, becoming an integral body. Though the surficial part of this area was disturbed and covered by the limestone debris rushing down from the upper slope, the quartz–sandstone debris and purple-red clayey soil with sandstone debris in the front step of Maojiayuan flat are original material remaining in place. No disturbing of shearing remarks is found in the dense mass. This indicates that the base of this area kept its stability during the landsliding.

(2) Eastern Part – Shallow Slide Zone (IIc). Loaded and dragged by the debris flow from Maojiayuan flat, the accumulations of this area slipped southward along slip planes at different depths. In general, the change of the topography upslope from borehole 9 is not significant. However, in the zone 200–250 m wide along the shoreline, the elevation of the ground surface has increased by 5–25 m and the volume by 620,000 m^3. The slip tongue in the river is 400 m wide and occupied 31–40 m of the water surface where the water level is 65 m. The volume of the sliding mass under water is about 1 million m^3.

(3) Sanyougou Gully – Rapid and Deep Sliding Zone (II$_6$). This was the path for the sliding mass rushing into the river. On June 10, about 600,000–700,000 m^3 mass covered the gully. On June 12, about 2 million m^3 of debris flow pounded into the gully, widened and deeply cut the head part of the gully and increased the middle and lower part by 10–25 m. Part of the mass rushed into water, forming a slip tongue 320 m wide which occupied 55–95 m wide of the water surface, creating a surge wave climbing up 49 m in height on the opposite bank. The volume of the sliding mass under water is about 1.6 million m^3.

Scope and Magnitude of the Landslide

The landslide occurred on the west part of the original slope overburden and is bounded on the west by the bedrock cliff. The east flank scarp runs N50–10E at the upper part and turns to S40N below elevation of about 400 m. The slide, 200 m in length from S to N, 220 m wide near to the main scarp, 380 m wide at its middle, and 720 m wide along the river band, covers 0.73 km^2 area and involves 2×10^7 m^3 of slope material, accounting for 66% of the total area and 60% of the total volume of slope accumulations, respectively.

The slide may be divided into four parts based on its mechanism (Fig. 17.7):

(1) Drive-sliding area (area I). This refers to the former Jiangjiapo slope and part of the Maojiayuan flat. The slip plane seems to be along the surface of the bedrock in general. The volume of the whole sliding mass of this area is about 13.8 million m^3: 4.8 million m^3 slipped away and 9 million m^3 left on the slip plane.

(2) Drag-failure area (area II). This is a part of Xintan slope between elevation 380 and 80 m, covering 39×10^4 m^2 in area which accounts for 55% of the total area of the whole landslide. The total volume of the accumulations is 17 million m^3. It is estimated that the mass that slid is about 5.34 million m^3, which accounts for 31% of the total volume above. Comparing the topography before sliding, the upper part of the ground surface is lowered and the lower part is raised. The volume of the accumulation is increased by 1.4 million m^3. As mentioned above, this area could be subdivided into three zones. At the quick-deep slide zone, i.e., Sanyougou gully, the mass that slid is about 1.14 million m^3 at the other two zones (II_a, II_0), the slid area volume is estimated to be 4.1 million m^3.

(3) Accumulating area (area VI). This area is situated on the former flood land, lower than elevation of 80 m, and the left side of the former riverbed. The tip of the material that slid occupies the major part of the river channel, being 200–300 m wide, more than 1 km long along the river, and 5–20 m thick, covering 190,000 m^2 of water area. The total volume of new accumulations reaches to 3.4 million m^3, 80,000 m^3 of it deposits on the former flood land above elevation of 65 m, 2.6 million m^3 of it is under water. At the cross section facing the mouth of the Sanyougou gully, the material that slid occupied one-third of the total former river section where the river water level is at an elevation of 65 m.

In addition to the three areas above, there is another belt-like disturbed area, 40–160 m wide, which developed on the east of the slope, and has been affected by dragging, pulling, and releasing actions.

Mechanism and Causes of the Landslide

1. The loads of the back talus and the accumulation of slope material are the key causes of the landslide of the Jiangjiapo slope.

   The fact that the Sanyougou gully exists on the west side of the Jiangjiapo slope indicates that at present, the volume of collapsed rock from the west cliff is less than the volume of the material which was transported through the gully and the slope material mainly originates from Guangjiaya cliff, north of the slope. The collapsed blocks of the Guangjiaya cliff partially load the talus cone and partially roll down the slope, resulting in an increase of the overburden of the Jiangjiapo slope. The talus cone with surface angles of 30–45 degrees is situated at elevation 740–910 m. The slope angles of the buried bedrock surface vary from 25 to 60

degrees and increase toward Guangjiaya cliff. The volume of the talus cone is about 1.5 million m³. Choosing the section in Fig. 17.6 as a representative one for the talus cone and assuming the unit weight of the talus to be 22 kN/m³, and adopting friction coefficient to be 0.38, $C = 0$, resulting from calculation, 800,000 T of horizontal surplus pushing force is obtained from calculation. This force and the gravity of the slope overburden are the main trigger, which resulted in the integral pushing-type sliding.

2. The typical boundary condition of the slide determines the special pattern of the failure. On the longitudinal section of the slope, as shown in Fig. 17.3, a steep surface which is located below the Maojiayuan flat divides the top of bedrock surface to two parts: upper and lower. The extension line of the upper part of the top of the bedrock meets the ground surface of the Maojiayuan flat. Therefore, the sliding surface existing along the top of the bedrock in the Jiangjiapo slope would develop further along the place where the shear stresses were concentrated and the counter shear force was lower, i.e., roughly following the extension line of the bedrock surface and daylights on the Maojiayuan flat. That is why the Xintan slope, for a long time before the major landslide, had not been pushed entirely by the Jiangjiapo slope and has been in stable condition although the latter had been intensively deforming.

On the cross sections of the slope, the bedrock surface inclines to the west in general. Naturally, the lower portion of the bedrock surface is situated close to the foot of the western cliff. The western part of the slope, possessing thicker overburden, more intensive groundwater activities, and a lower boundary surface, i.e., bedrock surface, should be less stable than the eastern part. Consequently, it is at the western part that the June 10 sliding took place and also from there that most of the sliding material of the major landslide on June 12 moved away. The steep eastward rise of the bedrock surface limited the eastward development of the landslide. Some evidences show that a low bedrock ridge probably exists under Gaojialin ridge and extends upslope, through the front step of the new Jiangjiapo slope to borehole 3. The ridge divides the bedrock surface into two longitudinal troughs. The western one is deep and narrow and has historically always been the path for the slip material transported from Jiangjiapo slope to the river channel. The eastern one is open, shallow, and gentle, and the slope accumulations on it were rather stable before the sliding. The slope accumulations of Gaojialing ridge and Maojiayuan flat probably protected by the bedrock ridge appear to be the most stable part of the whole slope. Comparing the location of each survey point (F_1–F_6) before sliding with that of after sliding shows that the moving direction of Jiangjiapo landslide was roughly parallel to the western cliff, which indicates that the rocky cliff limited the sliding.

In short, the shape of the bedrock surface buried in the slope controlled the shape and scope of the landslide. The characteristic that the bedrock surface is divided into two parts (upper and lower), the lower part consisting of one ridge and two troughs, determined the deformation pattern of the whole slope. The deformation of the upper slope fully differed from that of the lower slope, as the lower slope was broken up into three different portions.

3. Impact of the dual structure of the accumulations on the dynamics of sliding. The accumulations of the Jiangjiapo slope were divided into upper and lower layers

(Fig. 17.4). The upper one, 20–40 m thick, consists of limestone blocks; the lower one, being 10–40 m thick and thickening downslope, consists of blocks and debris mixed with clayish soil that contains local clayish lens. In the rainy season, the lower layer may have been saturated and became material ready for a dense mud flow.

Figure 17.7 shows the change of area and shape of the overburden section between survey points F_1 and F_6 before and after sliding. If sliding of the F_1F_6CD section was integral, its area should increase due to loosening effect, i.e., $F_1'F_6'C'D' > F_1F_6CD$. In fact, $F_1'F_6'C'D\prime$ was 44% smaller than F_1F_6CD. This can be only interpreted that the lower layer has been squeezed out sideways, flowing to the west ditch based on following reasons. First, the surface vegetation and features between F_1 and F_6 was preserved intact, which rules out the possibility that the reduction of the area was caused by surface sliding. Secondly overlaying $F_1'F_6'C'D'$ with F_1F_6CD shows that the reduction part is surprisingly similar to the lower layer. Finally, the back calculation found that the friction coefficient of the skip surface increased after sliding, which indicates that the lower weak material may be replaced by the upper layer. It is conceivable that the saturated lower layer under the load of the upper layer and the pushing force from the back talus of the slope would be a final stress condition. As soon as the great amount of material slides away from the west gully, the exposed lower layer would be squeezed out to the direction of depressurization. This sideways squeezing out of the lower layer, if it is verified by further explorations, should be a unique phenomenon which is beneficial to restabilization of the part of the slope that slides.

4. Impact of precipitation on the landsliding. Figure 17.8 shows that displacement of the Jiangjiapo slope, represented by survey points A_3 and B_3, has a period of high-rate deformation each year which closely corresponds to the rainy season. This relationship is characterized as follows:

(a) The start and end times of the high-rate deformation period lagged behind the start and end times of rainy season. The lagging start time decreased year by year and the lagging end time increased year by year.

(b) The precipitation–displacement relationship varied in different deformation stages, which reflects the degree of development of the slip plane and the variation of the strength of the slip plane. In the creep period, the slip plane had not initiated yet. Though the groundwater in rainy season reduced the stability of the slope, the shear stress had not reached the peak strength of the potential slip plane so that the deformation rate had no change in wet season, i.e., no high-rate deformation stage occurred yet. In the slow deformation period, the primary slip plane was formed but did not penetrate the full length of the slope. In the wet season, the groundwater that originated from rainfall reduced the strength of the slip plane and effective normal stress acting on it speeded up the slope deformation. However, the saturation process was very slow, due to the poor penetration of the incomplete slip plane. Therefore, the stage of high-rate deformation lagged remarkably behind the start time of the rainy season (for 3–4 months). On the other hand, due to the strength of the slip plane, deformation had not lowered down to its residual value and the surplus driving force
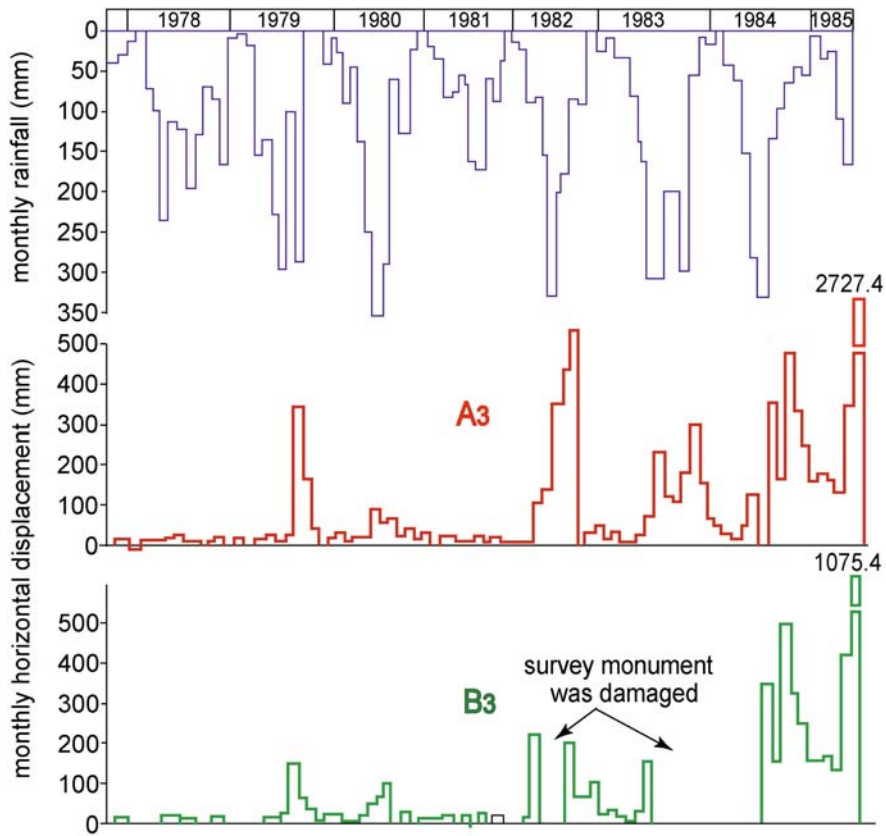
Fig. 17.8 Relationship between displacement and rainfall

was not great enough. As soon as the strength of the slip plane was partially recovered, the sliding rate slowed down and the period of the high-rate deformation ended only 1 month behind the end of the rainy season. In the integral pushing-type slide stage that started from rainy season of 1983, the slip surface fully penetrated the entire slope and gradually experienced long-distance shearing and grinding. As a result, its strength gradually decreased to the residual value and cohesion decreased nearly to zero. Therefore, in the rainy season, the groundwater may quickly penetrate along the slip plane so that the period of high-rate deformation and rainy season started almost simultaneously. But after the rainy season, due to the low strength of the sliding surface, the retardation process of the high-rate deformation lasted for a long period (3–5 months) and never completed during entire dry season (e.g., in 1984).

(c) In different stages of slope deformation, the critical value of rainfall to trigger high-rate deformation (which is related to the total precipitation since the beginning of the rainy season before the start time of the high-rate formation) was different and tended to decrease year by year.

It is noteworthy that the Jiangjiapo slope, though having experienced the extremely high-rate deformation stage in the rainy season of 1984, still decelerated in the dry season of the year. In the late dry season, i.e., from middle of March to the beginning of April 1985, the monthly horizontal displacement of A_3 and B_3 was rather great (about 130 mm) but only one-fourth or so of the maximum horizontal displacement (MHD) of the previous rainy season, which indicates that the slope tended to be stable if there was no more rain. However, in the first month (April) of rainy season of 1985 though there was no rainstorm coming yet, the trend of the displacements of A_3 and B_3 was still sharply reversed and the MHD reached to the value of about three times as that of the previous month (Fig. 17.8). The rainfall only slightly increased in May and early June, being about 150 m or so, the displacement increased tens of times more than those in the previous dry season, having led to the final failure of the slope.

The data above shows that the progressive failure of the Jiangjiapo slope was closely related with the amount of rainfall. The high and rather concentrated rainfall in this region favors the creep of the slope and speeds up the initiation and development of the slip plane and sliding, as well. As the movement of the slip plane progressed, the sensitivity of the landslide to the rainfall gradually grew. Though the landslide on June 12 was not triggered by a certain rainstorm, it is clear that the rainfall of the rainy season increased the groundwater activity, thus inducing the slope to finally fail.

The studies on the Xintan landslide revealed that whether or not the rainfall induces sliding depends not only on the intensity and quantity of rainfall but also on the developing stage that the landslide is in. If the conditions are not ripe enough for sliding, a heavy storm or long rains may not necessarily cause integral landslide. For example, in 1935, an exceptional rainstorm only generated some local slides at the Xintan area. The intensity and amount of rainfall needed for triggering a slide decreases as the slope progressively deforms. At the higher stage of slope deformation even rather low-level rainfall may trigger landsliding if it is strong enough to form underground water flow. Therefore, it is reasonable to take the "triggering rainfall" for the lower limit of rainfall which probably induces sliding during the year.

5. Failure of the lower slope. Xintan slope was caused by loading and dynamic surface-dragging action of the debris flow rushing down from Jiangjiapo slope.

The eastern part of Xintan slope (Zone IIc) below elevation of about 380 m had borne the loading and dragging forces caused by the debris flow of around 1.7 million m^3, i.e., 3.4 million T rushing in high speed along part of the slope. The shear stress created by the dragging force reduced quickly with the depth of the slope accumulations, as did the displacement of the slope. In the course of deformation shear slip planes could develop along some incompetent layers if they existed in the slope. The depth of the slip planes varied from place to place as a result of great differences of the occurrence of incompetent layers, variation of the block-size and density of scale, slip distance and slip-rate, and its structure and mechanism are more complicated.

6. Earthquakes were not the cause of the landslide. The Xintan area is situated in the Zigui–Yuyangguan Seismic Belt that is a small seismic region with only low-level magnitude and infrequent recurrence of earthquakes. The nearest seismic structures are the Xiannushan fault and the Jiuwanxi fault which are a few kilometers away from the slope. There was no destructive earthquake in the last 2000 years according to historical record. Some description about "earthquake and avalanches" is found in a local file but it distinguishes what is called earthquake with that caused by gravitational rockfall. The seismograms recorded by the seismic-station network in the Three Gorges region show that the area was microearthquake-free a half year before June 12, 1985 within 60 km distance from Xintan and earthquake-free from June 1 until the end period of the sliding and within a 200 km distance. This indicates that based on data available, there is no direct connection between earthquakes and Xintan landslide.

According to the seismic conditions, the maximum credible earthquake (MCE) of the Zigui–Yuyangguan Seismic Belt is found to be about M_S 5.5. Even if an earthquake with this magnitude takes place at the north tapering point of Xiannushan fault, the intensity at the sliding area, after 10 s, through at 8 km distance, will be estimated to be about 6 degree of intensity (in Chinese Seismic Intensity scale; the maximum value is 12 degrees) that indicates only low-level energy. The historical records show that the earthquake with this intensity does not have the sufficient and necessary triggering capability for large-scale landsliding in the Xintan area. Only when the sliding conditions are ripe enough and the stability is low enough would an earthquake with the average or maximum level estimated to occur may become a triggering factor. However, this has never occurred according to the data and is very unlikely to occur.

The analysis above demonstrates that the direct causes of the Xintan landslide are the gravitational force of the slope accumulations, the load of the back talus, favorable material and boundary conditions, and groundwater activities that resulted from the abundant rainfall.

Mechanical Analysis of Jiangjiapo Landslide

1. *Back calculation of the slip plane*: The central longitudinal section (Fig. 17.7) and its parallel section 50 m to the west of it are chosen for back calculation of the general strength of the Jiangjiapo landslide.

(a) *Slip plane under the back talus*: The back talus being self-stabilized after sliding downslope for a certain distance could be considered in a critical state. It is reasonable to ignore groundwater effect since the talus is highly permeable, thus being under good draining condition. Choosing $c = 0$ and $\gamma = 22$ kN/m^3 and using the residual driving force equation, the general friction coefficients of slip planes in the two sections are about 0.38.

(b) *Remainder of slip plane*: The remainder of the slip plane of Jiangjiapo slope is under the rock blocks and debris with soil and can be simplified to be a broken line. The same equation as above is used and two simultaneous equations are established based on the two sections being selected and the values of cohesions and friction coefficients could be obtained by solving the equations.

The strength of the slip plane is a function of space and time and depends on the degree of movement of the shear surface, slip distance and rate, and groundwater activities. Corresponding to different stages of slope deformation, the variation of the general strength of the slip plane can be divided into four stages. In the first stage, which corresponded to the creep period of the slope deformation, the strength of the potential slip plane was close to the peak value. In the second stage, which corresponded to the slow deformation period, the strength should be lowered between the peak and residual values. In the third stage, which corresponded to the intensifying acute deformation period, the general strength was gradually reduced to the residual value. In the fourth stage, which corresponded with a stabilizing period after the sliding, the strength recovered again, which probably was caused by the fault at the bottom of the accumulations that contains a relatively high content of soil that was replaced by the upper part that contained little soil. Only for the first and fourth stages are the data sufficient enough for back calculation.

For the first stage, choosing the natural unit weight $r = 22$ kN/m^3, saturated unit weight 23 kN/m^3, underwater unit weight 13 kN/m^3, and having known $f = 0.38$, $c = 0$ for the part of slip plane under the back talus, the general strength of the slip plane of the major part of Jiangjiapo slope was obtained to be $f = 0.27$ and $c = 125$ kPa which indicated that the clayish material played a major role on the slip plane.

For the fourth stage, assuming that the slope was in critical equilibrium state at the moment when the sliding stopped, and ignoring the super stabilizing effect caused by the high-speed slope movement and disregarding the groundwater activity (since there was no rainfall for 3 days before sliding and the original groundwater was almost drained away with the mud rock flow), taking other physic-mechanical conditions as the same as those on the first stage, $f = 0.34$ and $c = 17$ kPa found out from the back calculation, the friction coefficient jumped 25% above previous peak value and cohesion reduced by 75% of the previous peak value.

2. *Sensitivity analysis*: In order to define the factors which affect the slope stability and the degree of the influence, sensitivity analysis has been conducted based on the central longitudinal section.

Presenting the analysis results of the creep period, Fig. 17.9 shows that the driving force from the back talus and the strength of the potential slip plane are the most sensitive factors. However, in the last decade, the growth of the back talus was not notable. The movement of the Jiangjiapo landslide mainly depended on the decrease of the strength of the slip plane. The water level and unit weight of the slip body are not sensitive, which indicates that the impact of the groundwater on the sliding was mainly by means of seeping into the slip plane, thus reducing its strength.
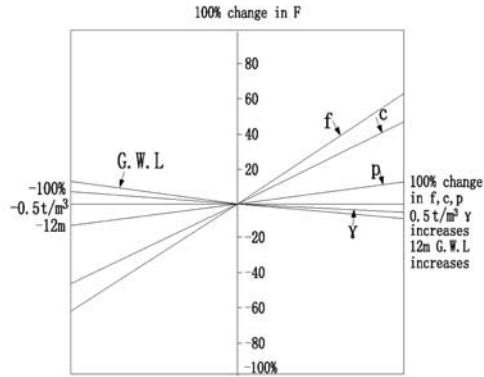
f. friction coefficient ; c. cohesion ; p. driving force from back talus ; γ. unit weight of

sliding mass ; G.W.L. groundwater level

Fig. 17.9 Sensitivity analysis of the stability of Jiangjiapo slope before sliding. *f* – friction coefficient; c – cohesion; p – driving force from back talus; γ – unit weight of sliding mass; G.W.L. – groundwater level

Figure 17.10 shows the sensitive analysis on the Jiangjiapo slope failure. To compare with that before sliding, the sensitivity of *f* rises and *c* goes down. As mentioned before, a part of the previous material on the slip plane was substituted by the upper layer that contained little soil, thus the sensitivity of the slope on groundwater should decrease. Besides, the slope being highly permeable, it should be under good drainage conditions, and the effect of groundwater on the slope stability has remarkably decreased.
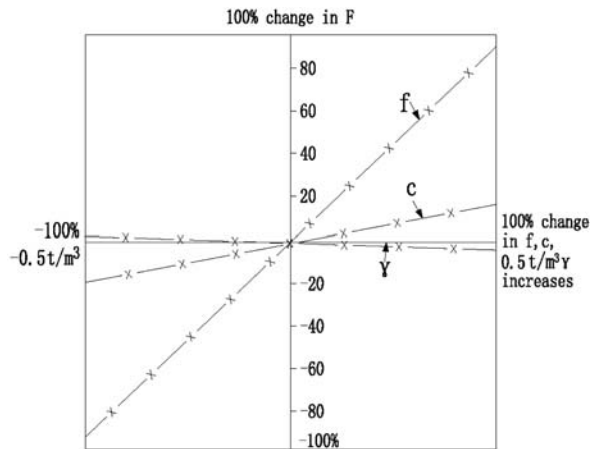
Fig. 17.10 Sensitivity analysis of the stability of Jiangjiapo after the sliding

Study of the Parameters of the Sliding Movements

1. *Estimation of the initial speed of the Jiangjiapo major sliding*: The locations of A_3 were surveyed on May 14, June 10 and at noon of June 11. Assuming that it moved in uniform acceleration in each period between each survey time and between June 11 and the starting time of the major sliding, the horizontal speed of the front part of Jiangjiapo slide at 3:45 h of June 12 can be calculated out as $V_0 = 0.00026$ m/s, 0.81 m/h, or 19.5 m/day.

2. *The maximum speed of the Jiangjiapo slide above the slip plane*: The seismogram of the landslide shows that the time period of the major slide was 41 s. The horizontal displacement of the front part of the Jiangjiapo landslide, which was represented by survey point F_6, is 193 m. Choosing the value of the initial speed V_0 as above, assuming the sliding to be of uniform acceleration, and neglecting its deceleration process, the maximum speed of Jiangjiapo sliding which was represented by F_6 is found to be 9.4 m/s. Correspondingly, maximum horizontal speed of the back part of the slope was found to be 8.2 m/s. The maximum speeds of each points of the slope increased from back to front.

3. *Entering river speed of the debris flow in the Sanyougou gully*: According to the work–energy transformation principle, the average speed can be calculated as follows:

$$V = \sqrt{2gh(1 - f \cdot ctg\,\theta)}$$

where θ is the general slope angle from the weight center of the debris flow above the exposed slip plane to the shoreline, equal to 22.4 degrees; f is the dynamic friction coefficient, selecting $f = 0.35$ based on experience; h is the height differential between the river water and weighted center of the debris flow when it passed the exposed slip plane, equal to 330 m; and g is the gravity acceleration. The average speed of the debris flow that passed the river water edge is about 31 m/s.

4. *Surge and its attenuation*: The maximum runup height of the wave surge on the opposite bank of Sanyougou gully is 49 m and the shape of the curve of the wave on the opposite bank is complicated due to the variation of trend, slope angle, and roughness of the bank.

Figure 17.11 is the attenuation curve of the wave upstream and downstream which shows that the diminution is rather sharp. Farther from Miaohe Village 10.5 km downstream from the landslide where the river channel is suddenly widened and farther from Zigui County Town 12.3 km upstream from the landslide where the river sharply bends, the wave became no longer of notable size. In the course of wave propagation, the surging height on the bank that the traveling wave initially runs up is greater than that on the corresponding opposite bank. At the places with the same distance to the landslide, the surging height upstream is greater than that downstream, which may result from the temporary impounding of the river water that was caused by the huge slip tongue suddenly narrowing the cross section of the channel by one-third in size.

Fig. 17.11 Attenuation curves of the water-wave surge
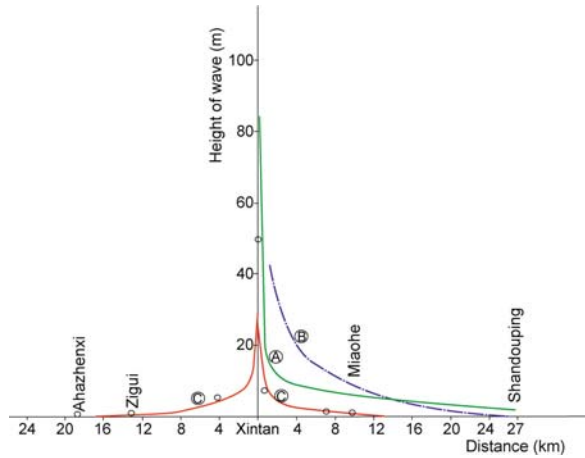
Considering the pattern of the slip tongue entering the river channel and the topographic characters of the riverbed, some empirical formula are selected to calculate the height of first surge which is calculated to be in the range of 33–39 m. The greater value is questionable since the average depth of water of this section of river is 33.6 m.

Slide Seismogram Studies

The Xintan landslide is within the geographic network of the seismic stations for Three Gorges Project. A perfect seismogram representing the process of the landslide has been recorded, although a rare occurrence for this kind of data to be seen in China.

The seismogram can be divided into three sections, each of which represents different type of movements.

Section A recorded the Jiangjiapo landsliding, following the debris flow and the dragging and sliding of the Xintan slope. The characteristics of this section differ greatly from the seismogram of the earthquake.

Section B, in which a high-frequency element occurs, shows another type of movement that takes place which most likely is the former caused by water surge. The time period of this part is 14 s that may represent the time for the surge to travel from its initial point to the opposite bank.

The sharp spurt in extreme amplitude is not the intrinsic feature of a seismogram of a landslide but earthquake occurred in section C and could be interpreted as the shock caused by the water wave striking the opposite bank.

Based on the analysis above, some specific time can be identified. The start time of the major landsliding is 3:51:58 h, stop time 3:56:5 h, i.e., the landslide lasting

for 0:4:7 h, the time of debris flow entering the river 3:53:23 h, and the time of water wave arriving at the opposite bank 3:53:37 h.

Monitoring and Prediction of Landslide Activities

Slope Deformation Monitoring

It is the long-term precision monitoring and detailed geological exploration that is the basis of landslide occurrence and characteristics prediction.

For a slope of such large scale and composed of loose material, only a multipoint survey system is able to monitor the variation and tendency of the deformation at its different stages and locations. Considering that the slope is long but relatively narrow and the bedrock is exposed on both sides, the collimation method is believed to be the best approach to monitor the horizontal displacements. Four collimation lines A, B, C, and D are arranged in parallel to the Yangtze River. Each line consists of five points and the end points are fixed in found bedrock. There are a total of 12 survey points representing the locations of deformation at different parts of the slope.

The monitoring survey, roughly once a month, started in November 1977. This collimation method is characterized by its rather high-precision, audio-visual read-out, and simple operation. The vertical displacements are surveyed by means of direct leveling with precision in accord with the national standard of the second-order leveling.

Up to 1982, the displacements of many survey points had reached a great value and still speeded up day by day, tending to void the requirements of the collimation method. The Xintan slope had little deformation. As a result of this situation, the survey system was modified in 1983:

(a) The type of system mounted on the Jiangjiapo slope was changed to be the intersection method and indirect leveling.
(b) Eight additional survey points $F_1, \ldots, F_3$ were set up from the back talus to the front part of the Jiangjiapo slope in order to determine whether the slope slid integrally.
(c) The monitoring method for the Xintan slope remained the same as before. However, a collimation line E was added between C and D to ascertain the effect of the sliding downward Jiangjiapo slope on the Xintan slope.

It should be mentioned that changing the collimation method to the forward intersection method for the Jiangjiapo slope was conducted at the right moment because (a) the intersection method could determine the direction of the movement which is one of the critical items for measuring sliding initiation and early warning; (b) there was no need for the surveyors to enter the dangerous area when the slope was in intensive deformation. Therefore, the surveying was convenient and safe, and the

data could be obtained without interruption. (c) The error of the location determined by the intersecting point did not exceed 5.9 mm which was about one-third of the daily displacement of $A_3\prime$ in the rainy season and about one-fourth of the monthly displacement of $A_3\prime$, and which was good enough for the monitoring purpose.

Prediction of the Landslide Occurrence

The prediction of the Xintan landslide occurrence may be divided into three stages: 1. Primary warning stage, in December 1969. Based on the report, "The Engineering Geological Report on the Slope Stability of Huayan Cliff of the Xintan" put forward by the Yangtze Valley Planning Office, Jiangjiapo slope was classified as dangerous and it was proposed that the inhabitants who lived on the Jiangjiapo slope and at both ends of the Xintan should be relocated. Since the end of 1977 when four collimation lines were put into operation, the data about the scope of the unstable slope, the magnitude, direction, speed, and seasonal variations of the slope deformation have been provided. Then, a great deal of additional geological investigation and exploration was completed and provided a deeper understanding of the characteristics of the slope material and its boundary conditions. Only by knowing the slope structure, boundary conditions and the slope deformation process both in time and space, did the landslide prediction became reliable. In 1982, in "The Findings Report on the Stability of the Huayan Cliff Area of Xintan" written by YVPO, it is reconfirmed that the unstable Jiangjiapo slope was in an active condition.

In this stage, which corresponded to the creep and slow deformation periods, there were no remarkable evidences of the ground deformation. Though the place and scope of potential landsliding had been defined, other items of landsliding prediction had not been determined.

This was the primary warning stage which indicated only the tendency of the slope deformation.

2. High-level warning stage. Considering that the essential change from an accumulating progression of sliding to integral push-type sliding was completed by the rainy season of 1983 and the magnitude and speed of displacement sharply increased, in May 1983, the Rockfall Investigation Division reported that the Jiangjiapo slope with 13 million m³ of accumulations was highly active and showing the mode of the integral slide, thus threatening the town of Xintan. Based on the warning, the provincial government started to withdraw the inhabitants from Xintan Town and the whole dangerous area and began to build the new settlement.

This was the high-level warning stage corresponding with the intensifying deformation period.

3. Impending slide warning. Based on the situation that the Jiangjiapo slope was still in intensive deformation in the dry season by the end of 1984, on March 1985 the YVPO reported to the provincial government, asking to speed up the relocation of the inhabitants at Xintan in order to complete evaluation before rainy season. They pointed out that the sliding was in the direction of south by west, i.e., leading to the eastern part to Xintan Town. In April, when the rainy season was arriving, the

slope deformation further intensified. On May 9, the Rockfall Investigation Division submitted an urgent report and raised an alarm that 13 million m^3 of the sliding mass of the Jiangjiapo slope being in state of integral slide, was moving toward the town of Xintan.

Both reports pointed out the time period, i.e., before the rainy season or after May 9 when the disastrous landsliding probably took place. This stage corresponded to the acute deformation period and the warning was an impending one.

Conclusions

A great deal of enlightenment was gained from the Xintan landslide. Since a landslide always has a long-term developing process and shows a series of warning signs, it should be known that given the aspects of space, the monitoring scheme should be changed with the progression of slope deformation. The scheme used in Xintan is unsophisticated but efficacious, thus easily duplicated. Earthquake, rainstorm, and long-duration rain does not necessarily cause an integral landslide; on the other hand, the quantity and intensity of the rainfall needed to trigger a landslide decreases with the degree of development of the slope deformation. Along a river channel, the attenuation of the huge water surge generated by sliding mass is very sharp. Based on the attenuation curves from calculation and testing of experiences, the dam-site selection and scope and scheme of evacuation both on river and land can be reasonably considered. In short, the abundant information accumulated before and after the Xintan landslide provides a chance to provide a break-through in the theory and prediction of the large-scale overburden landslide. As a result the event will deeply influence the study on ground failure in China.

References

Edil TB and Schultz MN (1983) Landslide hazard potential determination along a shoreline segment. Engineering Geology, 19(3): 159–177

Fookes PG, Sweeney M, Manby CND, Martin RP (1985) Geological and geotechnical engineering aspects of low-cost roads in mountainous terrain. Engineering Geology, 21(1–2): 1–152

Sauer EK (1984) A landslide in clay shale in the North Saskatchewan River valley, Canada. Engineering Geology, 20(4): 279–300

Chapter 18
Time Prediction of the Xintan Landslide in Xiling Gorge, the Yangtze River

Shangqing Wang

Abstract   The Xintan landslide is a large-scale landslide that occurred in Xiling Gorge, the last gorge upstream of the Three Gorges in the Yangtze River. It occurred on May 12, 1985. Through intensive monitoring and field investigation, the occurrence of this landslide was predicted successfully, and human loss was avoided in Xintan Town, which is located at the toe part of this landslide. In this chapter, the deformation property is described, and the monitoring data are presented to show the prediction process.

Keywords   Displacement monitoring · Time prediction · Colluviums · Reactivated landslide

Introduction

The Xintan landslide is located on the north bank of the Yangtze River, 56 km upstream from the Three Gorges dam. It is a reactivated landslide which had failed several times in history (Fig. 18.1). On June 12, 1985, in the early morning of 0352–0356 hours, a huge landslide occurred again in Xintan Town. The landslide had a total volume of $3.0 \times 10^7 \mathrm{m}^3$.

High-speed (10–30 m/s) debris destroyed the 1000-year-old Xintan Town and buried 481 family's 1,569 houses and 780 ha farmland. About one-tenth of the debris slid into river and caused a 54-m-high wave, and the wave traveled as far as 42 km. The wave sunk 13 auto-ships and 64 wooden boats in an 8-km stretch of the river. The front part of the debris had a volume of $3.4 \times 10^6 \mathrm{m}^3$, and it formed a sliding tongue of 93 m wide and 250 m long. It interrupted shipping for 12 days (Figs. 18.2, 18.3, and 18.4).

S. Wang (✉)
China Three Gorges University, Key Laboratory of Geological Hazards on Three Gorges Reservoir Area, Ministry of Education, Yichang, China, 443002
e-mail:wangsq@ctgu.edu.cn
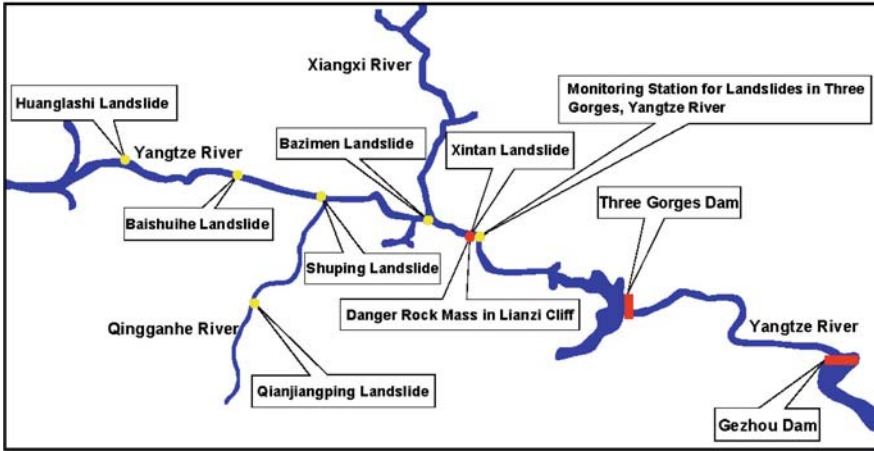
Fig. 18.1 Location of the Xintan landslide in Xiling Gorge, Yangtze River

Thanks to the accurate prediction and efficient evacuation, of all the 457 families, 1,371 people were evacuated from the landslide area before the sliding began and there was nobody injured. There were 11 ships in this area which had made a stop to take refuge. The geological disaster loss was reduced to a minimum extent (according to a loss estimation, the direct economic loss was reduced by 87 million Yuan).
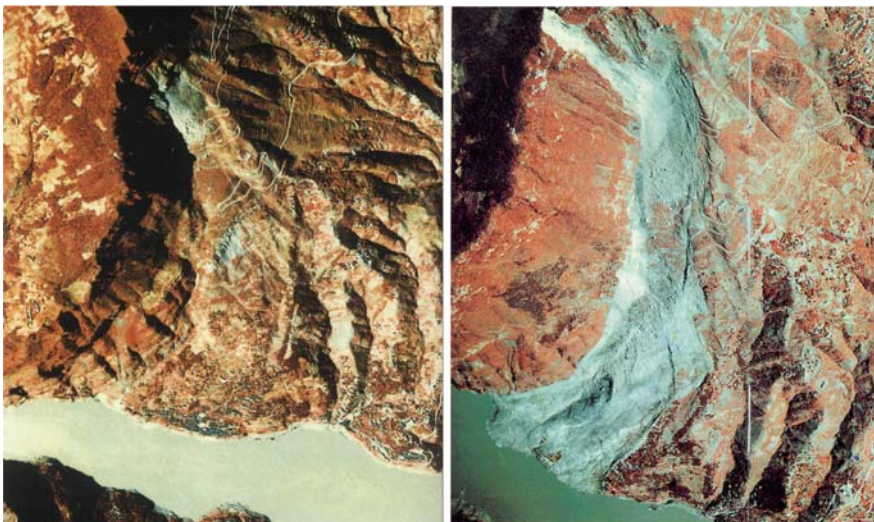
Fig. 18.2 A panoramic aerial view of the Xintan landslide before sliding (*left*) and after sliding
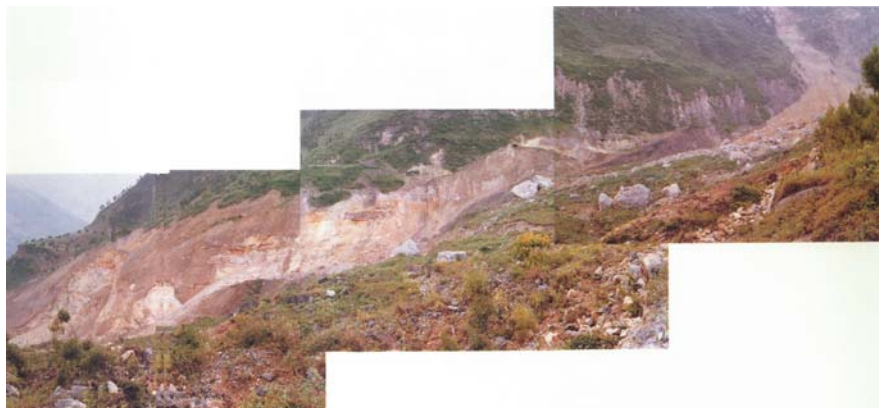
Fig. 18.3 The 80-m-high west flank of the Xintan landslide

Successful prediction has occurred infrequently in the history of landslide prediction in China and the experience accumulated invaluable expertise on the research of prediction and forecasting of landslides. Therefore, it is important to summarize the experiences of landslide development and prediction for improving the level of landslide prediction and as a result, promoting landslide mitigation and disaster prevention (Wang et al. 1999).

Fig. 18.4 Buildings destroyed by the landslide (Office building of the Rock Fall Survey Department of Xiling Gorge, Hubei Province)

The Sliding Process

Characteristics of Landslide Movement

The Xintan landslide is a pushing-type debris landslide. According to field investigation, the Jiangjiapo area in the upper part of slope slid first and sheared out of the bottom of Jiangjiapo at an elevation of 380 m (Wang et al. 1990). As a result of punching and loading of the upper debris, the lower Xintan slope began to slide in a large area with different depths and speeds. The landslide can be divided into two sections and four areas according to the characteristics of landslide movement and the differences of a sliding body in a failure process (Fig. 18.5).
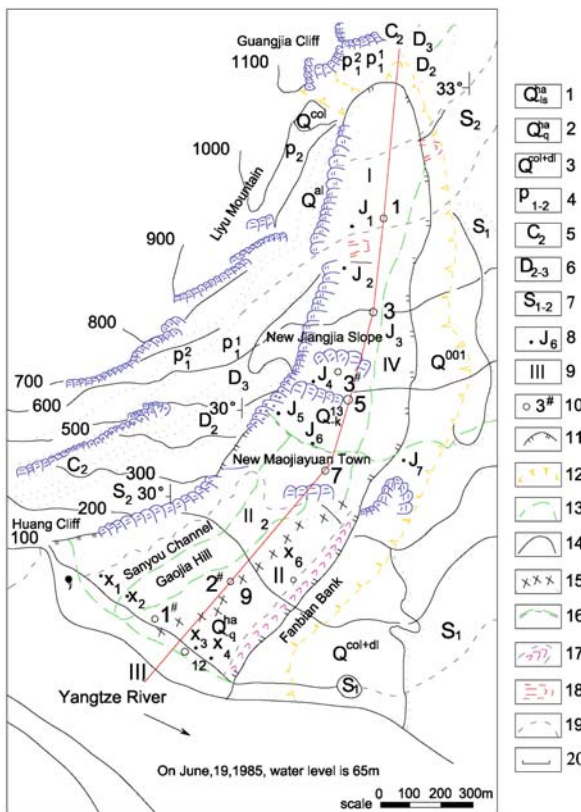
Fig. 18.5 Engineering geological map of the Xintan landslide. 1 – shiver of quaternary limestone; 2 – shiver of quaternary quartz sandstone; 3 – slope wash; 4 – Permian system; 5 – Carbonic system; 6 – Devonian system; 7 – Silurian system; 8 – survey point; 9 – divisional code of landslide; 10 – exploratory well or boring; 11 – borderline of landslide; 12 – borderline of rock fall; 13 – divisional line of landslide; 14 – borderline of underwater deposit; 15 – divisional line of shiver composition; 16 – sliding exit; 17 – ridge of debris edge; 18 – bad broken highway; 19 – debris flow valley; 20 – vertical section

(a) *Active sliding area of the upper section (I)*: This area is known as the Jiangjiapo slope which is above an elevation of 380 m. It slid along rock with an area of $3.3 \times 10^5 \, m^2$, and a volume about $1.4 \times 10^7 \, m^3$. There was $4.8 \times 10^5 \, m^3$ of sliding debris that slid out of this area and rushed into the Yangtze River along the Sanyou valley on the west side. Here, it formed a dry debris avalanche. The left side of the debris lay over the Maojiayuan flat area and its lower slope. The sliding distance is 50–400 m, and takes the shape of a short end and a long front.

(b) *Passive sliding area of the lower section (II)*: This is part of the Xintan slope at an elevation of 380–80 m with an area of $3.9 \times 10^5 \, m^2$, and a volume of about $1.7 \times 10^7 \, m^3$. It lost stability under the punching and loading of the upper area of sliding debris. It formed a ridge at the east edge with 400 m long and 3–15 m higher than the original slope at an elevation less than 600 m relative to the river bank. It can be divided to three sub-areas according to their features: Gaojialing, which is the relatively stable area of the middle part (IIa); the Sanyou valley which was a high-speed sliding area of west area (IIb); and a low-speed sliding area at the east area (IIc). IIa area is relatively stable and the original buildings and landform can be dimly distinguished. Its surface is covered by sliding debris from the upper part with a depth of 5–15 m, it was heavily deformed, slid down the slopes at a high speed and deposited material at a depth of 10–25 m. Some of its debris rushed into the river, and formed a deposit of 250 m in width and 93 m in length. Its slip surface reached the bedrock. The deposition in IIc area was divided into several blocks by the upper sliding load and slid at different depths and distances of 82–350 m. The slip surface is situated inside the old deposits, according to boring numbers 1 and 2 which were taken after sliding (Fig. 18.6).

(c) *Depositional area (III)*: This is the slope area under the elevation of 80 m. The whole debris has an east–west direction of 200–300 m width, along river 710 m in length, 5–20 m of thickness, and a total volume $3.4 \times 10^5 \, m^3$. Debris
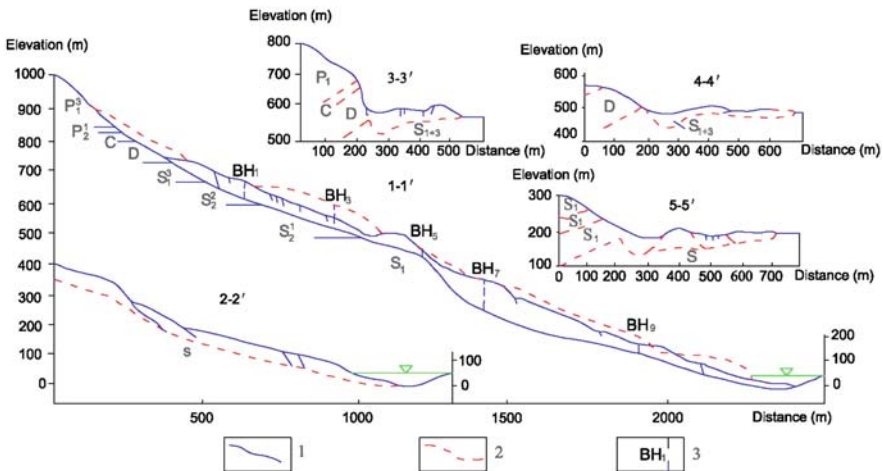
Fig. 18.6 Geological profile of the Xintan landslide. 1 – sliding surface; 2 – conjectural sliding surface; 3 – boring
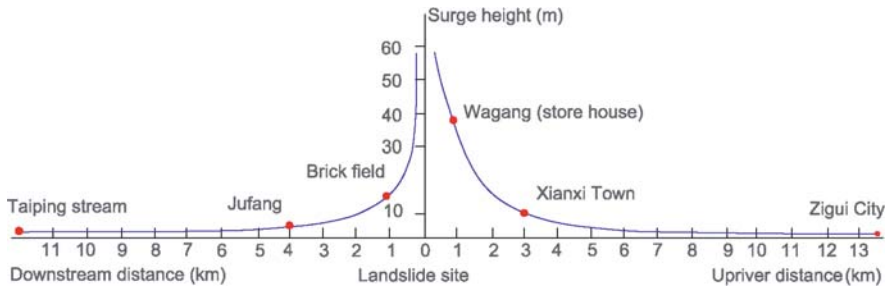
Fig. 18.7 Attenuation curve of ground swell caused by debris from the Xintan landslide

$(2.6 \times 10^5 \, \text{m}^3)$ rushed into the river underneath the water level. In Sanyou valley with a maximum deposited volume, the debris had dammed the river section for 1/3 width. According to the in situ investigation on June 14, 1985, the landslide rushed into the river and caused back flow for 13 km, and generated a wave of 54 m height. It destroyed two two-story storehouses of The Rockfall Survey Institute of Xiling Gorge, Hubei Province in thither bank of Xintan Town. The wave overturned ships along the lower and upper reaches of the river for a distance of 8 km. The wave reached the upper tributary streams 15.5 km from Zigui county and lower streams 26 km from Sandouping Town. Figure 18.7 shows the height of the wave and its attenuation curve.

(d) *Draught and jostle sliding area (IV)*: This area is situated in the east side of the main sliding body, and there were several small-scale sliding caused by draught and jostle from the upper main body.

Deformation Features of the Landslide

(a) *Deformation difference between the upper and the lower sections*: According to the 7-year survey (November 1977–June 1985) on displacement, the lower section of the Xintan slope was relatively stable, while the upper section of Jiangjiapo slope was in the status of quick deformation, and therefore was the source area of the Xintan landslide. The sliding debris was controlled by the boundary conditions of bedrock.

(b) *Development stages of deformation*: According to the analysis on the displacement curve of survey point A_3 in Jiangjiapo at the higher part of the slope and B_3 in the toe of landslide, the development stages of deformation of the Xintan landslide can be divided into four stages as follows: preliminary creeping, regular creeping, accelerating creeping, and rapid deformation.

(c) *Mechanical features of deformation*: The upper Jiangjiapo slope had loose, grading sliding features before the rainy season of 1983. The cracks on the slope surface took a shape of side lines, and draught from front to the back margin. Draught cracks in the back margin and west sides penetrated together after 1983 and it came into the stage of whole moving. The deformation rate from the survey points decreased from the back margin to the front edge therefore showed a process feature of sliding.

The Features of Sliding Debris

(a) *Landslide shape*: Slopes that were higher than 150–200 m decreased in height after sliding and the lower slopes became higher after sliding. The back margin of Guangjiaya rock and Jiangjiapo slope had the maximum subsidence as high as 50 and 75 m or so, as the Guangjiaya rock disappeared. The landform remained as the two ridges (Jiangjiapo, Maojiayuan ridges) and one mountain (Gaojialing mountain), and the front edge of Maojiayuan and Gaojialing remained in their original situation and landform.

(b) *Hydro-geological features*: The slope structures became loose after sliding and its permeability increased. Additionally, a filler-shaped lower depression formed in the west edge. Therefore rainfall can quickly gather and seep into the slope. According to the survey in #3 silo, material was dry in the places higher than 21.4 m but there was seepage along the top of the clay layers. It indicated quick drainage in deposited debris. In the east side area of the Xintan landslide, the landslide debris had a loose status and high permeability; therefore, the springs in the front of the sliding body disappeared before sliding. The surface discharge in the Sanyou valley was as high as greater than 10 l/s and ordinarily 3–6 l/s, minimum discharge 0.23 l/s. The peak value of discharge in the rainy season was 1–2 days later than the rainfall, making it clear that the groundwater mainly came from the deposited debris with short flow.

Essential Features of the Landslide

Topography

The landform of the Xintan landslide showed a slope that is higher north, lower in the south and a slope that is higher in the east and lower in the west. The west edge of Huangyan and north edge of Guangjiaya are a steep cliff of sandstone and limestone of Devonian–Permian Periods. The average gradient is 60° and the gorges are 300–450 m high. The east side is connected to a gentle mound of sandstone and shale of Silurian Period. The slope spreads in a direction of south to north with a 2 km length, and is shallow (300–500 m) in the north and wide (1,100 m along river bank) in the south. It heaves to the east in the middle of the slope, in a horn shape, with an area of 1.1 km². The elevation in the back margin is 900 m and in river bank is 65 m with an angle of 23°. There were two horizontal ridges in the middle part of the slope: one is the front ridge of Jiangjiapo which has an elevation of 500–560 m, an angle 50–60°, trends toward the N30E, and it divides the slope into the upper part (Jiangjiapo slope) and the lower part (Xintan slope) into two parts. Another ridge is the front ridge of Maojiayuan which has an elevation of 270–330 m, trend toward the N75E, the height and angle are similar to the former one, and it divides the lower part of the Maojiayuan plat. The lower part of the Xintan slope was divided into two parts of the west part of Sanyou valley and the eastern gentle slope by the Gaojialing ridge. Except for the abovementioned ridges, there are other 30–40° ridges such as the back margin of Guangjiaya rock and debris in the front near the river bank. In the

other part are gentle slopes of 10–15°. The slope inclined to the west is horizontal and is a U shape above Maojiayuan which is higher in the east–west area and lower in the middle. The gently sloping area of the east is higher and in the west is lower under the Maojiayuan area.

Materials and Structure

The depth of the Xintan landslide was 30–40 m and became thicker from east to west. The depth in west Jiangjiapo–Gaojialing was much thicker than 80 m and the maximum depth was 110 m with a total volume of $3.0 \times 10^7 m^3$. According to its formation, the components of the sliding body can be divided into the following three parts:

(a) *Guangjiaya dangerous rockfall*: The Guangjiaya dangerous rockfall consists of big rock of Permian limestone and several small stones. It formed rockfall deposits under Guangjiaya cliff which extended to Jiangjiapo with a depth of 20–30 m. The debris was loose deposits with no sorting and most of them are large stones. They deposited in a disorderly manner and protruded out of the slope. The content of clay was less than 5%.

(b) *Slope diluvium of rockfall*: Rockfall is distributed under the toe of Jiangjiapo with a depth of 10–40 m. The deposits mainly consist of limestone gravels while some consist of Devonian sandstone and Silurian shale detritus. The clay content was large and it showed a lens shape of in some areas and had a dense structure. The two kinds of detritus formed the double-layer structure of Jiangjiapo slope with a volume of $1.3 \times 10^6 m^3$.

(c) *Colluvial deposits*: These deposits were distributed in Maojiayuan and the area among Gaojialing, and the old Xintan school. The upper part consists of Devonian quartz sandstone and gravels of Silurian sandstone while there are several limestone gravels within. The deeper layer mainly consists of limestone gravels and their clay contents are higher while some are lens shaped. A three-layer structure can be seen in the cliff of Maojiayuan while the top layers are colluvial deposits of Silurian siltstone and shale with a depth of 30 cm; the middle part is colluvial deposits of Devonian quartz sandstone and the diameters are 2–20 cm. There is no clay inside and the structure is loose with a depth of 8 m and there are weathering layers of 5–10 cm above them. The bottom parts are colluvial deposits of Silurian siltstone with several limestone gravels with a depth of 30 cm. There is a 1 m weathering layer above them. In the whole slope body, there is a tendency toward clay content, density increase, and void ratio, and permeability decreases from surface to deep areas and from the front to the back margin.

Bedrock Structures

The terrain trends toward N10–30E, obliquity 25–38°. The Huangyan cliff at the west edge shows a converse slope and the Guangjiaya cliff in the north trend as

a horizontal slope which consists of a hard structure layer of Devonian–Permian sandstone and limestone and among them, the bottom consisting of Permian coal has a depth of 2–3 m. They are a shale-coal layer and distributed in the middle-bottom part of the south cliff area and they decrease to the bottom of the cliff toward the north. There are a few coal caves in this coal layer. Four faults in the bedrock can be divided into two groups. The NNW group has a big scale with an obliquity 55–70° and 20–200 m that is visible. The NNE group trends toward the SE with small obliquity. Four groups of fissures occur: N65–85E, N30–50E, SN, and N10–40 W. All of them have a steep inclination. The bedrock sliding surface mainly consists of Silurian sandy-shale and this is the layer of deep sliding.

Hydro-geological Conditions

The groundwater of the slope was mainly supplied by rainfall in the area. The bottom bedrock consists of shale. The sliding surface shows a shape that is higher in the east and lower in the west and in the western edge there is a deep trough. The groundwater flows toward the downslope while flow to the west edge occurs and is concentrated in the front margin of the landslide. There are several springs appearing at the elevation around 120–150 m because of the presence of water-block layers in this line. The discharge is 0.04–0.2 l/s normally and 0.15–0.83 l/s in the rainy season. The Sanyougou valley became the main drainage channel of surface flow.

Boundary Conditions

The back margin and west edge of the Xintan landslide is a bedrock cliff of Devonian–Permian sandstone. The east edge was fissured with colluvial deposits. The sliding body has a depth of 30–40 m and it increases from east to west. The debris depth in west Jiangjiapo to Gaojialing is more than 80 m and the maximum depth is 110 m. The sliding body mainly consists of colluvial detritus with some clay and of Silurian sandstone and shale showing a complex shape. The Xintan landslide slid along the clay layer under the debris. According to the survey in well #3 in Jiangjiapo of the main sliding area, the sliding clay is a brownish-red color. There are some gravels of well psephite with a diameter of 0.5–1.0 cm within. The sliding surface showed a wet nature and the thickness is 0.5–0.8 m. The bottom of the layer disturbed widely, and there are different colors in some areas. The upper layer has a high density and there are slickenside and scrape formations.

Formation Mechanism of the Landslide

The main factors of the Xintan landslide failure were the following: rockfall loading of Guangjiaya dangerous rock in the back margin of landslide, accumulation of colluvial deposits in main sliding area, sliding force of debris in the slope, static and dynamic water pressure.

Mechanism of Destabilization

(a) *History of the landslide*: According to the records in county annals of Zigui County, the old name of Xintan was "Hao Sanxia" and "original flat", "no big beach". The sliding debris rushed into the center of the river, forming a new beach during the Han dynasty and it was therefore named "Xintan (new beach)" (Fig. 18.8).

In AD 100, in summer April of Han dynasty Yongyuan 12th year, Zigui Mountain slide as high as 1,333 m, walled up the river, buried more than 100 people.

In AD 377, mountain slid again in Jintai second year. The river back flowed for more than 100 km on the day of sliding and it made a huge wave of 100 m in height.

In AD 1030, Tianshen seventh year of Song dynasty, mountain slid, damaged lots of ships, blocked river for 21 years.

In AD 1542, Jiajing 21st year of Ming dynasty, a large landslide occurred after a long time and heavy rainstorm which damaged more than 100 houses and blocked the river for 82 years. In 1558, a landslide occurred in Xintan area which damaged several tens of houses and killed more than 300 people. On June 3, 1935 on the lunar calendar, a landslide
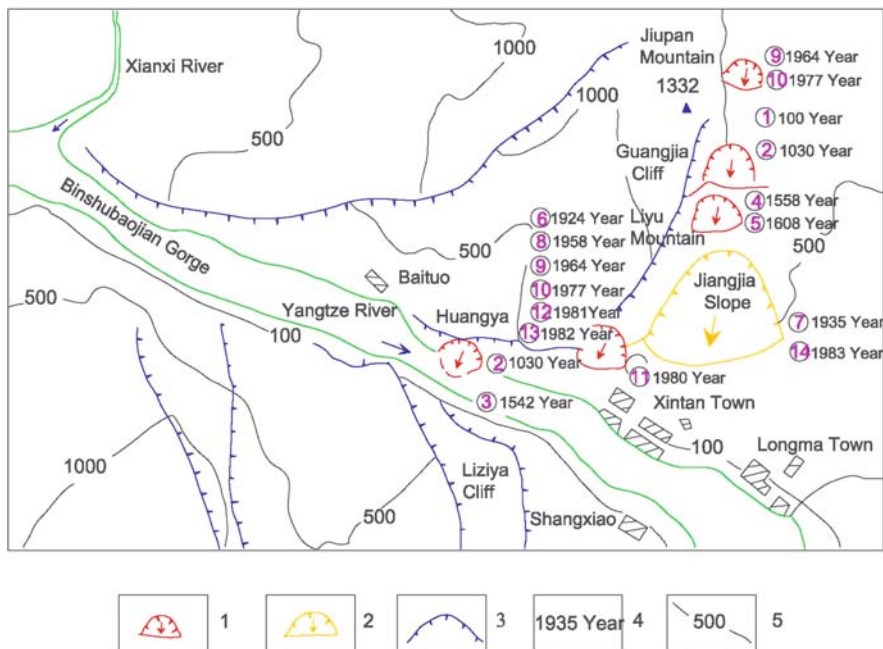
Fig. 18.8 Developmental history of landslides and rock falls in the Xintan area. 1 – falling; 2 – landslide; 3 – scarp; 4 – time of landslide and rock fall; 5 – contour and elevation

occurred from Jiangjiapo to Linjiang-Liulin after 7 days of rainstorm which cut off the east road of Xintan Town and pushed more than 20 houses into the river.

(b) *Mechanism of destabilization*: The mechanism of destabilization can be summarized as follows according to the history of landsliding, topography, and long-term surveys:

(1) The main factor for whole reactivation and local sliding in history is the rockfall loading in the back margin of the landslide.
(2) The colluvial deposits in the upper part of the landslide loaded by sliding debris from a higher place in the slope and then moved downslope.
(3) Some of the area which was pushed by moving debris was blocked because of a narrowing in the horizontal section, and then the Jiangjiapo area heaved upward after the increasing loading from the upper part.
(4) The sliding body becomes loose then formed a sliding debris flow area in the west trough of the Sanyou valley. The slide loading from the back edge of the east side or from the upper sliding debris pressed into the lower area, forming a sliding trough of high speed between the upper and lower parts of the landslide.

Falling Loading

Falling loading is the ultimate reason for the formation and reactivation of the Xintan landslide. The deposits and many landslides in the history of the Xintan slope were caused by the long-term continuous falling from cliffs at the western edge and the northern side. The accumulated falling debris reached $1.6 \times 10^6 \mathrm{m}^3$ during this century according to estimates. The fore area deformation of the reactivation of the Xintan landslide started from a $1.0 \times 10^5 \mathrm{m}^3$ fall in the northern side of Guangjiaya in 1964.

The Effect of Precipitation

The seepage from precipitation is an important factor accelerating the deformation and reactivation of the landslide. The Xintan landslide is situated in the rainstorm area of west Hubei province. The annual precipitation is 1,100 mm and 61% occurs from May to September. The surface flow occurs in a more than 2 km^2 catchment area of an old landslide and seepage into sliding body, groundwater level rises, and there is an increase in pore water pressure. Precipitation will soften the clay in the sliding surface and decrease the strength and then increases the deformation of the landslide. According to the analysis in Table 18.1, there is a positive correlation between the big displacement and annual precipitation in the survey points of A_3 and B_3 in the main sliding area of the front and toe of Jiangjiapo.

Table 18.1 Relationship between displacement changes and precipitation

Deformation stage	Year	Rainy season/month	High-speed deformation period: Months	High-speed deformation period: Continue time/months	Decelerate period (months)	High-speed deformation period (months) start/end	High-speed deformation period (months): Months	Initiation precipitation (mm): Accumulated precipitation during rainy season	Initiation precipitation (mm): Monthly precipitation	Continuous time before sliding: Start/end month	Continuous time before sliding: Months
Slow creeping	1977		Non-clear high-speed deformation period								
	1978	4/6								4/6	3
	1979	4/9	8/10	3	1	4	1	658	359.3	4/8	5
Constant creeping	1980	5/8	6/9	4	2	2	1	390.7	291.5	5/6	2
	1981	7/8	Low precipitation year, non-clear high-speed deformation period								
	1982	6/9	7/11	5	3	1	3	359.7	170	6/7	2
Accelerating creeping	1983	5/10	6/8	9	4	<1	4	292.7	195.4	5/6	2
	1984	5/9	5/8	11	5	<1	>5	103.1	103.1	5	1
	1985	4	4			<1		79.1		4	1

Annotate: rainy season is the continuous month of precipitation of more than 90 mm

1. Along with the increase of precipitation, displacement increases and high-speed deformation period occurs in the rainy season.
2. All the initiation time and stopping time of high-speed deformations are later than that of rainfall and the delay times are different in different deformation stages: In the constant creeping stage, the initiation time of high-speed deformation is 2–4 months later than the rainy season but the stopping time is only 1 month later than rainfall. In the accelerating creeping stage, the initiation time of high-speed deformation is shorter than 1 month but the stopping time is long after the rainy season. This shows that along with the increase of deformation speed, the sensitivity of deformation to rainfall is increased gradually.
3. The starting precipitation (accumulated precipitation during whole rainy season before acceleration) of high-speed deformation period and the precipitation of the initiation month decreases along with the increase of deformation stage. The starting precipitation in the constant creeping stage is more than 350 mm, and monthly precipitation is more than 200 m. The starting precipitation and monthly precipitation in the accelerating creeping stage are under 300 and 200 mm, respectively.

Landslide Monitoring and Prediction

Features of Deformation Monitoring

The monitoring of the Xintan landslide is the apotheosis of successful landslide prediction using a robust deformation monitoring method based on geological survey (Wang 1996).

The monitoring works on the Xintan landslide began in November 1977. The monitoring system consists of 5 survey lines on which there are 15 points of deformation survey, 15 triangle points of close observation, and 1 controlling net of 6 controlling points. The horizontal displacement of the slope toward the river is surveyed by collimation line method. Theodolite WILDT3 type and a special moveable target were used for survey. The small angle method was used if the horizontal displacement was bigger than the reading range of the target. The vertical displacement is surveyed by geometric level method and the type WILDN3 Theodolite was used. The three-dimensional displacement of cross-survey points (F_1–F_8 and A_3–B_4) were measured by the front intersection method and the accurate triangle-level survey method using T3 Theodolite. The features of the survey system are as follows (Fig. 18.9).

(a) *Monitoring net of point, line, and plan*: The distribution of survey points is placed in accordance with the deformation of the corresponding area. The accuracy of the survey meets the requirement for monitoring in different deformation stages. The time intervals of the survey are well distributed. The survey methods are practical with high credibility, simplicity, and safety. They are suitable for

Fig. 18.9 Monitoring system
of the Xintan landslide:
1 – triangle network;
2 – bench mark;
3 – cross-point; 4 – survey
point of cracks;
5 – residential area; 6 – cliff
of falling; 7 – divisional line
of bedrock; 8 – scarp
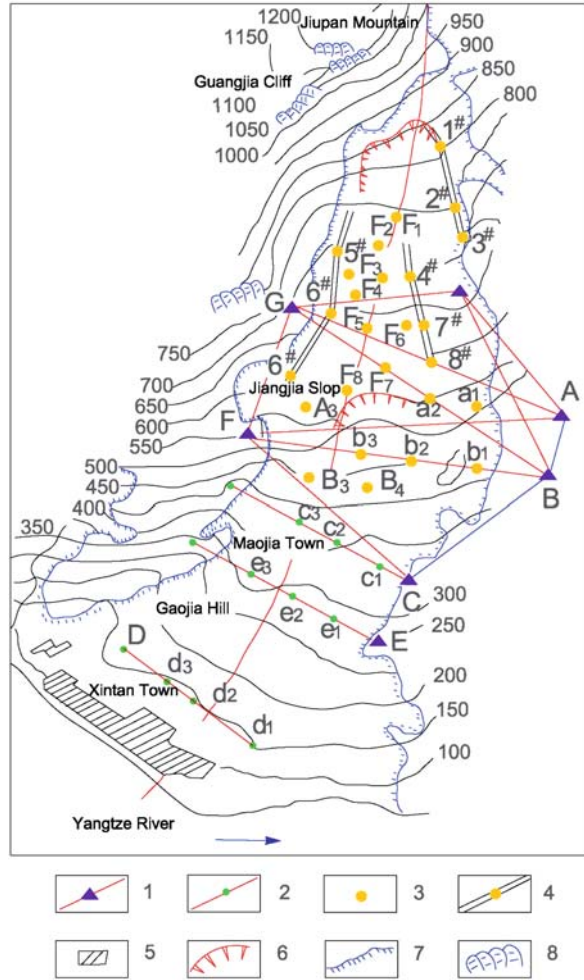
the hard natural environment and conditions in the landslide area. For instance,
the collimation line method used to monitor the horizontal displacement toward
the Yangtze River has the advantages of high accuracy (1.5 mm), being directly
perceived, easy operation, and speedy confirming of deformation area, etc. The
upper part of Jiangjiapo slope was confirmed quickly as the unstable slope
according to the analysis of survey data beginning with 5 years. The A_3 sur-
vey point (elevation 565 m) in the upper part of the west cliff of Jiangjiapo and
the B_3 point (elevation 461 m) in the toe of the slope are situated in the place
of stress concentration through slope deformation. They have large displace-
ments, typically 10–50 m/month, and there are the same moving features in the
upper part and the toe part which indicate that they are the same deformation
block. They are in the later period of the constant deformation stage and they

are progressing toward the accelerating stage. The survey points of C, D collimation line in the lower part of Xintan slope only recorded small accumulated displacement under 5 mm which indicated that the lower part of the slope was in relatively stable condition.

(b) *Adjustment of survey area and monitoring method on time*: According to the different parts and different stages of slope deformation, the survey area and monitoring method were adjusted three times: November 1977, June 1983, and May–July 1984 in order to confirm the direction of movement and scale of the slide.

   For instance, after the rainy season of August 1982, the deformation in upper Jiangjiapo area accelerated clearly and the fissures along the back margin and east–west edge developed and connected gradually forming a curve-shaped cracking. In order to confirm the landslide scale, the main sliding direction, place of shear out and the inference to the lower Xintan slope, the survey net was adjusted and increased in 1983. The displacement monitoring in the accelerating stage and pre-sliding was increased to eight survey points (F_1–F_8) in the area from Guangjiaya to Jiangjiapo then the horizontal displacement was measured by front intersection method. Because the deformation increased in the front and toe of Jiangjiapo, the displacement in A, B line became too large to be surveyed by collimation method and leveling method. Moreover, it became dangerous for survey people. Therefore the horizontal displacement was surveyed by the front intersection method and the vertical displacement was surveyed by triangle elevation method instead of level method. Meanwhile a six-point line-angle controlling net was established. The E collimation line was added inside the C, D line. The collimation line method and level method were still used in the lower slope because the displacements in these areas were small.

   According to the analysis of survey data of July–November 1984, the F_1–F_8 points in the back area from Guangjiaya colluvial deposits to Jiangjiapo slope had large displacements and it decreased from back to front gradually while the displacement of point F_1 in the back margin was 2.8 times that of F_8 in the front part. Therefore it can be seen that the landslide has the feature of pushing press deformation. The moving direction of F_1–F_8 was the same of south to west which is the direction toward Xintan Town and the tendency of whole sliding became obvious. Moreover, the three collimation lines of C, D, and E in the lower Xintan slope recorded small displacement which meant that they were relatively stable. At the same time, there were humidity, tympanites, shear phenomena, and so on in the western toe area of Jiangjiapo, which means the landslide may shear above the C line (elevation 380 m) at a high position. Therefore the landslide has high potential energy which will threaten the safety of Xintan Town directly.

(c) *Provide necessary conditions for effective monitoring in time and space*: The survey points of the monitoring system provided not only necessary condition of effective space monitoring on deformation features and key area (for instance, in main sliding area and surrounding cracks, western margin of Jiangjiapo) but also time monitoring of all deformation stages from slow creeping, constant

creeping, accelerating deformation to sudden deformation. It accumulated abundant valuable data for the landslide prediction of middle-long period, short time, and pre-sliding.

Progressing Development Features of the Landslide

The reactivation of the Xintan landslide indicated a failure process of accumulating deformation from quantitative change to qualitative change (Sun 1996). According to the analysis of horizontal displacement–time curve of survey points A_3 and B_3 in the western front and toe area (key area), the landslide deformation experienced not a flat change but a staggered variation which has rapid and slow changes. The deformation before sliding mainly occurred in the upper part of Jiangjiapo area. According to the survey data of displacement and field investigation during the 7 years from November 1977 to June 1985, the progressing development process can be divided into four stages: slow deformation, constant deformation, accelerating deformation, and rapid deformation (Fig. 18.10).

(a) *Slow deformation stage (before August 1979)*: The main sliding area of Jiangjiapo experienced punching and loading from rockfall in back margin and western Guangjiaya continuously. At this point, it began to deform. There were large cracks along the south–north direction and the slope had the tendency of downslope creeping. The deformation rate was smaller than 10 mm/month.

(b) *Constant deformation stage (August 1979–July 1982)*: The creeping curve reflecting the sliding speed was slow and constant. The deformation rate increased to 10–50 mm/month. The ground cracks became reactive in the rainy season, and caused the deformation to enlarge. There was a volume of $2.0–8.5 \times 10^5 \mathrm{m}^3$ of dangerous blocks that appeared conterminous in the front area of Jiangjiapo. The trees in this area tilted toward the south and there were several that had fallen over.
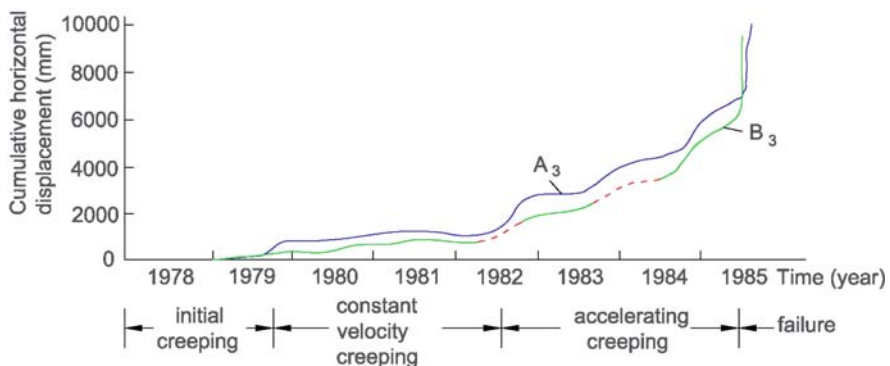
Fig. 18.10 Horizontal displacement–time relation curve of survey points A_2, B_2 before sliding

(c) *Accelerating deformation stage (July 1982–May 1985)*: The main features in this stage were as follows: The moving speed of survey points in the main sliding area increased, and the creeping curve increased continuously which showed an accelerating feature. Survey points A_3 and B_3 moved toward the south at a rate of 171.9 and 168.2 mm/month with an accumulated displacement as high as 5,845.3 and 5,718.8 mm, respectively. The deformation speed reached more than five times of previous stage. The ground deformation accelerated which showed a boundary condition for the whole sliding of the slope. The back margin cracked and fell down 15 m and the penniform fissure in the east and west edge connected together and loosened, subsidence occurred, and stepped cracks occurred. The dangerous block in the front area with a volume of $8.5 \times 10^5 \, m^3$ fell down a distance of 3–5 m. There was obvious shearing bouffant in back of Maojiayuan. The main sliding direction was south trending to the west, directly toward the Xintan Town.

(d) *Rapid deformation stage (May 1985–12 June 1985)*: The main features in this stage were as follows: The landslide deformed rapidly and it became dangerous according to instrumental monitoring and in situ investigation.

First, the deformation in the survey points from Jiangjiapo to the toe of Guangjiaya increased rapidly while the displacement reached a peak value. The creeping curve of points A_3, B_3, and F_1–F_7 showed inflexion in the same time before 28 days of sliding (May 15). The inclination of the deformation curve trended to as steeply as $90°$.

> May 14–June 10: A_3 point moved 2.318 m toward the southwest while B_3 point rapidly moved 10.764 m toward the southeast direction. There was subsidence of 0.793 and 2.946 m, respectively.
>
> May 15–June 11: F_1–F_7 points moved 3.07–15.77 m toward the southwest and subsidence of 0.63–2.47 m. The daily speed was 0.114–0.584 and 0.023–0.091 m. F_8 point data were lost because of its large subsidence. The deformation showed a feature of compression, sliding from north to south.
>
> June 10–11: A_3 point moved 6.083 m directly toward the west while B_3 point moved 2.961 m continuously toward the southwest.
>
> 8:00–8:45 AM June 11: F_1–F_7 moved 6.04–24.05 m toward south at a speed of 5.3, 4.7, 4.4, 4.0, 2.8, 1.9, 1.3 mm/min. The displacement was large in the back and small in front which showed a pushing-moving deformation feature.

Second, there was an obvious auspice of pre-sliding: The back margin in the toe of Guangjiaya failed 2 m on the one night of June 10. The extension subsidence area in the east–west edges enlarged to 10–35 m and failed 3–5 m then merged together and formed a curve-shaped cracking circle. The toe of Jiangjiapo became humidified and clearly showed tympanites.

The main sliding area from Wotangkeng to Jiangjiapo contained lots of sliding phenomena such as tympanites, highway stagger, and ground heaving. There were

other phenomena such as ground shaking, ground sound, ground heating, ground-water, and animal behavior abnormality. The long water bleb inside T3 Theodolite cannot be leveled repeatedly.

The area of falling and rockfall in the front part of Jiangjiapo became continu-ously bigger and bigger and the humidity in the toe increased. At 4 h 15 s June 10, the west part of Jiangjiapo cliff (elevation 520 m) fell down in an area of $7.0 \times 10^5 \mathrm{m}^3$ and piping occurred before 5 min had elapsed, and the whole slide experienced sand-blast which was sprayed as high as 10 m in elevation indicating the occurrence of a large landslide.

Landslide Prediction

The monitoring and prediction on the Xintan landslide has been ongoing for more than 5 years. The middle-long-term prediction, short-term prediction, and pre-sliding prediction were done by the mode of briefing, deformation reporting, danger-ous condition reporting, emergency telegram, and emergency telephone (fire alarm, flood alarm).

(a) Before accelerating deformation stage: Briefing on loading condition and defor-mation status, attention questions and working suggestions.
(b) Accelerating deformation stage: Middle-long-term prediction of the landslide by deformation reports and dangerous condition reports. The prediction was mainly for the trends and features of local deformation to whole deformation, notable deformation places, sliding scale, and possible damages. This informa-tion will supply the scientific basis for the local government to arrange remov-ing, relocation, etc.
(c) Rapid deformation stage: Prediction was communicated in the form of danger-ous condition reports, emergency telegrams, and emergency telephone to the government reporting the emergency conditions namely forecasting the sliding time, place, scale, main sliding direction, moving type, and the disaster area in a short time, for pre-sliding prediction. It will urge the government to make the final decision for taking measures of disaster prevention.

Deformation Features of Sliding Remains

The landslide monitoring system was re-built after sliding in order to assess the deformation condition of sliding remains. The triangle method of two directions and triangle leveling method were used to survey the horizontal displacement and vertical displacement. According to the analysis of the deformation monitoring data, there was residual sliding after the large landslide during 1 week in the slide remains. The accumulated displacement toward the river was 360–1,850 mm in June 14–17 with a daily rate of 120–617 mm. The speed decreased and the landslide came into a

Table 18.2 Macroscopic portion of each development steps and deformation (speed of monitoring points for the Xintan landslide)

Deformation stages Macroscopic portent	I. Slow deformation stage (before August 1979)	II. Constant deformation stage (August 1979–July 1982)	III. Accelerating deformation stage (July 1982–May 1985)	IV. Rapid deformation stage (May 1985–June 12, 1985)
1. Cracks	Long cracks in a south–north direction in main sliding area	Reactive of cracks in rainy season, new extension deformation	Feather cracks in back and side edge and extended to connecting show the margin condition of whole sliding	Extension circle of curve-shaped cracks, increasing in length, width, and subsidence
2. Upheaval sink	Non-clear upheaval and sink	Small upheaval and sink in some area	Sink in the back margin, upheaval in front area	Subsidence in the back area, clear upheaval in toe
3. Falling	Small falling in back cliff and western dangerous rocks	Falling loading in Guangjiaya reached a volume of $1.6 \times 10^6 \text{m}^3$, small fall in toe area	Small falling in toe area in rainy season	Large falling in back margin, falling in toe continuously, increasing scale
4. Deformation	Small deformation, <10 mm/month, downslope creeping	Increasing deformation, 10 mm ≤ monthly displacement <50 mm, nearly constant moving	Increased to 50 mm ≤ monthly displacement <100 mm, clear change in creeping curve	Rapid increasing of deformation reached peak value. Monthly rainfall ≥100 mm or more. Inflexion in creeping curve steep to 90°
5. Relation between deformation and precipitation	Not clear	When rainfall >200 mm/month, clear deformation	When rainfall <200 mm/month, sudden deformation	In phase relation
6. Ground water	No clear different change	Higher groundwater, discharge increase or decrease	Higher groundwater, spring became sandy, discharge changed rapidly, spring disappear in toe	Groundwater level changed obviously, wet area increase
7. Others	Back margin falling loading, creeping deformation start	Jiangjiapo cliff rock fall 30,000 m³ in March–May 1982	Trees tilted to south, small falling in toe	Ground shaking, ground sound, ground heating

Table 18.3 The criterion for synthetic prediction of the Xintan landslide

Type	Factor of safety	Possibility	Speed	Macroscopic portent information
Criterion	Fs ≤ 1.0	P≤95%	≥3,500 mm/day or ≥116 mm/month	Table 18.2

slow deformation condition. The slide remains deformed for 2.5 years (June 1985–December 1987) (for a total of three rainy seasons, and then it came into a stable condition).

Aspects of Successful Prediction for Failure of the Xintan Landslide

Landslide prediction is a difficult task. There are no prediction theories and methods experienced for in situ validating because of complexity, randomicity, and uncertainty. The accurate time prediction of landslide is even now scientifically difficult for disaster prevention. Lots of so-called "successful predictions" are based on judgment and past experience in assessing pre-slide phenomena. The prediction based on the theoretical prediction model is mainly validated after sliding has occurred. The critical aspects of landslide prediction are the prediction method and criterion. There are obvious macroscopic portions and other abnormal phenomena that occur during the progressive deformation of landslide failures such as ground deformation, groundwater change, ground sound, and animal behavior abnormality. Integrating prediction methods, which combine the macroscopic portions with speed criterion and its critical factors such as precipitation, reservoir fluctuation, human activities, and earthquake is an important aspect of landslide prediction (Xu et al. 2004).

The macroscopic portions of each deformation stages and deformation information and integrating predicting criterion in the Xintan landslide are shown in Tables 18.2 and 18.3 for landslide prediction reference (Hu et al. 1996).

Conclusions

It is an honor to experience the investigation and prediction of the Xintan landslide. There are some understandings as follows after reviewing and summarizing of prediction process on the Xintan landslide:

1. The Xintan landslide prediction was based on the geological investigation, quantity statistics on ground survey data, environmental engineering geology comparison, and expert consultation. It was a successful prediction based on predominating deformation features of all stages in time and according to the

criterion of inflexion in displacement curve and other pre-sliding macroscopic portent, pre-sliding prediction on the time, place, scale, and damages.

2. The Xintan landslide experienced four deformation stages: slow deformation, constant deformation, accelerating deformation, and rapid deformation. The deformation features and the increasing process of inclination in creeping curve of key survey points show the characteristics of falling loading landslide of pushing reactive type. Namely the whole tendency of creeping curve in different deformation stages show increasing steps which means it reached into the accelerating deformation stage. It is the pre-sliding auspice that there is a sharp inflexion in creeping curve. This is the typical phenomena of this kind of landslide and it can be a reference for the prediction of same kind of landslide.

3. The characteristics of deformation survey on the Xintan landslide are the adjustment of survey method according to the different area, different deformation stages. It adjusted the monitoring places and survey method to form a monitoring network of point, line, and plan which supply an effecting condition for monitoring landslide's progressing in time and place.

4. It consists in the principles of combining long-term survey with field investigation, qualitative analysis with quantitative analysis, experience criterion with theoretical analysis that became one of the experiences for successful prediction of the Xintan landslide.

5. According to the analysis on the deformation monitoring of sliding remains, there are after sliding in 1 week after main landslide and the displacement are notable. Then the speed decreased and it came into slow deformation condition. The sliding remains deformed 2.5 years or three rainy seasons, then it came into a stable condition.

6. There are clear macroscopic portents before landslide. Integrating prediction method which combines the macroscopic portents with speed criterion and its affecting factors such as precipitation, reservoir fluctuating, human activities, and earthquake is an important method of landslide prediction.

References

Hu GS, Wang SQ et al. (1996) Study on prediction criterion of Xintan landslide. Chinese Journal of Geological Hazard and Control, 7(Supplement Issue): 67–72 (in Chinese)

Sun GZ (1996) Historic monument of disaster mitigation. Chinese Journal of Geological Hazard and Control, 7(Supplement Issue): 1–4 (in Chinese)

Wang SQ et al. (1990) Study and analysis of landslide stability. Project of Monitoring and Control of Xintan Landslide and Lianziya Hazardous Rock Mountain of Three Gorges, Yangtze River. Investigation Report of Rockfall Institute of Xiling Gorge, Hubei Province, pp 19–38 (in Chinese)

Wang SQ (1996) Review on prediction of Xintan landslide. Chinese Journal of Geological Hazard and Control, 7(Supplement Issue): 11–19 (in Chinese)

Wang SQ et al. (1999) Landslide Monitoring and Forecast in Three Gorges, Yangtze River. Geological Publishing House, pp 13–20 (in Chinese)

Xu Q, Huang RQ, Li XZ (2004) Research progress in time forecast and prediction of landslides. Progress in Earth Sciences, 19(3): 478–483 (in Chinese)

Chapter 19
Back-Analysis of Water Waves Generated by the Xintan Landslide

Yang Wang and Guoqing Xu

Abstract The Xintan landslide, a fast-moving landslide that occurred on June 12, 1985, is located on the north bank of the Yangtze River at Xintan Town, Zigui County, Hubei Province, China. Investigations showed that this landslide travelled at a speed of about 20 m/s and induced a huge water wave with wave run-up of 54 m on the opposite shore. Back-analysis of water waves generated by the Xintan landslide is used to determine the friction angle of the sliding zone in a state of movement. Newton's second law and the basic principles of kinematics are used to obtain landslide velocity by the method of back-analysis, and the volume conversion law and the viscous force formula in flow fields are applied to calculate the initial height of the water wave. In terms of continuity equation, movement equation of transient flow and water head loss theory in open channels in hydrodynamics, the propagation process of the landslide surge is divided into two stages: the sharp-decay stage and the slow-decay stage. It is assumed that the sharp-decay stage is a kind of exponential decay and the slow-decay stage is a kind of water head loss with propagation distance in an open channel. Wave run-up on the opposite shore is calculated with the consideration of slope angle and run-up azimuth. It is concluded that an appropriate value of the reduction factor of friction angle of the sliding zone is between 0.8 and 0.9, and the results have significance for the selection of the friction angle of the sliding zone in a state of movement and calculation of landslide velocity.

Keywords Xintan landslide · Water wave · Back-analysis · Friction angle · Decay · Run-up

Introduction

Landslides along reservoirs may cause great water waves, which seriously threaten dams, ships and the lives and property of residents. Historically, there have been many examples of landslides forming dams and causing water wave events

Y. Wang (✉)
China University of Geosciences, Wuhan, Hubei, 430074, China
e-mail: wangyangcug@126.com

(Chai 1995; Yan 2006). Examples include the Tangyanguang landslide at Tuoxi reservoir in Hunan Province, China, that occurred on March 16, 1961 (Jin and Wang 1988), the Vaiont reservoir landslide in Italy that occurred on October 9, 1963 (Zhong 1993), the Jipazi landslide on the bank of the Yangtze River in China that occurred on July 17, 1982 (Li 1988), the Xintan landslide on the bank of the Yangtze River in China that occurred on June 12, 1985 (Wang and Liu 1986; Wang and Tan 1991) and the Qianjiangping landslide on the bank of the Qinggan River, a tributary of the Yangtze River in China that occurred on July 13, 2003, all of which caused a large amount of damage, resulting in enormous losses.

The sizes of water waves generated by landslides are calculated by experimental formula or numerical analysis and simulation. The experimental method mainly includes a number of formulas: the Slingerland and Voight, Noda, Huber and Hager, Panjiazhen, Chow, Synolakis and Hall and Watts (Wieczorek et al. 2003; Noda 1970; Pan 1980; Chen 1984). Numerical analysis and simulation mainly includes the Saint-Venant equation (G. Pérezl et al. 2006), finite element method (Christopher and Bruce 1977), finite difference method (Harbitz et al. 1993), boundary element method (Grilli et al. 2002), Navier–Stokes equation (Rzadkiewicz et al. 1996), wavelet transform method (Panizzo et al. 2002) and the DIF equation (Jiang et al. 2005).

Based on the engineering geology of the Xintan landslide, back-analysis of water waves generated by the Xintan landslide is used to determine the friction angle of the sliding zone in a state of movement. Newton's second law and the basic principles of kinematics are used to obtain landslide velocity, and the volume conversion law and the viscous force formula in flow fields are applied to calculate the initial height of the water wave. In terms of the hydrodynamic continuity equation, movement equation of transient flow and water head loss theory in an open channel, the decay process of landslide surge is divided into two stages: sharp-decay stage and slow-decay stage.

Engineering Geology of the Xintan Landslide

The Xintan landslide is located on the north bank of the Yangtze River at the exit of Bingshubaojian Canyon, Xintan Town, Zigui County, Hubei Province. It is 15.5 km away from Zigui County, 26.6 km away from the Sandouping Dam and 72 km west of Yichang City (Fig. 19.1).

Topography and Geomorphology of Xintan Landslide

The landslide area is a weathered and denuded bank slope landform with an average gradient of 23° and a thickness of 30–40 m. The northern part is higher than the southern part and the western is higher than the eastern along the river (Fig. 19.2). The west part is Huangyan Mountain and the north part is Guangjiaya and Jiupan mountains. The highest elevation is 1,332 m. The south part is the Yangtze River
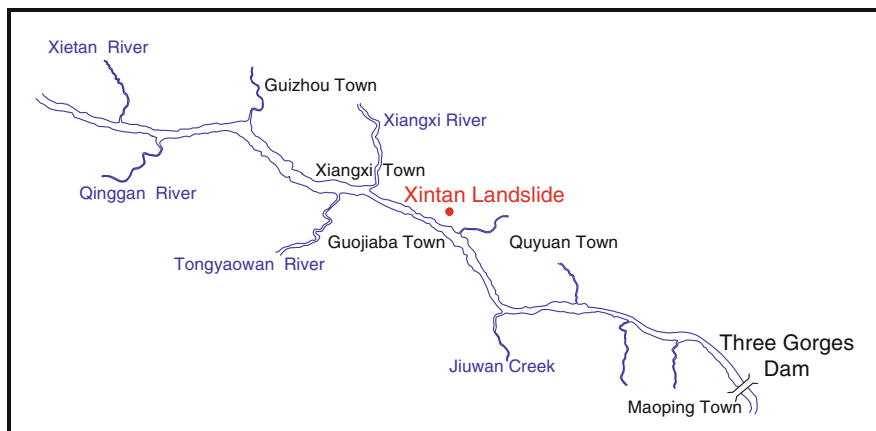
Fig. 19.1 A location figure of the Xintan landslide (Guo et al. 1991)

with the lowest elevation of about 56 m. There are three terraces of different elevations: 80–90, 120 and 160–165 m.

The Xintan landslide, about 2,000 m long, is an irregular quadrilateral plane, with an area of 0.75×10^6 m^2 and a volume of 3×10^7 m^3. The relative elevation difference between the back part of landslide and the bed of the Yangzte river is about 800 m. The average width of the landslide area is 450 m, with a narrower back part of about 300 m and a wider front of 500–1,000 m (Fig. 19.3). It has different gradients in different positions. Four steep parts, including the part near the river, the front part of Maojiayuan (elevation between 300 and 400 m), the front part of Jiangjiapo (elevation between 510 and 590 m) and Jiupanshan Mountain (between 750 and 900 m), have a slope angle of 35–40° and 50–60°. The graded areas include the back part of Xintan Town with an elevation of 200–270 m and the area between Maojiayuan and Wojukeng slopes, and have a slope angle of 15–20°.

Rock and Soil of the Xintan Landslide

Bedrock in the Xintan landslide was formed in the Silurian, Devonian, Carboniferous and Permian Periods. Among them, bedrock belonging to the Silurian Period contains the Luoerping Formation composed of yellowish green siltstone and shale and the Shamao Formation, characterized by brown purple sandstone, green siltstone and sandy shale, which mainly appear in dividing lines between colluvial and sloping deposits and bedrock in the west area of Maojiayuan. Bedrock from the Devonian Period includes the Yuntaiguan Formation featuring grey quartz sandstone containing siltstone and the Xiejingshi Formation featuring grey purple quartz sandstone, mostly appearing in the east of steep cliff between Liyu Mountain and Huangya. Bedrock from the Carboniferous Period includes the Huanglong Formation with thick, white, coarse-grained crystalline limestone containing dolomite limestone, of which the outcrop area is small. Bedrock belonging
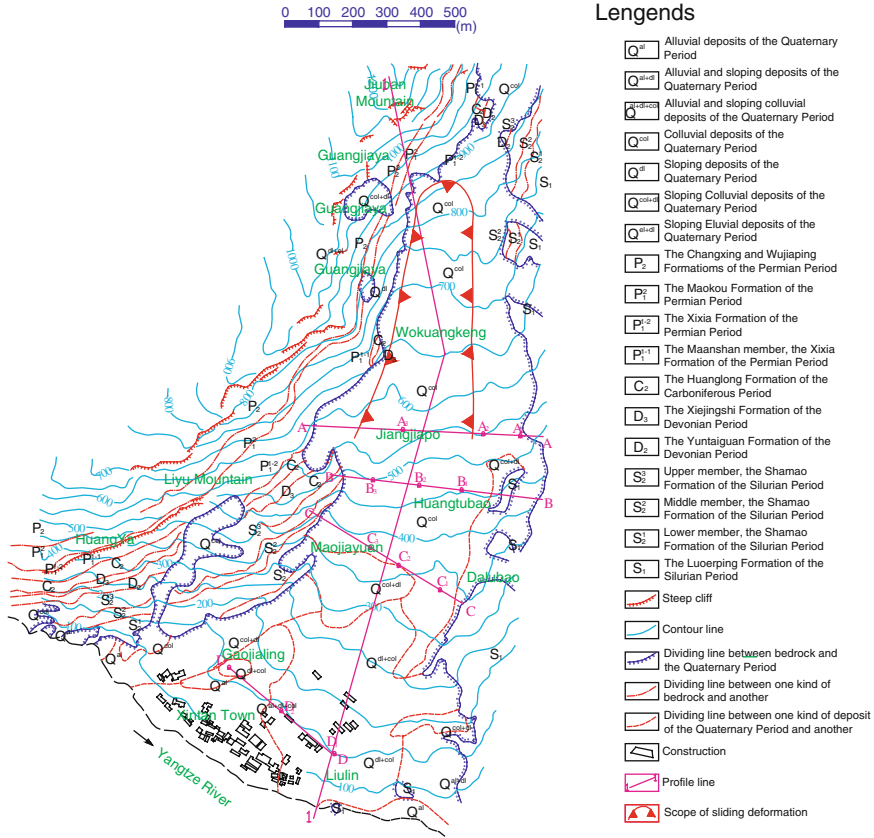
Fig. 19.2 Engineering geology of the plan of the Xintan landslide (rockfall investigation office of the Xiling Gorge in Hubei Province 1983)

to the Carboniferous Period includes the Maanshan Member, the Xixia Formation, characterized by black grey mudstone and carbonaceous shale containing a coal seam and Limestone Member, the Xixia Formation with alternative layers of dark grey limestone and mudstone, the Maokou Formation with grey black thick limestone containing chert nodules, the Wujiaping Formation with grey and grey yellowish thin-layer limestone containing a shale and chert layer and the Changxing Formation with dark moderately thick, grey limestone with nodules and bands, which appear in the Jiupanshan, Guangjiaya and Huangya (Figs. 19.2 and 19.3).

Colluvial deposits of the Quaternary Period are mainly distributed at the toe of Jiupan mountain and JiangJiapo slope, composed of broken stones and blocks of limestone from the Carboniferous and Permian Periods, with clay content of less than 5%. Sloping colluvial deposits, 10–40 m thick and compact, with high clay content, are mainly distributed at the bottom of Jiangjiapo slope, and mostly consist
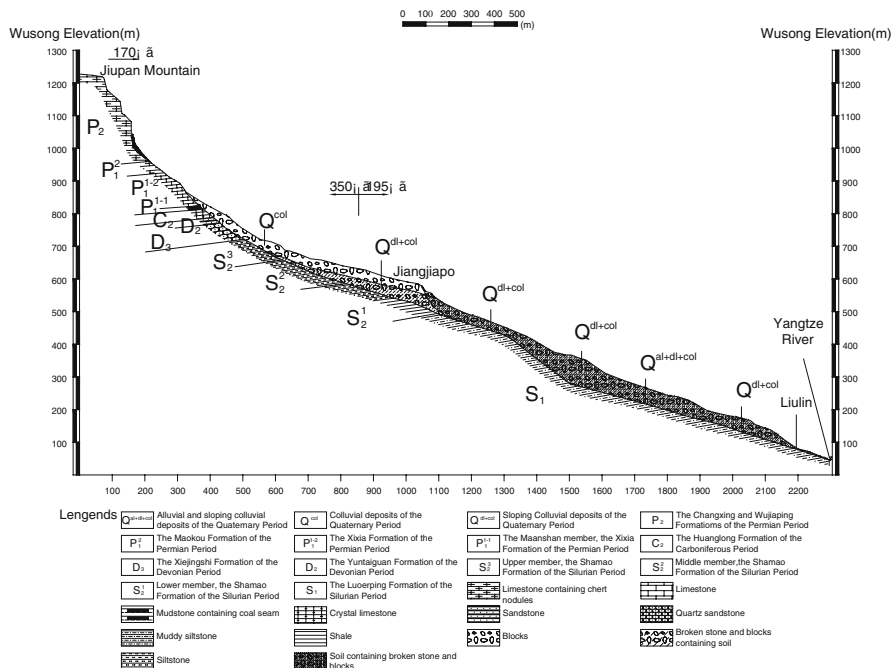
Fig. 19.3 Engineering geological profile of the Xintan landslide (rockfall investigation office of the Xiling Gorge in Hubei Province 1983)

of broken stones and blocks of limestone. Mainly distributed at Maojiayuan and Gaojialing, the sloping colluvial deposits are composed of blocks of quartz sandstone containing few blocks of limestone in the upper part, and blocks and broken stones of limestone, which contain a high clay content in the lower part. The alluvial, and sloping colluvial deposits, 10–30 m thick and compact, is mainly distributed over the area between Gaojialing and Xintan Town, and is primarily composed of broken stones and blocks of limestone containing calcareous nodules, sand, gravel, and cemented gravel (Figs. 19.2 and 19.3).

Calculations of Landslide Velocity and Water Wave

Calculation of Landslide Velocity

Based on the engineering geology of the Xintan landslide, the slope body between Jinagjiapo and Yangtze River is selected to be used as the experimental section. Two directions are selected for this section to analyze the mechanics of these sections. The first is the direction perpendicular to the slip surface and the second is the direction parallel to the slip surface (Fig. 19.4). The assumptions of
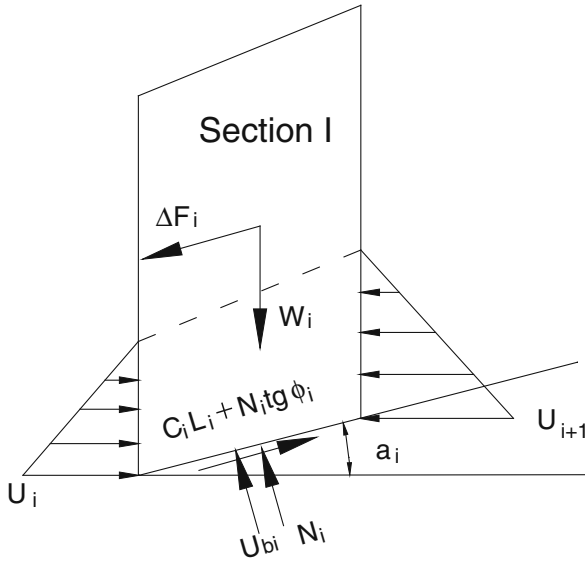
Fig. 19.4 Forces of section

the analysis are that the section in question is considered as a rigid body when it moves, the value of the acceleration perpendicular to the slip surface of the section is zero, and the direction of resultant forces from the front and back sections acting on the current section that is parallel to the slip surface. Newton's second law is used to establish the kinetics equation of the section and solve for acceleration. Then, the basic principles of kinematics are employed to solve for terminal speed.

According to Newton's second law and assumptions, the equations of the direction perpendicular to the slip surface and the direction parallel to the slip surface can be represented as follows:

$$W_i \cos \alpha_i - (U_{i+1} - U_i) \sin \alpha_i - U_{bi} - N_i = 0 \tag{19.1}$$

$$W_i \sin \alpha_i + \Delta F_i + (U_{i+1} - U_i) \cos \alpha_i - (C_i L_i + N_i tg \Phi_i) = M_i a_i \tag{19.2}$$

$$\sum_{i=1}^{n} \Delta F_i = 0 \tag{19.3}$$

According to these formulae

$$a_i = \frac{\sum\limits_{i=1}^{n} [(W_i \sin \alpha_i + \Delta U_i \cos \alpha_i - C_i L_i) - (W_i \cos \alpha_i - \Delta U_i \sin \alpha_i - U_{bi}) \, tg \, \Phi_i]}{\sum\limits_{i=1}^{n} M_i}$$

(19.4)

Here $\Delta U_i = U_{i+1} - U_i$, where α_i is the acceleration of section I, W_i is the weight of section I, M_i is the mass of section I, ΔF_i is resultant forces acting on the current section I, which are from front and back sections, U_i is the water pressure of lower lateral wall of section I, U_{i+1} is the water pressure of upper lateral wall of section I, U_{bi} is the water pressure of bottom surface of section I, C_i is the cohesion of the sliding zone of section I, φ_i is the internal friction angle of the sliding zone of section I, L_i is the length of bottom surface of section I and N_i is the positive pressure acting on the bottom surface of section I.

Velocity of section I can be calculated as follows:

$$V_{i2}^2 = V_{i1}^2 + 2 \cdot a_i \cdot L_i$$

(19.5)

where V_{i1} is the initial velocity of section I and V_{i2} is the terminal velocity of section I.

According to Eq. (19.5), landslide stops when the square of V_{i2} is less than or equal to zero, and the volume of landslide sliding into the reservoir is total volume of sections sliding into the reservoir.

Calculation of the Initial Water Wave Characteristics Generated by the Landslide

The volume conversion law means that water volume pushed away by the landslide is equal to the total volume generating water wave in the process of landslide movement on the assumption that the infiltration of the water in the pores of rock and soil mass is not taken into account.

The water wave spreads in a semi-circular form with the boundary of the reservoir bank at a certain speed at transitory time (Fig. 19.5). The volume of the water wave can be expressed as follows:

$$V_1 = \frac{\pi R^2}{2} h_1 = \frac{\pi (c_1 t_1)^2}{2} h_1$$

(19.6)

where c_1 is the spread speed of water wave, h_1 the height of initial water wave, h_0 the depth of the reservoir, V_1 the total volume of the water wave, t_1 the certain transitory time and R the spread distance within t_1.
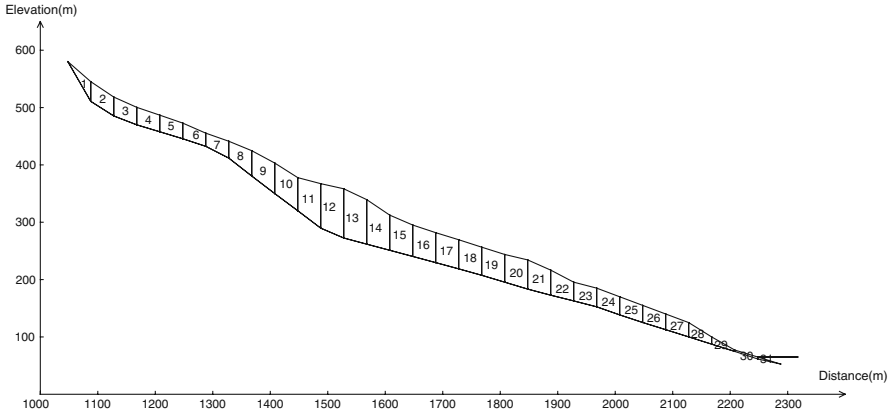
Fig. 19.5 Sketch of the distribution of the initial water wave

According to the continuity theory of the flow of a disturbed wave on water surface in hydraulics (Li and Xu 2000), the relationship between the height of wave and the speed of wave can be represented as

$$c_1 = (h_0 + h_1)\sqrt{\frac{2g}{2h_0 + h_1}} \tag{19.7}$$

When a section moves in liquid, it must overcome viscous force, and its kinetics equation can be expressed as follows:

$$m\frac{dv}{dt} = -\frac{1}{2}c_d\rho v^2 A \tag{19.8}$$

where m is the mass of section, v the movement speed of section, ρ the density of liquid, c_d the viscous resistance factor and A the area of head-on surface of section.

Based on the initial conditions that velocity of section is v_0, the velocity of section moving into water can be solved as follows:

$$v = \frac{v_0}{Bv_0t + 1} \tag{19.9}$$

Here,

$$B = \frac{c_d\rho A}{2m}$$

Displacement of the section moving into water can be calculated as follows:

$$S_2 = \int_0^t vdt = \int_0^t \frac{v_0}{Bv_0t + 1}dt = \frac{\ln(Bv_0t + 1)}{B} \tag{19.10}$$

Water volume displaced by the landslide sliding into water can be calculated as follows:

$$V_2 = A \cdot S_2 \tag{19.11}$$

The total volume generated by the water wave can be calculated as

$$V_1 = V_2 + V_0 \tag{19.12}$$

where V_0 is the volume of material sliding into the reservoir in the process of landslide movement.

Based on the volume conversion law, the initial water wave generated by the landslide can be calculated as

$$V_1 = g\pi t_1^2 \cdot \frac{h_1(h_0 + h_1)^2}{(2h_0 + h_1)} \tag{19.13}$$

where h_1 is the initial water wave generated by the landslide.

Calculation of the Propagation of Water Wave

In terms of continuity equation, the movement equation of transient flow and the water head loss theory in an open channel in hydrodynamics, the decay process of landslide surge is divided into two stages: sharp-decay stage and slow-decay stage.

It is assumed that the sharp-decay stage is a kind of exponential decay (Li 1982; Chen 1984; Wang 2005), and the propagation formula in this stage can be expressed as follows:

$$h_s(x, t) = h_1 e^{-\sqrt{k_1}x - \sqrt{\frac{g}{h_1}}t} \tag{19.14}$$

It is assumed that the slow-decay stage is a kind of water head loss with propagation distance in an open channel (Wang 2005). The propagation formula in this stage can be expressed as

$$h_s(x) = h_{s0} - \frac{2 g(h_0 + h_{s0})^2 \cdot n^2}{(2h_0 + h_{s0}) \cdot R^{\frac{4}{3}}} \cdot x \tag{19.15}$$

where h_{so} is the height of water wave at the start point of slow-decay stage, R the hydraulic radius, n the coarse factor and x the spread distance of slow-decay stage.

Calculation of the Run-up of the Wave

Wave run-up on the opposite shore is calculated with the consideration of slope angle and run-up azimuth (Wang 2005) as follows:

$$\Delta h = \left[\left(\sqrt{\frac{\pi}{2\alpha}} - 1 \right) \cos \beta + 1 \right] h \qquad (19.16)$$

where Δh is the height of wave run-up on the opposite shore, h the height of water wave, α the slope angle and β the run-up azimuth.

Back-Analysis of Water Waves Generated by the Xintan Landslide

The Shear Strength Parameters of the Sliding Zone of the Xintan Landslide

There is some research about the shear strength parameters of the sliding zone of the Xintan landslide. Residual strengths for the condition of natural water content and saturated water content of the Xintan landslide were obtained by direct shear test (consolidated quick shear). The total stress index and effective stress index were obtained by triaxial test (consolidated without drainage and consolidated drainage) (Zhu and Lu 1991). Wave method was used to solve shear strength parameters (Wu and Gao 1989); the back-analysis method was used to solve for friction factors (Xue et al. 1988; Wang et al. 1988). From the results above, the cohesion and internal friction angle of the sliding zone of Xintan landslide are determined as 21.0 kPa and 17.6°, respectively.

Back-Analysis of the Internal Friction Angle of the Sliding Zone in a State of Movement

The residual strength parameters of the sliding zone at rest are different from those in a state of movement. There is scant research concerning the residual strength parameters of a sliding zone in a state of movement and their values are not defined. Back-analysis of water waves generated by the Xintan landslide is used to solve for the friction angle of the sliding zone in a state of movement. On the assumption that the cohesion of the sliding zone is zero, the reduction factor of friction angle of the sliding zone in a state of movement is A, i.e., the ratio of internal friction angle in a state of movement to that at rest is A. The section method is used to solve for velocity (Fig. 19.6), and the Xintan landslide velocity and wave run-up on the opposite shore with different values of A are calculated (Table 19.1).
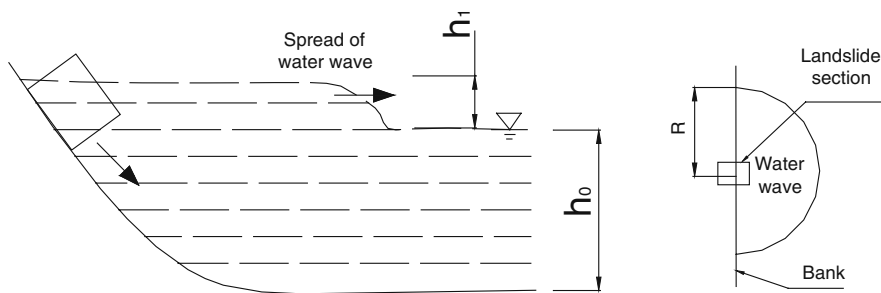
Fig. 19.6 Sections of the Xintan landslide

Table 19.1 Back-analysis results of water wave generated by the Xintan landslide

A	Landslide velocity (m/s)	Initial water wave (m)	Wave run-up (m)	Volume sliding into river (million m^3)
0.75	20.98	59	69.4	509.95
0.80	18.89	48.4	54.5	457.63
0.85	16.69	47.1	52.7	411.33
0.90	14.18	43.8	48.1	337.03
0.95	11.38	37.7	39.9	269.43

According to the data, the average velocity of the Xintan landslide was about 20 m/s, the volume of material that slide into the Yangtze River is about 3 million m^3 and wave run-up on the opposite shore is about 54 m. In combination with the calculation results (Table 19.1), an appropriate value of A is between 0.8 and 0.9.

Conclusions

Back-analysis of water waves generated by the landslide is used to solve for the friction angle of the sliding zone in a state of movement. In back-analysis, the Newton second law and the basic principles of kinematics are used to obtain landslide velocity, and the volume conversion law and the viscous force formula in flow field are applied to calculate the initial height of water wave. The propagation process of landslide surge is divided into two stages: sharp decay and slow decay. Wave run-up on the opposite shore is calculated with the consideration of slope angle and run-up azimuth. The data show that average velocity, the volume of the landslide sliding into Yangtze River and wave run-up on the opposite shore of the Xintan landslide provide an appropriate value for A derived. The results have significance for the selection of the friction angle of a sliding zone in a state of movement and the calculations of velocities of the landslide and water wave generated by the landslide.

References

Chai HJ, Liu HC, Zhang ZY (1995) The classification of Chinese landslide dam events. Journal of Geological Hazards and Environment Preservation 6(4): 1–9

Chen, XD (1984) Experiential method of surge triggered by landslide in reservoir and design of program. Science and Research School in Zhongnan Institute of Reconnaissance and Design of the Ministry of Water Conservancy and Electric Power, Changsha, 18 pp (in Chinese)

Christopher GK, Bruce L (1977) Finite element approach to waves due to landslides. Journal of the Hydraulics Division, ASCE 103(9): 1021–1029

Grilli ST, Vogelmann S, Watts P (2002) Development of 3D numerical wave tank for modelling tsunami generation by underwater landslides. Engineering Analysis with Boundary Elements 26: 301–313

Guo XZ, Zhang Y, Chu ZC, et al. (1991) Geological hazards of China and their prevention and control. Geological Publishing House, Beijing, 259 pp

Harbitz CB, Pedersen G, Gjevik B (1993) Numerical simulations of large water waves due to landslides. Journal of Hydraulic Engineering, ASCE 119(12): 1325–1342

Jiang ZB, Jin F, Sheng J (2005) Numerical simulations of water waves due to landslide. Journal of Yangtze River Scientific Research Institute 22(5): 1–3

Jin DL, Wang GF (1988) Tangyanguang landslide of Zhexi reservoir. In: Ground Rock Engineering Professional Committee of China′s Rock Mechanics and Engineering Academy & Engineering Geological Professional Committee of China′s Geology Academy (ed.) Typical Landslides in China. Scientific Press, Beijing, pp 301–307

Li W, Xu XP (2000) Hydraulics. Wuhan University of Hydraulic and Electricity Press, Wuhan, 469 pp (in Chinese)

Li WX (1982) Differential Equations of Hydraulics and its Application (Translated by Han, ZH, Zhen, KQ). Shanghai Science and Technology Press, Shanghai, 386 pp (in Chinese)

Li YS (1988) Jipazi landslide – An example of the reactivated old landslide in the three gorges region of Yangtze river. In: Ground Rock Engineering Professional Committee of China′s Rock Mechanics and Engineering Academy & Engineering Geological Professional Committee of China′s Geology Academy (ed.) Typical Landslides in China, Scientific Press, Beijing, pp 323–328

Noda E (1970) Water waves generated by landslides. Journal of the Waterways, Harbours and Coastal Engineering Division, ASCE 96(4): 835–855

Pan JZ (1980) Stability of Construction Against Sliding and Analysis of Landslide. Water Conservancy Press, Beijing, 238 pp (in Chinese)

Panizzo A, Bellotti G, Girolamo PE (2002) Application of wavelet transform analysis to landslide generated waves. Coastal Engineering 44: 321–338

Pérezl G, García-Navarro P, Vázquex-Cendón ME (2006). One-dimensional model of shallow water surface waves generated by landslides. Journal of Hydraulic Engineering, ASCE, 132(5): 462–473

Rockfall Investigation Office of the Xiling Gorge in Hubei Province (1983) The collection of research and investigation data about the Xintan Rockfall on the bank of the Xiling Gorge, the Yangtze River. Yichang, 424 pp (in Chinese)

Rzadkiewicz SA, Mariotti C, Heinrich P (1996) Modelling of submarine landslides and generated water waves. Physics and Chemistry of the Earth 21(12): 7–12

Wang DY, Liu SK (1986) Investigation of the surge effect caused by the Landslide at Xintan, Yangtze. Yangtze River 17(10): 24–27

Wang FW, Tan ZD (1991) The forming mechanism and sliding character of Xintan landslide. Journal of Yangtze River Scientific Research Institute 8(3): 28–34

Wang LS, Zhan Z, Su DG, et al. (1988) The preliminary studies of Xintan landslide's development characteristics and the mechanism of the starting and motioning and stopping. In: Ground Rock Engineering Professional Committee of China's Rock Mechanics and Engineering Academy & Engineering Geological Professional Committee of China's Geology Academy (ed.) Typical Landslides in China, Scientific Press, Beijing, pp 211–224

Wang Y (2005) The research on speed of the landslide and its surge hazard in reservoir (A Dissertation Submitted to China University of Geosciences for the Degree of Doctor of Philosophy). China University of Geosciences, Wuhan, 100 pp (in Chinese)

Wieczorek GF, Jakob M, Motyka RJ (2003) Preliminary assessment of landslide-induced wave hazards: Tidal Inlet, Glacier Bay National Park. U. S. Geological Survey Open-File Report 03-100: U.S. Department of the Interior and U.S. Geological Survey

Wu MB, Gao JG (1989) Measurement of wave action and mechanical analysis on the slope. Chinese Journal of Geotechnical Engineering 11(5): 70–77

Xue GF, Liu GF, Ren J (1988) The studies of Xintan landslide.In: Ground Rock Engineering Professional Committee of China's Rock Mechanics and Engineering Academy & Engineering Geological Professional Committee of China's Geology Academy (ed.) Typical Landslides in China, Scientific Press, Beijing, pp 200–210

Yan R (2006) Secondary disaster and environmental effect of landslide and collapsed dams in the upper reaches of Minjiang river (A Dissertation Submitted to Sichuan University for the Degree of Master of Engineering). Sichuan University, Chengdu, 143 pp (in Chinese)

Zhong LX (1993) Enlightenments from the accident of Vaiont landslide in Italy. The Chinese Journal of Geological Hazard and Control 5(2): 77–84

Zhu RG, Lu WX (1991) The study of clay strength characteristics at Xintan landslide. In: Huazhong University of Scientific and Technology (ed.) Proceedings of the International Landslide and Geotechnical Engineering, Huazhong University of Scientific and Technology Press, Wuhan, pp 14–19

Part III
New Methodologies Applied in this Area

Chapter 20
Intelligent Optimization of Reinforcement Design Using Evolutionary Artificial Neural Network for the Muzishu Landslide Based on GIS

Shaojun Li, Xiating Feng, Shunde Yin, and Youliang Zhang

Abstract Reinforcement measures are inevitably taken for most landslides in the reservoir area of Three Gorges, China. The reinforcement designs are often based on numerical analysis and land-use planners' experience, which will make them conservative in most cases. Obtaining a global optimum design which can guarantee both the landslide stability and lower costs of remedial works is a significant problem. This chapter presents a new method for the optimization of reinforcement design for landslides that is an integration of evolutionary artificial neural network algorithm, numerical analysis and GIS. Artificial neural network is used to build the nonlinear relationship between the parameters of reinforcement measures, factor of safety (FOS), and engineering cost; and network structure is optimized by genetic algorithm. Numerical analysis is used to create training and learning examples, and GIS technique plays the role of result visualization and data provision for numerical analysis. During the optimization procedure, the engineering cost is taken as a fitness function of genetic algorithm and FOS is regarded as a constraint condition. Accordingly, the optimized parameters of reinforcement measures, such as pile space, length, and the geometry and size of slide-prevention piles, will be obtained. Based on these optimized parameters and the intelligent prediction model, the reinforcement design will directly lead to more economical engineering costs. Finally, the reinforcement design will be visualized in a three-dimensional strata model of a landslide, which can contribute to land-use planners' synthetic decision-making. In addition, some integrating geological sections and local strata model can be generated in the GIS platform which will be used for numerical analysis for landslide stability. The proposed method is applied to the Muzishu landslide in the reservoir area of Three Gorges, China. The results provide a satisfactory optimum design which makes it possible to significantly reduce engineering costs.

Keywords Intelligent optimization · Reinforcement design of landslide · Evolutionary artificial neural network · GIS · Muzishu landslide

S. Li (✉)
State Key Laboratory of Geomechanics and Geotechnical Engineering, Insitute of Rock amd Soil Mechanics, The Chinese Academy of Sciences, Wuhan 430071, China
e-mail: sjli@whrsm.ac.cn

449

Introduction

As we know, landslides are severe geological hazards which occur frequently every year throughout the world. In China, losses due to landslide hazard are as much as 30 billion RMB according to some estimates (Hang 2007; Wang and Huang 2004). In the years after the impoundment of the Three Gorges Reservoir, the landslide hazard has especially become more serious. There are about 11,784 existing and potential landslides along the reservoir area of Chongqing city. As a result, the Chinese government has paid much more attention to landslide prevention and remediation. There has been more than 10 billion RMB invested for landslide investigation, engineering, and mitigation. However, mitigation has still been a challenging and important task in solving landslide problems. Slide-prevention piles and anchor cables that aim to reduce or eliminate landsliding are regarded as the most effective measures for landslide reinforcement in this area. However, the current design based on numerical analysis and planners' experience is often very conservative, which results in expensive engineering costs. The challenge is to evaluate problems effectively, so as to obtain a reasonable and optimum reinforcement design which can guarantee both the landslide stability and lower costs to do so.

Optimization of reinforcement design for landslides is a very complex problem which is limited by both landslide stabilization techniques and engineering costs. As such, the basic objective is to get the best parameters of reinforcement measures, such as configuration, geometry, and size of slide-prevention piles and anchor cables, for the lowest cost. There are some recent studies that address this problem. Xia and Zhu (1998) used analytic hierarchy process and fuzzy decision to choose reinforcement design of unstable slopes. Zhang (1999) adopted grey theory to get the optimum remedial design for a landslide. However, these methods only obtained relative optimum results through finite reinforcement designs; they could not adequately indicate the global optimal design. The relationship between reinforcement parameters and landslide stability and engineering cost is highly nonlinear. A suitable algorithm is required to recognize the highly nonlinear relationship. In addition, the search for the optimum reinforcement parameters' values is in a large space (parameters range) and is highly multimodal. A useful search algorithm to obtain global optimal solutions is required. Feng et al. (2000, 2002) recognized the mechanical parameters and constitutive model of rock by artificial neural network and genetic algorithm and obtained satisfactory results.

The method proposed in this chapter is to deal with the optimization problem of landslide reinforcement design, which is an integration of evolutionary artificial neural network, numerical analysis, and GIS. Artificial neural network will be adopted to build the nonlinear relationship between reinforcement parameters and factor of safety and engineering costs; genetic algorithm is used to solve the problem of global optimization and obtain the best network structure and reinforcement parameters. Numerical analysis is used to create training and learning examples, GIS technique will provide three-dimensional visualization for landslide strata information and reinforcement design, and it is also used to provide the basic analytic data. A local geological section and model is used for numerical analysis. The details

of all the techniques are discussed in this chapter. Finally, the method is applied in a practical reinforcement project for the Muzishu landslide located in the reservoir area of Three Gorges dam, China.

Integration Method for Optimization of Landslide Reinforcement Design

The method for optimization of landslide reinforcement design is based on an integration of evolutionary artificial neural network, numerical analysis and GIS, which is described as the following four parts.

Evolutionary Artificial Neural Network

Artificial neural network is a kind of computer learning technique, as it has the strong ability for function nonlinear mapping, the unknown relationship between inputs and outputs parameters can be built from a series of learning examples, and it has been widely used in the geotechnical research field (Wang and Rahman 1999; Wang and Feng 1997). As we know, the most popular model in artificial neural network is the back propagation (BP) algorithm (Kohonen 1998). However, there exist two problems with this algorithm which will greatly affect the generalization ability of the network for prediction outcomes of new cases. One is network structure, the other is "over-training" and local minima. Thus a new learning procedure referred to as genetic algorithm is proposed in this chapter to deal with this problem.

Genetic algorithm operates on the Darwinian principle of "survival of the fittest". An initial population of size m is created from a random selection of parameters in the parameter space. Each parameter set represents the individual's chromosomes. Each individual is assigned a fitness based on how well each individual's chromosomes allow it to perform in its environment. Through selection, crossover, and mutation operations, with the probabilities P_s, P_c, and P_m, respectively, the next generation is created. Fit individuals are selected for mating, whereas weak individuals die off. The process of mating and child creation is continued until an entire population of size m is generated. In practice, the average fitness of the population tends to increase with each generation. The fitness of each of the children is determined, and the process of selection/crossover/mutation is repeated. Successive generations are created until very fit individuals are obtained.

In the algorithm of evolutionary artificial neural network (ENN), genetic algorithm is used to optimize and obtain the optimal network structure (hidden layers and nodes) by the global search over a large space (parameters range), it can overcome the problem of "over-training" and local minima very well. Once the optimal neural network structure is obtained, both the corresponding reinforcement parameters and intelligent prediction model can be determined.

Construction of Nonlinear Relationship Between Reinforcement Parameters, Factor of Safety and Engineering Cost

In general, the nonlinear mapping relationship between reinforcement parameters, factor of safety and engineering cost is very difficult to be described by explicit expression. As a result, an artificial neural network model NN $(n, h_1, \ldots, h_p, m)$ is used to construct it in this chapter. The relationship is shown as follows:

$$\text{NN} \quad (n, h_1, \ldots, h_p, m): \quad R^n \to R^m \tag{20.1}$$

$$(Y) = \text{NN} \quad (n, h_1, \ldots, h_p, m)(X) \tag{20.2}$$

$$(Y) = (M, F) \tag{20.3}$$

$$(X) = (x_1, x_2, \ldots, x_n) \tag{20.4}$$

where output node is $(Y) = (M, F)$, F represents factor of safety, M is the engineering costs of remedial works. Input node of network $(X) = (x_1, x_2, \ldots, x_n)$, x_j are the reinforcement parameters to be determined, $j = 1, 2, \ldots, n$. For example, $(X) = (L, a, b, d, n, \ldots)$, where L is the length of slide-reducing pile, a is the width and b is the length of pile section, d represents the pile space, n is the main reinforcing steels. The network has total p hidden layers and the nodes is like $h_1, \ldots, h_p$.

Search of Optimal Reinforcement Parameters Using Genetic Algorithm in Global Space

The optimization of landslide reinforcement parameters is a typical restraint problem, as the application must satisfy both the desired landslide stability and the attempt to lower engineering cost. The basic objective is to obtain the lowest engineering cost whereas the design can guarantee the landslide stability. Based on the *ENN* technique described above, the outputs are assumed M (*ENN*) and F (*ENN*), which represent the engineering costs and factor of safety, respectively. The constraint condition is listed as follows:

$$\min f = M \quad (ENN) \tag{20.5}$$

$$\text{s.t.} F \quad (ENN) \geq Fs \tag{20.6}$$

where f represents the engineering cost of landslide reinforcement design, Fs is the factor of safety given by related specifications.

In this algorithm, the engineering cost is regarded as the evaluation index, fitness of genetic algorithm is based on the following equation:

$$Fitness = \min\{M[ENN(n,\ h_1, \ldots,\ h_p,\ m)]\} \qquad (20.7)$$

Once the neural network model representing the nonlinear relation is obtained, the model can be used for the recognition of the network structure and reinforcement parameters. The search procedure by genetic algorithm can be described as follows:

Step 1: Determine the initial parameters of artificial neural network and genetic algorithm as follows:

(1) The range of hidden layers and hidden nodes of artificial neural network.
(2) Number of parameters to be search N_p.
(3) Evolutionary generations N_{gen}.
(4) Population size P_{size}.
(5) Binary bits of every parameters N_{bit}.
(6) Probability of two-point mutation C_r.
(7) Probability of creep mutation J.
(8) Number of random seeds I_s.
(9) The range of parameters to be searched and a set of learning samples.

Step 2: Assume evolutionary generation $I=0$, and generate randomly P_{size} group of parameters at their given range. Each individual represents an initial solution.
Step 3: Input a set of parameters to the model NN ($n, h_1, \ldots, h_p, m$), use Eq. (20.7) to evaluate the fitness of the current individuals.
Step 4: Select each individual from the parent generation and encode it to binary chromosomes.
Step 5: Select randomly two individuals i_1 and i_2 from the parent generation. Carry out the crossover operation on the individuals i_1 and i_2 and generate a new chromosome. The new chromosome will pass on a two mutation and creep mutation at probabilities of C_r and J_r to generate a new parameter set.
Step 6: Decode the new chromosomes into parameters.
Step 7: Repeat Steps 4–6 until P_{size} new individuals are generated. They are used as offspring group.
Step 8: Replace randomly an individual in the offspring generation using the best parent's individual with the minimum *fitness*, take the offspring as parent.
Step 9: Execute the loop condition: $i_{gen} = i_{gen} + 1$.
Step 10: If the given evolutionary generation is reached, or the best individuals (the parameter to be back recognized) are obtained, then the evolutionary process ends. Otherwise, go to Step 3.

Three-Dimensional Visualization and Subsidiary Analysis for Strata Information and Reinforcement Design Based on GIS Technique

GIS (geographic information system) has been widely used in geotechnical engineering, as it provides a meaningful approach for optimum design of landslide reinforcement. An integrating system IGIAS[3D] for slope safety assessment has been developed based on GIS technique (Li et al. 2005), strata model, reinforcement measures and monitoring facilities are all visualized in this three-dimensional platform.

The fundamental data for strata modeling are geological sections, contour map, and borehole histogram. To build the three-dimensional strata model, some reasonable spatial interpolation algorithms and self-adaptive stratum control technique are applied. The model of reinforcement measures are added into the strata model as three-dimensional entities (Li et al. 2007). Some subsidiary analytic functions are also provided, such as information query of strata and all facilities, geological section generation, administration of construction and project materials, and so on. On the other hand, the arbitrary geological sections and strata model can be provided for numerical analysis through the three-dimensional synthetic geological model. The method will contribute much for the final synthetic decision-making by the planners.

Intelligent Optimization of Reinforcement Design for the Muzishu Landslide

Based on the methods described above, the Muzishu landslide is taken as the example for practical engineering application, and the optimum reinforcement design is given. The Muzishu landslide, locating on the south bank of the Yangtze River, is in Guojiaba town, Zigui County, Hubei province, China (Fig. 20.1). The landslide has a total potential slipping volume of $4.0u10^5$ m^3 with a length of 130–190 m and a width of 80–120 m. Because of the important location of this settlement in the Three Gorges, there are many residential houses and schools on the landslide body (Fig. 20.2).

Brief Description of the Muzishu Landslide

Muzishu landslide is a kind of quaternary accumulative landslide. Geologically, the bedrock originating from the lower Xiangxi group of the Jurassic Period is mainly made up of sandstone. The soil in the landslide body, with a maximum thickness of 25.0 m, consists of artificial macadam soil (thickness: 0.5–8.0 m), gravelly soil (thickness: 2.0–15.0 m), block stone, and macadam soil (thickness:
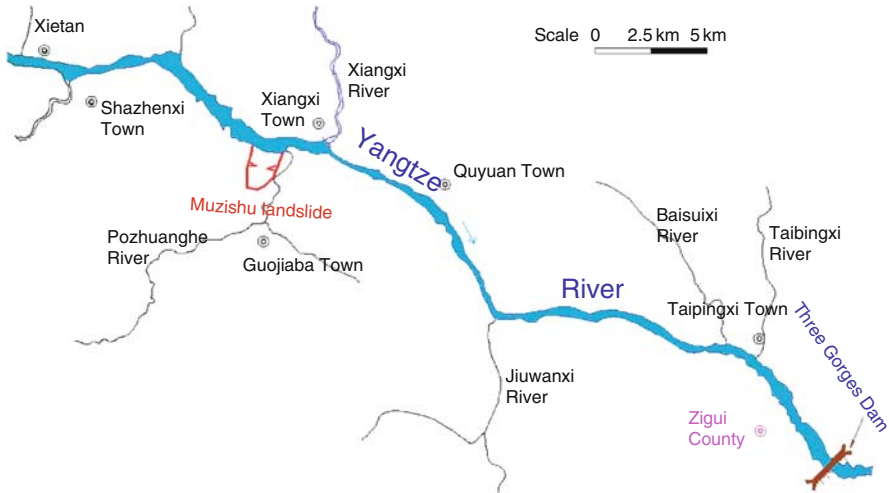
Fig. 20.1   Location of the Muzishu landslide

Fig. 20.2   Photograph of the Muzishu landslide (*Dashed red line* indicates landslide boundary)

0.5–13.0 m). The descriptions of soil and bedrock are listed in Table 20.1 and the typical geological section is shown in Fig. 20.3.

Reinforcement Design and Optimization Procedure

Through a series of previous studies and feasibility demonstrations, the reinforcement measures are determined to be two rows of slide-prevention piles distributed in middle-top and middle-bottom of the landslide body, respectively. Obtaining the

Table 20.1 Properties of gravelly soil in Muzishu landslide

Physical properties

Moisture content ω (%)	Bulk density (kN/m³)		Liquid limit WI (%)	Plastic limit Wp (%)	Plasticity index Ip (%)
	Wet	Dry			
18.8–21.9/*20.1	19.6–20.9/ *20.3	16.3–17.6/ *17.0	25.6–29.5/*17.8	14.8–18.0/ *16.9	10.2–11.5/*10.8

Mechanical properties

Consolidated fast shear		Residual shear	
Cohesive strength C (kPa)	Internal friction angle φ (deg.)	Cohesive strength C' (kPa)	Internal friction angle φ' (deg.)
6.0–18.0/*13.0	12.0*25.0/*19.3	0–6.0/#4.0	10.0–25.0/#18.0

*Mean value of five samples.
Mean value of three samples.
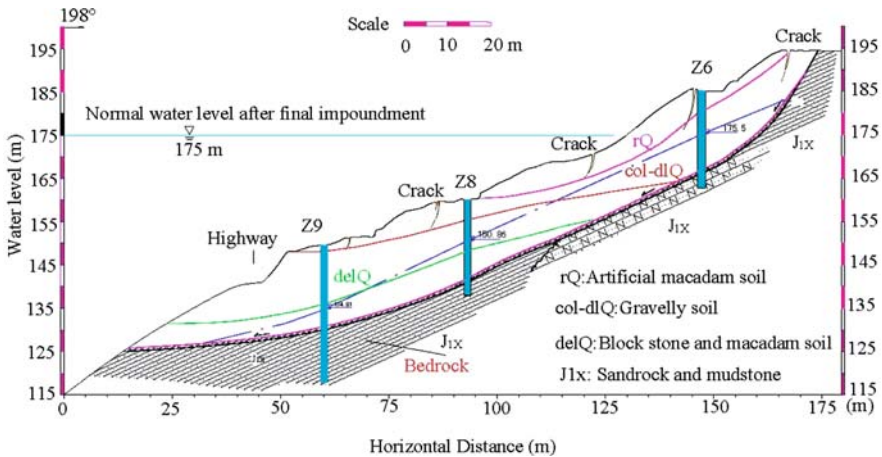
Fig. 20.3 A geological section of the Muzishu landslide

optimum design is based on the intelligent optimization algorithm and limiting equilibrium method which is used to calculate the factor of safety of each sample. Different pile length, section size, spacing, and number of main steel bars are taken into account. Sixty samples are constructed and are shown in Table 20.2.

The optimum model of artificial neural network design is shown in Fig. 20.4. Input parameters are the length of two rows of piles (L_1, L_2), width of pile section (a_1, a_2), length of pile section (b_1, b_2), space (d_1, d_2), number of main steel bar (n_1, n_2), output parameters, consisting of factor of safety (F) and engineering costs (M). Based on the samples mentioned above, artificial neural network is obtained for learning. The main optimization flow process is described as follows:

Table 20.2   The safety and economic index of each sample

	Middle-top piles					Middle-bottom piles						
		Pile section			Main		Pile section			Main		Cost
Sample no.	Pile length (m)	Width (m)	Length (m)	Space (m)	steel bars	Pile length (m)	Width (m)	Length (m)	Space (m)	steel bars	Factor of safety	(RMB) $\times 10^4$
1	35	2.1	2.6	4.8	103	36	2.4	2.9	6.3	119	1.1345	825.442
2	35	2.3	2.7	5.2	98	36	2.4	2.8	5.2	119	1.14	878.116
3	33	2.2	2.6	5.3	96	34	2.2	2.6	5.1	100	1.1271	742.548
4	34	2.3	2.7	5	109	37	2.4	2.8	5.2	128	1.1456	945.836
5	37	2.1	2.5	5	127	37	2.1	2.4	5.3	130	1.1328	954.965
6	38	2.4	2.8	5.7	138	38	2.5	2.8	5.5	140	1.1504	1043.156
7	36	2.8	3.1	6	127	37	2.2	2.6	4.6	128	1.1502	1027.443
8	37	2.5	3.1	5.6	126	35	2.2	2.5	4.2	106	1.1508	995.944
9	39	2.5	2.8	5.2	148	35	2.5	2.9	5.7	113	1.151	1027.772
10	37	2.5	2.9	4.6	127	37	2.2	2.6	5.5	125	1.1513	1048.147
11	38	2.2	2.5	5.5	139	38	2.6	3.2	5.7	136	1.1515	1036.986
12	39	2.3	2.5	5.5	154	39	2.4	2.7	5.1	149	1.1498	1156.967
13	34	2	2.4	4.2	94	39	2.5	3	5.5	147	1.1496	1008.388
14	37	2.1	2.6	6.2	123	40	2.7	3.1	5.7	156	1.1494	1014.847
15	37	2.6	2.9	5.5	114	39	2.5	3.1	6.1	138	1.1492	984.255
16	34	2.4	2.9	5.3	103	36	2.4	2.9	5.6	120	1.1437	863.654
17	36	2.5	2.9	5.6	121	37	2.5	2.8	5.4	131	1.1493	971.792
18	37	2.4	2.8	5.4	130	37	2.6	3.2	5.7	115	1.1511	979.062
19	35	2.2	2.7	6.3	109	36	2.3	2.8	6.2	117	1.1263	737.053
20	35	2.2	2.5	5.2	101	37	2.5	2.9	4.6	127	1.1496	984.119
21	38	2.2	2.5	5.5	139	36	2.1	2.9	6	110	1.1326	874.632
22	34	2.1	2.4	4.5	101	37	2.6	2.9	5.5	114	1.1378	896.852
23	38	2.4	2.8	6.3	137	40	2.5	3	5.6	146	1.1504	1040.234
24	36	2.8	3.1	6	127	37	1.9	2.5	5.2	121	1.1408	919.268
25	37	2.4	2.7	4.9	125	38	1.9	2.4	4.5	134	1.1452	1089.295
26	34	2.4	2.8	4.9	105	39	2.2	2.6	5	146	1.1482	1028.546
27	35	2.2	2.5	5.2	101	35	2.2	2.5	5	112	1.1295	821.655
28	33	2	2.6	5.3	88	40	2.3	2.6	5	151	1.1317	945.651
29	36	1.8	2.4	5.3	108	40	2.3	2.5	4.9	159	1.1361	1030.396
30	36	1.8	2.4	5.5	110	41	2.7	3.4	5.8	152	1.1506	1009.543
31	36	2.3	2.9	6.2	117	35	2.2	2.5	4.2	106	1.1395	892.349
32	37	2.6	3.1	5.6	124	37	1.9	2.5	5.2	121	1.1417	944.557
33	37	1.9	2.5	5.2	121	39	2.5	3.1	6.1	138	1.1447	953.121
34	40	2.5	3.1	5.3	147	37	2.1	2.6	6.2	123	1.1465	1019.225
35	40	2.6	3.1	5.4	151	35	2.3	2.8	6.1	109	1.1502	1004.648
36	40	2.6	3.1	5.4	153	38	2.3	2.6	5.4	141	1.1585	1162.758
37	41	2.5	2.8	5.4	159	40	2.6	3.3	6.2	150	1.1641	1206.557
38	38	2.3	2.6	5.4	140	40	2.7	3.2	5	149	1.1678	1217.762
39	39	2.5	3.1	6.1	138	35	2.3	2.8	5	109	1.1491	961.089
40	41	2.5	2.8	5.4	159	42	3	3.5	6.2	166	1.1752	1324.177
41	42	3	3.4	6.3	164	42	3	3.4	6	162	1.1825	1344.611
42	38	2.2	2.9	5.4	130	41	1.9	2.7	4.8	140	1.1496	1106.984
43	41	2.8	3.4	6.5	155	36	2.3	2.8	6	117	1.15	989.204
44	36	2.5	2.9	5	116	39	2.4	2.9	6.3	147	1.15	999.834
45	35	2.4	2.8	5.8	112	40	2.5	3.2	5.9	144	1.1502	964.184

Table 20.2 (continued)

| | Middle-top piles | | | | | Middle-bottom piles | | | | | | |
| | | Pile section | | | Main | | Pile section | | | Main | | Cost |
Sample no.	Pile length (m)	Width (m)	Length (m)	Space (m)	steel bars	Pile length (m)	Width (m)	Length (m)	Space (m)	steel bars	Factor of safety	(RMB) ×10⁴
46	38	2.2	2.6	5.3	136	41	2.4	2.8	5.3	151	1.1503	1135.286
47	35	2.3	2.8	6.1	109	41	2.8	3.4	6.5	155	1.15	954.931
48	37	2.4	2.8	5.6	130	39	2.6	2.9	6	154	1.1513	1034.194
49	35	2.4	2.7	6.4	113	40	2.8	3.4	6.3	152	1.1504	943.353
50	36	2.7	3.3	5.6	117	36	2.3	2.7	5.4	118	1.1511	938.094
51	36	2.3	2.6	6.1	121	41	2.6	3.1	5.6	155	1.1503	1033.643
52	37	2.3	2.6	6.7	129	41	2.7	3.2	5.7	154	1.1503	1026.546
53	38	2.2	2.5	5.8	139	37	2.7	3.1	5.5	136	1.1504	1017.632
54	38	2.2	2.4	5.7	146	39	2.6	3.1	5.7	149	1.1502	1070.558
55	39	2.2	2.4	5.7	159	40	2.5	3	5.5	151	1.1501	1141.867
56	39	2.2	2.4	5.6	160	39	2.5	3	5.5	146	1.1504	1125.861
57	37	2.1	2.7	5.5	121	39	2.7	3.1	6	152	1.1505	1009.875
58	37	2.2	2.7	5.6	125	39	2.6	3.2	6.2	146	1.1502	985.227
59	36	2.3	2.7	5.4	120	37	2.7	3.2	6	133	1.1506	952.176
60	36	2.3	2.7	6.5	119	42	2.8	3.5	6.5	156	1.1504	980.884
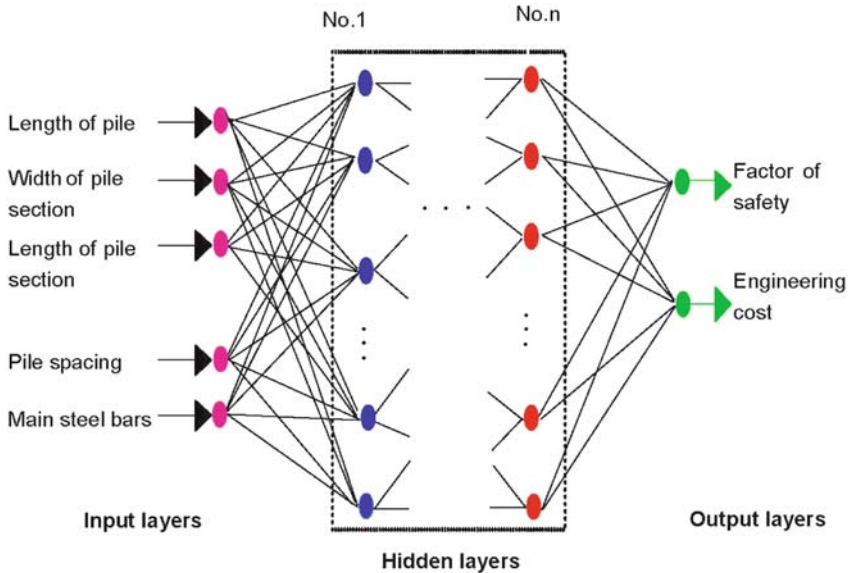
Fig. 20.4 The artificial neural network model for optimization of landslide reinforcement design

Step 1: Genetic algorithm is used to optimize the structure of artificial neural network. Accordingly, the parameters of genetic algorithm are set: $N_p = 60$, $N_{gen} = 50$, parameters of artificial neural network are set: input = 10, out-

put $= 2$, hidden layers $= 2$, nodes of hidden layers $= 1$–30. The former 58 samples in Table 20.2 are learning samples and the last two samples are test samples.

Step 2: After the computing search by genetic algorithm, the best structure of artificial neural network is obtained, the first layer $h_1 = 24$, the second layer $h_2 = 12$. Thus, the structure of artificial neural network is determined to be *ENN* (10, 24, 12, 2).

Step 3: Then the network model will substitute the numerical analysis for landslide stability, the range of reinforcement parameters are set as follows:

Pile length: 32–42 m; width of pile section: 1.8–3 m; length of pile section: 2.2–3.5 m; pile space: 4–7 m; number of main steel bars: 80–150.

Accordingly, the parameters of genetic algorithm are set as follows: $N_p = 10$; $N_{gen} = 60$; $P_{size} = 60$; $N_{bit} = 20$; $J_r = 0.2$; $C_r = 0.2$.

Step 4: Calculation of fitness is based on constraint condition. During the *ENN* optimum procedure, the engineering cost is assumed to be the evaluation index, and *fitness* of genetic algorithm is calculated as follows:

$$Fitness = \min\{M[ENN(10, 24, 12, 2)]\} \qquad (20.8)$$

According to the administrative requirements of slope design in Three Gorges, the factor of safety should be up to 1.15. Therefore, the constraint condition is listed below:

$$F[ENN(10, 24, 12, 2)] \geq 1.15 \qquad (20.9)$$

$$(Y) = ENN(10, 24, 12, 2)(X)$$

$$(Y) = (M, F), (X) = (L_1, a_1, b_1, d_1, n_1, L_2, a_2, b_2, d_2, n_2) \qquad (20.10)$$

Step 5: After a 60 generation search by genetic algorithm, the final reinforcement parameters are obtained as the following description:

Middle-top piles: pile length: 35 m; width of pile section: 2.3 m; length of pile section: 3.0 m; pile space: 5.5 m; number of main steel bars: 101.

Middle-bottom piles: pile length: 35 m; width of pile section: 2.6 m; length of pile section: 3.2 m; pile space: 5.5 m; number of main steel bars: 136.

Factor of safety is 1.1507 and the engineering cost is 9.0526 million RMB.

The optimized reinforcement parameters can verify the effectiveness of slide-prevention pile design. Based on these parameters, the factor of safety calculated by numerical method is 1.1502. Correspondingly, the engineering cost is 9.1394

Table 20.3 Comparison of ENN results and practical numerical solutions

Output parameters	Predicted result by ENN	Numerical result using recognized parameters	Relative error (%)
Factor of safety	1.1507	1.1502	0.045
Engineering cost (RMB) $\times 10^4$	905.26	913.94	0.950

million RMB. The comparison of calculated solutions and predicted results by ENN is shown in Table 20.3.

The result indicates that the method of evolutionary artificial neural network can create the complex nonlinear relationship between the reinforcement parameters, factor of safety and engineering cost. The relative error between predicted result and numerical solution is 0.045 and 0.95% for factor of safety and engineering cost, respectively.

Three-Dimensional Visualization and Subsidiary Analysis for Reinforcement Design

Based on the geological sections, contour map and borehole histogram of the Muzishu landslide, a series of virtual boreholes covering the whole landslide area is created for the requirement of strata modeling. The Kriging spatial interpolation method and self-adaptive stratum control technique are applied; three steps of strata modeling are implemented in the IGIAS^{3D} software (Li et al. 2007), which consist of strata division, generation of strata curved face and strata skirt. As a result, the three-dimensional strata model is built (Fig. 20.5). According to materials of the reinforcement design, the three-dimensional model of slide-prevention piles and their layout are displayed in the three-dimensional strata model, as shown in Fig. 20.6.
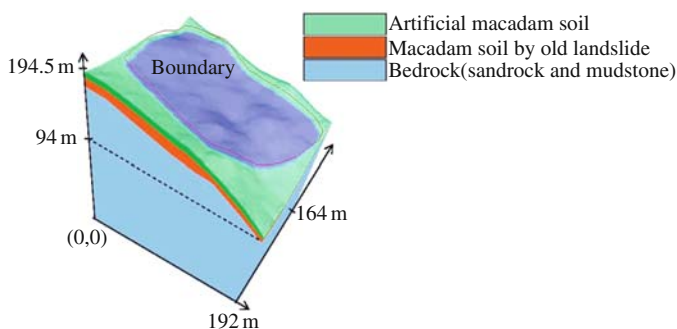

Fig. 20.5 Three-dimensional strata model of Muzishu landslide

Fig. 20.6 Three-dimensional visualization of reinforcement design
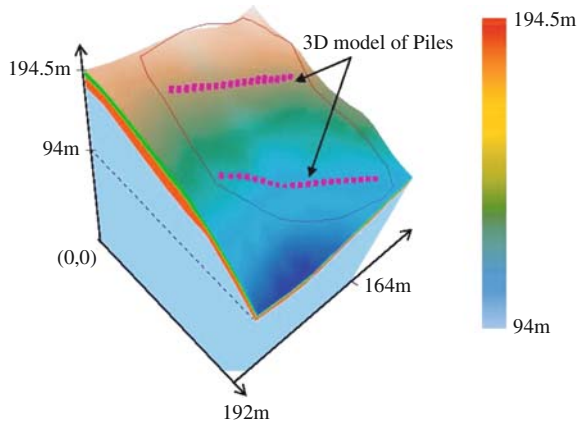
Subsidiary analysis includes an information query of slide-reducing piles and strata (Fig. 20.7), arbitrary geological section generation and numerical model output (Fig. 20.8), and synthetic design decision-making by planners. Through the three-dimensional analytic platform, the reinforcement design can be adjusted dynamically.

Fig. 20.7 Information query of strata and slide-prevention piles

Fig. 20.8 An arbitrarily selected geological section

Discussion and Conclusions

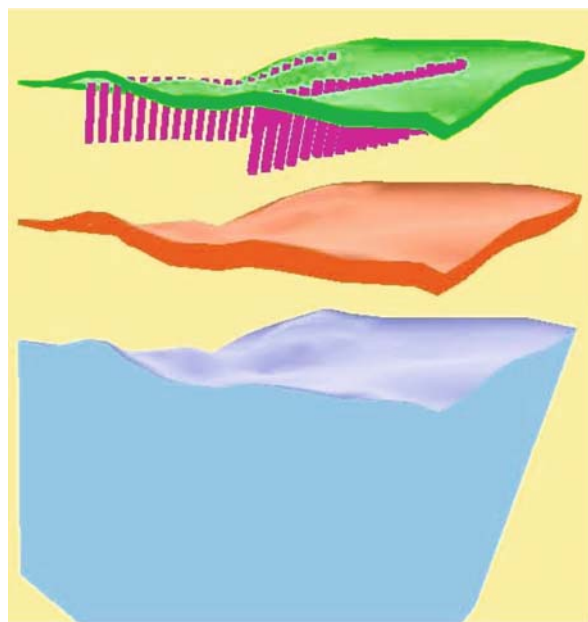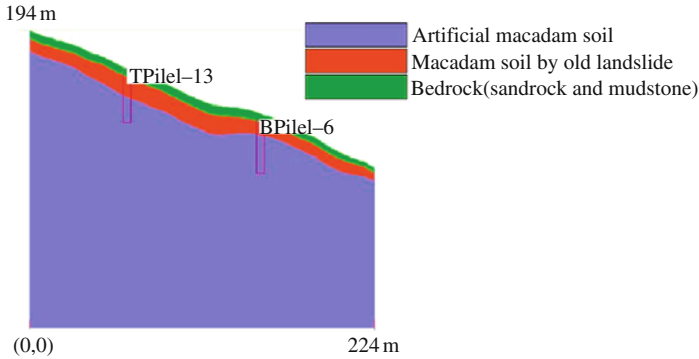Compared to previous designs for mitigation of the Muzishu landslide, the optimized design by ENN intelligent method not only guarantees the factor of safety but also saves a maximum 1.57 million RMB in engineering costs (14.63% of the total budget). For those landslides with higher reinforcement cost, the method will be even more effective.

According to the practical project conditions of this landslide, stress is different among the two rows of slide-prevention piles, and the middle-bottom piles have to bear larger pushing force. The optimized reinforcement design just agrees with this mechanical analysis, as the section of middle-bottom piles is larger than that of middle-top piles, it can provide much bigger reduced sliding force.

The intelligent method ENN introduced in this chapter has good performance in describing the nonlinear relationship; it can overcome the problems of over-training existing in the artificial neural network and can indicate the optimal of the final reinforcement parameters. Therefore, this method provides an effective approach for optimization problems in geotechnical engineering.

Intelligent optimization of reinforcement design is a significant problem for landslide projects. Based on the reasonable nonlinear relationship between reinforcement parameters, factor of safety and engineering cost, it can identify the optimum reinforcement parameters by intelligent search in a global space and provide a safe and economical remedial design for a landslide.

GIS technique plays an important role in the optimization of reinforcement design, which makes it possible for the landslide strata information and reinforcement design to be visualized in a three-dimensional platform. It will also provide some essential data for numerical analysis during the optimizing procedure. The planners can adjust the reinforcement designs dynamically and get a better decision-making ability in this three-dimensional visual environment.

References

Feng XT, Zhang ZQ, Qian S (2000) Identifying geo-material mechanical parameters of Three Gorges Project permanent shiplock using intelligent displacement back analysis method. International Journal of Rock Mechanics and Mining Sciences 37(7): 1039–1054

Feng XT, Li SJ, Liao HJ, Yang CX (2002) Identification of nonlinear stress-strain-time relationship of soils using genetic algorithm. International Journal for Numerical and Analytical Methods in Geomechanics 26: 815–830

Hang RQ (2007) Large-scale landslide and their sliding mechanisms in China since the 20th century. Chinese Journal of Rock Mechanics and Engineering 26(3): 433–454

Kohonen T (1998) An introduction to neutral computing. Neural Networks 1: 3–16

Li SJ, Feng XT, Zhang XW (2005) Study on the development and application of three dimensional intelligent information analysis for three slope safety assessment. Chinese Journal of Rock Mechanics and Engineering 24(19): 3419–3426

Li SJ, Feng XT, Wang W (2007) Spatial analysis based on three dimensional strata grid model for geotechnical engineering. Chinese Journal of Rock Mechanics and Engineering 26(3): 104–109

Wang J, Rahman MS (1999) An artificial neural network model for liquefaction-induced horizontal ground displacement. Soil Dynamics and Earthquake Engineering 18: 555–568

Wang SJ, Huang DC (2004) Centurial achievements of engineering geology in China. Beijing: Geological Press, pp 1–30

Wang YJ, Feng XT (1997) Intelligent rock mechanics: Development and application. In: Proc. of 9th International Conference of the Association for Computer Methods and Advances in Geomechanics. Rotterdam: A A Balkema

Xia YY, Zhu RG (1998) Intelligent subsidiary decision system for design selection of hazard slope. Chinese Journal of Rock Mechanics and Engineering 17(4): 453–458

Zhang SB (1999) The method to select landslide reinforcement designs using grey system. Hazard Methodology 114(4): 36–39

Chapter 21
The Application of Fractal Dimensions of Landslide Boundary Trace for Evaluation of Slope Instability

Shuren Wu, Huabin Wang, Jinliang Han, Jusong Shi, Lin Shi, and Yongshuang Zhang

Abstract   Fractal phenomena are a naturally occurring characteristic of landslides. In the process of landsliding, a series of traces of the rupture surface on the ground surface extends progressively, as various types of slope failure occur. After this enlarging of the surface of rupture is completed, mass movements increase the volume of material because the displaced material dilates. After landslide occurrence, geometrical features of the rupture surface appearing on the ground surface are one way of providing information to evaluate slope instability. Correspondingly, fractal dimensions of the landslide boundary trace can reach a maximum in view of its geometry, which indicates that the landslide is in a critically stable state. In the case of changes of external factors, slide masses are likely to reactivate. This chapter addresses fractal dimensions of the trace of a landslide outline and its application in evaluating slope instability. In the vicinity of Badong County Town on the south shore of the Three Gorges Reservoir, fractal dimensions of 11 landslides with respect to boundary trace were calculated using a box-counting method. Six landslides were chosen as a case study to distinguish the relationship between fractal dimensions of boundary trace and slope instability. Compared with previous work in calculating the factor of safety, a landslide has the potential to reactivate if the value of fractal dimensions is between 1.4 and 1.5. A landslide is stable overall but minor slope failures are likely to occur in small areas, if the value of fractal dimensions is 1.1–1.3. A value of fractal dimensions of 1.0 indicates that the landslide is in a stable state. In summary, landslides with larger fractal dimensions in view of the boundary trace were evaluated as not being in a stable state.

Keywords   Fractal dimensions · Landslide · Slope instability · Three Gorges Reservoir · China

S. Wu (✉)
Geomechanics Institute of China Academy of Geological Sciences, Beijing 100081, P.R. China
e-mail:shrwu@sohu.com

Introduction

Landslides are a natural hazard, defined as the movement of a mass of rock, debris, or earth down a slope (Cruden and Varnes 1996). In many countries, landslides have caused many deaths and considerable damage to, and in some cases the destruction of, elements of the worldwide economic infrastructure.

Landslides can be initiated by various external triggering factors. These include intense rainfall, earthquakes, groundwater-level changes, storm waves, or rapid stream erosion, which cause an increase in shear stresses or decrease in shear strengths of slope-forming materials. Slope failures represent the outcome of a steady-state process in an open, complex, nonlinear system. If any external parameter is changed, the steady state is usually re-established by means of a corresponding change of other parameters. For landslides, they may occur in steps of various magnitudes in area and volume, which can be represented by boundary traces in landslide mapping by both remote sensing interpretation and field investigation.

The fractal character of landslides has been used for its geometrical description and characterization. Considerable progress has been made in understanding physical processes associated with landslide hazards, using fractal dimensions and a self-criticality (SOC) concept (e.g., Guzzetti et al. 2002; Rouai and Jaaidi 2003; Turcotte and Malamud 2004). Based on an original "sandpile" model proposed by Bak et al. (1988), the frequency of landslide occurrence as a function of their size can be described by a power law, which confirms the existence of scale-invariant distribution of landslide area (Guzzetti et al. 2002).

However, progressive failure of slopes occurrence presents continuous changes in the geometry of landslide boundary. In timescale, the slope geometry relates to slope instability. Some literature focuses on the study of the relationship between the trace of landslide boundary and slope instability (Yin et al. 1989; Liu 1996; Zhou and Ou 1997; Tan et al. 1999). For landslide geometry, little progress was made on its quantitative description (Wu et al. 2002a). Moreover, numerous methods were proposed to evaluate slope instability (Nash 1987; Duncan 1996), such as limit-equilibrium methods, circular failure-surface methods and noncircular failure-surface methods, finite-element or finite-difference methods. In these models, many variables are involved in evaluation of slope instability, and calculations of the factor of safety (FS) require geometrical data, physical data on geologic materials and their shear strength parameters (cohesion and angle of internal friction), information on pore-water pressure, etc. However, it is very difficult to get the above information for landslides at a regional scale.

As noted in Bak et al. (1988), a sandpile model has large numbers of degrees of freedom and its behavior is sensitive to its initial conditions; these conditions are termed "complex". To evaluate slope instability, the complexity of a slope system requires employment of new methods that are efficient in predicting this nonlinear characteristic of natural landslides.

In this chapter, we investigated various landslides located in the vicinity of Badong County Town on the south shore of the Three Gorges Reservoir, China (Fig. 21.1). Fractal dimensions of traces of landslide boundaries were obtained, and
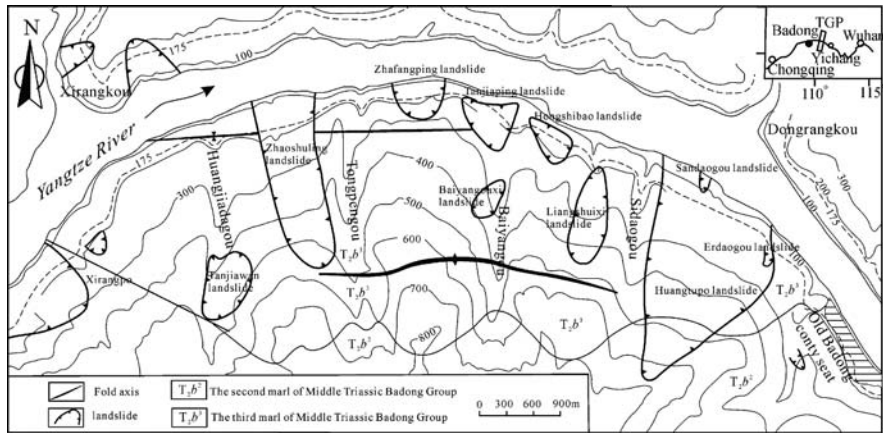
Fig. 21.1 A sketch map of the landslide trace pattern in the vicinity of Badong County Town

the relationship between the extension of the surface of rupture on the ground surface boundary and slope instability was then determined.

Features of Landslides in the Study Area

A new town was initially established at Huangtupo in early 1982, due to inundation of the former location, by the rising reservoir water level, which was a planned outcome of the construction of the Gezhouba Dam at Yichang City (Fig. 21.1). However, intensive urban development, without adequate investigation of engineering geological conditions, reactivated several large and composite landslides (Deng et al. 2000; Liu et al. 2002). The Three Gorges Project accelerated the development of a new Badong county town, which was relocated to Xirangpo, 6 km west of Huangtupo. Slope stability in this area is of importance for new settlements, and towns and roads are clearly visible in these high-risk areas. Therefore, more than 20 landslides in the Badong block were investigated, after detailed geological reconnaissance was conducted by the Yangtze River Commission and other researchers (e.g., Zhong 1995; Cui 1996; Cai et al. 2002; Liu et al. 2002; Tang et al. 2002; Wu et al. 2002b). The boundaries of these landslides are shown in Fig. 21.1.

These landslides were located in the same geological environment. One of the most significant geomorphological characteristics affecting slope instability is the strata dip toward the slope faces along the Yangtze River. Five valleys perpendicular to the main stream divide the area into five blocks from the old county-seat town to the new county town, which makes the topographic structure of slopes more complex. The average slope angle of the landslides was 20–30°, and step-like morphology was found within masses. Several upper masses of most of the landslides are composed of loose Quaternary deposits with soils and fractured rocks as a layer with high permeability, while some of lower masses consisting of limestone

or mud-limestone of the Badong Formation, resulting in aquifuges. This hydrological structure is thus susceptible to landsliding. The bedrock of mid-Triassic mud-limestone of the Badong Formation dips northward at 10–30°.

Most of the landslides are palaeo-landslides, which were identified by continuous boundary traces. They are outlined in the forms of gullies, scarps, cracks, and interfaces between various bedrock units. Particularly, the geometry of the boundary of the Huanglashi landslide is more complicated, as shown in Fig. 21.2. At the Huanglashi site, a swarm of landslides is composed of a palaeo-landslide and a recent activated mass. The area of the whole landslide is 1,580,000 m^2, and its volume is up to 40,000,000 m^3. The palaeo-landslide occurred 20,000 years ago, while the recent slide mass was formed after a variety of slope failures that have occurred since the 1980s. The landslide swarm has been classified into east and west masses. The east concentration of landslides consists of various old and recent landslides. For the western concentration of active masses as the main slide body of the Huanglashi landslide, the total volume is about 26,000,000 m^3. This swarm of landslides is composed of the Hengping landslide and the Dashiban-Taizhijiao landslide, of which the boundaries have partially overlapped.
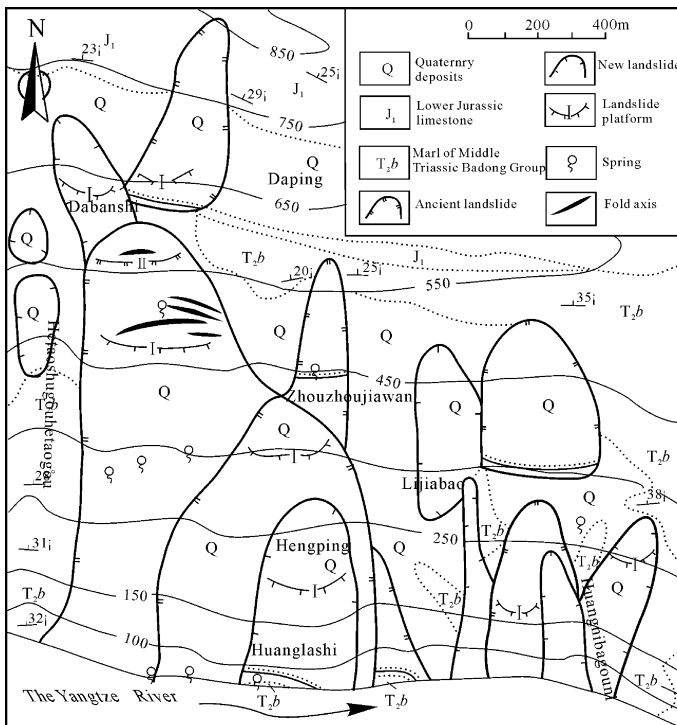

Fig. 21.2 A sketch map of the Huanglashi landslide trace pattern

Methodology

Fractal dimensions of an object are calculated by an algorithm called "box-counting", which includes many calculation methods, such as capacity, correlation, and information dimensions. In the method here used, a variety of smaller squares with a dimension of ξ was applied to cover the geometry of the landslide boundary as a line, and the number of pieces needed to cover the original square was then obtained as N (ξ). If a D-dimensional object was used in place of the line, a relationship of N (ξ) = $1/e^D$ was observed, where D is the box-counting dimension for a noninteger. As mentioned above, an expression can be written for the fractal dimension of the landslide boundary as follows:

$$D = -\lim_{\xi \to 0} \lg N(\xi)/\lg(\xi) \qquad (21.1)$$

By plotting a number of such pairs of $N(\xi)$ and ξ in a log-scale graph, a tangent value was obtained by a least-square fit, which was designated as a fractal dimension of the landslide boundary.

Results and Discussion

Fractal Dimensions of Landslides

As shown in Fig. 21.3, fractal dimensions of 11 landslides were obtained as a variety of tangent values by a least-square fit, after plotting a number of such pairs of $N(\xi)$ and ξ in a log-scale graph. It was seen that the Zhagnfangping landslide, the Huanglashi landslide and the Hongshibao landslide are greater than 1.40 fractal dimensions, while the Huangtupo landslide and the Zhaoshuling landslide have smaller fractal dimensions.

Relationship Between Fractal Dimensions and Slope Instability

Qualitative Analysis of the Relationship Between Landslide Boundary Traces and Slope Instability

Traditionally, geometrical data have played an important role in geotechnical modeling of slope instability. Differences in geometry of slopes will, to a great extent, influence the result of slope instability evaluations in three dimensions. Much attention was herein paid to three types of landslide boundary traces as shown in Fig. 21.4, of which fractal dimensions were used to evaluate slope instability.

In Fig. 21.4, traces A_1, A_2, and A_3 are at the same magnitude of fractal dimensions; however, they represent different progressive evolutions of slope failure. Trace A_1 indicates that a main scarp was not formed, and thus the slope does not
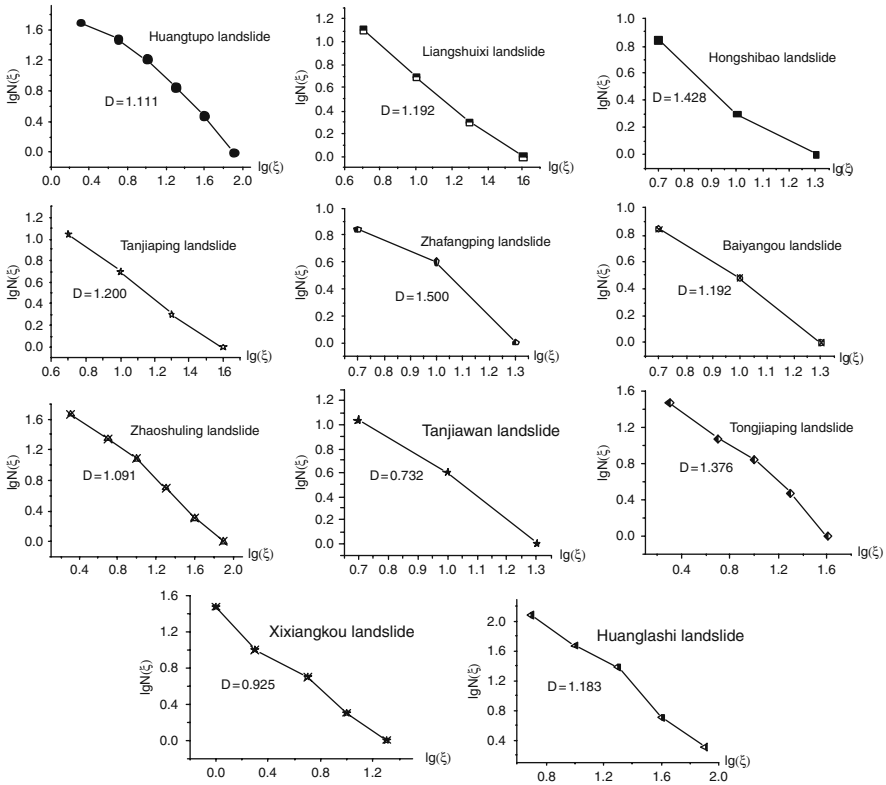
Fig. 21.3 Fractal dimensions of the boundary traces of major landslides

have potential to fail. The length of the boundary trace is smaller than or equal to the length of a discontinuous boundary. It was also found that the length of the boundary trace in type A_2 is greater than that of a discontinuous boundary. It is suggested that this kind of slope is more prone to failure than slopes with terrace A_1. If the boundary is progressively connected as shown in type A_3, it is concluded that the slope is unstable and that landslides will occur due to changes in external factors.

Traces B_1, B_2, and B_3 show that the rupture surfaces on the ground surface are connected after slope failure. Type B_1 of landslide boundary indicates that landslides are in a large area; thus it is in a stable state, while the slope in type B_2 is unstable but the area of displaced materials is huge. Slopes in type B_3 are in a small area, and have more potential to fail.

Landslide boundary traces of types C_1, C_2, and C_3 are more complicated than those mentioned previously. In this case, a continuous boundary is presented with various geometrical features. A landslide boundary of type C_1 is continuous, which indicates that this kind of landslide is relatively stable, compared with other landslides with boundary traces of types C_2 and C_3. In boundary traces of type C_2, it can be seen that a variety of small landslides occurred after the main landsliding.

Fig. 21.4 Visualization of landslide boundary traces
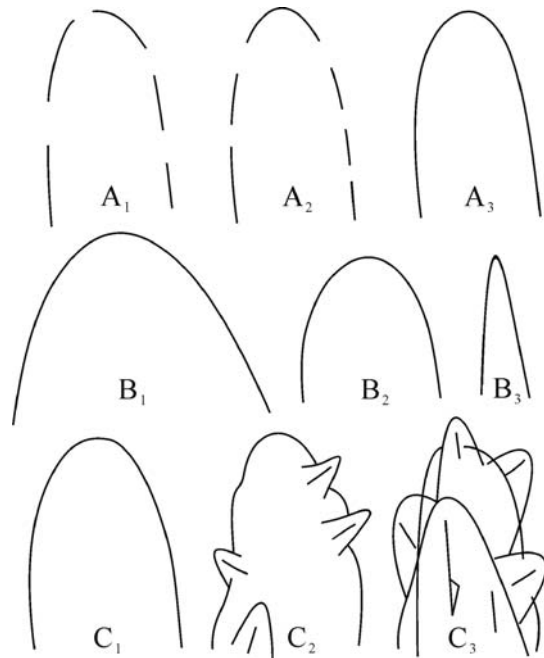
This kind of landslide is explained by a process of successive failure. Moreover, the boundary trace of type C_3 is the most complicated. This trace can be overlaid by the boundaries of smaller or secondary landslides. It thus suggests that landslides of type C_3 are more likely to reactivate.

From qualitative analyses mentioned above, it can be concluded that the boundary traces of landslides, to a great extent, are related to their instability. The boundary of a landslide results from successive extensions of the surface of rupture, and its trace becomes complicated. This type of landslide is prone to failure. It is worthwhile to note that only the geometry has been taken into account in slope instability analysis, while other environmental factors, such as geological conditions, slope types and structures, geotechnical aspects, hydrology and human activity, have been ignored.

Quantitative Description for Slope Instability Using Fractal Dimensions of Landslide Boundary Traces

A variety of landslides can be presented in different boundaries as shown in Fig. 21.4. Using fractal theory, fractal dimensions of landslide boundaries were calculated. In view of fractal dimensions, they are not the same as the familiar Euclidean dimensions, measured in discrete whole integers 1, 2, or 3, but are a different kind of quantity. Usually noninteger, a fractal dimension indicates the extent to which the fractal object fills the Euclidean dimension in which it is embedded.

For fractal dimensions of landslide boundary traces, their values in types A_1, A_2, and A_3 range from 0 to 1, while those in types C_1, C_2, and C_3 are between 1 and 2.

As shown in Fig. 21.3, the fractal dimensions of the Huanglashi landslide, the Zhafangping landslide, and the Hongshibao landslide range from 1.40 to 1.50, which are the largest of all the samples. For the Huanglashi landslide, the factor of safety (FS) is 1.0, which indicates that the landslide is in a critical equilibrium state (Li and Zhong 1993). From our fieldwork, various deformations were found in the Huanglashi slide mass, and it has the potential to fail again. In addition, a variety of slope failures of a small magnitude was likely to occur in the Zhafangping landslide and the Hongshibao landslide (Geological Survey Bureau of Yangtze Water Resource Commission 1994).

Values of FS were obtained using different simplified methods for the Tongjiaping landslide (Liu et al. 2002). The value of FS for its middle-lower segment was evaluated to be 1.1 by the simplified Janbu method, while the minimum FS was about 1.0 along a potential sliding surface, which suggested that the landslide was in a critical equilibrium stage. It was recorded that after intensive rainfall, slope failures occurred at the Tongjiaping site in the summer of 1998 (Liu et al. 2002). Our field investigation conducted in 2002 also identified various falls and slides in the sliding body after heavy rainfall. In view of a fractal dimension of 1.376, indications are that this landslide was stable. However, slope failures can occasionally occur in the case of a change of external factors, which coincides with the results from geotechnical modeling (Liu et al. 2002).

Values of fractal dimensions for the Huangtupo landslide and the Zhaoshuling landslide were about 1.0. It suggested that these landslides are stable, which can be verified by the results of using 3D finite-element methods (Tan et al. 1999; Tang et al. 2002).

Conclusions and Remarks

The patterns formed by fractal phenomena are a naturally occurring characteristic of landslides. This chapter addresses the relationship between landslide boundary traces and slope instability. In the process of landsliding, boundary shear surfaces extend progressively, and they are likely to be present in slope failures in a small area. After this extension of rupture surface onto the ground surface is completed, movement increases the volume of the material being displaced because the displaced material dilates. After landsliding, the geometry of the rupture surface thus provides information in evaluating slope instability. Correspondingly, fractal dimensions of the landslide can reach a maximum in view of boundary geometry. This indicates that the landslide is in a critically stable state. In the case of a change of external factors, it is likely to reactivate. In the vicinity of Badong County Town, fractal dimensions of 11 landslides were calculated using a box-counting method. Six landslides were chosen as a case study to distinguish the relationship between fractal dimensions of landslide boundaries and slope instability. Compared with

previous work in the calculations of FS, a landslide is potential to reactivate if its fractal dimensions are between 1.4 and 1.5, while a landslide is stable overall but small slope failures occasionally are likely to occur locally, if its value of fractal dimensions is 1.1–1.3. A value of fractal dimensions of 1 indicates that the landslide is in a stable state. To sum up, landslides with larger fractal dimensions were evaluated as being in an unstable state.

References

Bak P, Tang C, Wiesenfeld K (1988) Self-organized criticality. Physical Review A 11:364–374

Cai YJ, Guo QL, Yu YZ (2002) The reservoir-induced slope failure mechanism and prediction. Chinese Journal of Hubei Geology & Mineral Resources 16:4–8

Cruden DM, Varnes DJ (1996) Landslide types and processes. In: Turner, AK, Schuster RL (Eds.), Landslides Investigation and Mitigation. Transportation Research Board Special Report 247, National Research Council. National Academy Press: Washington DC, pp 36–75

Cui ZQ1 (1996) The main geological problem in the city of Badong county and its urgent countermeasures. Proceedings of International Symposium on Geological Environment of the Three Gorges Reservoir Area and Second Sino—Japan Strata Environment Mechanics. China Coal Industry Publishing House: Beijing, pp 15–22

Deng QL, Zhu ZY, Cui ZQ, Wang XP (2000) Mass rock creep and landsliding on the Huangtupo slope in the reservoir area of the Three Gorges Project, Yangtze River, China. Engineering Geology 58:67–83

Duncan JM (1996) State of the art: limit equilibrium and finite element analysis of slopes. Journal of Geotechnical Engineering 122:577–596

Geological Survey Bureau of Yangtze Water Resource Commission (1994). Report on the geological survey for the resettlement of Badong County Town in the Three Gorges Reservoir, unpublished

Guzzetti F, Malamud BD, Turcotte DL, Reichenbach P (2002) Power-law correlations of landslide areas in central Italy. Earth Planetary Science Letters 195:169–183

Li YS, Zhong YQ (Eds.) (1993) Large-scale landslides and rockfalls in the reservoir of Three Gorges project of Yangtze River. Guangdong Travel and Tourism Press: Guangzhou, China, pp 55–176

Liu B, Zeng QF, Yin ZL, Hu YJ (2002) The stability analysis and treatment study of Badong-Tongjiaping landslide. Chinese Journal of Hubei Geology & Mineral Resources 16:33–38

Liu CZ (1996) On some basic problems in evaluation of slope stability. Chinese Journal of Geological Hazard and Control 3:55–59

Nash D (1987) A comparative review of limit equilibrium methods of stability analysis. In: Anderson MG, Richards KS (Eds.), Slope Stability for Geotechnical Engineering and Geomorphology. John Wiley & Sons: New York, pp 11–75

Rouai M, Jaaidi EB (2003) Scaling properties of landslides in the Rif mountains of Morocco. Engineering Geology 68:353–359

Tan CX, Wang RJ (1999) Analysis on landslide stability by using three-dimensional numerical simulation. Chinese Journal of Changchun University of Science and Technology 29:267–271

Tang HM, Ma SZ, Liu YR, Jia HB (2002) Stability and control measures of Zhaoshuling landslide, Badong County, Three Gorges Reservoir. Chinese Journal of Earth Science 27:621–625

Turcotte DL, Malamud BD (2004) Landslides, forest fires, and earthquakes: examples of self-organized critical behavior. Physica. A, Statistical Mechanics and its Applications 340: 580–589

Wu SR, Shi L, Tan CX, Hu DG, Mei YT, Xu RC (2002a) Fractal analyses of the Huanglashi and Huangtupo landslides in the Three Gorges, Yangtze River China. Chinese Journal of Earth Science 25:61–65

Wu YF, Shi L, Wu MY, Huang SH (2002b) Questions in stability factor on control of large scale landslides of the Three Gorges Reservoir region. Chinese Journal of Hubei Geology & Mineral Resources 16:87–91

Yin TZ, Wu FQ, Yin KL (1989) Static and dynamic regularity of landslides and space-time prognosis of slope instability. Chinese Journal of Earth Science 2:119–133

Zhong YQ (1995) Study of prediction method by synthetic information for Huanglashi landslide. Chinese Journal of Geological Hazard and Control 4:68–80

Zhou PG, Ou ZD (1997) Stability estimation of the different types of gentle slope in the reservoir area of Three Gorge Project. Chinese Journal of Geological Hazard and Control 2:24–32

Chapter 22
Uncertainty Evaluation of the Stability of the Huanglashi Landslide in the Three Gorges of the Yangtze River

Huiming Bao, Xuan Mo, Wencheng Yu, Wei You, and Xiaohui Kang

Abstract This chapter evaluates the stability of the Huanglashi landslide in the Three Gorges of the Yangtze River. By means of the uncertainty evaluation model for the Huanglashi landslide, this chapter calculates and evaluates the stability of the landslide at present and after water storage, and then analyzes the stability after the completion of the Three Gorges project. The stability analysis can be used for predicting the stability tendency and the prevention of future disasters.

Keywords Huanglashi landslide · Uncertainty · Stability · Probability

Introduction

A large number of geological disasters have developed in the Three Gorges reservoir region of Yangtze River, particularly the landslides that are threatening the stability of the Three Gorges project and will be more dangerous after the water storage operations (Wang 1999).

The Huanglashi landslide is located on the north bank of the Yangtze River, which is 2 km to the east of Badong county town and 66 km upstream from the Three Gorges dam. It is ranked as one of the three most dangerous landslides in the Three Gorges reservoir region because of its large scale, reactivation, and the short distance from the Three Gorges dam (Bao 1993).

A number of parameters for stability evaluation of landslides including cohesion, friction angle, underground water table, bulk density, and so on are random and uncertain. The landslide stability evaluation is affected by many factors, and it is referred to as a probability process. The traditional mathematical and mechanical models for calculating landslide stability cannot work without certain parameters, so the above factors need to be comprehensively analyzed and evaluated while

H. Bao (✉)
Department of Civil Engineering, Guilin University of Technology, Guilin 541004, Guangxi, China
e-mail: bhm@glite.edu.cn

evaluating the landslide stability. Given the random and test error of parameters, the heterogeneity of the geological body, the random and fuzzy effect for the land-slide exterior factors, it is difficult to quantify the effects of these factors on land-slides, hence the method of uncertain analysis is used in the landslide evaluation (Wang et al. 2007).

Characters and Geological Environment of the Huanglashi Landslide

General Characters of the Landslide

The Huanglashi landslide is a landslide group distributing from the east to the west between Lijiabao and Benlongxi, and forming a longitudinal extended concave for-mation. The back margin of the main scarp is at 836 m asl, the frontal margin at the toe is at 66 m asl where it is under the reservoir of the Yangtze River. The landslide is 260 m wide at the top, 820 m wide where it is close to the river, and 1,500 m long, covering an area of 1.15 km^2. The thickness is 8–100 m and the total volume is about 22.8 million m^3. Based on the origin, failure mechanism, shape and material composition, the landslides group is divided into the Hengping tangential landslide, Dashiban and Taizijiao colluvium landslides (Figs. 22.1, 22.2, and 22.3) (Bao 1993).

Character of the Hengping Landslide

As a bedrock tangential landslide, the Hengping landslide forms a circular chair-shaped landform. The back margin is at 490 m asl and 300–620 m wide, the frontal

Fig. 22.1 Full view of the Huanglashi landslide
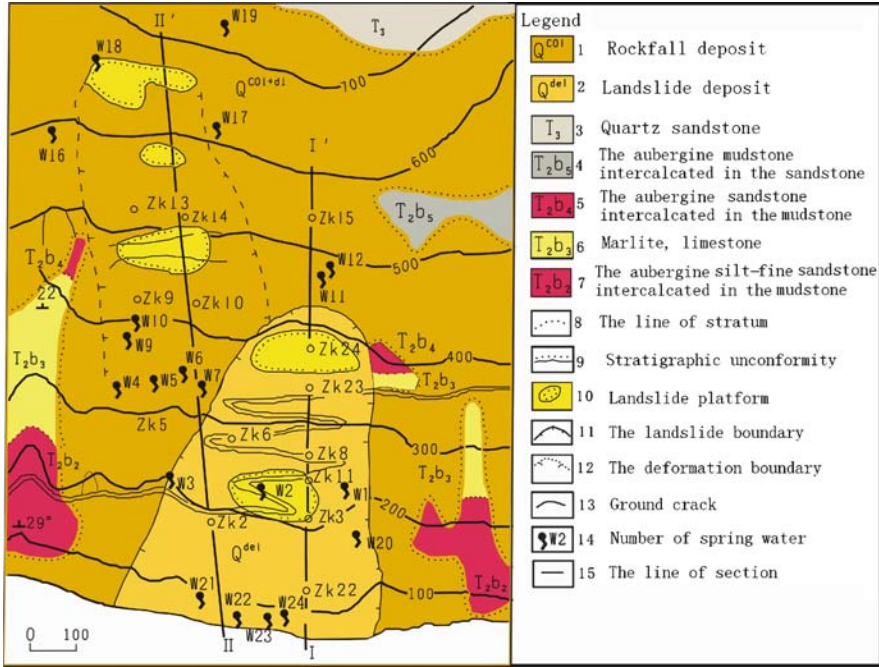
Fig. 22.2 The geological map of the Huanglashi landslide
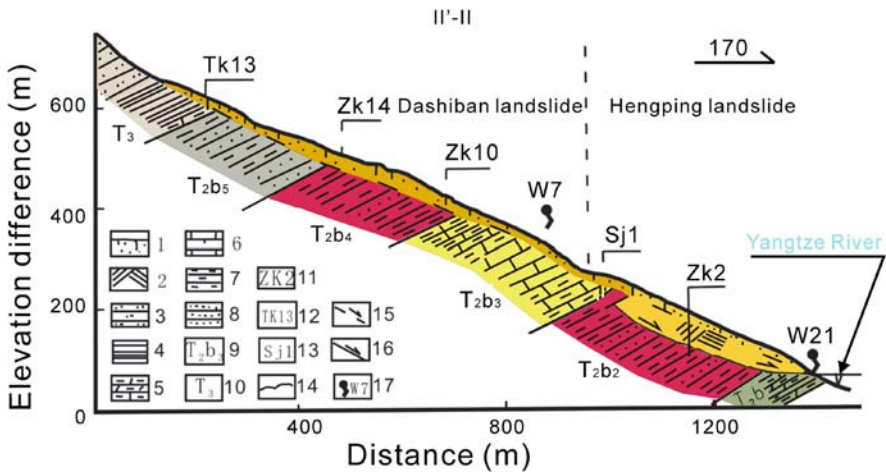
Fig. 22.3 Geological cross section of the Huanglashi landslide. 1 – gravelly soil; 2 – cataclasite by landslide; 3 – gray white quartz sandstone; 4 – gray shale; 5 – marlite; 6 – marlite and limestone; 7 – aubergine mudstone; 8 – aubergine silt and fine sandstone; 9 – code of Badong group stratum; 10 – code of Xiangxi group stratum; 11 – number of drilling; 12 – number of open test pit; 13 – number of shaft; 14 – ground crack; 15 – speculate sliding surface; 16 – sliding surface; 17 – number of spring water

margin is at 65–70 m asl. The landslide is 1,700 m long, covering an area of 0.3 km^2. The volume totals about 17 million m^3. The landslide body consists of block, detritus, and clay, forming a soil–rock mixture type of structure. The upper stratum is a loose accumulation without stratigraphic succession, while the lower stratum is mainly cataclastic rock with clear stratigraphic succession, the outcropping part being lower than the surrounding normal rock. The strength of the sliding zone composed of purplish red detritus and clay is characterized as follows: c =0.01– 0.37 MPa, φ=25–35°.

Character of the Dashiban Landslide

The landslide is 700 m long in direction S–N and 250–350 m wide with the back margin at about 800 m asl, covering an area of 0.22 km^2. The volume totals about 4 million m^3 (Fig. 22.3). It is divided into three steps at different elevations (Fig. 22.2).

The upper part of the landslide body consists of yellow gray block, detritus, and clay. The primary composition of detritus is quartzose sandstone; the lower part consists of purplish red clay and detritus mainly composed of siltstone, shale, and marl. The strength of the sliding zone is denoted as such: c=0–5 kPa, φ=23–29.5° (Yang et al. 1991).

Character of the Taizijiao Landslide

The back margin is connected to the frontal margin of the Dashiban landslide and the frontal margin is beneath the water level of the reservoir. The landslide is 560 m long in the longitudinal direction, 180 m wide in the latitudinal direction, and 10–25 m thick, with an area of 0.1 km^2 and a total volume of 1.8 million m^3. The landslide body mainly consists of purplish red siltstone, gray green marl, and clay. The strength of the sliding zone soil is characterized as follows: c=25–51 kPa, φ=19.8–31.8° (Yang et al. 1991).

Geological and Environmental Characters

The Huanglashi landslide is located in the mountain valley area of western Hubei Province, where the Yangtze River strikes SE 100°. The valley top is at 800–850 m asl and the river bottom is at 20–50 m asl, with a difference in elevation of 750–800 m. The landslide is a longitudinal valley reversed slope. In this location, the Yangtze River before dam construction is 200–250 m wide during the low-water period. The highest flood water level is at 112.5 m and the lowest water level is at 54.77 m. In the landslide area, Benlongxi lies in the west and Lijiagou lies in the east; a number of gullies develop including five evident gullies that are 10–20 m deep.

The bedrock consists of the Badong formation, Xiangxi group of Medium Triassic period, and Quaternary Period sediment. The Badong formation is divided into four units:

(1) T_2b^1 – gray green calcareous and argillaceous shale, thin-bedded limestone and marl, 69 m thick;
(2) T_2b^2 – siltstone lenticular intercalcated in the purplish red shale, 257 m thick;
(3) T_2b^3 – gray yellow and gray green thin-bedded limestone containing mud, gray medium-bedded limestone, 245 m thick;
(4) T_2b^4 – the upper is shale intercalcated in the purplish red siltstone, the lower is calcareous siltstone intercalcated in the purplish shale, 364 m thick.

The Xiangxi group (T_3–J_1) appears on the top and back margin of the landslide with a thickness of 400 m. The upper stratum is gray thick-bedded quartzose sand stone, the lower stratum is gray black carbon limestone, medium-bedded limestone, and lime shale containing a coal seam.

Quaternary Period sediment is divided into colluvium (co1-d1q) and the accumulation (de1Q) is composed of detritus and clay, 10–87 m thick generally with a maximum thickness of 102 m.

The east–west Shazhenxi-Baifuping anticline is to the south of the landslide area with the Zigui and Guandukou synclines to the east and west, respectively. The bedrock strikes 265–280°, dips 355–10° with a slope of 25–35°.

Four joint sets have been recognized: trending E–W with a southerly dip of 65–85°; trending NE–SW with a southeasterly dip of 40–80°; trending NW–SE with a northeasterly dip of 55–88°; and trending N–S with an easterly dip of 50–80°.

The landslide lies at the edge of the rainstorm area of western Hubei Province with an average annual precipitation of 1,100 mm, a maximum annual precipitation of 1,522 mm (1952 and 1983, respectively) and a maximum daily precipitation of 193.3 mm (July 5, 1962). The rainy season is from May to September when 70% of annual rainfall occurs.

The pore water in colluvium, accumulation, and heavily weathered strata dominates in the landslide area, except for the karst fissure water in T_2b^3 stratum. Five groups of spring appear at 65–80, 200–215, 330–350, 450–480, and 600–700 m asl, with a maximum discharge of more than 400 dm^3/min. These springs have a long-term effect of softening and argillation on the sliding zone that is the waterproof stratum, decreasing the greatly, the stability of landslide.

Deformation and Failure Mechanism of the Landslide

Huanglashi landslide develops on a reversed slope of longitudinal valley composed of Badong formation that is a combination of soft and hard strata but is soft primarily. The purplish red siltstone and marl with low strength is helpful to the

development of landslides. The characteristics of the landslide depend on the high-strength gray medium- and thick-bedded limestone distributing in the middle.

The Hengping Landslide

After the river began undermining in a concave formation the slope foot became free and the slope rockmass deformed under the influence of gravity. Subsequently, tension cracks developed and expanded with the original structural joints and unloaded the cracks, gradually causing deformation and a tracing slip plane. The slope will be in the state of limiting equilibrium once the tracing sliding plane is formed ultimately, and will slide emergently along the plane if induced by rainstorm and other factors.

Hence the way of failure is defined as bend–tension crack–failure along the tracing slip plane.

The Dashiban Landslide

Colluvium crept along the bedrock plane, bending the underlying bedrock. Following that, the consequent structure was formed on the slope surface, which is conducive to creep. The stress concentration surged at the slope foot and shoulder due to the cumulative effect of slope deformation. As a result, the tension failure occurred where the tension strength was low, reflected by the occurrence of a tension crack at about 560 m asl in 1975. In July 1983, induced by the heavy rain, the tension cracks appeared where the stress concentrated with part of the cracks penetrating the landslide and the cracks at both sides arranging like feathers, and a small slump occurred at the frontal margin. In recent years, the cracks at the back margin of the top platform evidently deformed and the center of the slope became depressed, indicating that the deformation is more serious.

The potential slip plane, composed of the tension section on the top, the locked section in the middle, and the creeping section at the slope foot, has been formed in the landslide at present. If the locked section fails, the landslide will fail emergently. Hence the way of failure is defined as creep–tension crack–shear.

Taizijiao Landslide

Colluvium crept along the bedrock plane, bending the underlying soft mudstone and sandstone. Following that, the consequent structure was formed on the slope surface, which is conducive for water to permeate and accelerate the softening and argillation, until the slip plane is formed and a landslide occurs.

Hence the way of failure is defined as creep–shear.

Uncertainty Analysis on the Stability of the Huanglashi Landslide

At present the evaluation of the stability and development is primarily based on the factor of safety. However, the factor of safety just indicates the stability compared with the average value, as it is common that the slope with high factor of safety fails but the slope with low factor of safety remains stable. Hence this chapter evaluates the stability of Huanglashi landslide using the method of combining the factor of safety and failure probability.

Uncertainty Analysis on the Stability of the Hengping Landslide

Determination of Safety Coefficient

Based on the character of landslides and the geological model of failure, this chapter calculates the factor of safety with the method of transitive coefficient. The section is given in Fig. 22.4, and the parameters are indicated by laboratory tests and engineering analogy as follows: $c=50$ kPa, $\phi=22°$, $\gamma=22.6$ kN/m^3, and the others are given in Tables 22.1 and 22.2. With the pool level at a normal level, 99.59 m (the highest flood level historically), 150 and 175 m, the factor of safety is 1.036, 1.003, 0.935, and 0.913, respectively.

Uncertainty Analysis of the Hengping Landslide

The factors affecting the stability of the landslide include c, φ, R, h, etc. The factor of safety (K) is defined as follows:

$$K = G(c, \varphi, R, h, \ldots)$$

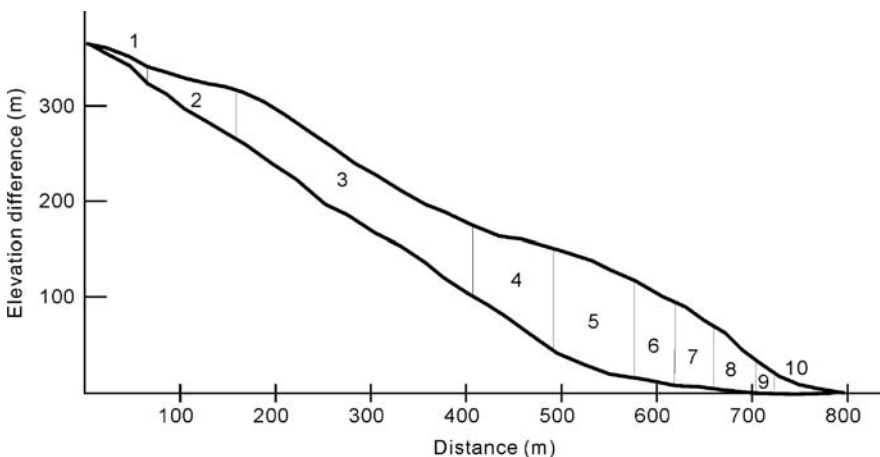**Fig. 22.4**   Section of the Hengping landslide used in calculation

Table 22.1 Shearing strength of the Hengping landslide

			Shearing strength			
			Peak value		Residual value	
	Natural water	Natural bulk	cp	p	cr	r
Name of soil	content (%)	density (g/cm^3)	(kPa)	(°)	(kPa)	(°)
Purplish red gravel soil	11.3	2.21	52	24°	30	21°
Yellow clay loam	15.2	2.19	40	21°30′	28	20°
Purplish red gravel soil	13.2	2.08	42	22°	35	20°30′

Table 22.2 Calculating date of the Hengping landslide

	1	2	3	4	5	6	7	8	9	10	11
YT (m)	348	326	304	170	149	118	96	72	38	20	8
YB (m)	348	316	358	97	49	19	9	4	3	4	8
YW (m)	348	316	258	97	49	20	10	7	6	6	6
L (m)	50	90	240	80	80	40	40	40	20	32	–

where the parameters acquired by survey and test are random variables as well as K. Assuming the density function of random variables is f(K), the failure probability (Pf) of landslide is given by

$$Pf(K < 1) = \int_0^1 f(f)dK$$

Monte Carlo simulation method, which could acquire the parameters without a large number of sampling tests, is used to calculate the failure probability in three steps:

(1) Determine the distribution of random variables

With the level under the slip plane, the underground water table is excluded as well as the bulk density slightly affecting the slope stability. Just two variables, C and φ, are included in the calculation. The values of C and φ of the soil at sliding zone distribute normally.

(2) Sample the random variables of normal distribution with the equation given by Naylor et al. (1966) as follows:

$$X = (\text{Var}[x])^{\frac{1}{2}} \left(\sum_{i=1}^{12} Ri - 6.0 \right) + E(x)$$

where Var[x] is the variance of samples; $E(x)$ is the mean value of samples; R(i) is random numbers of interval.

Substitute the equation $(\text{Var}[x])^{\frac{1}{2}} = V \times E(x)$ into the above equation to obtain

$$X = \left[1 + V\left(\sum_{i=1}^{12} Ri - 6.0\right)\right] E(x)$$

where V is the deviation coefficient.

The deviation coefficients of c and φ are 0.4 and 0.2, respectively, according to the study of Bao (1988):

$$C = \left[1 + 0.4 \times \left(\sum_{i=1}^{12} Ri - 6\right)\right] \times 50$$

$$\phi = \left[1 + 0.2 \times \left(\sum_{i=1}^{12} Ri - 6\right)\right] \times 22$$

(3) Calculate the failure probability

Substitute the value of random samples into the expression $K=G$ (c, φ, R, h,...) to obtain enough value of K. Then calculate the distribution of K and obtain Pf. If the number of sampling is limited in practice, divide the number that $K<1$ by the total number of samples to calculate the failure probability.

The failure probability is 50%, a medium probability according to the classification given by Bao (1988).

Preliminary Elevation of the Stability of the Hengping Landslide

The factor of safety of the Hengping landslide is 1.036 with a medium failure probability of 50%, indicating that the landslide is still stable.

After the water storage of the Three Gorges reservoir and the pool level rises to 175 m asl, the factor of safety decreases to 0.913, and failure is possible.

Analysis of the Stability of the Dashiban Landslide

Character of Deformation Development

The deformation has been developing since July 1983 when a large number of tension cracks occurred. New tension cracks with a strike of N75°W and a width of 0.5–2 cm appeared at 650 m asl after the rainfall season in 1987. The cracks in the middle also changed, but the cracks at 380 m asl did not change, according to the monitoring data over a year.

Hence the landslide has been evaluated as having an accelerating deformation.

The Probable Location of Shear Outlets

The probable location of shear outlets, while it fails at 330–350 m asl and strikes SSE, has a serious effect on the stability of Hengping landslide.

Analysis on the Stability of the Dashiban Landslide

This chapter calculates the stability of the Dashiban landslide based on the estimated location of shear outlets, the primary section and the long-term strength of bedrock contact zone. The factor of safety is 1.003 with a failure probability of 80%, indicating the landslide has been in the state of limiting equilibrium.

The Effect of the Dashiban Landslide Failure on the Hengping Landslide

If the Dashiban landslide fails in the estimated way, most of the west part of the Hengping landslide will be involved, primarily by the loading and impact of high potential energy.

According to the analysis of static load, the Hengping landslide will be in the state of limiting equilibrium if 5% volume of the Dashiban landslide is involved, and the factor of safety decreases, evidently as the load rises. Given the dynamic load and impact of high potential energy, the stability will decrease further. Hence it is possible for the Hengping landslide to react as soon as the Dashiban landslide fails.

Analysis on the Stability of the Taizijiao Landslide

There is no crack on the ground of the Taizijiao landslide with little slumping, and no reactivity according to indications from the monitoring of ground deformation. However, it is possible for the Taizijiao landslide to react due to the failure of the Dashiban landslide.

Conclusions

(1) The Huanglashi landslide is still safe currently and has different stability between the upper and lower parts. The factor of safety of the upper landslide is low with a high failure probability while the stability of the Hengping and the Taizijiao landslides is higher with a medium failure probability. Generally speaking, the Huanglashi landslide is potentially unstable.
(2) The overall stability development mainly depends on the development of the Dashiban landslide.
(3) The way the Huanglashi landslide begins to fail is that the Dashiban landslide starts initially, causing the Hengping and the Taizijiao landslides to fail.
(4) The possibility that the Hengping landslide fails will rise after the water storage operations of the Three Gorges reservoir.

References

Bao HM (1993) Stability evaluation of Huanglashi landslide in Three Gorges region of Yangtze River. Journal of Guilin College of Geology 13(3):258–264

Bao HM (1988) Geological Model and Stability Analysis of Huanglashi Landslide in Three Gorges Region of Yangtze River. Master Thesis of Changchun College of Geology

Naylor TH, Balintfy JL, Burdick DS, Chu K (1966) Computer Simulation Techniques. New York, Wiley.

Wang L, Deng QL, Li DY, Yang HJ (2007) Appraisal on landslide stability by probability analysis method. Safety and Environmental Engineering 14(2):1–3

Wang SQ (1999) The monitoring and prediction of the slope in the three gorges region of Yangtze River. Geological Publishing House, Beijing, 1 pp (in Chinese)

Yang TM, Yan YZ, Sun YZ, Xu FX (1991) Analysis of stability deformation characteristic of Huanglashi landslide. The Chinese Journal of Geological Hazard and Control 2(3): 31–41 (in Chinese)

Chapter 23
Recognition of Lithology and Its Use in Identification of Landslide-Prone Areas Using Remote Sensing Data

Zhongping Zeng and Huabin Wang

Abstract   Remote sensing data provide not only information about landslide characteristics, such as landslide locations, scarp shapes, but also the related environmental factors, such as lithology, tectonic structure and land cover, which have significance for landslide occurrence. This chapter aims to use remotely sensed data to extract lithology information, and to relate this to landslide incidence. A variety of digital image techniques were applied to remote sensing data, and several image lithostratigraphy units were delineated by the identification elements such as weathering manifestations, drainage patterns, weathering, erosion characteristics, and surface morphology. Landslide location was identified by image interpretation and from field survey data. Other landslide-related factors, such as altitude and slope, were derived from digital elevation models. A method of generalized likelihood ratio was then utilized to analyze the relationships between landslide occurrence and lithology factors. Based on these data, causal factors, contributing to landslide occurrence, have been combined into a binary logistic regression model, and landslide probabilities are then calculated cell by cell. The results state that the rate of regression model classification has successfully increased from 71.5 to 92.6% of the overall slopes after "lithostratigraphical unit" variable was added. The study shows that remote sensing data can provide a quantitative causative factor source for landslide hazard assessment.

Keywords   Recognition of lithology · Remote sensing · Landslide · Hazard zonation Binary · logistic regression model

Introduction

Landslides are one of the most destructive natural phenomena, which cause damage to both property and life every year, particularly in the developing countries, where the economic loss due to the impact of natural hazards often makes

Z. Zeng (✉)

College of Public Administration, HuaZhong University of Science and Technology, Wuhan 430074 P. R. China

e-mail: z.p.zeng@tom.com

the difference between economic growth and stagnation (Fournier d'Albe 1976; Swiss Reinsurance Company 1990; Van Western 2000). From July to September 2007, it is estimated that about 21,602 geological hazards have occurred in China except Beijing, Tianjin, and Shanghai. Geological hazards included landslides, rockfalls, mud and rock flows, ground collapses, ground fissures and land subsidence, among them there were 12,880 landslides, resulting in 358 deaths, 142 injured, and 66 missing, with up to 0.238 billion dollars of direct economic losses (http://www.cigem.gov.cn/ReadNews.asp?NewsID=12977). Therefore, it is essential to carry out studies to identify landslide-prone areas for landslide hazard mitigation. Landslide hazard zoning, being one of the effective landslide management methods, has been widely accepted by geoscientists, engineering professionals, local communities, and all levels of government in many parts of the world (Aleotti and Chowdhury 1999; Guzzetti et al. 1999).

A landslide hazard mapping method consists of two different aspects: assessing the susceptibility of the terrain for slope failure and then determining the probability of a specific triggering event occurring. Traditionally, landslide hazard assessment was laborious and time-consuming because of the time and effort required for field surveys, especially over large areas. Remote sensing technology, which allows a rapid acquisition of quantitative data over wide areas at low cost and high accuracy, has drawn greater attention from geoscientists and engineering professional in recent years (Van Westen and Getahun 2003; Metternicht et al. 2005; Cheng et al. 2004). Aerial photography and high spatial resolution satellite images have been used extensively to characterize landslides and assist in landslide inventory and hazard mapping programs (Saha et al. 2005; Nichol et al. 2006). Remote sensing data provide not only information about landslides characteristics, such as landslides location and scarp shapes, but also the environmental factors, such as soil and rock material, linear tectonic structure, land cover, etc. From a single, high-resolution satellite image in digital format, together with multi-spectral information, a range of ground surface features related to landslide occurrence can be identified, classified, and mapped directly. Remote sensing data and techniques can play a more important role in information extraction of landslide causative factors. In the Three Gorge areas, landslides are associated with certain kinds of lithological units composed of certain soil and rock material (Qiao et al. 2004). This chapter provides examples of the capability of remote sensing fusion techniques for extracting lithological information and relating this to landslide incidence.

The Study Area

The study area selected is located at the watershed of the Longchuangou River in Badong City of Hubei Province, China, which is about 60 km west of the Three Gorges Dam, on the Yangtze River (Fig. 23.1). The lithotectonic setting and the regional geographical map of the area show that the main geological unit is characterized as unconsolidated materials, sandstone, marls and is predominated by limestone formed during the Triassic Period. In field investigations, a total of 23 landslides were identified around the basin (Fig. 23.2). These landslides are
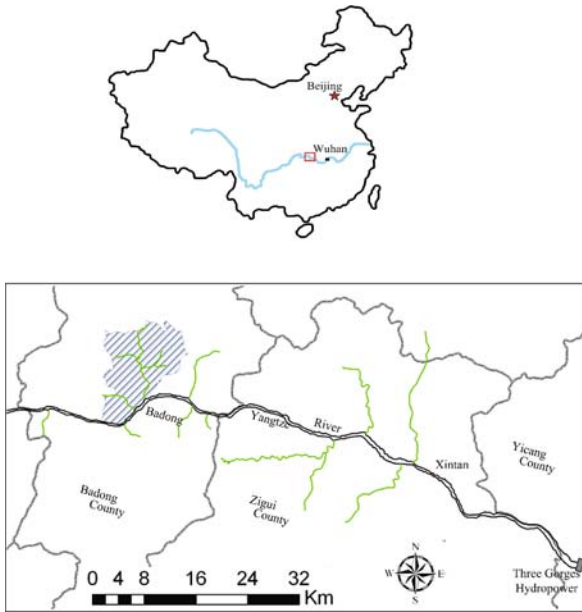
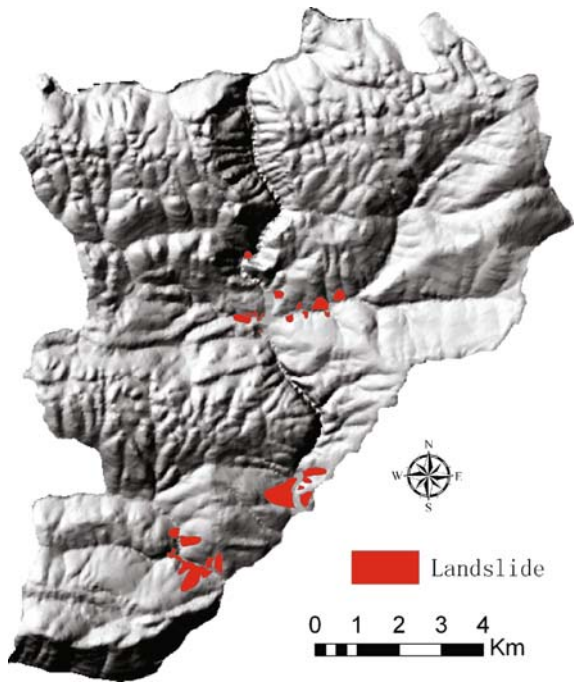**Fig. 23.1** Location of the study area

Fig. 23.2 Landslide inventory map of the study area

differentiated according to the kind of soil and rock material, and topographic settings. Along the Longchuangou River, landslides occur mainly in unconsolidated materials such as massive Quaternary loose units and sandstone or marl with intercalated clays, especially in the stratum unit named Badong Group sandstone sediments. That means that landslides occur where the lithology is a factor. Lithological unit is one of the most important causative factors of landslide activity.

Recognition of Lithology Using Remote Sensing Data

Preparation of Remote Sensing Data

Multi-spectral LandSat ETM+ images were used in this study. The acquisition date was on January 2002. The image, consisting of four visible bands (Band 1–4), one near infrared (NIR) (Band 5), one infrared (Band 7) with 30 m spatial resolution, and one panchromatic band with 15 m spatial resolution, was preprocessed by radiation correction, geometry rectification, and image registration before further processing. A shape file for the border of the study area was also created, and was then used to subset or clip the image.

A variety of image processing methods, such as histogram equalization and image data fusion have been performed in order to increase the quality of the resulting information. Image data fusion can be defined as "the combination of two or more different images to form a new image" (Van Genderen and Pohl 1994). Most image fusion methods combine complementary image data at the pixel level and can be grouped into the categories of color-related techniques and numerical/statistical techniques (Duggin and Pught 2005). In this chapter, principal components analysis (PCA) statistical transformation method was applied to merge the multi-spectral images (band 5–4–3) with the panchromatic image (band 8) of ETM+ sensor (Fig. 23.3). Compared to the red–green–blue (RGB) false-color image stacked by band 5–4–3 images, the fusion image had higher space resolution and provided more valuable information about lithological units and land cover. The higher enhanced texture information in the merged image enabled us to determine different types of sedimentary rock more exactly.

Interpretation of Lithology Units Using Remote Sensing Images

Traditionally, lithology and its spatial relationships can be distinguished by geological mapping or by field investigations, which is usually laborious and time-consuming over an extensive area. Remote sensing data record the electromagnetic energy reflected from, or emitted by earth's surface. Such images are very useful to sense the properties of objects on the earth surface, including exposed lithology. For instance, visible or near-infrared data provide texture features as well as spectral features, while interferometric synthetic aperture radar (SAR) data contribute

**Fig. 23.3** The merged images of the study area
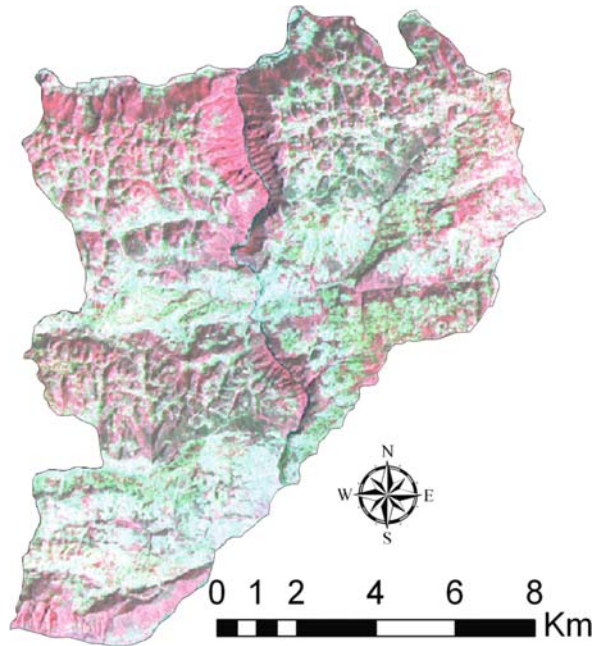
much to rock texture or surface roughness information. Multiple data sources can be integrated to provide a comprehensive view of the lithostratigraphy.

In terms of remote sensing geological interpretation principles and lithological information is always identified by the color, weathering and erosion characteristics (whether the rock is resistant or recessive), drainage patterns, and thickness of bedding. However, in the temperate and tropical region, such interpretation procedures may be problematic because dense forest covers much of the landscape, which may restrict interpretation of lithology or rock features. Fortunately, we can still use remote sensing data to infer underlying rock materials by drainage and vegetation patterns. This concept is called as geobotany (Rose et al. 1979). The underlying principle is that the sedimentary constituents of the bedrock may control or influence the condition of vegetation or drainages. In addition, identification elements such as weathering manifestations, weathering and erosion characteristics, and surface morphology may be apparent on high- or medium-resolution imagery and air-photos, even if the area of interest is covered by high-density forest.

The study area is predominantly covered by these types of rock, e.g., limestone, which is resistant to erosion, sandstone, and unconsolidated materials, which are more likely to be eroded. These two types of rock show different feature characteristics of texture, differential weathering, and surface morphology in the merged satellite image. The former is blocked with steep hummocky topography, while the latter is smooth with gently undulating terrain. Furthermore, field observations show

Fig. 23.4 Lithostratigraphy
interpretation results from the
merged image
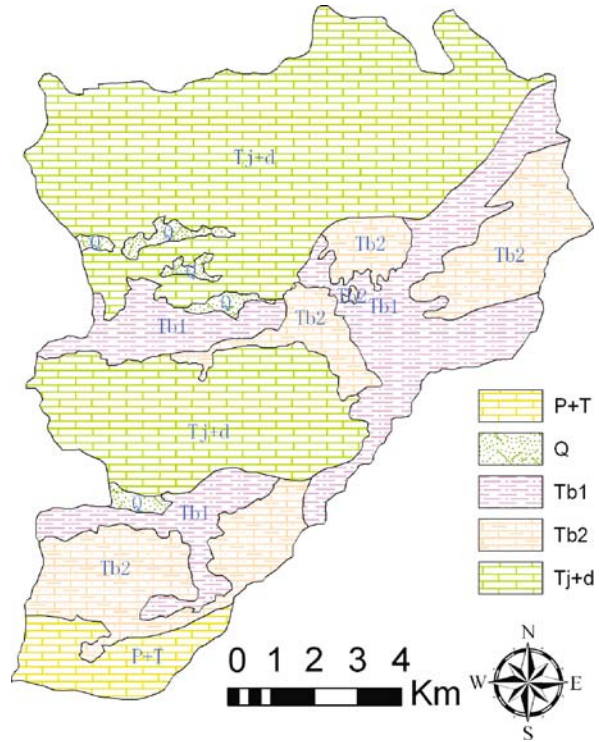
that the limestone rock is covered with thin soils which are suitable for shrubs or
trees, giving an advantage for lithostratigraphic interpretation.

Five "image lithostratigraphic" units consisting of carbonate rock strata units,
sandstone strata units, and unconsolidated units, were delineated according to their
spectral reflectance signatures, the structure of the bedding planes, and the surface
morphology (Fig. 23.4). In order to validate the interpretation results, a map of
the lithological units derived from field survey was digitized using geographical
information system (GIS) tools. The map comparison states that the "image lithos-
tratigraphic" units from images were well coincident with the stratigraphic map,
confirmed by field surveys.

Analysis of the Lithostratigraphic Factor in Landslide Hazard Zonation

Logistic regression modeling has proved to be useful in examining the relation-
ship between a set of independent variables and a dependent variable that uses
only two dichotomous values, here representing the presence or absence of land-
slides (Dai and Lee 2003; Lee 2004; Ayalew and Yamagishi 2005). Quantitatively,

if P is the estimated probability of landslide occurring, the relationship between the occurrence and its dependency on several variables can be expressed as follows:

$$P = \frac{1}{(1 + e^{-z})} \tag{23.1}$$

The probability varies from 0 to 1 on an S-shaped curve, and Z is the linear combination. It follows that logistic regression involves fitting an equation of the following form to data:

$$Z = b_0 + b_1 x_1 + b_2 x_2 + \cdots + b_n x_n \tag{23.2}$$

where b_0 is the intercept of the model, b_i $(i = 0,1,2, \ldots, n)$ is slope coefficients of the logistic regression model, and x_i $(i = 0, 1, 2, \ldots, n)$ are independent variables. The linear model formed is then a logistic regression of presence or absence of landslides (present conditions) on the independent variables (pre-failure conditions).

Several different options, such as stepwise regression and backward stepwise regression, are available during logistic regression model creation. In the stepwise regression process, variables can be entered into the model in the order specified by the researcher, and the logistic regression can test the fitness of the model after each coefficient is added or deleted. In the backward stepwise process, the analysis always begins with a full or saturated model and variables are eliminated from the model in an iterative process. The backward stepwise regression appears to be a preferred method of exploratory analyses because the fitness of the model can be tested immediately after the elimination of each variable. Therefore, using the backward stepwise process, the logistic regression model can also provide the valuable information on the relation between the possibility of landslide occurrence and influencing factors.

The likelihood ratio (LR) changes can be used for variable inclusion or elimination when a logistic regression model is created (David and Lemeshow 1989). The LR statistic is defined as two times the log of the ratio of the likelihood functions of two models evaluated at their maximum likelihood estimates (MLE). The MLE uses the ratio of the maximized value of the likelihood function for the full model (L_1) over the maximized value of the likelihood function for the simpler or the reduced model (L_0). One can compute a chi-squared statistic, χ^2. to represent deviance for this comparison as follows (Dai and Lee 2003):

$$\chi^2 = -2[\log(L_0) - \log(L_1)]$$

The value of adding parameter to a logistic model can be tested by subtracting the deviance of the model with the new parameter from the deviance of the model without the new parameter, this difference is then tested against a chi-square distribution with degrees of freedom equal to the difference between the degrees of freedom of the old and new models. Generally, a larger value of $-2 \log(L_0/L_1)$ indicates a poor fit of the model.

In the study area, landslides occur where lithological or morphological conditions are conducive to their occurrence. In order to analyze the incorporative interactions after the lithological factors were included in a logistic regression model, two morphological condition factors, slope angle and elevation, were considered. A series of 1:50,000-scale topographical maps were digitized to create a DEM at a spatial resolution of 25 m. The model was constructed by an iterative maximum likelihood procedure and the backward stepwise method was adopted.

The change of estimated MLEs for the model with or without the lithostratigraphic unit variables was calculated. When slope and image lithostratigraphic units were considered, the LR statistic in the model was 3245.758. Adding the lithostratigraphic unit variables produced a decrease of 724.568. The result showed that lithostratigraphic units did improve goodness of fit to the model.

A classification table, which provides a mechanism for classifying new cases based on previously existing data, is another kind of statistics in logistic regression analysis. The table shows the observed versus predicted responses. The results of classification for both full model and reduced model are presented in Table 23.1. Clearly, the overall success rate classification has improved from 71.5 to 92.6% after the lithostratigraphic unit variable was included.

Table 23.1 Classification table showing the comparison between the full regression model and the reduced regression model

Observed	Reduced model prediction			Full model prediction		
	1/0		Percentage	1/0		Percentage
	0	1	correct	0	1	correct
	2,457	1,505	62	3,645	317	92.0
	470	2007	81.0	160	2,317	93.5
Overall percentage		71.5			92.6	

A landslide susceptibility map was made using three kinds of factors as follows: slope angle, elevation, and lithostratigraphic unit (Fig. 23.5). The result shows that almost all known landslides correspond well with a "high" area in the hazard map.

Results and Discussions

Aerial photographs, satellite images, and radar images have been a primary data resource for landslide hazard zonation since the mid-1970s of the 20th century. Not only can remote sensing technology enable us to map a landslide with varying forms and spectral characteristic but it also can provide the surface information related to landslides, such as lithological and structural settings, drainage and vegetation patterns, and soil humidity. This study demonstrated an example of lithology

Fig. 23.5 Landslide hazard zonation of the study area (only slope, lithology, and elevation factors are considered)
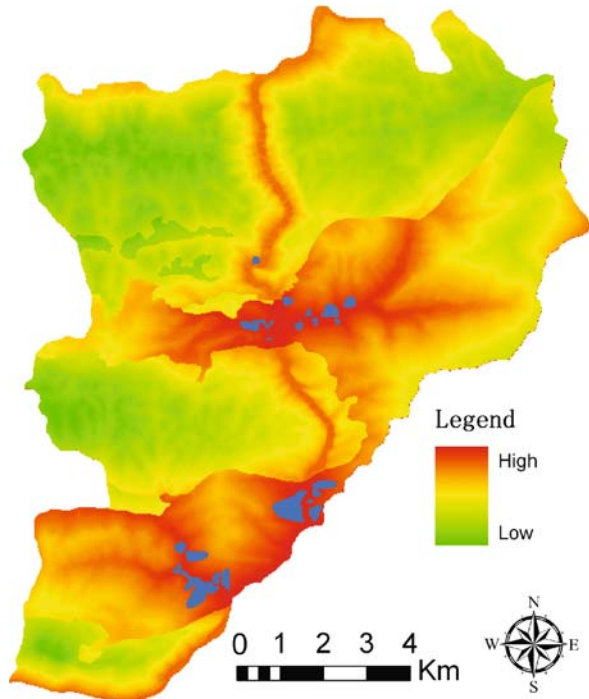
recognition by remote sensing for landslide hazard zonation. We restricted our investigation to the Longchuangou River in the Three Gorges areas and used LAND-SAT ETM+ data. Although the resolution of the image was too coarse for landslide inventory and the characteristics of the landslides could not be recognized and analyzed, some of the terrain conditions associated with landslides, lithology can still be done by remote sensing technology. The lithology recognition results seem less significant because a more detailed ground survey had been performed around the watershed due to the importance of the Three Gorges Project, but such finding is important to predict landslide-prone terrain for those regions where the landslide hazard zonation will start. The capabilities of remote sensing data should be utilized more fully in landslide studies. The availability of multi-spectral and high-resolution data as well as the advanced capabilities of digital image processing techniques in generating enhanced and interpretable images will further enhance the potential of remote sensing in determining predisposing factors for landsliding in greater detail and with better accuracy.

References

Aleotti P, Chowdhury R (1999) Landslide hazard assessment: summary review and new perspectives. Bulletin of Engineering Geology and the Environment, 58: 21–44

Ayalew L, Yamagishi H (2005) The application of GIS-based logistic regression for landslide susceptibility mapping in the Kakuda-Yahiko Mountains, Central Japan. Geomorphology, 65: 15–31

Cees J. Van Western (2000) The modelling of landslide hazards using GIS. Surveys in Geophysics, 21: 241–255

Cheng KS, Wei SC, Chang SC (2004) Locating landslides using multi-temporal satellite images. Advances in Space Research, 33: 296–301

Dai FC, Lee CF (2003) A spatiotemporal probabilistic modelling of storm-induced of shallow landslide using aerial photograph and logistic regression. Earth Surface Process and Landforms, 28: 527–545

David H, Lemeshow S (1989) Applied Logistic Regression. John Wiley and Sons, Inc., New York

Duggin MJ, Pught ML (2005) Data fusion: a consideration of metrics and the implications for polarimetric imagery. Polarization Science and Remote Sensing II, edited by Joseph A. Shaw, J. Scott Tyo, Proceedings of the SPIE, Vol. 5888

Fournier d'Albe EM (1976) Natural disasters. Bulletin of Engineering Geology and the Environment, 14: 187

Guzzetti F, Carrara A, Cardinali M, Reichenbach P (1999) Landslide hazard evaluation: a review of current techniques and their application in a multi-scale study, Central Italy. Geomorphology 31:181–216

Lee S (2004) Application of likelihood ratio and logistic regression models to landslide susceptibility mapping using GIS. Environmental Management, 34(2): 223–232

Metternicht G, Hurni L, Gogu R (2005) Remote sensing of landslides: an analysis of the potential contribution to geo-spatial systems for hazard assessment in mountainous environments. Remote Sensing of Environment, 98: 284–303

Nichol Janet E, Ahmed Shaker, Man-sing Wong (2006) Application of high-resolution stereo satellite images to detailed landslide hazard assessment. Geomorphology, 76: 68–75

Qiao JP, Wu CY, Tian HL (2004) Contribution rate research of stratum to landslide growth of Yunyang-Wushan segment in three gorges reservoir region. China Journal of Rock Mechanic and Engineering, 23(17): 2920–2924

Rose AW, Hawkes HE, Webb JS (1979) Geochemistry in Mineral Exploration. Academic Press, New York

Saha AK, Gupta RP, Sarkar I, Arora MK, Csaplovics E (2005) An approach for GIS-based statistical landslide susceptibility zonation – with a case study in the Himalayas. Landslides, 2(1): 61–69

Swiss Reinsurance Company (1990) Economic Losses and Insured Losses Due to Natural Disasters 1960–1989, Sigma 2/90

Van Genderen JL, Pohl C (1994) Image fusion: issues, techniques and applications. Proceedings EAR SeL Workshop, Strasbourg, France, pp 229–234

Van Westen CJ, Getahun FL (2003) Analysing the evolution of the Tessina landslide using aerial photographs and digital elevation models. Geomorphology, 1347: 1–13

Chapter 24
Construction and Application of a Real-Time Monitoring System for Landslides

Youlong Gao, Hongde Wang, Gang Li, Junyi Zhang, and Xiuyuan Yang

Abstract Monitoring and early warning is an important measure for geological disaster mitigation, the goal being to avoid or reduce major casualties and huge property losses. The information obtained for landslide deformation process is valuable for analysis and for the understanding of deformation law and landslide process. Real-time monitoring can achieve automatic continuous monitoring data collection, and this timely information is critical for analysis and for decision-making to avoid lengthy response times which can delay emergency measures, causing serious consequences. A more rapid response capability has been regarded as important by more and more people and has become the inevitable trend for monitoring of geological disasters. The research results are systematically summed up by the Research and Demonstration for Technology and Method on Geologic Hazard Monitoring and early warning investigations of the Ministry of Land and Resources P.R.C. The goals are to demonstrate the components and benefits of real-time monitoring, including implementing the methods of single-chain construction of the real-time system, the subsequent monitoring network, data collection system, data transmission system, and the data processing and information dissemination system. The goal is also to introduce and demonstrate the construction and implementation of the system and to show measures to deal with failure. This work will have implications for the installation of future real-time monitoring systems.

Keywords Landslide · Real-time monitoring · Data collection · Remote data transmission · Demonstration in Wushan

Introduction

The purpose of landslide monitoring is to quantify landslide deformation change, make forecasts, and attempt to prevent the disaster, if possible. At present, the basic

Y. Gao (✉)
China University of Geosciences, Wuhan 430074; Center for Hydrogeology and Environmental Geology, CGS, Baoding, Hebei 071051
e-mail: gemcgao@163.com,gemcgaoyl@263.net

landslide monitoring in China follows this pattern: Arranging a certain number of monitoring points on the landslide body, installing monitoring equipment, regular observation, data processing and analysis in a room, compilation of a results' report, and then sending of the information to the local management to decide on response measures. The disadvantages of this method are that it requires large amounts of manpower and material resources, is of low efficiency, introduces a large human error factor, and also causes a slow response to unobvious precursors to failure, because of the longer observation time interval which slows response. Thus, it is of practical significance to find a real-time monitoring system to track the deformation process of landslides continuously, which will enhance the usability of remote monitoring (Yin 2007; Wang and Gao 2007). While the real-time system is not like the live broadcast of television or stock transactions, as these are strict real-time systems, it is technically feasible to implement full automation of the landslide remote monitoring system, which having a certain lag phase has relied on modern technology. If the time lag can be controlled in a very small rang, the real time monitoring can be achieved.

An in-depth study of the construction of a real-time monitoring system was done in the course of the geological survey project known as "Research and demonstration of method and key technology of geological disaster early warning".

The first demonstration of geological hazard real-time monitoring and early warning was begun in the city of Wushan. The monitoring subjects included four landslides and three bridges. The methods used for real-time monitoring are the displacement monitoring of the deep (slip zone) by borehole inclinometer, displacement monitoring of the deep zones by TDR, monitoring of pore water pressure, monitoring of rainfall, and flow monitoring of adit (Gao et al. 2004). In this report, the building process and research results of the demonstration system will provide a guideline for future, similar system construction.

Signification and Characteristic of Real-Time Monitoring

Real-time monitoring is the remote-continuous immediate observation of landslide process. The real time monitoring system actually relies on the supporting technologies.

The main advantage and unique characteristic of this real-time monitoring system is the fact that it is real time, with which all monitoring information for the landslide can be accessed by management (or the public), located in remote areas, and analysis and decision-making can as a result be rapidly implemented. The process is automatic, without the need for human intervention. Clearly, real time can maximize the economy of labor and reduce operating costs. Because of the entire process of automation, it can easily be a continuous, tracking observation, and the period of data collection can be set for a very short duration, such as a few hours or less. It is important to track deformation process and the inversion of the deformation mechanism of landslide at the time that it occurs (Han and Xue 2000)[4].

   To achieve real-time monitoring, it must be ensured that the monitoring data can be collected automatically, processed immediately, and released quickly.

   At present, monitoring instruments are generally associated with a data acquisition instrument, which can collect and store data automatically as the cycle is set. Automated data collection is as easy to achieve as the rapid development of the universal data acquisition.

   Normally, a monitoring control center (referred to as "control center") is founded in an urban area some distance away from the landslide and is economical. Located between the landslide and the control center is the transmission medium to make the monitoring data available for management and analysis. According to the distance between the landslide and the control center, the transmission apparatus is divided into close quarters data transmission (usually less than 1 km in length) and remote data transmission (Gao et al. 2004; Reid and Lahusen 1998). The former is connected by cable because of the shorter distance while the latter uses a remote data transmission system. The transmission system is divided into two kinds by the medium, wired and wireless transmission, and the method is shown in Fig. 24.1 . As communications cable is set up between the monitoring point and the control center, the network line is vulnerable and can be damaged easily. Repairs are difficult and cause system vulnerability and have an impact on other components. When the distance is long, the transmission has an inadequate signal attenuation without the implementation of relay equipment. Because there are many disadvantages existing in the cable transmission method, the cable transmission method is gradually replaced by wireless transmission method.

   The processing of various types of monitoring data in the control center includes the conversion of raw data, database input, secondary processing, and comprehensive analysis. To ensure that information can be processed and disseminated immediately, the systems should be made available to management through a means of information and real-time Internet access. Recently, it became apparent that the information management and decision-support system of geological disasters is going to be based on GIS. A real-time disseminated system provides the monitoring data, curve, and analysis results and other information (by Internet) to the management (or public) rapidly, which is useful for decision-making and socio-economic concerns.
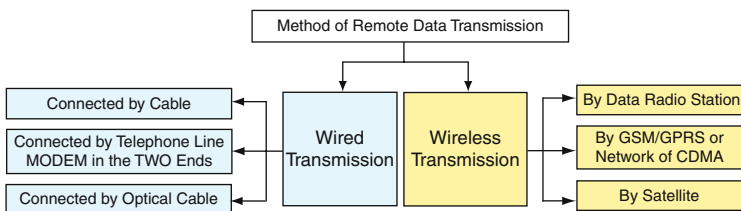

Fig. 24.1 Common method of remote data transmission

The basic functions of this real-time monitoring system are data collection, transmission, processing, automatic dissemination of information, all of which coordinate with each other and work together.

System Structure

As shown in Fig. 24.2, the real-time monitoring system is composed of a single chain of monitoring points (sensors, monitoring drilling, monitoring pier, etc.) and the data acquisition system in the landslide, the data transmission system between the landslide and the control center, and the data processing and dissemination system in the control center (Reid and Lahusen 1998; Chen et al. 2004).
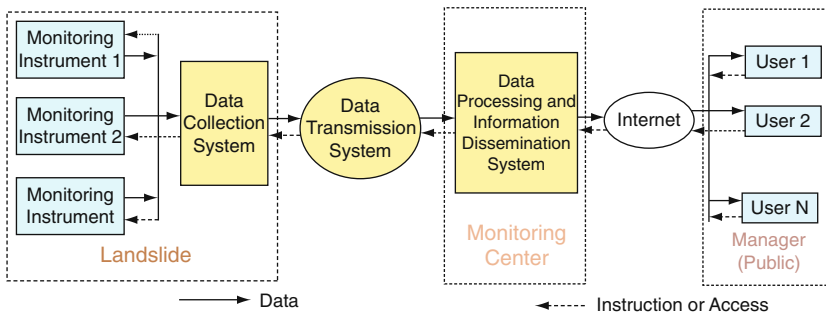

Fig. 24.2 Foundation of a real-time monitoring system

Data Collection System

Data acquisition system, as its name implies, is to collect and store various types of monitoring data, which are collected by a group of data acquisition instruments coordinating with the monitoring transducers or a general data acquisition instrument. Through the standard interface, data can be easily downloaded to a PC for further analysis. This is a typical relationship of the host and slave computers. Software for acquisition and control is installed on the host computer (PC), and by setting time and time interval, the acquisition instrument (the slave computer, usually SCM) is directed to complete acquisition, download data and save them in the hardware. The logic of the slave is to simplify the structure of the acquisition and solidification program, which is well established.

Data acquisition systems are not only to command and collect but also to accept the control of the control center, regulate time and cycle of collection, send data to the center on time, and thus acts like a "transfer station". The acquisition system should back up the original data to ensure their safety. A data acquisition system is installed on the landslide and is connected to the monitoring equipment by cables.

It is installed in a protective box or room, with a reliable power supply system to ensure that it works for a long time.

Data Transmission System

The data transmission system is used for data transfer between collection instruments, monitoring center, and the management (or public). In fact, transfer between the monitoring center and the management (public) is implemented through the Internet and the issuance system (Fig. 24.2).

Long-distance data transmission is through the use of wireless. With the development of wireless modern communications technology, the application is becoming diversified, stability is improved, and speed has also had a qualitative improvement. The biggest advantage of wireless transmission is that it is not subject to restrictions from space, so that the monitoring center could be established anywhere in the world, the system can be extended indefinitely, and the information can be centralized and publicized. The advantage brought by the technology is enormous from a national perspective.

Data are usually transferred as documents in the data collection between a PC and the server monitoring center. Wireless communication systems establish a virtual channel for sending documents. Transmission control procedures are used to complete the file transfer tasks, which are divided into server-side (Monitoring Center server) and client (PC data acquisition instrument). Server-side control procedures include the function of the collecting client which is sent to the control center receiving monitoring data. Client control procedures include the functions of connecting a wireless network, sending the data files to the server, and backing up the original data. The reliability of the transmission data depends on the strength of the wireless network signal and speed and control procedures for failsafe operation. Experience confirms that when the wireless network coverage has good signal strength based on the circumstances, the transmission error rate and stability are in line with the requirements.

Information Processing and Distribution System

Monitoring information processing will have a direct outcome on the quality of the decision. GIS-based intelligent information management of landslide monitoring systems can be used not only for the database management of various informational and multi-monitoring data but also for predicting deformation trends and forecasting stability of the situation and for evaluation of the landslide through a numerical model. The system makes slide space, multi-attribute data, and monitoring data collection into one, in accordance with the logic of a strict mathematical algorithm, which is a quantitative evaluation result. Their accuracy depends on the model of

science. In order to improve the accuracy of the analysis, a variety of comprehensive evaluation models can be joined.

A monitoring database management system is based on the landslide information management system, and the external databases play a role in the management of systems and the operation of the system background. This is known as the bottom of the database. Bottom databases are mainly used for the management of monitoring stations, the monitoring of drilling, monitoring points, and so forth, on the basis of information and various types of monitoring data. They provide real-time data sources for B/S framework for the information dissemination system.

Information dissemination provides all the landslide information to management (or the public) by the way of WEB Home. It includes geological conditions, the development characteristics, monitoring data, multi-curve over time, notification information, and relevant images and video. It has static and dynamic information according to the relative fixed information content. Static information is relatively fixed data and seldom changes, for example, landslide geological conditions, development features, and the descriptive text of monitoring. Dynamic information increases over time, such as monitoring data and curve. Real-time information is more dynamic and automatically updates Home, and the data reflect the latest changes (Han and Xue 2000). The B/S structure of the system and the database change will be reflected from the dynamic response on the home page. This is just in time to update the database data, so that real time can be achieved.

An information dissemination system provides solutions for any person in the world who can master landslide monitoring information anytime and anywhere. It allows landslide remote monitoring to be available on any Internet server, which maximizes the effectiveness of information.

Key Technologies and Solutions

The key to real-time monitoring is that monitoring data can be automatically transferred, processed, and warehoused rapidly. In the concept of time, the requirement of collection, transmission, processing, and dissemination system is not "lazy delay". The system can automatically operate in accordance with control instructions without manual intervention. In addition, in order to make the entire system extend indefinitely and have more of a diverse number of landslide monitoring information, we must also ensure that the data are designated correctly with the type, place, time, and other "labels" to avoid conflict.

As data acquisition, wireless, information processing and dissemination systems constitute a single chain of real-time system, once a system failure occurs, it would lead to the loss of real time. Therefore, the independence of the normal operation of real-time monitoring system is guarantee for an accurate outcome.

Acquisition System and the Automatic Convergence of the Transmission System

A data acquisition instrument computer (PC) controls the entire process of data collection. After download, the datum is stored in the designated address (folder) on the disk in the form of files. Transmission control client programs are installed on the PC. In order to "remove" in time, the data files will be in the control of the client, and transmission procedures will indicate whether the specified address has timely documents. If this condition exists, then transmission is started. Completing this process of judgment is extremely easily performed through the development of a high-process language timer. The time interval of the timer should be neither too long nor too short. Generally, 5–10 min is suitable. With the existence of multiple data files, the recommended transmission method is to line them up one by one. It is not necessary to compress, as the uploaded packaging will increase compression–decompression process, and if the file is too big to compress, it will increase the probability of transmission failure. It may be appropriate to extend the interval time with time to avoid time conflict. The data transmission control client program flowchart is shown in Fig. 24.3.

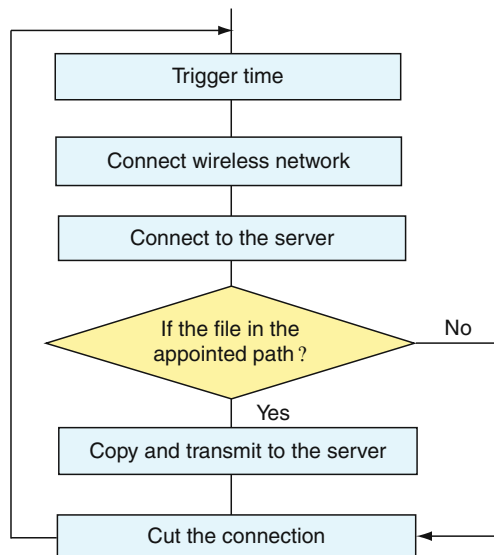It is advisable to back up a counterpart to ensure data security in the PC before data transmission.

Fig. 24.3 Data transmission control client program flowchart

Servo Data Processing and Storage Procedures

Data files are stored at designated disk address after transferring to the monitoring center server. Servo data handling and storage procedures judge for the existence of rapidly acquired documents, the distinction between data types, select the appropriate processing module to complete the conversion, and record the results in the underlying database for analysis by the information management systems and information release system. This process is shown in Fig. 24.4.

Servo data handling and storage procedures decide document form by using the timer control and the timer interval which is about 10 min (which is suitable). The function model for data conversion, calculation and treatment is prepared individually according to the processing modules and calibration methods for each monitoring instruments. Servo data handling and storage procedures flowchart is shown in Fig. 24.5.
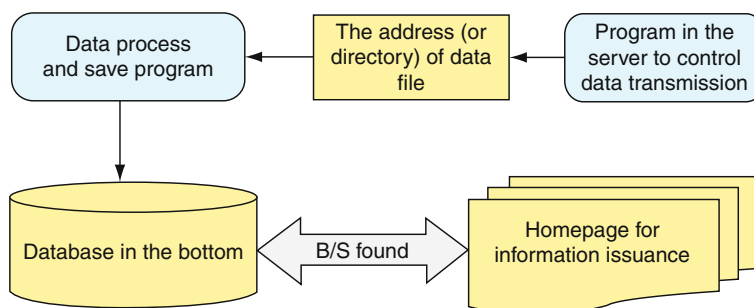

Fig. 24.4 The process of data exchange in the server in the control center

Data File Names Agreement

Monitoring center server data files are stored in a fixed address in the disk. In order to ensure a real-time monitoring system with unlimited scalability and more remote monitoring points data, the data files of different landslides must be differentiated. Servo data processing and storage procedures should correctly identify as to which landslide is which. The simplest possible solution is to agree on the data files name and labeling protocol which can identify the site, monitoring data (equipment) type, date and time of acquisition, and other important information.

Data file names have the agreed format of "XXXYYYYNNNNNNNN NNNN.dat". "XXX", three characters, identifies the monitoring methodology (equipment) types, e.g., "TDR" and "KXS", respectively, identify monitoring equipment for the TDR and pore water pressure monitor. "YYYY", four characters, indicates station number, e.g., "XJG2" identifies the formation landslide on the second stations, "YHG1" the Yuhuangge landslides on the first set of stations. Figure 24.6 is a front photo of the Yuhuangge landslide. In order to facilitate identification of differing monitoring points, the label can be extended to eight or more characters.
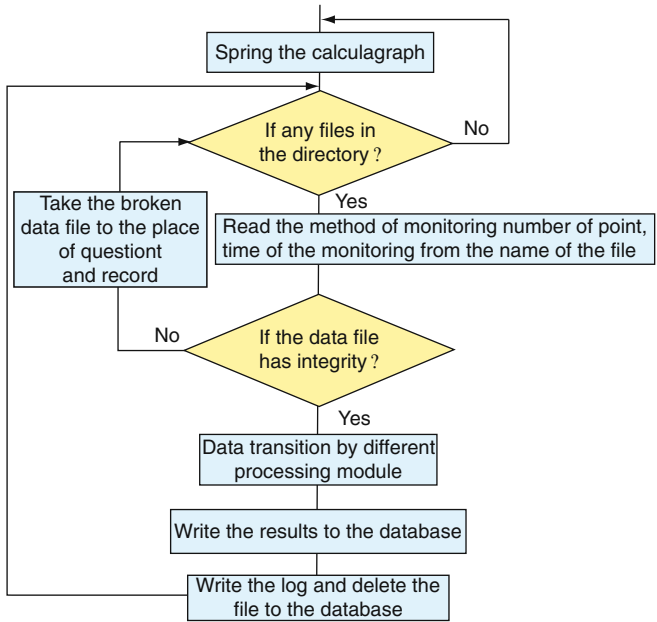
Fig. 24.5   Servo data handling and storage procedures

Fig. 24.6   Front view of the Yuhuangge landslide in Wushan County

"NNNNNNNNNNNN", 12 characters, shows date and time of the acquisition, e.g., "200508201020" shows the time for data acquisition to be 10:20 on August 20, 2005. This agreement prevents duplication of the same location or different locations at different collection sites.

Servo data handling and storage procedures identify the monitoring methodology (equipment) by means of reading the sequence from the document. They apply the appropriate conversion calculation module to compute and then put the results into the appropriate database table.

Application and Evaluation

The geological hazard monitoring and early warning demonstration station of Wushan County is the first geological hazard real-time monitoring station in our country. It lies in the hinterland of the Three Gorges Reservoir region, on the left riverbank of the Yangtze River. In this region, the geological formations are very complex and subject to geological hazards, and this region is one of the most dangerous regions. By demonstrating and contrasting 4 landslides such as Xiangjiagou landslide from a total of 27 landslides, real-time monitoring effectiveness was tested. This project began in 2003 and was finished in 2005. The real-time monitoring system is running properly now.

Monitoring Method and Monitoring Instruments

The four landslides are all deeply packed layers, and most of the sliding surfaces are interfaces between packing layers and bedrock layers. Some of them are weak inter-layers in a packing body. At present, the engineering mitigation for the landslides has been finished. Demonstrative stations lie in a region of heavy rainfall. The landslide micro-topography has suffered intense change due to large-scale engineering activities, intense construction has been taking place on the slope, and the large number of buildings increased the landslide load. After the increase of water level, groundwater activity further intensified, together with the phenomenon of an unstable cutting slope. As such, the stability of the slope decreased, and it is easy for the slope to fail. In order to master the 3-D measurement of the deformation of the landslide and to understand the process of development, the monitoring instruments are on the landslide surface and in the deep part (sliding zone) displacement. Other instruments are for measuring pore water pressure, rainfall, reservoir water level, and so forth; at the same time engineering information is collected, and the macroscopic geological investigation is conducted in appropriate areas.

In order to show the advantage of the demonstration station, a small displacement of the landslide was determined as the creep deformation stage, and monitoring methods and instruments, which were applicable and in good working order, were chosen to be the landslide monitoring demonstration instruments. All of them are shown in Table 24.1. They include a pair of high-accuracy frequency GPS earth′s

Table 24.1 Wushan demonstration station monitoring method

Monitoring content	Monitoring method	Monitoring instrument	Monitoring parameter	Significance
3-D landslide displacement	Surface displacement	GPRS method	Ashtech UZ_CGRS GPS	Horizontal and vertical displacement	Master 3-D landslide displacement
	Deep displacement	TDR	TDR monitor system	Displacement of deep deformation layer	Mainly used in judging the depth of sliding surface
		Drilling tiltmeter deep displacement	Sinco fixed drilling tiltmeter	① Horizontal displacement	Master the direction of slips and the change of temperature
				② Ground temperature	
				③ Air temperature	
Water regime	Pore water pressure	Pore water pressure monitoring method	Pore water pressure monitoring instrument	① Pore water pressure	Master the pore water pressure and water level in different depths
				② Ground temperature	
				③ Water content rate (non-satiety)	
				④ Water level	
	Rainfall	Hyetometer method	Automatic hyetometer method	① Rainfall	Master the condition of rainfall, analyze the effect of rainfall
				② Strength of rainfall	
	Water level	Collection		Water level of the Yangtze River	Analyze the deformation developments of landslide

Table 24. 1 (continued)

Monitoring content	Monitoring method	Monitoring instrument	Monitoring parameter	Significance
	Triangular Weir method	Ultrasonic open channel automatic flowmeter	Landslide groundwater flow	Analyze the relationship between deformation of landslide and groundwater
	Landslide adit drainage flow			
Strain	Fiber strain sensing analysis	BOTDR	Strain change of fiber distribution direction	Demonstrative application, feasibility, and foreground
	Strain of landslide and bridge			

surface displacement monitors, technology (TDR) reflecting monitors, BOTDR monitors, fixed deep location in-place inclinometer, pore water pressure monitors, rainfall monitors, rate of flow in landslide, and warehouse water level monitoring of the reservoir.

GPS and BOTDR report at regular intervals and, due to factors such as construction cost and socio-economic concerns, the other monitor methods are all real-time monitoring.

Management

In order to protect monitor instrument facilities against damage, buildings (guarantee protecting boxes) are set up at the monitor spots where different types of monitor instrument facilities are installed. They are called sub-stations. The sub-stations total five. The monitoring control center is called center station or main station. So it is a two-stage management system.

The advantages of using a two-stage management system than a one-step management system are obvious.

First, its construction cost is lower; the differences are shown in Figs. 24.7 and 24.8. In a two-stage management system, the different function monitor points closely in position are centralized at one place; then wireless GPRS transmission system is used for data transmission.

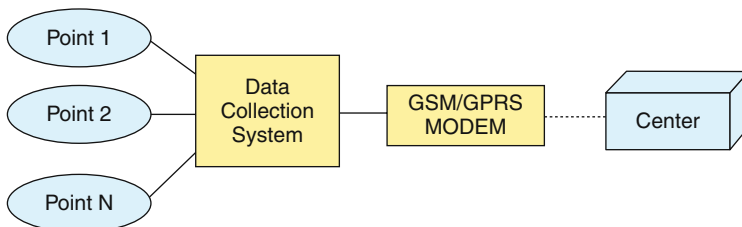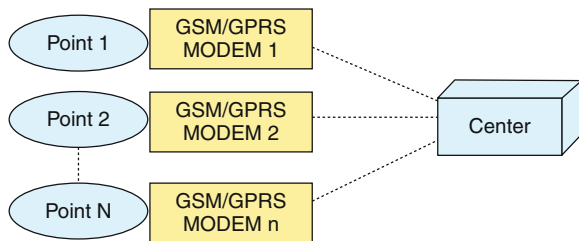**Fig. 24.7** The sketch map of one-step management of wireless transmission

Fig. 24.8 The sketch map of two-step management of wireless transmission

Second, it reduces risk in losing transmission data. Every sub-station data collect instrument may work automatically according to established procedures when the main station does not work in order.

Third, it is convenient to maintain software and hardware. Make the structure of the monitoring system clear and correct.

Fourth, it safeguards monitor instruments against damage.

Demonstrative Station Data Collection System

Some monitor instruments own storage facilities for monitoring data, such as fixed inclinometer in the hole, TDR, pore water pressure monitoring instrument, and automatic hyetometer. Among them, the TDR's storage facility is an industry-controlling machine (PC), which can be used as a control machine for downloading and storing data from other monitor instruments and also for transferring data from sub-stations to main station by extended serial port. Figure 24.9 shows how to install monitor instruments, data collection instruments, GPRS-MODEM, etc.

The data collection system is assembled in sub-station and supported by 220 V alternating current. Another online UPS is available long time.

Fig. 24.9 Demonstrative station data collect system hardware linking way sketch map
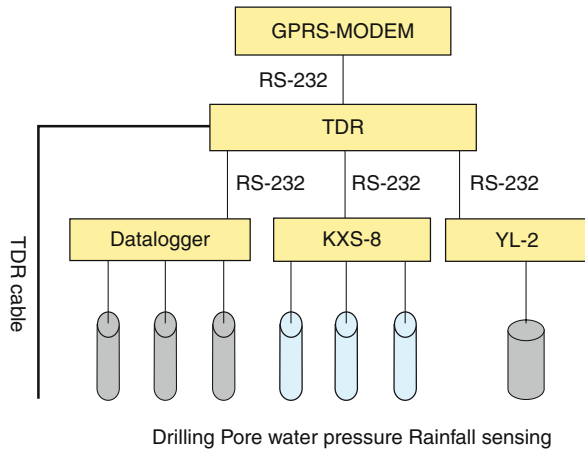
GPRS Remote Wireless Transmission System

The demonstration station monitoring center from landslide line distance 0.6 to 2.74 km was set up in the Wu Shan County land and resources bureau office building. It connects with the GPRS network wireless transmission monitoring data. GPRS (General Packet Radio Service) is a China mobile the 2.5 developing on

GPRS uses the TCP/IP agreement and may write the data in the central server (being appointed as a fixed IP address).

GPRS data transmission hardware is a commercial GPRS-MODEM. The software for transmission is compiled and composed autonomously. The software controlling transmission composes two parts. One part is for server unit, and the other for client unit. The two units cooperate each other. The transmission under the control of the customer is used to accept instruction and to upload data on a holding procedure installation charging machine in sub-station.

Since GPRS is a wireless communications business of global overcast, the main station can be built anywhere in the world theoretically.

Demonstrative Station Information Issuance System

Demonstration station information system hardware is composed of two mini-type servers and two PC terminals, way links, and switches in ADSL Internet format, with the local area network. The Database Server is used to store monitoring data. The Web server is used first to accept and handle monitoring data and then display Internet-facing monitoring information, and second, between the M bandwidth equity net linked up with 1000, which ensures that the data exchange is rapid and has external safety. The links are shown in Fig. 24.10.

The server operating system is Microsoft Windows, the Server 2003 Standard; the database system is Microsoft SQL Server 2000 SP4. The network is equipped with a firewall, which prevents viruses from invading. On the Web server, the important application programs include: (1) transmission software for the client unit, (2) Servo Data Processing and Storage Procedures, (3) bottom database, and (4) host page procedure. All of them are worked out by ourselves. Among them, the bottom database and host page is the core of the information releasing system. All of them are worked out by ourselves. Among them, information indicates that the systematic core is bottom database as is the host page procedure.
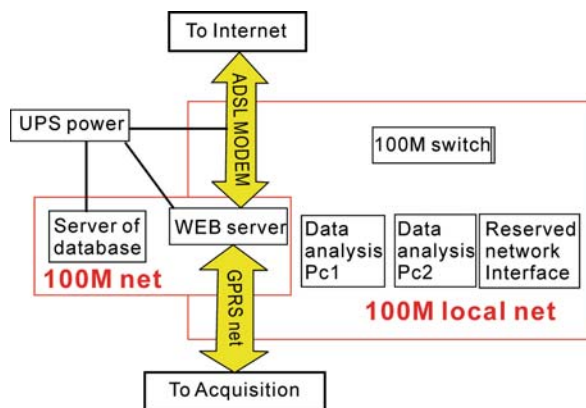

Fig. 24.10 A sketch map of link mode of equipment of information issuance program

Bottom Database System

A bottom database system is the basis of an information publishing system, and it can be divided into basis information management, data management, and auxiliary information management. The content of basis information management includes monitoring stations (center station and local station), monitoring drill, monitoring point, publishing information, publishing picture, and so forth. Data management content includes a fixed drilling tilt meter deep displacement (sliding zone), GPS surface displacement, TDR deep displacement, BOTDR strain variable quantity, pore water pressure, ambient temperature, rainfall, reservoir water level, and so forth. The content of auxiliary information management includes a classified user password, download information, statistical time access, and so forth. The database system structure is shown in Fig. 24.11.
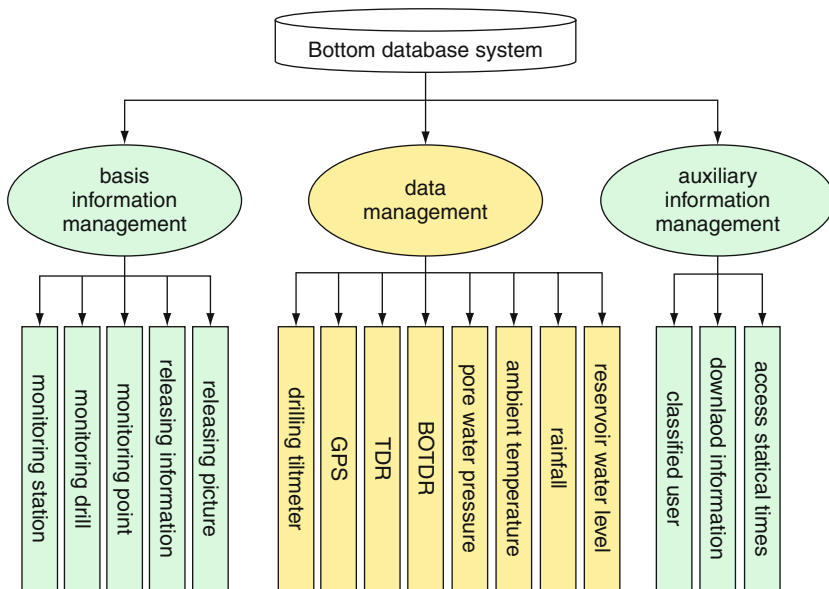
Fig. 24.11 The form of the database of the demonstration

Information Issue Homepage

The information homepage provides all the necessary information for remote users, including overview of the demonstration station, the progress of construction, real-time monitoring curve, and monitoring data. The homepage is compiled by ASP.NET, and the connection is established through SQLDB and the bottom database exchanges the data bi-directionally. From the aspect of releasing the information content, accessibility, and management maintenance, the homepage is designed with a navigation area, releasing area, managing area, and downloading

area for the connection between the remote user and administrator (shown in Fig. 24.12). Among them, the core contents are RTM and Data Query in the releasing area. RTM is used to display all types of real-time monitoring curves, and data query is used to download various types of monitoring data.

From the aspect of convenience, RTM adopts a step-by-step way to display: "select the landslide–select the monitoring section–select the monitoring points–select the monitoring period–display the monitoring curve". And each grade is linked with the figure as shown in Fig. 24.13. While looking into the curve, we can isolate and extract any given monitoring period to see the deformation trend in a certain period. Since the curve is shown in the form of a picture, users can easily download it into their PC.

Regarding security considerations, the data query is encrypted, and the users need authorized user name and password to sign up before inquiring. Similar to RTM, the data query adopts a combined sieving way, which is "Select monitoring methods – Select monitoring points – Select monitoring starting time – Display data tables" (shown in Fig. 24.14). Users can paste and save them to MS Word in the form of a table by choosing the option of all or partial inquiry. The information issuing system has both Chinese and English versions.

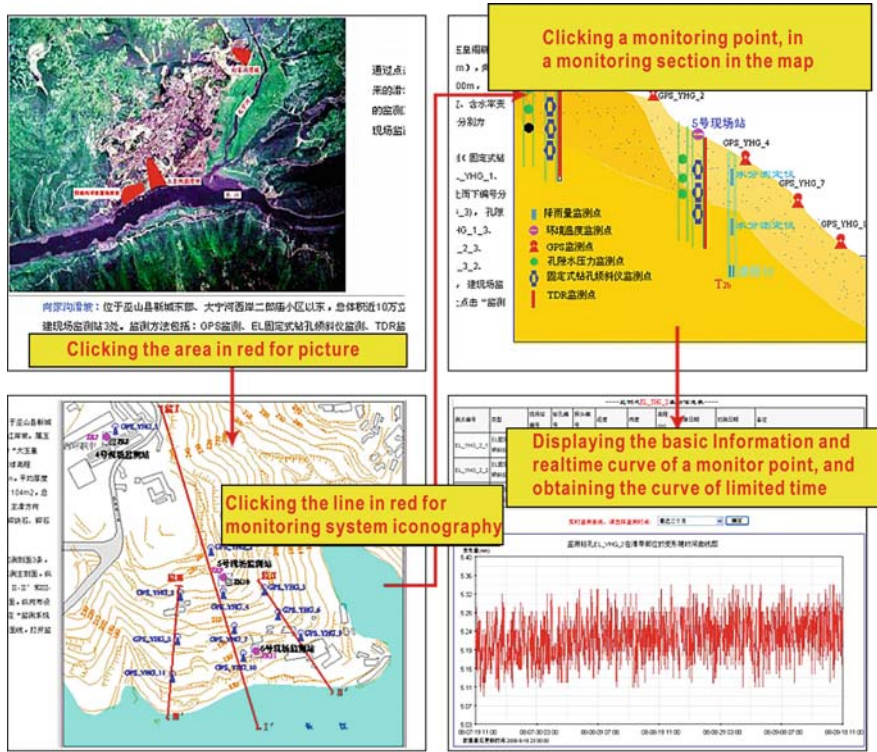**Fig. 24.12** Information issue homepage of the Wushan Demonstration Station

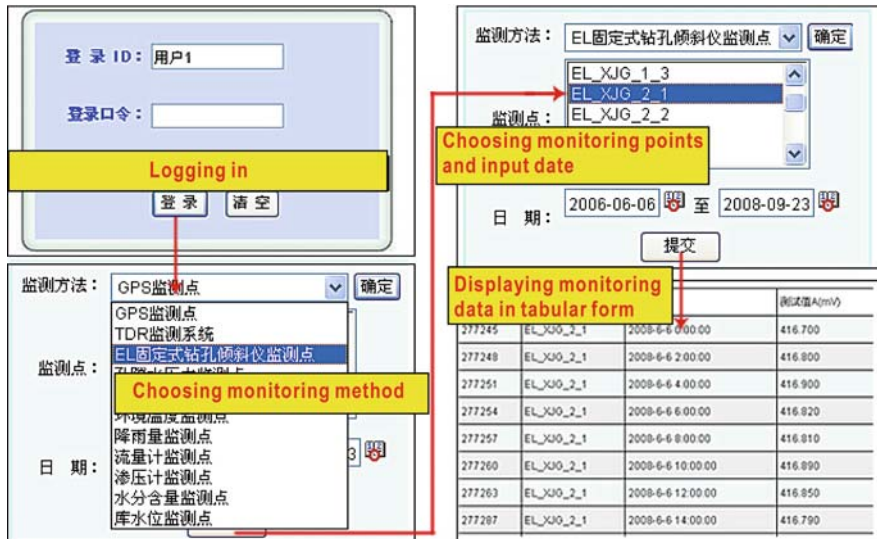**Fig. 24.13** The process for inquiring the RTM curve

Fig. 24.14 The process for inquiring monitoring data

Assessment

At the end of 2006, the demonstration station had finished 85,000 monitoring in all, and obtained nearly 2,850,000 pieces of monitoring data (calculated with the total number of database records). There were about 620 types of failures in total. Generally, the system failures include two aspects: first, there is damage or destruction to monitoring sensors and auxiliary facility for various reasons, so that the monitoring point is unable to work normally, causing interruption in monitoring, and loss of monitoring data, such as damage of the probe, fiber fracture, and GPS mark destruction; second, the integration of monitoring data collection, transmission, processing, etc., had some problems with post-processing technology, so that the monitoring data could not be released in time and as a result, the monitoring system lost its real-time character.

There are some phenomena that damage or destroy monitoring sensors and auxiliary facilities, such as strong thunder, engineering activity, and artificial damage. But equipment life, poor quality, etc., can also cause problems. These problems can generally be solved through replacing or rebuilding (except in the case of concealing the installed equipment).

The failure between cooperation and post-processing technology mainly takes place in the transmission system, at a total of more than 500 times. Some failures are the customer cannot pull out a number or cannot connect to the server after pulling out the number, or loses the response while transmitting the data; the server does not respond when it receives the procedure. The main reason for the failure lies in the local GPRS signal if it is unstable and the signal of a location is weak; second, failure-tolerant, error-correcting ability and stability of control procedure of data transmission is not good enough.

In addition, blackouts and power failures occasionally happen. In situations where there is a loss of electrical power for a long time, UPS systematic battery depletion will cause the monitoring system to stop working.

The countermeasure against this malfunction includes installing a simple lightning rod and protecting the equipment from the probability of monitoring equipment being struck by lightning; increasing the UPS battery power and backup power; strengthening the mutual communication among the local Ministry of Land and Resources officials, urban construction department, engineering company owners, and operation team; strengthening the training of geology disaster prevention common sense and public information for monitoring equipments protection, optimizing transmission control procedures, etc.

The failure statistics show that the electric power system is complete, the communication signal is stable, the countermeasure is adopted aptly, the real-time monitoring system runs steadily, with a low failure rate, and it can basically meet the purpose of observing in real time for a long time.

Conclusion

The traditional monitoring mode of regular observation not only is time-consuming but can also easily cause oversights, resulting in serious consequences. Therefore, it is significant to establish a real-time monitoring system, which can continuously track the landslide deformation process and also represent the future trend of monitoring development. RTM is a remote-continuous real-time observation. Real time is able to not only minimize the workforce and reduce the operating cost but also track the landslide deformation process and inverse landslide deformation mechanism.

The RTM system consists of a monitored site, data collecting system, data transmission system, data processing and an information issue system with a single-chain structure. The key to the real-time monitoring system is that the monitoring data can be transmitted, dealt with, and stored automatically, as soon as possible. Transmission control procedure, controlled by a time recorder with a suitable 5–10 min interval, automatically senses the connection between the data collecting system and the transmission system. When there are multiple data files, we recommend transmission one by one in a line. The data servo process and storage procedures connect the transmission system and the information issue system, function to fulfill the calculation of all kinds of primitive data conversion by transferring corresponding processing module rapidly, and save the results into the bottom of the database. The procedure time interval of the time recorder is suitable for about 10 min. In order to guarantee the real-time monitoring system with limitless expandability and input more data from different monitoring points, the agreed-upon naming rule of the data file is a brief, valid solution, which is "XXXYYYYNNNNNNNNNNNN.dat".

The geology disaster demonstration station in Wushan County adopted a second management mode and constructed the first real-time monitoring system in China through the connection and integration of the collecting system, GPRS wireless transmission system, data servo processing system, storage procedures, bottom database system, and information issue system. The application confirms that, in a given situation, the electric power system is complete, the communication signal is stable, the countermeasure is adopted aptly, and the real-time monitoring system runs steadily, with a low failure rate, and it can basically meet the requirements of observation in real time for a long time.

Despite the fact that this chapter discusses the real-time monitoring of landslides, it is not difficult to understand that the program can also be applied to other types of disasters such as mud-rock flows, ground subsidence, land subsidence, which are just different from the monitoring network. Moreover, this program can also be applied to other fields, for instance, environmental protection, meteorological phenomena, hydrology, and groundwater monitoring. The one thing worth pointing out is that the monitoring net is essential for the whole monitoring system. On the basis of deep geology analysis, confirmation of the main monitoring content (parameter), selection of the monitoring method scientifically, and rational arrangement of the monitoring site can make the monitoring system work well.

References

Chen MJ, Ouyang ZX, Shi JS (2004) Radio remote monitoring system for geological disaster based on GPRS technology. Journal of Natural Disasters, 13(3): 65–69

Gao YL, Zhang JY, Xue XQ (2004) The application of the real-time monitoring technology in geologic hazard prevention – taking the demonstration station of real-time monitoring and early-warning for geological hazard in Wushan country for example. Proceedings of Geological Hazard Investigation and Monitoring Technology and Method, China Bureau of Geological Survey, pp 121–128

Han ZY, Xue XQ (2000) Status and development trend of monitoring method and technology for geological hazard. Proceedings of Geological Hazard Investigation and Monitoring Technology and Method, China Bureau of Geological Survey, pp 47–52

Reid EM, Lahusen GR (1998) Real-time monitoring of active landslides along highway 50, El Dorado County. California Geology, 51(3):17–20

Wang HD, Gao YL (2007) Research and achievement paper of the key technology and method of geological hazard early-warning. Center for Hydrogeology and Environmental Geology of China Bureau of Geological Survey

Yin YP (2007) Initial study on the hazard-relief strategy of geological hazard in China. The Chinese Journal of Geological Hazard and Control, 15(2):1–7

Chapter 25
Entropy-Based Hazard Degree Assessment for Typical Landslides in the Three Gorges Area, China

Zongji Yang and Jianping Qiao

Abstract   With the development and expansion of landslide research, quantitatively conducting typical landslide hazard assessment is demonstrated to be an effective method in assessing landslide hazard. This study sets up an index system for landslide hazard assessment by means of intensity factors and probability factors of landslide occurrence. Based on the information entropy method, subjective weight was calculated for 21 typical landslides in Wushan County, located in the Three Gorges Reservoir area, and a qualitative typical landslide hazard degree assessment model was established. This model was then used in evaluating the hazard degree of the landslides in Wushan County, and the results were contrasted and confirmed through field investigation. The accuracy rate of the investigation is as high as 90.4%. As a result, this model demonstrates a useful application of a new methodology and provides a basis for future warning and hazard evaluations of a typical landslide.

Keywords   Entropy · Typical landslide · Hazard degree · Assessment · Three Gorges

Introduction

As one of the world's largest hydropower projects, the Three Gorges Dam Project has attracted attention for its potential impact on ecosystems and socio-economic issues. Because of the adverse geological conditions and rugged terrain, the Three Gorges area is one of the most susceptible areas for the occurrence of frequent landslides and it is also, one of the most densely populated terrains in China (Fig. 25.1). A total of 2,500 landslides have been identified in the area, and after filling of the reservoir, where impounded water has risen to a higher and higher elevation, the frequency and magnitude of landslides are expected to increase through the reactivation of old landslides and the triggering of new ones. As a result, landslide hazard

J. Qiao (✉)
Institute of Mountain and Environment, Chinese Academy of Science, Chengdu, Sichuan, 610041, China
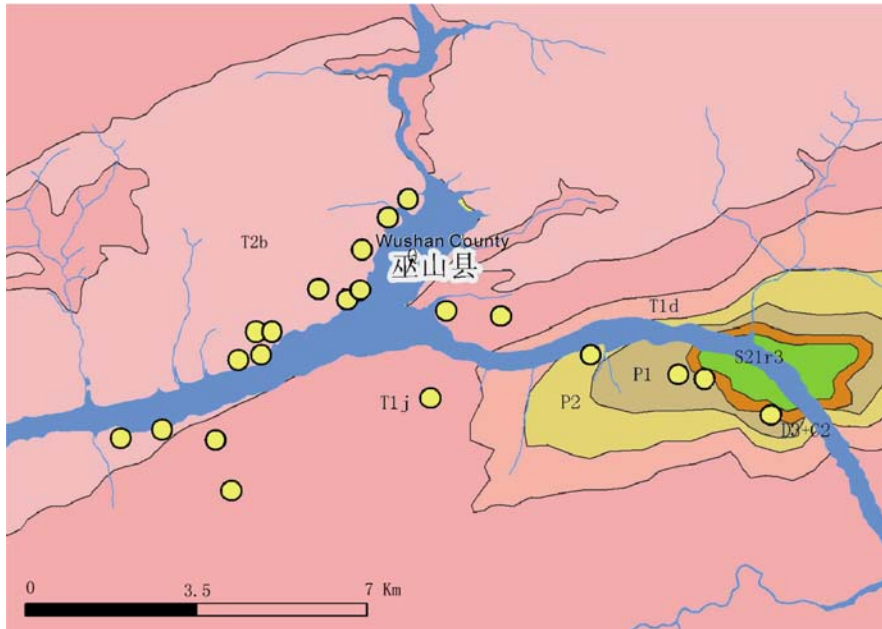e-mail: jpqiao@imde.ac.cn

Fig. 25.1 Distribution of landslides and geological map in Wushan County, Three Gorges

assessment is concentrated in this area and through years of research, regional evaluation and site-specific zonation of landslide hazard has achieved admirable development and success (Wu et al. 2001; Liu et al. 2004; Qiao et al. 2006; Fourniadis et al. 2007).

Compared with the achievements of regional-scale landslide assessment and zonation, research on typical landslide assessment is relatively rare, and development of methodology and implementation lags behind. At present, the analysis on a typical landslide is commonly calculated by the stability coefficient K using limit equilibrium principle (or LEP) based on the assumption for homogeneous materials, a situation which is not applicable for heterogeneous rock or slope deposits. Due to the uncertainty of parameters C and φ, empirical value was often introduced to fix it, and therefore the objectivity of LEP was deficient. Moreover, the results show only the state of the stability of ($K>1$) or unstable ($K<1$), two conditions which cannot reflect the many details which affect and cause unstable slope conditions. As a result, the LEP model was unable to satisfy the present demand for typical landslide quantitative analysis.

Conducting a quantitative, typical landslide hazard degree assessment is attracting more attention along with the development of landslide assessment research. Previous studies on typical landslide hazard assessment mainly use factors of superposition of the qualitative and semi-quantitative models (Qiao 1991; Wang and Kong 2001). By using AHP method, subsequent studies have gradually introduced index

weights based on expert experiences, and utilized this model to appraise the hazard degree of the Baota landslide in the Three Gorges area (Fan et al. 2004).

The entropy application originated from thermodynamics in 1948. Information entropy is a quantitative degree of system confusion, and it can forecast the development trend of a system, so it was quickly applied to valley system simulation (Ai 1987). At present, the information entropy method has been widely used to determine the weight index in natural hazards, and in environmental, integrated assessment of natural processes such as debris flow, drought, and sandstorm (Li et al. 2002; Ren 2000; Yi and Shi 1994; Mon et al. 1994).

A landslide is an open system for exchanging materials and energy with the environment, so it can be measured and described by the information entropy method. The entropy of a landslide refers to the extent of various factors influencing the landslide development. Important factors provide more entropy in the index system. As a result, the value of entropy can be used to calculate objective weights of the index system.

This chapter describes the setup of an index system for a typical landslide hazard degree assessment. Based on the information entropy method, the subjective weight of each index factor was calculated by the basic data for 21 typical landslides in Wushan County, Three Gorges, and then a qualitative typical landslide hazard degree assessment model was established. Afterwards, this model was applied to evaluating the hazard degree of the landslides in Wushan County, and eventually the results were confirmed and verified by means of field investigation.

Method

Index Selection

Hazard analysis formally consists of determining the probability of a damaging event, of intensity equal to or greater than a threshold value (Varnes 1984). Based on the statement above, landslide hazard assessment analysis should require: (1) the intensity assessment of the landslide event and (2) its probability of occurrence (Romeo et al. 2006). Therefore the index group should be composed of factors reflecting the possibility and intensity of landslides.

Data Standardization

Various factors in an index system are not the same attributes and dimension, and therefore a direct comparison is not possible, so it is necessary to conduct a standardization application before comparing the calculations

$$\text{Positive effect: } r_{i,j} = \begin{cases} 1 & x = x_{\max} \\ \frac{x - x_{\min}}{x_{\max} - x_{\min}} & x_{\min} < x < x_{\max} \\ 0 & x = x_{\min} \end{cases} \quad (25.1)$$

$$\text{Negative effect: } r_{i,j} = \begin{cases} 1 & x = x_{\min} \\ \frac{x_{\max} - x}{x_{\max} - x_{\min}} & x_{\min} < x < x_{\max} \\ 0 & x = x_{\max} \end{cases} \quad (25.2)$$

Then, the eigenvalue matrix R was formed by m landslide samples and n index system:

$$R = \begin{bmatrix} r_{1,1} & r_{1,2} & \cdots r_{1,n} \\ r_{2,1} & r_{2,2} & \cdots r_{2,n} \\ \vdots & \cdots & \\ r_{m,1} & r_{m,1} & \cdots r_{m,n} \end{bmatrix}$$

Entropy Calculations

$$E_j = -K \sum_{i=1}^{m} p_{i,j} \ln p_{i,j} \quad (25.3)$$

$$p_{i,j} = \frac{r_{i,j}}{\sum_{i=1}^{m} r_{i,j}} \quad (25.4)$$

where E_j is the entropy value, $p_{i,j}$ the specific density of eigenvalue, $r_{i,j}$ the eigenvalue, and $K = (\ln m)^{-1}$.

Weights of Index

The weights have attributed the role the factors play in the synthesis assessment, and the bigger value indicates that the factor's function is more important in this index system

$$W_j = \frac{V_j}{\sum_{j=1}^{m} V_j} \quad (25.5)$$

where W_j is the weight of index factors and $V_j = 1 - E_j$.

Model

After weights of index factors have been determined, a typical landslide hazard degree assessment model can be defined as follows:

$$H_i = \sum_{j=1}^{n} w_j \bullet r_{i,j} \quad (25.6)$$

where H_i is the landslide hazard degree, W_j the weight of index factors, and $r_{i,j}$ the eigenvalue.

Application

The Study Area

Wushan County lies in the hinterland of Wushan Mountain and is located on the east edge of the Sichuan Basin. It is to the north of Daba Mountain. The length from north to south of the whole area is 80.3 km, and the width from east to west is 61.2 km. Wushan County is located in the eastern section of the Three Gorges Reservoir, and it is the key city which the Three Gorges Projects displaced immigrants relocate to. Because of the particular geological environment, Wushan County is seriously threatened by the geological calamity of landslide. Forty percent of the landslides in the Three Gorges Reservoir are centered in the areas from Yunyang to Wushan district. After the final impoundment of the reservoir, the highest water level will be 175.4 m in height, along the banks of the Yangtze River. This rising water

Table 25.1 Landslides database in the Wushan County, Three Gorges

| Landslide name | Factor signs | | | | | | | | |
	G_d (m)	S_t	L	O_d (°)	S_d (°)	G (°)	S_f	V (m³)	K (%)
Renzicun	310	T_1j	Dolomite	70	–4	31	Convex	270,000	45
Majiawu	80	T_2b	Mudstone	5	8	29	Convex	320,000	85
Houping	80	T_2b	Marlite	1	–9	26	Convex	360,000	65
Houpinglu	15	T_2b	Marlite	10	0	45	Straight	12,000	55
Jiguanshibei	90	T_2b	Marl	5	0	40	Stair	70,000	40
Longmenqiao	145	T_1j	Limestone	0	3	35	Concave	120,000	40
Longmenqiaoyi	120	T_1j	Limestone	20	–8	24	Straight	170,000	60
Yangoupo	50	T_2b	Marl	160	15	31	Convex	12,000	60
Tongzipingnan	50	T_1j	Limestone	22	1	33	Straight	21,600	40
Fengtousi	70	T_2b	Marl	70	–14	26	Stair	300,000	40
Guanjiaqi	55	T_2b	Mudstone	100	–22	18	Straight	24,000	60
Caiziba	125	T_2b	Marl	85	–8	30	Convex	144,000	80
Dawanli	100	T_2b	Marl	60	–25	35	Convex	72,000	25
Zhangjiawn	200	T_2b	Marlite	158	23	40	Stair	500,000	20
Weiqiangcun	500	T_2b	Mudstone	30	–30	20	Stair	60,000	50
Baizhangpo	200	P_1	Marlite	85	15	40	Convex	3000,000	80
Dabaoxun	300	D_3	Marlite	120	21	35	Convex	400,000	60
Caiyuanba	500	T_1j	Limestone	155	45	60	Convex	800,000	70
Zhongnancun	500	T_2b	Sandstone	5	16	38	Convex	250,000	30
Wangjiawan	80	P_2m	Limestone	75	7	25	Convex	840,000	25
Shaojituo	80	P_1	Limestone	75	14	45	Stair	200,000	50

Intensity factors: volume (V): total volume of landslide material; height difference (G_d): the height from the vertex to the bottom of landslide; rock content (K): the percentage ratio of rock comprising landslide material. Probability factors: gradient (G): the slope angle of the landslide; orientation difference (O_d): the discrepancy between slope and stratum orientation; structure (S): the discrepancy between slope and stratum angle; slope form (S_f): the different types of slope section shape; strata (S_t): the different geologic time periods of strata; lithology (L): the different types of lithology of landslide material.

level will increase the instability of pre-existing landslides and of the surrounding slopes. Due to the Three Gorges Project, the situation of disaster prevention and reduction for Wushan County is critical, based on the severity of the hazard.

Data and Index Selection

This study selects data from 21 typical landslides in Wushan County from the Landslide Database of the Institute of Mountain Hazards and Environment, Chinese Academy of Science. After correlation and cluster analysis, nine independent landslide susceptibility factors were selected and placed into the index system (see Table 25.1 for basic data and index factors).

Model Established

The contributing ration method (Qiao et al. 2006) was employed to assign the values of factor lithology, strata, and slope form (see Fig. 25.2), others remain as the basic data. Equations (25.1) and (25.2) were employed to standardize the basic data into eigenvalue matrix R.

$$R = \begin{bmatrix}
0.61 & 0.36 & 0.00 & 0.35 & 0.56 & 0.31 & 1.00 & 0.09 & 0.38 \\
0.13 & 1.00 & 0.40 & 0.51 & 0.97 & 0.26 & 1.00 & 0.10 & 1.00 \\
0.13 & 1.00 & 0.80 & 0.28 & 0.99 & 0.19 & 1.00 & 0.12 & 0.69 \\
0.00 & 1.00 & 0.80 & 0.40 & 0.94 & 0.64 & 0.00 & 0.00 & 0.54 \\
0.15 & 1.00 & 0.80 & 0.40 & 0.97 & 0.52 & 0.14 & 0.02 & 0.31 \\
0.27 & 0.36 & 1.00 & 0.44 & 1.00 & 0.40 & 0.43 & 0.04 & 0.31 \\
0.22 & 0.36 & 1.00 & 0.29 & 0.88 & 0.14 & 0.00 & 0.05 & 0.62 \\
0.07 & 1.00 & 0.80 & 0.60 & 0.00 & 0.31 & 1.00 & 0.00 & 0.62 \\
0.07 & 0.36 & 1.00 & 0.41 & 0.86 & 0.36 & 0.00 & 0.00 & 0.31 \\
0.11 & 1.00 & 0.80 & 0.21 & 0.56 & 0.19 & 0.14 & 0.10 & 0.31 \\
0.08 & 1.00 & 0.40 & 0.11 & 0.38 & 0.00 & 0.00 & 0.00 & 0.62 \\
0.23 & 1.00 & 0.80 & 0.29 & 0.47 & 0.29 & 1.00 & 0.04 & 0.92 \\
0.18 & 1.00 & 0.80 & 0.07 & 0.63 & 0.40 & 1.00 & 0.02 & 0.08 \\
0.38 & 1.00 & 0.80 & 0.71 & 0.01 & 0.52 & 0.14 & 0.16 & 0.00 \\
1.00 & 1.00 & 0.40 & 0.00 & 0.81 & 0.05 & 0.14 & 0.02 & 0.46 \\
0.38 & 0.09 & 0.80 & 0.60 & 0.47 & 0.52 & 1.00 & 1.00 & 0.92 \\
0.59 & 0.00 & 0.80 & 0.68 & 0.25 & 0.40 & 1.00 & 0.13 & 0.62 \\
1.00 & 0.36 & 1.00 & 1.00 & 0.03 & 1.00 & 1.00 & 0.26 & 0.77 \\
1.00 & 1.00 & 0.00 & 0.61 & 0.97 & 0.48 & 1.00 & 0.08 & 0.15 \\
0.13 & 0.00 & 1.00 & 0.49 & 0.53 & 0.17 & 1.00 & 0.28 & 0.08 \\
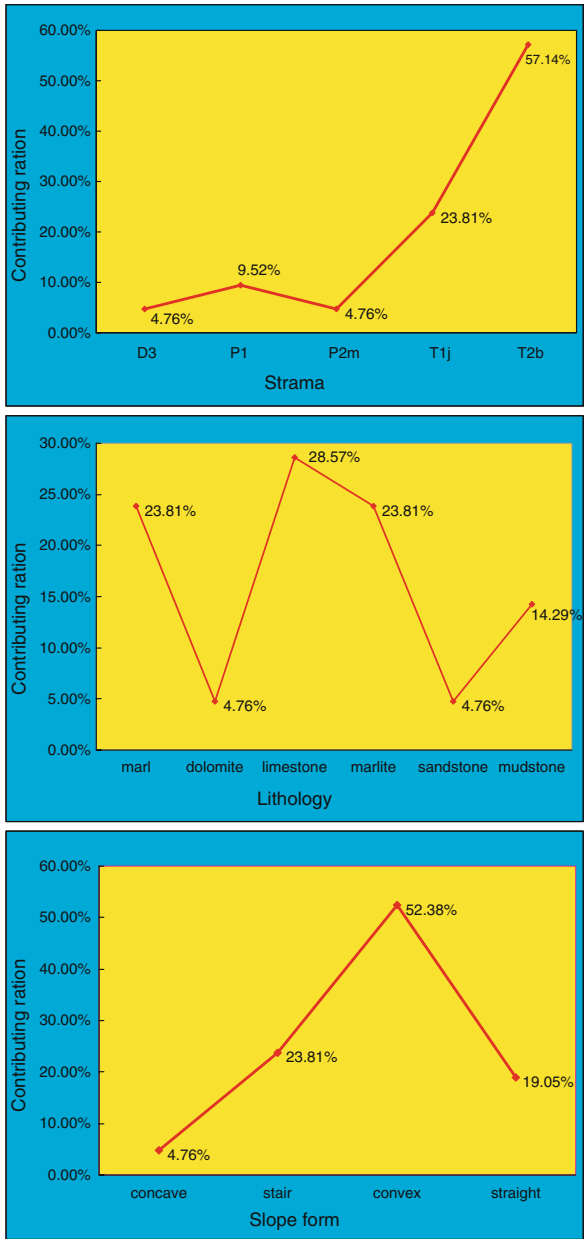0.13 & 0.09 & 1.00 & 0.59 & 0.53 & 0.64 & 0.14 & 0.06 & 0.46
\end{bmatrix}$$

Fig. 25.2 Distribution of the contributing rate of each factor

Entropy values and weights can be calculated by Eqs. (25.3, 25.4 and 25.5)

$$E_j = [0.87, 0.97, 0.96, 0.94, 0.93, 0.94, 0.87, 0.72, 0.93]$$
$$W_j = [0.15, 0.03, 0.05, 0.08, 0.06, 0.07, 0.15, 0.32, 0.08]$$

And according to the weight of each index, the typical landslide hazard assessment model (25.6) can be changed into

$$H = 0.15^*G_d - 0.03^*S_t - 0.05^*L - 0.08^*O_d - 0.06^*S_d - 0.07^*G - 0.15^*S_f$$
$$- 0.32^*V - 0.08^*K$$

$$(25.7)$$

Equation (25.7) shows that volume (V) weight is the largest, followed by slope form (S_f) and height difference (G_d). The volume directly reflects the intensity and the hazard scale of the landslide, and should occupy the dominant position in the hazard recognition. Slope form provided for the slope-free surface, which is an important index to reflect the possibility of landslides occurrence, and the height difference which indicates potential energy of the slope is also one of the principal indexes of a landslide. As a result, the objective weight of the index indicated by information entropy method is consistent with the general rules of discrimination and development of landslides.

The levels of landslide hazard are commonly divided into three or four grades; in this study the division levels were based on four grades by tolerance 0.25 (see Table 25.2).

Table 25.2 Landslide hazard degree and activity characteristic

Score range	Hazard grade	Hazard evaluation
0–0.25	Low	Minor-scale landslides ($V<1$ Mm^3), occasional occurrence
0.25–0.50	Middle	Middle-scale landslides ($V<100$ Mm^3), the moderate frequency
0.50–0.75	High	Large landside (100 Mm$^3 \leq V < 1{,}000$ Mm^3), high frequency
0.75–1.0	Extreme	Giant landside ($V \geq 1{,}000$ Mm^3), very high frequency

Hazard Assessment

The hazard degree of the 21 typical landslides in the Wushan County can be assessed by applying Eq. (25.7), and afterward, a field investigation was launched to verify the reliability of results (see Table 25.3 for results of hazard assessment and validation).

The results show that 3 landslides accounting for 14.2% of the total belong to a high hazard degree, 14 accounting for 66.7% of the total belong to the middle hazard degree, and 4 accounting for 19.1% of the total belong to a low hazard degree. According to verification by field investigation, the accuracy rate is as high

Table 25.3 Results of typical landslides hazard assessment in the Wushan County, Three Gorges

Landslide name	Score	Hazard grade	Field validation
Renzicun	0.40	Middle	Unanimous
Majiawu	0.46	Middle	Unanimous
Houping	0.44	Middle	Unanimous
Houpinglu	0.26	Middle	Unanimous
Jiguanshibei	0.28	Middle	Unanimous
Longmenqiao	0.21	Low	Lower
Longmenqiaoyi	0.26	Middle	Unanimous
Yangoupo	0.34	Middle	Unanimous
Tongzipingnan	0.22	Low	Unanimous
Fengtousi	0.24	Low	Lower
Guanjiaqi	0.15	Low	Unanimous
Caiziba	0.42	Middle	Unanimous
Dawanli	0.34	Middle	Unanimous
Zhangjiawn	0.28	Middle	Unanimous
Weiqiangcun	0.33	Middle	Unanimous
Baizhangpo	0.75	High	Unanimous
Dabaoxun	0.46	Middle	Unanimous
Caiyuanba	0.64	High	Unanimous
Zhongnancun	0.52	High	Unanimous
Wangjiawan	0.40	Middle	Unanimous
Shaojituo	0.27	Middle	Unanimous

as 90.4%, which demonstrates that the method is credible for a typical landslide hazard degree assessment.

Discussion

Index factors selection and weight determination were the nucleus of a typical landslide hazard degree assessment. In eliciting the objective weight of the index, the information entropy method is based on the premise that a certain amount of available information exists, and a given set of landslides with explicit, known factors, are the best candidates for entropy analysis. Therefore, lack of data can lead to some factors not being introduced, such as hydrological and artificial factors, which are not included in this study. Furthermore, area-scale factors that are not differentiated between samples such as seismic intensity and precipitation in the same region have not been introduced into the index system. Therefore, the next phase of work will focus on how to introduce these indexes when data are insufficient.

Conclusion

Typical landslide hazard degree assessment is a comprehensive assessment method. The physical significance of the index system and weights for each landslide were

distinct, and used and applied from basic landslide data, which reflect the general characteristics of landslide process, and regional features of landslide development in the study area. As a result, this approach is an objective quantitative model of hazard degree assessment. After the model was created, it was applied, in the assessment of the hazard degree of the 21 landslides in the Wushan County study area. The accuracy rate of results is as high as 90.4% after validation of the model by field investigation. Additionally, this model is not exclusive for Wushan area but is also applicable to analogous geological regions.

Despite the scarcity of data based on information entropy method, this study has shown convincing success for the ascertainment of typical landslide hazard in the Three Gorges area, and the simplicity of the model is favorable in terms of cost-containment of landslide assessments, and can be undertaken without a time-consuming geological investigation. This work has also demonstrated that the information entropy method is very useful for objective weight determination of the index system.

Accordingly, this study serves to demonstrate a new method of hazard assessment and by its success, advocates for and promotes its utilization. The study also provides a basis for future warning methods and hazard evaluations for typical landslide in the Three Gorges area.

References

Ai NS (1987) Comentropy in erosional drainage –system.*Journal of Soil and Water Conservation* 1(2):1–7

Fan XY, Qiao JP, Chen YB (2004) Application of analytic hierarchy process in assessment of typical landslide danger degree. *Journal of Natural Disasters* 13(1):72–77

Fourniadis IG, Liu JG, Mason PJ (2007) Landslide hazard assessment in the Three Gorges area, China, using ASTER imagery: Wushan-Badong. *Geomorphology* 84:126–144

Li XJ, Chen YN, Ouyang H (2002) Analysis on sand disaster with disaster entropy method. *Arid Land Geography* 25(4):350–353

Liu JG, Mason PJ, Clerici N (2004) Landslide hazard assessment in the Three Gorges area of the Yangtze River using ASTER imagery: Zigui-Badong. *Geomorphology* 61:171–187

Mon DL, Cheng CH, Lin JC (1994) Evaluating weapon system using fuzzy analytic hierarchy process based on entropy weight. *Fuzzy Sets and Systems* 62(2):127–134

Qiao JP (1991) Judgment of danger degree of instable slope. *Mountain Research* 9(2):117–122

Qiao JP, Zhu AX, Wu CY (2006) Bottom factors applied to the zoning study of the risk level of landslides in the Three Gorges Reservoir area. *Wuhan University Journal of Natural Sciences* 11(4):761–766

Ren LC (2000) Disaster entropy: conception and application. *Journal of Natural Disasters* 9(2):26–31

Romeo RW, Floris M, Veneri F (2006) Area-scale landslide hazard and risk assessment. *Environmental Geology* 51(1):1–13

Varnes DJ (ed.) (1984) Landslide hazard zonation: a review of principles and practice. UNESCO, 63

Wang CH, Kong JM (2001) The differentiating danger slope occurring high-speed landslide. *Journal of Engineering Geology* 9(2):127–132

Wu SR, Shi L, Wang RJ (2001) Zonation of the landslide hazards in the fore-reservoir region of the Three Gorges Project on the Yangtze River. *Engineering Geology* 59:51–58

Yi CX, Shi PJ (1994) Entropy production and natural hazard. *Journal of Beijing Normal University (Natural Science Edition)* 30(2):276–280

Chapter 26
The Conceptual Model of Groundwater Systems in a Large-Scale Landslide – A Case Study of the Baota Landslide in the Impoundment Area of Three Gorges Project

Pinggen Zhou and Heping Ma

Abstract In a case study of the Baota landslide in the impoundment area of the Three Gorges project, the conceptual model of groundwater systems in this large-scale landslide was established by integrating the data from hydraulics, physical–chemical characteristics, environmental isotopes, and temperatures of the groundwater in the landslide. The conceptual model of groundwater systems includes the recharge, seepage, discharge condition, and trend of groundwater which is in turn controlled by the environmental factors (e.g., rainfall, reservoir impoundment, and artificial surface water recharge). This is one of the keys to predict the slope stability and to apply countermeasures to mitigate landslides.

Introduction

The purpose of studying conceptual models of groundwater systems is to discover the recharge, seepage, discharge condition, the trend of groundwater systems, the environmental factors (e.g., rainfall, reservoir impounding, and artificial surface water recharge), and to zone the groundwater systems. This is the basis and key to landslide prevention and mitigation. The previous studies were mainly concentrated on the mathematical modeling of the groundwater level with the various environmental factors mentioned above (Hodge and Freeze 1977; Rulon and Freeze 1985; Iverson and Major 1987; Leach and Herbert 1982; Sangrey and Harropwilliams 1984; Valore and Farulla 1996). In Japan, some studies were made using geo-chemical methods (e.g., physical–chemical characteristics, environmental isotopes, and temperature) to identify the source and flow path of groundwater in the

———————————
P. Zhou (✉)
China Institute of Hydrogeology and Engineering Geology Exploration, Beijing 100081, China
e-mail: zhoupg@mail.cigem.gov.cn

landslide, especially in the landslide area that occurs along with geothermal activities (Sato et al. 1989; Watanabe et al. 1996; Yoshioka et al. 1986; Yoshioka and Kitaoka 1989; Yoshioka 1990a,b). The case studies were also reported in Canada, and state that the recharge from the surface water to groundwater was identified by groundwater chemical analysis data (Eyles and Howard 1988). It is less reported that the integrating data of hydraulics, physical–chemical characteristics, environmental isotopes, and temperatures of the groundwater systems of the landslide were used to establish the conceptual model of groundwater systems within large-scale landslides in the previous studies. In a case study of the Baota landslide – a large-scale landslide in the impoundment area of the Three Gorges project, the integrating data were applied to establish the conceptual model of groundwater systems. The recharge, seepage, discharge conditions of groundwater in the landslide, which are controlled by the environmental factors (e.g., rainfall, reservoir impounding, and artificial surface water recharge) were identified in this conceptual model.

The Characteristics and the Conceptual Model of the Groundwater Systems of the Landslide

Geological Setting and Hydro-geological Structure

The Baota landslide is surrounded by the Dahegou stream in the east, the Jipazi landslide in the west, and the Yangtze River in the south. The altitude of the upper boundary of the landslide is within 200–400 m, and the altitude of the lower boundary of the landslide is within 45–70 m. The difference of elevation is about 330–350 m. The total area of the landslide is about 1.26 km^2. The landslide can be divided into two parts – the upper and the lower, and it is made of loosely consolidated sediments. Many trenches cut deeply throughout, and two to three terraces due to the multi-time activities of the landslide can be seen in the landslide. Since 1986, the remarkable deformation has become obvious in the upper part of the landslide: creeping motion in the upper boundary and tension cracks in the middle of the landslide can be seen. It has been indicated by the monitoring data in situ that the deformation occurred mainly in the rainy season (from May to August) in the years 1986, 1989, 1993, which were coincident with the local precipitation. Therefore, the occurrence and development of fissures in the landslide relate directly to precipitation (Figs. 26.1, 26.2, and 26.3).

The aquifers of the landslide can be divided into two types. Aquifer I consists of an upper loosely consolidated sandy-clayey layer with a depth varying from 0 to 58.7 m, and is distributed over all the areas of the landslide. Aquifer II consists of the lower fissured rocky gravel layer with an average depth of 50 m. Aquifer II is far more permeable than Aquifer I. The upper part of the landslide is mainly made of Aquifer I, the lower landslide is mainly made of aquifer II. The porosity in the upper part of the landslide is greater than that in the lower because of their differing content of sand. The bed of the slide is made of Jurassic Period series of an inter-layer of sandy-rock layer and a clayey-rock layer, with minimal fissuring.
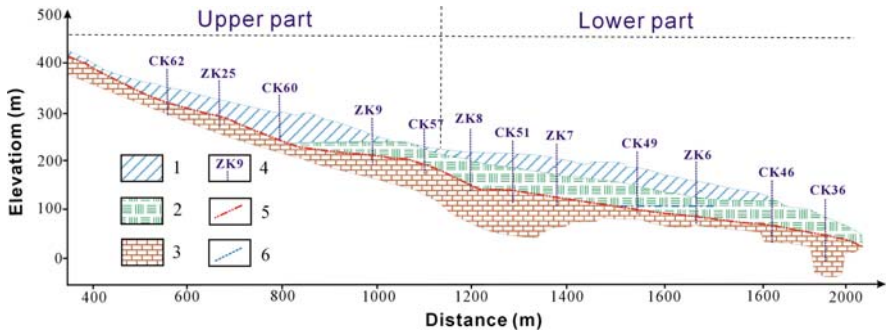
Fig. 26.1 The geological map of the Baota landslide. 1 – loose sandy-clayey layer; 2 – fissured rocky gravel layer; 3 – Jurassic series of the inter-layer of sandy-rock layer and clayey-rock layer (J_{3P}); 4 – borehole; 5 – slide surface; 6 – groundwater table
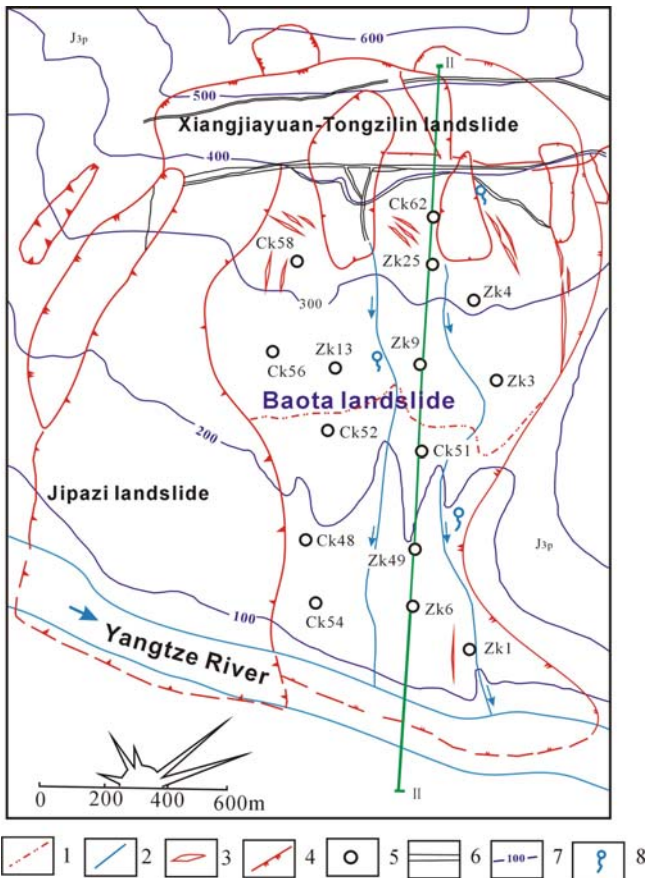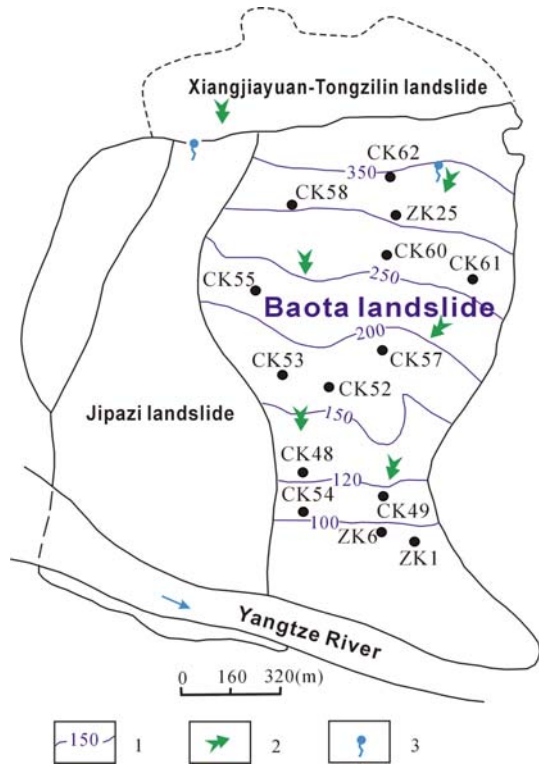

Fig. 26.2 The geological section map of the Baota landslide (Aquifer sections II-II): 1 – boundary of two parts of landslide; 2 – boundary of landslide; 3 – crack; 4 – boundary of ancient landslide; 5 – borehole; 6 – drain; 7 – contour line of elevation; 8 – spring

The Flow Field and the Regime of the Groundwater Systems

The contour map of the groundwater level of the landslide can be drawn from the observation data. From this map, it can be seen that groundwater flow from the upper to the lower and discharges into the Yangtze River.

The various amplitudes of the groundwater level were different. The regime of groundwater changed with the Yangtze River level in the rainy season (May–October) in front of the landslide (e.g., borehole of ZK1, ZK6, ZK54, and ZK49). The maximum various amplitudes respond to the Yangtze River level (more than 20 m), the other peaks of the groundwater level originate from the recharge of the precipitation. The amplitude of the middle of the landslide is lower than 2–3 m. The various amplitudes of the groundwater level in the upper part of the landslide are about 6–8 m. These peaks all respond to the precipitation. The arrival time of the peak value of the groundwater level in the lower landslide area is 2 months later than that in the upper landslide area and is 1 month later than that in the middle area (seen Fig. 26.4).

The maximum outlet flow of the springs is about 0.2 L/s in the rainy season, and the seepage is reduced to about 0.001 L/s or it becomes a wetland area, in the dry season.

Fig. 26.4 The groundwater level of the Baota landslide as shown in a borehole and the water level of the Yangtze River (January–December 1995)
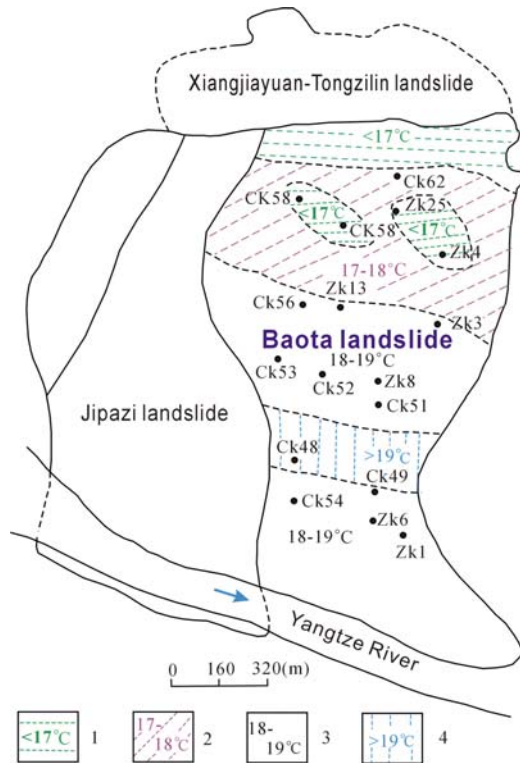
The Chemical Characteristics and Temperature Fields of the Groundwater Systems in the Landslide

Two types of groundwater are Ca–HCO^{3-} and Ca–Mg–HCO^{3-}, as indicated from the chemical tri-linear diagram (Fig. 26.5). The total hardness of groundwater is about 0.29–0.56 g/L. The groundwater is similar to rain water and the Dahegou stream water in chemical constituents. The pH varies from 6.9 to 8.2. In some places, the groundwater is rich in K^+, Na^+ resulting from the cation exchange or the recharge of the surface sewage.

From the contour map of the groundwater temperature measured in December 1995, the temperature increased along the direction of groundwater flow, but some abnormal low-temperature areas resulted from the surface water recharge which coincided with the location of a fish pool (Fig. 26. 6).

The Environmental Isotopes of the Groundwater

1. *The H^3 of the groundwater*: The H^3 of the groundwater varies in slope from 19.4 to 23.1 TU with an average value of 20.97 TU. The difference in variation is 3.7 TU, and the system error can reach 2 TU. It can be concluded that the age of the
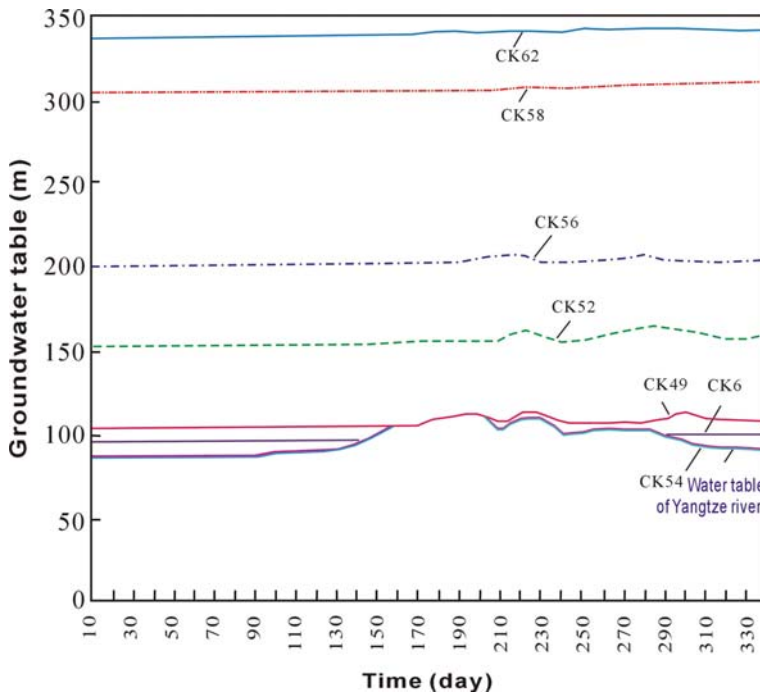
Fig. 26.5 The triangle graph of the groundwater chemistry of the Baota landslide (December 1995)

groundwater in the Baota landslide is the same as that of the Yangtze River water and local stream water (Table 26.1), which means the groundwater were replenished very recently.

2. *The characteristics of the stable isotopes of the groundwater*: The stable isotopes curve ($\delta^{18}O$ versus δD) of rain water of the Sichuan basin was obtained from 38 samples of rain water (Table 26.1, Fig. 26.7), in which the effects of temperature, altitude, and longitude have been considered sufficiently. The average value of δD is $-57\permil$. The average value of ^{18}O is $-8.6\permil$. This curve of $\delta^{18}O$ versus δD can be presented as follows:

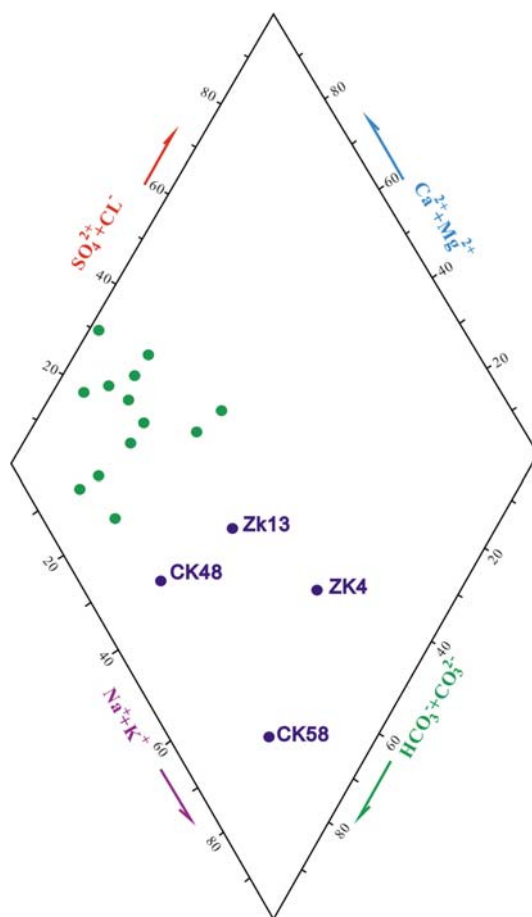$$\delta D = 7.2\delta^{18}O + 5.2 \tag{26.1}$$

The standard stable isotopes curve (^{18}O versus δD) of global rainfall is shown in Fig. 26.6, and it can be presented as follows:

$$\delta D = 8\delta^{18}O + 10 \tag{26.2}$$

The effects of temperature (T) and altitude (H) in the southwest region of China can be presented as follows:

$$\delta^{18}O = 0.30\, T - 12.72 \tag{26.3}$$

Fig. 26.6 The contour map
of the groundwater
temperature of the Baota
landslide (December 1995)

$$\delta^{18}O = -0.0018\,H - 6.86 \qquad\qquad (26.4)$$

The results of stable isotope analyzing the groundwater in the Baota landslide are
presented in Fig. 26.6. According to the analysis data of $\delta^{18}O$, the effect of relative

Table 26.1 The analysis results of the H^3 of groundwater and other water samples (December 14, 1995)

Sampling location	Sampling depth (m)	H^3 (TU)
ZK_6	69	19.8
ZK_9	51	19.4
ZK_{25}	11.30	22.6
CK_{52}	66.50	23.1
Yangtze River		21.0
Dahegou stream		19.9

Fig. 26.7 The stable isotopes of the groundwater of the Baota landslide
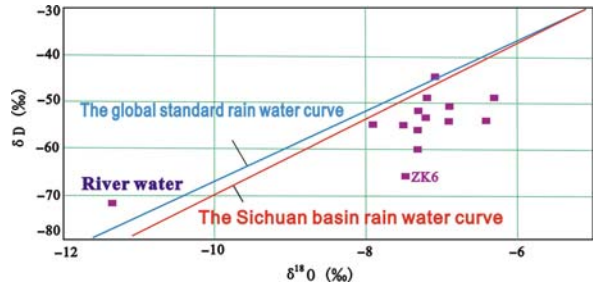
altitude (within 500 m) to the value of $\delta^{18}O$ is 0.9‰ (within 2‰ of the errors of the
test system). Therefore, the effects of temperature and altitude can be omitted. The
data of the stable isotopes of the groundwater in the Baota landslide are located near
the rainfall stable isotope curve of the Sichuan basin and the standard stable isotope
curve of the global rainfall, which means that the groundwater in the landslide origi-
nates from the local rainfall (Fig. 26.8). The value of $\delta^{18}O$ of the groundwater in the
borehole of ZK6, which was located in front of the landslide, is between the values
of the other groundwater samples and the river water sample. So the groundwater in
front of the landslide can be regarded as the mixture of groundwater and river water.
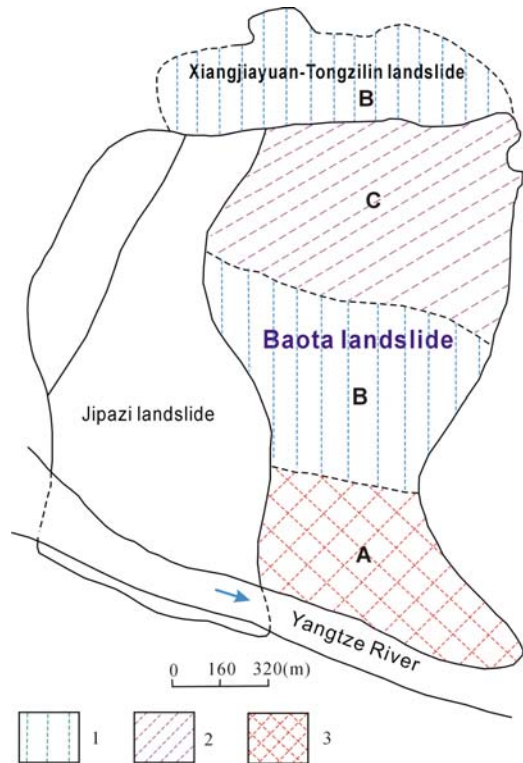

Fig. 26.8 The groundwater
system zoning of the Baota
landslide: 1 – groundwater
flow zone; 2 – rain and
surface water infiltration
zone; 3 – Yangtze River
influence zone

Conclusion and Discussion

According to the studies of the geological setting, the characteristics of the ground-water system above, the zonation of the groundwater system of the landslide can be simplified as shown in Fig. 26.8.

The groundwater in the Baota landslide originated from the local rainfall and the artificial surface water infiltration. In front of the landslide, there exists the mixture of Yangtze River water and groundwater, with a remarkable variation of groundwater level, especially during rain and flooding season. The rainfall and artificial surface water infiltration occurred mainly in the upper part of the Baota landslide. The middle of the landslide is the seepage area of the groundwater. The water-level changes in the upper part are bigger than that in the middle.

The conceptual model of the groundwater system is not only one of the keys to predict the landslide stability but is also useful to mitigate the landslide. The main deformation, which is primarily affected by the infiltration of precipitation and surface water, occurred in the upper part of the Baota landslide, and therefore, the surface drainage system should be used to prevent rainfall and the artificial surface water infiltration, as this has been verified by test results.

References

Eyles N, Howard KWF (1988) A hydro-chemical study of urban landslides caused by heavy rain: Scarborough Bluffs, Ontario. Canadian Geotechnical Journal 25:455–466

Hodge RA, Freeze RA (1977) Ground water seepage system and slope stability. Canadian Geotechnical Journal 14:466–476

Iverson RM, Major JJ (1987) Rainfall, ground water seepage, and seasonal movement at Minor Creek landslide, Northwestern California: physical interpretation of empirical relations. Bulletin of Geological Society of America 99:579–594

Leach B, Herbert R (1982) The genesis of a numerical model for the study of the hydrogeology of a steep hillside in Hong Kong. Engineering Geology Quarterly Journal 15:243–259

Rulon JJ, Freeze RA (1985) Multiple seepage faces on layered slope and their implication for slope stability analysis. Canadian Geotechnical Journal 22:347–356

Sangrey DA, Harrop-williams KO (1984) Predicting ground water response to precipitation. Journal of Geotechnical Engineering, ASCE 110:857–975

Sato O, yoshida S, Inaba K (1989) Chemical aspect of ground water in landslide area. Proceedings of the Japan-China Symposium in Landslide and Debris Seepages, pp 99–104

Valore C, Farulla CA (1996) Evaluation of safety conditions of slopes by drainage galleries. Proceedings of the International Symposium on Landslides, pp 1817–1822

Wang DC, Zhang RQ, Shi YH (1980) The Principles of Hydrogeology. Chinese Geological Publish House, Beijing, pp 5–55

Watanabe N, Oki Y, Sato O, Kusakabe M (1996) Landslide generated by geo-pressured hydrothermal system in the Northern Fossa Magna Region of Japan. Proceedings of 30th International Geological Congress (17-2), August 4–15, Beijing, China

Yoshioka R, Koizumi N, Kusakabe M (1986) Chemical and isotopic compositions of natural waters from an area of large-scale landslide caused by the western Nagano Prefecture earthquake. Disaster Prevention Research Institute Annuals, Kyoto University, Japan, 29(B-1):379–390

Yoshioka R, Kitaoka K (1989) Variation in chemical and isotope components of ground water from the Otabaru landslide in the area of hydrothermal alteration, Beppu City. Bulletin of the Disaster Prevention Research Institute 32(B-1):211–228

Yoshioka R (1990a) Landslides and groundwater geochemical. Journal of Groundwater Hydrology 32(3):147–162 (in Japanese)

Yoshioka R (1990b) Landslides and groundwater, geochemical investigation. Journal of Groundwater Hydrology 32(4):253–272 (in Japanese)

Chapter 27
Bank Collapse Along the Three Gorges Reservoir and the Application of Time-Dependent Modeling

Qiang Xu, Minggao Tang, Jianguang Bai, Jianjun Chen, and Simeng Dong

Abstract   After the Three Gorges reservoir impoundment water level changed, the groundwater dynamic stress field and the rock mass stress field changed considerably. As the water level changes, wave erosion as well as rain storm, causes bank collapse to often occur along the reservoir area. This chapter aims to find the mechanism causing bank collapse and apply this type of information using models which can then describe these mechanisms for later research. In order to find out the relationships between bank collapse and bank width, slope angle, property of bank soil, and intensity of rainfall, some modeling tests were carried out and the results showed that the width of the bank is the main factor affecting bank collapse. Another conclusion is that the process of bank collapse can be characterized as time-dependent. It is proposed that the process be divided into four characteristic phases: surface erosion, shallow erosion, deep erosion, and termination of slope movement. Deep erosion is the key phase of the four, for which the velocity and scale of bank collapses can be calculated.

Keywords   Reservoir bank collapse · Modeling test · Effect-of-time of bank collapse · Effect factors of bank collapse · Width of bank · Time-dependent

Introduction

The area of the Three Gorges Project reservoir is shaped like a long bar which crosses the eastern area of Sichuan Province to the western area of Hubei Province. There are many cities and towns located along the banks of the reservoir area. After the reservoir project began the process of impounding water, the water level varied from 145 to 175 m in height, every year. Due to water storage, water merged and eroded the banks. Rainfall impacted the area, and as a result, the rock mass

Q. Xu (✉)
State Key Laboratory of Geo-hazard Prevention and Geo-environment Protection,
Chengdu University of Technology, Chengdu 610059, China
e-mail: xq@cdut.edu.cn

and groundwater stress fields changed a great deal and caused bank collapse. The sequences not only caused the reactivation of ancient landslides but also caused new landslides which are dangerous to people living in those areas and have a large impact on their properties (Physical modeling for examination of bank collapse in the Three Gorges area).

Bank collapse is a progressive process. One method that can be carried out is to have an overview of bank collapse mechanisms in order to summarize similar cases in other reservoirs which already have experienced bank collapse after a long history of water storage. Another method is to carry out modeling tests (Physical modeling for examination of bank collapse in the Three Gorges area). This chapter chooses to take the latter method and presents a method of simulating the geological property of rock and soil, groundwater condition, and slope types in the Three Gorges area. The method includes building models, in order to find out the bank collapse mechanism and to understand which factor effect is the key factor. Finally, the chapter used the models to analyze the time-dependent mechanism of bank collapse.

Modeling Test Design and Procedure

The facilities of the modeling test are all designed by the State Key Laboratory of Geo-hazards Prevention and Protection in Chengdu University of Technology. The modeling test system includes two main simulation systems: the reservoir water storage model and the rainfall simulation model. The reservoir water storage model includes a manually adjusted testing trough which is 2 m in length, 1.5 m in width, and 0.6 m in height, some other equipment which is also manually adjusted for measuring displacement, water level, and pore-water pressure. The rainfall simulation model includes circuit checking systems for several pore-water pressures and overlapping insufflations simulating rainfall system. All the data setting and collecting are controlled by computers.

According to the information from the site investigation, it can be found that the soil composition on the banks in the Three Gorges reservoir is loosely consolidated material which includes fine sand, coarse sand, silt, silty clay, and clay. Due to the fact that the test requires a large amount of testing materials, it is hard to collect the real sample from site; materials are prepared in the test similar to sand composition of the site.

In order to find out the bank collapse mechanism and which factor effect is the key factor, three types of test models are designed:

(1) Mono-factor model: One variable was chosen for sand property, slope angle, reservoir water level, and the intensity of rainfall and then tested to find out which factor effects the scale and type of bank collapse the most.
(2) Multi-factor model: Finding the mechanism of bank collapse by comprehensive analyzing for every factor of sand property, slope angle, reservoir water level, and the intensity of rainfall; calculate the scale of the bank collapse.

(3) Time-dependent model of bank collapse: find out the bank collapse development process.

Mono-factor Model Test

The mono-factor model test focuses on figuring out the contributing factor for bank collapse process among sand property, slope angle, reservoir water level, and the intensity of rainfall. From the history found in geological records in the Three Gorges area and some records in other similar reservoirs, it can be concluded that the sand properties on the collapsed bank are mainly formed by clay, silt, fine sand, and coarse sand (The National Laboratory of Geological Hazard Prevention and Geological Environment Protection, Chengdu University of Technology 2005). The average natural resting angle of these four materials with natural moisture content is 53° and the average underwater resting angle is 32°, so the designed slope angles are 12, 22, 32, 53°, respectively, for four levels. By referring to the water storage records, the water levels are chosen as 139, 145, 156, 175 m, respectively, for four levels (Study on influence factors of bank collapse in the Three Gorges Reservoir with physical modeling). The intensities of rainfall design are 12, 24, 36, and 48 mm/h by following the rainfall records in the Three Gorges area (Ecology and Environment Project Leader Group of the Three Gorges Project of Chinese Academy of Sciences 1988). More details are shown in Table 27.1.

Due to the amount of soil loss related to the grain composition (especially in sand composition), the test materials are chosen as the sand which has grain diameters

Table 27.1 Design scheme of mono-factor model test

Test group	Material	Slope angle (°)	Water level (m)	Intensity of rainfall (mm/h)
(1)	Fine sand	32	145	12
	Coarse sand	32	145	12
	Silt sand	32	145	12
	Silty clay	32	145	12
(2)	Fine sand	53	145	12
	Fine sand	32	145	12
	Fine sand	22	145	12
	Fine sand	12	145	12
(3)	Fine sand	32	139	12
	Fine sand	32	145	12
	Fine sand	32	156	12
	Fine sand	32	175	12
(4)	Fine sand	32	145	12
	Fine sand	32	145	24
	Fine sand	32	145	36
	Fine sand	32	145	48

between 0.075 and 2 mm (Kong 1992). The percentage of grain compositions are as follows: fine sand 93.71%, coarse sand 78.4%, silt 59.4%, and silty clay 34.78%.

Values of surface area and the volume of the model slopes depend on the slope angles. After analyzing the relationships between amount of loss of unit's volume and every four effect factors and the relationships between amount of loss of unit's surface area and every four effect factors, it has been found that the relative coefficient is higher in the relation between amount of loss of unit's volume and every four effect factors (Table 27.2). Therefore, the amount of loss of unit's volume is chosen to represent the amount of loss on the banks (see Table 27.3).

With the calculated data, five curves are created to reflect the relationships between the amount of loss and every four effect factor, see Figs. 27.1, 27.2, 27.3, 27.4, and 27.5.

It can be indicated from Fig. 27.1 that when the grain composition of sand which has a particle diameter between 0.075 and 2 mm is less than 40%, the sand property

Table 27.2 Relative coefficients of relationships between the amount of loss of unit's volume (kg/m^3) and each effect factor

Test factor	Relative coefficient
$0.075 < d < 2$ mm sand composition (%)	0.800
Slope angle (°)	0.949
Water level (m)	0.867
Intensity of rainfall (mm/h)	0.873

Table 27.3 Results of mono-factor model test

Test group	0.075–2 mm grain percentage (%)	Slope angle (°)	Water level (cm)	Intensity of rainfall (mm/h)	Amount of loss (kg/m^3)
1	93.71	32	145	12	13.225
	78.4	32	145	12	2.252
	59.4	32	145	12	1.151
	34.78	32	145	12	0.234
2	93.71	53	145	12	62.709
	93.71	32	145	12	13.225
	93.71	22	145	12	4.267
	93.71	12	145	12	1.414
3	93.71	32	139	12	11.725
	93.71	32	145	12	13.225
	93.71	32	156	12	2.295
	93.71	32	175	12	1.353
4	93.71	32	145	12	12.595
	93.71	32	145	24	13.667
	93.71	32	145	36	16.452
	93.71	32	145	48	31.905

cannot influence the amount of loss of unit's volume too much; but when the percentage exceeds 80%, the influence increases sharply, for which it can be concluded that when the soil on the banks is mainly composed of sand, the banks are prone to collapse easily, and the real case also reflects this conclusion.

However, there are two conditions to be considered where the grain composition is outside 0.075–2 mm. The first condition is where the diameters of grains which

Fig. 27.1 Relational curve for the amount of loss of a unit's volume and content grain composition between 0.075 and 2 mm in diameter
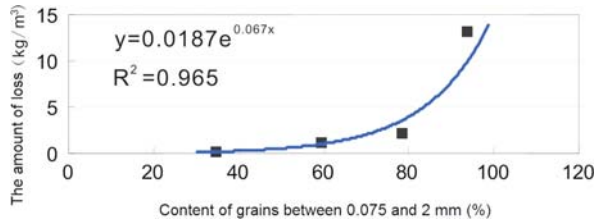

Fig. 27.2 Relational curve for the amount of loss of a unit's volume and content percentage of grain that is less than 0.075 mm in diameter
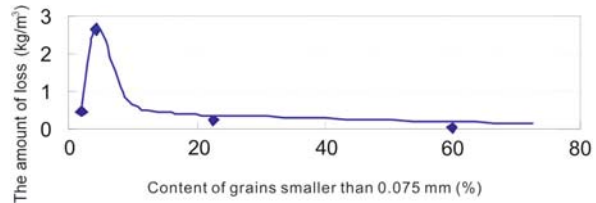

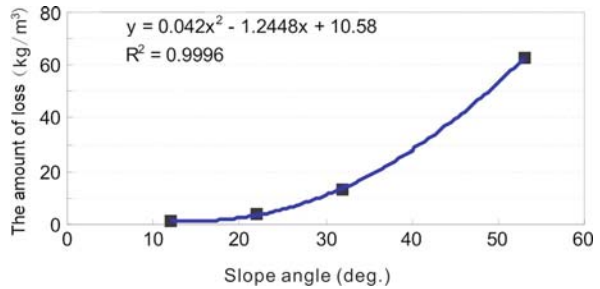**Fig. 27.3** Relational curve for the amount of loss of a unit's volume and angle of the slope

Fig. 27.4 Relational curve for the amount of loss of a unit's volume and rainfall intensity
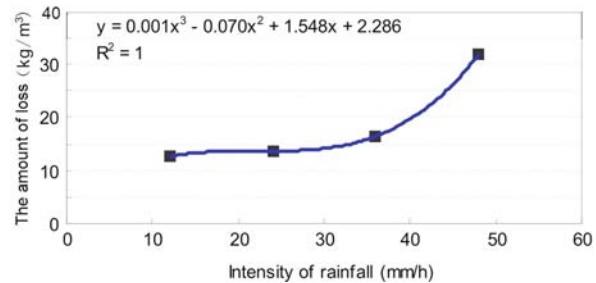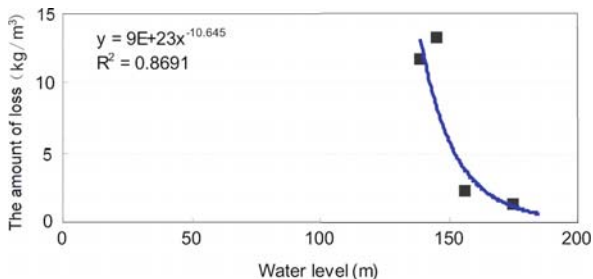
Fig. 27.5 Relational curve for the amount of loss of a unit's volume and water level of reservoir

are smaller than 0.075 mm and comprise the major percentage, and the banks are composed of silt and clay. Because of the large cohesive force, the banks do not collapse easily. The second one is where the grain diameters are larger than 2 mm and comprise the major percentage, and the banks are composed of breccia and block-granules, where gravities are exceeded by the carrying ability of water. In this case, the banks do not collapse easily. These conclusions are indicated in Fig. 27.2.

Figure 27.2 illustrates the relation between the amount of loss of a unit's volume and grain composition of which particle diameters are smaller than 0.075 mm. The points on the x-axis represent coarse sand, fine sand, silt and silty clay, from left to right, respectively. It can be concluded from Fig. 27.2 that the bank which is composed mainly of fine sand prone to collapse most under the same condition. This is because of the larger gravity of coarse sand and the larger cohesive force in silt and silty clay. The results reflect the similar situation in the real case along the banks of the Three Gorges reservoir.

Figure 27.3 illustrates the relation between amount of loss of unit's volume and a slope angle which is a direct ratio. When the slope angle is smaller than 22° (same as the natural resting slope angle above water in the Three Gorges area), with the slope angle getting deeper, the speed of loss of unit's volume becomes slower; when the slope angle is bigger than 22°, the effect toward the loss of volume from the slope angle becomes obvious. Therefore, it can be concluded that when the slope angle exceeds a certain value (>22°), the effect cannot be ignored.

Figure 27.4 shows the relationship between water level and the amount of loss of a unit's volume. According to the curve, it can be concluded that with the intensity of rainfall increasing, the loss of volume is also increasing gradually. When the intensity of rainfall is less than 36 mm/h, the effect to the loss amount is less, and vice versa.

Figure 27.5 shows the relationship between the water level and the loss of the unit's volume as an inverse ratio. This result seems against the order of nature, but the reason might be the results due to the confined test models. The change in water level is related to the dynamic stress field inside the slope.

Figure 27.6 shows that when water level is high, as when it reached level 1, the difference in water head inside the slope is h1 from the top A point to level 1, the value is less than h2, which stands for the difference in water head inside the slope

Fig. 27.6 Change of moving
water pressure inside bank
soil mass at different water
levels
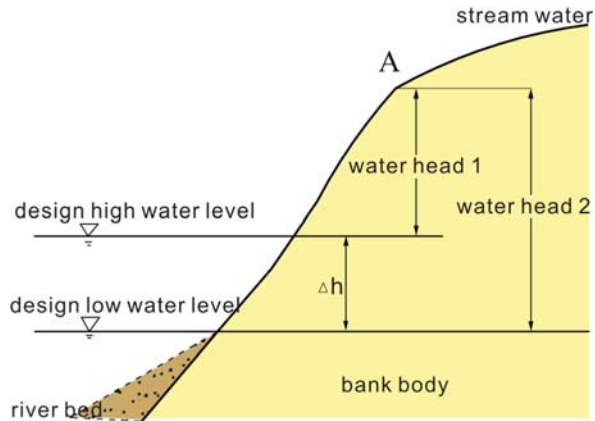
from the top A point to level 2; the smaller the difference is, the weaker the dynamic
stress field is, so less soil will be lost from the bank, and vice versa.

It also can be concluded from Fig. 27.5 that when the water level is below 166
m, changing the amount of loss of the unit's volume will be directly affected by the
water level in a direct ratio. When the water level is above 166 m, the influence from
water level causing loss of a unit's volume will become weak.

By studying the relational curves for every four factors, the inflexion of slope
can be found in the curves and the point can be considered as the limit value of
each effect factor. When the value of one factor exceeds the limit point on curve,
it would reflect this factor becoming the major factor for the total. In conclusion,
focus should be on finding the inflexion of the curve when checking which factor
influences the bank collapse the most.

Multi-factor Model Test

Design and Procedure of the Multi-factor Model Test

This model test is based on the mono-factor model test which considers the four
effect factors which are the slope angle, water level, intensity of rainfall, and the
sand property. Furthermore, it proposed four levels to describe every effect factor.
Similar to the mono-factor test, the design average natural resting angle of four types
of test materials is 53° under natural moisture content, natural resting angle under
water is 32°, and slope angles are 15, 25, 40, 55°, respectively, for four levels; the
design water levels are 139, 145, 156, 175 m for four levels; the design intensity of
rainfall is 12, 24, 36, 48 mm/h for four levels. The test materials are composed of
silty sand, fine sand, coarse sand, and silt. Following the normal distribution theory,
it is in the design to apply the orthogonal method to match each factor and four
levels together, the results of which are shown in Table 27.4.

Table 27.4 Design procedure of the multi-factor model test

Test time	Slope angle (°)	Water level (m)	Intensity of rainfall (mm/h)	Sand property
1	15	139	12	Silt
2	15	145	24	Silty sand
3	15	156	36	Fine sand
4	15	175	48	Coarse sand
5	25	139	24	Fine sand
6	25	145	12	Coarse sand
7	25	156	48	Silt
8	25	175	36	Silty sand
9	40	139	36	Coarse sand
10	40	145	48	Fine sand
11	40	156	12	Silty sand
12	40	175	24	Silt
13	55	139	48	Silty sand
14	55	145	36	Silt
15	55	156	24	Coarse sand
16	55	175	12	Fine sand

Model Test in Different Types of Bank Collapse

There are two types of bank collapse due to loss of materials along the Three Gorges
reservoir area: the erosion type and the sliding type.

1. *Erosion type*: This can be described as the soil on the banks being carried away by
erosion and washing out of the reservoir water, waves, and rainfall. At this point the
bank collapses and moves backward. By the test, it can be found that when the slope
angle is small or the c, ϕ in sand property is small, and the intensity of rainfall is
small, the main type of bank collapse is the erosion type. This kind of bank collapse
has the characteristics of being slow, long-lasting, and small in scale. Figures 27.7
and 27.8 show this type of bank collapse.

2. *Sliding type*: This can be described as the soil mass moving along a sliding plain,
triggered by the heavy rainfall or some other factors. The test model is shown in
Figs. 27.9 and 27.10. During the test, it can be found that this type of bank collapse
often occurs when the water level varies a lot affecting the dynamic stress field
inside the deep slopes.

Sensitivity Analysis for Effect Factors

When the particle diameter of the test materials is smaller than 0.075 mm, due to the
large cohensive force, bank collaspe would not happen; while the particle diamater
is larger than 2 mm, the gravity of the material is too large to sustain the water,
the bank collapse also would not happen. Therefore, the material of which particle

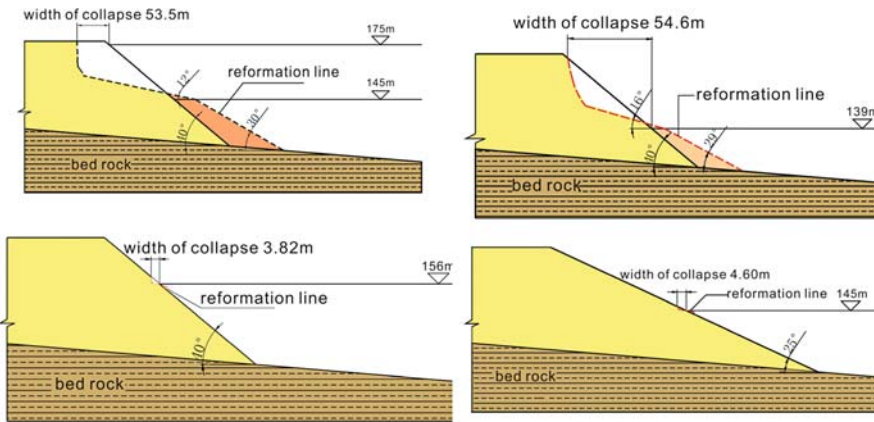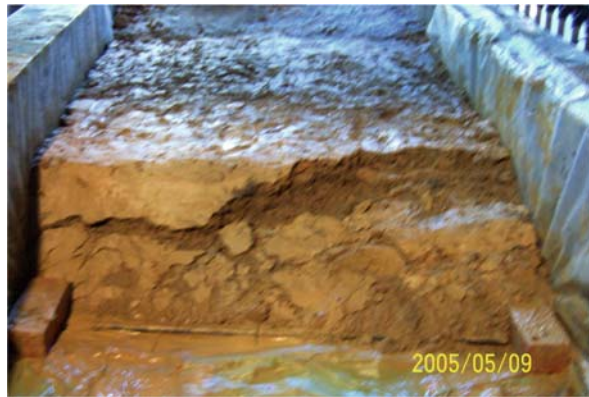**Fig. 27.7** Bank collapse for
the erosion type

Fig. 27.8 Cross section of bank collapse for the erosion type

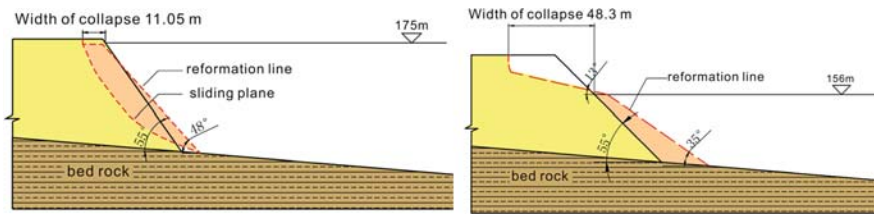**Fig. 27.9** Bank collapse for
the sliding type

Fig. 27.10 Cross section of bank collapse for the sliding type

diameter is between 0.075 and 2 mm is chosen to be the test material. The proportion of sand is the main concern in preparing the test material. The results of the test show that bank collaspe would not happen in silty clay slope, so it is proposed to reduce the test time from 16 groups in Table 27.4 to 12 groups in Table 27.5, and the collaspe widths are transited to the real case by scale.

According to the results in Table 27.5, the sensitivity coefficient of collaspe width to each effect factor can be calculated for the purpose of evaluating the effect factor quantitatively.

Here is one part of the calculation by slope angle to introduce the application of the sensitivity coefficient calculation method (Li and Yu 2004).

First, the average width of collapse by slope angles is calculated:

$$15° : (3.95 + 3.30 + 4.20)/3 = 3.82$$
$$25° : (84.47 + 4.60 + 8.45)/3 = 32.51$$
$$40° : (54.6 + 53.35 + 3.82)/3 = 37.26$$
$$55° : (46.41 + 48.3 + 11.05)/3 = 35.25$$

Second, in the changing area of slope angle, the sensitivity coefficient is calculated:

Table 27.5 Processing form about data of multi-factor test

Time	Slope angle (°)	Water level (m)	Intensity of rainfall (mm/h)	Sand property(%)	Collapse width (m)
1	15	145	24	59.4	3.95
2	15	156	36	93.71	3.30
3	15	175	48	78.4	4.20
4	25	139	24	93.71	84.47
5	25	145	12	78.4	4.60
6	25	175	36	59.4	8.45
7	40	139	36	78.4	54.60
8	40	145	48	93.71	53.35
9	40	156	12	59.4	3.82
10	55	139	48	59.4	46.41
11	55	156	24	78.4	48.30
12	55	175	12	93.71	11.05

$$15-25° : (32.51 − 3.82)/(25 − 15) =   2.87$$
$$25-40° : (37.26 − 32.51)/(40 − 25) =   0.32$$
$$40-55° : (35.25 − 37.26)/(55 − 40) = −0.13$$

Then the average value of sensitivity coefficient from every slope angle group is calculated:

$$(2.87 + 0.32 − 0.13)/3 = 1.02$$

By following the same method, the sensitivity coefficient of water level, intensity of rainfall, and the sand properties are –2.48, 0.79, and 0.87, respectively.

It can be concluded from the results that the water level is the most sensitive factor affecting the width of bank collapse; slope angle and sand property are less sensitive than water level, but the intensity of rainfall is the least sensitive factor.

Time-Dependent Model Test

So far as it has been told, every prediction method about bank collapse can only predict the width of bank collapse when the slope stops moving, without taking the whole development process of slope movement into consideration. However, the bank collapse is a process of development, which also includes the stages of initiation, development, and cessation. Therefore, in order to provide a previous prediction of bank collapse, it is necessary to study the whole process of bank collapse.

Based on the above research results of the model test, a time-dependent model has been prepared to study the rules of slope development after a long duration of impoundment of reservoir water.

Design Procedure of the Time-Dependent Model Test

The slopes in the Three Gorges reservoir area are almost all soil slopes. In order to find out the development process as time passes, it is proposed that a certain slope angle and a certain water level be used as components of the model. The test model geometry ratio is 1:130, the testing through is 0.6 m in height, 1.5 m in width, and 1.8 m in length. The original slope angle is 40°, the height of the design slope is as 50 m, the water level is 156 m, the design heights of waves is between 1 and 1.5 m. By manually simulating wave action on the design banks regularly for certain periods, the data for slope angle underwater, width of the erosion belt, and deformation on the crown on the slopes have been collected and the width of the collapse bank has been calculated. The results are used to analyze the development process of bank collapse taking into consideration of a time-dependent component.

Test Results and Analysis

The duration of the test is about $5\frac{1}{2}$ months. The phenomena of bank collapse has stopped after 3 months; however, in order to get the more precise results from the test, the duration has been prolonged for another $2\frac{1}{2}$ months.

The erosion started from the surface and deepened into the slope body gradually. By the action of waves, a niche formed on the slope in the test (Figs. 27.10 and 27.11). The materials that have been washed away have sediment at the slope toe and formed a discharge underwater.

Due to the niche that was enlarged by the wave erosion as time passed by, the bank would collapse by gravitational effect. Lots of cracks appeared on the crown of the slope. At the same time, the angle of slope changed because of the sediment materials from the collapse. The wave stopped its effect on the slope when the erosion belt reached 35 m and the slope above water was stable, and it is also the stop signal of the test. Some selected data from the test are shown in Table 27.6.

The width of bank collapse, erosion belt, and the displacement of the slope (include the length under water) are the most important data in the test. Figure 27.12 illustrates the development trend of each data by the time which has passed.
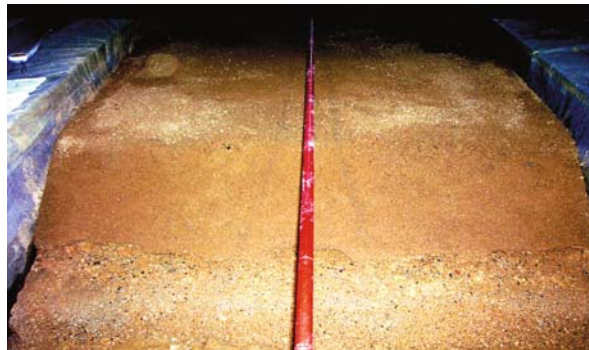

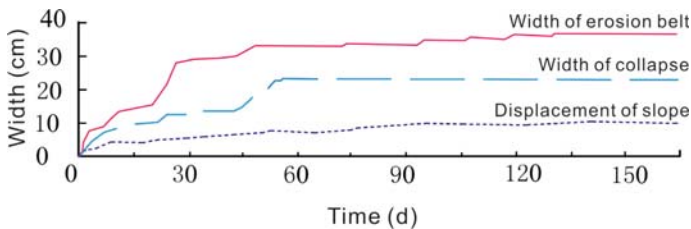**Fig. 27.11** Scouring at the face layer

Fig. 27.12 The development current of the bank collapse

Table 27.6 Results of bank collapse modeling test

Duration (min)	Displacement on the toe of slope (cm)	Slope length underwater (cm)	Slope height underwater (cm)	Slope angle underwater (°)	Slope eroded width (cm)	Bank collapse width (cm)
0	0	25	20	38.65	0	0
3	2	25	19	37.23	7	4
6	3	26	17.5	33.94	9	7
9	4	26	17	33.17	11	8
12	4	26	17	33.17	13	9
15	4	26.5	17	32.68	14	9.5
18	4.5	28	17	31.26	15	10
21	5	27	17	32.19	16	10.5
24	5	23.5	16	34.24	21	12.5
27	5	20	16	38.65	24.5	12.5
30	5.5	20	16	38.65	28	12.5
33	5.5	19	16	40.10	29	13.5
36	6	20	15	36.87	29	13.5
39	6	20	15	36.87	29	13.5
42	6	20.5	15	36.19	29.5	14
45	6.5	21.5	15	34.90	30	15
48	6.5	21.5	15	34.90	32	19
51	7	22	16	36.02	33	20
54	7.5	22.5	15.5	34.56	33	22
60	7.5	22.5	15.5	34.56	33	23
72	7.5	22.5	15.5	34.56	33	23
75	8	22.5	15.5	34.56	33.5	23
90	8	22.5	14.5	32.80	33.5	23
96	8.5	22	14	32.47	34.5	23
99	8.5	22	14	32.47	34.5	23
108	8.5	21.5	14	33.07	35	23
117	8.5	21.5	13.5	32.12	35	23
120	9	21	13.5	32.73	36	23
129	9	21	13.5	32.73	36	23
132	9.5	21	13.5	32.73	36.5	23
150	9.5	21	14	33.69	36.5	23
165	9.5	21	13.5	32.73	36.5	23

Analysis of Bank Collapse Development Process

General Process of Bank Collapse

There are four stages that can be organized by the characteristics in the process: (1) surface erosion, (2) shallow erosion, (3) deep erosion, and (4) termination of slope movement (Figs. 27.13 and 27.14).

1. *Surface erosion*: Waves destroyed the bank by carrying the intensely weathered materials away (Fig. 27.11). A discharge was formed on the slope toe area, and an exception occurred when the slope angle was too big or the water level was too deep. A steep terrace formed on the top of the erosion belt, see Fig. 27.15.

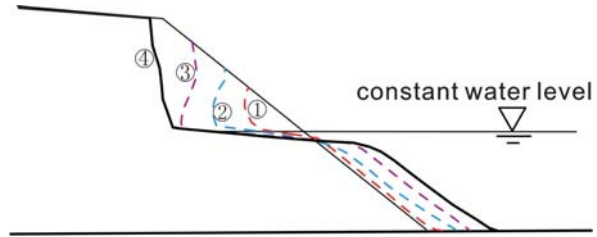**Fig. 27.13** The typical cross-sectional plane of the bank collapse seedtime

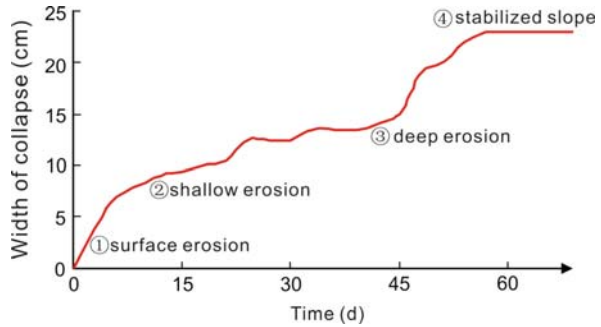**Fig. 27.14** The curve of the bank collapse width changing with time

Fig. 27.15 Steep terrace formed by shallow erosion

The characteristics of this stage are as follows: high velocity of erosion, narrow erosion belt, direct effect by waves, long run-out distance of eroded materials, niches formed under water, and decrease in slope angle.

2. *Shallow erosion*: Due to a tighter structure than that of the materials on the surface, the materials on the shallow part of slopes are not easily washed away. The velocity of erosion decreased. However, when time passed, the collapse also occurred due to the effect of gravity on the upper slopes. Several niches formed on part of the banks (Fig. 27.16).

The characteristics of this stage are as follows: slow velocity of erosion, wide erosion belt, and shallow erosion occurring on slopes, niches formed underwater and continued a decrease in slope angle.

Fig. 27.16 The niche eroded
by wave action on the back of
the slope

Fig. 27.16 The niche eroded by wave action on the back of the slope

Fig. 27.17 The perpendicular wall after the collapse

3. *Deep erosion*: Due to niches and the width of the erosion belts that continued to enlarge, the effect of waves becomes smaller. With niches enlarging continually, the upper part of the slopes would collapse on a large scale, and would occur suddenly (see Fig. 27.17). Because of such a large amount of collapsed materials they cannot be carried away quickly, and the slope angle underwater would increase afterwards.

The characteristics of this stage are the developing pattern of the erosion, appearing like a ladder, width of erosion belt increases continually, niches are enlarged continually, and the shape of slope under water is protruded.

4. *Slope movement stopped*: When the width of erosion belt exceeds certain values, the wave cannot affect the part of the slope which is above water anymore, which means the slope comes into a stable stage when no more new sediment materials from the erosion are processed. However, this will happen only if other factors do not affect the slope stability other than the erosion.

The characteristics of this stage are as follows: the velocity of the bank collapse slows down, and the movement of the slope becomes slow until it stops.

Although the general process can be divided into four different stages according to a time-dependent effect, it is not easy to find out the clear distinguishing point. Actually, every stage may include the washed, erosion, collapse phenomena, for it maintains the order of the development process. Therefore, a conclusion can be

drawn as the erosion on the surface of slope occurs more often than the shallow erosion, and the velocity of bank collapse is slow when the erosion belt is wide. The sudden collapse will occur when the erosion reaches the deep part of the slope.

The varying heights on the water level only affected the erosion belt, and it also followed the general regulation of the development process, of which the development pattern also can be described as a ladder pattern.

Stage 3 is found to be the most important stage of the general process. The duration, pattern, and the scale of bank collapse vary too much when stage 3 occurs under different conditions. When the slope is composed of loose materials such as sand, it is hard to form a niche underwater due to the low cohesive force, and the slope will collapse gradually without pause in the process. When the slope is composed of clay or silt, the bank collapse will take a long time to cover the whole development process, and the slope will collapse in the pattern of a ladder. When the slope angle is big, large-scale collapse would occur suddenly. The velocity of bank collapse, the collapse pattern, and scale are evident by this stage.

Evidence of Bank Collapse Termination

By studying the geometrical form of slopes, it can be found that the evidence of bank collapse stopped, the calculation are shown as below, see Fig. 27.18. The width of bank collapse can be counted as follows:

$$s = a + b + c - d - e$$

The width of stopped slope after erosion can be counted as follows:
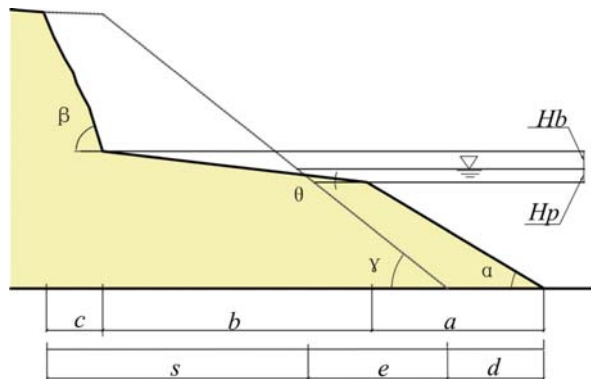
$$b = (Hp + Hb + \Delta H)ctg\,\theta$$

Fig. 27.18 The cross section of the bank when collapse ended

where ΔH is the height difference of water level, θ the stable slope angle on the erosion belt, *a* the width of the slope under water, *b* the width of the stopped slope, *c* the changing width of the slope above water, *d* the width difference of the slope toe underwater, *e* the original width of the slope underwater, *s* the width of the bank collapse, *Hb* the height of waves effecting, and *Hp* the depth of the waves effecting.

Conclusion

(1) It can be concluded from the mono-factor model test that the bank width, slope angle, property of bank soil, intensity of rainfall would affect the bank collapse on different levels and the sand property and slope angle play the most important roles of the four factors. Relationships between the amount of loss of volume on slopes and slope angle, sand property, and intensity of rainfall are in a direct ratio. When one of the factors exceeds a certain limit value, the bank collapse will occur.

(2) It can be concluded from the multi-factor model test that the most sensitive factor which affects the width of collapse is water level, in the following order: slope angle, sand property, and intensity of rainfall.

(3) The process of bank collapse shows an obvious time-dependent pattern. It will experience the surface erosion, shallow erosion, deep erosion, and slope stability. Stage 3 is the most important stage among the four stages. The velocity of collapse and the scale and pattern of collapse can be calculated in this stage.

(4) The evidence of bank collapse ending can be found from the model test: when the slope angle both above and below water arrives at certain values, the waves cannot affect the erosion belt anymore.

A statement should be made that the model test is designed for homogeneous slopes, where the results only represent the general evolution of the slope-failure development process. Further research is necessary to find out the evolution of the development of slope failure in anisotropic slopes that are usually found in the Three Gorges reservoir areas.

References

Ecology and environment project leader group of the Three Gorges project of Chinese Academy of Sciences (1988) The research on status and countermeasures of influence of the Three Gorges project on ecology and environment. Science Press, Beijing, pp 1–8 (in Chinese)

Kong DF (1992) Engineering Geotechnics. Geological Publishing House, Beijing, pp 33–37 (in Chinese)

Li SG, Yu Q (2004) Technical Economics. Harbin Institute of Technology Press, Harbin (in Chinese)

The National Laboratory of Geological Hazard Prevention and Geological Environment Protection, Chengdu University of Technology (2005) Study on pattern, prediction parameters, range evaluation and prediction of bank collapses in Three Gorges area, Chengdu (in Chinese)

Appendix A
Stratigraphic Column in the Three Gorges Area (Modified from Yin 2004)

Stratum unit

Erathem Era	System Period	Series Epoch	Formation (group)	Stratum Code	Thickness (m)	Description
Cenozoic	Quaternary			Q	0–140	Clay, silt, sand, gravel, cobble, colluvium, and sliding debris
Mesozoic	Jurassic	Upper	Penglaizhen	J_3p	215–1,000	Red mudstone, sandy mudstone sandwiching sandstone. At the lower part, gray quartz sandstone and feldspathose sandstone, with discontinuing coal seam
			Suining	J_3s	300–514	Alternative layers of brown mudstone and calcic siltstone, muddy siltstone, and siltstone. Generally contains calcium
		Middle	Shangshaximiao	J_2s	790–1,703	Alternative layers of amethystine and brown mudstone, sandy mudstone, and gray feldspathose sandstone in different thickness, sandwiching mixed color sandstone and siltstone
			Xiashaximiao	J_2xs	335–498	Yellow or green conchostracan shale at the top. Amethystine mudstone, gray or brown feldspathose sandstone at different thickness, sandwiching calcareous nodule
			Xintiangou	J_2x	240–350	Red mudstone, carbonaceous shale, mudstone and quartz sandstone, and muddy siltstone
		Lower	Ziliujing/Niejiashan	$J_{1-2}z/J_{1-2}n$	165–217	Mixed color mudstone, shale sandwiching gray quartz sandstone, siltstone, shell-limestone, and marlite
			Zhenzhuchong	$J_{1-1}z$	109–230	Yellow and black mudstone, shale with gray quartz sandstone, siltstone, with hematite, carbonaceous shale and conglomerate at the bottom

Stratum unit

(continued)

Erathem Era	System Period	Series Epoch	Formation (group)	Stratum Code	Thickness (m)	Description
	Triassic	Upper	Xujiahe/Xiangxi/ Shazhenxi	$T_3xj/T_3xx/T_3s$	338–650	Consists of two sub-formations. The upper sub-formation is feldspathose quartz sandstone, gray-black mudstone, sandy mudstone with siltstone, thin coal seam, with sandy quartz sandstone at the bottom; the lower sub-formation is feldspathose quartz sandstone, quartz sandstone, sandy mudstone with shale, siltstone, thin coal seam, with carbonaceous shale at the bottom
		Middle	Badong/Leikoupo	T_2b/T_2l	97–470	The Badong formation consists of four layers. The first and third layers are limestone, marlite, with a little dolomite limestone, muddy limestone, and muddy stone; the second and fourth layers are calcareous muddy stone, sandwiching siltstone, sandy mudstone. The Leikoupo formation consists of limestone, muddy limestone, dolomite limestone, dolomite sandwiching Karst breccia, with illite claystone at the bottom
		Lower	Jialingjiang	T_1j^2	547–707	Mainly consists of limestone, secondary of dolomite, Karst breccia, and dolomite limestone. Stylolite structure can be seen in limestone
			Feixianguan/Daye	T_1f/T_1d	466–657	The Feixianguan formation consists of amethystine and brown calcareous mudstone, siltstone and limestone, only distributes near Chongqing City. The Daye formation consists of limestone, oolitic limestone, muddy limestone, and little calcareous shale

(continued)

Stratum unit					
Erathem Era	System Period	Series Epoch	Formation (group)	Stratum Code	Thickness (m)	Description
Paleozoic	Permian	Upper	Changxing/Dalong Longtan/Wujiaping	P_2c/P_2d P_2l/P_2w	104–180	Limestone containing chert nodules, sandwiching carbonaceous shale and dolomite limestone. Thin coal seam is sandwiched in Longtan formation
		Lower	Maokou Xixia Liangshan	P_1m P_1x P_1l	127–188	Bulky limestone, biolite, limestone containing chert nodules, coal seam at the bottom
	Carboni-ferous	Upper	Huanglong	C_2h	<38	Dolomite, limestone, and brecciate dolomite
	Devonian	Upper	Xiejingshi Huangjiadeng	D_3x D_3h	50–120	Boundstone, mudstone, quartz sandstone, siltstone, sandstone with gravel, and conglomerate
		Middle	Yuntaiguan	D_2y		
	Silurian	Middle	Shamao Luoerping Longmaxi	S_2s S_2l S_1l	1,280	Shale, silty shale containing siltstone and boundstone
		Lower				
	Ordovician	Upper	Wufeng Linxiang	O_3w O_3l	11	Black silica shale, carbonaceous shale sandwiching chert layer, gray shale, and mudstone containing pyrite
		Middle	Baota Miaopo	O_2b O_2m	78	Dolomite limestone with fissure structure, bulky mudstone, and calcareous mudstone
		Lower	Meitan Honghuayuan Tongzi Nanjinguan	O_1m O_1h O_1t O_1n	315	Shale, boundstone dolomite, and limestone

(continued)

Stratum unit

Erathem Era	System Period	Series Epoch	Formation (group)	Stratum Code	Thickness (m)	Description
	Cambrian	Furon-gian	Sanyoudong	$Є_3s$	564	Crystallized dolomite, dolomite limestone, muddy dolomite, and calcareous shale
		Middle	Qinjiamiao	$Є_2q$	130–204	Silica dolomite limestone, mudstone, dolomite, and shale
		Lower	Shilongdong Tianheban Shipai Shuijingtuo	$Є_1$	373–561	Shale, dolomite, alternative layers of dolomite limestone and silty shale and carbonaceous shale containing phosphate mine layer
	Silian	Upper	Dengying Doushantuo	Z_2d	218–626	Bulky dolomite limestone, dolomite, medium-bulky sandstone, sandy shale, and phosphorite rock
		Lower	Nantuo Liantuo	Z_1l	106–182	Glacial deposits of muddy conglomerate, sandstone, sandy conglomerate, sandy shale, and conglomerate
	Pre-Silian		Konglin formation	$AnZ\delta o^2$	>5,418	Quartz diorite, quartz syenite, biotite trondhjemitic gneiss, mica schist, quartz schist, and migmatite
Note	Contact relation of the strata					Discordance Disconformity Conformity

Yin YP (2004) Major Geological Hazards and the Prevention on Relocation Sites of the Three Gorges Reservoir, the Yangtze River. Geological Publishing House, Beijing (in Chinese).

Appendix B

Distribution of main landslides
in the Three Gorges Reservoir

0 5 15km

Chongqing

Yichang

Legend:

Sandstone & shale with coal seam

Mud limestone interlayer with sandstone and shale

Limestone & dolomite interlayer with shale

Igneous & Metamorphic Rock

City

Village

River

Submerged region

Landslide

Rock fall

Peak